



**HAL**  
open science

# Development of fluorescent platforms for the design of multifunctional compounds for in vitro and in vivo applications in molecular imaging

Jacques Pliquet

► **To cite this version:**

Jacques Pliquet. Development of fluorescent platforms for the design of multifunctional compounds for in vitro and in vivo applications in molecular imaging. Optics / Photonics. Université Bourgogne Franche-Comté, 2018. English. NNT : 2018UBFCK067 . tel-03030365

**HAL Id: tel-03030365**

**<https://theses.hal.science/tel-03030365>**

Submitted on 30 Nov 2020

**HAL** is a multi-disciplinary open access archive for the deposit and dissemination of scientific research documents, whether they are published or not. The documents may come from teaching and research institutions in France or abroad, or from public or private research centers.

L'archive ouverte pluridisciplinaire **HAL**, est destinée au dépôt et à la diffusion de documents scientifiques de niveau recherche, publiés ou non, émanant des établissements d'enseignement et de recherche français ou étrangers, des laboratoires publics ou privés.



**THESE DE DOCTORAT DE L'ETABLISSEMENT UNIVERSITE BOURGOGNE FRANCHE-COMTE  
PREPAREE A L'INSTITUT DE CHIMIE MOLECULAIRE DE L'UNIVERSITE DE BOURGOGNE  
(ICMUB)**

Ecole doctorale n°533  
Ecole Doctorale Carnot-Pasteur

Doctorat de chimie

Par  
Jacques Pliquett

Development of fluorescent platforms for the design of multifunctional compounds for  
*in vitro* and *in vivo* applications in molecular imaging

Thèse présentée et soutenue à Dijon, le 30/11/2018

Composition du Jury:

Dr. FROCHOT, Céline	Directrice de recherche <i>Université de Lorraine, Nancy</i>	Rapportrice
Dr. MAURY, Olivier	Directeur de recherche <i>École Normale Supérieure de Lyon, Lyon</i>	Rapporteur
Pr. GASSER, Gilles	Professeur des Universités <i>Université Paris-Sciences-et-Lettres, Paris</i>	Examineur
Pr. HISSLER, Muriel	Professeure des Universités <i>Université de Rennes 1, Rennes</i>	Présidente du Jury
Dr. BERTHET, Cyril	Directeur de l'unité Pharmaco-imagerie <i>Société OncoDesign®, Dijon</i>	Membre invité
Pr. DENAT, Franck	Professeur des Universités <i>Université Bourgogne – Franche-Comté, Dijon</i>	Directeur de thèse
Dr. BODIO, Ewen	Maître de conférences <i>Université Bourgogne – Franche-Comté, Dijon</i>	Co-directeur de thèse
Dr. GOZE, Christine	Maître de conférences <i>Université Bourgogne – Franche-Comté, Dijon</i>	Co-encadrante de thèse
Dr. PAUL, Catherine	Maître de conférences <i>EPHE – Université de Bourgogne Franche Comté, Dijon</i>	Co-directrice de thèse



## Acknowledgements

This thesis has been prepared in three labs at the University of Burgundy (UB) in Dijon. The bulk of the work has been done at the “Institut de Chimie Moléculaire de l’Université de Bourgogne” (ICMUB – UMR 6302), a joint research unit between the University of Burgundy and the “Centre National de la Recherche Scientifique” (CNRS) in the two teams OCS (OrganoMétallique, Catalyse et Stéréochimie) and P2DA (Polyamines, Porphyrines, Développements et Applications). The biological investigations were performed at the LIIC- (EA 7269), the “Laboratoire d’Immunologie et Immunothérapie des Cancers”, a division of the EPHE, “École Pratique des Hautes Études” situated at the UB. All three teams are warmly acknowledged for having received me in their midst. This thesis was financed by the Conseil Régional de Bourgogne (PhD JCE grant # 2015-9205AAO033S04139 / BG0003226) with the stewardship of Oncodesign and the European Union through the PO FEDER-FSE 2014/2020 Bourgogne program, their support for this project is gratefully acknowledged.

First of all I would like to extend my sincere gratitude towards Professor Muriel Hissler of the University of Rennes 1 and Professor Gilles Gasser of the PSL University of Paris for kindly accepting to examine my work, Dr. Céline Frochot of the University of Lorraine, Nancy and Dr. Olivier Maury of the ENS Lyon for agreeing to review my thesis.

This Ph.D. thesis has of course not been prepared in solitude but is the result of great teamwork and cooperation between a multitude of individuals.

Most notably I would like to thank my four Ph.D. supervisors, Professor Franck Denat, Dr. Ewen Bodio, Dr. Christine Goze (all three ICMUB) and Dr. Catherine Paul (LIIC). All four of you are laudable supervisors and have been extremely supportive throughout my thesis. I am blessed and honored to have had such invested and caring supervisors who knew how to enable me to provide the work that I did, adapt to my style and be present, supportive and challenging in just the right, balanced amount. Christine and Ewen, especially you two have always been accessible at any time of the day or night for my silly requests and ideas, for brainstorming and fruitful discussions, both of scientific as well as personal matter.

I would also like to thank all the persons who have contributed (in a practical fashion by performing experiments for me) to this work; most notably the scientific and technical staff of the “Plateforme d’Analyse Chimique et de Synthèse Moléculaire de l’Université de Bourgogne” (PACSMUB) as well as the quantum chemistry team and other persons in various areas of expertise for their help, counsel and the numerous analyses they performed for me: Marie-Jo Penouilh, Quentin Bonnin (NMR and Mass Analyses), Myriam Laly and Laure Giancarlo (ICP-MS analyses), Yoann Rousselin (Single cristal X-ray analyses), Paul Fleurat-Lessard and Miguel Ponce-Vargas (Quantum chemical simulations).

I would like to thank Anthony Romieu for his expertise and counsel in practical matters concerning fluorescence and optical analyses.

Fluorescence imaging was performed by Souheila Amor who spent countless hours bent over culture dishes and microscopes on my behalf to provide us with great images.

I also appreciate the help and contributions of Cindy Racœur, Nesrine Mabrouk as well as Pierre Simon Bellaye for performing the preclinical study on my bioconjugates, as well as Lucile Dondaine who spent a great amount of time teaching me how to perform IC<sub>50</sub> analyses.

This thesis would probably have been a psychological nightmare without the great friendship and support that I experienced throughout my thesis by all the former and present Ph.D. students who work(ed) at the ICMUB and LIIC at the same time as me and by whom I was so well integrated. Thank you Coline, Audrey, Mario, Johan, Robin, Sarra, Antoine, Anne, Valentin, Alix, Adrien, Léa, Garence, Emma, Océane and everybody else I have forgotten for the great time we spent together both at the ICMUB and LIIC as well as outside of it; for the vacations we had together; the culinary reunions, movies, partys and sportive events. All of you always had 5 (or 50) minutes to spare to chat and joke with me. All of you are the heart and soul of both labs.

Last but not least I would like to thank my girlfriend Marie for her patience during the last three years and for supporting me through the ups and downs of this thesis.



## Table of Contents

Acknowledgements .....	3
Table of Contents .....	6
Abbreviations .....	10
Preface.....	13
Introduction.....	17
0.1    Cancer .....	17
0.2    Imaging and Molecular imaging .....	18
0.2.1    Optical imaging.....	21
0.2.2    Metal based anti-cancer agents.....	32
0.3    Objectives of the thesis: towards the development of fluorescent platforms .....	35
Chapter I – BODIPY .....	41
1.1    Choice of the platform.....	41
1.1.1    Synthesis and functionalization of BODIPY-dyes .....	42
1.2    Gold in biology: a brief overview.....	49
1.2.1    Auranofin.....	49
1.2.2    Chemical biology of Gold.....	49
1.3    BODIPY-Platform.....	53
1.3.1    Towards double functionalization.....	59
1.3.2    Synthesis of BODIPY-acid .....	60
1.3.3    Functionalization of trifunctional BODIPY-acid <b>8</b> .....	61
1.3.4    Introduction of a thioglucose tetraacetate moiety.....	63
1.3.5    Quantum chemical investigations.....	66
1.3.6    Trifunctionalization of the dichloroBODIPY acid.....	67
1.4    Characterization of the BODIPYs properties .....	73
1.4.1    Introduction of a simplified graphic representation.....	73
1.4.2    Photophysical characterization of obtained BODIPY-dyes .....	73
1.4.3    Biological investigations .....	77
1.4.4    Compounds Localization by Confocal Imaging.....	80
1.4.5    Lipophilicity and Gold uptake: generalities.....	82
1.4.6    Establishing structure-activity relationships .....	83
1.5    Summary and outlook .....	85
1.5.1    Summary and Conclusion.....	85
1.5.2    Outlook.....	86
Chapter II – AzaBODIPY .....	91
2.1    Introduction to azaBODIPY-dyes .....	92

2.1.1	Synthetic access to azaBODIPYs .....	92
2.2	1,7-di(phenol)-3,5-di(phenyl)-azaBODIPY .....	94
2.2.1	Photophysical characterization .....	100
2.2.2	Activation of hydroxy-azaBODIPY <b>34</b> for bioconjugation .....	101
2.3	Hydrosolubilization of azaBODIPYs .....	104
2.3.1	Hydrosolubilization of BODIPY and azaBODIPY – an overview .....	104
2.4	E-aza-BODIPYs.....	106
2.4.1	First system: 1,7-di(phenol)-3,5-di(phenyl) E-azaBODIPY.....	108
2.4.2	New platform molecules .....	111
2.4.3	E-azaBODIPY : Second system .....	119
2.4.4	Third system: 1,7-di(phenyl)-3,5-di(methoxyphenyl) E-aza-BODIPYs.....	122
2.4.5	Activation of the compounds for bioconjugation .....	126
2.4.6	Photophysical characterization of E-azaBODIPYs and precursors .....	128
2.5	Biological investigations .....	133
2.5.1	Choice of vector.....	133
2.5.2	Bioconjugation .....	136
2.5.3	Characterization of <i>in vitro</i> -properties of the obtained bioconjugates.....	139
2.5.4	<i>In vivo</i> investigations .....	142
2.6	Summary and Outlook.....	150
2.6.1	Summary .....	150
2.6.2	Outlook.....	153
General Conclusion .....		159
Materials and Methods .....		163
4.1	Materials and Methods .....	163
4.1.1	NMR spectra .....	163
4.1.2	Spectroscopic properties.....	163
4.1.3	Analytical HPLC.....	164
4.1.4	Semi preparative chromatography .....	164
4.1.5	MALDI .....	164
4.1.6	Determination of cytotoxic properties .....	164
4.1.7	Determination of logP .....	165
4.1.8	Cell lines and culture conditions .....	165
4.2	Synthetic procedures.....	165
4.2.1	BODIPYs .....	165
4.2.2	AzaBODIPYs .....	184
4.3	Gold uptake .....	213
4.4	Bioconjugation.....	214

## Table of Contents

4.5	In-vitro confocal microscopy experiments .....	214
	References.....	216
	Table of Figures .....	235
	ANNEX I .....	243
7.1	Quantum Yield .....	243
7.2	Computational Details .....	245
7.2.1	Results and Discussion .....	245
7.3	Details for the determination of distribution coefficients (logD) .....	246
	ANNEX II – Photophysical Spectra.....	250
8.1	Spectra of BODIPYs.....	250
8.2	Spectra of azaBODIPYs.....	253
	Annex III – single crystal X-Ray data.....	259
9.1	Compound 4b .....	259
9.1.1	Summary .....	259
9.1.2	Extended Experimental .....	259
9.1.3	Reflection Statistics .....	260
9.2	Compound 6 .....	261
9.2.1	Summary .....	261
9.2.2	Extended Experimental .....	261
9.2.3	Reflection Statistics .....	262
9.3	Compound 7 .....	263
9.3.1	Summary .....	263
9.3.2	Extended Experimental .....	263
9.3.3	Reflection Statistics .....	264
9.4	Compound 8 .....	265
9.4.1	Summary .....	265
9.4.2	Extended Experimental .....	265
9.4.3	Reflection Statistics .....	266
9.5	Compound 10 .....	267
9.5.1	Summary .....	267
9.5.2	Extended experimental .....	267
9.5.3	Reflection Statistics .....	268
	Résumé.....	269
	Abstract .....	270



## Abbreviations

Abbreviation	Meaning	Abbreviation	Meaning
Abs	absorption	MALDI-TOF	Matrix Assisted Laser Desorption Ionisation - Time of Flight
ACN	acetonitrile	MDSC	myeloid-derived suppressor cell
ADC	antibody-drug-conjugate	MICoE	Molecular Imaging Center of Excellence
anhyd.	anhydrous	MRI	Magnetic Resonance Imaging
approx.	approximately	MRS	Magnetic Resonance Spectroscopy
azaBODIPY	4,4-difluoro-4-bora-3a,4a,8a-triazas-indazene	MSI	mass spectrometry imaging
BBN	bombesine	MTS	(3-(4,5-dimethylthiazol-2-yl)-5-(3-carboxymethoxyphenyl)-2-(4-sulfophenyl)-2H-tetrazolium)
Boc	tert-butyloxycarbonyl	n.d.	none detected/unsuccessful analysis
Boc-TOTA	1-(t-Butyloxycarbonyl-amino)-4,7,10-trioxa-13-tridecanamine	n.t.	not tested
BODIPY	4,4-difluoro-4-bora-3a,4a-diaza-s-indazene	NADPH	nicotinamide adenine dinucleotide phosphate
Bz	benzyl	NBS	N-Bromosuccinimide
cat.	catalytic	NCS	N-Chlorosuccinimide
CEO	Chief executive officer	NHS	N-Hydroxysuccinimide
CT	computed tomography	NIH	National Institute of Health
CTLA4	cytotoxic T-lymphocyte-associated protein 4	NIR	near-infrared
Cy5	Cyanine 5	NMR	nuclear magnetic resonance (spectroscopy)
Cys	Cysteine	NODAGA	1,4,7-triazacyclononane,1-glutaric acid-4,7-acetic acid
DCM	dichloromethane	OAc	acetate
DDQ	2,3-Dichloro-5,6-dicyano-1,4-benzoquinone	p.i.	post injection
DEA	diethylamine	PBS	phosphate buffered saline
DFT	density functional theory	PD-1	Programmed Cell death 1
DIPEA	<i>N,N</i> -diisopropylethylamine	PDITC	phenyl di(isothiocyanate)
DMAP	<i>N,N</i> -Dimethylpyridin-4-amine	PD-L1	Programmed cell death ligand 1
DMF	dimethylformamide	PDT	photodynamic therapy

DMSO	dimethylsulfoxide	PE	phycoerythrin
DNA	deoxyribonucleic acid	PEG	polyethylene glycol
DOL	degree of labelling	PET	Positron Emission Tomography
DOTA	1,4,7,10-Tetraazacyclododecane-1,4,7,10-tetraacetic acid	ppb	parts per billion
EDC	1-Ethyl-3-(3-dimethylaminopropyl)carbodiimide	ppm	parts per million
EGFR	Epidermal growth factor receptor	PSMA	Prostate specific membrane antigen
Em	emission	<i>p</i> TSA	<i>para</i> -toluene sulfonic acid
EN	Electronegativity	QY	quantum yield
EPR	Enhanced Permeability Retention	RF	radio frequency
eq	equivalent	RNA	ribonucleic acid
ESI	electrospray ionization	ROS	Reactive Oxygen Species
Et	ethyl	RP	reversed phase
<i>et al.</i>	<i>et alius (lat.)</i> , and others	rt	room temperature
FA	formic acid	SD	standard deviation
FDA	US Food and Drug Administration	SDS	sodium dodecyl sulfate
FDG	Fluorodeoxyglucose	SDS-PAGE	sodium dodecyl sulfate–polyacrylamide gel electrophoresis
FPLC	fast protein liquid chromatography	<i>S<sub>N</sub>Ar</i>	nucleophilic aromatic substitution
Hb	Hemoglobin	SNM	Society of Nuclear Medicine
HbO <sub>2</sub>	oxygenated Hemoglobin	SPECT	Single Photon Emission Computed Tomography
HBTU	(2-(1H-benzotriazol-1-yl)-1,1,3,3-tetramethyluronium hexafluorophosphate	TBAF	tetrabutylammonium fluoride
HER-2	Human epidermal growth factor Receptor 2	TBDMS	tert-butyl-dimethylsilane
HIV	human immunodeficiency virus	TEA	triethylamine
HOMO	Highest Occupied Molecular Orbital	TEAB	triethylammonium bicarbonate
HPLC	high performance liquid chromatography	TFA	trifluoroacetic acid
HR-MS	High resolution mass spectrometry	THF	tetrahydrofuran
HSAB	Hard and Soft Acids and Bases	tht	tetrahydrothiophene
HSGlu(OAc) <sub>4</sub>	$\beta$ -thioglucose tetraacetate	TLC	thin layer chromatography
IC	Internal Conversion	TRIS	2-Amino-2-(hydroxymethyl)propane-1,3-diol
IC <sub>50</sub>	inhibitory concentration 50	TrxR	Thioredoxin reductase
ICG	indocyanine green	TSTU	<i>N,N,N',N'</i> -Tetramethyl-O-( <i>N</i> -succinimidyl)uronium tetrafluoroborate
ICMUB	Institut de chimie moléculaire de l'Université de Bourgogne	Tyr	Tyrosine

## Abbreviations

---

ICP-MS	inductively coupled plasma-mass spectroscopy	UK	United Kingdom
IgG	Immunoglobulin G	UV	ultraviolet
IR	infrared	vbr	very broad
ISC	Inter System Crossing	VIS	visible
IUPAC	International Union of Pure and Applied Chemistry	WHO	World Health organization
LUMO	Lowest unoccupied Molecular Orbital	$\beta$ -Gal	$\beta$ -Galactosidase

## Preface

Cancer describes a multifaceted body of diseases that originates in the unchecked and dysregulated growth and proliferation of cells. Cancerous growths impede the regular function of affected organs which, if left untreated, leads to the death of the host. [1] It is the the second leading cause of death globally (after cardiovascular diseases) with an estimated 18.07 million new patients annually in 2018, 9.55 million of which will succumb to their disease [2]. In 2010 the WHO estimated the global economic impact of cancer to at least 1.16 trillion US\$, corresponding to 2% of the world's gross domestic product [3].

Researchers around the world seek to develop new drugs and tools to improve diagnosis, response assessment and patient care in order to increase the rates of success as well lessen the impact of current treatment plans on the affected patients. Common treatment plans include operative care and chemotherapy that employes cytotoxic metal complexes, in recent years immunotherapies have been developed that recruit the immune system of the patient to fight cancer: for this pioneering approach James P. Allison and Tasuku Honjo were awarded the Nobel Prize in medicine and physiology in 2018 [4].

A cornerstone in the diagnosis of cancer and the assessment of response to treatment plans is the use of imaging and molecular imaging techniques. Molecular imaging is a set of techniques that permits the visualization, characterization and quantification of biological processes in living organisms [5]. It includes clinically established methods such as Computed Tomography (CT), Positron Emission Tomography (PET), Single Photon Emission Computed Tomography (SPECT) and Magnetic Resonance Imaging (MRI) [6,7]. In recent years optical imaging has emerged as promising modality for molecular imaging. It has proven its potential in pre-clinical applications and is being developed more and more towards clinical use, mainly because of the recent emergence of fluorescence guided surgery. However, due to the elaborateness of the compounds employed for this type of imaging the development of new probes and their modification is often difficult and time consuming. The demand for more versatile approaches and new tools for the continued advancement of this modality is thus evident.

This PhD thesis is in line with these concepts and provides new, versatile tools for the design of fluorescent probes and trackable therapeutical agents.



# Introduction



# Introduction

## 0.1 Cancer

Cancer is a large, heterogeneous body of malignant diseases. It can be defined as “an abnormal growth of cells caused by multiple changes in gene expression leading to a dysregulated balance of cell proliferation and cell death and ultimately evolving into a population of cells that can invade tissues and metastasize to distant sites, causing significant morbidity and, if untreated, death of the host.” [1]

A cancer in itself is non-lethal. However, as the abnormally growing cells gain mass (formation of tumors) and become invasive (formation of metastases), they displace healthy, normally functioning tissue. This impedes the affected organ to execute its tasks properly. The result is (multi-)organ failure and ultimately death of the host.

To reduce this impact and increase the rate of treatment successes many countries have installed systematic screenings as well as prevention and early-diagnosis programs. Figure 1 highlights the necessity of such screening and prevention schemes: an earlier diagnosis significantly improves the rates of success for the treatment.

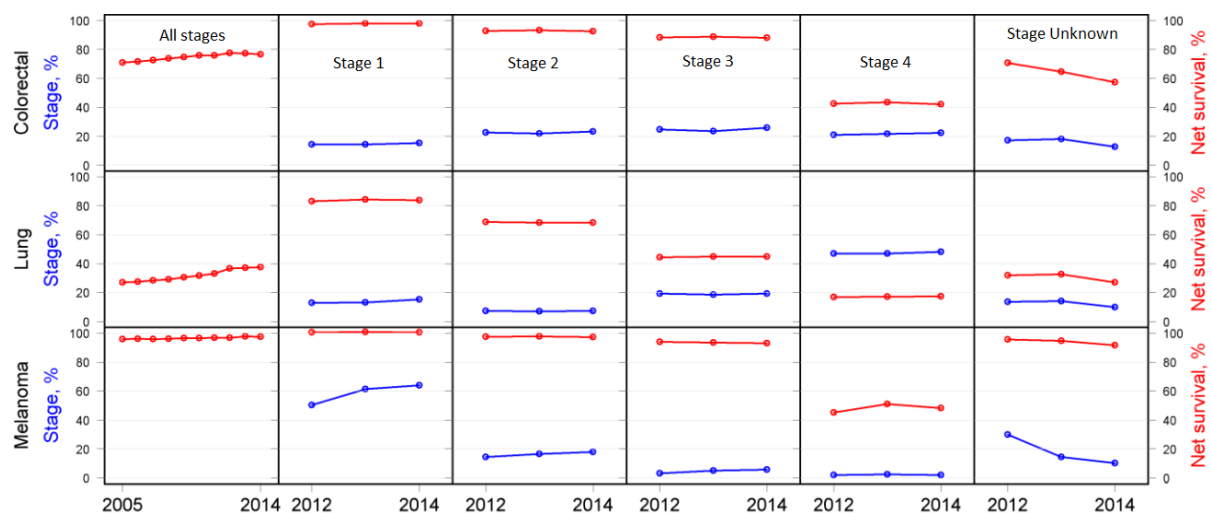


Figure 1: 1-year survival vs stage of initial diagnosis for the NHS (UK) from 2012-2014 for selected cancers. Red denominates % survival, blue % of cancers diagnosed at that stage. Figure adapted from [8]

Common prevention and early diagnosis schemes include blood tests, biopsies, the use of imaging techniques (MRI, CT) and visual inspection (e.g. colonoscopy) [9]. However, as can also be seen in Figure 1 the rates of early-stage diagnosis have not significantly improved between 2012 and 2014 (for the UK), highlighting the need for continued research in early diagnosis.

In 2011 Hanahan and Weinberg defined 10 properties that cells must acquire to classify as cancerous cells: among others they include sustained proliferative signaling, angiogenesis, genomic instability and avoidance of the immune system (Figure 2).

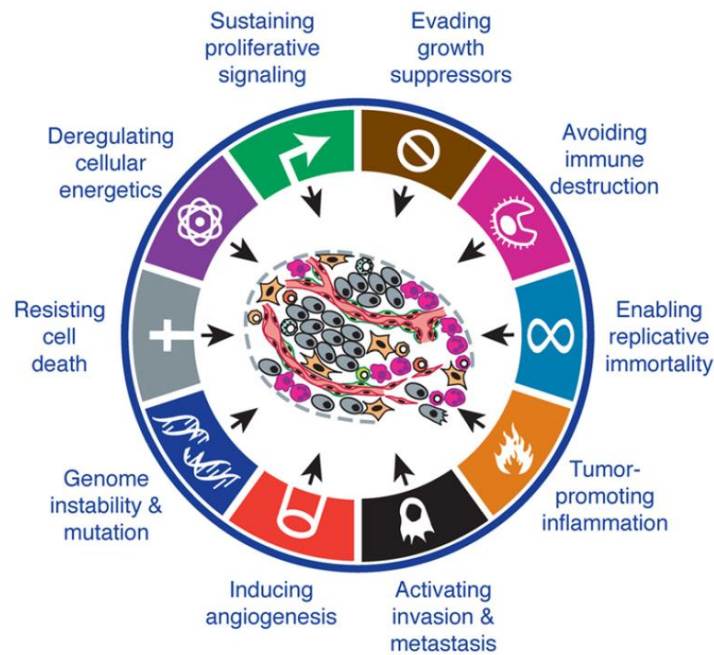


Figure 2: The Hallmarks of cancer. Adapted from [10]

Although cancerous growths combine all of the properties displayed in Figure 2, these properties are acquired over time. Many of the above mentioned characteristics appear at specific stages of tumor development. Each characteristic is associated with deregulation of associated processes and the development of specific antigens that appear or are overexpressed in cancerous tissue. A review on the matter was published by Nair *et al.* in 2018 [11] and summarizes various molecular markers that are overexpressed or tumor specific and have predictive value. Examples include:

- PSMA (Prostate specific membrane antigen): prostate cancer
- HER-2 (human epidermal growth factor receptor 2): breast cancer
- EGFR (Epidermal growth factor receptor): colorectal cancer
- PD-L1 (Programmed cell death ligand 1): various aggressive cancers, including metastatic melanoma, renal cell carcinoma and non-small cell lung cancer

These antigens can be used for immunohistochemical determinations after a biopsy. More interesting however is their use for non-invasive techniques such as diagnostic imaging. Indeed, the antigen can be used as a target for specific probes that enable the evaluation of their presence/absence/overexpression, their systemic distribution and their quantification to verify if a certain pathology is existent. If so, it permits the evaluation of its progression and help to select the treatment plans that are likely to succeed.

## 0.2 Imaging and Molecular imaging

*Imaging* describes a set of techniques aimed at providing visual representations of a system. For biological systems, the obtained image offers anatomical or functional insight. To physicians and researchers alike this insight is the basis to diagnose pathologies, understand biological processes and select treatment options.

In 2007 the members of the Molecular Imaging Center of Excellence (MICoE) and the Society of Nuclear Medicine (SNM) board defined *Molecular imaging*, a subspecialty of imaging, as follows:

*“Molecular imaging is the visualization, characterization, and measurement of biological processes at the molecular and cellular levels in human and other living systems. To elaborate; molecular imaging typically includes 2- or 3- dimensional imaging as well as quantification over time. The techniques used include radiotracer imaging/nuclear medicine, magnetic resonance imaging, magnetic resonance spectroscopy, optical imaging, ultra-sound, and others.”*[5]

It permits the mapping of functional differences, variations in metabolic processes or apparition of pathology-specific markers that are already present in early stages, thereby increasing a patient’s chances to be treated successfully [12]. In modern medicine molecular imaging is not only used to diagnose an illness and delineate for example a tumors’ or ulcers’ expansion, it has become a cornerstone towards the development of personalized medicine.

Today a wide variety of (both classical as well as molecular) imaging techniques is available. Except for ultrasound-based techniques, they all employ electromagnetic radiation in wavelength-windows in which tissue is more or less transparent. A representation of normal attenuation of electromagnetic radiation of biological tissue as function of the employed wavelength is given in Figure 3. It shows that  $\gamma$ - and X-rays, the far-red/near infrared radiation and radio-waves experience little absorption in biological tissue, leading to wavelength-windows in which the body is mostly transparent and that are thus predestined for use in various imaging modalities.

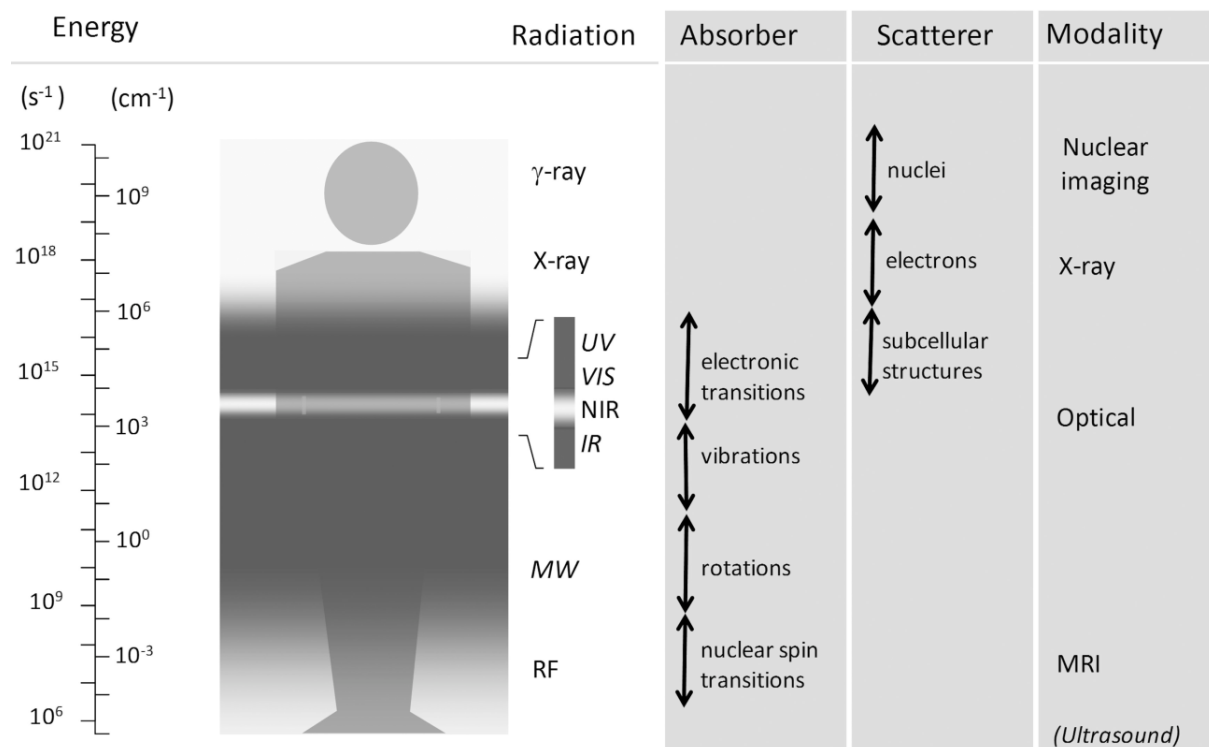


Figure 3: Attenuation of electromagnetic radiation by biological tissue [13]

## Introduction

The imaging techniques can be distinguished along several criteria. They can be differentiated by their:

- energy ( $\gamma$ -, X-rays, VIS/IR-radiation, RF or soundwaves)
- attainable spatial resolution (microscopic, *mesoscopic*, macroscopic)
- type of provided information (anatomical/structural, physiological, cellular, molecular)

Each imaging modality possesses intrinsic advantages and disadvantages that depend on the energy that is used, the way an image is obtained and the information that is provided [6,7]. An overview of the strengths and weaknesses of some techniques are given in Table 1.

Table 1: Examples for imaging modalities. Adapted from [6] and [7]

Technique	spatial resolution	temporal resolution	depth of penetration	primary contrast	Contrast/Imaging agent	Cost	information obtained	main use
<b>CT</b>	50 $\mu\text{m}$	minutes	no limit	tissue density	iodinated molecules, Barium infusions	\$\$	anatomical, physiological	clinical, pre-clinical
<b>SPECT</b>	1-2mm	minutes-hours	no limit	-	$^{99\text{m}}\text{Tc}$ , $^{111}\text{In}$ labelled molecules	\$\$\$	physiological, molecular	clinical, pre-clinical
<b>PET</b>	1-2mm	minutes-hours	no limit	-	$^{18}\text{F}$ , $^{64}\text{Cu}$ , $^{11}\text{C}$ , ( $^{68}\text{Ga}$ ), ( $^{89}\text{Zr}$ )-labelled molecules	\$\$\$	physiological, molecular	clinical, pre-clinical
<b>MRI</b>	10 - 100 $\mu\text{m}$	minutes-hours	no limit	water content, oxygenation reflection, tissue interfaces	paramagnetic Chelates, magnetic particles	\$\$\$	anatomical, physiological, molecular	clinical, pre-clinical
<b>Ultrasound</b>	50 $\mu\text{m}$	seconds-minutes	mm-cm	reflection, tissue interfaces	microbubbles	\$	anatomical, physiological, (molecular)	clinical, pre-clinical
<b>photoacoustic imaging</b>	10 $\mu\text{m}$ – 1mm	seconds-minutes	6mm – 5cm	hemoglobin	chromophores	\$	physiological, molecular	clinically translatable
<b>optical fluorescence imaging</b>	2-3mm	seconds-minutes	1-2cm	-	fluorophore-labelled molecules	\$	molecular	preclinical, emerging clinical

CT (computed tomography scan) for example grants excellent spatial resolution, combined with the advantage of unlimited depth of penetration of the used X-Ray radiation. However, the main drawbacks of this technic concerns the high radiation dose, as well as the low sensitivity, which requires very often the use of contrast agent, such as iodine based systems. Due to the large administered doses, patients with damaged kidneys are excluded from such diagnostics. Even with this precaution, contrast agents cause side effects in 0.15% of all patients of which 2.62% are serious (and potentially lethal) [14].

The same applies for MRI (Magnetic Resonance Imaging): it grants excellent anatomical insight but requires large doses of paramagnetic contrast agents (usually Gd-based) for physiological or molecular examinations. As for CT the large required doses of contrast agent restrict their administration and may cause severe side effects (0.3-0.5% of all patients, depending on the contrast agent [15]). SPECT (Single Photon Emission Computed Tomography) and PET (Positron Emission Tomography) are both based on the detection of decay radiation of radioactive nuclides. Both techniques adhere to the tracer-principle: very little probe is administered, which results in a very limited disturbance of the observed system and thus, from a chemical point of view, no toxicity or side effect. Both techniques intrinsically yield molecular and physiological information and permit good resolution. However, the obvious risk that is associated with handling radioactive material as well as the requirements for equipment and technical staff make these techniques extremely expensive and restrict their use to highly specialized diagnostic centers.

Currently the most commonly employed and clinically proven techniques for performing molecular imaging are PET and MRI:  $^{18}\text{F}$ -FDG-PET is routinely used to detect increased glucose uptake in the patient's body to find metastases. MRI can be used to detect the oxygen content of tissues through changes in relaxivity. MRS (Molecular resonance imaging, comparable to NMR) is used to determine concentrations of biomolecules such as choline to N-acetylaspartate and their ratios to determine cancers' aggressiveness [16].

In recent years optical imaging has emerged as promising technique for molecular imaging. It has proven its potential in pre-clinical applications and is being developed more and more towards clinical use, mainly because of the recent advances in fluorescence guided surgery. This thesis inscribes itself in this field of research, it is therefore worth providing a brief overview of currently existing techniques and the underlying principles they are based on.

### 0.2.1 Optical imaging

Optical imaging describes a set of techniques that is based on the detection of radiation in the visible and near infrared part of the electromagnetic spectrum. Various techniques have been developed that rely on its detection, examples include optical tomography, photoacoustic imaging, intravital microscopy, bioluminescence -, Cerenkov- and fluorescence imaging (Table 2).

*Table 2: Examples for imaging modalities that depend on visible and NIR-light*

<b>Optical imaging modality</b>	<b>Image derived from</b>
Optical tomography	Backscattered light
Photoacoustic imaging	Pulsed excitation and localized heating of tissue; detection by ultra-sound device
Bioluminescence imaging	Direct imaging of luciferase/luciferin couple or secondary imaging of chromophores excited by luciferase/luciferin couple
Cerenkov-imaging	Excitation of a fluorophore by Cerenkov radiation from radioactive decay.
Fluorescence imaging	Excitation of a fluorophore, detection of the fluorescence light at longer wavelengths

Among the different optical imaging modalities, optical fluorescence imaging uses photoluminescent compounds as traceable unit to obtain information about the examined system. Fluorophores may be coupled to vectors and other molecules to be used as probes for molecular imaging. The detected "light source" in tissue corresponds then to the fluorophore and thus yields information about its localization and concentration. Before diving deeper into the subject, a brief account of the photophysical processes it depends upon will be given.

## Introduction

### 0.2.1.1 Basic concepts of optical processes

Ultraviolet, visible and (near-)infrared light describe the part of the electromagnetic spectrum in which electronic transitions of outer electrons are possible (Figure 4).

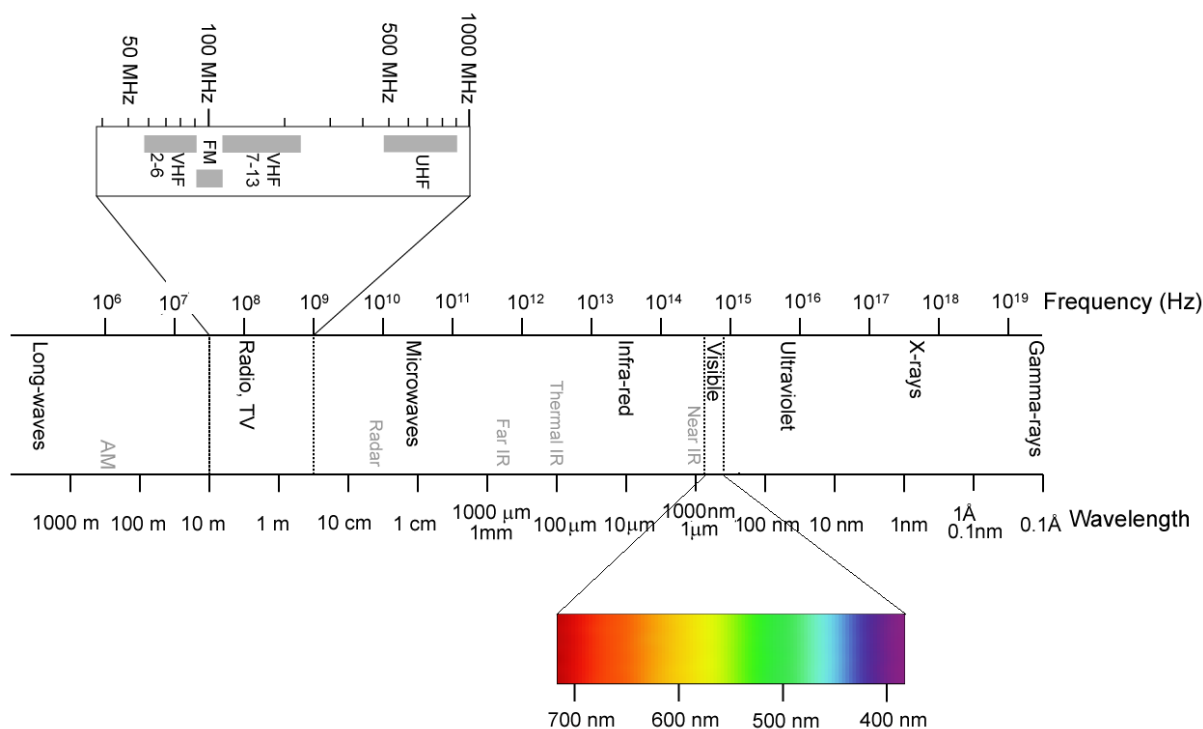


Figure 4: The Electromagnetic spectrum. Adapted from [17]

When such an electronic transition occurs, an electron is excited through interaction with the electromagnetic field of light which results in its excitation from an occupied (usually the highest occupied molecular orbital, HOMO) to an unoccupied (usually the lowest unoccupied molecular orbital, LUMO) molecular orbital of the absorbing species. The energy required for such electronic transitions lies in the range of  $100\text{-}600\text{ kJ mol}^{-1}$  ( $1\text{-}6.2\text{ eV}$ ), corresponding to the  $200\text{-}1200\text{ nm}$  window.

After excitation the system has several pathways to release its energy and fall back into the ground state. The possibilities are shown in the Perrin-Jablonski diagram in Figure 5 and are

#### (2, 3, 4) Internal Conversion (IC) and Intersystem Crossing (ISC)

These are processes were isoenergetic, radiationless conversions of states with the same (IC) or different multiplicity (ISC) take place

(5) Vibrational relaxation (thermalization). The molecule loses its energy to the surrounding medium by collisions with other molecules

#### (6) Fluorescence

A Radiative process between electronic states having the *same* multiplicity

#### (7) Phosphorescence

A radiative process between electronic states having *different* multiplicity

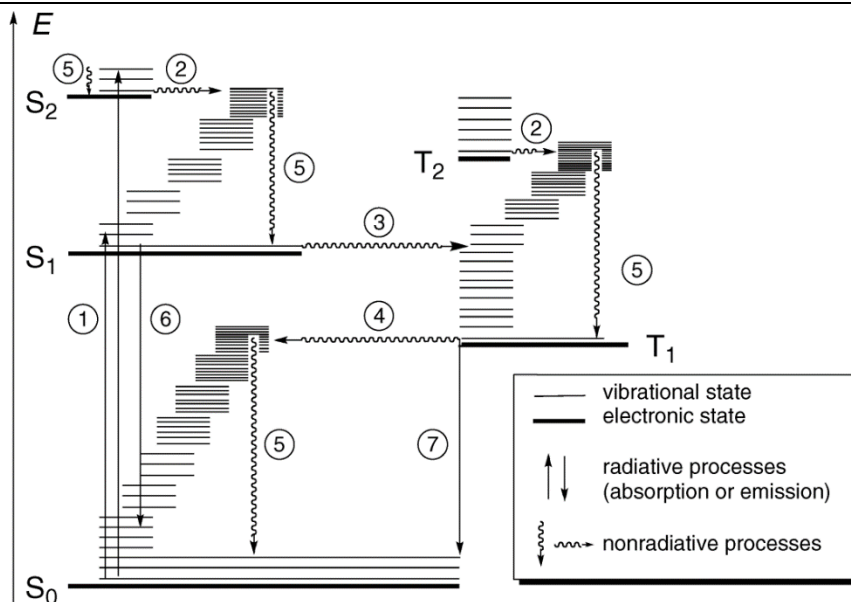


Figure 5: A Perrin-Jablonski Diagram of a given optically active system [18] 1- Absorption, 2- Internal Conversion, 3,4-Intersystem crossing, 5-vibrational relaxation, 6-Fluorescence, 7-Phosphorescence

The timescale at which the different processes occur are summarized in Table 3.

Table 3: Timescale of energetic transitions in excited molecules. Numbers refer to processes shown in Figure 5. Adapted from [18]

Process	Name	Time scale $\tau=1/k_{\text{process}}$ [s]
1	Absorption	$10^{-15}$
2	Internal conversion	$10^{-12}$ - $10^{-6}$
3	Intersystem crossing ( $S \rightarrow T$ )	$10^{-12}$ - $10^{-6}$
4	Intersystem crossing ( $T \rightarrow S$ )	$10^{-9}$ - $10^1$
5	Vibrational relaxation	$10^{-13}$ - $10^{-12}$
6	Fluorescence	$10^{-9}$ - $10^{-7}$
7	Phosphorescence	$10^{-6}$ - $10^{-3}$

The quantum efficiency (also called quantum yield) with which fluorescence occurs is defined as the ratio of emitted to absorbed photons and is proportional to the ratio of lifetimes of the excited state ( $\tau_s$ ) and radiative processes ( $\tau_r$ ) (equation (I))

$$\Phi = \frac{N_{\text{emitted}}}{N_{\text{absorbed}}} \sim \frac{\tau_s}{\tau_r} \quad (\text{I})$$

The fluorescence quantum yield is determined either by measuring the fluorescence lifetimes (i.e. time resolved measurements) or through comparison of the fluorescence intensity of an unknown compound (uk) to a reference (k) in the steady-state regimen using equation (II)

$$\Phi_{uk} = \frac{A_{0,k} \int i_{F,uk} n_{uk}^2}{A_{0,uk} \int i_{F,k} n_k^2} \Phi_k \quad (\text{II})$$

where A is the absorption of the compound,  $\int i$  is the integrated fluorescence intensity and n the refractive index of the employed solvent (a mathematical deduction can be found in ANNEX I - 7.1).

## Introduction

---

In molecular imaging, a fluorophore is characterized by the following photophysical properties:

- Brightness describes the product of quantum efficiency multiplied by molar absorption coefficient ( $\Phi \times \epsilon_{\text{abs}}$ ). It permits the direct comparison of two fluorophores. Concerning the fluorescence properties, a commonly encountered problem in the development of fluorophores is the quenching of fluorescence. Several phenomena can be responsible; two of them (encountered in this thesis) are photoinduced electron transfer and the aggregation of the probes.  
Quenching through photoinduced electron transfer may appear in systems where an acceptor and donor are present in the same molecule. This static quenching may be caused by electron-rich groups such as amines, alcohols or phosphorous substituents with free electron pairs [19]. When the fluorophore in question is poorly soluble in the used solvent, aggregation and molecular stacking can occur. Two types of stacking interactions are possible, J and H-type stacking. Depending on the type of interaction, constructive or destructive interference of single molecule excitons may occur [20]. Compared to monomeric chromophores H-type stacks result in flattened emission peaks, lowered quantum yields and the appearance of a blue-shifted absorption band due to out-of-phase excitonic coupling. J-type stacking displays in-phase excitonic coupling, resulting in bathochromically shifted absorption peaks. Both types of stacking may coexist in solution [21].
- The Stokes shift is the result of vibrational relaxation of a fluorophore into a lower excited state before the occurrence of a radiative transition. Larger Stokes shifts reduce reabsorption of emitted photons due to smaller spectral overlap. Large Stokes shifts permit the use of cheaper filters for the imaging equipment and reduce the background noise in imaging applications.
- Photobleaching describes the phenomenon that fluorophores lose brightness over time under irradiation. It is caused by photochemical reactions that occur with the excited fluorophore and that lead to its permanent inactivation. Reactions of triplet-states and photooxidation are possible causes for this behavior [22]

The absorption and emission wavelengths of the fluorophore represent another important property that need to be tailored for the targeted application.

### 0.2.1.2 Transparency windows

Light (and thus including fluorescence light) is subject to interferences in tissues that affect the attainable depth of penetration, resolution and requirements for equipment.

Three main sources of noise or interference exist in biological tissue

- The absorption coefficient of tissue

Four wavelength windows are distinguished in fluorescence imaging: the visible part (350nm-650nm), the far-red- near infrared I (NIR I) window (650-900nm) and the NIR II (1000nm-1700nm) window that is subdivided into NIR IIa (1100-1300nm) and NIR IIb (1500nm-1700nm) (the specific values vary from source to source) [23,24]. The specific absorption of tissue and common biomolecules for various wavelengths are shown in Figure 6. Especially the NIR I window displays very little absorbance and is therefore often called optical therapeutic window.

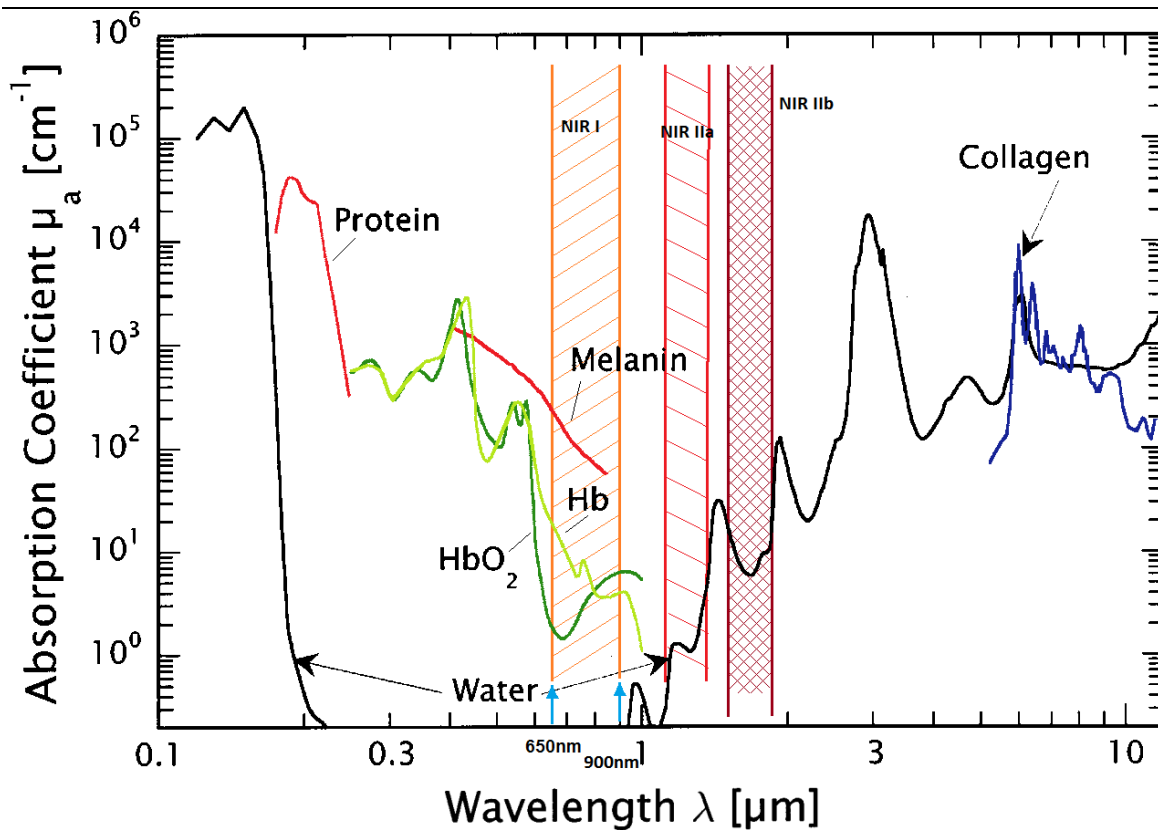


Figure 6: Double logarithmic plot of absorption coefficients of biological tissues in the UV/Vis - infrared range. The optical therapeutic window is highlighted in orange. Hb: Hemoglobin, HbO<sub>2</sub>: oxygenated hemoglobin. Adapted from [25]

The other two main influences are

- autofluorescence of ubiquitous biomolecules such as hemoglobin, melanin and lipids and
- Rayleigh-scattering on particles. Rayleigh-scattering decreases with  $\lambda^{-4}$  of the used wavelengths (blue light scatters far stronger than red light) which leads to higher physically achievable resolutions when longer fluorescence-wavelengths are used.

As mentioned before, each targeted application has optimum requirements for the employed fluorophore: for *in vitro* applications such as confocal/fluorescence microscopy and flow cytometry very little tissue has to be traversed; fluorescence emission in the visible spectrum is thus sufficient and desirable due to lower requirements for the used equipment. *In vivo* fluorescence imaging on the other hand is commonly executed in one of the transparency windows (far red-NIR I and NIR II) due to the higher relative transparency of tissue in this region.

### 0.2.1.3 Classes of Fluorophores and their application

Several classes of fluorophores exist; e.g. nanoparticles and quantum dots [26,27], fluorescent proteins [28,29] and organic and inorganic fluorophores. Biological, biochemical and medical research has become unimaginable without the use of fluorescence microscopy and the staining of specific organelles to establish the localization of various agents in cells and tissue alike.

A wide choice of organic fluorophores exists from which a suitable candidate can be selected, depending on the intended application and required properties (Figure 7).

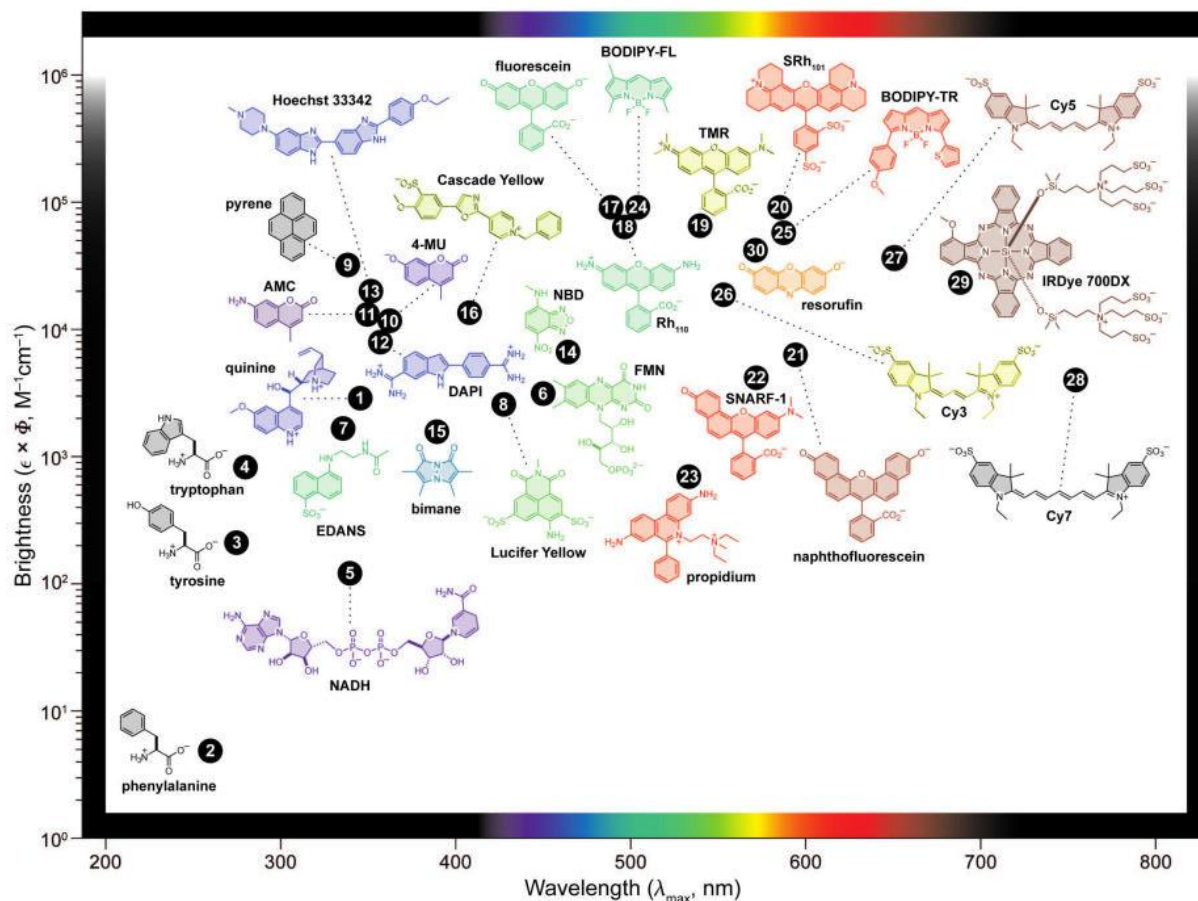


Figure 7: Plot of brightness vs. emission wavelength for various fluorophores [30]

Owing to their high brightness, cyanines, xanthene dyes such as rhodamine or fluorescein and BODIPYs are highly sought after fluorophores. They can be applied as they are to stain specific organelles or be coupled to other molecules to act as a probe.

Some commercial examples for routinely used organelle-specific stains that permit the labelling of life and fixed cells alike are given in Figure 8.

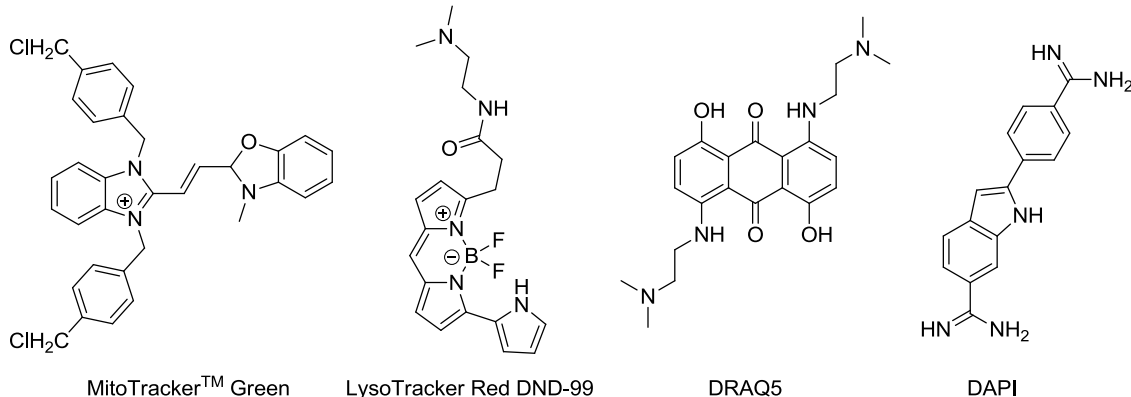


Figure 8: Examples for commercial, organelle specific dyes: MitoTracker™ Green specifically labels mitochondria, LysoTracker Red DND-99 fluoresces in acidic organelles (usually Lysosomes), DRAQ5 stains DNA through intercalation; DAPI intercalates into the minor groove of DNA and thus stains the nucleus [31–34]

Other than organelle specific dyes Xanthene dyes such as fluorescein and Invitrogens Alexa series are the most used dyes for *in vitro* techniques; they are used to label antibodies, peptides, DNA/RNA sequences and many more. When selected with care to reduce spectral overlap many dyes can be used in parallel for multi-colour labelling of an analyzed sample [35] (Figure 9).

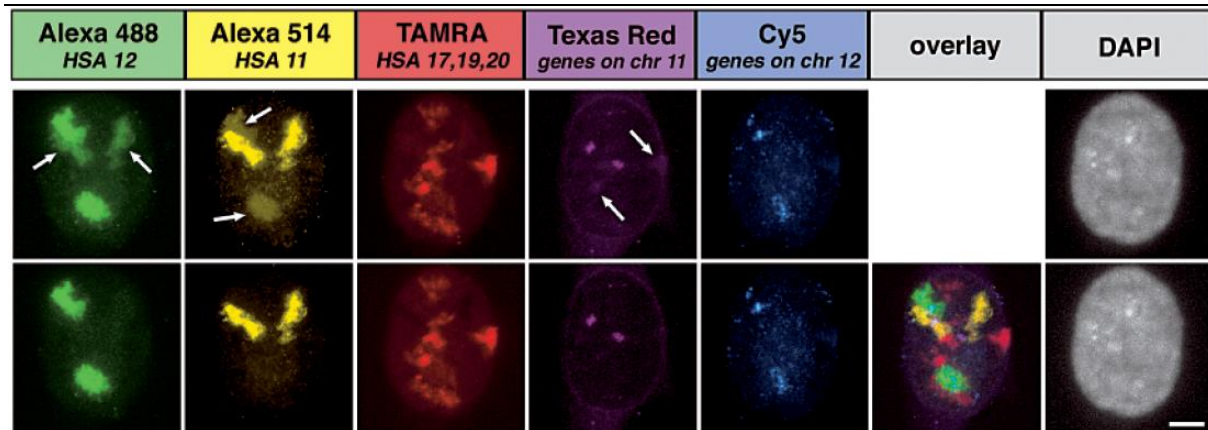


Figure 9: Multi-color fluorescence in situ hybridization of human chromosomes in the cells nucleus. Top row: untreated images for each channel; arrows indicate channel –bleed through. Bottom: spectrally unmixed channels and overlay of unmixed channels [35]. Except for Cy5 all used dyes are Xanthene-derivates

Fluorophore-labelled probes are routinely used for the development of molecular imaging agents to gain insight into biochemical mechanisms and evaluate and quantify cellular processes. Examples include the development of  $\beta$ -lactamase-activated fluorophores to evaluate bacteria's resistance to penicillin by fluorescence activation [36] or the evaluation of  $\beta$ -galactosidase activity by turn-on probes ( $\beta$ -galactosidase is a cellular marker for cellular senescence) [37,38] (Figure 10).

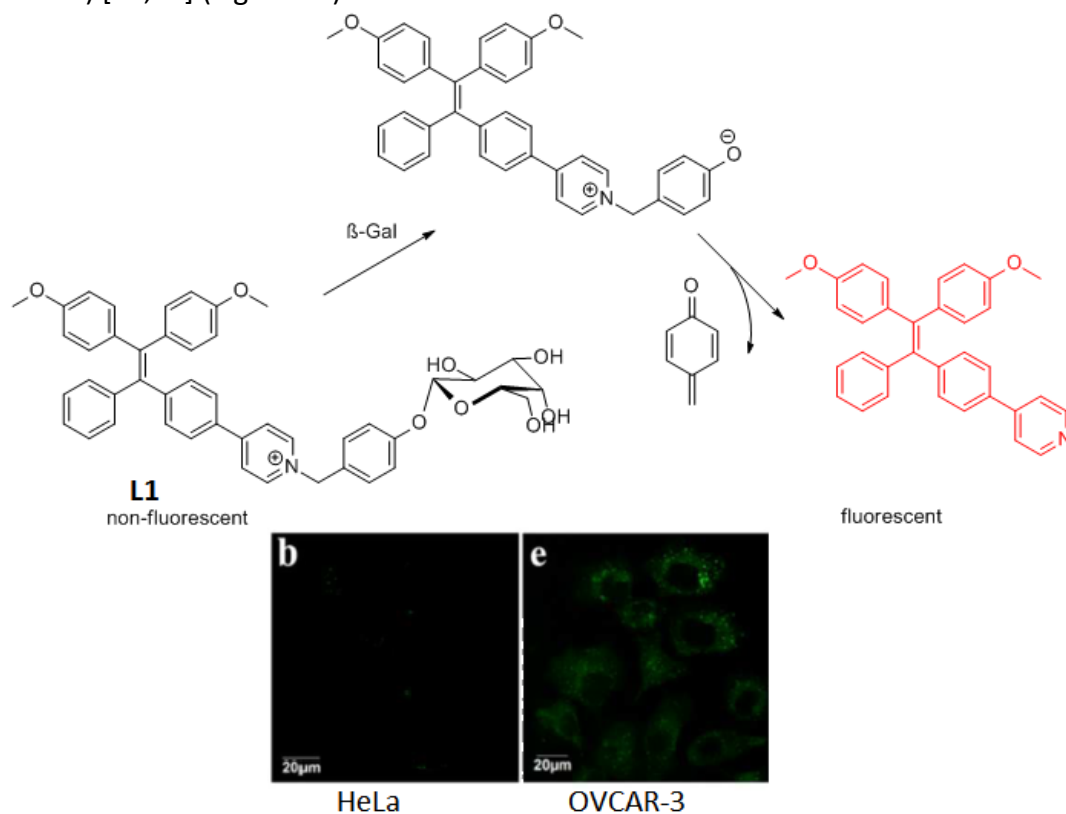


Figure 10: Turn-on fluorescent probe for the detection of  $\beta$ -Galactosidase activity. Image bottom left: fluorescence image of  $\beta$ -Gal negative HeLa cells; bottom right: fluorescence image of  $\beta$ -Gal-positive OVCAR-3 cells. Both were incubated with  $10\mu\text{M}$  L1 for 40min [38]

In 2018 Conic *et al.* applied a variety of Alexa-488 labelled antibodies against nuclear protein targets on electroporated life cells. Using super resolution imaging the labelled antibodies enabled them to study cellular trafficking of newly synthesized proteins and transcription factors and their transport and organization in the cell's nucleus as well as post translational modification events in real time [39].

## Introduction

Whereas *in vitro* applications are dominated by xanthene-dyes such as fluorescein and rhodamine (the routinely employed and commercially available Alexa Fluor series are to ¾ xanthene derivatives [40]) most fluorophores that are used in medical imaging emit in the red end of the visible spectrum or in the infrared. Due to low attenuation by the tissue and very little Rayleigh scattering the largest depth of penetration and best resolution is achieved using the NIR II window. However, the development of organic fluorophores that emit in this region has proven difficult; the existing examples are large polyaromatic donor-acceptor-donor assemblies that have very unfavourable behavior in solution [41]. For this reason most organic fluorophores in *in vivo* imaging emit in the NIR I region, the most commonly used fluorophores are cyanine derivatives such as Cyanine 5 (Cy5), indocyanine green (ICG), IRDye® 800, 5-Ala/Protoporphyrin IX and xanthene-derivates such as fluorescein (Figure 11). Of the above mentioned dyes fluorescein is somewhat of an exception due to its emission far outside of a transparency window. It does however excel in superficial applications such as fluorescence guided surgery [42].

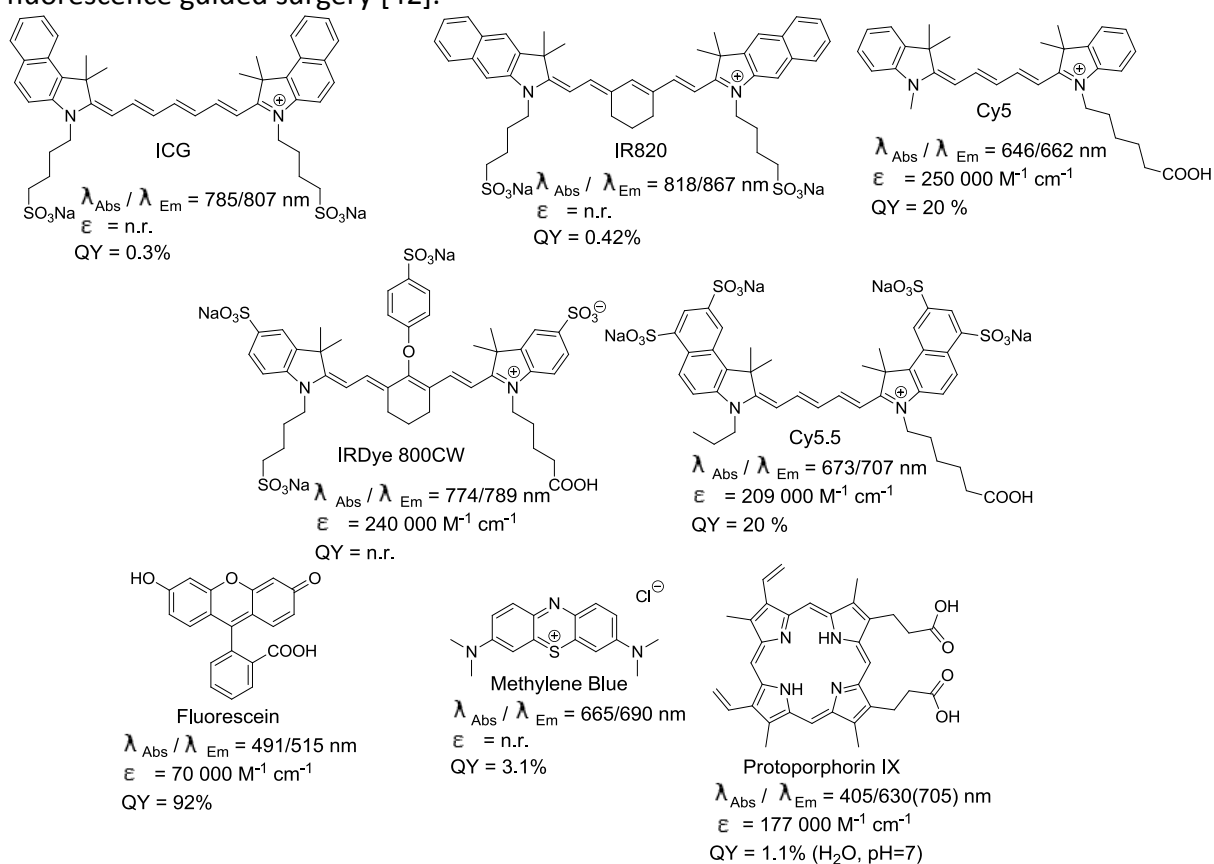


Figure 11: Some examples for fluorophores or fluorescent motives that are currently used in the clinic or in clinical trials (photophysical data of cyanines taken from [43], Fluorescein from [44], methylene blue from [45], Protoporphyrin IX [46,47]). n.r.= not reported

As shown in recent reviews [42,43,48] the field of *in vivo* applications is dominated by cyanine dyes due to their long emission wavelengths and excellent molar absorption coefficients. These translate into good brightnesses even with mediocre quantum yields as seen for the FDA approved ICG. IRDye® 800 CW-bioconjugates are being/have been evaluated in 24 clinical trials (01/2019) against various cancers (Table 4)[49].

Table 4: Status of clinical trials employing IRDye® 800 CW derivatives [49]

Completed	Terminated	Active	Recruiting/unknown
7	3	1	13

However, due to the presence of a multitude of non-aromatic double bonds, cyanine dyes are prone to photobleaching and possess limited chemical stability. Most importantly however they are difficult to functionalize multiple times once assembled. In order to obtain a stable, easy-to-functionalize dye for our purposes we took interest in another class of dyes, BODIPYs.

#### 0.2.1.4 BODIPYs in optical fluorescence imaging

BODIPYs (boron-dipyrromethene dyes) have caught researchers' interest due the combination of good optical properties and excellent chemical and photostability.

BODIPYs, short for 4,4-difluoro-4-bora-3a,4a-diaza-s-indazenes can be considered as annulated cyanine dyes. They possess a boron atom to rigidify the backbone and ensure the planarity of the molecule.

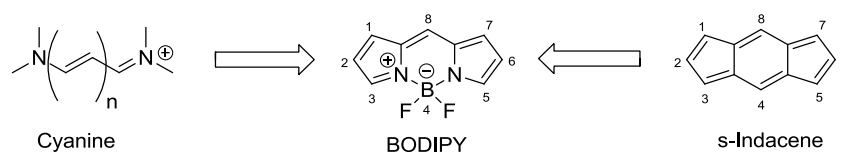


Figure 12: Nomenclature of BODIPYs

The base compound in itself is highly fluorescent and emits at around 500-530nm, depending on the substituents. As for fluorescein this emission is outside of the optical therapeutic window. Just like fluorescein or Alexa-488 they have found their main use in *in vitro* imaging or other light-depending applications such as photodynamic therapy (PDT). In terms of emission wavelength, quantum yields and absorption coefficients, both the commercial Alexa-488 and BODIPY™-FL are interchangeable; BODIPYs however have the advantage of displaying very narrow emission peaks which makes them advantageous for multicolor imaging due to easier spectral unmixing (Figure 13).

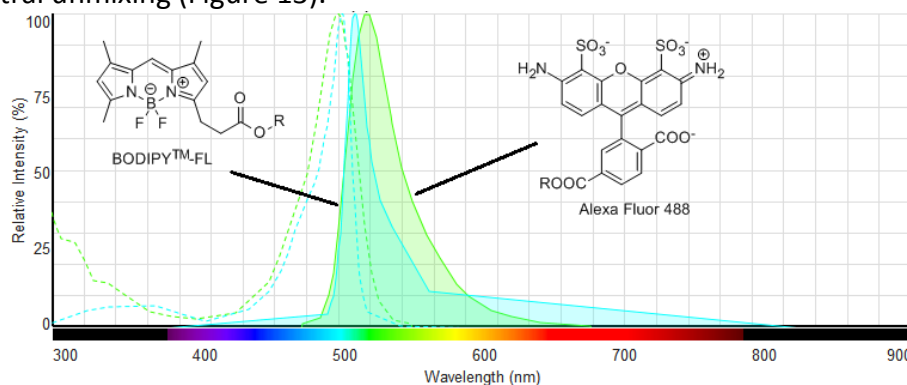


Figure 13: Spectral comparison of the commercial dyes BODIPY-FL(cyan) and Alexa 488 (green) [50]

Besides classic labelling of compounds of interest (as would be possible using other fluorophores) BODIPYs have successfully been used to study membranes [51], lipid droplets in skeletal muscles [52] or monitor the activity of the redoxactive enzymes using cysteine-conjugated BODIPY [53], taking specifically advantage of neutral BODIPYs' properties. For the design of non-commercial dyes they are a well liked class of dyes due to their versatile modifiability.

## Introduction

Besides classic *in vitro* applications more recently they have been applied for *in vivo* imaging and to design bimodal imaging agents that permit fluorescence and PET/SPECT imaging. In these bimodal probes the BODIPY can be coupled to a polyazamacrocycle for the use of radioactive metallic isotopes [54–57]; other examples include the use of  $^{125}\text{I}$  (**L4**)[58] and isotopic exchange of  $^{19}\text{F}$  for  $^{18}\text{F}$  (**L3**)(Figure 14).

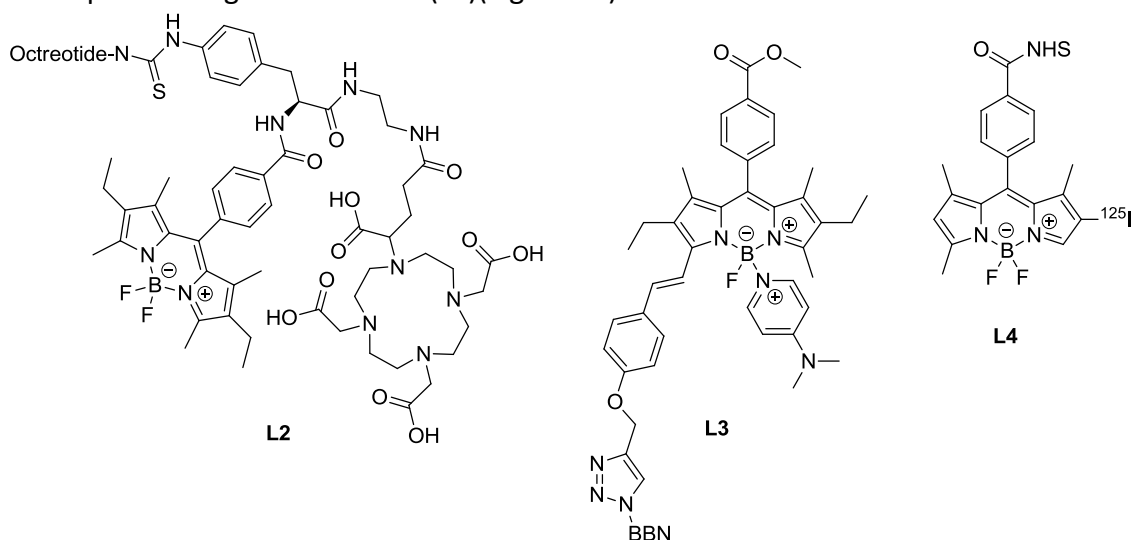


Figure 14: Examples for BODIPY based bimodal probes that combine the advantages of BODIPYs *in vitro* and strengths of PET *in vivo*: **L2** [55] **L3** [57], **L4** [58]

Despite the short emission wavelength classical BODIPYs have been used in numerous instances to perform *in vivo* imaging studies (Figure 15)[59–61].

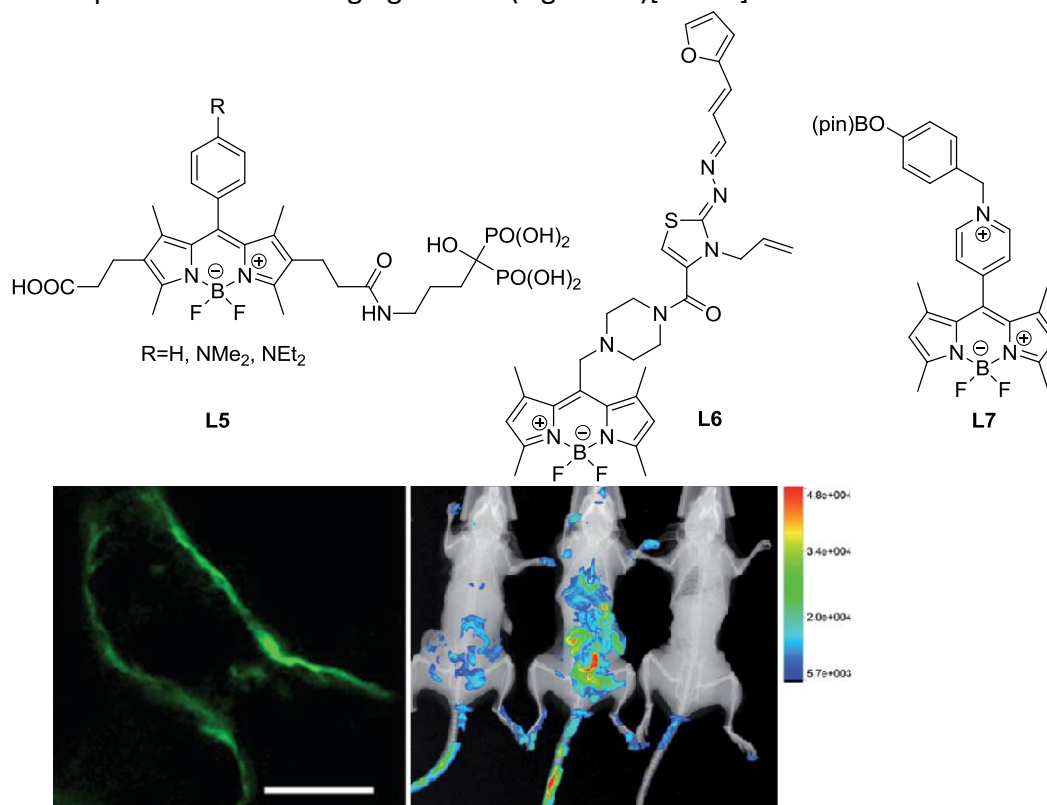


Figure 15: Examples for BODIPY-use in *in vivo* studies. **L5**: on/off-probe for studying osteoclasts in intravital microscopy on mice [59](intravital microscopic image of **L5** beneath); middle: whole body imaging in mice to track anti-Chagas agent **L6** *in vivo* [60] (whole body mice images of **L6** beneath; left mouse 120min p.i. with **L6**-vesicle emulsion, middle mouse 120min p.i. with **L6**-DMSO/ $\text{H}_2\text{O}$ -solution, right mouse: control mouse injected with PBS). **L7**: selective *in vivo* detection of  $\text{H}_2\text{O}_2$  in angelfish [61]

Other examples for their *in vivo* application can be found in [62–66]. Due to the limited transparency of tissue in the used wavelength-window the *in vivo* applications of classical BODIPYs as *in vivo* tracers remain scarce.

For this PhD project we selected this class of fluorophore for the development of a trackable molecular platform that mostly aims at facilitating the required *in vitro* investigations of metal based therapeutic drugs.

In order to overcome the spectral shortcoming of classical BODIPYs, several strategies have been developed to extend the  $\pi$ -system of the BODIPY core in order to reach further into the far red/infrared part of the electromagnetic spectrum. Usually this fine-tuning is done by introduction of styryl-substituents as shown in 2009 by Akkaya's group [67] (L8-L12, Figure 16).

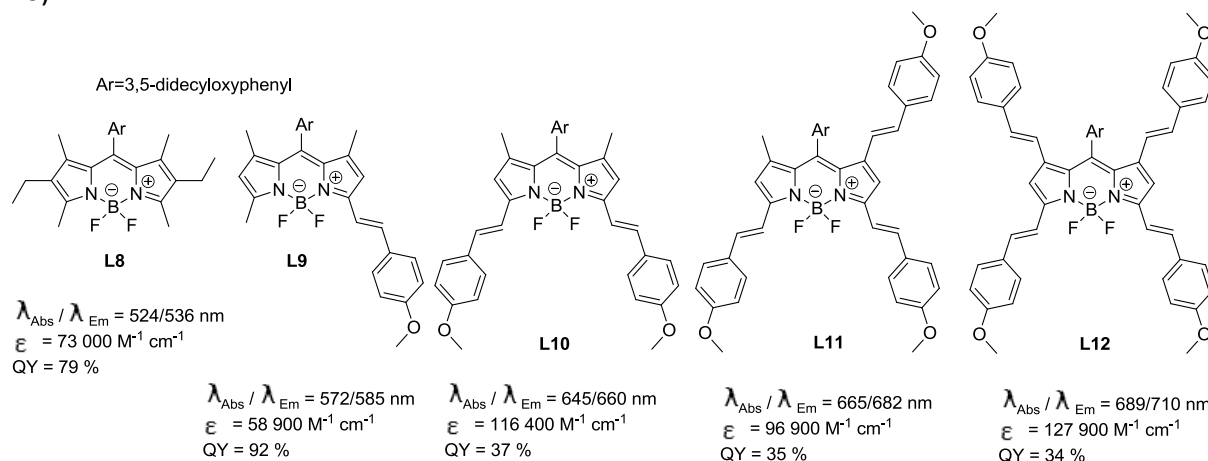


Figure 16: Fine-tuning of optical properties BODIPYs by Knoevenagel reaction. Photophysical data for **L8** in EtOH [68], styrylBODIPYs **L9-L12** in  $\text{CHCl}_3$  [67]

As shown in Figure 16 all resulting BODIPYs maintain excellent optical properties, independent of the number of styryl-substituents that were introduced.

$\pi$ -extended BODIPYs have found widespread pre-clinical use as tracers [69–72], imaging agents for photoacoustic imaging [73] and especially for photodynamic therapy (a good review was recently published by Lee *et al.* [74]). Other strategies for the extension of the  $\pi$ -system are extensively reviewed in the literature (e.g. by Lu *et al.* [75]) and show the great versatility of this class of fluorophores.

Since 2005 azaBODIPYs, a close relative of BODIPY dyes, have received much attention: the replacement of the 8-carbon (*meso*-carbon) by a nitrogen atom red-shifts the absorption and emission maxima by 120-150nm to 650nm and beyond. They possess equally good optical properties (high molar absorbencies, high quantum yields and brightnesses) as their relatives while being more resistant to photobleaching than styryl-BODIPYs due to the absence of free double bonds. Their synthetic accessibility, functionalizations, properties and published applications are shown in detail in Chapter II – AzaBODIPY. Due to the great versatility we selected this class of fluorophore for the development of *in vivo*-trackable agents.

## 0.2.1.5 Theranostics and trackable drugs

Even though the usefulness of classical (non  $\pi$ -extended) BODIPYs as trackable agents for *in vivo* purposes remains relatively limited due to the low wavelength of emission of approx. 530nm they excel during the development-stage of drugs: to gain insight into subcellular processes they are great assets.

The BODIPY-part of the molecule can play out its strength in the *in vitro* techniques such as confocal imaging, flow-cytometry and even intravital microscopy. This permits excellent, subcellular/submicron resolution during the development phase to gain insight into a drug's mechanism of action to distinguish e.g. bound from unbound fluorophore (Figure 17).

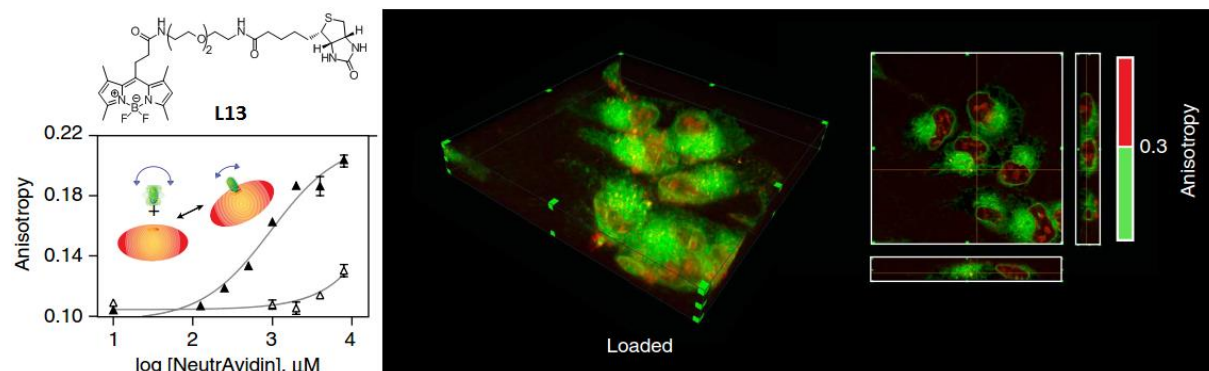


Figure 17: Fluorescence anisotropy imaging of a BODIPY-Biotin derivative (**L13**). Binding of **L13** reduces molecular movement which results in increased fluorescence anisotropy. Green: unbound fluorophore, red: bound fluorophore [76]

The combination of therapeutically active agents with trackable units is also called “theranostics”. Theranostics is an artificial combination of the words therapy/therapeutic and diagnosis/diagnostic. This term was first coined in September 1998 as a sales-pitch by PharmaNetics CEO John Funkhouser when marketing his company's business model: Their approach was to commercialize both the treatment and the diagnostic tool to evaluate treatment efficiency [77,78]. Both the test and the treatment were independent of each other and had to be performed separately, allowed however the personalization and adjustment of the treatment by yielding standardized information about the treatment progress.

The definition and understanding of theranostics has changed over time: nowadays it can incorporate anything between personalized medicine, trackable therapeutic agents as well as diagnostic agents that can be transformed with little effort into their therapeutic counterparts (e.g. changing the radionuclide attached to the tracer from a  $\beta^+$  emitter like  $^{64}\text{Cu}$  to a  $\beta^-$  emitter like  $^{67}\text{Cu}$ ). We decided to use the theranostic approach in order to design a variety of closely related trackable, metal based anti-cancer agents whose localization may change depending on the substituents and substitution pattern exhibited by the molecule. It is therefore worth providing a brief account of metal based anti cancer agents and showcase, how their trackability may facilitate the elaboration and optimization of such compounds.

## 0.2.2 Metal based anti-cancer agents

Nowadays the most common anti-cancer treatment plans include metal based anticancer drugs, 46% of them on the basis of Platinum [79].

The first platinum-drug, cisplatin, was introduced into cancer treatment after the accidental discovery of its cytotoxic properties by Barnett Rosenstein in 1965 [80]. In 1978 the FDA

approved its use as anti-cancer agent [81]. Treatment with cisplatin often leads to severe side effects such as nausea, vomiting, nephrotoxicity and loss of hearing [82].

However, treatment with cisplatin often leads to development of resistances [83,84]. To improve the specificity and reduce side effects a multitude of platinum-drugs has been developed over the last decades. Amongst thousands of failures a variety of compounds has been found that are now available for therapies (or in clinical trials). Some examples and interesting leads are given in Figure 18 (more examples can be found in [85]).

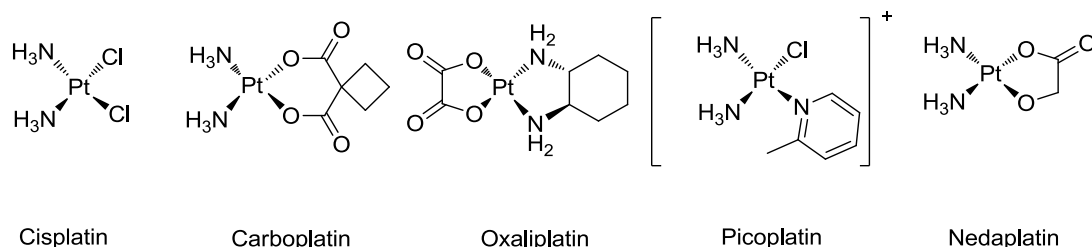


Figure 18: Some Platinum-based drugs that are currently used in therapy or in clinical trials [85]

Due to the frequent resistances the scope of drug development has also widened and shifted from improving platinum drugs towards the discovery of motifs based on other metals and ligands. This limits the development of resistances due to different molecular targets and grants the possibility of dual (or oligo) treatments. A multitude of leads that are based on metals such as ruthenium, titanium, iridium and gold has been discovered [85,86] (Figure 19).

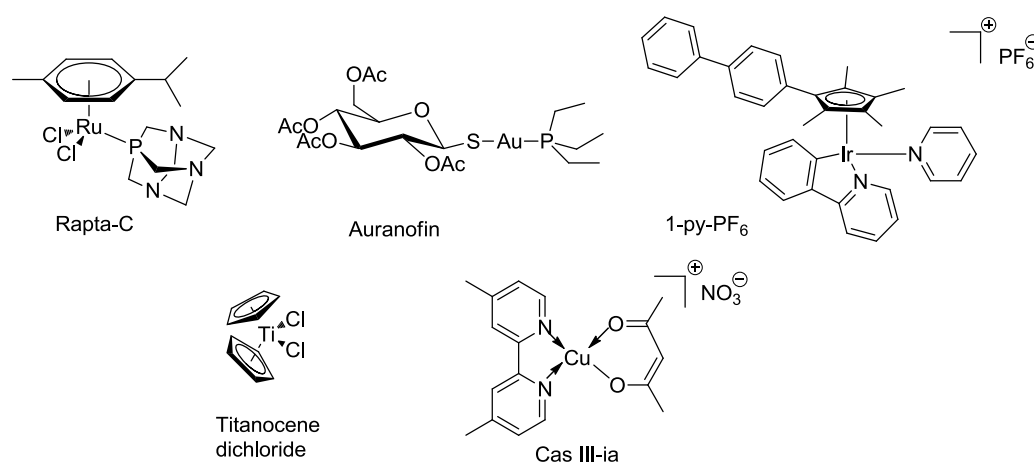


Figure 19: Some lead-motives of therapeutically active metals other than Platinum that are currently in clinical trials [85,87] or showing interesting *in vivo* activity [88]

### 0.2.2.1 Metal based theranostics

Complicated experiments have to be designed to follow the drugs fate *in vitro* (an *in vivo*) and to determine their mechanism. This knowledge however is the base for a rational design and improvement of drugs. The introduction of a trackable moiety to the drug facilitates that task as it intrinsically permits to determine cellular compartments and targets. This approach is the basis of trackable metal based anticancer drugs (metal based theranostics).

Taking the lead motifs from Figure 19 above various BODIPY analogues have been developed by our group as well as others (Figure 20)[89–94].

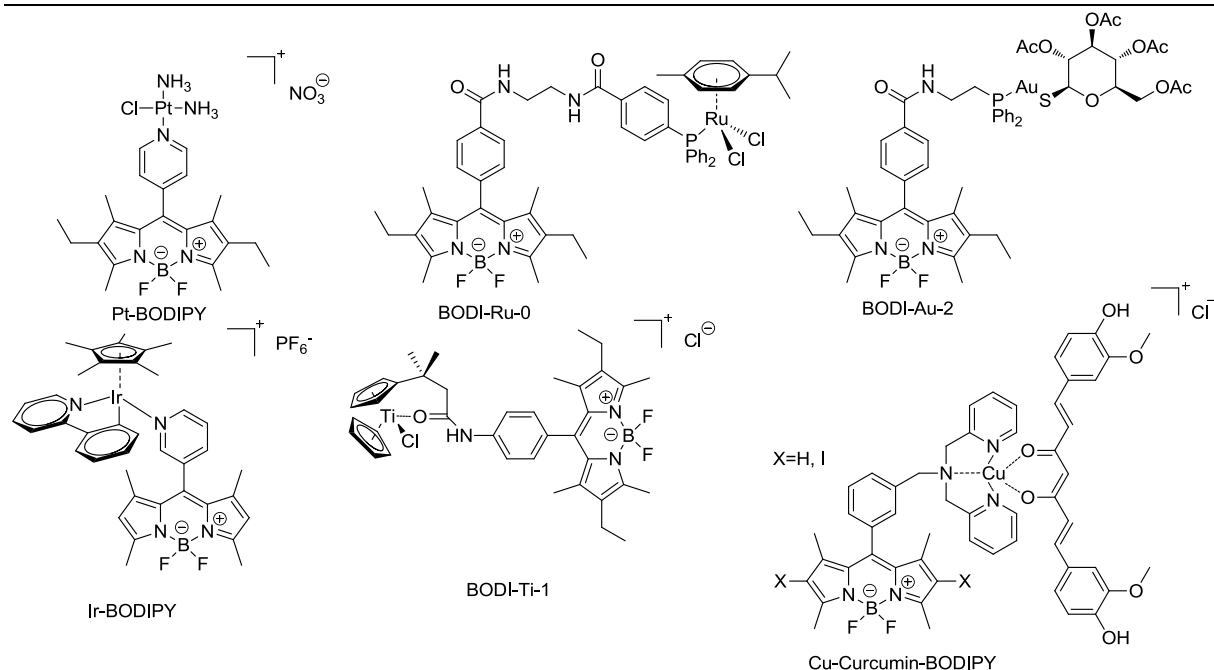


Figure 20: Examples of BODIPY theranostics that have been developed using the leads of Figure 19. Pt-BODIPY [89], BODI-Ru-0 [90], BODI-Au-2 [91], IrBODIPY[92], BODI-Ti-1 [93], Cu-Curcumin-BODIPY for PDT [94]

Recent advances have been thoroughly reviewed by our group [95] as well as others [96]. It is worth noting the non-innocent role of the probe, e.g. in the case of Pt-BODIPY shown in Figure 20: while cisplatin is localized and acts in the cell's nucleus its BODIPY-analogue is localized in the mitochondria. Moreover, it does not enter the nucleus but still maintains good cytotoxicity compared to cisplatin [89]. The influence of the imaging moiety on the biological behavior becomes even more evident when different gold-based, trackable therapeutics that we developed in our group are compared to one another. Indeed, despite a very similar therapeutic moiety (phosphine-gold(I)-complex), the compounds display very different localization and antiproliferative properties (Figure 21).

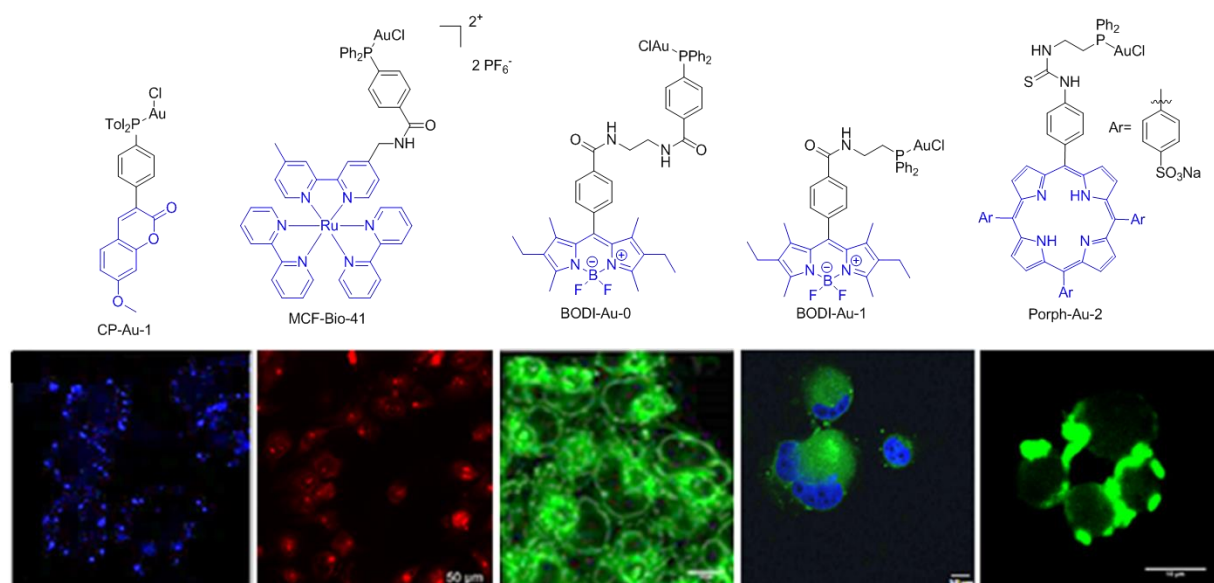


Figure 21: Influence of trackable moiety on cellular localization [95]. Cellular localizations: CP-Au-1: raft domains; MC-Bio-Au-1: nucleus; BODI-Au-0: membranes; BODI-Au-1 (in green, DAPI in blue): cytosol; Porph-Au-2: membranes

Especially the difference between BODI-Au-0 and BODI-Au-1 is striking: The addition of a single benzamide-group results in a different localization whereas no marked change in cytotoxicity was observed.

Consequently, it is obvious that the probe needs to be introduced at the beginning of the optimization process and not when a non-labelled lead has been identified. The problem is that it is very difficult to predict, which combination of probe and therapeutic agent will give good results. Moreover, the design of syntheses providing these sophisticated compounds are often time consuming and lead to a limited number of analogues. Thus, if we want to move this theranostics from a research curiosity to a drug design strategy, it is urgent to find a solution that permits to easily fine-tune and optimize these objects. That is why we decided to conceive platforms suitable for the efficient and rapid synthesis of a large number of optical theranostics. Indeed, a stepwise, controlled and site-specific introduction of moieties of interest would enable to study the individual influence of each component on the final biological behavior. With this information in hand, it is or should be possible to predict general trends in reactivity, selectivity, photophysical properties and biological behavior of a resulting theranostic agent depending on the site of substitution. Moreover, using this information it is possible to rationally design and improve selected properties of the theranostic agent.

### 0.3 Objectives of the thesis: towards the development of fluorescent platforms

“Platform approach” is a well-known strategy aiming at linking more than two compounds together thanks to an additional compound: the platform. This key element must fulfill several requirements, such as:

- be commercially available or cheap to synthesize (few synthetic steps, short reaction time, simple purification, cheap starting material...)
- be available in large scale
- be as simple as possible
- be chemically and thermally stable to enable chemical functionalization
- enable selective stepwise functionalization by at least three substituents

In this study, we target biological applications. More precisely, we want to be able to introduce onto the platform an optical probe, a therapeutic agent, a biologically relevant vector and an additional group for either tuning the physico-chemical properties of the final object (e.g. solubility) or introducing a second modality of imaging (e.g. radioactive probe) (Figure 22).

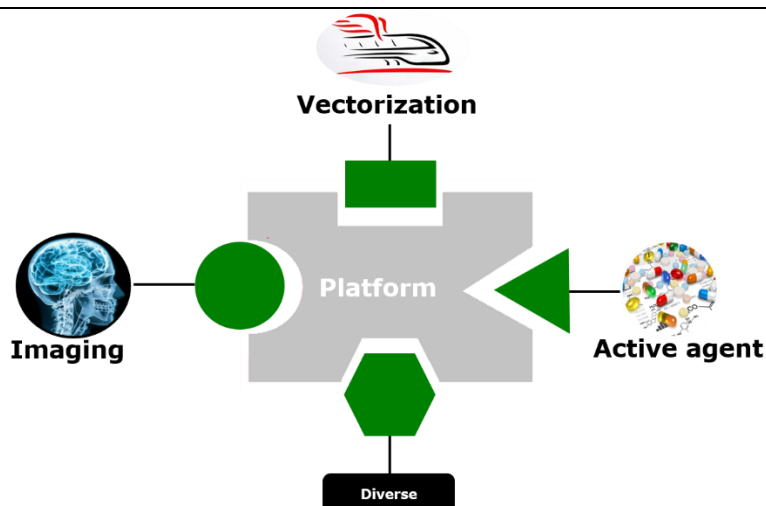


Figure 22: Platform approach

Thus, additional characteristics are required for the platform:

- enable introduction of readily available substituent in mild conditions (ideally nucleophiles such as amine, alcohol, thiol...)
- create biologically stable bonds such as C-C bonds or amides between the platform and the substituents
- do not quench the fluorescence

Numerous platforms are reported in the literature; among them some common examples are the use of amino acids (e.g. lysine), benzotrifuranone (**L15**), dichlorotetrazine (**L17**)... (Figure 23).

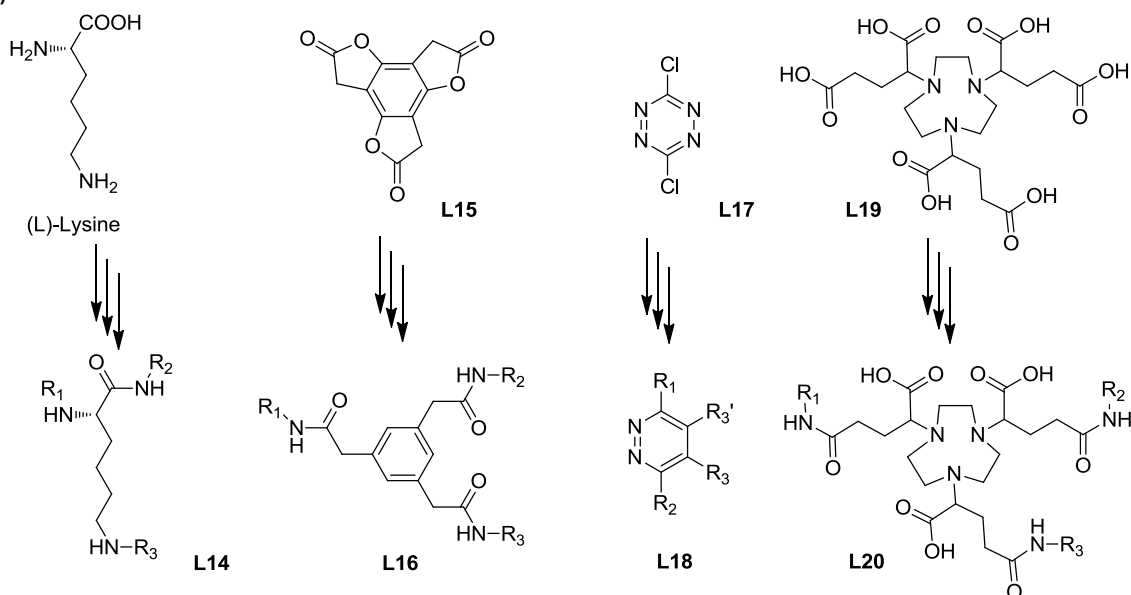


Figure 23: Examples for molecular platforms [97,98]

Most of the reported examples deal with trifunctionalizable platforms, while we envision the combination of four “modalities” (imaging, therapy, vectorization, modification of the hydrophile/lipophile balance). Moreover, it is, in our view, unfortunate that the platform skeleton does not bring any valuable property to the final compound. Thus, we decided to develop a platform, which is itself fluorescent. Nevertheless, it implies that the platform possesses very favorable optical properties (high brightness, resistance to photobleaching) and retains these properties after functionalization.

Although scarce, there are some examples of fluorophores that are used as scaffolds and can be modified or conjugated to vectors without too much trouble as shown by the use of BODIPY (**L21**) [99], Virginia Orange (**L23**) [100] and porphyrin (**L26**) [101] in Figure 24.

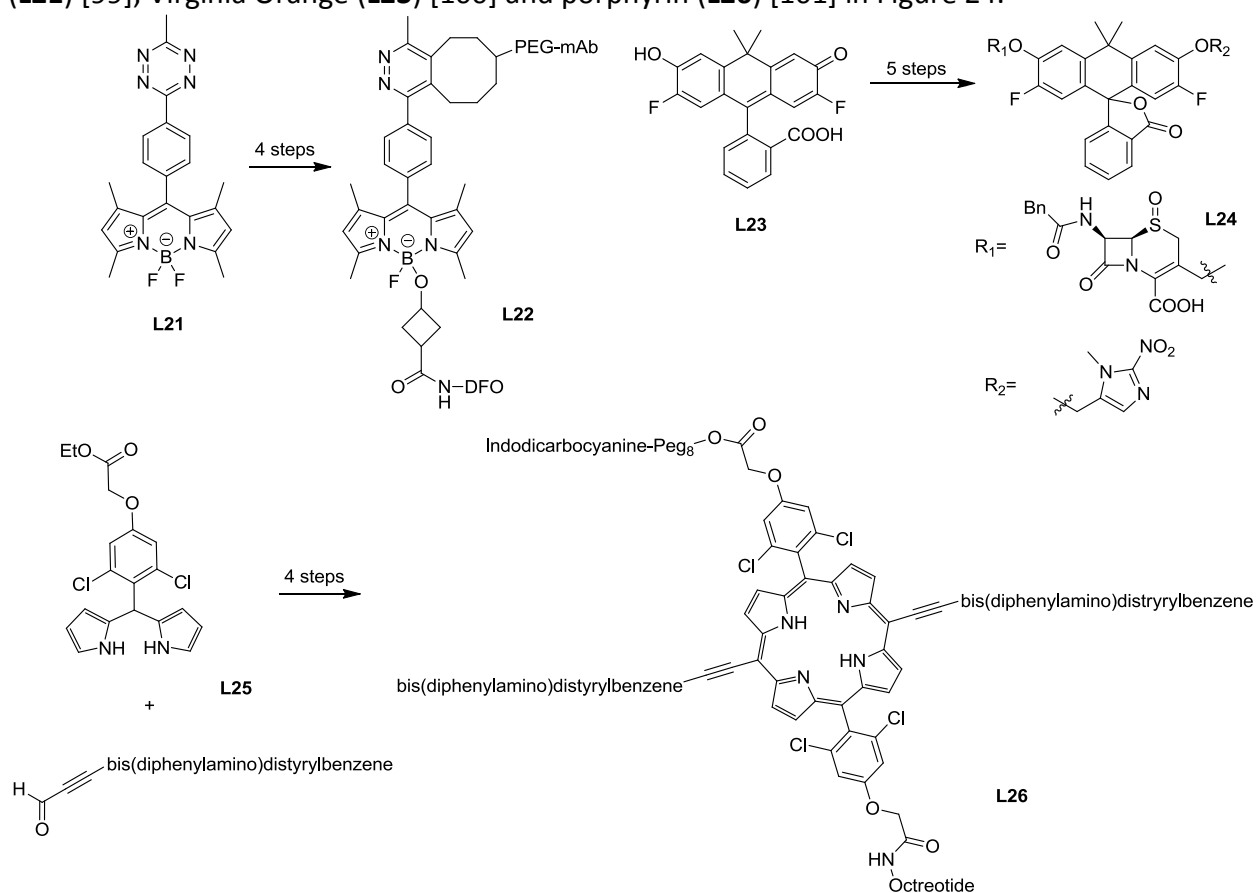


Figure 24: rare examples of fluorophores that are used as platforms: BODIPY (**L21**, top left) [99] Virginia Orange (**L23**, top right) [100] porphyrin (**L26**, bottom) [101]

All the work developed during my PhD was developed around this platform approach, and particularly around BODIPY-based fluorescent platforms. Specifically, we worked on two different BODIPY systems with the following objectives for my thesis:

- Development of a simple and trifunctionalizable BODIPY-based fluorescent platform for *in vitro* application, in order to be able to test of a large family of gold(I)-based optical theranostics.
- Design of a water soluble AzaBODIPY fluorescent platform for the development of an *in vivo*-compatible optical trackable therapeutic agent.

The first chapter of the manuscript will describe the synthesis of the first trifunctional platform, as well as its functionalization investigations, and the different applications, which could be realized, starting from this very versatile BODIPY-based compounds.

The second chapter will be dedicated to the development of a new family of very promising water soluble azaBODIPY platforms.



# Chapter I - BODIPY



## Chapter I – BODIPY

The work developed in this first chapter aims at proving the interest and the feasibility of using a fluorescent platform to rapidly and efficiently design a family of metal-based theranostics. We decided to use gold(I) complexes as therapeutic moiety for proving this concept. Indeed, we noticed in previous studies that gold(I) presents the great advantage to not quench the fluorescence of fluorophores [90,91,102]. First we will explain why BODIPY dyes meet all the criteria required for the conception of a fluorescent platform. This will be followed by a brief focus on the therapeutic potential of gold complexes. After this introduction an account and description of the synthesis and the use of a bi and a tri-functionalizable fluorescent platforms will be provided, as well as their use to reach a large panel of metal-based trackable therapeutics. To finish, an *in vitro* evaluation of the biological properties of these theranostics will be reported.

### 1.1 Choice of the platform

As reported earlier, the first part of this thesis aims at developing a multifunctional molecular platform that can be used for *in vitro* (and to a limited degree *in vivo*) investigations and possesses a therapeutic potential thanks to the presence of biologically active, metal based agents (Figure 25).

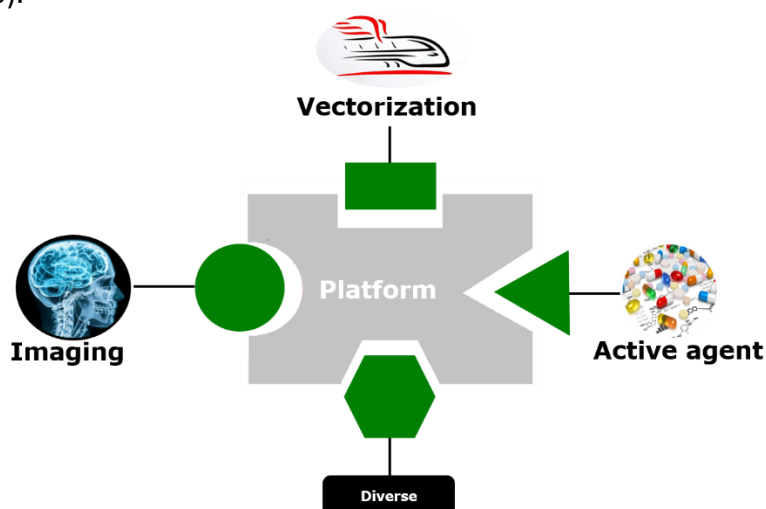


Figure 25: The multifunctional platform approach

The selected platform should be

- suitable for the introduction of three different substituents (in order to be able to introduce a vector, a therapeutic moiety, and another group for tuning the molecule like a water solubilizing group)
- suitable for a selective, stepwise introduction of the various substituents,
- suitable for the grafting of the substituents *via* nucleophilic substitution (numerous amines and thiols are commercially available, easy to synthesize, and require simple reaction conditions),
- reactive under mild reaction conditions to be suitable for the introduction of metal-based complexes and biomolecules

Additionally, for the reasons shown in the general introduction, the platform should intrinsically fulfill the task of being the trackable moiety. We have identified BODIPY dyes as potential platforms due to their versatility, various ways to access the base compound and a great variety of possible functionalizations of this class of dyes. We decided to first investigate the bifunctionalizable platform developed by Dehaen and Boens [103]: a dichloroBODIPY (Figure 26) to check if it meets the three last criteria we defined.

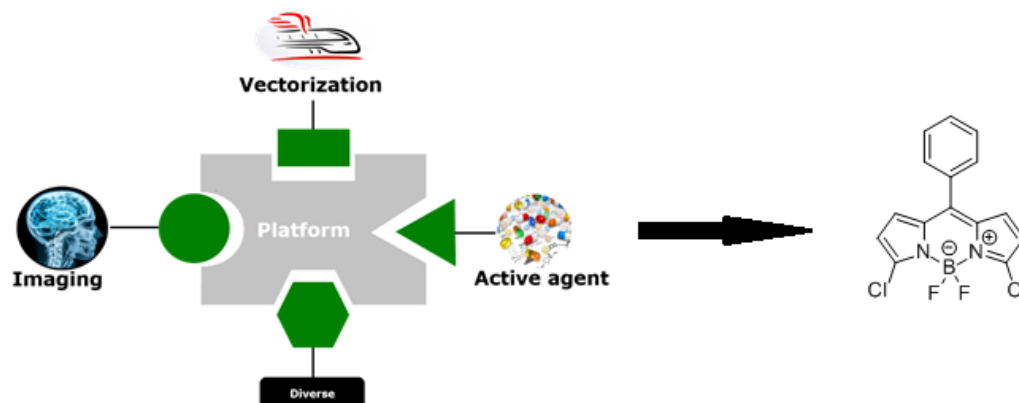


Figure 26: dichloro-BODIPY - the selected multifunctional platform

In addition to the bifunctional platform that we had chosen we wanted to retain the possibility of supplementing our bifunctional platform with a carboxylic acid function in order to widen its scope.

A brief overview over possible transformations as well as selected works involving the functionalization of both carboxylic acid based as well as dihalogenated BODIPYs will be provided in the next section.

## 1.1.1 Synthesis and functionalization of BODIPY-dyes

### 1.1.1.1 Accessing the base-compound

BODIPY's were first described in 1968 by Treibs and Kreuzer [104], when they investigated acylation techniques of pyrroles in presence of  $\text{BF}_3$  as Lewis-acid for substrate activation. To their surprise, they obtained a brightly fluorescent compound to which they managed to attribute the structures **L27** and **L28** shown in Figure 27.

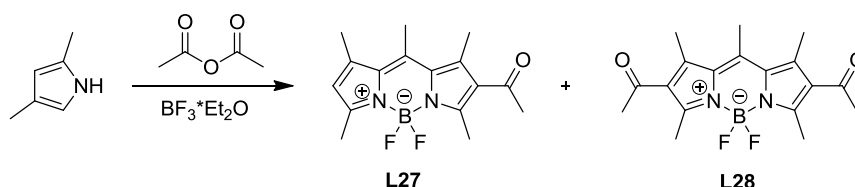


Figure 27: First synthesis of BODIPY-dyes [104]

Keeping in line with IUPAC rules the new compound was called BODIPY, short for 4,4-difluoro-4-bora-3a,4a-diaza-s-indazene (Figure 28).

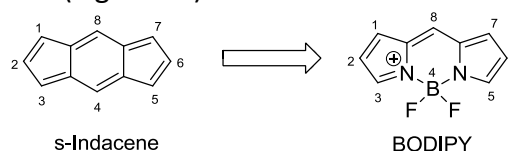


Figure 28: Nomenclature of BODIPYs

Due to the thermal instability above  $-40^{\circ}\text{C}$  of the precursor dipyrin the unsubstituted title compound was not actually been discovered until 2008/2009 when three groups independently from one another reported the successful synthesis [105–107].

Due to said instability, BODIPYs are usually decorated with varying substituents to prevent polymerization at the dipyrin-state. Two main synthetic protocols have been established using either aldehydes or acid chlorides as electrophiles (Figure 29).

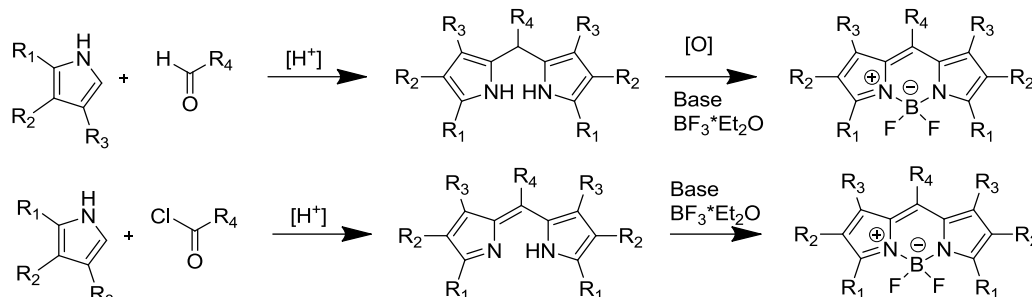


Figure 29: General Synthesis of symmetrical BODIPYs

The strategy is divided in three steps: 1) formation of the dipyrin/dipyrromethane, 2) oxidation of this intermediate using oxidizers such as DDQ or chloranil, and 3) complexation of the boron in presence of a base such as  $\text{Et}_3\text{N}$ .

In order to access unsymmetrical BODIPYs the pyrrole unit can be acylated first and reacted with a second pyrrole in a next step as described below (Figure 30).

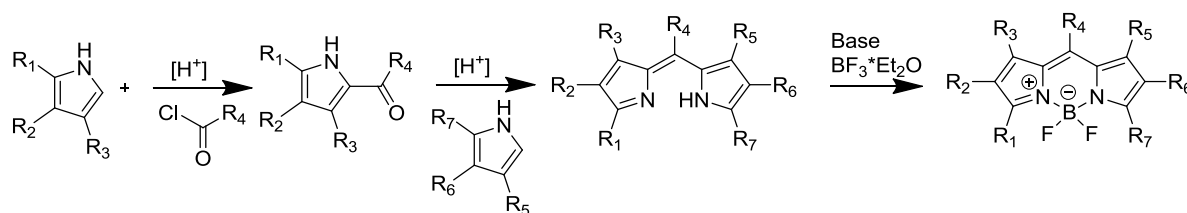


Figure 30: Synthesis of unsymmetrical BODIPYs

In 2007, Burgess and coworkers developed a third synthetic strategy; this strategy grants access to symmetric BODIPYs *via* decarbonylation of formylpyrroles using  $\text{POCl}_3$  [108] (Figure 31).

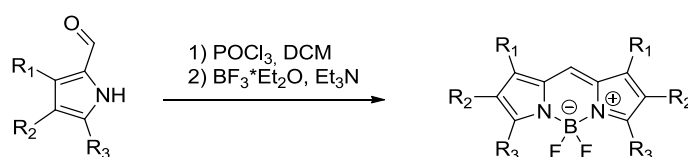


Figure 31: Accessing symmetric BODIPYs *via* decarbonylation reaction [108]

This approach can be advantageous when the required substitution pattern inaccessible at the dipyrromethane or BODIPY stage as well as for substrates that do not support treatment with DDQ.

One of the main advantages of BODIPY over classic fluorophores is its versatility in terms of substitution. Indeed, almost any substituents can be envisioned for group  $\text{R}_1\text{--R}_7$  either introduced during the synthesis of the BODIPY core or during post modification. Moreover, depending on the substituents, the photophysical properties of the dye can and have been finely modulated, in particular their absorption and emission wavelengths, Stokes shift, quantum yield... This ability is key when looking at a fluorescent platform scaffold. Some important transformations will be shown in the next paragraph in order to permit an informed selection of BODIPY that can serve as a viable platform molecule.

## 1.1.1.2 Functionalization of the primary BODIPY

The easiest way to access BODIPYs that possess interesting photophysical properties and carry different transformable functions is to introduce the desired substituent in the *meso*-position during the assembly process of the BODIPY core by using commercial aromatic aldehydes such as nitro-, carboxy- or hydroxy benzaldehyde. However, the BODIPY core in itself is highly versatile as well. Due to the electron-impooverishing character of the BF<sub>2</sub>-moiety the BODIPY core largely behaves like an electron-poor aromatic compound and can undergo functionalizations such as Pd-catalyzed cross coupling reactions, halogenations and aromatic substitution reactions [109] (Figure 32).

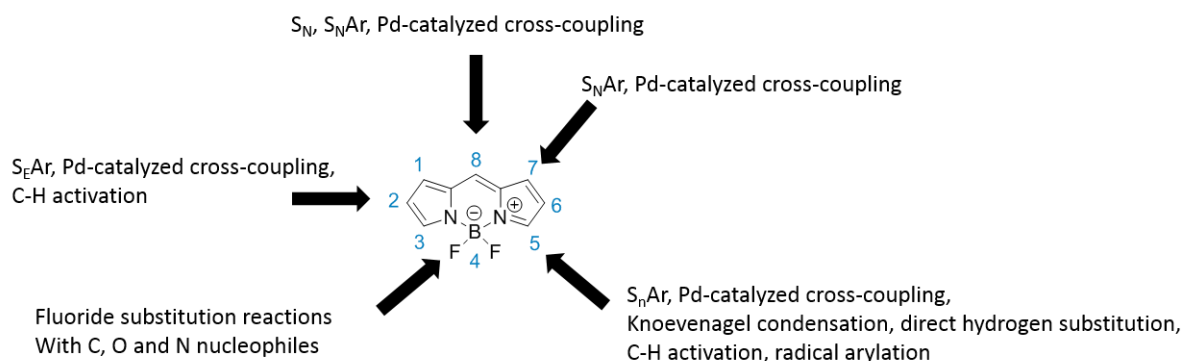


Figure 32: Possible functionalizations of the BODIPY-base structure [109]

We will focus our attention on functionalizations that rely on carboxylic acid functions (for the formation of amide-bonds) and (nucleophilic aromatic) substitution reactions on the BODIPY-core.

## 1.1.1.3 Functionalization and reactivity of the 3,5-positions of the BODIPY

BODIPYs carrying carboxylic acid functions on a *meso*-phenyl substituent can be accessed through several possible pathways. They are directly accessible by use of both unprotected [110] as well as protected carboxylic acid derivatives [111] that are subsequently hydrolyzed to give the free carboxylic acid. In 2009 Ziesel used Pd(PPh<sub>3</sub>)<sub>2</sub>Cl<sub>2</sub> catalyzed carboalkoxylations (that were developed by Heck in 1974 [112]) of **L29**, followed by hydrolysis to introduce the carboxylate in the *meso*-phenyl [113,114] (Figure 33).

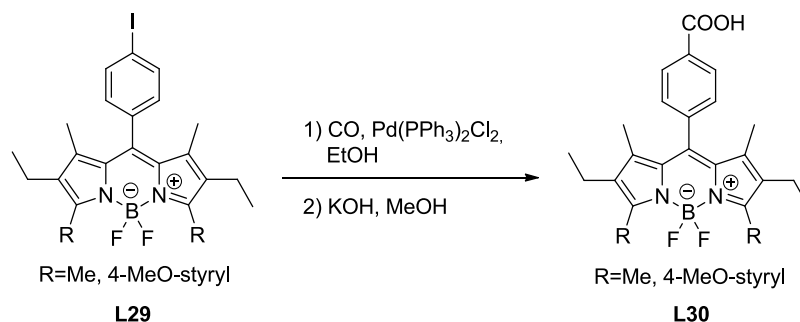


Figure 33: Accessing BODIPY-carboxylates via Pd-catalyzed carboalkoxylation [113,114]

*Meso*-phenyl carboxylate functionalized BODIPY derivatives are commonly used as they permit easy functionalization through the formation of amides and esters.

In previous works of our group BODIPY-carboxylic acids have found widespread use to elaborate a variety of compounds. Applications included the study of the properties and

versatility of BODIPY-phosphine based theranostics (**L32-L34**) [90], the influence of the vector on biological properties of gold(I)-BODIPYs (**L35a - L35c**) [91] or the design of multimodal tools for use in PET/SPECT (**L36a, L36b**) [115,57] (Figure 34).

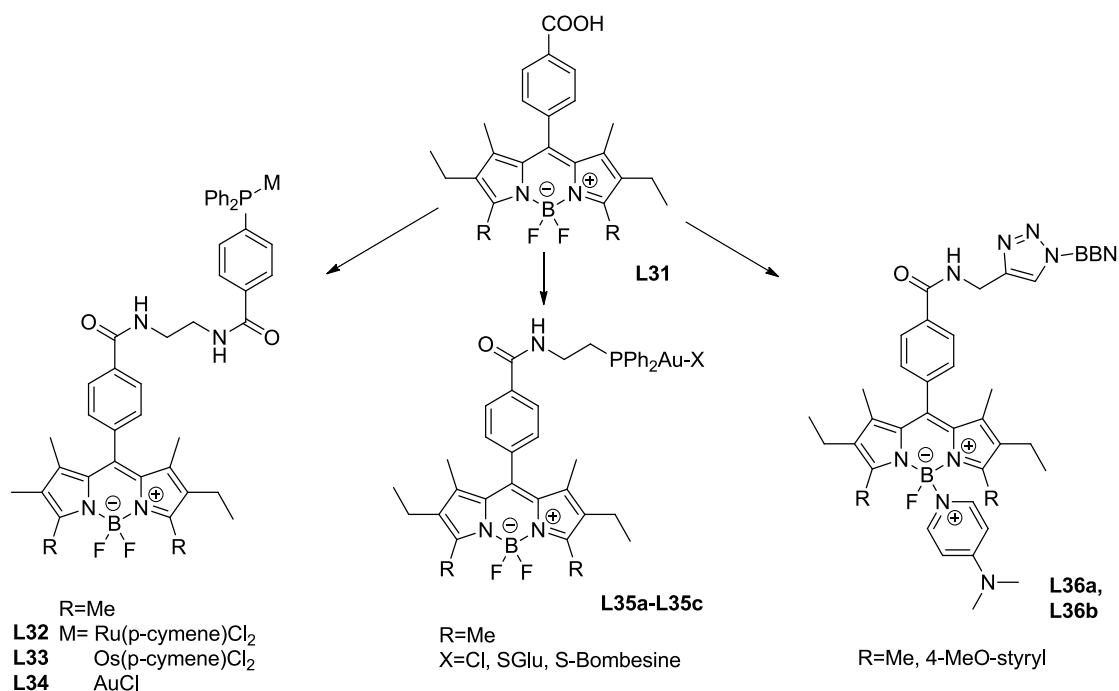


Figure 34: Use of BODIPY-carboxylic acid in previous studies from our group [57,90,91]

The electron-richness of pyrroles often leads to unwanted side-reactions such as oligo- and polymerization during the BODIPY assembly. This prompted many groups to use alkyl-substituents in one of the 2-positions of the starting pyrrole(s) to prevent those reactions. Using alkyl-carboxylic acids is an easy way to render the target-BODIPY functional. This technique was pioneered by Haughland *et al.* in 1988 [116] and is commonly applied to render the BODIPY reactive towards biological molecules. It is also the go-to strategy for most commercial BODIPYs and is covered by numerous patents, notably by Fisher Scientific's Invitrogen [116,117].

The starting pyrrole is transformed using a Vilsmeier-Haack formylation. The formylated pyrrole **L37** is then reacted under Wittig-conditions to obtain an ethenyl-pyrrole (which can be directly used to construct BODIPYs as well) [116–118] (Figure 35).

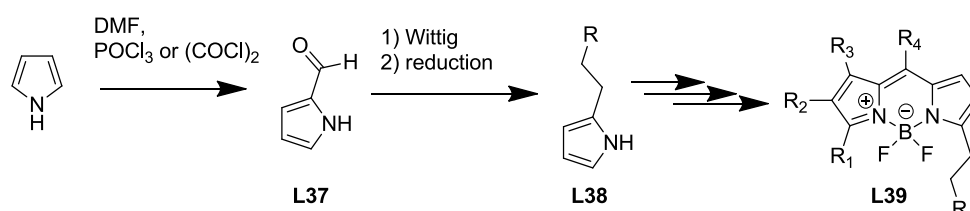


Figure 35: Functionalized BODIPY-dyes by pyrrole decoration [116,118]

Reduction of the double bond then gives the base pyrrole which in turn is transformed using the common techniques. This way any Wittig-compatible substituent can be introduced into the 3 and/or 5 positions of the final BODIPY, granting access to a wide variety of possible structures.

BODIPYs carrying activated alkyl-acid substituents in the 3 position such as propionic/pentanoic acid succinimidyl ester are commercialized [119] and commonly used in biological application as N- and S-reactive probes.

Methyl groups in the 3,5-position are not only used to prevent side reactions. They can be oxidized by halogenating agents (e.g. NBS) or strong oxidizers such as nitric acid to introduce oxygen- or nitrogen bearing substituents that are not conjugated to the BODIPY core in order to e.g. increase the hydrosolubility of the final dye [120–123] (Figure 36).

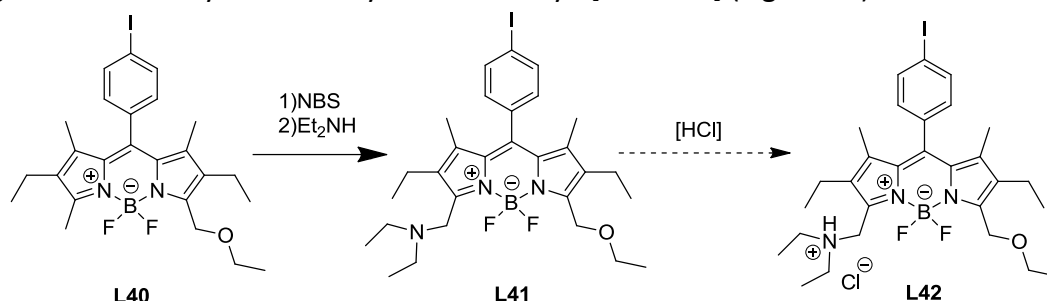


Figure 36: Use of  $\alpha$ -pyrrolic methylation of BODIPY to increase solubility [121]

In 2005 Akaya discovered that the CH acidity of a 3-methyl-group is high enough to be used as substrate for Knoevenagel like reactions [124]. This granted access to highly red-shifted BODIPYs by adding styryl groups to the core of the dye [124–126] (Figure 37).

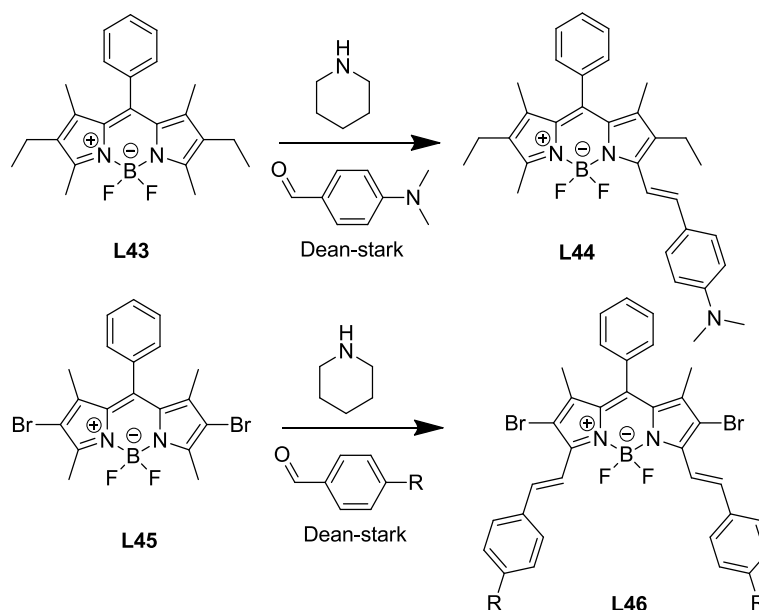


Figure 37: Accessing styryl and distyryl-BODIPYs by Knoevenagel-reaction. Discovery by Akaya in 2005 (L44) [124]. First accounts of distyryl-BODIPY (L46) [125,126]

This approach permitted the design of far red/NIR-shifted BODIPYs while avoiding the use of naphtho-fused or other types of extended pyrroles which exhibit very unfavorable solubility and stacking behavior.

Styryl-extended BODIPYs have been used for many biological applications and were successfully used in sensing [127–129], in *in vitro* as well as *in vivo* applications as shown by the synthesis of very elaborated structures by others [114,130,131] as well as by our own group [57,132] (Figure 38). Unfortunately, styryl-extended BODIPYs are prone to photobleaching and often display unfavorable solubility as well.

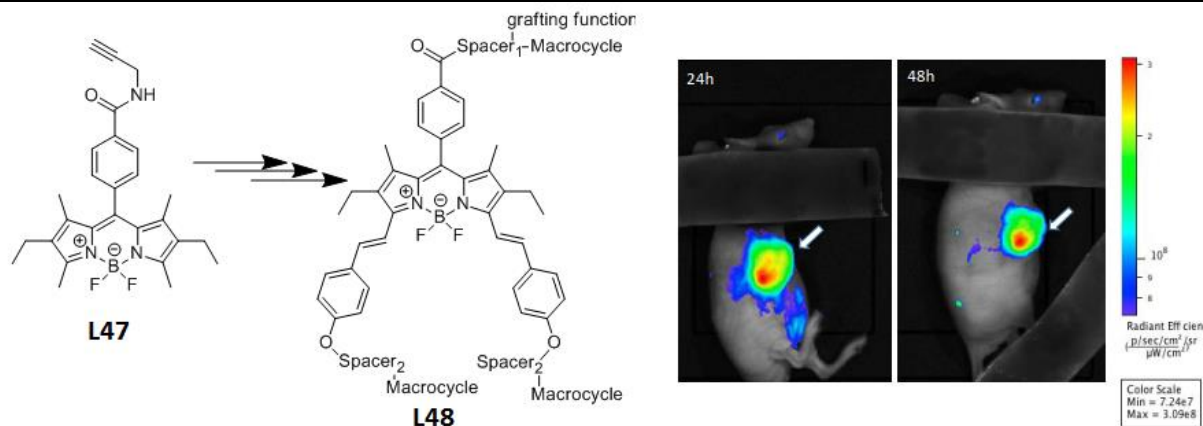


Figure 38: Application of distyryl-trisDOTA-BODIPY L48 in molecular imaging [132]

#### 1.1.1.4 3,5-halogenated BODIPYs

##### 1.1.1.4.1 Halogenation of BODIPYs and their precursors

BODIPY dyes have extensively been modified using different electrophilic aromatic reactions to introduce halogens, sulfonates or acyl substituents.

With electrophiles the unoxidized dipyrromethane behaves a lot like its precursors, pyrroles, favoring an  $\alpha$ -pyrrolic attack [133].

Depending on the stage at which the halogenation occurs different selectivities can be observed: chlorination and bromination of the dipyrromethane stage occurs in the order  $5 \rightarrow 4 \rightarrow 3$ -position when using NBS, NCS or  $\text{Br}_2$  [134,103], whereas for the finished BODIPY the 2/6-position is substituted first, followed by the 5/3-positions and finally the sterically hindered 7/1-positions [135,136]. Mono-iodination occurs in the 2/6-position first too [137], much like Friedel-Crafts acylations [138]. Interestingly, any substitution occurs in a step-by-step fashion, hinting on continuously reduced reactivity towards the next electrophilic attack. This makes selective functionalization and the isolation of any mono- to perhalogenated BODIPY possible (Figure 39).

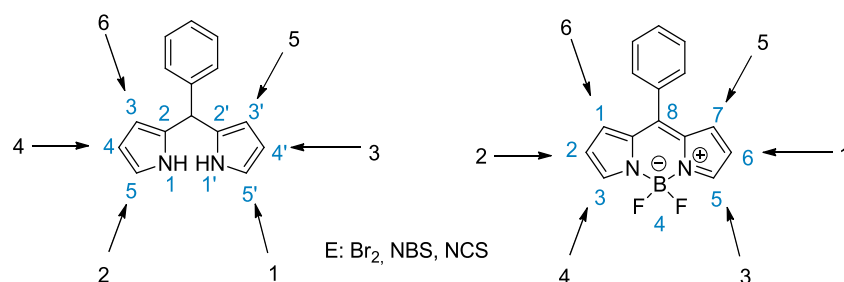


Figure 39: Substitution order during halogenation. The order of halogenation is shown in black, the IUPAC-conform molecular positions are given in blue. Dipyrromethane is shown on the left, bora-dipyrromethane (BODIPY) on the right

In order to access 1-3/5-7-chlorinated BODIPYs, chlorination has to occur at the pyrrole-level (before steric hindrance) [136].

##### 1.1.1.4.2 Reactivity of 3,5-halogenated BODIPYs towards nucleophiles

The halogenated dyes can act as versatile substrates for Pd-catalyzed organometallic coupling reactions in order to extend the carbon skeleton. Due to the electron-poor nature of the

BODIPY-core, halogenated BODIPYs can also directly be engaged in nucleophilic aromatic substitution reactions ( $S_NAr$ ).

Dehaen and Boens pioneered both the halogenation as well as the exploration of the resulting reactivity. For 3,5-dihalogenated dyes they were able to introduce a variety of N-, S- and O-nucleophiles [103] selectively. Using secondary or aromatic amines they observed a distinct decrease in reactivity for the second substitution. This required them to use refluxing conditions whereas the first substitution is feasible at room temperature (Figure 40).

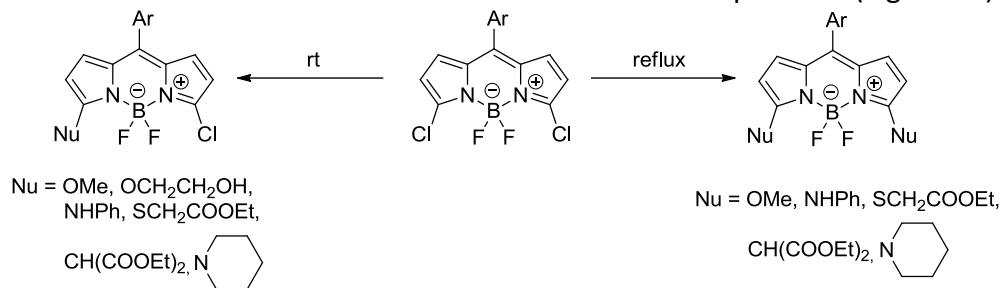


Figure 40: Nucleophilic aromatic substitutions using a variety of nucleophiles [103]

Li *et al.* investigated the selectivity to nucleophilic attack towards hard (C-nucleophiles) and softer nucleophiles such as S, N, and O-based compounds. They found that in accordance with Pearson's HSAB-concept C-nucleophiles show a preference for the hard boron center whereas softer nucleophiles prefer the nucleophilic aromatic substitution [139].

Since their development dichloroBODIPYs have found widespread applications in the elaboration of compounds whose use ranges from sensing and detection of analytes such as chemical warfare agents [140] all the way to *in vitro* applications such detection of sulfides [141] and glutathione [142] in life cells.

Judging from literature the displayed reactivity of dichloroBODIPYs appears perfect in order to permit their use as platforms: they are reactive towards a large panel of nucleophiles (Figure 40) while the change in reactivity between mono- and disubstituted compound should permit a selective and stepwise functionalization with high-value nucleophiles.

In our group we have already gained some experience with the use of dichloroBODIPYs, notably for the synthesis of macrocycle-substituted BODIPYs for the detection of copper ions (**L49**) [143] as well as for the synthesis of gold(I)-containing theranostic agents (**L50**) [102].

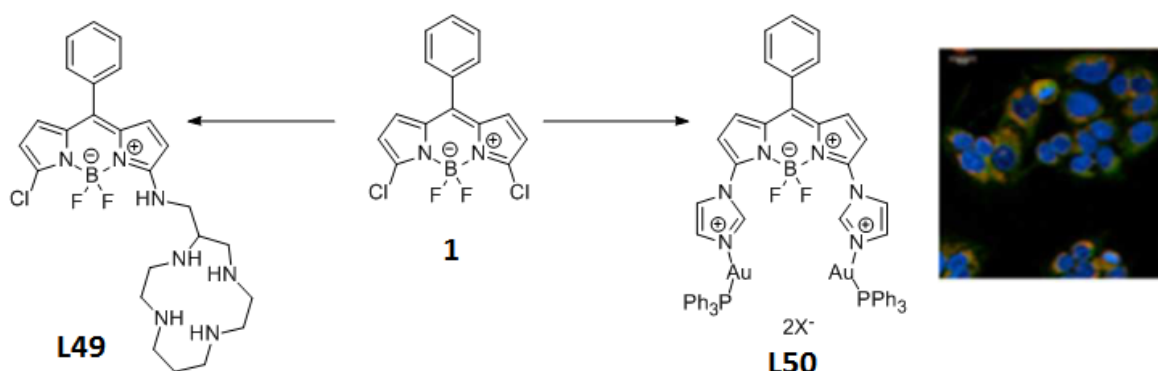


Figure 41: Previous uses of BODIPY-Cl<sub>2</sub> **1** in our group [143,102]. The fluorescence image on the right shows the merged image of BODIPY **L50** and organelle-stains for colocalization

Even though a variety of trackable, gold-containing agents (based on BODIPYs [90,91,102] or other fluorophores [144,145]) have been synthesized in our group, however, up to now, the aim was only to design small families of 2-4 compounds. The developed approaches did not

allow the rapid access to a large panel of compounds, making a structure-activity relationship study difficult.

The first part of this thesis seeks to remedy this by using a platform approach.

## 1.2 Gold in biology: a brief overview

### 1.2.1 Auranofin

Today, Auranofin (Figure 42) – commercialized under the brand name Ridaura® – is certainly the most famous gold complex in medicine.

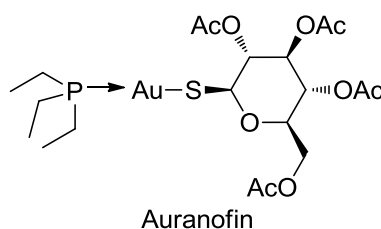


Figure 42: Structure of Auranofin

Auranofin was introduced in 1982 as an arthritis medication and to treat related chronic inflammatory diseases [146,147]. Nowadays its risk/benefit balance is questioned, but it is still FDA approved. Mainly due to the extreme cost implied in drug development and discovery (that can easily surpass 1 billion dollars) the NIH (National Institute of Health) launched a campaign to reinvestigate the potential of old drugs [148,149]. The reasoning behind and advantages of that strategy are obvious as the (re)investigated drugs are:

- available
- well described
- their pharmacological profile (pharmacokinetics, metabolites etc.) is known

Auranofin was included in this program and has caught researchers' attention due to its activity against a variety of illnesses such as cancer, viral infections (HIV), neurodegenerative disorders (Alzheimer's and Parkinson's) as well as parasitic and bacterial infections [149].

This has led to the recent renewed interest in gold containing compounds, especially auranofin-like complexes (i.e. [Au(I)(phosphine)thioglucose tetraacetate]), either in the development of innovative complexes or in the comprehension of their mechanism of action.

### 1.2.2 Chemical biology of Gold

Before going deeper into my PhD subject, it is worth providing some pieces of information on gold's biological behaviour, and especially of the state of the art of gold-based drug's mechanism of action.

#### 1.2.2.1 General Information

Gold is the 79<sup>th</sup> element in the periodic table and consists to 100% of the nuclide  $^{197}_{79}\text{Au}$ . It is the noblest metal, displaying redox potentials of  $\epsilon_0(\text{Au}/\text{Au}^+) = +1.69\text{V}$ ,  $\epsilon_0(\text{Au}/\text{Au}^{3+}) = 1.5\text{V}$  and  $\epsilon_0(\text{Au}^+/\text{Au}^{3+}) = 1.4\text{V}$ . Due its electronic configuration of  $[\text{Xe}] 4f^{14} 5d^{10} 6s^1$  the chemistry of gold is governed by the oxidation states +1 and +3 (Oxidation states between -1 and +5 are known). The 6s orbital experiences tremendous relativistic orbital contraction that influences all of the

properties gold exhibits: this is the reason why gold possesses the highest electron affinity (-2.31V) and Pauling electronegativity (EN=2.4) among all metals. The orbital contraction also results in very strong aurophilic interactions between the  $d^{10}$  orbitals of  $Au^I$  atoms that, depending on the interatomic distance experience stabilization between 100kJ/mol (2.73 Å) and 10kJ/mol (3.48 Å).

$Au^I$  is a relatively large, diffuse ion, resulting in weak Lewis-acidity. Without stabilizing complexes  $Au^I$  dissociates spontaneously into  $Au^0$  and  $Au^{III}$  in aqueous media. Soft ligands such as phosphines, thiols/sulfides, selenides and cyanides are able to stabilize the +1 oxidation state [150].  $Au^I$  prefers linear, bicoordinate geometry.

The second stable oxidation state,  $Au^{III}$  is a stronger Lewis acid than  $Au^I$  but still considered soft (between  $Cu^{2+}$  and  $Ag^+$ ) [151]. It is isoelectronic to  $Pt^{II}$  and (like Pt) prefers a square-tetraplanar coordination geometry.

### 1.2.2.2 Biological behavior

Many efforts have been spent on the clarification of the role of gold in the biological environment. Depending on its speciation it is a more or less toxic heavy metal that does *not* possess any biological function.

Gold is reactive enough to be used as a catalyst (e.g. in C-C bond formation of alkenes and alkynes[152]), however, in biological environments its actions seem to be governed by its capacity to bind naturally occurring ligands and inhibit the active sites of essential proteins. Common soft ligands to which gold can bind are for example cysteine, selenocysteine and nitrogen donors such as histidine. With cysteine gold forms very stable complexes with conditional equilibrium constants of  $K=10^{24}$  [153]: this makes them thermodynamically favorable enough to even displace other metals such as copper ( $K=10^{16}$ ) or zinc ( $K=10^{17}$ ) from biologically essential complexes [154]. Abundant proteins that present accessible cysteine are for example albumin, glutathione and metallothionein.

Numerous researchers, e.g. Kean *et al.* [155], have asserted that gold ligands are quickly released in biological media and that any gold species is rapidly reduced *in vivo*, essentially demoting the attached ligands to drug delivery vehicles. This claim is not obvious to prove and various gold-containing compounds (gold(III)-corrole [156], gold(III)-porphyrin [157], gold(III)-phenanthrene[158]), which present excellent cytotoxic properties, seem to remain (biologically and redox-)stable in the biological environment. This is the reason why our group developed an “ON/OFF” smart theranostic system (gold(I)-phosphine-coumarin), which is fluorescent when the P-Au bond is intact and which switches off as soon as this bond is broken [144]. We proved that for these complexes, the P-Au bond is stable at least 48 h in cells and at least 24 h *in vivo*. This discovery increases the interest of developing gold-complex with fine-tuned ligands.

Both the modes of coordination as well as the redox-behavior of gold in its various oxidation states raise the question of which cellular compartment(s) and molecular target(s) are effected by gold-containing agents. Analyzing the “Catalytic Site Atlas” database [159] Kumar *et al.* found in 2011 that the active sites of 23.26% of all eukaryotic membrane enzymes and 22.78% of all eukaryotic non-membrane enzymes contain either cysteine or histidine [160], making them potential targets for gold drugs. Depending on the degree of oxidation of the gold-center and type of ligands various preferences seem to emerge. Due to intensive research in the field the state of the art evolves constantly and is thus regularly reviewed [161–163], a brief summary will be given in the next paragraph.

## 1.2.2.3 Molecular targets of Gold

As shown earlier in chapter 1.2.1 gold(I) is unstable in aqueous solutions without sufficient stabilization and spontaneously disproportionates into  $\text{Au}^0$  and  $\text{Au}^{\text{III}}$ .  $\text{Au}^{\text{III}}$  in turn is readily reduced in biological media, rendering the formation of gold clusters and nanoparticles possible.

Gold nanoparticles are investigated as new treatment options in cancer therapy. When administered as such they are usually used as drug delivery vehicles (EPR-effect), radiosensitizers, contrast agents or for thermal therapy [164]. However,  $\text{Au}_{55}$ -gold clusters have been shown to irreversibly attach to the major groove of double strand DNA and proved effective against 11 cancer cell lines, displaying cytotoxicity in the 0.1-1  $\mu\text{M}$  range [165].

In several studies evidence for direct gold-agent-DNA interaction was found. This interaction strongly depended on the ligands: compounds possessing a terpy moiety **L51** showed irreversible DNA intercalation (thus impeding replication) (Figure 43) [166]. Gold(III)-porphyrin led to DNA fragmentation (**L52a-e**, Figure 43) [157] and dithiocarbamate (**L53**, Figure 43) formed gold(III)-DNA-adducts [167].

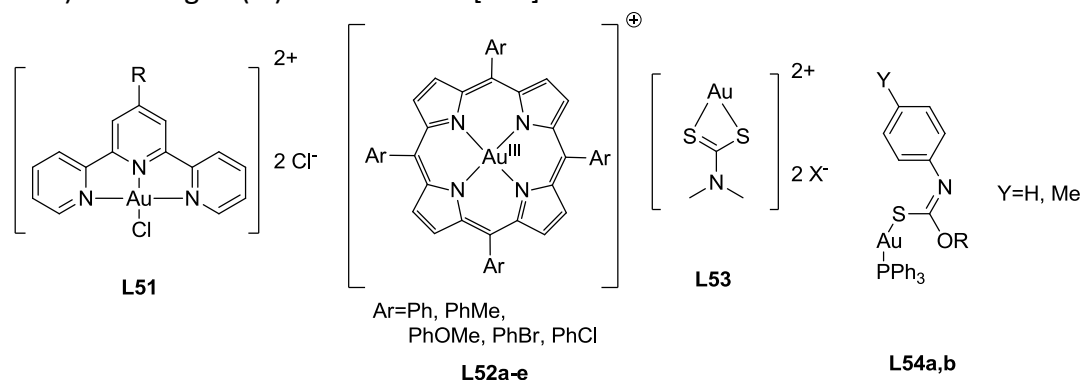


Figure 43: DNA-damaging gold-based agents. **L51** [166] **L52a-e** [157], **L53** [167], **L54a,b** [168]

Not only gold(III)-compounds have been developed that target DNA; indeed, the gold(I)-phosphine thiocarbamate **L54a,b** was found to cause DNA fragmentation and induces apoptosis by induction of p53 [168]; all compounds displayed cytotoxicities in the nM to low  $\mu\text{M}$  range.

Of the above mentioned compounds the gold(I)-phosphine **L54a,b** is somewhat of an exception as more commonly gold(I)-compounds seem to be unable to sufficiently stabilize DNA and instead impede the function of other targets such as disulfide reductases, cysteine proteases, or tyrosine phosphatases [162,169].

Disulfide reductases (amongst them Thioredoxin, Thioredoxin reductase (TrxR), glutathione reductase and others) display cysteine and selenocysteine in the active center which makes them perfect ligands for gold(I). Disulfide reductases are present in every cell of every organism and are essential to keep oxidative stress to the cell in check: they are essential in reducing and destroying Reactive Oxygen Species (ROS) that are generated in the respiratory chain during normal cell processes as well as ROS generated by other sources. The active center of TrxR consists of a selenocysteine (it is one of currently 23 selenoproteins known in the human genome, 11 of which are implied in redox active proteins: 5 Glutathione-peroxidases, 3 Thioredoxin reductases and 3 Iodothyronine deiodinases [170]) and a cysteine that are reduced by NADPH to render the enzyme active.

Investigations on purified TrxR samples showed that gold compounds show high inhibitory potential (nM range) and readily inhibit the enzyme by coordinating the active center

[149,171,172]. This results in TrxR depletion and consequently lower inactivation of ROS. The ROS buildup leads to oxidative damage of DNA, fatty acids as well as glutathione depletion and compromised mitochondrial integrity and can ultimately result in induction of apoptosis [173].

However, gold(I)-based agents do not only possess the potential to inhibit disulfide reductases: when screening a large panel of gold(I)-phosphines Karver *et al.* found 11 compounds that strongly (low  $\mu\text{M}$  range) inhibit protein tyrosine phosphatases [174] which play a crucial role in cell growth, differentiation, immunology and metabolism.

More recently several groups have also found evidence that gold(III)-based agents such as gold(III)-thiomalate can inhibit the ubiquitin/proteasome system [175]. Thanks to its tetraplanar coordination geometry and gold(III) compounds have also been used to inhibit the aquaporine system [158,176] which regulates the cellular water flux (and thus osmotic pressure) amongst other functions (Figure 44).

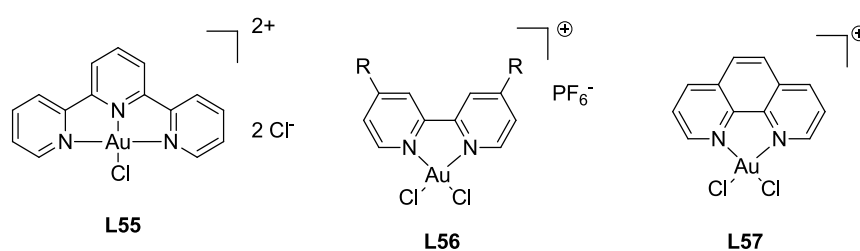


Figure 44: Au(III)-pyridiniums that have been shown to inhibit aquaporines and can interact with zinc-finger enzymes [176]

Many of the studies shown above have the common shortcoming that binding to a certain target is usually proven using purified samples of the target-to-(dis)prove. Due to the complexation behavior shown in 1.2.2.2 and the frequency of possible ligands in the active sites of enzymes this approach may strongly bias the result and lead to incorrect assumptions. For auranofin it was pointed out that due to the reactivity towards sulphur containing ligands it is likely to inhibit to some extent any single (purified) enzyme system it is presented to [177]. In the complex environment of a life cell (i.e. *in vitro*) or small animal (i.e. *in vivo*) it is however unclear if the molecule reaches the designated target organelle. This suspicion was recently confirmed by Quero *et al.* [175]: using purified TrxR they showed that their gold(III) thiomalate strongly inhibits TrxR. However, *in vitro* this behavior could not be reproduced; instead of a TrxR-inhibition they found that their compound displayed strong ubiquitin/proteasome system-inhibition whereas TrxR-inhibition did not play any significant role.

Due to the many variables and large panel of possible targets with which gold based compounds can interact, gold-based therapeutic agents represent interesting targets for drug development, both to find more efficient and selective compounds as well as to gain a deepened understanding of the mechanisms and cellular systems involved.

Having trackable compounds greatly facilitates this research as they intrinsically reveal information about a compounds cellular localization: this permits in particular to exclude molecular targets as main point of action when the compound cannot be detected in the target's organelle.

In our group we have developed a variety of trackable gold-based therapeutic agents that display excellent cytotoxic properties [90,91,102,178–181]. However, all previously

developed molecular entities have the common shortcoming to be difficult or tedious to modify. Up until now this prevented the facile modification and tweaking of the compounds and restricted easy access to a larger panel of compounds for structure-activity-relationship studies.

The goal of the first part of this thesis is thus not to develop *the* perfect gold-based therapeutic agent but rather the development of new tools; more specifically a multifunctional platform that grants easy access to a larger panel of compounds to more easily permit the modulation of molecular properties through the sequential introduction of various substituents. The obtained compounds will be based on BODIPYs and gold(I)-phosphines, both of which have been routinely used in our lab for the last decade.

### 1.3 BODIPY-Platform

During my PhD, one of the main objectives was to design metal-based optical theranostics. Thus, the first criterion we wanted to validate is the suitability of introducing metal complexes on the BODIPY platform. Moreover, we would like to investigate the relevance of the bioinorganic therapeutic strategy called “multinuclearity”. This strategy relies on the fact that many studies claim that the efficiency of a metal complex is only due to the quantity of metal entering the cells (ligands would have a single “transport role”). For example, our group recently published a study based on phosphine-ruthenium complexes, where a direct correlation can be made between the quantity of ruthenium entering the cells and the cytotoxicity of the compound [182]. Taking advantage of this hypothesis, several groups, amongst them our team, have designed multimetallic complexes to improve the cytotoxicity of their metal-based drugs. Depending of the studies, the cytotoxicity was significantly improved or almost not changed [179]. In the present work, we would be able to study this aspect: the step-by-step introduction of the metal complex moiety would permit the synthesis of mono and bimetallic theranostics.

As previously indicated, we chose gold(I) complexes due to their biological relevance and their limited impact on the fluorescence of the BODIPY dye. In the team, we are used to introduce phosphine gold moieties thanks to the commercially available 2-amino-ethylidiphenylphosphine. Even if this phosphine is quite sensitive to oxidation reactions (manipulation in glovebox is strongly advised), once coordinated to gold(I) center, the complex is stable and easy to handle.

The BODIPY-Cl<sub>2</sub> starting material used for these preliminary essays had been synthesized at gram scale by predecessors – namely Dr. Martin Ipuy and Dr. Julia Volkova following established protocols [103]. In short, the starting benzaldehyde is brought to reaction in pyrrole in presence of TFA, followed by chlorination with NCS at low temperature. The resulting dipyrromethane is then oxidized using DDQ, followed by complexation with BF<sub>3</sub>\*Et<sub>2</sub>O to access the BODIPY-Cl<sub>2</sub> **1** (Figure 45).

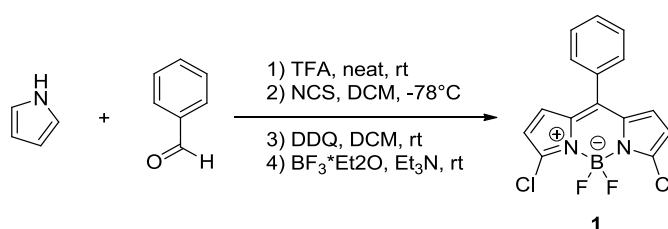


Figure 45: Synthesis of dichloro-BODIPY **1** starting material following established protocols. Synthesis executed by Dr. Martin Ipuy and Dr. Julia Volkova following the procedure published in [103]

The gold(I)-amine phosphine **3** was synthesized using reported protocols [91]: The chloroauric acid hydrate was reduced in presence of tetrahydrothiophene (tth) to yield (tth)AuCl **2**. (tth)AuCl was used to aurate the commercial diphenylphosphineethylamine (Figure 46) to obtain the gold(I)-complex **3**.

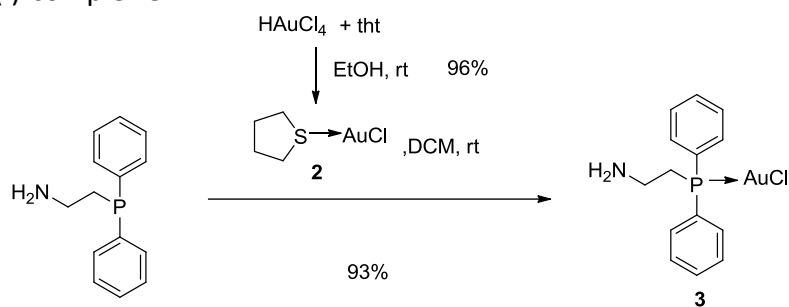


Figure 46: Synthesis of gold(I)-amine phosphine **3** [91]

We first targeted the double substitution of derivative **1**. As a consequence, 2 equivalents of the gold-phosphine **3** and BODIPY **1** were refluxed in dry ACN using  $\text{K}_2\text{CO}_3$  as a proton-scavenger (Figure 47).

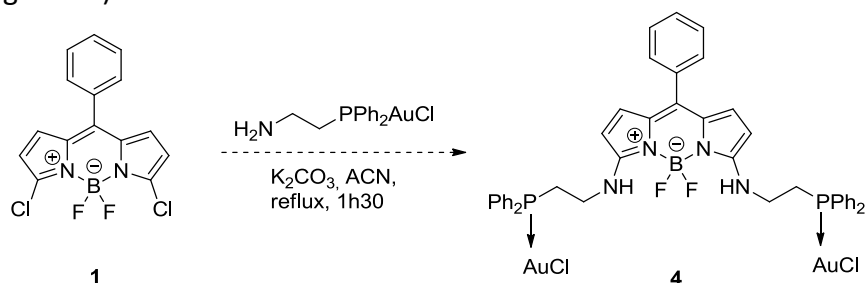


Figure 47: Attempt at double substitution of dichloro-BODIPY **1** using gold(I) amino phosphine **3**

Figure 48 shows the  $^1\text{H}$ -NMR-spectra of the starting materials and the compound that we obtained.

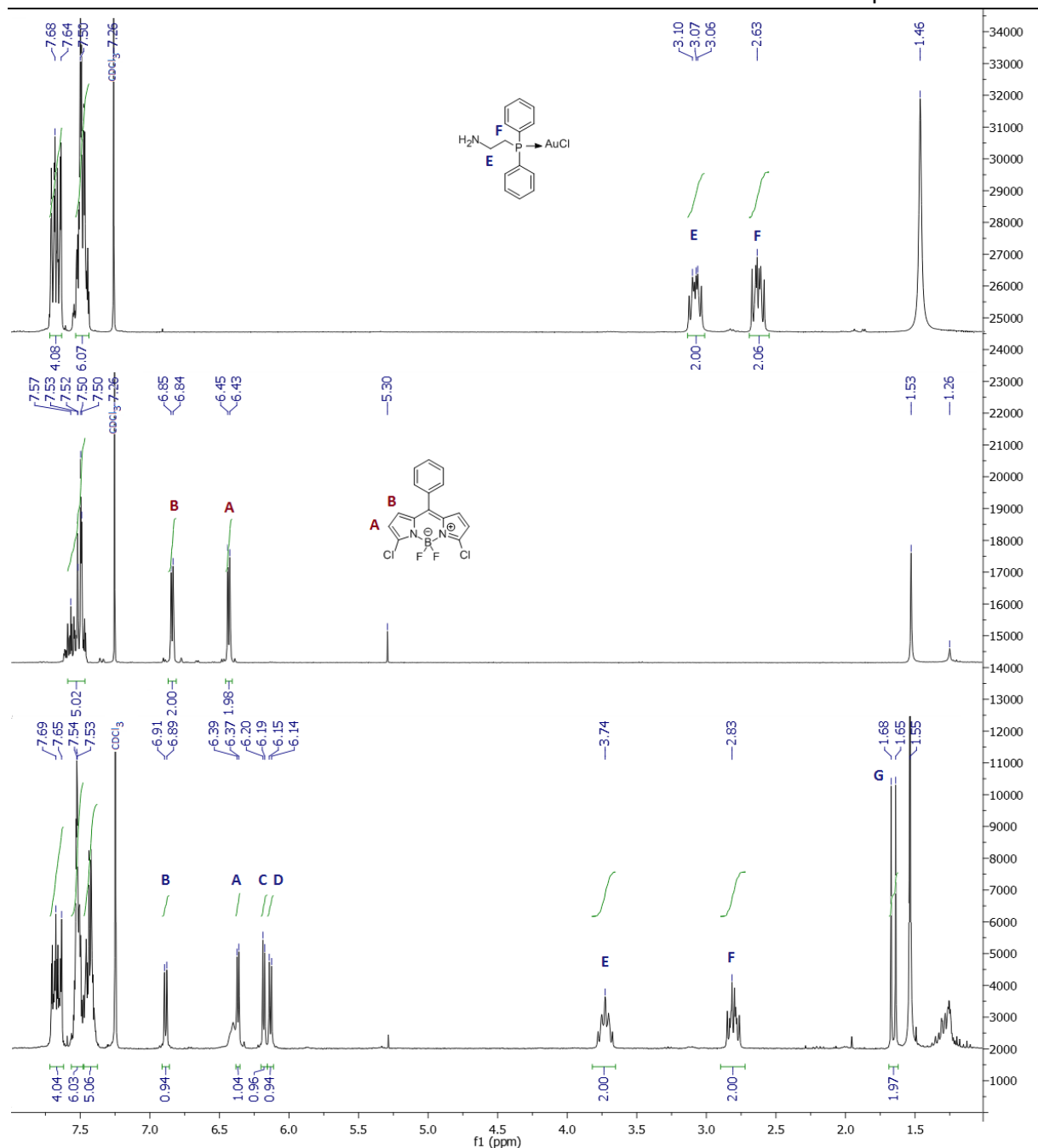


Figure 48:  $^1\text{H-NMR}$ -spectra of the starting materials gold(I)amino phosphine **3** (top), BODIPY-Cl<sub>2</sub> **1** (middle). The bottom  $^1\text{H-NMR}$  shows the spectrum obtained for the product that we obtained for the attempted double substitution of dichloro-BODIPY **1**. All spectra were recorded in  $\text{CDCl}_3$  at 300 MHz and 300 K.

The signals between 6 and 7 ppm show that the pyrrolic protons had become unsymmetrical, which led us to the conclusion that only one gold(I)-amino phosphine **3** had been introduced onto the BODIPY (which thus explains signals C and D of the aromatic region in Figure 48). Signal G (1.67 ppm) however was inconsistent with the targeted compound. In addition to the unexpected NMR high resolution mass analysis (HRMS) also held a surprise (Figure 49).

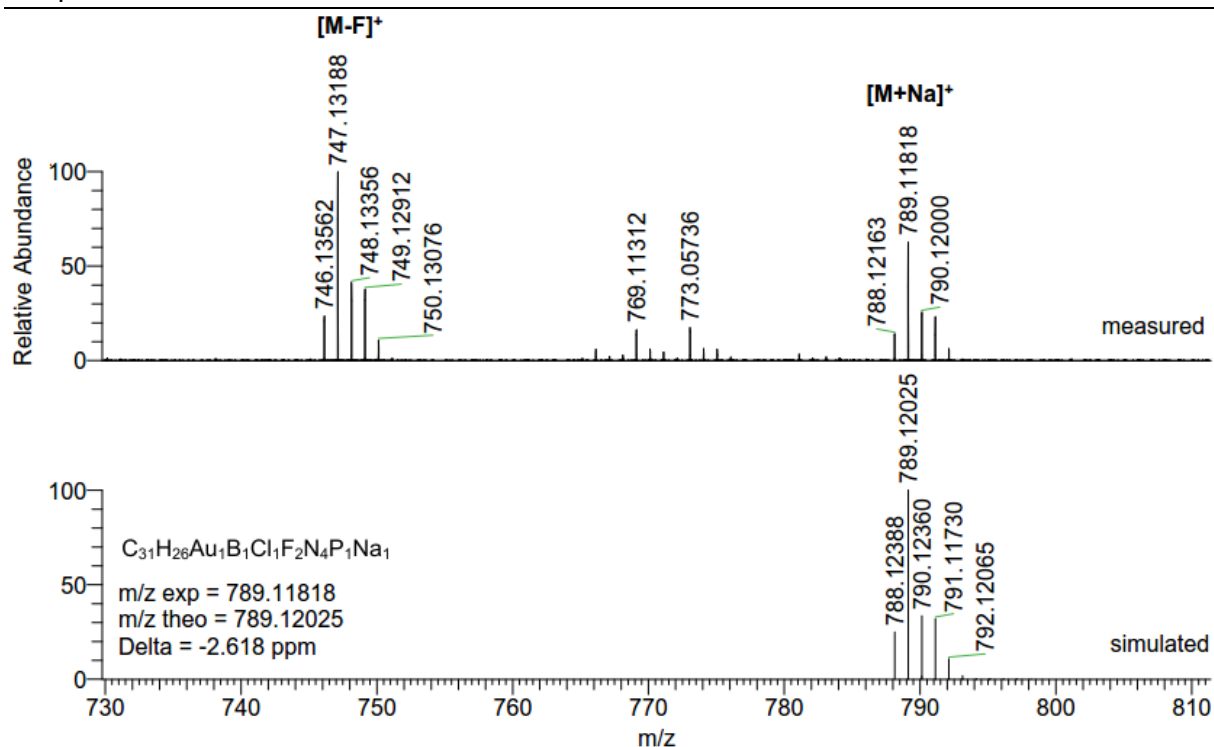


Figure 49: HRMS spectrum of the reaction product of the attempted double substitution of **1**

Indeed, the mass spectrum shown in Figure 49 presents a peak massif centered around  $m/z = 789$  instead of the expected  $m/z = 784$  (monosubstituted product) or  $m/z = 1187$  (double substituted product). In conjunction with the NMR-signal at 1.66 ppm (bottom NMR in Figure 48) we concluded that the dichloroBODIPY **1** had

- undergone only a single substitution (no double substitution was observed at all)

and that

- the solvent participated in the reaction by being deprotonated by the carbonate, leading to substitution of the chlorine that was attached to the gold atom (Figure 50).

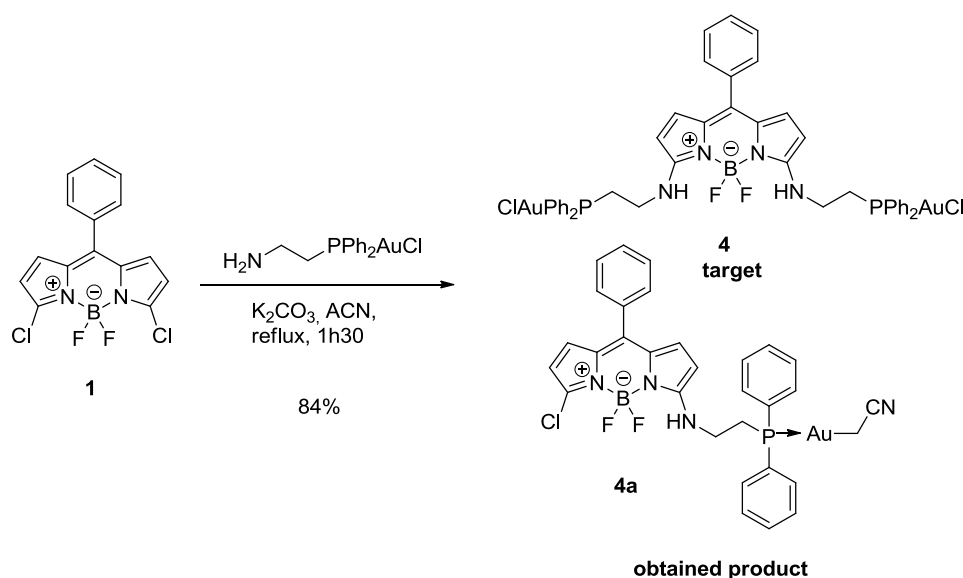


Figure 50: Introduction of Gold(I)-amino phosphine **3** onto the BODIPY core of **1** by nucleophilic aromatic substitution in acetonitrile

The introduction of cyanomethyl and other activated species such as malonitrile onto the gold-atom is not unknown in the literature. However, in all published cases either strong bases such as BuLi, organic super-bases [183] or halogen-abstractors ( $\text{Ag}_2\text{O}$ ) have been used to deprotonate the acetonitrile. In the following we first focused our efforts on the synthesis of the monosubstituted compound **4b** to establish a viable synthetic protocol.

The reaction conditions were thus slightly modified to prevent the substitution of the chloride ligand borne by the gold(I)-center.

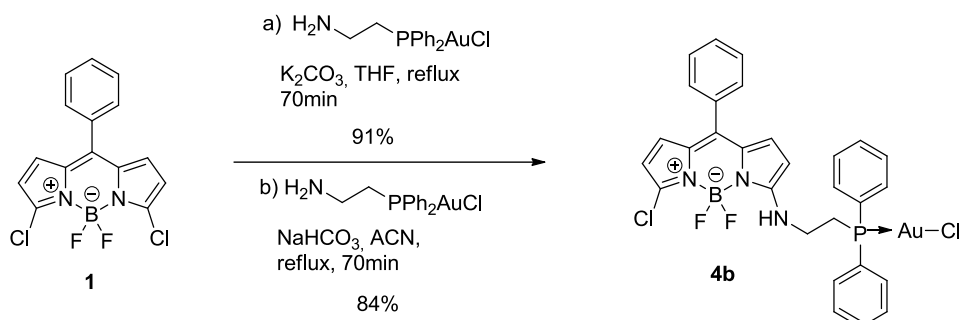


Figure 51: Modified reaction conditions for the synthesis of monosubstituted BODIPY

The use of either THF/ $\text{K}_2\text{CO}_3$  or ACN/ $\text{NaHCO}_3$  led to the desired monosubstituted product in good yields and prevented reactions with the solvents (Figure 51). We were able to obtain crystals of **4b** in sufficient size and quality to perform single crystal X-ray scattering. This compound crystallizes as a dimer with an aurophilic bond between the gold(I)-centers.

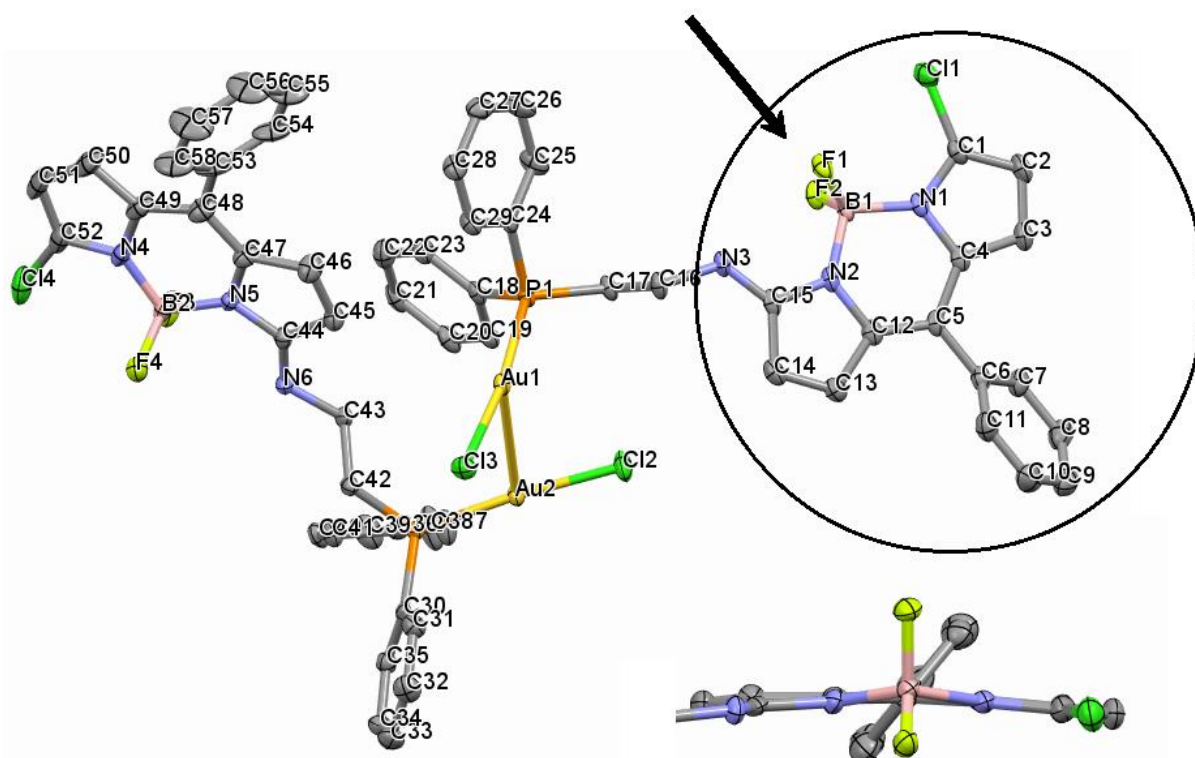


Figure 52: X-Ray structure of BODIPY **4b**. The circled part is shown in the bottom right along its  $\text{B} \rightarrow \text{meso-C} \rightarrow \text{meso-phenyl}$  axis (molecule is flipped, view direction is indicated by the arrow). The ellipsoids are drawn at 50% probability level. Hydrogen atoms and solvent molecules are omitted for clarity. The molecule was drawn using CIF data

The view along the  $\text{B1-C5-meso-phenyl}$  axis (bottom right, Figure 52) shows that the phenyl substituent is rotated out of the molecular plane of the BODIPY-core which results in very limited conjugation between the two subunits.

The shape-analysis of the aurophilic bond shows that both Au(I)-metal centers are found in a T-shape-environment (mer-trivacant octahedron) with a local  $C_{2v}$ -symmetry. The structural parameters for both subunits are almost identical (Table 5).

Table 5: Selected bond-lengths and dihedral angles for BODIPY **4b**. Bond-lengths are given in Å, angles in °

Bond	Length [Å]	Angle	Angle [°]
Au1-Au2	3.13975(19)	P1-Au1-Cl3	171.97(3)
Au1-Cl3	2.2961(8)	P2-Au2-Cl2	174.45(3)
Au1-P1	2.2330(8)	P1-Au1-Au2	102.29(2)
Au2-Cl2	2.3021(8)	P2-Au2-Au1	105.93(2)
Au2-P2	2.2344(8)	Cl3-Au1-Au2	82.53(2)
		Cl2-Au2-Au1	79.62(2)

With 3.13975(2) Å the gold(I)-gold(I) bond is in the range of reported aurophilic bonds of 2.5-3.5 Å [184,185]. The dihedral angle between the P-Au-Cl of 171.97° and 174.45° infer that the bond is very weak.

Literature suggested that this weak aurophilic bond is only present in the solid, at room temperature in solution it is overruled by solvation [186]. An attempt at using Raman-spectroscopy to observe the Au-Au-bond [187] was unsuccessful due to the incompatibility of the used laser. However, Nomiya *et al.* [186] showed that the formation of the dimeric species can be observed using low-temperature phosphorus-NMR. In their case a new peak developed upon formation of the dimeric species at -90°C/183K. The new dimeric species displayed shifts between -0.6ppm and -1ppm respectively compared to the monomeric gold-phosphine.

We therefore performed low temperature  $^{31}\text{P}$ -NMR of **4b** in deuterated DCM. The NMR (Figure 53) shows that the peak of the gold(I)-amino phosphine broadens significantly and shifts upfield at low temperatures.

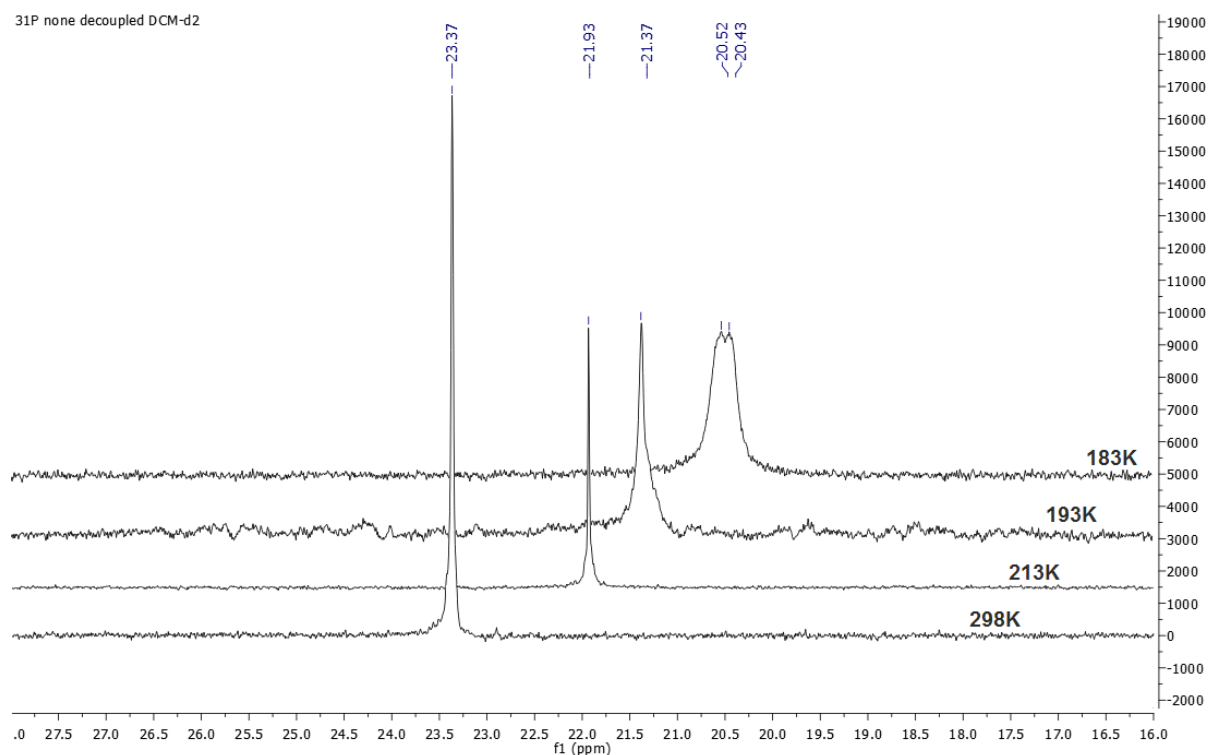


Figure 53:  $^{31}\text{P}$ -NMR-spectra of BODIPY **4b**. Overlay of NMR recorded at different temperatures. The traces are **not** stacked at an angle or x-offset. The NMR was recorded in DCM- $D_2$  at 500MHz

Upon lowering the temperature the peak gradually shifts upfield. At 193K only a single (if broad) peak can be observed.

At 183K a broadening and splitting of the peak seems to begin, indicating that indeed the Au-Au-bond is forming. However, 183K is only 7K above the freezing point of DCM-D<sub>2</sub>; at this temperature the solvent's viscosity is already strongly increased due to the formation of solvent-clusters. Decreasing the temperature even further is not possible due to solvent restraints and the risk of damaging the apparatus. Nonetheless we were able to confirm the absence of the dimeric species in solution at room temperature and show that the aurophilic bond that we observed by X-ray scattering is overruled by solvation.

### 1.3.1 Towards double functionalization

So far our attempts to synthesize a multinuclear gold-based compound were unsuccessful. With the monosubstituted compound **4b** in hand we thus focused our efforts on introducing two gold(I)-moieties into the BODIPY **1**. In order to achieve the double substitution of the BODIPY core (Figure 54) a numerous conditions were tested.

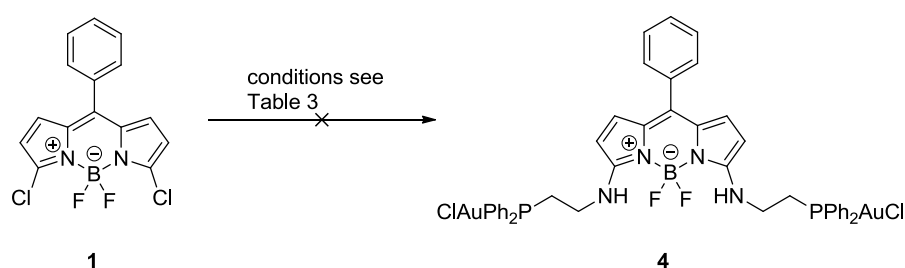


Figure 54: Double substitution of the BODIPY-Cl<sub>2</sub> **1** with gold(I)-amino phosphine

The tested conditions are summarized in Table 6 and included the reaction in presence of Pd-based catalysts, irradiation with microwaves, absence of base as well as presence of acid. The use of acid was attempted in the hope to protonate the formed secondary amine so as to form an ammonium. This would reduce the electron density at the BODIPY core and reactivate it towards nucleophilic aromatic attacks, thus enabling a second substitution.

Table 6: Tested conditions for the double substitution of BODIPY-Cl<sub>2</sub> by gold(I)-amino phosphine **3**. No product observed=no double substitution occurred. Catalytical amount of pTSA means 1 grain

Equivalents of gold(I)-phosphine <b>3</b>	Base/acid	Catalyst	Solvent	Temperature (heating)	Reaction time	Observation
2	K <sub>2</sub> CO <sub>3</sub>	-	THF	reflux	60h	no product formation
3	K <sub>2</sub> CO <sub>3</sub>	-	THF	160°C (microwaves)	15min	formation of nanogold
3	2eq Et <sub>3</sub> N	0.1eq Pd(OAc) <sub>2</sub> , 0.3eq PPh <sub>3</sub>	DMF	90°C	24h	degradation
2	2eq Et <sub>3</sub> N	0.1eq Pd(OAc) <sub>2</sub> , 0.3eq PPh <sub>3</sub>	ACN	reflux	24h	degradation
4	-	-	THF	reflux	90min	no reaction
3	-	cat. pTSA	ACN	reflux	2h	formation of

3	-	cat. <i>p</i> TSA	THF	reflux	2h	nanogold formation of nanogold
---	---	-------------------	-----	--------	----	--------------------------------

All the tested conditions led either to starting material or to unwanted/degradation products. As previously indicated, some examples of double substitution of dichloro BODIPYs using aniline derivatives, secondary amines [103], or even hydrazine have been reported. Only one account has succeeded in introducing a primary aliphatic amine twice onto the BODIPY core. In this case the authors used the amine as a solvent, performed the reaction at reflux and the double substitution required prolonged reaction times [188]. However, the use of gold(I)-amino phosphine in large excesses is self-prohibitive for obvious reasons.

Faced with these difficulties, we decided to directly move to the trifunctionalizable platform, as described above. Our idea was simple: design a dichloroBODIPY carrying a carboxylic acid function at the *meso*-phenyl substituent. Thus, the BODIPY would be able to undergo functionalization in a step-by-step fashion and permit the introduction of sensible substituents such as peptides that might not resist the refluxing conditions used to introduce the gold-bearing unit.

### 1.3.2 Synthesis of BODIPY-acid

The BODIPY-ester **7** was synthesized using usual conditions: reaction of pyrrole with the desired aldehyde under acid catalysis – the carboxylic acid function was protected as its methyl ester form – to yield the dipyrromethane in good yields. The dipyrromethane **5** was chlorinated using NCS, followed by oxidation to obtain the dipyrromethene **6**. Dipyrromethene **6** was then deprotonated at the pyrrolic nitrogen using Et<sub>3</sub>N, followed by the addition of BF<sub>3</sub>·Et<sub>2</sub>O to introduce the BF<sub>2</sub> moiety (Figure 55).

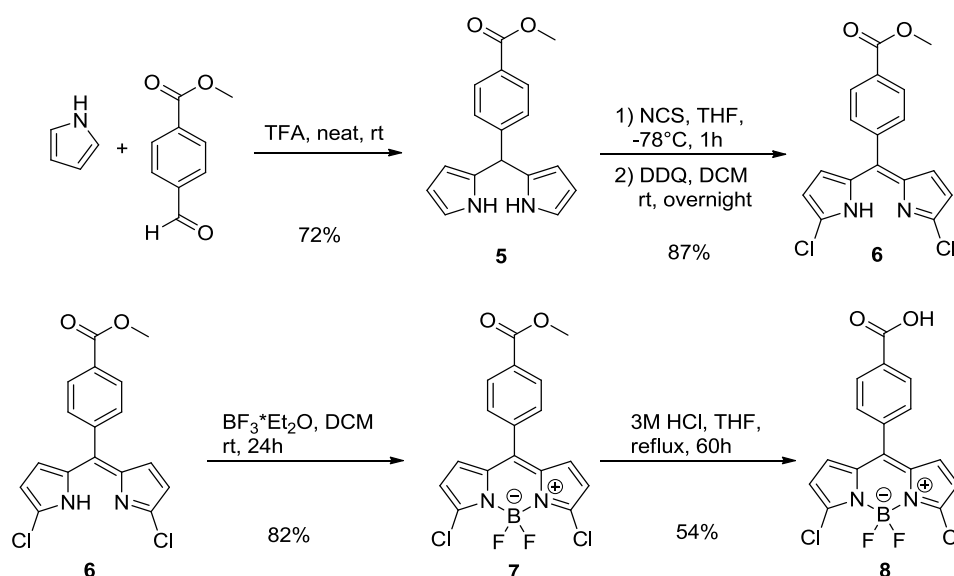


Figure 55: Synthesis of BODIPY-Cl<sub>2</sub> acid **8**

In order to obtain the trifunctional platform the ester function was hydrolyzed. Several conditions were tested: the obvious choice was the use of dilute aqueous base (e.g. LiOH, NaOH, KOH or K<sub>2</sub>CO<sub>3</sub>). Usually this strategy gives good results for BODIPYs that only carry alkyl or aryl substituents [189–191]. In our case however it led to degradation of the BODIPY-core

due to deboration and nucleophilic attack of the OH on the chlorines that are situated on the BODIPY-core. The basic hydrolysis was therefore abandoned and acidic conditions were investigated.

TFA in DCM proved inadequate as well as the effective acid concentration leads to protonation of the pyrrolic nitrogen and loss of the boron moiety. A compromise was devised and the hydrolysis executed in a partially biphasic system using equal volumes of THF and 3M HCl. Refluxing for several days then yielded the free acid-BODIPY **8** in acceptable yields (Figure 55). The synthetic procedures of the starting material proved very robust and were scaled up to 8g of BODIPY-ester **7** and 2.5g of BODIPY-acid **8** without significant decreases in yield.

We were able to grow monocrystals for the compounds **6**, **7** and **8** and confirm their identity by X-Ray diffraction (Figure 56).

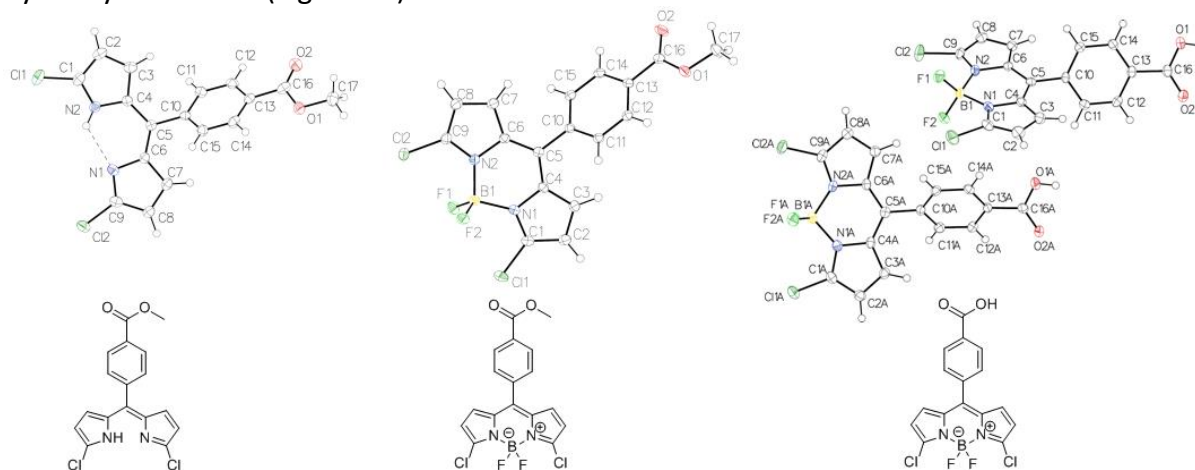


Figure 56: X-Ray diffraction of dipyrromethene **6** (left) and BODIPYs **7** (middle), **8** (right)

For all three compounds the X-Ray diffraction did not reveal any surprising structural features. The dipyrromethene crystallizes in a monoclinic crystal system with the space group  $P2_1/c$  whereas both the BODIPY ester **7** and the free acid **8** crystallize in a triclinic crystal system (both in the space group  $P\bar{1}$ , in the case of the free acid **8** with two molecules per asymmetric unit).

### 1.3.3 Functionalization of trifunctional BODIPY-acid **8**

Following the successful synthesis of the free acid BODIPY **8**, its regioselective functionalization with gold complex **3** was performed. Application of the optimized conditions for the synthesis of **4b** to the synthesis of **9** proved effective and yielded the monosubstituted BODIPY **9** in good yields of 80% (Figure 57). As for BODIPY **1** no double substitution was observed.

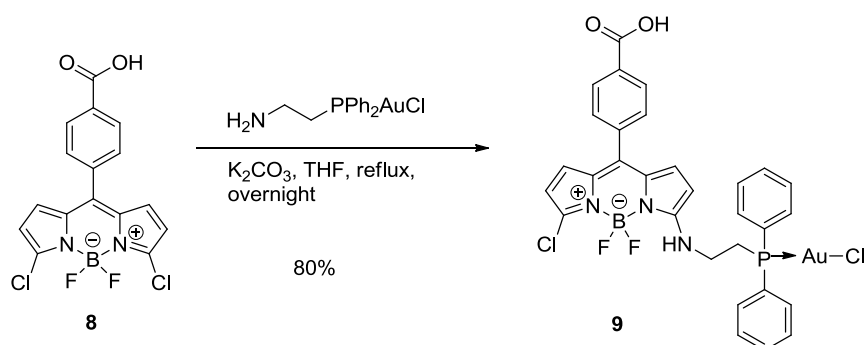


Figure 57: Synthesis of BODIPY **9**

In order to prove the BODIPY's usefulness as a platform-molecule the selective functionalization of the acid-function was attempted. For this purpose, the acid function was activated as an acyl chloride and reacted at room temperature with the auriphosphine **3** (Figure 58).

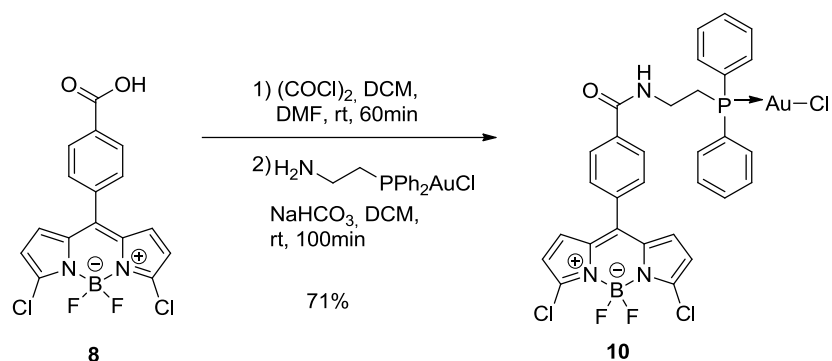


Figure 58: Functionalization of meso-acyl by activation as acyl chloride to synthesize BODIPY **10**

The reaction proceeded smoothly and yielded the target compound in good yield. Small losses were sustained during the precipitation. No core-substituted byproduct was observed, which confirms the chosen synthetic strategy as a valid pathway for the selective functionalization in the *meso*-position.

To attach two gold bearing moieties to BODIPY **8** the previously established procedures were applied in combination: first the carboxylic acid was activated in DCM using  $(\text{COCl})_2$  as the chlorination agent, followed by addition of an excess (2.1 equivalents) of gold-complex **3** in THF and reflux in presence of a proton scavenger ( $\text{K}_2\text{CO}_3$ ). This approach yielded the desired double substituted compound **11** in very good (93%) yield (Figure 59).

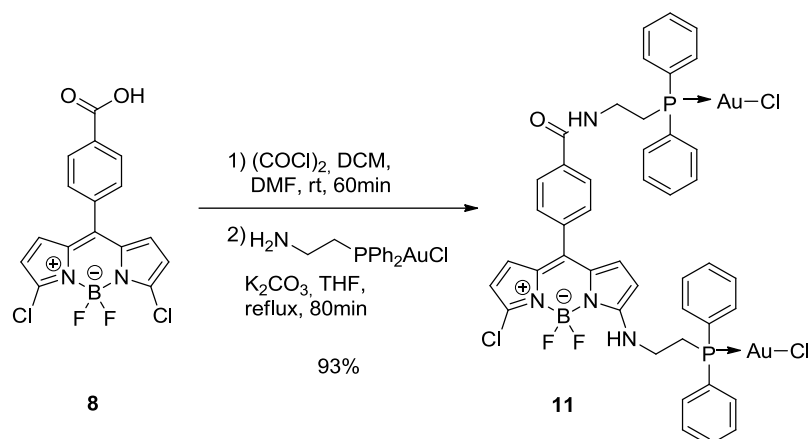


Figure 59: Double substitution of BODIPY **8** with two gold(I)-amino phosphine moieties

Special attention has to be paid to the evaporation of excess  $(\text{COCl})_2$  and drying of the acyl chloride: in one instance incomplete removal of the solvents/agents and incomplete scavenging of the liberated HCl resulted in hydrolysis of THF and subsequent reaction to form the ester. In that instance the HCl prevented the reaction of the gold(I)-amino phosphine **3** due to protonation, leading to the unexpected compound **12** (Figure 60).

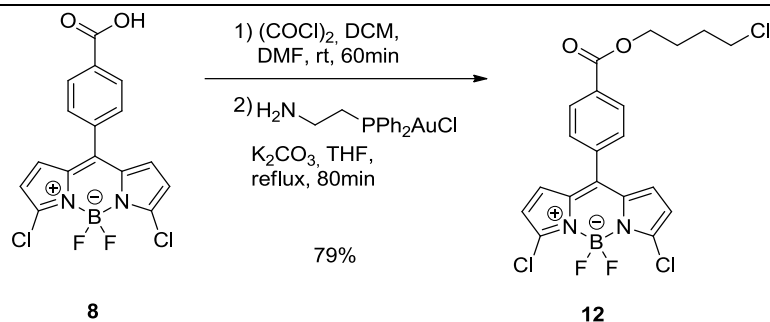


Figure 60: Opening of THF with subsequent chlorination by HCl

A complete removal of all solvent traces reliably prevented such unwanted side reactions.

In earlier experiments (not shown in this thesis), we found that the gold-complex was unstable in presence of  $(\text{COCl})_2$ . The double substitution with gold(I) bearing moieties was therefore never attempted, starting from the mono-functionalized BODIPY (**9**).

Following the successful synthesis of the four theranostic compounds **4b**, **9**, **10** and **11**, each compounds' photophysical and biological properties were then characterized. The results are shown and discussed in detail in chapter 1.4.2 - Photophysical characterization of obtained BODIPY-dyes and 1.4.3 - Biological investigations.

Having established the general feasibility of site-specific substitutions using the relatively delicate gold(I)-moiety **3** we were interested to explore the potential of the selected BODIPY platforms by synthesizing a large panel of compounds.

### 1.3.4 Introduction of a thioglucose tetraacetate moiety

In previous works we had observed that, as for Auranofin, the introduction of thioglucose could increase the antiproliferative properties of the gold complexes [91]. We were therefore interested to study if our compounds would display the same effect.

For this aim the thioglucose derivate was introduced on compounds **4b**, **9**, **10** and **11**. The substitution of the chlorido-ligand was straightforward: after deprotonation of  $\beta$ -thioglucose-tetraacetate using 1M NaOH in acetone, the solution was added to a solution of gold(I)-BODIPY and reacted for a short period of time. This yielded the desired compounds almost quantitatively for three of the four BODIPYs (small losses were sustained during the removal of the formed NaCl and the following precipitation) (Figure 61).

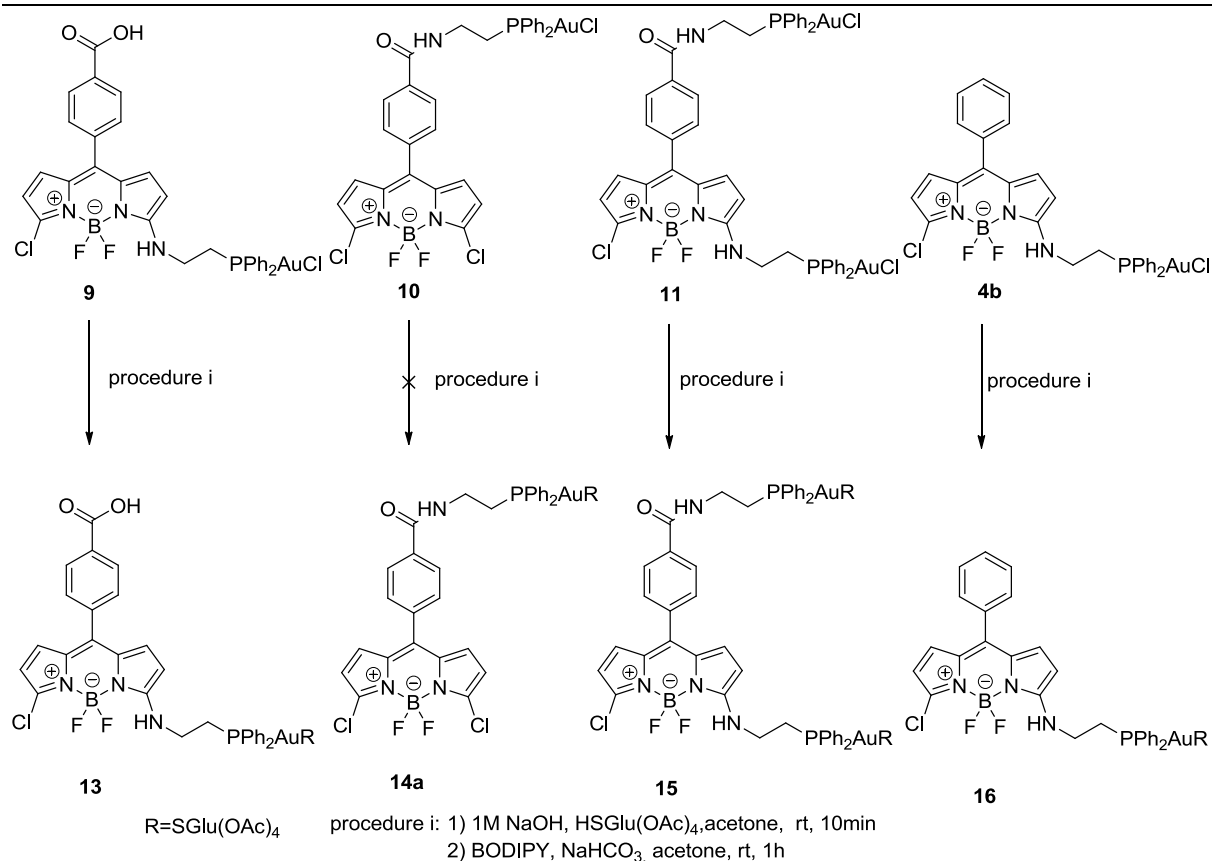


Figure 61: Introduction of thioglucose tetraacetate onto the gold bearing moiety

In the case of BODIPY **10**, a rapid change of color from orange-red to pink appeared, indicating that a reaction at the BODIPY-core had taken place. Indeed, analysis by HPLC-MS showed that up to three thiosugar-moieties had been introduced to the molecule, meaning that a double-core-substitution must have taken place (**14b**, Figure 62).

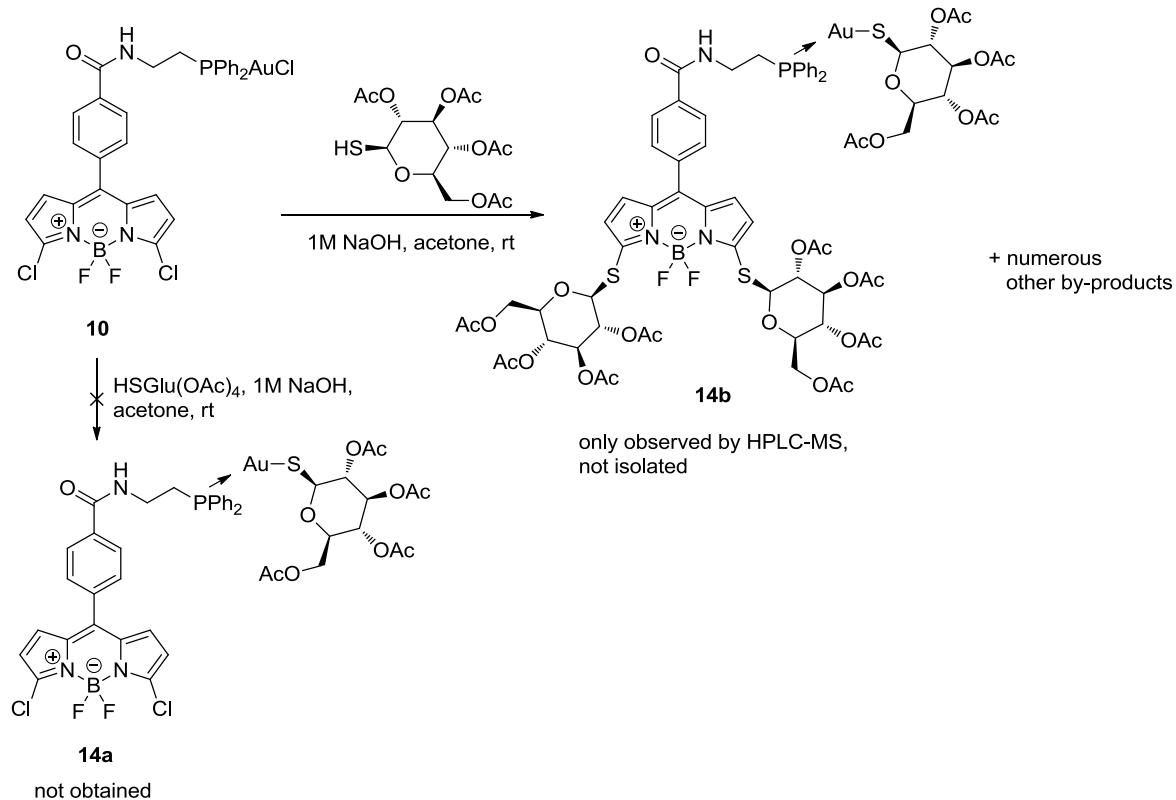


Figure 62: Intended reaction (left) and one of the observed products (**14b**, right)

Although this means that **14a** was inaccessible by the chosen method we were curious to investigate this reactivity. To confirm our observation we engaged BODIPY-Cl<sub>2</sub> **8** under the same reaction conditions (Figure 63).

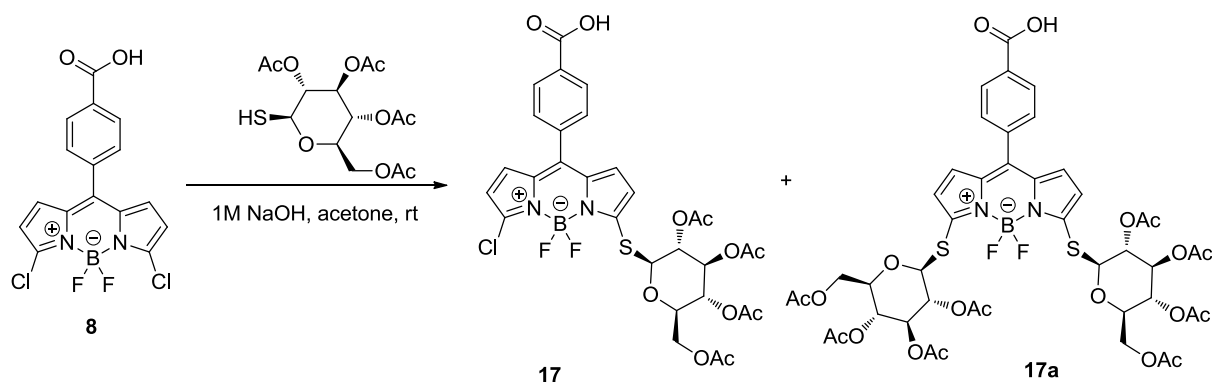


Figure 63: Reaction of BODIPY **8** with thioglucose tetraacetate

Once again the color changed swiftly from red-orange to the same pink that we had observed previously, showing that the same transformation had taken place. HPLC-MS analysis of the crude reaction mixture indicated that the BODIPY core readily underwent nucleophilic aromatic substitution.

Moreover, HPLC-MS showed that we had obtained a seemingly statistical mix of the mono- (**17**) and double substituted (**17a**) compounds. This hinted on the fact that unlike with *N*-substituents the introduction of a *S*-nucleophile does not significantly reduce the reactivity of the BODIPY-core.

In order to explain this unexpectedly high reactivity we performed DFT-calculations for some model-systems in collaboration with Prof. Paul Fleurat-Lessard and Dr Miguel Ponce-Vargas (ICMUB).

## 1.3.5 Quantum chemical investigations

The DFT calculations were performed at the M06-2X/6-31G(d) level to determine the lowest unoccupied molecular orbital energy ( $E_{\text{LUMO}}$ ) for some model systems containing amino- and thio- groups. This value can be associated with the electrophilicity of the molecule [192,193]. Therefore, the higher  $E_{\text{LUMO}}$ , the lower the probability of the molecule to experience a nucleophilic attack.

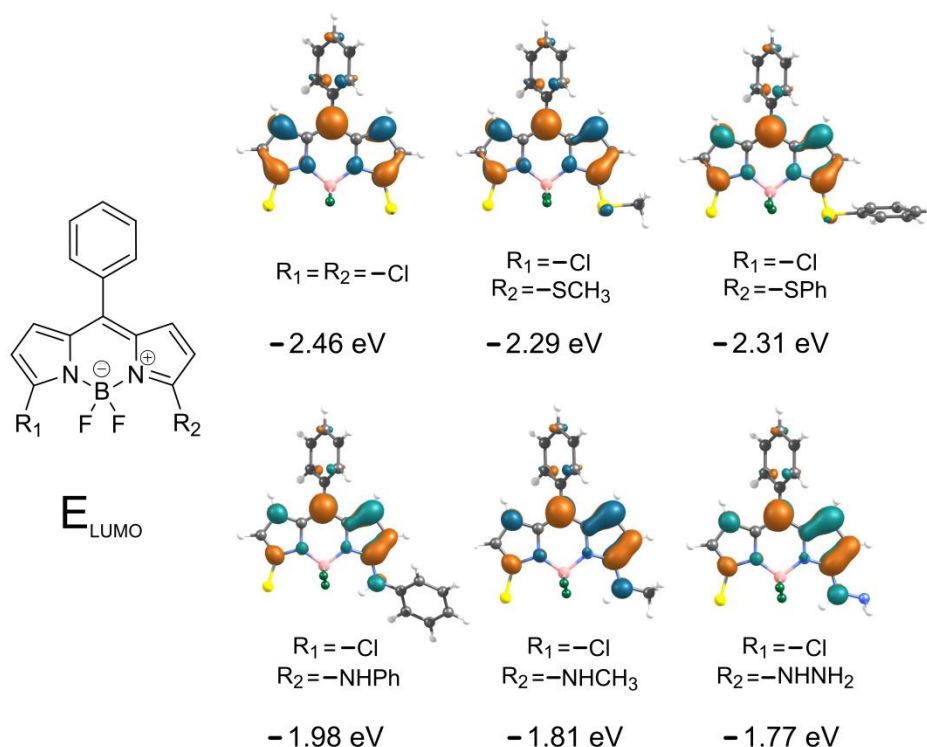


Figure 64: LUMO energies (eV) for some model systems

The graphical representation of the LUMO, which is mainly distributed over the dipyrromethene core in all systems is represented in Figure 64. The  $\text{BF}_2$ -moiety does not take part in the LUMO. This highlights its role as a sole stiffener of the BODIPY-backbone. The small contribution of the phenyl ring at the *meso* position evidences the poor conjugation between this fragment and the boron-dipyrromethene moiety given the broad dihedral angle between them (this angle is in good agreement with the X-Ray structures that we obtained for compounds **4b** and **6-8** (Figure 52 and Figure 56) in chapter 1.3.2).

The replacement of a chlorine atom by an amino-/thio- substituent leads to an  $E_{\text{LUMO}}$  increase with respect to the dichloride- starting compound. This effect is more pronounced for the amino-substituted BODIPYs ( $\Delta E_{\text{LUMO}} \sim 0.61$  eV) than for their thio-substituted counterparts ( $\Delta E_{\text{LUMO}} \sim 0.16$  eV).

The DFT-calculations confirmed our observation that the introduction of a first *S*-nucleophile does not significantly increase the electronic density at the BODIPY-core, therefore not preventing the introduction of a second substituent, including *N*-nucleophiles. A similar behavior was observed by Lincoln *et al.* [194]; following their work we found a qualitative trend between the LUMO energies of the compound and the Hammett parameters: the lower the  $\sigma_p$  (and or  $\sigma_m$ ) value, the higher the LUMO energy of the compound (Table 7).

Table 7: Literature values of selected Hammett-parameters for various substituents [195] (left) and calculated LUMO energies of BODIPY carrying substituents in 3,5 positions (right)

Substituent	$\sigma_m$	$\sigma_p$	Substituent 1	Substituent 2	LUMO energy
Cl	0.37	0.23	Cl	Cl	-2.46 eV
SMe	0.15	0.00	Cl	SMe	-2.29 eV
SEt	0.18	0.03	Cl	SPh	-2.31 eV
NHMe	-0.21	-0.70			
NH(CH <sub>2</sub> ) <sub>3</sub> CH <sub>3</sub>	-0.34	-0.51	Cl	NHMe	-1.81 eV
N(Me) <sub>2</sub>	-0.16	-0.83	Cl	NPh	-1.98 eV
NPh	-0.02	-0.56	Cl	NHNH <sub>2</sub>	-1.77 eV
NHNH <sub>2</sub>	-0.02	-0.55			

We also calculated the released energy that is associated with each secondary substitution. Two processes were distinguished: (a) the incorporation of an aminomethyl group in the thio-substituted BODIPY and (b) the incorporation of a thiomethyl in the amino-substituted BODIPY; both processes lead to the same product (Figure 65).

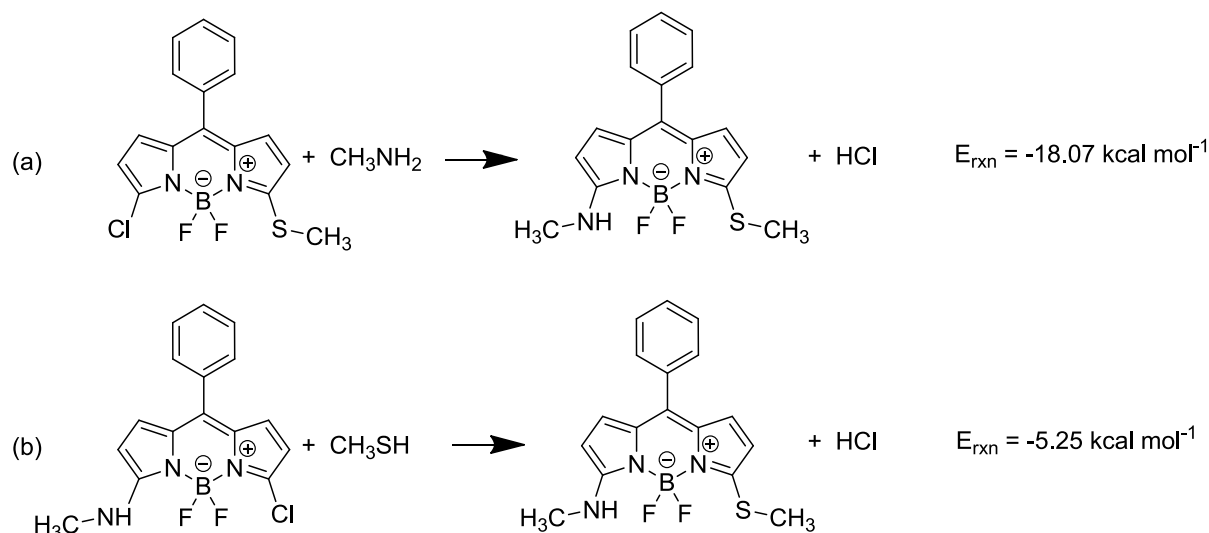


Figure 65: Some hypothetical reactions involving the model system

We found that reaction (a) is the more exothermic process of the two. It releases more than three times the energy of (b).

All calculated values are in good agreement with the observed behavior of dichloroBODIPYs and showcase the great difficulty/unfeasibility to incorporate a second primary amine to the amino-substituted BODIPY.

### 1.3.6 Trifunctionalization of the dichloroBODIPY acid

Since the substitution of the chloro-ligand of the gold-atom requires an anionic sulfide, the required compound **14a** is not accessible *via* the chosen pathway.

However, the high reactivity of the chloro- and dichloroBODIPY towards the presented S-nucleophile woke our interest as it opened up a multitude of possibilities for further diversification of the chosen platform.

We thus decided to widen the scope of our work and synthesize a whole family of closely related BODIPYs that possess different substitution patterns. First we focused our efforts on the optimization of the synthesis of **17**. In order to be able to form mostly the targeted mono thiosugar derivative, starting from the precursor **8**, the reaction conditions were optimized as follows:

- By limiting the *S*-nucleophile present in the reaction (slow addition) and using the agent in default, we were able to almost completely suppress double substitution.
- By optimizing the separation conditions: indeed, using classic chromatographic conditions the removal of the small amount of byproduct formed during the reaction was impossible: even semi preparative reversed-phase HPLC turned out to be insufficient. The addition of formic acid to the eluent finally aided the separation using normal phase chromatography and the optimization of both the reaction conditions and the chromatographic system enabled us to obtain the (pure) mono-substituted product in excellent yields (95% with regard to  $\beta$ -thioglucose-tetraacetate) and purity (Figure 66).

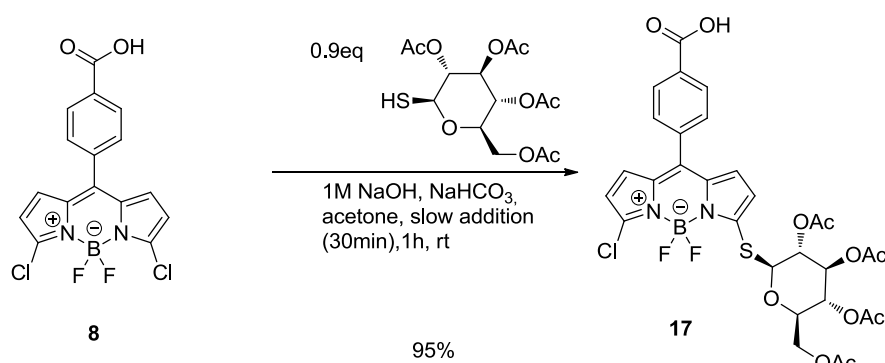


Figure 66: Monosubstitution of BODIPY-Cl<sub>2</sub> **8** using HSGlu(OAc)<sub>4</sub>

The same conditions were also applied to the mono-substitution of BODIPY-Cl<sub>2</sub> **1**. Unfortunately, the reaction proceeded far less smoothly and yielded significant amounts of double substituted BODIPY **18a** (Figure 67).

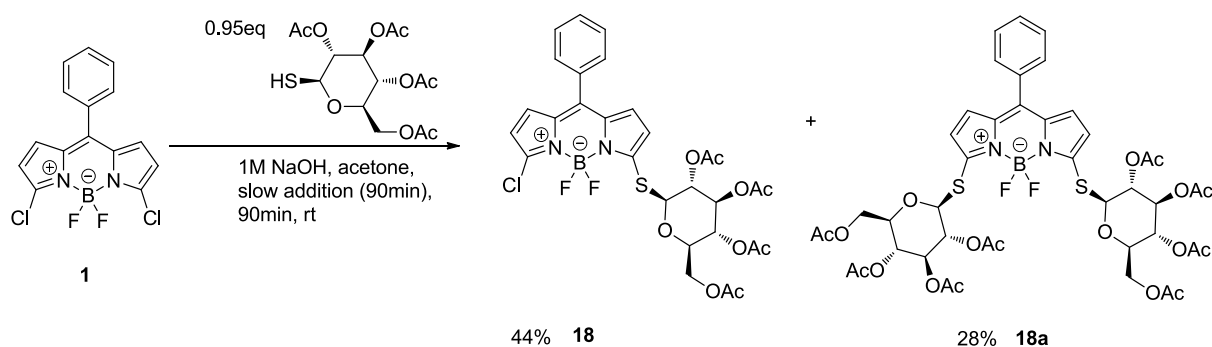


Figure 67: Substitution of BODIPY-Cl<sub>2</sub> **1** with HSGlu(OAc)<sub>4</sub>. Yields are given with regard to BODIPY. Using thioglucose tetraacetate as reference the yields are 44% and 56% respectively

For this reaction 44% and 56% of the thioglucose tetraacetate ended up in the monosubstituted (**18**) and double substituted (**18a**) compound respectively. (The derivate **18a** was identified by analytical HPLC-MS but neither isolated nor characterized). Interestingly, in absence of NaHCO<sub>3</sub> the selectivity of the reaction is even poorer (For the synthesis of **17** NaHCO<sub>3</sub> was primarily added to prevent protonation of the thiolate by the carboxylic acid).

In the next step, the mono-substituted BODIPYs **17** and **18** were reacted with the gold complex **3**. To that end, the two agents were dissolved in THF and refluxed for 60min in presence of a proton scavenger providing access to the desired products in good (82%, **19**) and excellent (95%, **20**) yields (Figure 68).

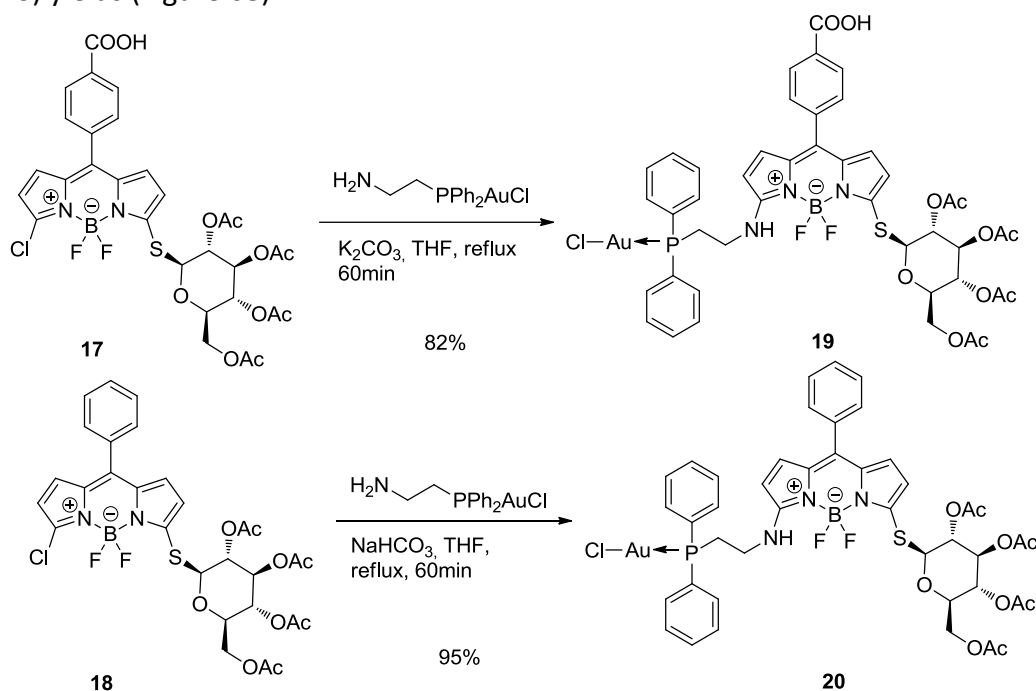


Figure 68: Secondary substitution of the thioglucose-functionalized BODIPYs

It is worth noting that we were able to selectively obtain the mono gold(I)-BODIPY complex **19** displaying a double functionalization on the BODIPY core. Conversely, we did not succeed in making the second functionalization occur exclusively on the carboxylic acid position. Indeed, even activating this function *via* the formation of the corresponding acyl chloride is not sufficient to overcome the reactivity of the second chlorine born by the BODIPY core. However, the BODIPY **21** carrying two gold-moieties was obtained in a very high yield using an excess of gold complex **3** (Figure 69).

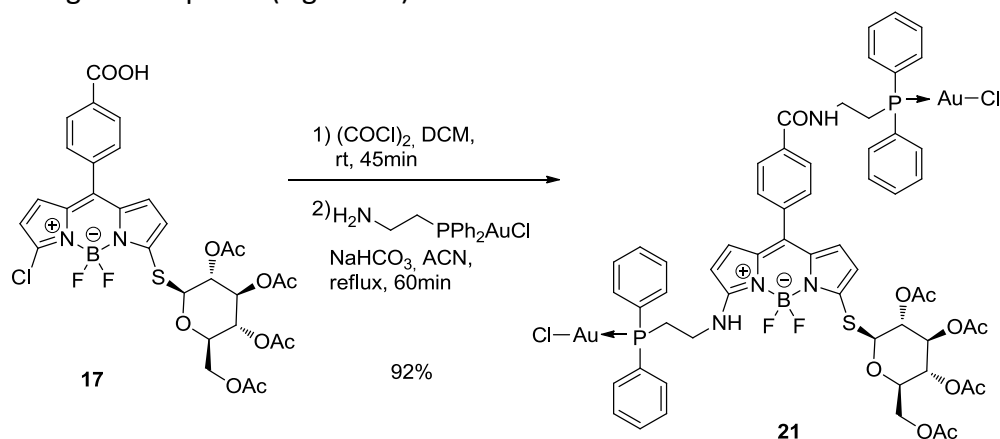


Figure 69: Attempt at introduction of the gold-bearing moiety onto the carboxylic acid function

The most important point of the synthesis of **21** is the fact that we proved that our platform can be functionalized by three nucleophiles under mild conditions. Keeping in mind the four criteria we defined for our ideal platform, only one requirement is not yet validated. It is the ability of introducing three **different** nucleophiles **step-by-step**.

Towards that end, we chose a third substituent that may influence/change the biological behavior of the final system. We opted for a phosphonium derivative. Indeed, this class of compounds can increase the water solubility of the theranostic, bring an additional mode of cytotoxicity, and/or induce a targeting of mitochondria, which contain the enzymes which are believed to be inhibited by gold(I) complexes. Triphenylphosphoniummethylamine **22** was chosen as the phosphonium of interest: the starting materials triphenylphosphine and bromoethylammonium hydrobromide are cheap, easy to handle and do not require the use of a protective atmosphere. The synthesis of the chosen compound was straightforward and followed known synthetic procedures [196] (Figure 70).

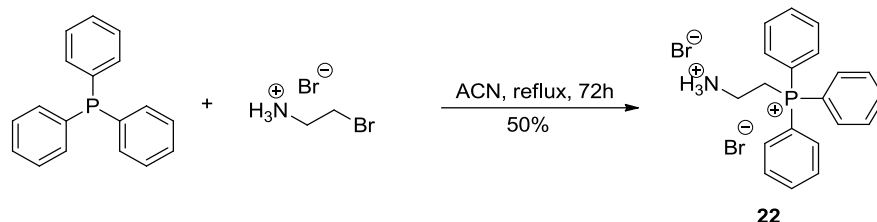


Figure 70: Synthesis of phosphonium **22**

Next, the synthesized aminophosphonium **22** was reacted with the BODIPY-acid. BODIPY **23** was then modified by introduction of thioglucose-tetraacetate. As observed during the synthesis of BODIPY **17** the small difference in reactivity between unmodified and mono-core-substituted product made it necessary to add the thioglucose tetraacetate slowly to the reaction to prevent excessive formation of byproducts (Figure 71).

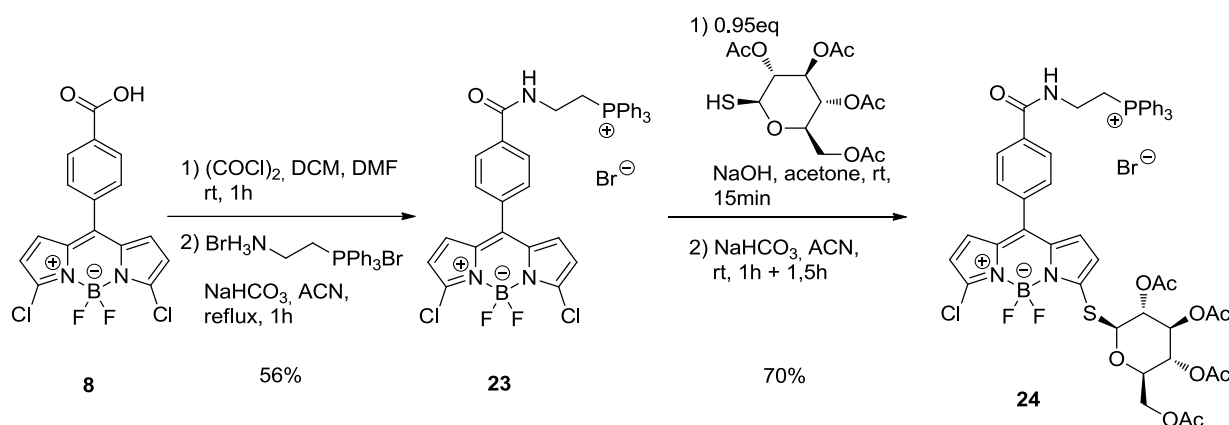


Figure 71: Formation of amid between BODIPY-Cl<sub>2</sub> **8** and phosphonium **22** and synthesis of BODIPY **24**

Following the addition of thioglucose to the BODIPY-core, BODIPY **24** was reacted with gold complex **3** to introduce the 3<sup>rd</sup> substituent using the optimized conditions (ACN, NaHCO<sub>3</sub> and reflux). Unfortunately, the chosen conditions were not appropriate for the compound as they led to total degradation of the starting materials after 90min.

The reaction was repeated using shorter reaction times (reflux for 30min). Unfortunately the obtained product mixture proved again too difficult to separate by classical chromatography on silica gel. An attempt to separate the desired compound from the product mixture by semi preparative HPLC failed however as the product was unstable under HPLC conditions and lost a phenyl during purification.

We therefore switched both the order and site of functionalization of both substituents. Inserting first the phosphonium **22** in the 5-position, followed by the introduction of the gold(I)-moiety **3** in the *meso*-acyl position at room temperature would enable us to use less harsh conditions during the last synthetic step and thus limit the risk of degradation.

Therefore the previously synthesized BODIPY **17** was modified using phosphonium **22** to yield **25** (Figure 72).

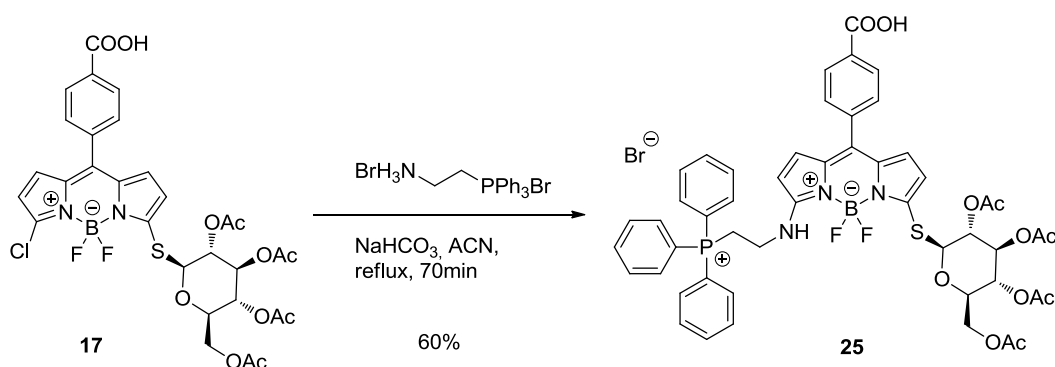


Figure 72: Introduction of phosphonium **22** in the 5-position of thioglucose-tetraacetate-substituted BODIPY **17**

In the next step the carboxylic acid was activated as acyl chloride using oxalyl chloride. Unfortunately these conditions led to heavy formation of a multitude of byproducts. Therefore, the functionalization was attempted using a coupling agent system typically used for peptide synthesis: HBTU/DIPEA (Figure 73).

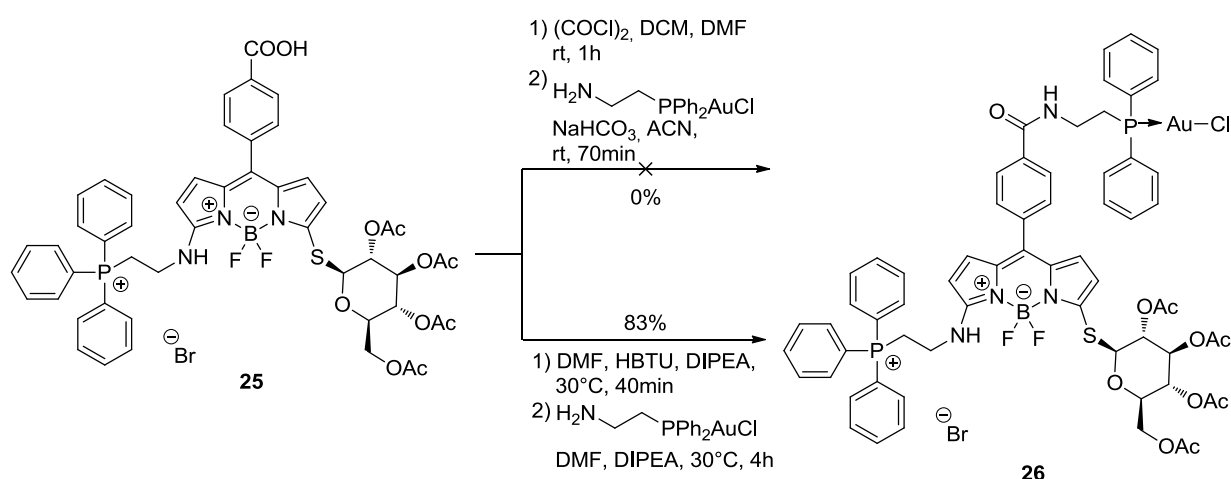


Figure 73: Introduction of the third substituent

Even the use of coupling agents led to formation of several byproducts, rendering the purification by column chromatography tricky: Addition of formic acid to the eluent was necessary. Under these conditions all byproducts visible under UV-light were removed successfully. However, NMR-analysis of the final product indicated that the compound had undergone ion exchange during reaction, trapping  $\text{PF}_6^-$  (initially present in HBTU) and one equivalent of the ion-pair  $\text{DIPEA-H}^+\text{PF}_6^-$ . Removal of  $\text{DIPEA-H}^+\text{PF}_6^-$  was attempted by repeating the purification using a slower gradient, without success. Different assays were performed for obtaining pure trifunctionalized BODIPY **26**, but we never succeeded in removing all the salts originating from coupling agents. Attempts to purify **26** by semi preparative RP-HPLC succeeded in removing salts from coupling agents, led however also to a continuous loss of phenyl (Figure 74).

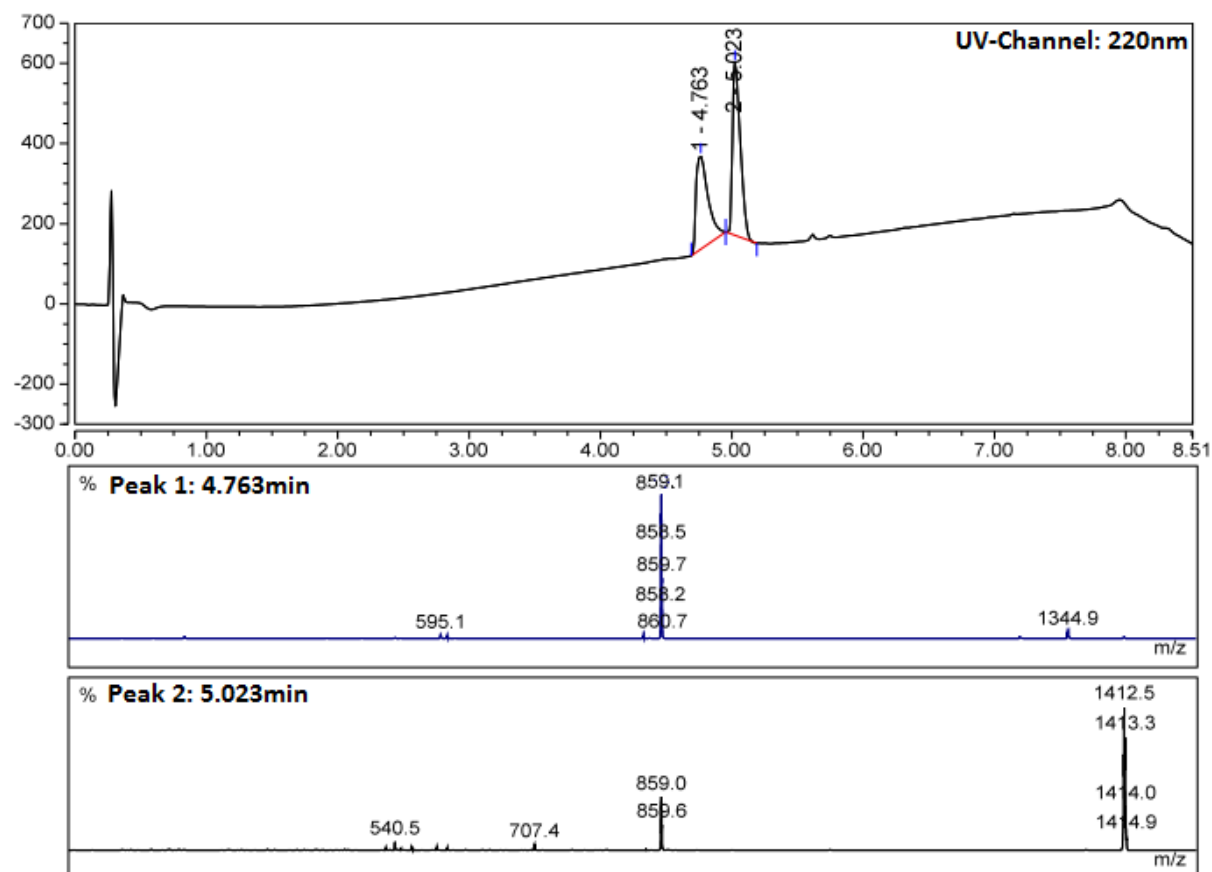


Figure 74: Analytical RP-HPLC/MS-Chromatogram from purification attempt of **26**. The first product is continuously formed during semipreparative RP-HPLC purification and corresponds to [**26-Ph**]. The shown UV-Channel (top) is recorded at 220nm.

The best result is a purity a bit superior to 85%.

Even if this product was not totally pure, it is clear that this issue is intrinsic to the sophisticated and sensitive substituents we have chosen and that we proved that it was possible to functionalize our platform **stepwise** by three **different** nucleophiles under mild reaction conditions.

More than just a chemical challenge, the synthesis of this new large family of BODIPYs aims at granting a rapid access to easily fine-tuned optical theranostics. Thus, we evaluated their photophysical properties and their ability to be efficient anti-proliferative agents that can be tracked *in vitro* by optical imaging.

## 1.4 Characterization of the BODIPYs properties

### 1.4.1 Introduction of a simplified graphic representation

In the following paragraphs we are going to describe and discuss each BODIPYs properties. For the sake of clarity, most of the time the structure of each compound will be replaced by a simplified depiction (Figure 75). The BODIPY-core is represented by three strokes to which each substituent is attached.

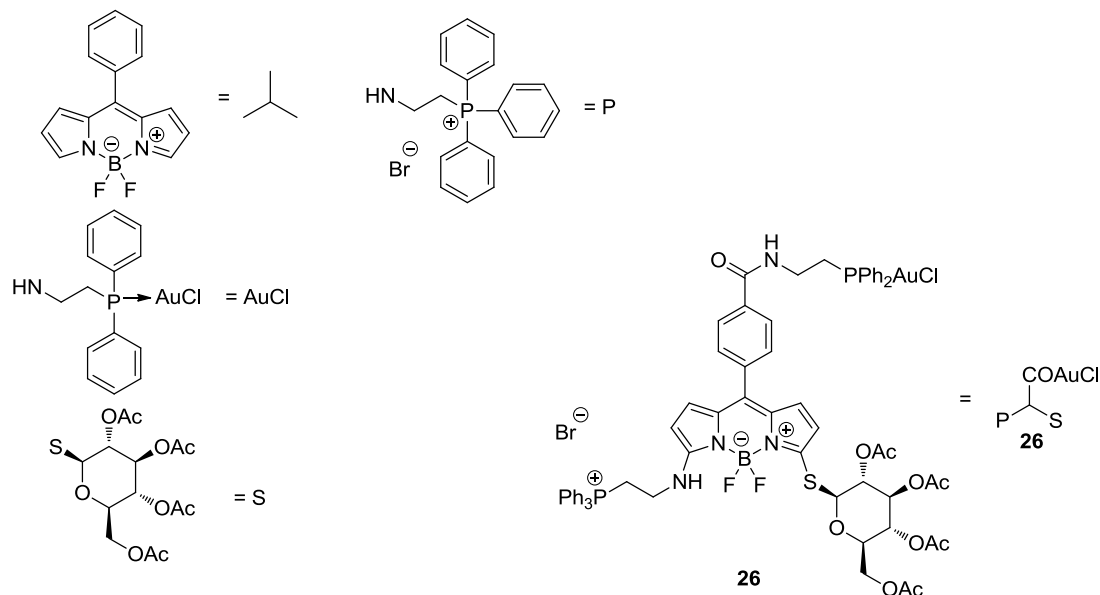


Figure 75: Simplified depiction of the obtained BODIPYs

Thioglucose tetraacetate will be abbreviated by S, the “X-substituted” gold-phosphine moiety by AuX and phosphonium **22** by P. Chlorine remains Cl and carboxylic acid COOH. Each simplified structure is accompanied by the molecules unique identifier.

### 1.4.2 Photophysical characterization of obtained BODIPY-dyes

All synthesized BODIPYs were characterized photophysically by measurement of their absorption and fluorescence spectra as well as their respective fluorescence quantum yields. Quantum yields were determined in the steady-state regime.

All compounds showed high molar absorption coefficients and good to excellent brightnesses (Table 8).

Table 8: Photophysical properties of the synthesized BODIPYs. All measurements were executed in DMSO. Rhodamine 6G in EtOH ( $\Phi=0.94$ ,  $\lambda_{exc}=488\text{nm}$ ) [197] was used as the standard for quantum yield measurements

Compound	$\lambda_{abs,max}$ [nm]	$\epsilon_{\lambda,max}$ [mol l <sup>-1</sup> cm <sup>-1</sup> ]	$\lambda_{em,max}$ [nm]	QY %	Brightness [mol l <sup>-1</sup> cm <sup>-1</sup> ]	$\Delta\lambda$ [nm]	Stokes-Shift [cm <sup>-1</sup> ]
<b>1</b> 	514	75 600	530	13	9 500	16	256
<b>4a</b> 	476	32 000	538	21	6 900	62	587
<b>4b</b> 	476	32 900	538	24	8 000	62	2 421
<b>7</b> 	518	69 300	538	5	3 300	20	2 421
<b>8</b> 	517	65 900	537	6	3 900	20	718
<b>9</b> 	480	29 900	546	15	4 400	66	720
<b>10</b> 	516	80 900	533	8	6 100	17	2 518
<b>11</b> 	479	30 500	544	21	6 500	65	618
<b>13</b> 	480	26 200	546	18	4 600	66	2 494
<b>15</b> 	479	34 100	543	24	8 000	64	2 518
<b>16</b> 	476	35 100	538	23	8 100	62	2 461
<b>17</b> 	540	75 300	555	26	19 700	15	2 421
<b>18</b> 	538	72 900	553	39	28 100	15	501
<b>19</b> 	513	24 000	570	15	3 700	57	504
<b>20</b> 	508	31 200	565	28	8 800	57	1 949
<b>21</b> 	511	31 300	569	24	7 500	58	1 986
<b>23</b> 	516	125 000	531	8	9 600	15	1 995
<b>24</b> 	541	48 100	559	23	11 000	18	547
<b>25</b> 	525	28 800	567	21	6 000	42	595
<b>26</b> 	523	16 200	569	21	3 400	46	1 411

To showcase general trends and influences of each substituent in the observed spectra, Figure 76 illustrates spectra of representative BODIPYs, having each possible combination of *N*- and *S*-core-substitution.

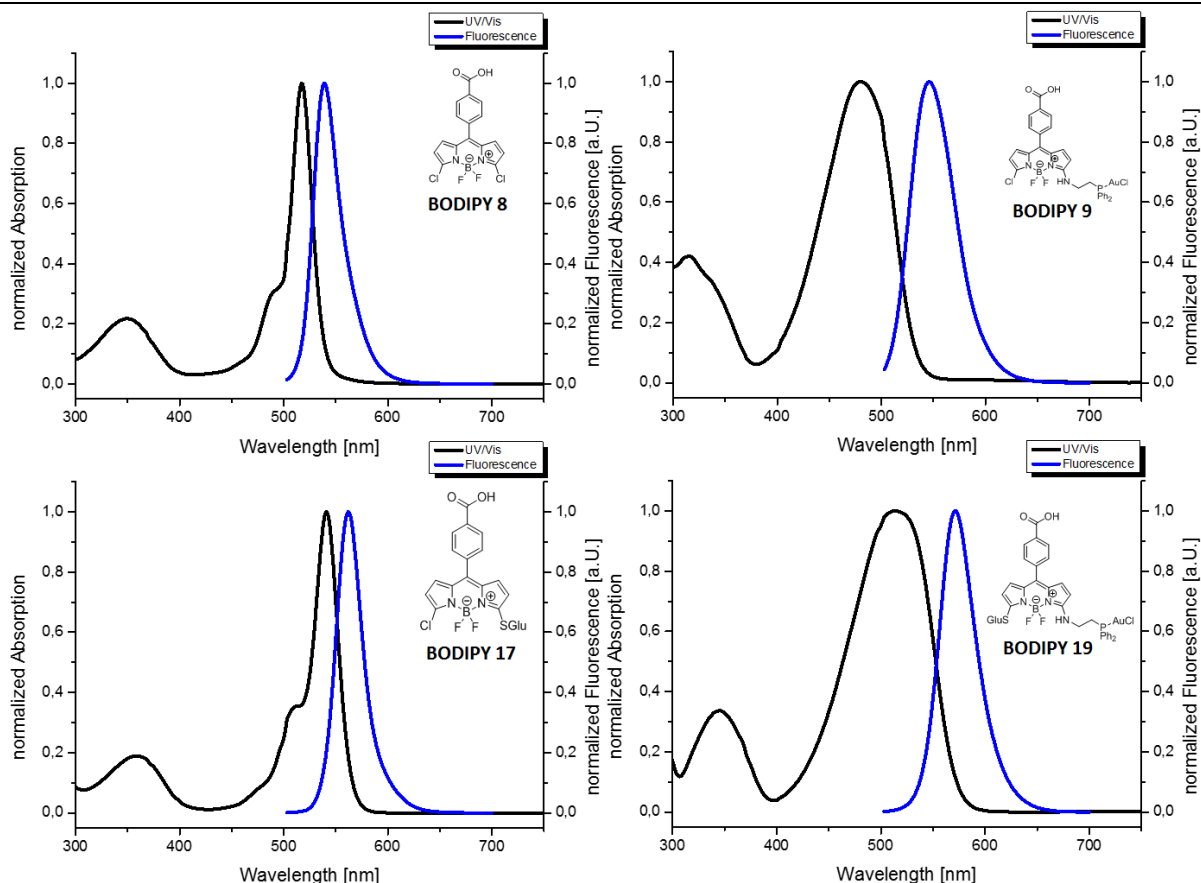


Figure 76: Representative spectra for all obtained BODIPYs. Substitution pattern: top left: Cl/Cl (**8**), top right: Cl/N (**9**), bottom left: Cl/S (**17**), bottom right: S/N (**19**)

The maximum absorption wavelength of either starting BODIPY (**1** and **8**) is at 515-520 nm. All dichlorosubstituted BODIPYs display very sharp absorption and emission bands (they emit at around 535 nm, resulting in spectral shifts of ca. 20 nm) with high molar absorption coefficients and relatively low quantum yields of 13 and 5-6%. The low quantum yield is not surprising as the two chlorine-substituents are expected to exhibit a (small) heavy atom effect.

The introduction of a gold-carrying moiety at any position in the molecule does not negatively influence the optic properties. Unlike commonly observed with other metals such as  $\text{Cu}^{2+}$ ,  $\text{Ni}^{2+}$ ,  $\text{Co}^{2+}$ ,  $\text{Fe}^{3+}$  [198] the gold(I) center does not quench the fluorescence.

The substitution of the *meso*-phenyl group (**10**, **19**, **23**, **26**) does neither induce any significant spectral shifts for both absorption and emission (<10 nm), nor does it influence the shape or peak-widths of the resulting dye. The presence of a free carboxylic acid function reduces the observed quantum yields significantly.

The introduction of an amine-substituent onto the BODIPY core results in a significant enlargement and a hypsochromic shift of around -30nm of the absorption-peak (**4a**, **4b**, **9**, **11**). The molar absorption coefficient is reduced by a factor of 2-3.

This behavior has already been investigated by our group [143] and can be explained by the additional available resonance structure of an amine-containing BODIPY (Figure 77).

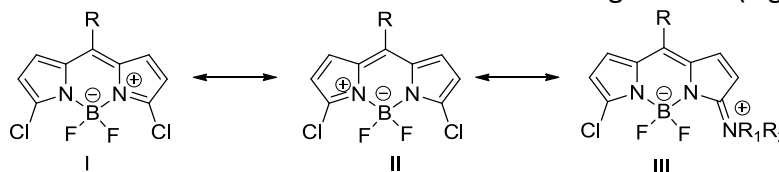


Figure 77: Resonance-structures of. Dichloro-substituted BODIPYs show only resonance structure I and II whereas for amine-substituted BODIPYs the nitrogen can participate in the conjugation (III)[143]

The additional resonance structure induces asymmetric electronic effects on the BODIPY core which results in its distortion. This distortion is visible in the single crystal X-ray diffraction that we obtained for BODIPY **4b** (Figure 78).

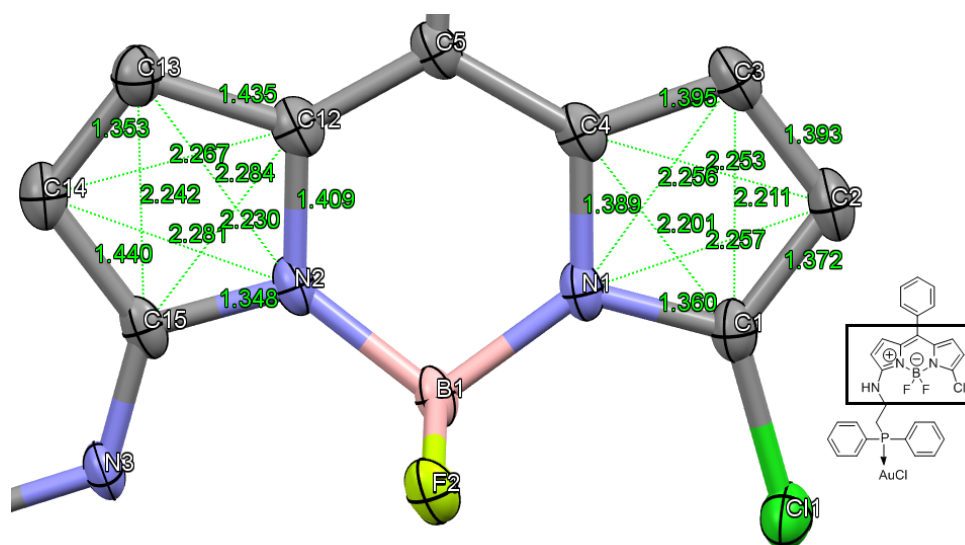


Figure 78: Interatomic distances in the pyrroles of BODIPY **4b**. All distances are given in Å. The black rectangle highlights the shown part of the molecule. Hydrogens and solvent molecules are omitted for clarity. Drawn with CIF data

The average bond lengths of both pyrroles are fairly equal with 1.397Å (amine substituted pyrrole) and 1.382Å (chlorine substituted pyrrole). The bond lengths in the chlorine substituted pyrrole show a narrow distribution. In the amine substituted pyrrole the bonds between C12-C13 and C14-C15 are significantly (2.8% and 5%) larger than their counterparts (C3-C4 and C1-C2 respectively) whereas N2-C15 and C13-C14 are shorter (-0.9% and -2.8% respectively). The amine not only distorts the molecule but also increases the LUMO-energies and therefore blue-shifts absorptions. This is supported by the quantumchemical investigations that we executed previously (Figure 64 and Figure 79).

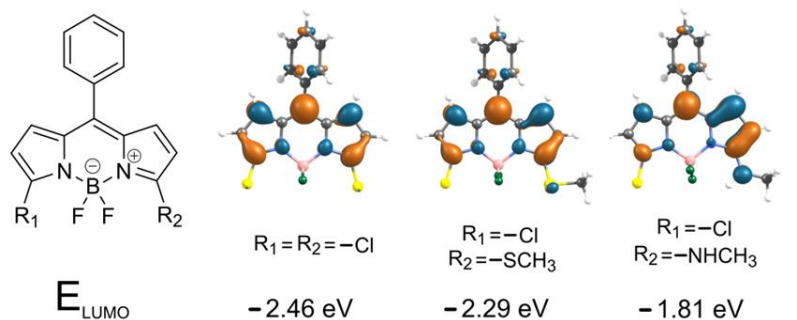


Figure 79: LUMO-energies of 3 model-BODIPYs. The LUMO-coefficients are shown as blue and orange isosurfaces for each atom.

Figure 79 shows the graphical representation of the each atoms orbital participation in the LUMO, for the amine-substituted compound the asymmetry between both pyrroles is evident, thus supporting the distortion-theory.

The observed changes in the absorption spectra of amino-substituted BODIPYs go together with a bathochromic-shift of the emission peak of about +10 nm and a significant increase in quantum yields of again a factor 2 to 3. The results are good brightnesses that are as high as or higher than those of the BODIPY-Cl<sub>2</sub> starting material.

The introduction of a thio-substituent results in a bathochromic shift of both the absorption and emission peak of ca. +20-25 nm and +30 nm respectively (**17** and **18**). For meso-(4-methoxyphenyl)-3,5-dichlorobodipy Boens and Dehean found the same trend; for their BODIPY the first substitution by aliphatic thiol resulted in an increase of +28 nm/+31 nm (Abs/Em) and an additional +28 nm/+29 nm (Abs/Em) for the second substitution [103].

The substitution of one chlorine by thiols significantly increases the quantum yield of the resulting dye (**17** and **18**).

For mixed double substitutions the influences of both substituents overlap: the enlargement of the absorption-peak that is caused by the amine is still present and both peaks are red-shifted compared to solely amine-substituted compounds while the larger stokes-shift caused by amine-substitution is maintained.

Irrespective of their substitution pattern all compounds show good enough optical properties for *in vitro* investigations.

### 1.4.3 Biological investigations

We took advantage of the numerous compounds that we synthesized to establish preliminary structure-activity relationships. Thus, we studied the impact of several parameters (lipophilicity, presence/absence of vector, number of gold atoms) on the antiproliferative properties, the cellular localization and the gold uptake of the compounds.

#### 1.4.3.1 Antiproliferative properties

To begin, all compounds underwent an evaluation of their antiproliferative properties. In this paragraph, we will use the term  $IC_{50}$  to designate the concentration of the tested product that is required to inhibit the proliferation of the population of a chosen cell line by 50% (compared to untreated cells).

A multitude of different techniques has been developed to detect cellular viability. Each test has unique strengths and shortcomings, the values that are obtained with each test may even differ [199]. Due to the easiness of application (and to keep the values comparable to earlier works that we have done) we chose the MTS-based approach to determine the overall effectiveness of the synthesized BODIPYs.

The MTS-assay evaluates the overall metabolic activity displayed by the cells in comparison to untreated specimen; it does not yield any information as to whether a compound has a cytotoxic (cell killing) or cytostatic (mitosis inhibiting) action.

To determine the  $IC_{50}$  each well were seeded with  $1 \cdot 10^5$  cells of one of the following three cancer cell lines:

- murine B16-F10 melanoma cells,
- murine EMT6 mammary carcinoma cells
- human MDA-MB-231 breast cancer cells

Each cell type was treated for 48h with each compound, followed by analysis by MTS assay to determine each compounds'  $IC_{50}$ . The obtained values are shown in Table 9 and Figure 80.

Table 9: IC<sub>50</sub> values of the synthesized BODIPYs. For better readability the compounds structures are shown using the simplified depictions introduced in chapter 1.4.1. The values are mean±SD of 3 independent experiments. All values are given in μM and were determined by MTS assay; data treatment was performed using GraphPad Prism 5.0.

Compound	MDA [μM]	EMT6 [μM]	B16 [μM]	Compound	MDA [μM]	EMT6 [μM]	B16 [μM]
1 	75.1 ±0.22	50.2 ±0.44	74.9 ±0.16	17 	75.0 ±0.16	49.6 ±0.25	74.9 ±0.20
4b 	25.2 ±0.12	10.6 ±0.09	50.0 ±0.13	18 	19.8 ±0.22	19.8 ±0.15	19.9 ±0.12
8 	74.8 ±0.30	49.8 ±0.40	50.1 ±0.12	19 	50.1 ±0.15	50.1 ±0.14	24.9 ±0.27
9 	25.2 ±0.15	20.0 ±0.12	49.9 ±0.14	20 	75 ±0.19	49.9 ±0.18	74.9 ±0.17
10 	75.2 ±0.21	74.9 ±0.39	75.1 ±0.20	21 	100.2 ±0.20	49.9 ±0.17	100.1 ±0.13
11 	50.0 ±0.19	74.8 ±0.31	74.9 ±0.18	23 	25.2 ±0.09	24.9 ±0.14	25.0 ±0.09
13 	10.1 ±0.19	9.9 ±0.10	10.3 ±0.21	24 	74.9 ±0.28	50.2 ±0.21	100.0 ±0.11
15 	50.0 ±0.18	49.9 ±0.19	49.8 ±0.17	26 	75 ±0.19	40.4 ±0.24	100.2 ±0.14
16 	29.8 ±0.13	19.7 ±0.18	20.2 ±0.31	Auranofin	5.23 ±0.09	4.87 ±0.12	4.68 ±0.16

When analyzing the IC<sub>50</sub> values, two types of compounds emerge, those with IC<sub>50</sub> in the 40 to 100 μM-range (**1**, **8**, **10**, **11**, **15**, **17**, **20**, **21**, **24**, **26**) and those that are more effective and display IC<sub>50</sub> in the 10 to 30 μM-range (**4b**, **9**, **13**, **16**, **18** and **23**). In this latter category, four molecules displayed high cytotoxicity whatever the cell line (**13**, **16**, **18** and **23**), while molecules **4b** and **9** displayed IC<sub>50</sub> values of respectively 10 and 20 μM only on breast cancer cell lines.

As a general trend all tested compounds show the least effect on B16-F10 whereas EMT6 are the most sensible towards treatment.

The general analysis of structural elements that are present in the molecule and their influence on IC<sub>50</sub> values shows several general tendencies:

- When the gold moiety is introduced onto the BODIPY-core a significant increase in cytotoxicity is induced (**4b**, **16**, **9**, and **13**), while its grafting onto carboxylic acid function led to a very limited effect (**10**, **11**, **15**, and **26**).
- The chlorido-gold moiety seems to be efficient against breast cancer cell lines but not against melanoma cell line (**4b** and **9**).
- Introduction of thioglucose tetraacetate onto the gold center increased the cytotoxicity of the complexes on B16-F10, leading to compounds as efficient on breast cancer cell lines as on melanoma (**16** and **13**), while
- interestingly, introducing the thioglucose derivative directly onto the BODIPY core did the reverse effect, it decreased the global activity of the complexes (**19** and **20**).

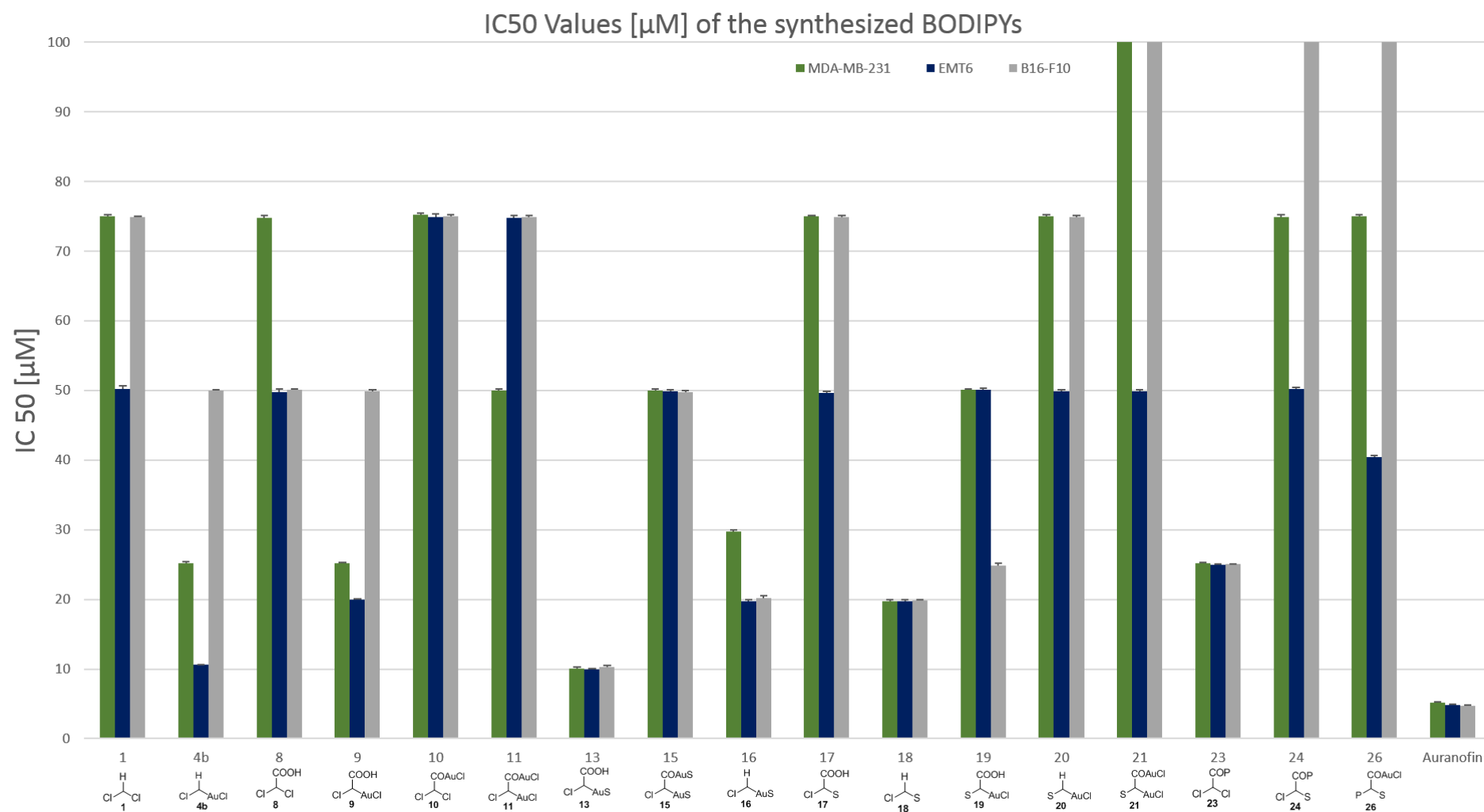


Figure 80: IC<sub>50</sub> Values for all tested BODIPYs. For better readability the compounds structures are shown using the simplified depictions introduced in chapter 1.4.1. The values are mean+SD of 3 independent experiments. All values are given in  $\mu$ M and were determined by MTS assay; data treatment was executed using GraphPad Prism 5.0.

We were unable to obtain IC<sub>50</sub> values for compound **25** since the supposedly most soluble compound formed aggregates upon contact with culture medium.

Among the multitude of compounds that we synthesized, **13** appeared to be the most potent compound with equal toxicity (~10 μM) towards all three cell lines, with an IC<sub>50</sub> in the same range as the ones of auranofin.

The most surprising compound is probably BODIPY **18**. Indeed, this compound displays an IC<sub>50</sub> of ca. 20 μM while it does not carry any metal nor phosphonium. An explanation could be its high reactivity toward nucleophiles. Thus, it could act as an alkylating drug. This behavior needs to be deeply investigated in the future. It would be especially interesting to understand why BODIPY **17** and **24** do not display similar activity.

#### 1.4.4 Compounds Localization by Confocal Imaging

As previously reported in the introduction, one of the main key when researchers look for the mechanism of action of a molecule is the determination of its localization. For example, today there are still numerous studies, which hypothesize a mechanism of action implying interactions with DNA based on studies performed on purified DNA but without any proof that the molecule enters the cell nucleus. Being able to track the molecules in cells is a first step. Thus, we took advantage of the fluorescence properties of our molecules for performing confocal imaging for all BODIPYs on all three cell lines in order to gain a more thorough insight into the cellular processes involved and possibly correlate certain cellular localizations of the compound to the exhibited cytotoxicity.

However, optical imaging studies can also be biased by several factors. The main one is the time of incubation of the molecules. Indeed, depending of the incubation time the molecules can be localized at different organelles. We tackled this issue by imaging the BODIPY derivatives after different periods of incubation: 1h, 4h, and 24h. This incubation for selected periods of up to 24h followed by imaging permitted to gain an idea of different kinetic behaviors as well as select suitable incubation periods to obtain images that are representative for the studied compound.

As can be seen for the example of BODIPY **4b** strong variations of the cellular localization are detectable over timer (Figure 81).

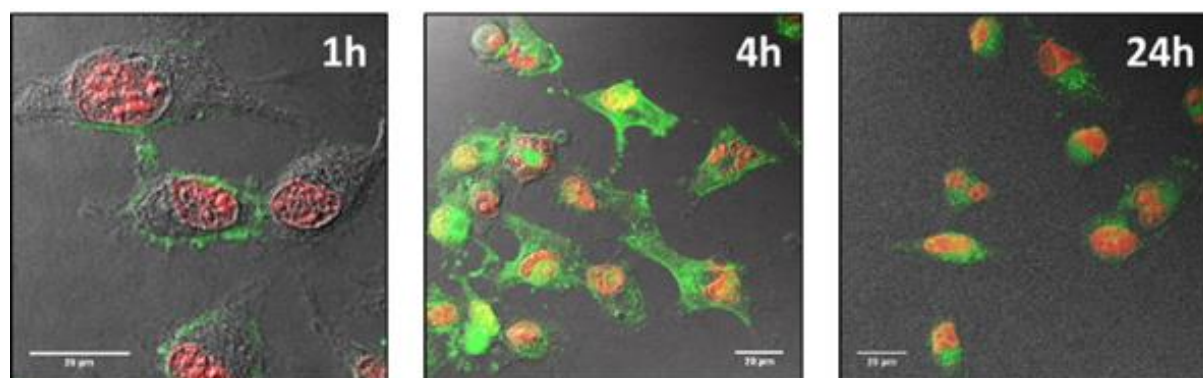


Figure 81: Confocal immunofluorescent analysis (merge) of MDA-MB-231 labelled with BODIPY **4b**. Cells were incubated with 10 μM BODIPY **4b** (green) for 1, 4 and 24h at 37°C, then fixed, followed by permeabilization with iced methanol. The nuclei are counterstained with DRAQ5 (red, fluorescent DNA dye)

At 1h the compound is localized on the cellular membranes, at 4h it is found in the cytoplasm and at 24h the cells' shapes have changed, which is characteristic for cells which are dying.

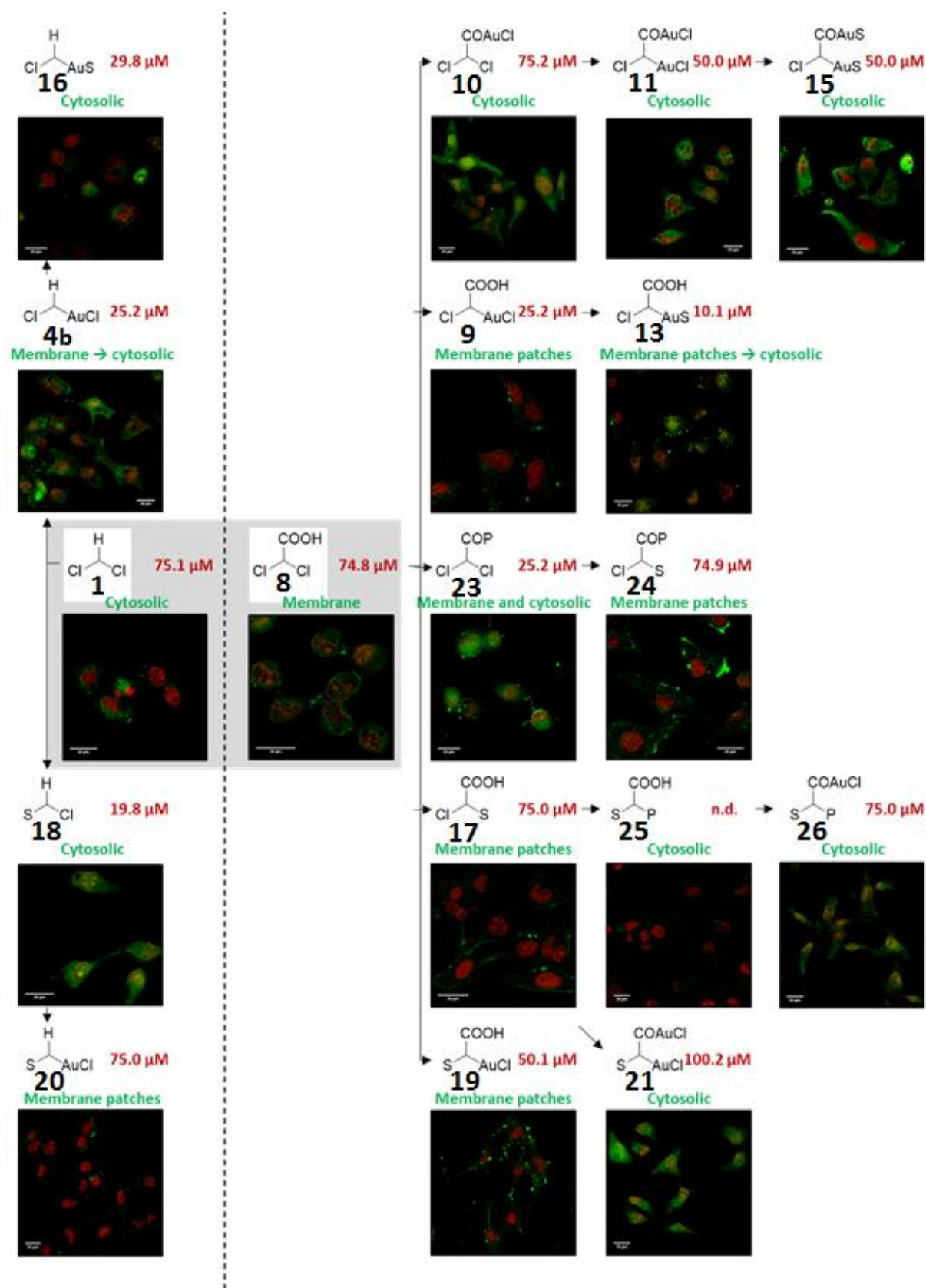


Figure 82: Confocal immunofluorescent analysis (merge) of MDA-MB-231 labelled with the different BODIPY derivatives. Cells are incubated with 10  $\mu\text{M}$  BODIPY derivatives (green) for 4h at 37°C then fixed, permeabilized with iced methanol. The nuclei are counterstained with DRAQ5 (red, fluorescent DNA dye)

A general analysis for all compounds showed a strong tendency for a localization mainly either in the cytosol and/or at the plasma membrane. Some products exhibited cytosolic or membrane (see Figure 82) (continuous or discontinuous staining) location.

Even though we found no clear correlation between the subcellular location of the products and their degree of cytotoxicity, it is worth noting that the presence of a free carboxylic group on the phenyl in *meso* position seems to favor accumulation on membrane (**8**, **9**, **13**, **17**, **19**, and **25**) whereas the introduction of a thioglucose tetraacetate onto the gold(I) center speeds up accumulation in cytoplasm (**13** and **16**). Interestingly, we did not observe any selective mitochondrial localization for the phosphonium-carrying compounds **23**, **24**, **25** and **26**.

#### 1.4.5 Lipophilicity and Gold uptake: generalities

Even though the already executed biological investigations gave some insight into the biological behavior and permit the formation of some theories to rationalize and predict the influence of each group and its position in the molecule on the final properties we were unable to correlate some of the results that we obtained to certain structural features (e.g. why the addition of thioglucose tetraacetate onto the gold atom of BODIPY **9** → BODIPY **13** leads to a strong increase in cytotoxicity whereas in case of BODIPY **11** → BODIPY **15** the cytotoxicity remains constant). Numerous studies reported on the fact that cytotoxicity and metal cell uptake can be directly correlated, leading to the conclusion that the role of the metal ligands may be limited to cell delivery. Moreover, it is often claimed that the key parameter for a good cell uptake is a fine tune of the lipophilicity. In order to gain a more complete picture we decided to investigate each compounds lipophilicity and perform gold-accumulation studies.

##### 1.4.5.1 Distribution coefficients (*logD*)

In order to check for correlations between the compounds hydro/lipophilicity and the observed cytotoxicity distribution coefficients were determined. Distribution coefficients describe the ratio of concentrations of a compound dissolved in two solvents at equilibrium. Any system of two immiscible solvents can be used, the most common however is the system water/1-octanol. When the investigated compound is nonionizable or only the nonionized part of the compound is used to calculate the ratio of concentrations, the obtained value is called partition coefficient *logP* and calculated as follows (equation III):

$$\log P = \log \left( \frac{C_{solute\ octanol}^{non-ionized}}{C_{solute\ water}^{non-ionized}} \right) \quad (III)$$

When the investigated compound is ionizable and/or all forms of the compound are included in the ratio the obtained value is called distribution coefficient *logD* and calculated as follows (equation IV):

$$\log D = \log \left( \frac{C_{solute\ octanol}^{non-ionized} + C_{solute\ octanol}^{ionized}}{C_{solute\ water}^{non-ionized} + C_{solute\ water}^{ionized}} \right) \quad (IV)$$

In case of 1-octanol and water the solvents are a good approximation of the aqueous cytosol and the lipid-based cell membranes. The obtained value therefore correlates with the lipophilicity of a compound and is a useful tool to predict its pharmacological behavior:

The lipophilicity of a compound will influence its bioavailability and elimination behavior.

For a compound that does not experience directed transport into a cell or a given

compartment of the body (e.g. the brain) its distribution coefficient gives an idea of how well the compound will enter that compartment by unspecific transport (mostly diffusion).

The logD's were determined using the HPLC-method, the results are shown in Table 10, experimental details are given in ANNEX I - 7.3.

### 1.4.5.2 Gold uptake

Gold uptake has been determined by ICP-MS measurement, after incubation of 40  $\mu\text{M}$  solution of the different gold(I)-complexes for 4h on MDA-MB-231 (BODIPYs **1**, **8**, **18**, and **25** have been tested as negative controls). ICP-MS analysis confirmed that gold complexes accumulate in cells (values ranged between 3.1 and 12.6 [Au] ppb/ $10^5$  cells). The results are shown in Table 10 and discussed in detail in the next chapter.

## 1.4.6 Establishing structure-activity relationships

Following the determination of each compounds hydrophilic balance and the corresponding gold accumulation in the MDA-MB-231 cell line we attempted to correlate the results to determine structure activity relationships and general trends of the influence of each functionalization.

### 1.4.6.1 Results of Lipophilicity and Gold-Uptake experiments

Table 10: Overview over logD, gold uptake and corresponding IC<sub>50</sub> values (both gold uptake and IC<sub>50</sub> are obtained for MDA-MB-231). n.d.: not determined (unsuccessful measure); n.t.: not tested (experiment not performed); a: value under detection limit; b: compounds containing two gold atoms. For easier readability the structures are depicted in the simplified representation (introduced in chapter 1.4.1)

Compound	Structure	logD pH=2,7 (pH=7)	[Au] ppb/ $10^5$ cells)	IC <sub>50</sub> , MDA ( $\mu\text{M}$ )	Compound	Structure	logD pH=2,7 (pH=7)	[Au] ppb/ $10^5$ cells)	IC <sub>50</sub> , MDA ( $\mu\text{M}$ )
<b>1</b>		4.7	- <sup>a</sup>	75.05 $\pm 0.22$	<b>17</b>		4.52 (1.46)	n.t.	74.96 $\pm 0.16$
<b>4a</b>		4.7	n.t.	n.t.	<b>18</b>		4.63	- <sup>a</sup>	19.76 $\pm 0.22$
<b>4b</b>		n.d.	4.46	25.24 $\pm 0.12$	<b>19</b>		3.93 (2.87)	3.14	50.10 $\pm 0.15$
<b>7</b>		4.7	n.t.	n.t.	<b>20</b>		5.44	4.67	75.00 $\pm 0.19$
<b>8</b>		3.94 (1.26)	- <sup>a</sup>	74.83 $\pm 0.30$	<b>21</b>		n.d.	5.88 <sup>b</sup>	100.20 $\pm 0.20$
<b>9</b>		4.21 (3.16)	8.96	25.17 $\pm 0.15$	<b>23</b>		3.85	n.t.	25.19 $\pm 0.09$
<b>10</b>		3.62	5	75.23 $\pm 0.21$	<b>24</b>		3.47	n.t.	74.92 $\pm 0.28$
<b>11</b>		5.03	5.57 <sup>b</sup>	49.97 $\pm 0.19$	<b>25</b>		4.55 (3.10)	- <sup>a</sup>	n.d.
<b>13</b>		4.18 (3.84)	10.74	10.07 $\pm 0.19$	<b>26</b>		4.8	6.52	75.00 $\pm 0.19$
<b>15</b>		n.d.	4.46 <sup>b</sup>	50.03 $\pm 0.18$	auranofin	Et <sub>3</sub> PAuS	n.t.	21.38	5.2 $\pm 0.09$
<b>16</b>		5.09	12.64	29.79 $\pm 0.13$					

Surprisingly, we did not find any obvious correlation between a compounds lipophilicity, its gold uptake and the cytotoxicity. Moreover BODIPYs **11**, **15** and **21** that contain each two gold atoms did not display an improved gold accumulation.

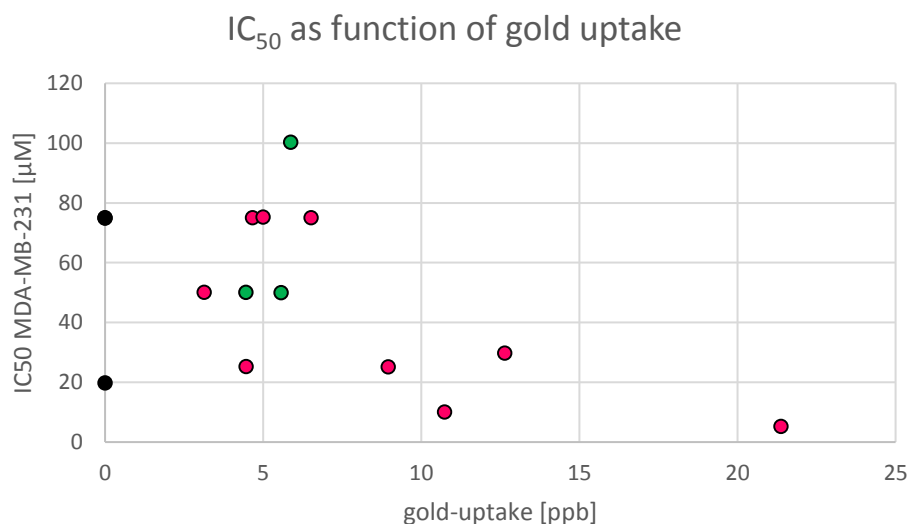


Figure 83: Influence of gold uptake on  $IC_{50}$  (for MDA-MB-231). Black dots represent gold-free compounds, red dots compounds carrying 1 gold atom and green dots compounds carrying 2 gold atoms

The *general* trend “higher gold uptake equals higher toxicity” seems to hold true, the strong variations in cytotoxicity of compounds exhibiting gold uptakes of around 5ppb are however a strong argument towards the fact that the gold uptake alone is not an appropriate variable to predict or fine tune a compounds efficacy. However, BODIPYs **9**, **13** and **16**, which display the highest gold-uptake are also amongst the most cytotoxic complexes (Figure 83). When all compounds are taken into consideration no correlation can be deduced between a compounds  $\log D$  and neither a compounds  $IC_{50}$  nor its gold uptake (Figure 84).

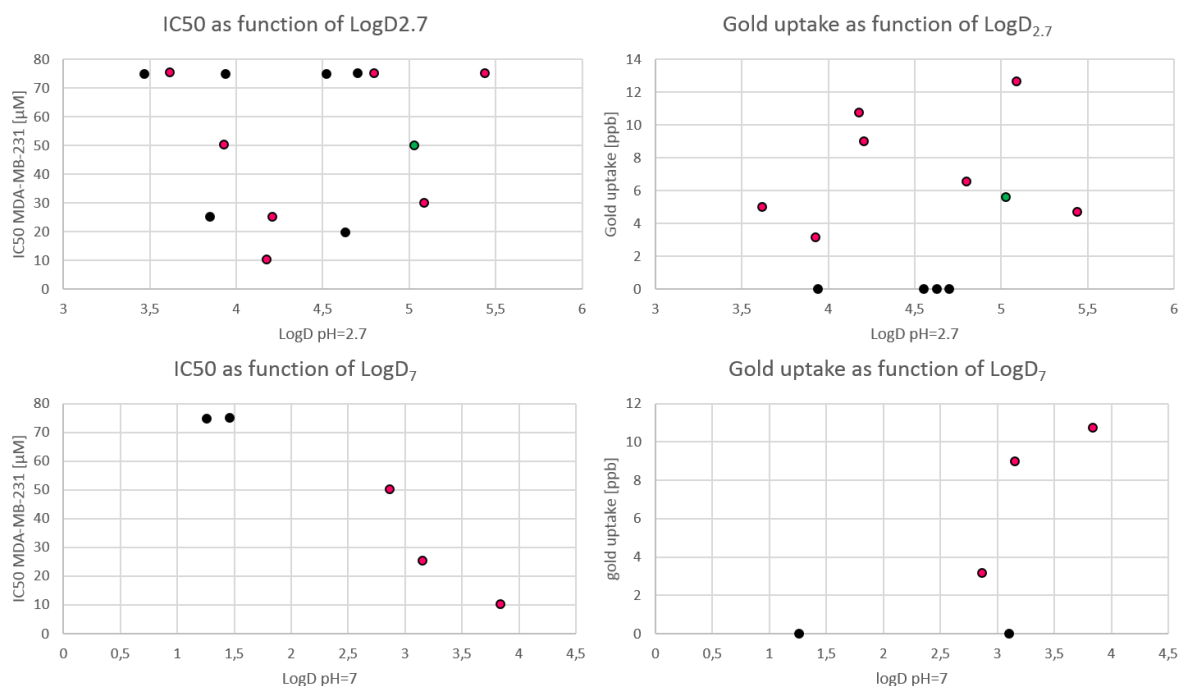


Figure 84: Influence of  $\log D$  on  $IC_{50}$  (left) and gold uptake (right). Both  $IC_{50}$  and gold uptake were determined for MDA-MB-231 cells. Black dots are gold-free, red dots represent compounds that contain 1 gold atom, green dots represent compounds with 2 gold atoms

However, when only the subset of compounds that carry a free carboxylic acid function (**8**, **9**, **13**, **17**, **19**; **8** and **17** do not carry a gold moiety) are analyzed an interesting trend shows: for the fully deprotonated compound (i.e.  $\log D_{\text{pH}=7}$ ) an *increase* in lipophilicity leads to an *increase* in cytotoxicity. At the same time an *increase* in lipophilicity also leads to an *improved* gold-uptake into the cells. No such correlation can be found neither for compounds that do *not* possess a free carboxylic acid function, nor for phosphonium-containing BODIPYs (**23**, **24**, **25**, and **26**) (data not shown).

## 1.5 Summary and outlook

### 1.5.1 Summary and Conclusion

The first part of this thesis dealt with the development of *in vitro*-compatible, fluorescent platforms for the design of metal based, trackable anti-cancer agents.

Two platform molecules were investigated; a difunctional *meso*-phenyl dichloro-BODIPY (**1**) and the trifunctional *meso*-benzoic acid dichloroBODIPY (**8**). Each designated platform molecule underwent a series of functionalizations with three nucleophiles; a gold(I)-phosphine (**3**), the thiosugar  $\beta$ -thioglucose tetraacetate and the phosphonium triphenylphosphonium-ethylamine. Combinations of the three nucleophiles have been used throughout the first chapter to explore the reactivity of the platform molecules and design 20 fluorescent compounds that display different substitution patterns, both in terms of number and positioning of the selected nucleophiles. We found that the core-substitution of either BODIPY-Cl<sub>2</sub> with an amine substituent results in non-reactivity of the BODIPY-core towards other nucleophiles (thus preventing a second substitution), whereas the introduction of a thio-nucleophile permits a second nucleophilic aromatic substitution with either *S*- or *N*-nucleophile. These findings were corroborated by DFT-simulation. This permits site-specific, selective functionalization using high-value substituents. We were thus able to perform the selective, site-specific functionalization of the starting material with up to three different substituents, thus validating the selected dichloro-BODIPYs as viable platform agents.

Following the successful syntheses each compound underwent a characterization of their photophysical properties. All synthesized compounds displayed absorption/emission maxima between 480-540 nm and Stokes-Shifts between 15-66nm in DMSO, depending on the substitution. All compounds are strongly fluorescent and display optical properties that are entirely sufficient for *in vitro* investigations.

The entire panel of compounds underwent an evaluation of their biological properties: We determined their respective antiproliferative properties (IC<sub>50</sub>) on three cancer cell lines (B16-F10, MDA-MB-231 and EMT6), investigated their lipophilic balance ( $\log P/\log D$ ) and their gold-accumulation into MDA-MB-231 cells. All compounds were then used to perform confocal microscopy on B16-F10, MDA-MB-231 and EMT6 for 1-24h to establish their respective cellular localization at various points in time. After evaluation of their biological behavior we established preliminary structure-activity relationships.

Four compounds displayed good antiproliferative activity (the three gold-containing agents **4b**, **9** and **13** as well as gold-free **18**); the three gold-containing agents displayed activities that are in the range of auranofin and will be investigated further in future studies.

To conclude, in first chapter of this thesis we successfully developed two versatile fluorescent platforms that can be functionalized as required with limited effort, thus granting rapid access to a large panel of compounds in short timeframes.

The developed methodology is not limited to biological/medicinal applications but can be extended to other fields.

## 1.5.2 Outlook

The following paragraph will offer several possible studies as well as modifications to either gain a deeper insight into the compounds' biological behavior and mechanism of actions or to improve the properties of the developed platform.

### 1.5.2.1 Follow-up studies for the existing compounds

The studies that we executed in this chapter (IC<sub>50</sub>, imaging study on 3 cell lines, analysis of the lipophilic balance, cellular gold uptake) provide some insight into the properties that are displayed by the developed compounds. Although we were able to determine general trends in the compounds behavior as well as draw some conclusions about general structure activity relationships, some information is still missing that needs to be investigated in the future.

The most important is an evaluation of each compounds stability in biological media. We attempted such an evaluation by incubating each compound at 37°C in growth medium (+bovine fetal serum). The proteins were removed by precipitation with ice cold ethanol and the supernatant analyzed; unfortunately this test displayed very poor repeatability. More importantly however this procedure resulted in incomplete removal of proteins which clogged the HPLC and prevented us from obtaining any useful data. Here a better protocol needs to be found.

Just as important would be an investigation to determine, if the obtained compounds have a cytotoxic (cell killing) or a cytostatic (mitosis arresting) action (and if that differs for the various substituents that are present in the molecule).

This study can be executed e.g. using Annexin V+propidium iodide staining, followed by flow cytometry [200]. Propidium iodide stains depolarized cells whereas Annexin V reacts with phosphatidylserine, a marker expressed during apoptosis. A double positive labelling thus indicates apoptosis. In order to test if cell cycle arrest has occurred the BrdU (bromodeoxyuridine) assay can be used to quantify DNA replication in the colony.

Beyond that many molecular markers have been developed that are indicative for various forms of cytotoxic or cytostatic action [201,202], depending on the general results the data can be refined by additional tests as needed. Once the exact form of action has been determined assays can be performed to determine the exact origin of the displayed properties; examples include tests for ROS and determination of mitochondrial changes have taken place.

Another way to gain additional insight into the cellular processes and how they are influenced by each compound is a proteomic analysis: for that the cells are incubated, lysed and the proteome analyzed by 2D gel electrophoresis [203]. The comparison of treated and untreated cells should provide new insight into the specific target(s) that is/are inhibited by the applied treatment.

Due to the high demand in labor for each of the proposed tests they should only be executed on a selected few of the obtained BODIPYs; e.g. **4b**, **9**, **13** and **18**.

Although we have executed a gold-uptake study for the entire cell, a subdivision into the displayed uptake in various organelles is of interest. This can be achieved by incubation of the cells with the tested compound, followed by fractionation of each selected organelle. Both, protocols as well as fractionation kits have been developed and are available [204,205]; this way the cellular gold uptake can be subdivided into gold accumulation by e.g. the nucleus, mitochondria and membranes to name but a few.

Each of the studies that we proposed so far aims at deepening the understanding of the displayed biological properties. However; it would also be interesting to see if our platform, as well as the derived theranostics possess other properties that we did not yet evaluate. Especially the derivatives that carry chloro-substituents on the BODIPY-core may prove active in photodynamic therapy (PDT) under irradiation with light due to the development of singlet oxygen.

Using the compounds that display good activities as well as high gold-uptake, an interesting study would be an elemental mapping of the cell and the superposition of the gold-distribution with the fluorescence that was detected in order to check if the two coincide. The metal mapping can be done using mass spectrometry imaging (MSI) [206] or X-Ray fluorescence [207]. Especially the second can provide excellent resolution, combined with unambiguous, quantitative information about the elemental distribution. Moreover, the colocalization with other elements can yield valuable information as to whether the gold atoms have *replaced* metals in their respective enzymes.

## 1.5.2.2 Possible modifications to the platform

Although the developed platform molecules (as well as the theranostic agents that are derived from them) display interesting properties, an improvement of their characteristics is of course possible.

The most pressing issue for the developed compounds is probably their high lipophilicity; for easier manipulation and better solubility in aqueous media the introduction of polar, hydrosolubilizing groups is desirable. Possibilities include (but are not limited to) the use of sulfonated amino acid-sequences, sulfonation e.g. of the 2,6-positions or the introduction of alkyne-ammoniums either on the boron center or in the 2,6-positions (the latter transformation requires the iodination or bromination of the 2,6-positions, followed by Sonogashira cross coupling reaction; the site specificity may prove difficult).

Using the platform as it is its reactivity as well as the effect of other substituents should be explored. Here possibilities include the introduction of vectors such as PSMA, Bombesin or its grafting to antibodies.

Last but not least we propose the development of smart-probes, comparable to the gold(I)-coumarine that we developed in 2015/2016 [144,145].

In 2016 Vasiuta and Plenio showed for a system used in catalysis that the introduction of diphenylphosphine onto the BODIPY-core of **L58** totally quenches the fluorescence [208] (**L59**, Figure 85).

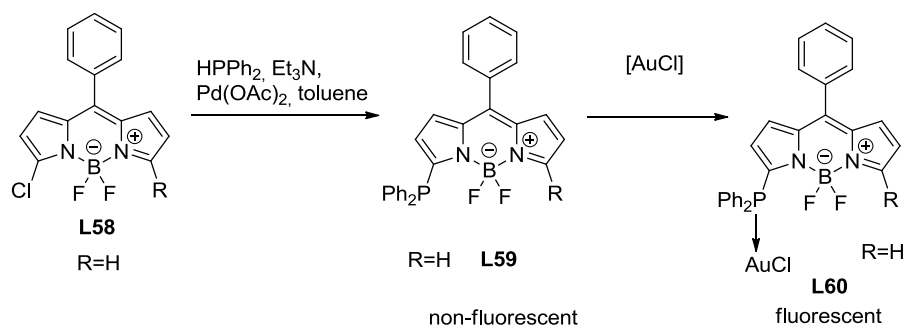


Figure 85: Proposition for a phosphine-gold(I) smart-probe. For R=H the molecule has been synthesized by [208]

Upon addition of gold(I) the metallated BODIPY **L60** emits at 531nm with 9% quantum yield. Just like the coumarine system that we developed previously this system could be used as a smart probe to detect if loss of metal occurs in a specific biological system or organelle.

Other molecular entities that possess the potential to be used as smart probes are pyridine ligands (for the development of gold(III)-based smartprobes); here the loss of metal would likely not quench the fluorescence but shift the maximum emission wavelength.

## Chapter II – AzaBODIPY



## Chapter II – AzaBODIPY

As we observed in the previous chapter classic BODIPYs have excellent optical properties and are very versatile in terms of functionalization. However, their fluorescence properties are not optimal for *in vivo* investigations. Indeed, their fluorescence emission of ca. 530-550nm does not reach far enough into the far red/infrared region of the electromagnetic spectrum to fall into one of the transparency windows (Figure 86).

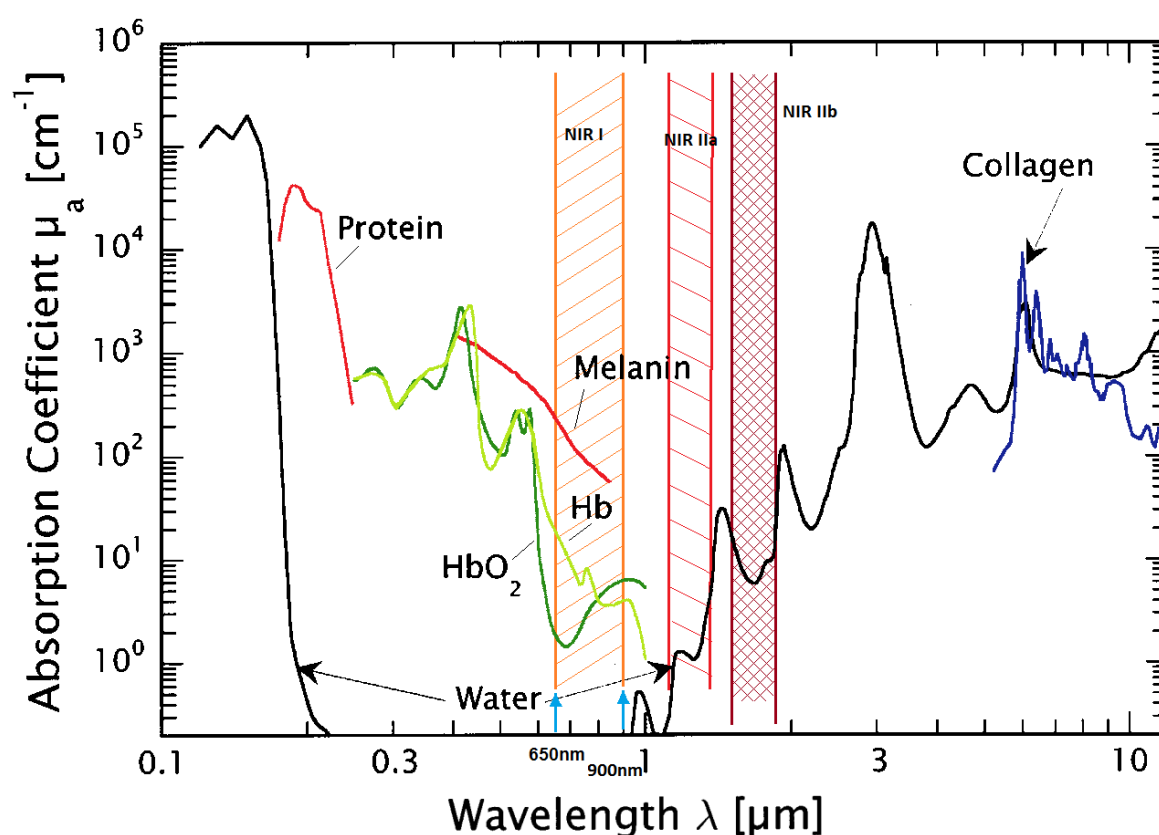


Figure 86: Absorbance of various tissues and biomolecules in the visible, red/infrared spectrum. The position of optical transparency windows has been added as orientation. Adapted from [25]

In order to optimize the BODIPY structures for *in vivo* biomedical applications,  $\pi$ -extended BODIPYs can be developed. For example, benzo- and naphtho-fused BODIPYs as well as the introduction of styryl-groups in the  $\alpha$ -pyrrolic positions using Knoevenagel like reactions [124] have been used to redshift the emission of the obtained fluorophores. This grants access to red- and highly red-shifted BODIPYs that have found widespread use in research and preclinical applications (Figure 87).

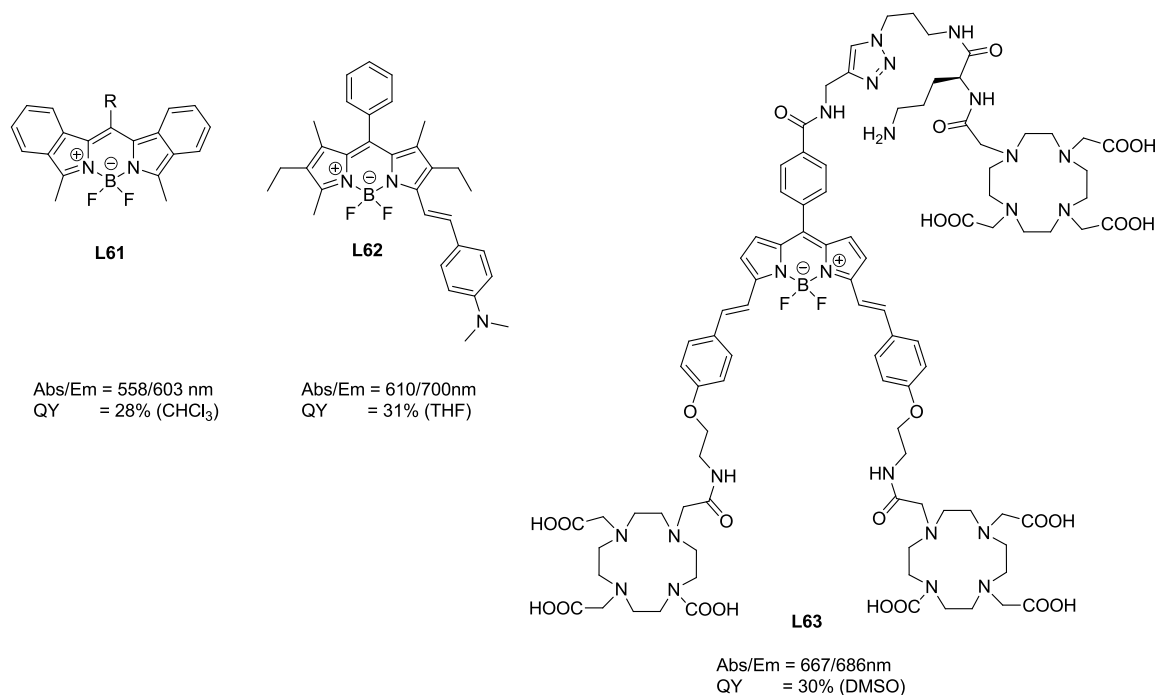


Figure 87: Examples for  $\pi$ -extended BODIPYs: isoindoline-based BODIPY by retro-Diels-Alder reaction (**L61**, left) by Wada et al. 2001 [209], access to styryl and distyryl-BODIPYs by Knoevenagel-reaction (**L62**, middle) by Akaya in 2005 [124] and example for a distyryl-BODIPY carrying polyazamacrocycles developed by our group [132] (**L63**, right)

However, very often, these  $\pi$ -extended BODIPY-dyes have very unfavorable solubility in water or/and stacking behavior: for example, although the compound **L63** shown on the right in Figure 87 is soluble in water without any problems, stacking and partial quenching of fluorescence occurred in PBS at concentrations higher than 5 nM. Another common problem with the styryl and distyryl-BODIPYs derivatives we developed for *in vivo* imaging is their lowered stability compared to classic BODIPYs: the accessible non-aromatic double bonds make this class of fluorescent dyes prone to photobleaching. For these reasons we decided to look into another family of BODIPY dyes, azaBODIPYs.

## 2.1 Introduction to azaBODIPY-dyes

### 2.1.1 Synthetic access to azaBODIPYs

Aza-dipyrromethenes were first described by Rogers in 1943 [210,211] and have since attracted a considerable, increasing interest. Just as BODIPY dyes, AzaBODIPYs retain the nomenclature that is derived from s-indacene (Figure 88).

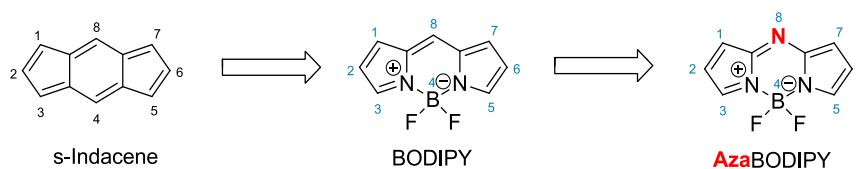


Figure 88: Structure and nomenclature of BODIPYs and azaBODIPYs

AzaBODIPYs strongly resemble BODIPYs in many aspects. However, thanks to the addition of a nitrogen atom in the *meso*-position the absorption and emission of the base compound is shifted to 650nm and beyond (Figure 89).

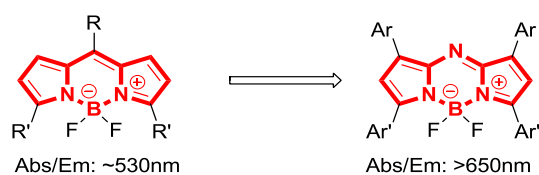


Figure 89: Base-structure of azaBODIPYs

Two major synthetic pathways were established by O'Shea in 2004 [212] to access aza-dipyrromethenes.

The first one is commonly used to access symmetrical azaBODIPYs. It consists in the use of nitromethane substituted chalcones that are submitted to condensation in presence of an ammonia-source (Figure 90).

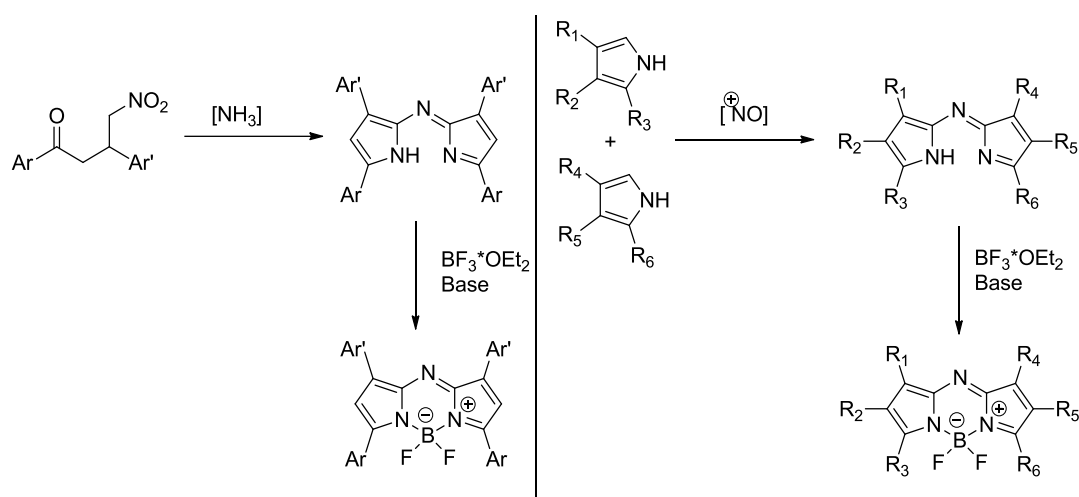


Figure 90: General synthetic pathways to azaBODIPYs. Left: chalcone based synthetic access to symmetrical azaBODIPY dyes. Right: access to unsymmetrical azaBODIPYs using nitrosylation reactions

The second strategy employs nitrosylation reactions on pyrrole-derivates and grants access to asymmetric and ring-fused azaBODIPYs such as thiophene-fused azadipyrromethenes [213]. So far, the access to alkyl-only substituted azaBODIPYs and the unsubstituted title compound has proven unreachable. The use of aromatics with various functionalities such as hydroxy- or halogens has however granted access to a vast choice of transformations. A comprehensive review on the synthesis and functionalization of azaBODIPYs has been published by Ge and O'Shea in 2016 [214].

AzaBODIPYs show very good optical properties, such as high molar attenuation coefficient and high quantum yield (and thus high brightness). Moreover, electron donating and withdrawing groups can be introduced to the aromatic substituents to fine-tune the absorption and emission-wavelengths. Indeed, the establishment of a push-pull effect in the molecule led to significant bathochromic shift [215]. Other key advantages of the azaBODIPYs are their high chemical and photochemical stability.

Because of all these properties, a variety of accounts has been published, that successfully use azaBODIPYs for biological applications both *in vitro* [216–219] as well as *in vivo* [219–221]. Additionally, it has also been reported that stacking and other solubility-related problems could be limited by the introduction of polar groups such as sulfonates and PEGs [216,219].

In the general introduction and in section 1.1 we have established requirements for the development of an ideal molecular platform.

Among them there are the following:

- the suitability for a selective, step-wise introduction of various substituents in order to be able to introduce vectors, therapeutic moieties and (if possible) groups that permit to tune the molecules properties (such as solubility in water),
- reactivity under mild reaction conditions to be suitable for the introduction of fragile moieties such as metal based complexes and biomolecules,
- the platform molecule itself should fulfill the function of fluorescence tracer and possess good optical properties, emit in the far red/infrared spectrum
- the platform should be accessible in “large” scale.

Due to the problems that we previously encountered in our group [132,222] additional requirements were

- the absence of stacking
- (high) stability, both towards photobleaching and biological as well as chemical influences

Judging from the information available to us from literature azaBODIPYs seem to fulfill all the requirements. We therefore chose this class of dye to transpose the results from the BODIPY study onto a system that would be suitable for *in vivo* studies. The first step consists in the design of the platform.

## 2.2 1,7-di(phenol)-3,5-di(phenyl)-azaBODIPY

Our group is specialized for years in the design and the development of innovative and sophisticated BODIPY derivatives. However, I was the first in the team to move to the design of azaBODIPYs. Thus, we began by synthesizing simple azaBODIPY derivatives. Our objective was not only to reproduce syntheses reported in the literature but also to optimize them to make them suitable for reaching gram scale of products.

The azaBODIPY we chose for this purpose is dihydroxy-azaBODIPY **30** shown in Figure 91 and carries the hydroxy-functions on the 1,7-phenyl substituents (as opposed to the 3,5-phenol-azaBODIPY **L64** that is commonly used in the literature by O’Shea, Burgess and others [216,218,219,221]).

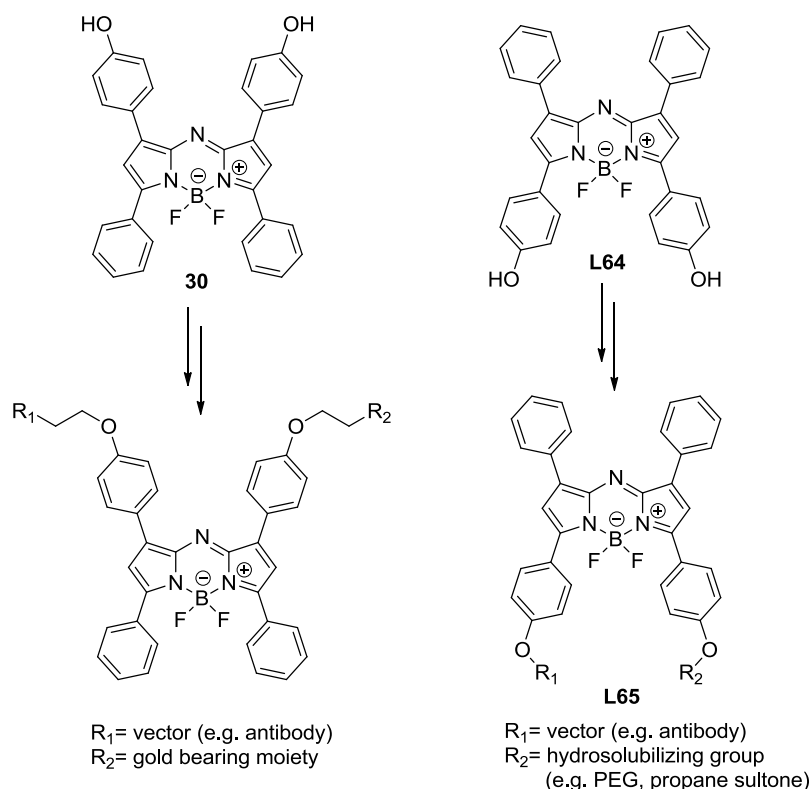
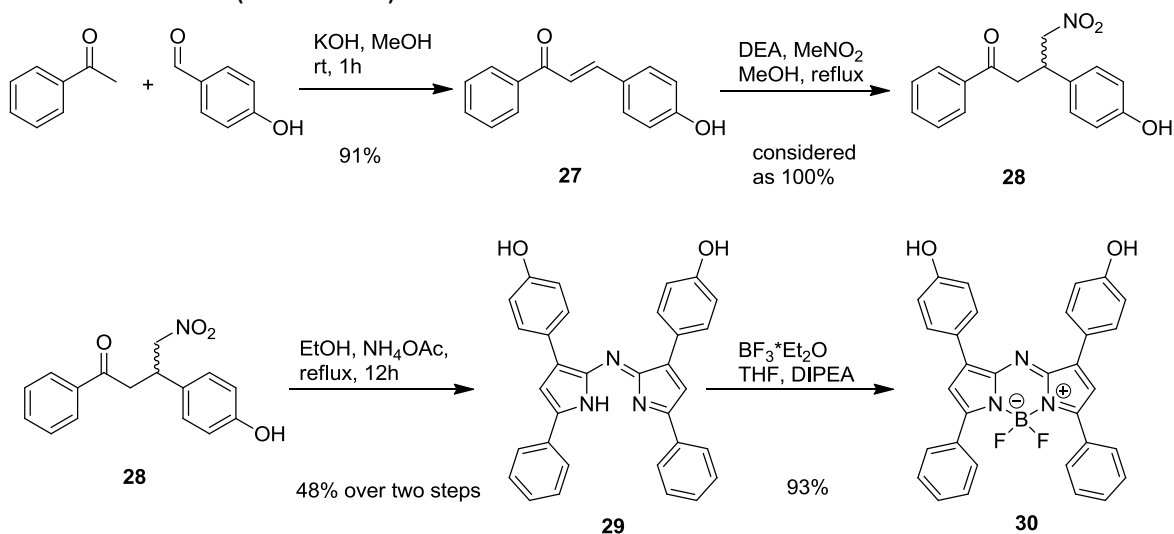


Figure 91: Selection of the first platform molecule (left). Right: commonly employed dihydroxy-azaBODIPY **L64** [219,218]

This azaBODIPY is easily accessible in 4 steps starting from cheap, commercially available starting materials. Choosing this analogue could be interesting to compare our results to the ones of the literature and see if the position of the functionalization impacts the properties of the molecule. The 1,7-diphenol-azaBODIPY **30** could then be desymmetrized following the approach established by O'Shea [216,223] and others [224,225] to obtain a bioconjugable fluorophore.

First, the chalcone **27** was formed in presence of KOH and MeOH. After neutralization the hydroxy-chalcone **27** precipitated readily and was then transformed into the nitromethane-Michael adduct **28** (Scheme 92).



Scheme 92: Preparation of azaBODIPY **30** starting from hydroxy-benzaldehyde and acetophenone

Nitrocompound **28** is then refluxed in EtOH in presence of a large excess of  $\text{NH}_4\text{OAc}$ . For this synthetic step, *n*-BuOH is often used as the solvent to permit stronger heating and to accelerate the formation of azadipyrrromethene **29** [226]. This is followed by partial evaporation, filtration and washing with EtOH. Our tests with BuOH did neither result in shortened reaction times nor in increased yields. This step is followed by complexation of boron in presence of DIPEA to rigidify the azaDIPY (**29**) backbone and obtain azaBODIPY **30**.

In the next step we performed the mono-functionalization of the azaBODIPY **30**.

A multitude of reaction conditions was attempted to form acetic acid ethers and preferentially obtain the monofunctionalized compound. Due to the electroattractive nature of the BODIPY-core we theorized that the pKa of the phenolic groups would be low enough to employ carbonates to form phenolates, followed by reaction with *t*Bu-bromoacetate. (Figure 93).

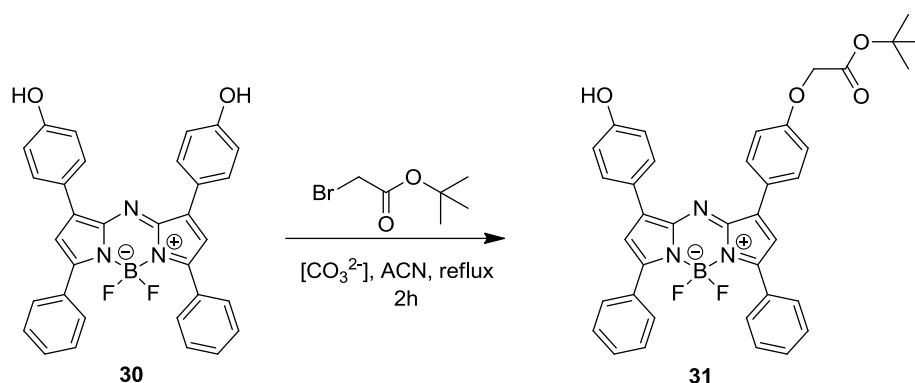


Figure 93: Envisioned formation of acetic acid ester **31** by simple nucleophilic substitution using a carbonate source as base

In fact, for the 3,5-phenolic azaBODIPY **L64**,  $\text{K}_2\text{CO}_3$  is commonly used as base and proton scavenger to drive the reaction towards the functionalized azaBODIPY [216,227]. Tests using  $\text{NaHCO}_3$  in refluxing acetonitrile led however to degradation of the azadipyrrromethene. We therefore screened a variety of base- and solvent-systems that are summarized in Table 11 below.

Table 11: conditions used for formation of azaBODIPY-ether **36** using a variety of different bases

Conditions used	Result
1.5 eq $\text{BrCH}_2\text{COO}^t\text{Bu}$ , $\text{NaHCO}_3$ , ACN, reflux, 2 h	degradation
1.5 eq $\text{BrCH}_2\text{COO}^t\text{Bu}$ , DIPEA, ACN, reflux, 2 h	no product observed
1.5 eq $\text{BrCH}_2\text{COO}^t\text{Bu}$ , $\text{NaHCO}_3$ , acetone, reflux, 2 h	no reaction
1.5 eq $\text{BrCH}_2\text{COO}^t\text{Bu}$ , $\text{K}_2\text{CO}_3$ , DMF, $90^\circ\text{C}$ , 2 h	degradation

Unfortunately none of the used conditions afforded the desired product. Literature however suggested that the use of anhydrous  $\text{CsF}$  in anhydrous DMSO as a mild base could remedy the encountered problem [223]. The fluorine behaves as an acceptor for hydrogen bonds, thus activating the phenol [228] (Figure 94).

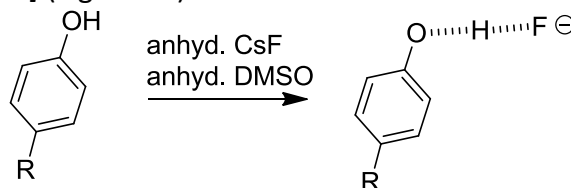


Figure 94: Principle of activation of aromatic hydroxy groups through  $\text{CsF}$

Indeed, the phenol-activation is visible to the naked eye thanks to a significant color-change (ultramarine blue to green-turquoise) upon addition of CsF to the azaBODIPY in anhydrous conditions. The now activated phenolic groups reacted readily with the offered electrophile without displaying selectivity; upon slow addition of 1 equivalent of *t*Bu-bromoacetate we observed almost exclusively double substitution and starting material. The conditions were therefore optimized by testing different combinations of addition-speed and amount of the engaged electrophile (Table 12).

Table 12: Primary optimization of reaction conditions for the monosubstitution of **30**

Conditions used	Result
1eq. BrCH <sub>2</sub> COO <sup>t</sup> Bu (slow addition), DMSO, 3eq CsF, rt, 2h	Double substitution +starting material
1eq. BrCH <sub>2</sub> COO <sup>t</sup> Bu (fast addition), DMSO, 3eq CsF, rt, 1h	Double substitution +degradation
2eq. BrCH <sub>2</sub> COO <sup>t</sup> Bu (fast addition), DMSO, 3eq CsF, rt, 20min	mono+double substitution, degradation
2eq. BrCH <sub>2</sub> COO <sup>t</sup> Bu (fast addition), DMSO, 3eq CsF, rt, time optimization	mono+double substitution

The continuous formation of double substituted product and observation of very little monosubstituted azaBODIPY **31** indicated that possibly the electron donating character of the added alkyl substituent led to a higher reactivity of the second hydroxy group present in the molecule. Shorter reaction times seemed to be a way to catch the intermediate monosubstituted product, as is the case for the conditions reported by O'Shea. We therefore performed an optimization study. This study showed that the substitution occurs extremely fast: in order to isolate the monosubstituted product the reaction had to be quenched by addition of water after 2.5 minutes to form a water cage around the fluorine and effectively neutralize it (Figure 95).

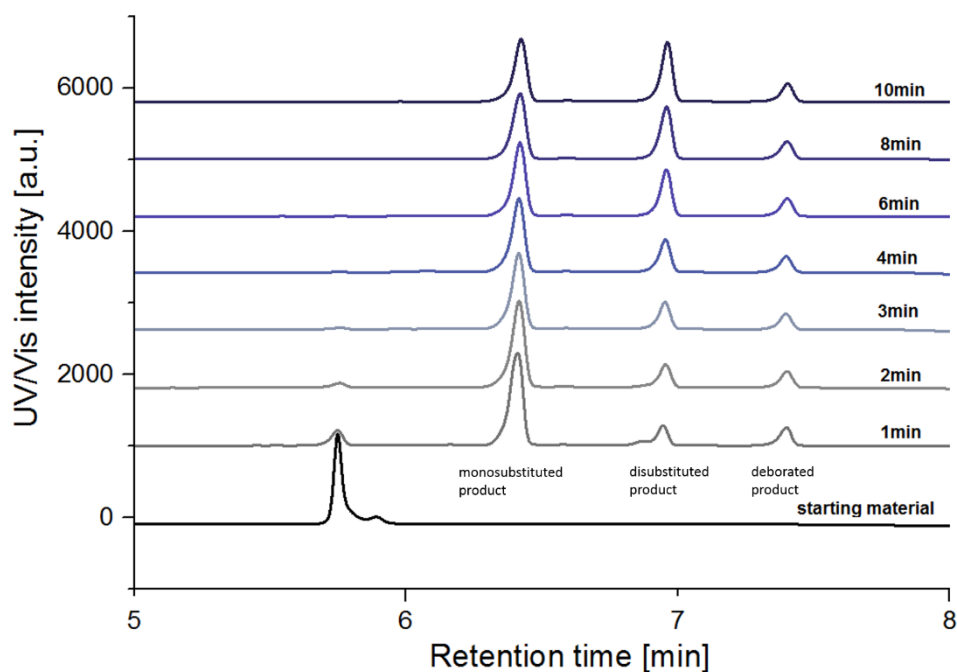


Figure 95: Optimization of monofunctionalization of **30** using CsF and *t*Butyl bromoacetic acid. The channel shown is the UV/Vis channel at 625 nm

In order to isolate mono- and disubstituted products and eliminate the deborated byproducts the DMSO had to be removed. Extraction with water or unsaturated brine resulted in formation of emulsions while the collected organic fractions still contained DMSO. Extraction with PBS-buffer yielded a very good phase separation and enabled the easy removal of DMSO. The separation of mono- and double substituted azaBODIPYs by column chromatography was then straightforward and granted easy access to the desired product **31** in 52% yield.

In the next step the ester had to be deprotected. The deprotection was attempted in DCM using TFA [218]. This approach led to deboration of the azaBODIPY core. In a next attempt, the hydrolysis was executed using 3M HCl and a variety of solvents. Acetonitrile was not able to solubilize the azaBODIPY well enough to obtain a homogenous solution. Therefore, DMF and DMSO were tested, in neither of which any hydrolysis was detected after 96h. We then focused our attention on the use of THF as solvent: first the starting material was totally solubilized in THF and then 3M hydrochloric acid added to the point where the starting material almost precipitated. These conditions finally permitted the desired hydrolysis. Using regular checks by HPLC-MS, the crude mixture was found to contain 91% of the desired product **32** after 5h hydrolysis at room temperature. Unfortunately, the deboration that we observed when TFA in DCM was used also took place using HCl (although much slower). This resulted in the gradual formation of an undesired byproduct and consumption of the target material for prolonged reaction times (Figure 96).

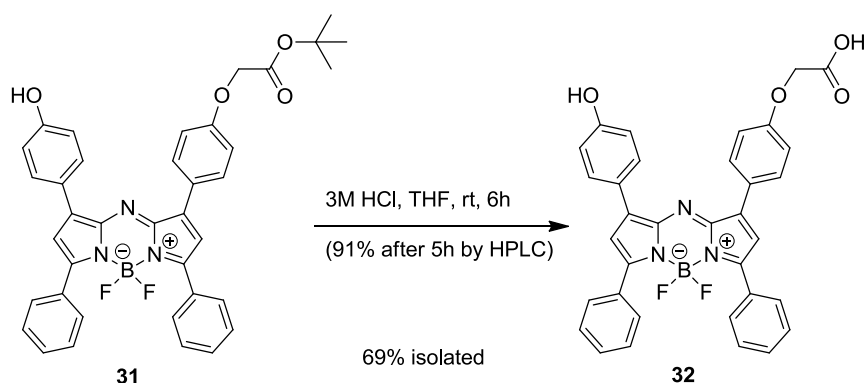


Figure 96: Acidic hydrolysis of the *t*-Butyl ester **31**

Literature suggested that the free acid could be isolated by extraction using basic aqueous solutions followed by back-extraction with acid [219]. For our 1,7-substituted compound **32** this did not yield any product. Any attempt of purification by regular column chromatography was unsuccessful due to the poor migration behavior on silica gel. Therefore, a purification by reversed phase semi preparative HPLC was attempted. Isolation of the pure **32** using this way was possible but tedious since

- it required several repeats to obtain a pure product
- the product precipitated repeatedly in the HPLC-column during injection and purification.

We finally managed to find a solvent system that resolved this issue by using an eluent of aqueous 50 mM TEAB (triethylammonium bicarbonate) and acetonitrile on an automated flash-chromatographic system.

The monoacid **32** was then used to introduce the pseudo-PEG TOTA-Boc as a spacer to distance the fluorophore from a vector such as antibodies or small peptides. The carboxylic

acid function was therefore transformed into an acyl chloride using oxalyl chloride in presence of DMF. Unfortunately, the resulting acyl chloride did not exhibit any reactivity towards the amine-spacer. Addition of the coupling agent HBTU then yielded the desired TOTA-Boc substituted azaBODIPY **33** (Figure 97).

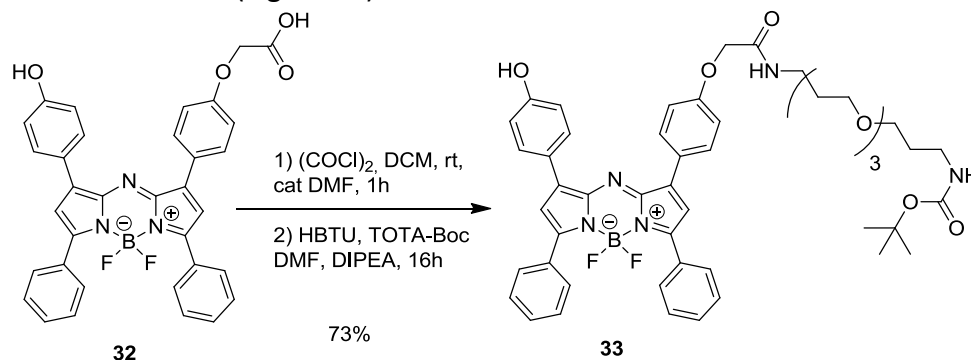


Figure 97: Introduction of TOTA-Boc using peptide coupling conditions

Although HPLC indicated that the reaction proceeded smoothly with almost quantitative yield, the purification presented a major challenge as the compound precipitated during reversed phase semi preparative HPLC both on injection and in the column. This led to an isolated yield of 10%. Classic chromatography was not possible either as the compound did not migrate at all on silica gel. In a next attempt the crude product was purified using size exclusion chromatography on Bio-Beads™. The crude eluate had to be partitioned between dilute hydrochloric acid (pH=3) and DCM, followed by repeated washing with DCM/pentane to remove residual coupling agent and stabilizers of the solvents. This approach afforded the desired product **33** in acceptable yield (73%) and purity to continue the synthesis.

Next, the Boc-protective group was removed using equal amounts of 3M hydrochloric acid and THF (Figure 98). The reaction was left to stir over night. According to HPLC it proceeded smoothly, was however not finished after 18h at room temperature (17°C). An increase in temperature to 35°C pushed the reaction to near completion in 4h (95%+3% starting material). Due to the onset of the formation of small amounts (2%) of byproduct, we decided to stop the reaction at this point and purify the product by semi preparative HPLC.

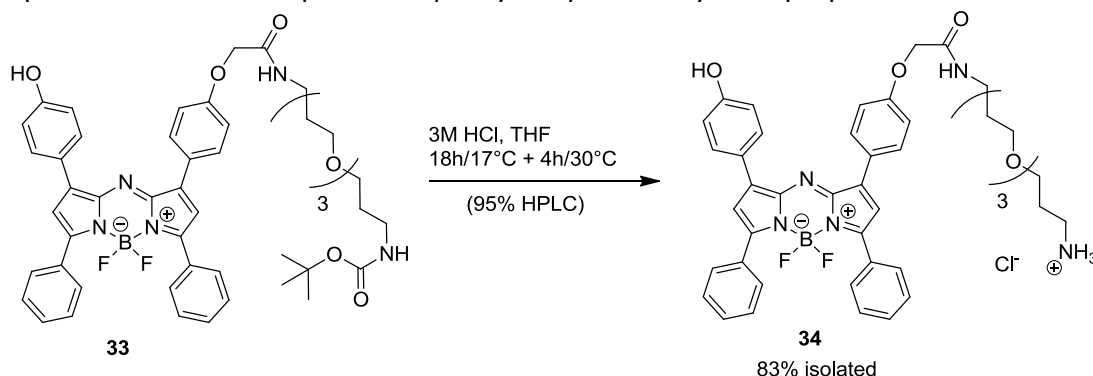


Figure 98: Removal of Boc from azaBODIPY **33** using 3M HCl

As for the earlier stages, we again encountered heavy problems during purification (precipitation upon injection and inside of the column) but were able to isolate 83% of the target compound. The photophysical properties of all azaBODIPYs that we obtained to this point were characterized and are shown and discussed in the next section 2.2.1 - Photophysical characterization.

## 2.2.1 Photophysical characterization

The azaBODIPYs that we obtained up to this point were characterized by UV/Vis and Fluorescence spectroscopy (the spectra of all compounds are shown in **ANNEX II – Photophysical Spectra**).

The values are summarized in Table 13. Interesting features of the compounds will be discussed in the following paragraph.

Table 13: Photophysical properties of tested azaBODIPYs. azaBODIPY **44** (section 2.4.2) in  $\text{CHCl}_3$  is used as the QY-reference ( $\Phi=0.36$  in  $\text{CHCl}_3$ ,  $\lambda_{\text{exc}}=670\text{nm}$ ) [44]. Compounds were excited at 670nm. n.d.=none detected

compound	Solvent	$\lambda_{\text{max, Absorption}}$ [nm]	$\epsilon\lambda_{\text{max}}$ [ $\text{M}^{-1}\text{cm}^{-1}$ ]	$\lambda_{\text{max, Emission}}$ [nm]	QY	Brightness $\Phi \times \epsilon_{\text{max}}$ [ $\text{M}^{-1}\text{cm}^{-1}$ ]	$\Delta\lambda$ [nm]	Stokes-Shift [ $\text{cm}^{-1}$ ]
<b>30</b>	DMSO	678	41 900	749	4%	1 510	71	1 398
<b>31</b>	DMSO	676	52 400	741	7%	3 400	65	1 298
<b>32</b>	DMSO	676	63 200	743	4%	2 290	67	1 334
<b>34</b>	DMSO	672	50 000	725	4%	2 220	53	1 088
<b>34</b>	PBS	700	35 900	n.d	-	-	-	-

All compounds were characterized in DMSO. AzaBODIPY **34** is an exception to this rule; the characterization was also executed in PBS to permit the direct comparison to azaBODIPYs that are presented in later sections of this thesis.

All compounds of the series show low quantum yields of 4-7% in DMSO and possess molar absorption coefficients between  $41\,900\text{ M}^{-1}\text{ cm}^{-1}$  and  $63\,200\text{ M}^{-1}\text{ cm}^{-1}$ . Their maximum absorption is centered on 675 nm. With emission maxima of around 725-750 nm, they display very large Stokes shifts of up to 71 nm.

The spectra of di(phenol)-azaBODIPY **30** displayed an interesting feature: the absorption and excitation spectra overlap relatively poorly (Figure 99).

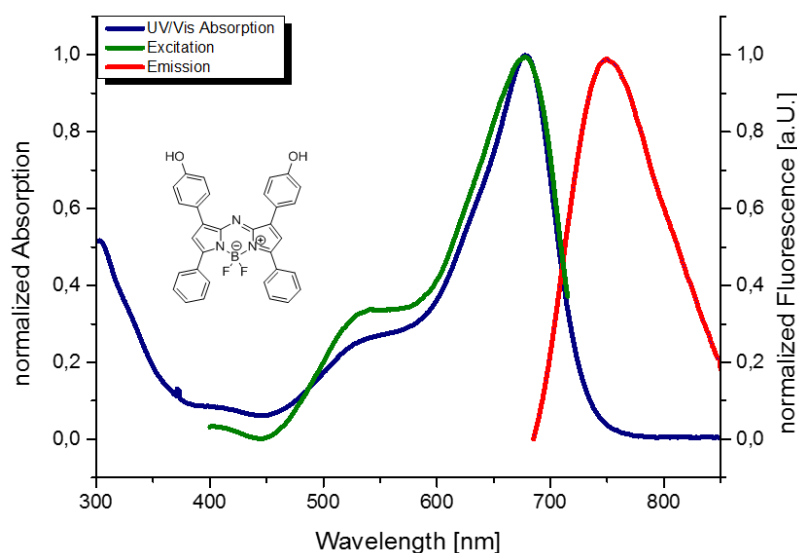


Figure 99: UV/Vis and fluorescence spectra of di(phenol)-azaBODIPY **30** in DMSO. Blue: Absorption spectrum, Green: excitation, Red: fluorescence Spectrum. Spectra were recorded at  $\sim 10^{-6}\text{ M}$  concentrations

This is quite common for compounds that have protonable/deprotonable substituents such as hydroxy groups whose apparent pK changes drastically due to the optical excitation. This was only observed for the azaBODIPY carrying two free hydroxy groups, none of the monosubstituted hydroxy-azaBODIPYs displayed similar behavior.

As mentioned above Aza-BODIPY **34** was characterized both in DMSO and PBS to permit the comparison to compounds that are shown in later sections of this thesis. AzaBODIPY **34**'s properties in DMSO are comparable to earlier synthetic steps of that derivate: just as **30**, **31** and **32** it possesses a molar attenuation coefficient of  $50\,000\text{ M}^{-1}\text{ cm}^{-1}$  and a quantum yield of 4%. However, due to stacking/aggregation the compound does not display any fluorescence in PBS (Figure 100).

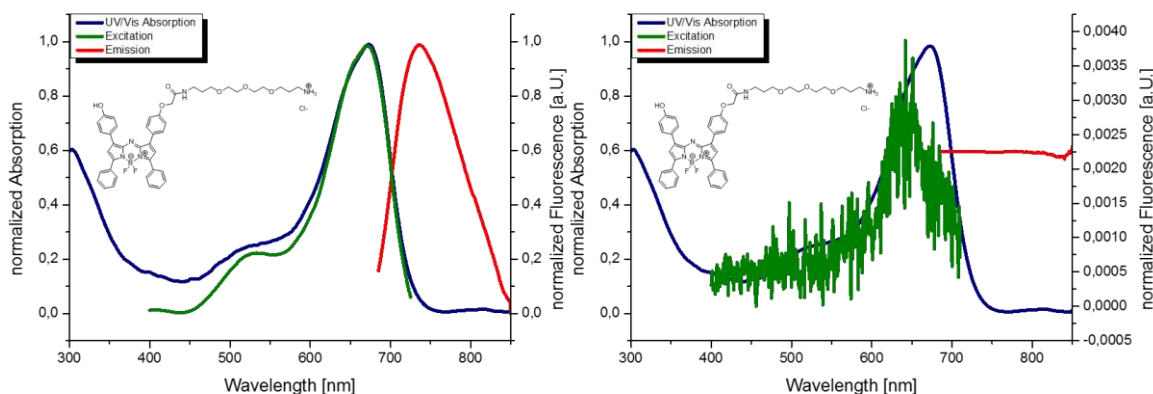


Figure 100: UV/Vis and Fluorescence spectra of azaBODIPY **34**. Left: Spectra recorded in DMSO, Right: spectra recorded in PBS. Blue: UV/Vis absorption. Green: Excitation spectra. Red: Fluorescence Emission. Spectra were recorded at  $\sim 10^{-6}\text{ M}$  concentrations

Contrary to what is commonplace in the literature, we did not add surfactants such as Triton-100X, SDS, Tween 80 and others to break up aggregates since for our purposes the fluorophore needs to remain fluorescent in aqueous solutions without any additive.

## 2.2.2 Activation of hydroxy-azaBODIPY **34** for bioconjugation

We hoped that in its final application the azaBODIPY would not stack/aggregate due to greater dilution and the sterical hindrance brought on by the antibody. We thus decided to push onwards and synthesize the fluorophore-antibody conjugate despite the displayed mediocre optical properties.

### 2.2.2.1 Choice of grafting function

In order to do so the amine function of the azaBODIPY-TOTA-ammonium had to be activated to be used for bioconjugation. Due to good experiences in earlier projects [115,132] we opted for the use of isothiocyanates as grafting function. Isothiocyanates are mainly reactive towards amines ( $\epsilon\text{-NH}_2$  of lysine and  $\alpha\text{-NH}_2$  of terminal amino acids). They do react with other nucleophiles such as tyrosinate or cysteinate. However, the formed thionouretanes and thiocarbamates are less stable than thioureas and gradually react with amines. This shifts the equilibrium towards thioureas (Figure 101).

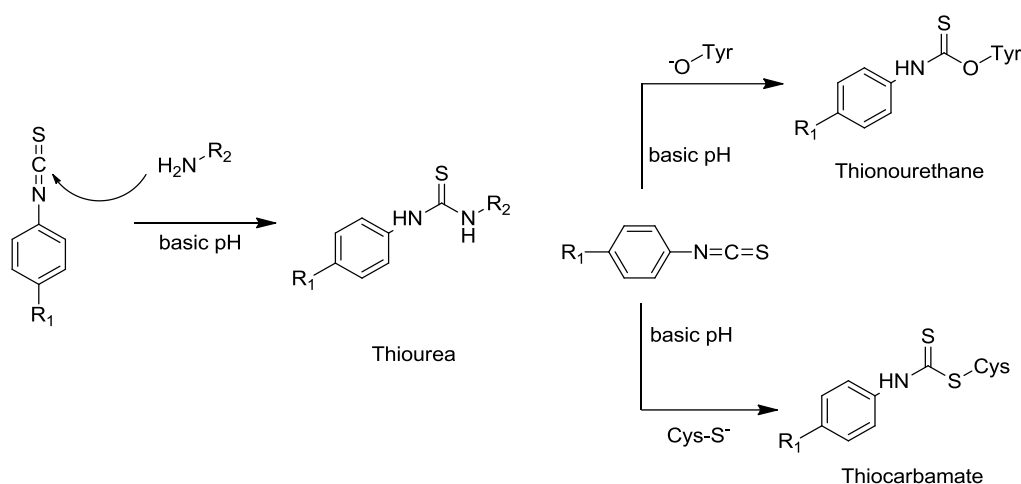


Figure 101: Reactions of isothiocyanates with nucleophiles that are present in biological media

Even though the resulting thiourea bond is slightly less stable than esters formed by the commonly used NHS-activated ester methodology they provide sufficiently stable bonds for relatively slow biological processes such as antibody mediated processes [229]. Isothiocyanates are bench-stable and reactive enough to be used for bioconjugation purposes while resisting hydrolysis in aqueous solutions. Using homobifunctional agents such as PDITC amines can be activated directly without prior transformation into other grafting functions.

#### 2.2.2.2 Activation of azaBODIPY **34** for bioconjugation

The activation of azaBODIPY **34** was carried out in presence of base and using a large excess (20 equivalents) of PDITC to prevent dimerization (Figure 102).

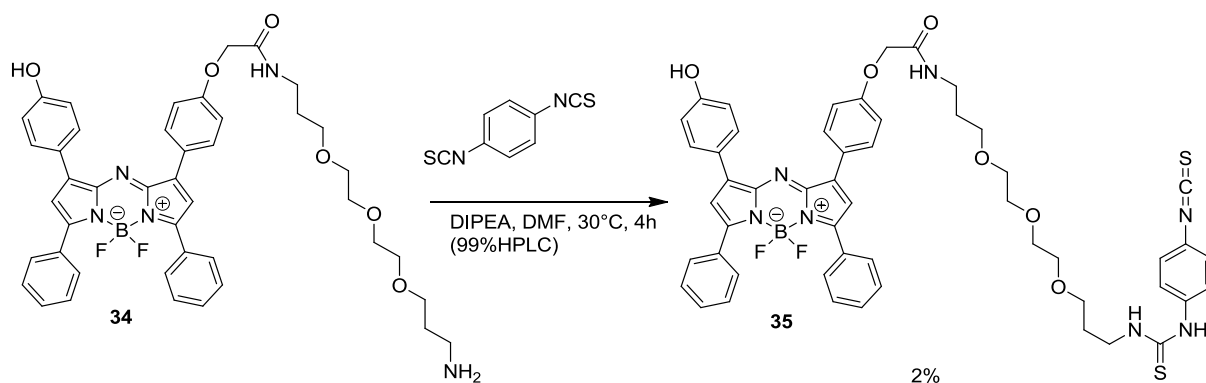


Figure 102: Activation of azaBODIPY **34** using PDITC

The reaction yielded the desired product without formation of byproducts. The removal of excess PDITC however posed significant challenges: Removal of excess PDITC by simple washing was prohibited because of the good solubility of **35** in common organic solvents. As for previous stages the activated azaBODIPY **35** did not migrate on common silica gel and precipitated/clogged the semi preparative HPLC. Despite these challenges we managed to isolate a minuscule amount of **35** by semi preparative HPLC. However, in addition to the “common” problems the obtained pure fractions containing 140µg (2% yield) of the desired product also exhibited excessive aggregation: once the solvents were removed the compound behaved like a pigment and formed aggregates that proved insoluble in every solvent, including DMF and DMSO.

Using sonication for prolonged periods of time (30min) we were able to obtain a solution that was used for bioconjugation to the humanized monoclonal anti-HER2 antibody TrastuzumAb. However, even though we were able to conjugate our fluorophore to the antibody, solubility issues prevented us to properly purify the bioconjugate.

At this point of the project, it was clear that the main challenge we had to take up is to render the azaBODIPYs water soluble.

## 2.3 Hydrosolubilization of azaBODIPYs

During the entire synthetic process we were surprised of how unfavourably the hydroxy-azaBODIPYs behaved; both in terms of aggregation and solubility issues as well as optical properties (see paragraph 2.2). Extrapolating from the literature published by O'Shea and others we expected that the introduction of the pseudo-PEG TOTA in conjunction with the highly polar carboxylate and the free hydroxy-group would solve or at least improve any tendency of the fluorophore to aggregate [223,227,230]. We were also surprised by the poor optical properties exhibited by our system since for the 3,5-phenolic azaBODIPY **L64** the liberation and deprotonation of a hydroxy group leads to an *increase* in quantum yields [219,224,231,232]. Our 1,7-phenolic azaBODIPY **30** however showed poor optical properties as well as pronounced aggregation and solubility issues that seemed to get worse with each step.

We therefore decided to first improve the solubility of our compounds before advancing any further towards the goal of obtaining a versatile platform.

### 2.3.1 Hydrosolubilization of BODIPY and azaBODIPY – an overview

A multitude of different strategies has been developed over the years to render BODIPYs soluble in aqueous solutions. They can be divided into two major strategies: either the BODIPY is rendered water soluble while remaining neutral, that is through introduction of hydrophilic groups such as PEGs. The other strategy consists of introducing polar, charged groups such as sulfones, ammoniums, phosphates and peptide sequences (Figure 103).

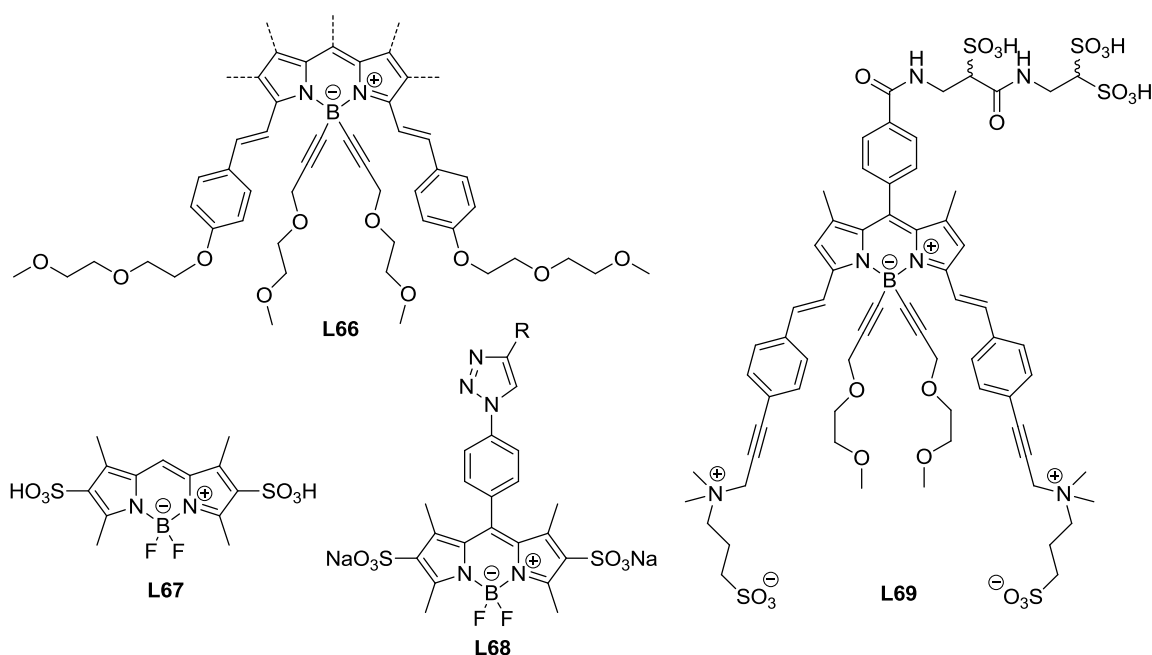


Figure 103: Hydrosolubilization of BODIPY-dyes. **L66** (top-Left): example for a strategy employing exclusively PEGs [233]. **L69** (right): an extreme example combining PEGs, sulfobetaines and sulfonated amino acids for hydrosolubilization [234]. **L67** (bottom left): first example of core-sulfonated BODIPY [235]; **L68** (bottom middle): example from Li et al. for functionalizable, water soluble core-sulfonated BODIPY-dyes [236]

Other commonly used techniques include the direct sulfonation of the  $\beta$ -pyrrolic positions of the BODIPY core using chlorosulfonic acid and B-O functionalization of the boron center with PEGs (see for example **L70-L72** [237,238] in Figure 104).

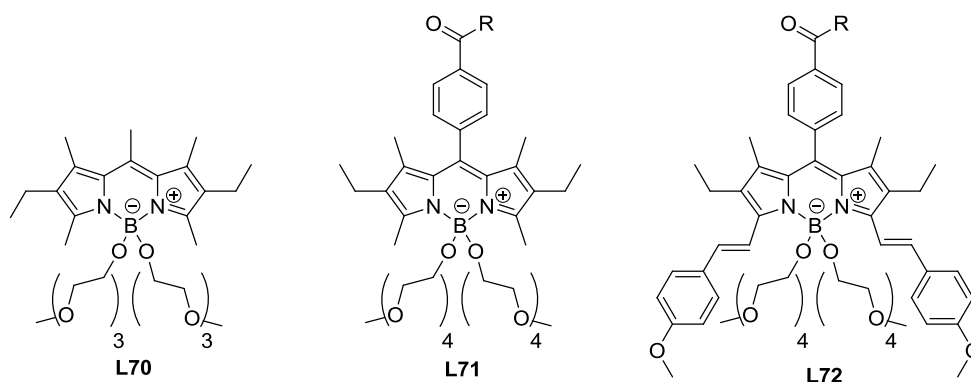


Figure 104: example for B-O functionalized BODIPYs for hydrosolubilization purposes. **L70** (left) [237], **L71** (middle) and **L72** (right) examples from our group [238]

For both the sulfonation approach as well as the B-O based hydrosolubilization strategies no successful syntheses have been published for azaBODIPYs so far. Instead, two major strategies are predominant for azaBODIPYs in the literature: authors either introduce PEG-groups with varying molar masses (one can find anything from small PEGs such as PEG-3 (**L73**) [239] to PEG-5000 (**L74**) [219]) (Figure 105).

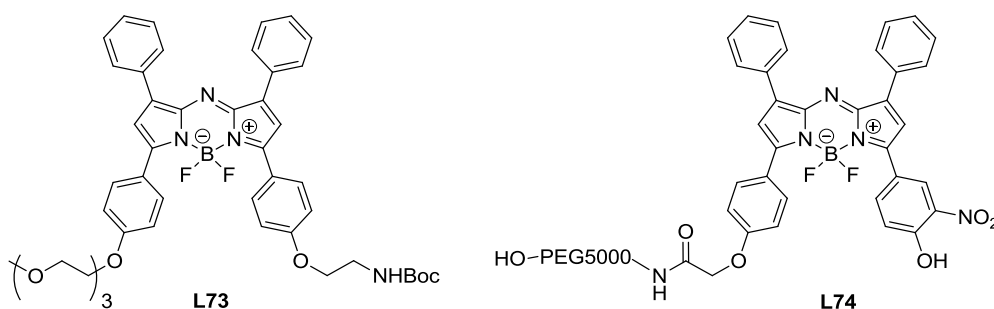


Figure 105: Hydrosolubilization of azaBODIPYs using PEG of small (**L73**, left, [239]) and very large (**L74**, right, [219]) masses

or the introduction of charged groups such as sulfone substituents (e.g. in the form of propane sulfone), carboxylic acids or ammoniums [216] (Figure 106).

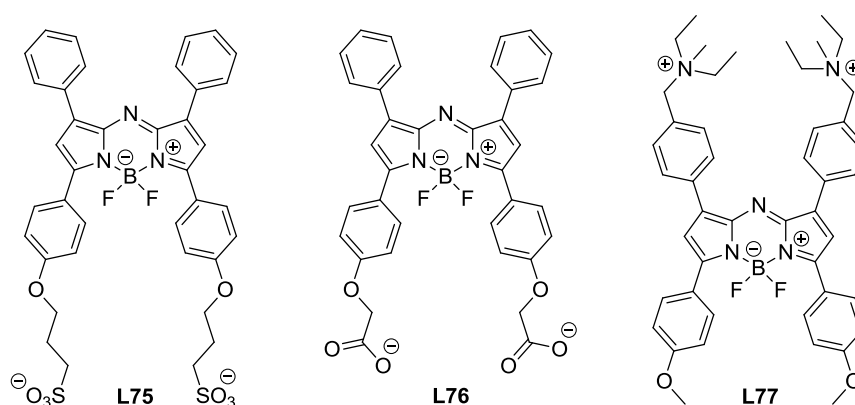


Figure 106: Hydrosolubilization of azaBODIPYs through introduction of polar groups such as sulfones (**L75**), carboxylic acids (**L76**) or ammoniums (**L77**) to the periphery of the azaBODIPY [216]

Variations thereof have been published that employ combinations of the two strategies such as the use of PEG+ammoniums (**L78**) [240], PEG+sulfone+sugars (**L80a-f**) [241] or short peptide chains and sulfone groups (**L79**) [225] (Figure 107).

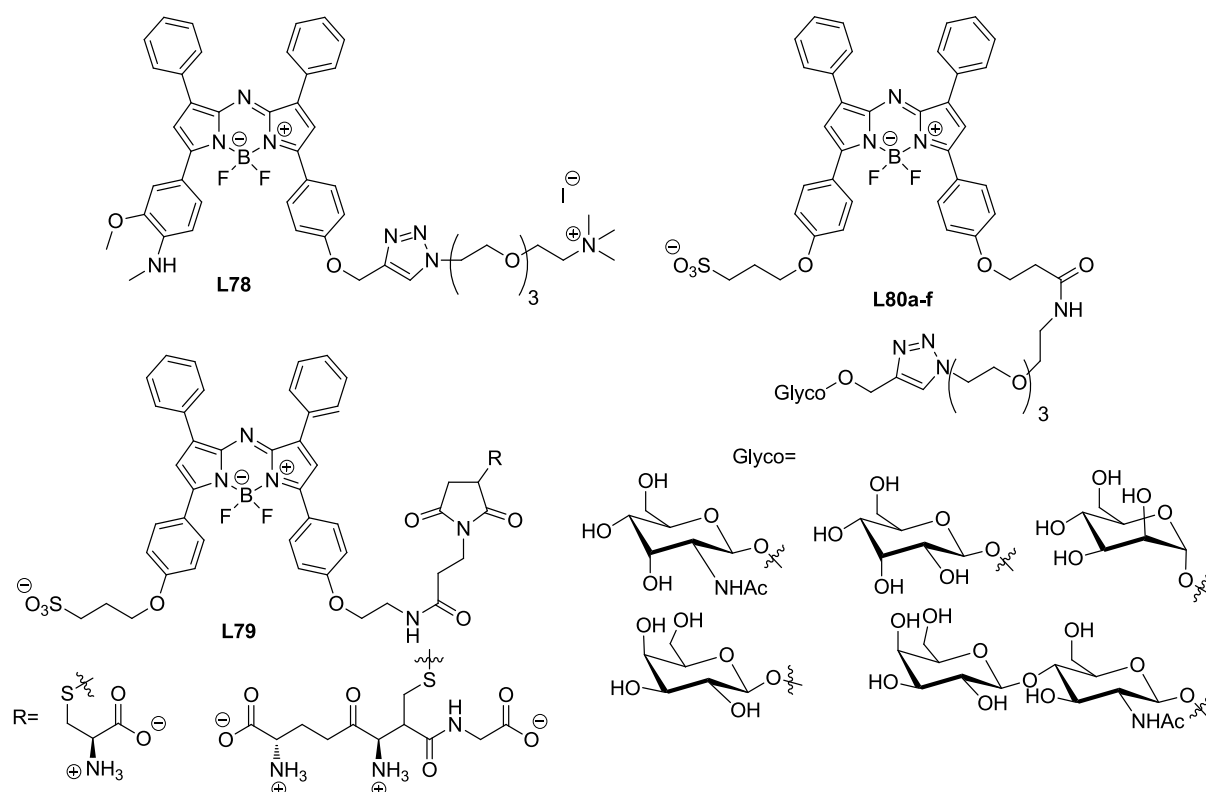


Figure 107: Hybrid hydrosolubilization strategies that employ various solubility enhancing groups: PEG+ammonium (top left) [240], Sulfone, PEG and various sugars (right) [241] and sulfone and amino acids or short peptide sequences [225]

At first glance, the direct sulfonation of the BODIPY core is attractive, but a thorough literature research revealed that this reaction had been attempted by Burgess, and that he did not succeed in obtaining the desired product [242]. He theorized that the highly electroattractive nature of the added sulfone-groups destabilizes the azaBODIPY-core. This leads to deboration; something that is not observed in classic BODIPYs due to the lack of the core-impoverishing *meso*-nitrogen atom. Due to its straightforwardness we still had an attempt of this strategy, which did not meet with more success.

The poor water solubility of azaBODIPYs is due both to their high lipophilicity and their high propensity to aggregate *via*  $\pi$ -stacking. Thus, we want to tackle these two aspects at the same time by functionalizing the boron. Indeed, introducing water solubilizing groups on the boron will prevent aggregation due to steric hindrance of the faces. For classical BODIPYs this type of transformation has been investigated extensively by Zissel and Ulrich both for rendering the resulting molecules water-soluble as well as to introduce light-harvesting groups. Our group recently reviewed this strategy [243].

## 2.4 E-aza-BODIPYs

In 2005 Zissel and coworkers investigated the feasibility of boron functionalization on classical BODIPY-dyes. The resulting dyes and dyads were used for light-harvesting purposes: dipolar interactions such as FRET depend on close proximity of the donor and acceptor dyes. The smallest obtainable distances were achieved by adding acceptor dyes to the boron center and replacing the fluorine atoms with various C-nucleophiles [244–246] (Figure 108).

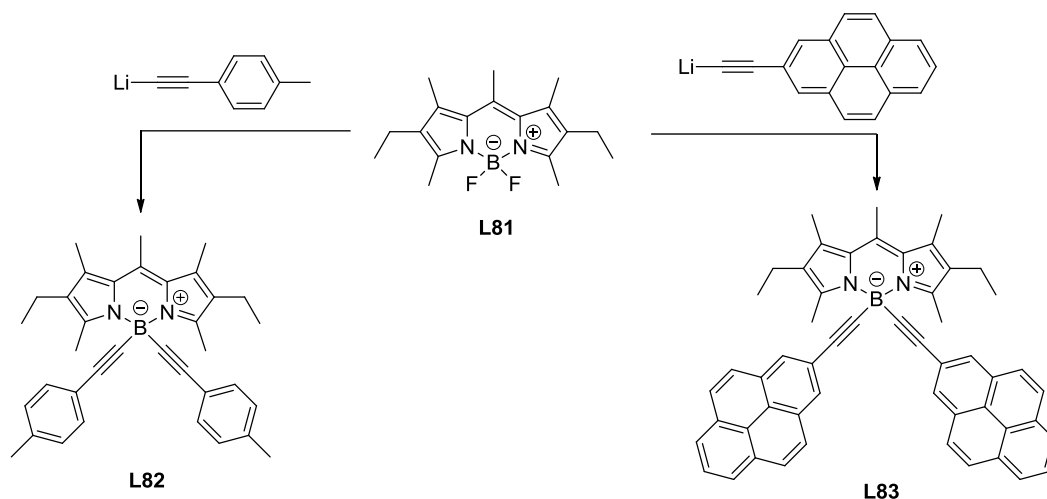


Figure 108: B-functionalization of BODIPY using organolithium compounds [244–246]

They found that the introduction of an ethynyl substituent did not affect the optical properties adversely, i.e. the exchange of the fluorine atoms did not result in significant spectral shifts or loss of brightness. This principle has since been applied to other nucleophiles such as  $sp^2$  or  $sp^3$ -hybridized carbon species (phenyl/polycyclic aromatics [247,248], methyl, ethenyl [249]) as well as oxygen-nucleophiles such as alcohols [250] or carboxylic acids [251,252].

By judiciously choosing the substituents, the boron functionalization was equally used to reduce the lipophilic character of the dyes as this lipophilicity can cause problems for biological applications. Employing hard nucleophiles such as organomagnesium and organolithium compounds the boron center was successfully used to introduce hydrosolubilizing groups such as dimethylaminopropyne. The amine in turn can be methylated or quaternized as required [114] (Figure 109).

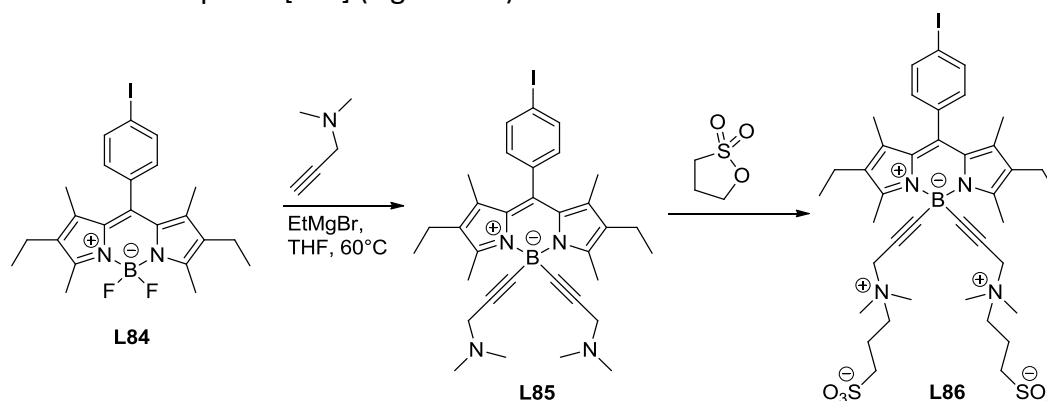


Figure 109: Hydrosolubilization strategy employed by Niu et al. [114]

We draw our inspiration from this strategy to improve the solubility and prevent stacking interactions of azaBODIPY derivatives. Of note, very little work has been done using azaBODIPY dyes with alkyne-functionalized boron centers: so far only 3 publications [253–255] and 1 patent [256] have been published. While the publications investigated the use of alkyne-substituents exclusively to exploit the resulting optical properties of added molecules, the patent specifically aims at improving the solubility in water by adding and quaternizing dimethylpropargylamines (the patent had not yet been published at the time when we started our work on functionalization of the boron atom).

## 2.4.1 First system: 1,7-di(phenol)-3,5-di(phenyl) E-azaBODIPY

Encouraged by the apparent general feasibility of boron substitution in azaBODIPYs, we selected triethyl propargylammonium as the substituent that we planned on introducing on the boron atom. This small, cationic molecule would permit the synthesis of a positively charged azaBODIPYs with voluminous substituents on the boron atom to prevent stacking while also strongly increasing the solubility in water. The synthesis was straightforward using propargyl bromide and triethylamine in chloroform, which yielded the corresponding ammonium (Figure 110).

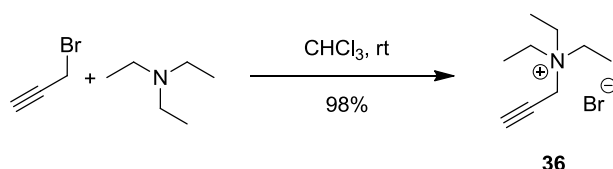


Figure 110: Synthesis of the ammoniumalkyne **36**

In the next step, the alkyne was lithiated using *t*BuLi to obtain the C-nucleophile. AzaBODIPY **30** was deprotonated as well using *t*BuLi prior to addition to prevent acido-basic reaction between alkyne-lithium derivatives and phenols. The deprotonated azaBODIPY was then added to the alkyne solution. Product formation could be observed after 30 minutes of reaction at low temperatures, but even after 1h30 at room temperature the reaction control by HPLC-MS showed that the reaction was not yet finished. Continued stirring over the weekend led to a surprise as the HPLC indicated that the reaction partially receded back towards the starting material. After quenching with aqueous methanol, the product was purified to afford **37** in 20% yield (Figure 111). Several additional attempts did not improve this disappointing result.

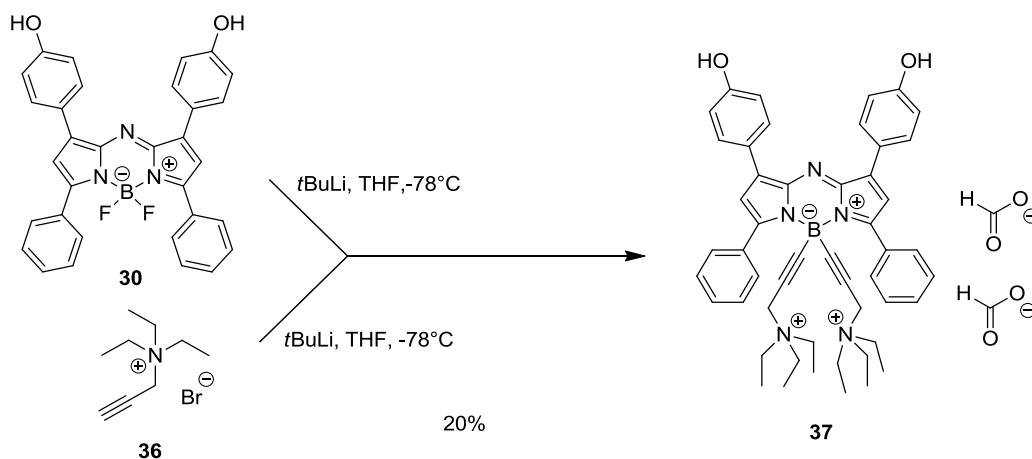


Figure 111: Synthesis of B-functionalized azaBODIPY **37**

We therefore decided to protect the hydroxy groups using TBDMSCl in DCM in presence of base and catalytic amounts of DMAP (Figure 112).



Dropwise addition of protected azaBODIPY **38** then led to a rapid color change that is shown in Figure 114.

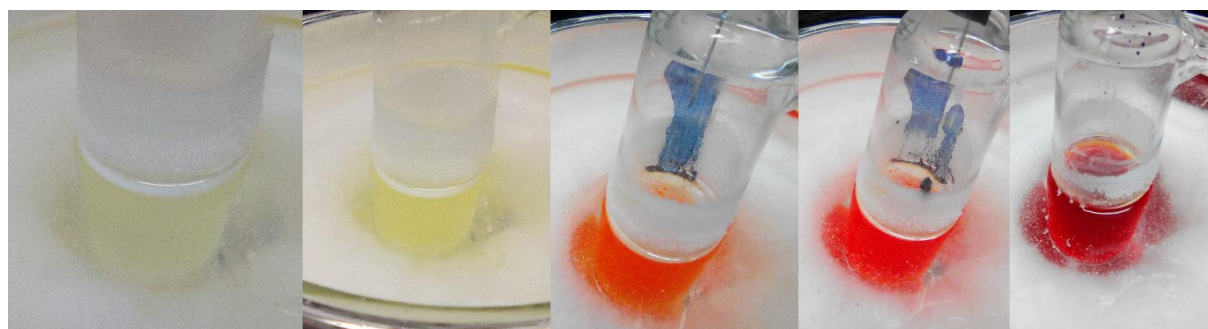


Figure 114: Color change upon addition of azaBODIPY to the lithium-alkyne. From left to right: Li-alkyne **36**, dropwise addition of (blue) azaBODIPY **38** to organolithium solution after 1-4 minutes

Compared to the unprotected azaBODIPY **30** the reaction proceeded in a much cleaner fashion: after 30 minutes at  $-78^{\circ}\text{C}$  only starting material, mono- and disubstituted product were observed (Figure 115).

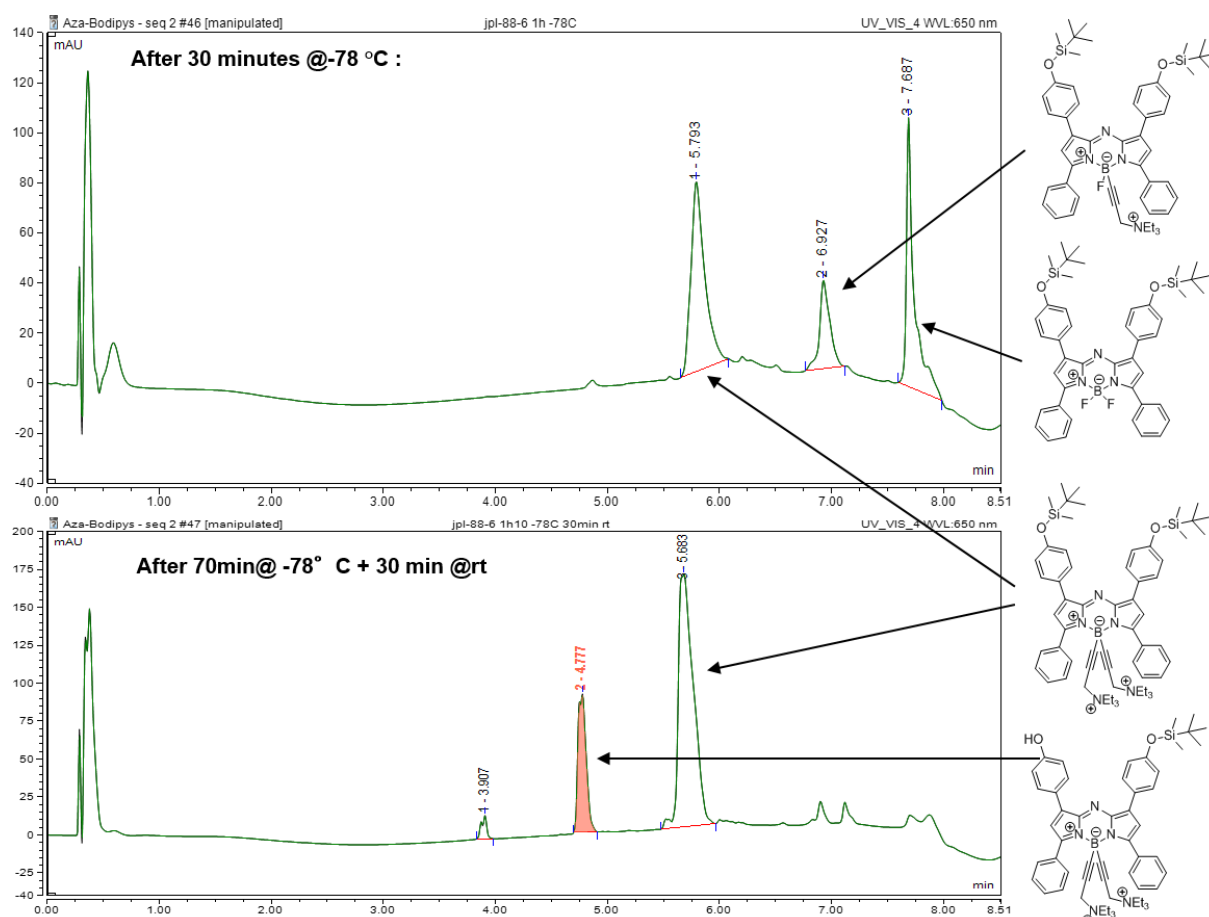


Figure 115: Evolution of HPLC-profiles (HPLC-conditions are given in section 4.1.3, page 164) observed during boron functionalization of TBDMS-protected azaBODIPY **38**.

A slow increase in temperature to ambient temperature pushed the reaction towards completion, leading to exclusively double substituted compounds **39a,b**. Due to the liberation of the fluoride anion during the reaction, the azaBODIPY was already partially deprotected during reaction as observed by HPLC-MS (Figure 115). We therefore decided to execute both

the substitution (+quenching) and hydrolysis one-pot. The addition of a fluorine source such as TBAF or CsF at room temperature led to the total degradation by loss of boron and appearance of a multitude of byproducts. The use of 1M HCl limited the apparition of side products but did not prevent deboration. The product **37** was isolated and purified by semi preparative HPLC in varying modest yields (from 10% to 50%). The attempt of boron-functionalization of using alkyne-Grignards did not lead to better results (no consumption of starting material was observed after 2h).

Nevertheless, the little obtained amounts of **37** were then used to be functionalized *via* the hydroxy group (it is worth noting that **37** is totally water soluble). For this reaction, the optimized conditions for the synthesis of **31** were employed (Figure 116).

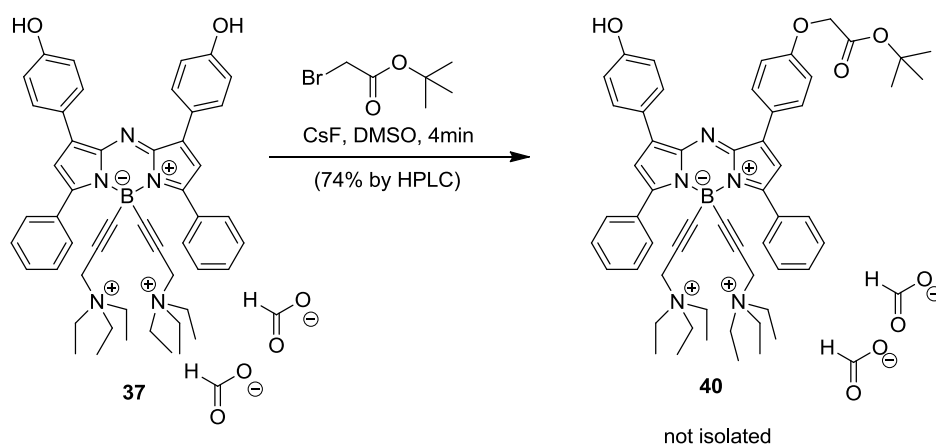


Figure 116: O-functionalization of the hydrosoluble azaBODIPY **37**

Product formation was observed by analytical HPLC but we never succeeded in isolating it. Hydrolysis of the ester directly after the formation of the ether may lead to better results.

We acknowledge that this synthetic pathway may be successful. However, it is clear that it is a too time consuming and low yielding strategy to be suitable for the development of a platform. It is worth noting that the boron functionalization is easy and led to a water soluble product. Thus, we decided to base our entire strategy on the functionalization of this position.

The photophysical properties of all compounds that were obtained (and isolated) in this section are shown and discussed in detail in chapter 2.4.6 - Photophysical characterization of E-azaBODIPYs and precursors.

## 2.4.2 New platform molecules

Since literature suggested that the optical properties are not noticeably influenced by the introduction of aliphatic alkyne-substituents (which we confirmed by our investigations of the functionalization of azaBODIPY **30**), we were curious to investigate if both the functionalization and the vectorization could be executed using the boron-substituents while choosing (and not altering) an azaBODIPY. This approach would have the added benefit that the “final” optical properties can be chosen beforehand while, thanks to the introduction of spacers and grafting functions, the boron-substituents would become even more bulky, thus successfully preventing stacking or aggregation of the final probe. It would also permit the use of neutral azaBODIPYs that do not present deprotonable groups for the boron functionalization with alkyne.

As explained in the introduction one goal of the second part of this thesis was to design trackable compounds that possess therapeutical activity. In order to do so we have chosen an azaBODIPY-system that can undergo Pd-catalyzed cross coupling reactions. This system was selected to introduce therapeutically active drugs (such as gold(I) and gold(III) based compounds) onto the azaBODIPY using pyridine- and phosphine ligands. Using the metallated compounds we planned to introduce vectors in order to obtain vectorized, trackable drugs such as antibody-drug-conjugates (ADC).

For this new approach we thus added three new azaBODIPYs to the investigated panel of compounds.

The compounds that we selected for these transformations are 1,7-di(phenyl)-3,5-di(methoxyphenyl)-azaBODIPY **44** and the two bromine-substituted azaBODIPYs 1,7-di(bromophenyl)-3,5-di(methoxyphenyl)-azaBODIPY **48** and the 1,7-methoxyphenyl-3,5-bromophenyl-azaBODIPY **52** (Figure 117).

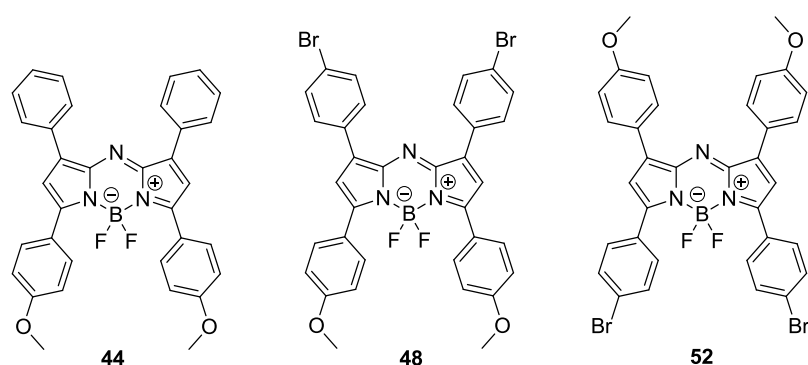


Figure 117: New base compounds for the development of *E*-azaBODIPY-platforms

#### 2.4.2.1 Synthesis of base-compounds for boron functionalization

To obtain the azaBODIPY **44**, we started from *p*-methoxyacetophenone and benzaldehyde. Both compounds underwent a Michael-addition in presence of KOH to obtain chalcone **41** as a fluffy precipitate in quantitative yield. The isolated chalcone **41** was redissolved in MeOH and reacted with a large excess of nitromethane in presence of diethylamine under reflux to obtain the Michael-adduct **42** (Figure 118).

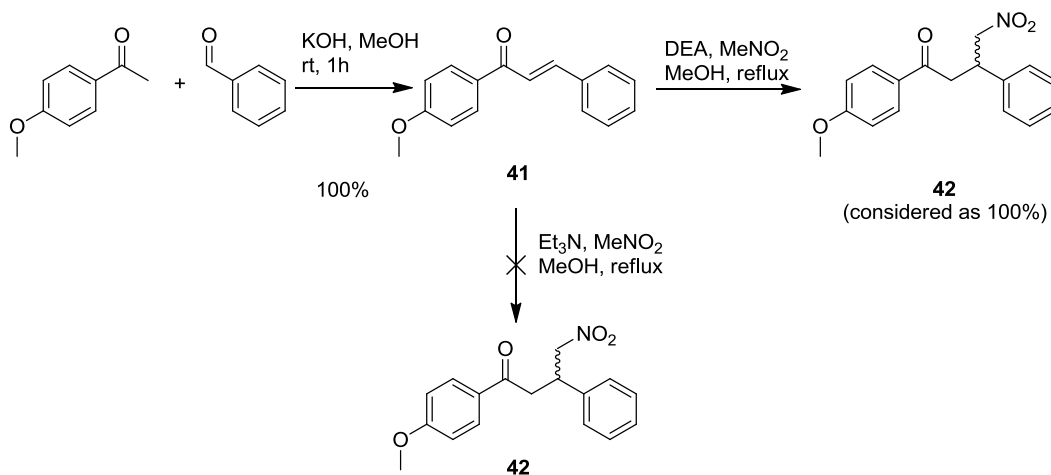


Figure 118: Formation of Michael-adduct **42**

Triethylamine was also tested as base but did not result in product formation. In the next step Michael-adduct **42** was refluxed in EtOH in presence of a large excess (20 equivalents) of  $\text{NH}_4\text{OAc}$  to obtain the very poorly soluble azadipyrrromethene **43**.

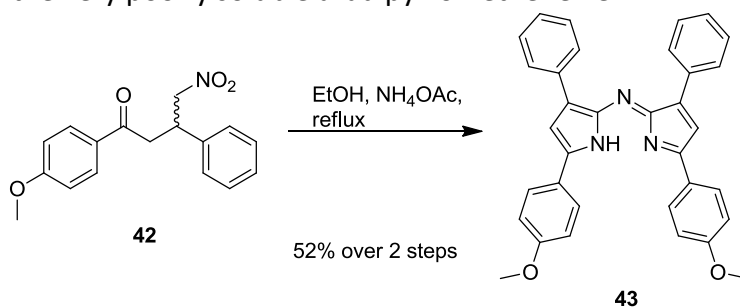


Figure 119: Formation of the azadipyrrromethene core

The removal of excess ammonium acetate can be difficult, Burgess employed filtration followed by washing to remove  $\text{NH}_4\text{OAc}$ . For us filtration tended to clog the filters and resulted in overall poor purity. Aqueous washing did not give good results either as the azaDIPY is poorly soluble in most solvents. This resulted either in aggregates in the aqueous phase and loss of compound or incomplete removal of salts. Purification by column chromatography was attempted but is very tedious and solvent-consuming. The method of choice turned out to be extensive and repeated washing with EtOH, followed by centrifugation.

In the next step the boron atom was introduced using an excess of  $\text{BF}_3 \cdot \text{Et}_2\text{O}$  and DIPEA (Figure 120).

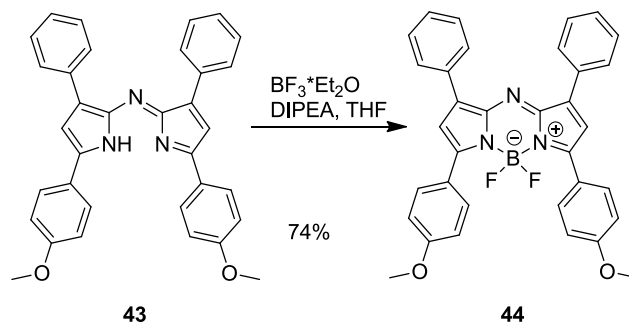


Figure 120: Introduction of the  $\text{BF}_2$ -moiety to form the model-compound azaBODIPY **44**

This reaction sequence was optimized by using THF as solvent, instead of  $\text{CH}_2\text{Cl}_2$ , which causes solubility issues at gram scale, and scaled up to 5 g of final azaBODIPY **44**. The purification of azaBODIPY **44** does not require any column chromatography, all impurities can be removed by repeated washing and recrystallization with MeOH. Using this strategy, we were able to reliably remove the  $\text{BF}_3 \cdot \text{DIPEA}$ -adduct that is formed in the last step and which presents a significant challenge in removal by chromatography.

To resume, we are able to synthesize more than 5 g of azaBODIPY in less than 3 days including purification thanks to the optimization of the reaction and purification conditions.

#### 2.4.2.2 Synthesis of bromophenyl substituted azaBODIPYs

The synthesis was carried out using the classic approach, e.g. synthesis of the chalcone, followed by Michael-addition of nitromethane and formation of the azaDIPY with subsequent introduction of the boron moiety (Figure 121).

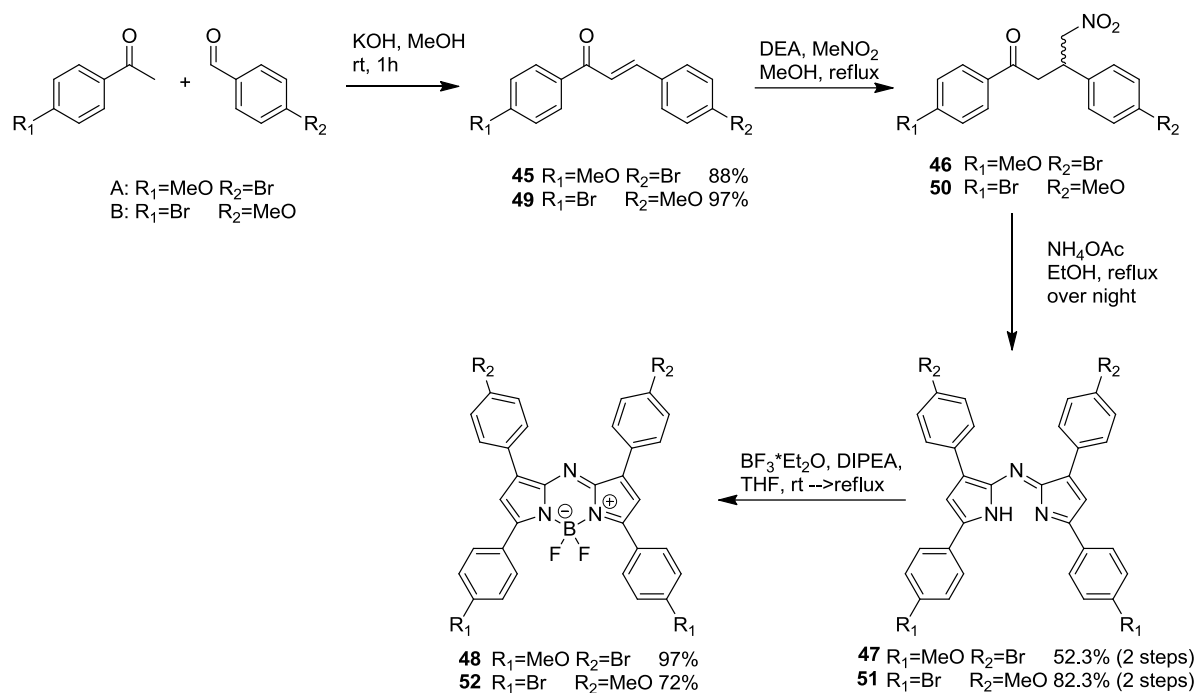


Figure 121: Synthesis of Br-MeO functionalized azaBODIPYs **48** and **52**

This synthesis enabled us to isolate 4.6 g of the desired azaBODIPY **48** in an overall yield of 45% and 6.7 g of **52** with an overall yield of 57%. In both cases, as for azaBODIPY **44** the reaction of the last step is quantitative. However, as observed for **44**, a significant amount of BF<sub>3</sub>\*DIPEA is formed during the reaction and has to be removed (thus requiring some sort of purification). The difference in efficiency of the last synthetic step stems from the simpler purification of azaBODIPY **48**: due to its poor solubility in MeOH the BF<sub>3</sub>\*DIPEA complex can be removed easily by simple washing with MeOH. Its isomer on the other hand requires difficult purification by column-chromatography, with significant losses due to co-elution of product and the BF<sub>3</sub>-adduct.

When the proton NMR (Figure 122) of the azaBODIPYs **44**, **48** and **52** are compared three major pieces of information stand out:

- even though both methoxy-bromo substituted azaBODIPYs **48** and **52** are isomers and only mirror each other's phenyl-substituents, a difference in solubility was observed. This is the basis of the purification of **48**; this effect is also visible by the poorly resolved spectrum of azaBODIPY **48** compared to **52**.
- the phenylic protons do not show any major difference in terms of chemical displacements for either of the two compounds **48** and **52**
- the comparison between the two azaBODIPYs that carry a methoxy substituent in the 3,5-positions (**44** and **48**) shows a significant shift for the 1,7 substituents

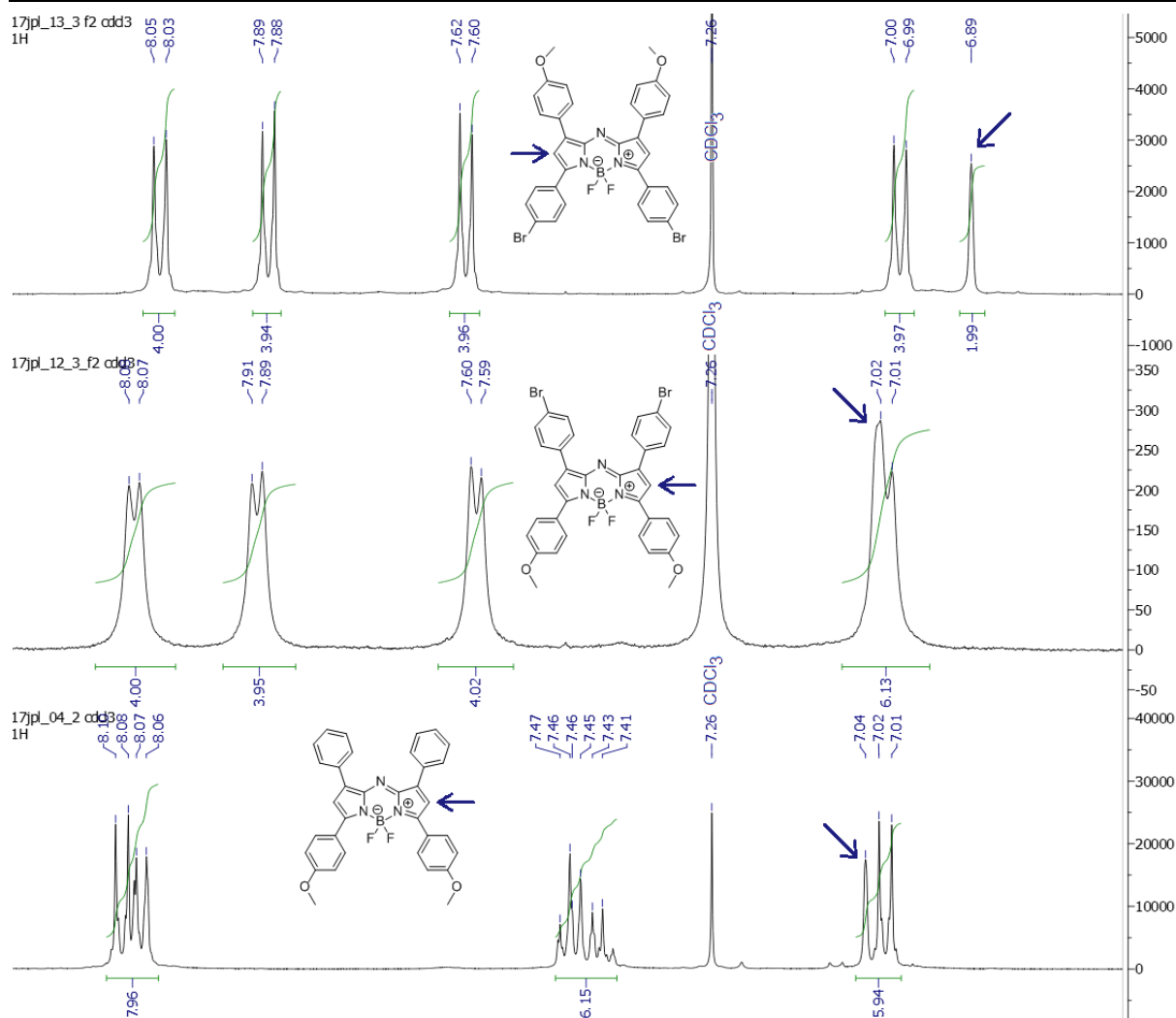


Figure 122: Comparison of the  $^1\text{H-NMR}$ -spectra of the aromatic zone of bromo-methoxy-substituted azaBODIPYs **52**, **48** and their comparison to methoxy-azaBODIPY **44**. The signal of the  $\beta$ -pyrrolic hydrogens are highlighted by flashes. The NMR were recorded in  $\text{CDCl}_3$  at 500MHz

- a significant difference for the  $\beta$ -pyrrolic H-atoms is visible depending on the direction of the intramolecular push-pull effect that is exerted by the methoxy and bromine substituents. Their signals are displaced by  $\Delta=0.13$  ppm
- this influence seems to be directed by the methoxy groups as visible when comparing spectra 2 and 3. The absence or presence of bromine does not significantly influence the exhibited electronic effects on the  $\beta$ -pyrrolic H-atoms.

This information can be used in the following in order to analyze possible electronic effects that are exerted by the introduction of different substituents into the azaBODIPY. A reversal of push-pull effects in the molecule leads to a shift of the signal observed for the  $\beta$ -pyrrolic H-atom whereas changes in the electronic structure of the phenyl-substituents significantly change the observed signals of the corresponding phenylic protons.

The photophysical properties of all three azaBODIPYs-dyes were characterized in DMSO and are shown and discussed in the following paragraph.

## 2.4.2.3 Photophysical characterization

The azaBODIPYs that we obtained in the previous paragraph were characterized by UV/Vis and Fluorescence spectroscopy to select the best candidate for further functionalizations (the spectra of all compounds are shown in **ANNEX II – Photophysical Spectra**).

The values are summarized in Table 14. Interesting features of the compounds will be discussed in the following sections.

Table 14: Photophysical properties of tested azaBODIPYs. azaBODIPY **44** in  $\text{CHCl}_3$  is used as the QY-reference ( $\Phi=0.36$  in  $\text{CHCl}_3$ ,  $\lambda_{\text{exc}}=670\text{nm}$ ) [44]. Compounds were excited at 670nm.

Compound	Solvent	$\lambda_{\text{max}}$ , Absorption [nm]	$\epsilon_{\lambda_{\text{max}}}$ [ $\text{M}^{-1}$ $\text{cm}^{-1}$ ]	$\lambda_{\text{max}}$ , Emission [nm]	QY	Brightness $\Phi \times \epsilon_{\text{max}}$ [ $\text{M}^{-1}$ $\text{cm}^{-1}$ ]	$\Delta\lambda$ [nm]	Stokes- Shift [ $\text{cm}^{-1}$ ]
<b>44</b>	$\text{CHCl}_3$	688	80 700	721	36%	29 050	33	665
<b>44</b>	DMSO	702	86 700	738	27%	23 740	36	695
<b>48</b>	DMSO	711	66 600	749	23%	15 570	38	714
<b>52</b>	DMSO	683	55 000	739	13%	6 950	56	1 109

All compounds were characterized in DMSO. AzaBODIPY **44** is an exception to this rule as it also served as quantum yield reference for all investigated azaBODIPYs.

2.4.2.3.1 The “model compound” azaBODIPY **44**

The “model” compound azaBODIPY **44** exhibits excellent optical properties in DMSO: both the maximum absorption and emission are in the far-red/NIR region (702/738nm) (Figure 123).

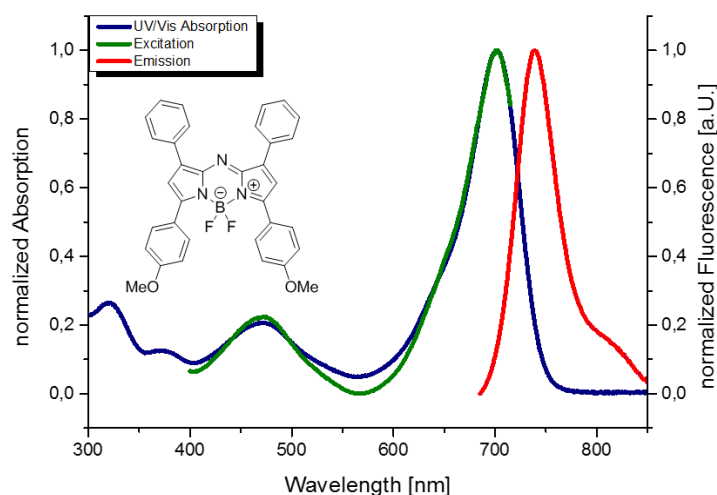


Figure 123: UV/Vis and fluorescence spectra of azaBODIPY **44** in DMSO. Spectra were recorded at  $\sim 10^{-6}$  M concentrations

Both peaks are relatively thin and show a Stokes-shift of 36 nm. With a molar absorption coefficient of  $\epsilon_{\lambda_{\text{max}}} = 86\,700 \text{ M}^{-1} \text{ cm}^{-1}$  in DMSO the model compound **44** absorbs strongly in the NIR-I-region of the electromagnetic spectrum. Using  $\text{CHCl}_3$  as solvent this compound **44** was used as quantum yield reference [44] for all other azaBODIPYs that were synthesized during this thesis.

2.4.2.3.2 Bromine-substituted azaBODIPYs **48** and **52**

## 2.4.2.3.2.1 Steady-state characterization

Both bromine-substituted azaBODIPYs **48** and **52** show good photophysical properties with

molar absorption coefficients of  $55\,000\text{ M}^{-1}\text{ cm}^{-1}$  (azaBODIPY **52**) and  $66\,600\text{ M}^{-1}\text{ cm}^{-1}$  (**48**) respectively, absorb and emit in the far red/NIR and possess good to large Stokes shifts of 56 and 38 nm. Their spectra in DMSO are shown in Figure 124.

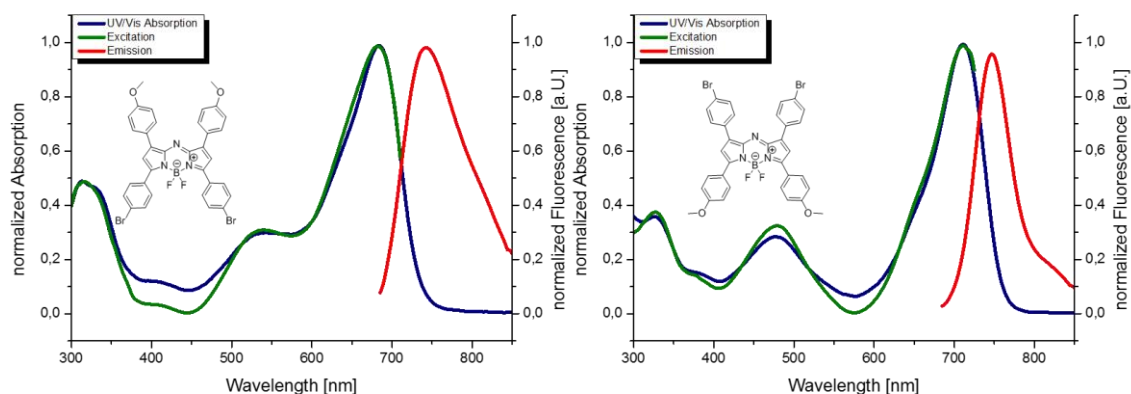


Figure 124: Absorption (blue), excitation (green) and emission spectra (red) for (**52**, left) and (**48**, right) in DMSO. Spectra were recorded at  $\sim 10^{-6}\text{ M}$  concentrations

Although the spectra resemble each other, an obvious difference is visible to the naked eye when looking at the two compounds in solution: whereas **52** (methoxy in 1,7-phenylic position) is of a strong blue color, the isomer **48** is green (Figure 125).



Figure 125: Comparison of azaBODIPY **52** (left) and azaBODIPY **48** in DCM

This can be attributed to a more efficient push-pull effect. Vicente investigated this behavior on azaBODIPY **44** in 2014 [215], their simulations showed greater orbital-coefficients for the 3,5-positions of simple azaBODIPYs than for the 1,7-positions (Figure 126).

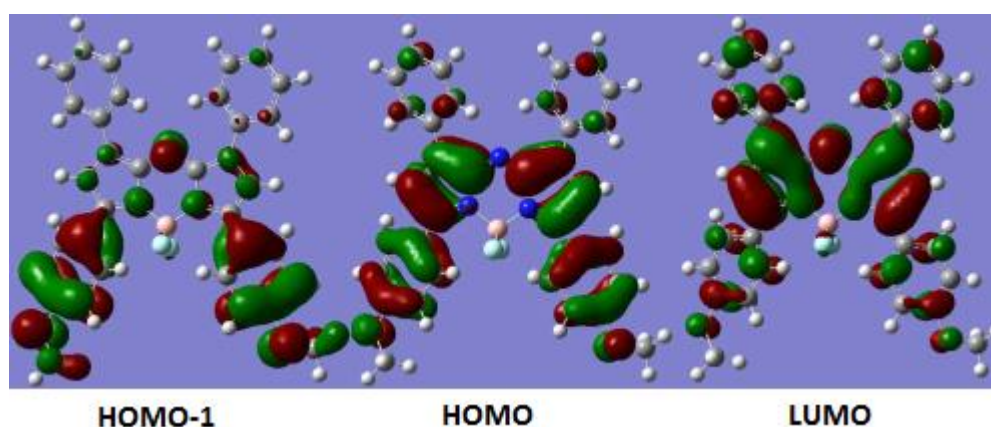


Figure 126: Frontier orbitals of aza-BODIPY **44** [215]

A methoxy-substituent in the 3,5-positions has therefore a greater effect on the optical properties than in the 1,7-positions. Compared to an unsubstituted tetraphenyl-azaBODIPY the absorption maximum of azaBODIPY **52** thus experiences a smaller bathochromic shift than the isomer **48**. This results in **52**'s blue color, compared to the green of **48** where a bigger part of the maximum-peak is “hidden” outside of the viewing capacity of the naked eye.

#### 2.4.2.3.2 Time resolved photophysical characterization

Both the compounds **48** and **52** are currently being investigated by a collaboration of ours (Dr Sofia Garakyraghi of Prof. Felix N. Castellano's group at North Carolina State University). Preliminary results show a marked difference in fluorescence lifetimes of the two investigated compounds. They found excited state lifetimes of 3.2 ns (azaBODIPY **48**) and 1.4 ns (azaBODIPY **52**) respectively (Figure 127).

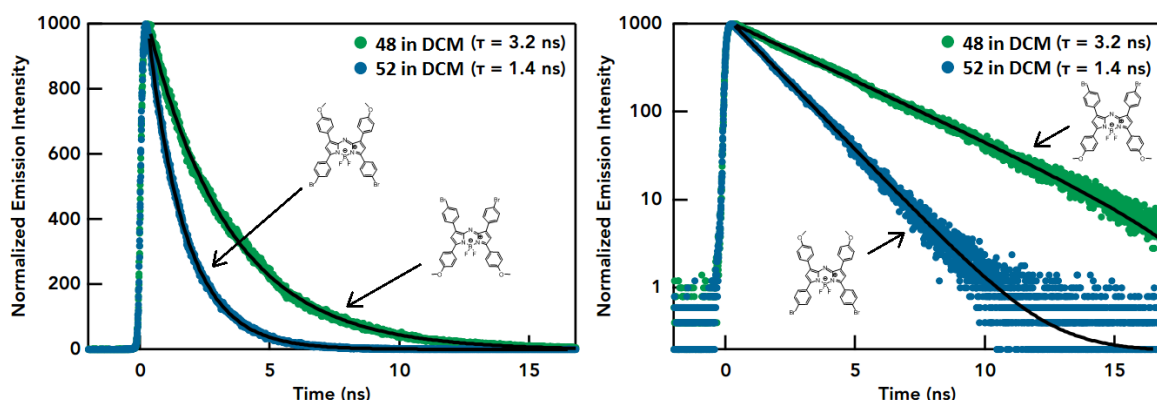


Figure 127: Fluorescence lifetime measurements of **48** and **52** in DCM. Green shows azaBODIPY **48** (methoxy substituent in the 3,5-phenylic positions), blue azaBODIPY **52** (methoxy-substituent in the 1,7-phenylic positions). Left: Y-values plotted linearly, right: logarithmic plot. Both graphs show the same data.

For two compounds that are this similar one to another this difference is remarkable. Interestingly, the excited state lifetimes correlate well with the observed quantum yields of 23% (azaBODIPY **48**) and 13% (azaBODIPY **52**). This indicates that the bromine in the 3,5-phenylic positions speeds up nonradiative relaxation processes. This is consistent with the simulations executed by Vicente that show that for the 3,5-phenylic substituents the frontier orbitals have greater orbital coefficients (Figure 126 and [215]).

The investigations are still ongoing and expected to yield further insight into the studied systems' photophysical properties.

#### 2.4.2.3.3 Overview and conclusion

From the data that we obtained so far, several general trends are discernable:

- an electron donating group in the 3,5-phenylic positions results in an absorption maximum that is bathochromically shifted compared to its 1,7-phenylic counterpart.
- the influence of a bromine atom on the spectral properties appears limited
- electron donating groups in the 3,5-phenylic positions result in lower Stokes-shifts than in the 1,7-phenylic positions
- the quantum yields of **44** and **48** are very similar; between the two bromine substituted azaBODIPYs **48** and **52**, **48** possesses a higher quantum yield and brightness.

For these reasons **44** and **48** were the compounds that were retained for further development of the platform.

### 2.4.3 E-azaBODIPY : Second system

Using the azaBODIPY **48** the boron-functionalization was attempted using 3-dimethylaminopropyne. When *t*BuLi was used to activate the alkyne the reaction exhibited overall poor reactivity (reaction times of several hours were required to observe the formation of traces of product) and very unclear results (Figure 128).

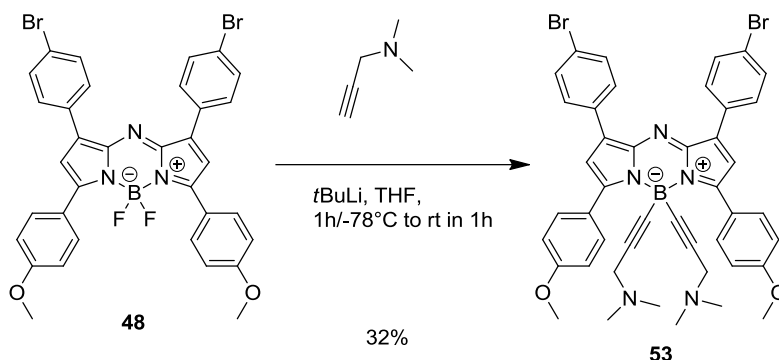


Figure 128: Boron functionalization of azaBODIPY **48** using organolithium agents

This can be explained by the strong tendency of organolithium reagents to form oligomers. The inverse correlation between degree of aggregation and their reactivity is well known [257–259]. Having a coordinating ligand such as dimethylpropargylamine in the reaction mixture may privilege the formation of tetra- or oligomeric lithiates and stabilize the compounds against dissociation, resulting in very poor reactivity.

Grignard reagents are known as an efficient alternative to lithium derivatives for introducing alkyne groups on boron of BODIPYs. Despite the non-reactivity displayed in the functionalization of **38**, we transformed the dimethylamine propyne into the corresponding Grignard-reagent using EtMgBr. To our delight, the Grignard reagent then reacted with the azaBODIPY and yielded the desired product without formation of side products (Figure 129).

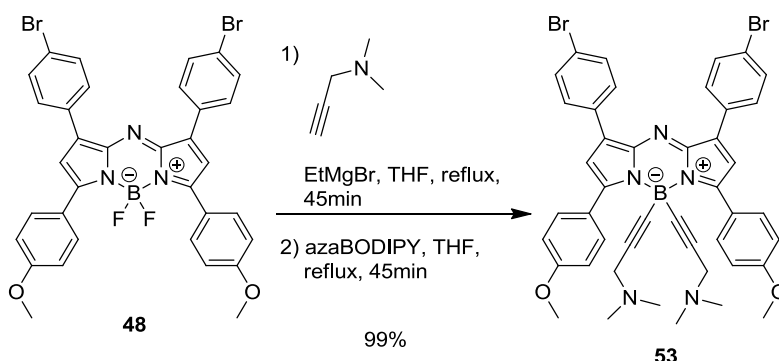


Figure 129: Improved synthesis of boron-functionalized azaBODIPYs using Grignard-agents

Improving on the synthesis of the starting material and using only minimal excesses of Grignard agents we were able to push the yields to almost 100% at the 0.5 g scale. The obtained product can be used further after a simple aqueous washing that aims at removing the magnesium salts. The boron-substituted compound **53** was transformed into the corresponding carboxylic acid by reaction with bromoacetic acid. Using dry chloroform, we

hoped that monoacid would precipitate due to the formation of charged ammonium species. In fact, what we did observe was that the mono-substituted compound **54** only just remains in solution. However, upon reaction with a second equivalent of bromoacetic acid the compound **55** precipitates and pulls the equilibrium. This results in significant amounts of double substituted product **55** (Figure 130).

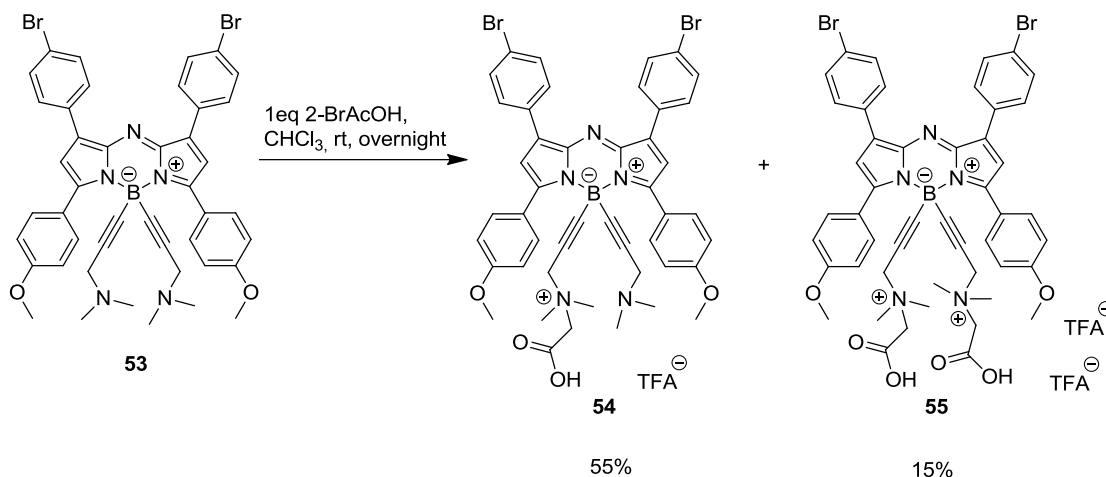


Figure 130: Desymmetrization of azaBODIPY **53** using 1 equivalent of bromoacetic acid

The product mixture had to be purified using semi preparative HPLC. We were pleased to see that the compound did not show any of the unfavorable solubility-behavior of their 1,7-phenolic counterparts (azaBODIPY **31**, **40**). Compound **54** was well soluble and did not pose any major challenge during the purification; the separation of mono- from diacid proceeded smoothly as can be seen in the  $^1\text{H}$  NMR spectrum shown in Figure 131.

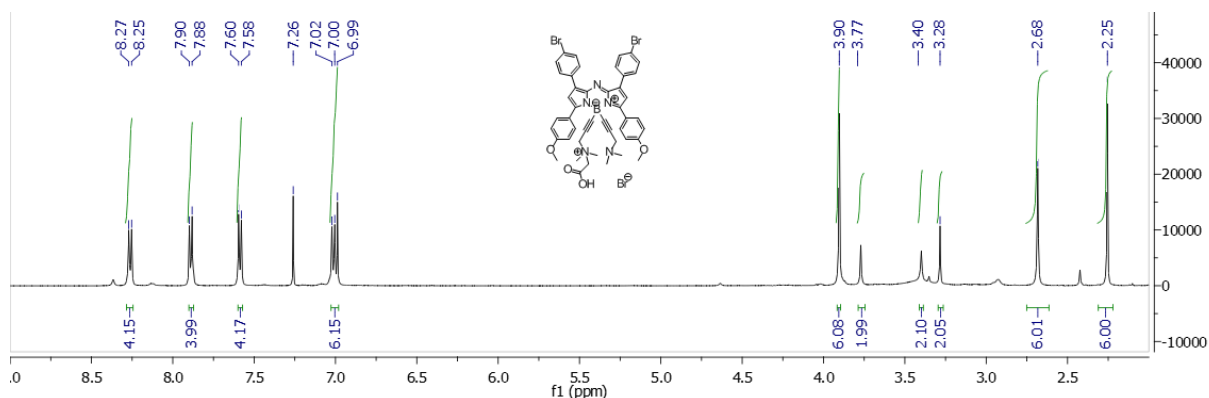


Figure 131:  $^1\text{H}$ -NMR-spectrum of the successfully desymmetrized azaBODIPY **54**. The NMR was recorded in  $\text{CDCl}_3$  at 500 MHz

Having the acetic acid derivatives in hands, we attempted peptidic coupling-reactions in order to react the compound with amines. Using benzylamine as a model compound, we succeeded in introducing two moieties into diacid **55** (Figure 132).

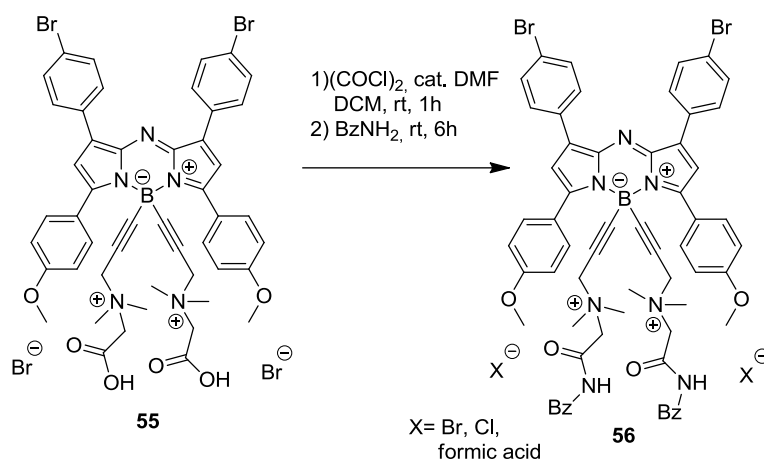


Figure 132: Reaction of azaBODIPY **55** with benzylamine

The attempt to couple a bulkier substituent, such as the previously used TOTA-Boc did not succeed, not even when coupling agents such as HBTU were employed. This might be explained by the close proximity of the acid function to the rest of the molecule which leads to steric hindrance and prevents efficient nucleophilic attacks on an activated carboxylic acid.

To remedy this problem, we tried to use 4-(bromomethyl)benzoic acid to increase the distance between the plane of the molecule and the carboxylic acid function (Figure 133).

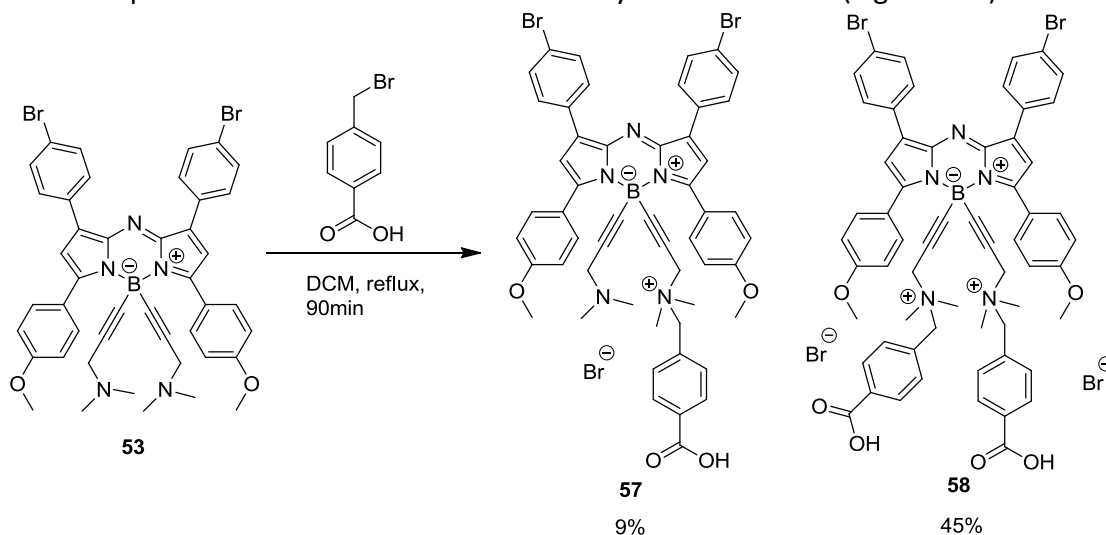


Figure 133: Desymmetrization of azaBODIPY **53** using 4-(bromomethyl)benzoic acid

Using one equivalent of acid, the reaction gave rise to both the mono(**57**)- and the disubstituted (**58**) products. Their separation was however quite simple: the disubstituted product **58** precipitates in DCM whereas the monosubstituted azaBODIPY **57** stays (in its majority) in solution. Repeated washings with DCM removes the mono-acid and unreacted 4-(bromomethyl)benzoic acid from the precipitate.

Using the diacid we executed a number of small-scale tests of the activation and amid-formation using TOTA-Boc to determine viable conditions (Figure 134).

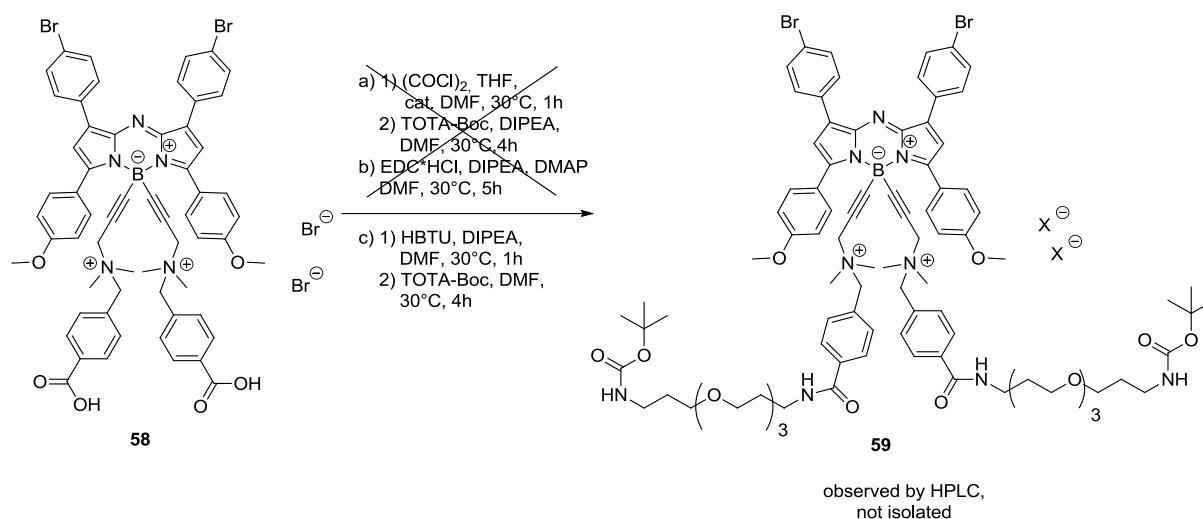


Figure 134: Successful activation of **58** and conjugation to TOTA-Boc

The activation of the carboxylic acid functions was attempted using oxalyl chloride, EDC and coupling agents for peptide synthesis. The attempts using oxalyl chloride or EDC did not result in the desired reactivity. The use of coupling agents then resolved this issue and permitted the formation of TOTA-containing amides in good yields. The compound was however never isolated due to the decision to switch to a bromine-free azaBODIPY. Indeed, the study was carried out with the two fluorophores **44** and **48** in parallel, and some tests - not reported in this manuscript – revealed the difficulty of functionalizing the bromine position.

[The photophysical properties of all isolated compounds were characterized in DMSO. The results are shown and discussed in detail in the section 2.4.6. - Photophysical characterization of E-azaBODIPYs and precursors]

#### 2.4.4 Third system: 1,7-di(phenyl)-3,5-di(methoxyphenyl) E-aza-BODIPYs

We applied the strategy optimized for the bromine-substituted derivative **48** (see section 2.4.3) with the 3,5-di(methoxyphenyl)-azaBODIPY **44**. We were able to isolate the boron-functionalized azaBODIPY **60** in excellent yield. A simple purification over a silica gel plug using EtOAc is required to remove the impurities that are formed during the reaction (Figure 135).

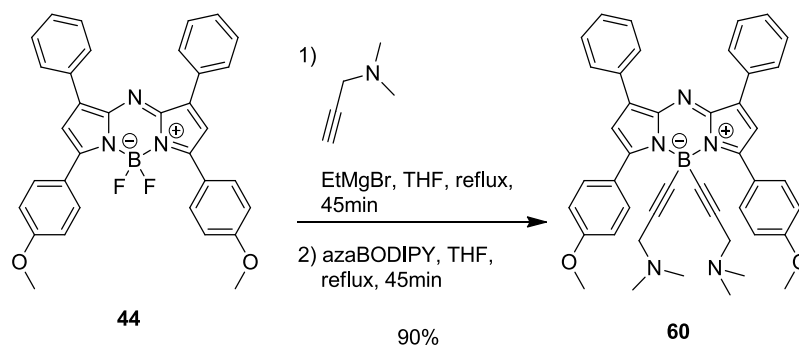


Figure 135: Introduction of 3-dimethylamino propyne onto azaBODIPY **44**

In the next step, we “desymmetrized” the B-substituted compound by addition of 4-(bromomethyl)benzoic acid (Figure 136). The use of DCM led to a major formation of double substituted product **62**. Any attempt at purification by semi preparative HPLC or automated Flash-chromatography resulted in failure as both the mono- and the diacid elute at exactly the

same time and are thus inseparable by RP-chromatography. Since we were interested in obtaining the mono-substituted compound, we tried other solvents. The best results were obtained using THF in strong dilution.

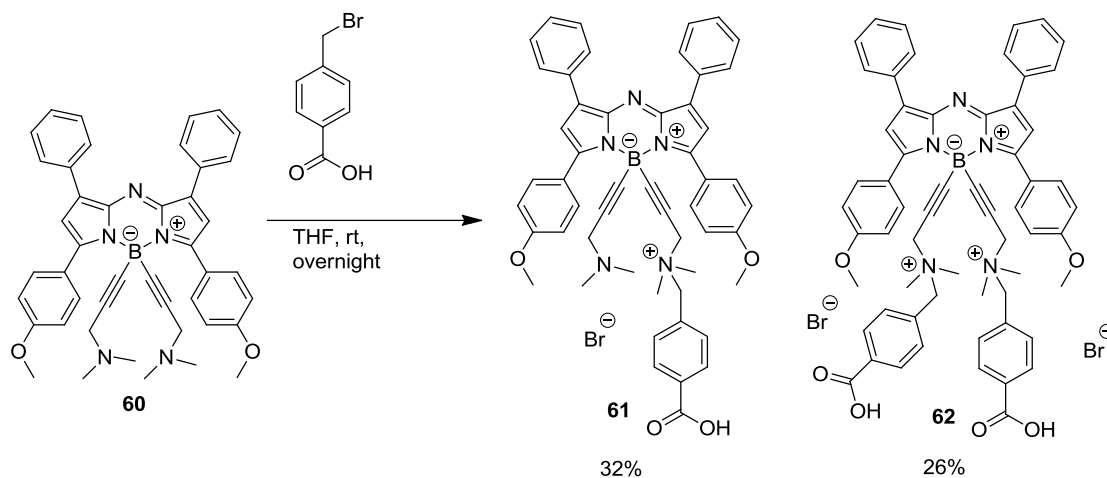


Figure 136: Desymmetrization of azaBODIPY **60** by reaction with 4-(bromomethyl)benzoic acid

The separation of the two products is difficult; after numerous attempts the best method that we found takes advantage of the difference in solubility in boiling THF to isolate pure **62** and contaminated **61**. The contaminated fraction can then be purified by column chromatography on silica gel using methanol and formic acid as eluent.

Although the general methodology remained unsatisfactory it enabled us to separate and isolate both compounds in sufficient amounts to proceed onwards. Moreover, this procedure permits the isolation of very pure monoacid which is the key-intermediate that is henceforth required for the synthesis of asymmetric, boron substituted azaBODIPYs.

If the objective is to exclusively isolate the double substituted azaBODIPY, the starting material needs to be reacted with more than two equivalents of 4-(bromomethyl)benzoic acid in presence of a carbonate base (Figure 137). A base is required in order to prevent spontaneous protonation of the second amine. The choice of base is important as well: when carbonate is used the diacid is formed (and can be isolated as described previously), the use of organic bases such as triethylamine led to the formation of the ester **63**.

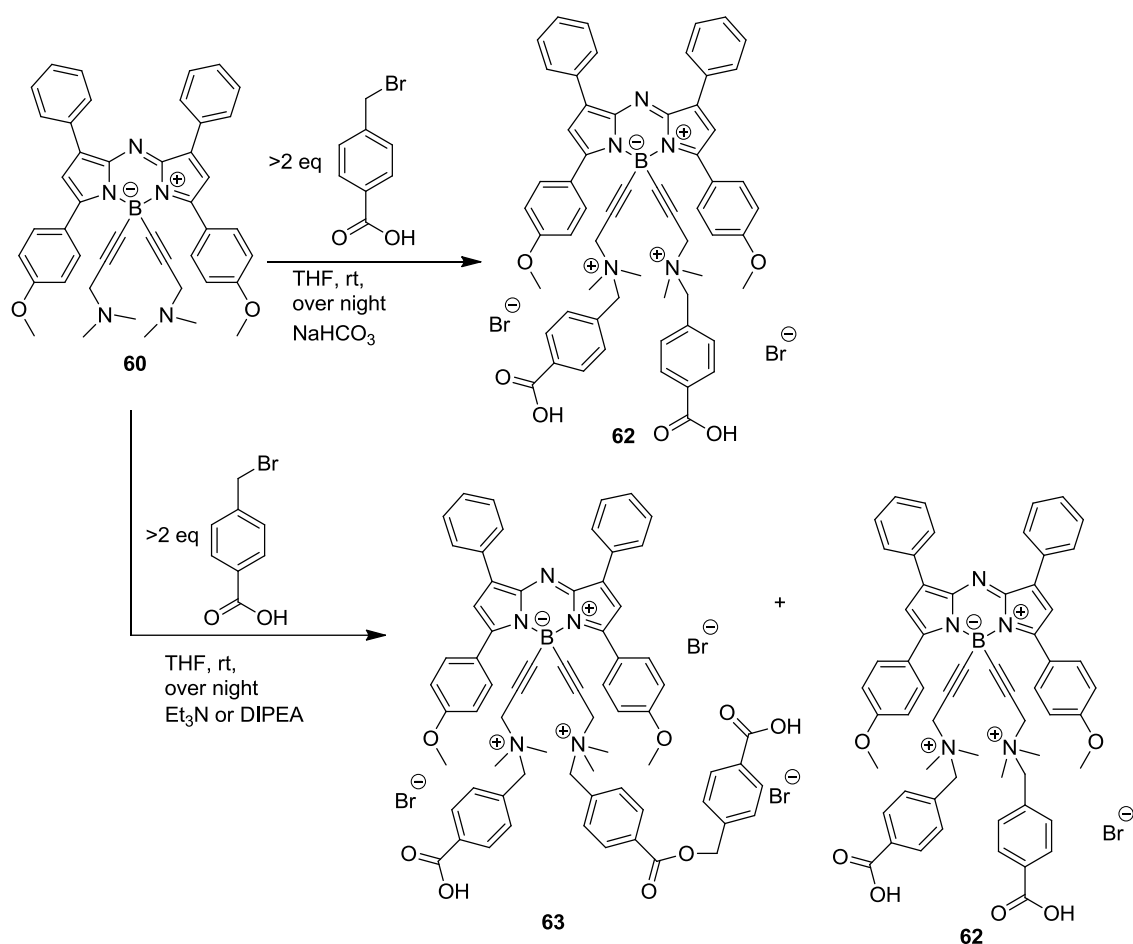


Figure 137: Introduction of 4-methyl benzoic acid as handle for further functionalization

In order to isolate the pure diacid **62** from this mix, the mixture has to be refluxed with dilute hydrochloric acid to hydrolyze the ester **63**. When bases such as KOH or NaOH were used the azaBODIPY core lost the boron moiety.

In the next step, monoacid **61** was activated using coupling agents to form the TOTA-Boc azaBODIPY **64** (Figure 138). HBTU or TSTU were used to carry out this reaction, both coupling agents yielded the desired product. We obtained less consistent results when using HBTU (compared to TSTU). The use of HBTU occasionally required the addition of the coupling agent in a large excess (up to 5 equivalents) in order to push the reaction to completion; TSTU on the other hand reliably yielded the desired product with only small excesses of coupling agent.

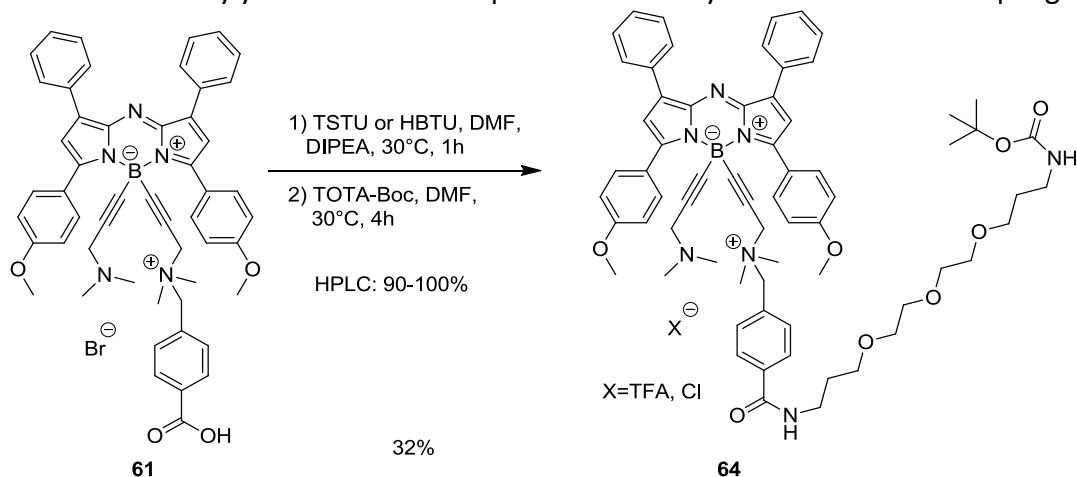


Figure 138: Synthesis of Boc-spacer containing azaBODIPY **64**

The compound can be purified using either normal phase column chromatography on aluminum oxide or semi preparative RP-chromatography. While the reaction control indicates reaction yields of 90-100%, we were only able to isolate 32% of the product.

This azaBODIPY can then be used as a platform through addition of functions to the amine, followed by hydrolysis and activation of the TOTA-Boc in order to obtain a bioconjugable compound. This proof of concept was executed using hydrosolubilizing groups.

For the hydrosolubilization, the tertiary amine was quaternized using two different approaches:

- first by use of methyl iodide
- second by use of propane sultone.

The alkylation is carried out at room temperature in presence of a carbonate base ( $\text{NaHCO}_3$ ) to ensure that any protonation that may have happened during earlier purification processes is reversed. Once HPLC-MS indicates that the reaction is complete, the Boc-group can be hydrolyzed using 1M HCl (Figure 139).

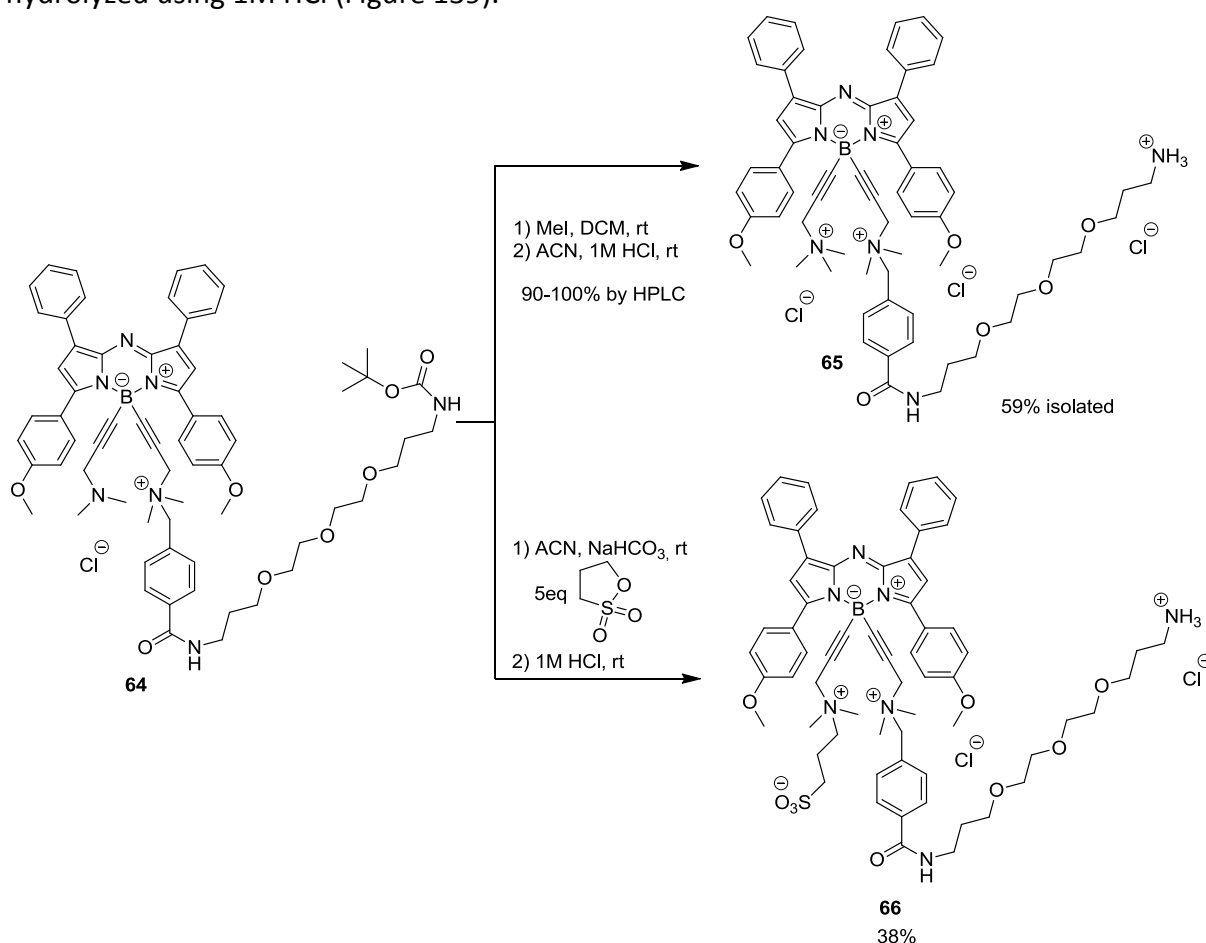


Figure 139: N-quaternization of azaBODIPY **64** using methyl iodide (top) and propane sultone (bottom)

The removal of MeI is straightforward: simple evaporation is sufficient to remove the alkylating agent. The alkylation by propane sultone on the other hand is very slow and incomplete after 6h, even when the reaction is refluxed. We therefore engaged an excess of propane sultone. In order to deactivate the excess of propane sultone to prevent alkylation of the TOTA after removal of Boc two strategies were tested. The use of ammonia for deactivation resulted in deboration of the desired compound **66**. Using 1M HCl instead worked

just fine as the newly formed amine was directly protonated, rendering it inert towards attack by the alkylating agent.

Both compounds are hydrophilic (the sulfobetained compound **66** is extremely hygroscopic: drying by lyophilization did not succeed in total removal of water). Thus we decided to investigate the possibility of introducing a bioconjugatable handle before evaluating their photophysical properties.

The photophysical properties of all isolated compounds were characterized in DMSO. The results are shown and discussed in detail in the section 2.4.6. - Photophysical characterization of E-azaBODIPYs and precursors.

### 2.4.5 Activation of the compounds for bioconjugation

The first bioconjugation-agent that we tried out was the same as previously, PDITC). As for hydroxy-azaBODIPY **34** the reaction of PDITC and **65** proceeded smoothly as indicated by HPLC, but again the removal of excess PDITC from the resulting compound proved extremely difficult (Figure 140).

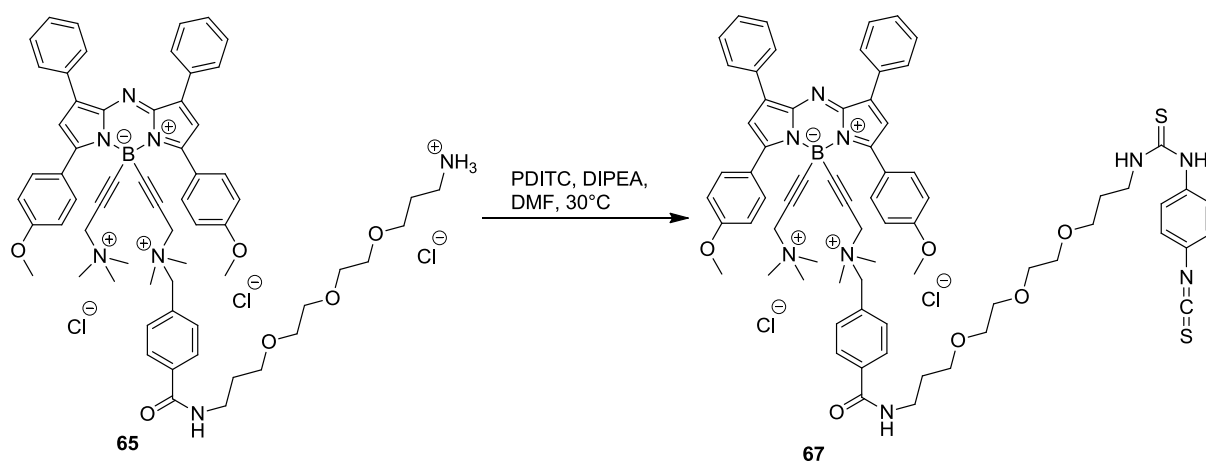


Figure 140: Activation of azaBODIPY **65** using PDITC

When injected into a semi preparative HPLC we observed the same behavior as before for **35**: the compound precipitated and clogged the HPLC. A purification on normal phase silica gel or aluminum oxide was rendered impossible as the compound did not migrate at all, even when harsh conditions (MeOH, MeOH+formic acid, MeOH+HCl DMF, DMSO and combinations thereof) were employed. We did manage to isolate 3 mg by using preparative thin layer chromatography (TLC) with MeOH+formic acid as eluent, but even then, the compound did not migrate but had to be isolated from the TLC-start.

In order to reduce the impact of the grafting function we looked for an alternative linker. A wide choice of different molecules and functions exist that have been tested and used for bioconjugation and *in vitro/in vivo* applications. Koniev and Wagner published an extensive review on the virtues and disadvantages of existing activation and bioconjugation methods [229].

Our requirements for the new grafting function were straightforward: the chosen compound should be hydrophilic, polar or charged and not undergo stacking with aromatic systems that

are present. Due to good experiences in Dr. Goncalves' group we identified diethylsquarate as promising linker. Indeed, squarates form stable bonds with amines, yielding bonds that behave like amides. Their small molecular mass and high polarity enable the formation of hydrogen-bonds to polar solvents such as water. They display good resistance towards acids and bases [260] and permit the use of nontoxic solvents such as ethanol during the activation process. In addition to that the monoamine squarate shows a marked difference in reactivity compared to the diethyl squarate which limits the reaction of a second probe with the bioconjugation handle. All these properties make this compound an easy-to-handle amine-activating group.

The activation procedure is straightforward: the starting material is solubilized in EtOH in presence of a base to ensure that the amine is deprotonated, followed by addition of an excess of diethylsquarate. 5 equivalents of the squarate are sufficient to ensure a clean reaction. The activation is slightly slower than with PDITC and requires slight heating.

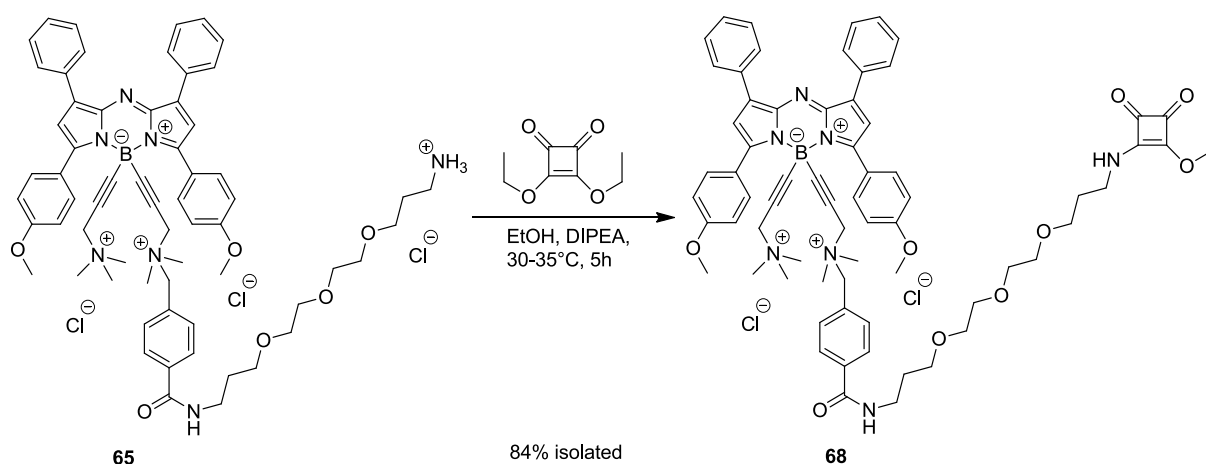


Figure 141: Activation of azaBODIPY **65** using diethyl squarate to obtain bioconjugable azaBODIPY **68**

After the activation compound was purified without any trouble using RP-semi preparative HPLC to remove excess squarate. When the reaction was repeated with reaction temperatures maintained at 30-35°C, excellent yield (84%) can be obtained (Figure 141). The same procedure was applied to the sulfonated derivative **66**: again, the reaction temperature was kept at 30-35°C both during the reaction and solvents were removed. This resulted in an activation yield of 85% after purification and ion exchange (Figure 142).

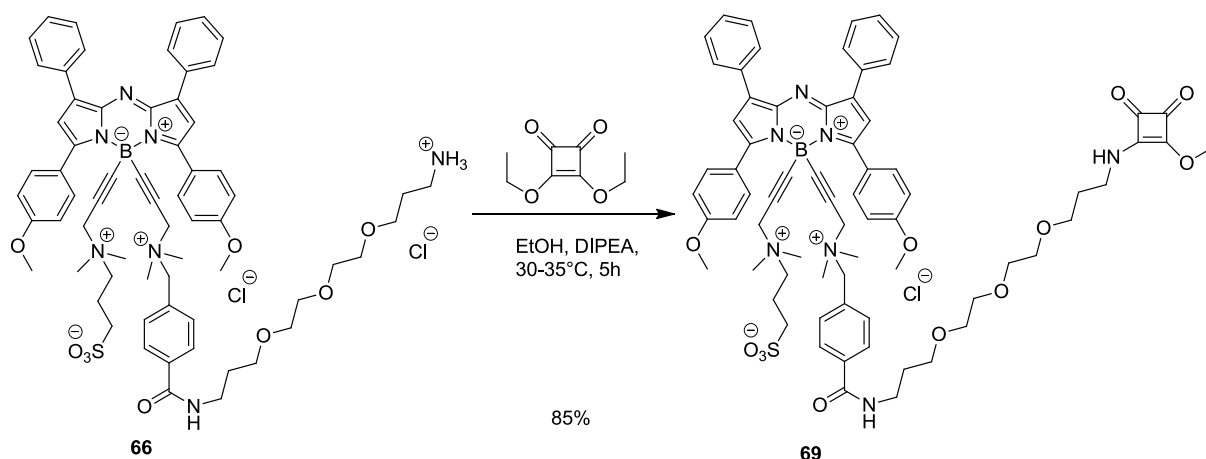


Figure 142: Activation of azaBODIPY **66** with diethylsquarate

The photophysical properties of all isolated compounds were characterized in DMSO. The results are shown and discussed in detail in the next section.

The azaBODIPYs obtained this way were then used for bioconjugation to tag antibodies (see chapter 2.5.2).

## 2.4.6 Photophysical characterization of E-azaBODIPYs and precursors

All E-azaBODIPYs that we obtained as well as their respective precursors were characterized by UV/Vis and Fluorescence spectroscopy in DMSO. The compounds destined for bioconjugation as well as their precursors **65** and **66** were also characterized in PBS to investigate their optical properties, as well as their solubility and stacking behavior in aqueous solutions. As beforehand azaBODIPY **44** was used as the quantum yield reference. The characteristics are summarized in Table 15.

Table 15: Photophysical properties of E-azaBODIPYs synthesized in this chapter. azaBODIPY **44** in CHCl<sub>3</sub> is used as the QY-reference [44]. Compounds were excited at 670nm

compound	Solvent	$\lambda_{\max}$ , Absorption [nm]	$\epsilon_{\lambda_{\max}}$ [M <sup>-1</sup> cm <sup>-1</sup> ]	$\lambda_{\max}$ , Emission [nm]	QY	Brightness $\Phi \times \epsilon_{\lambda_{\max}}$ [M <sup>-1</sup> cm <sup>-1</sup> ]	$\Delta\lambda$ [nm]	Stokes- Shift [cm <sup>-1</sup> ]
<b>30</b>	DMSO	678	41 900	749	4%	1 510	71	1 398
<b>38</b>	DMSO	668	77 400	704	10%	7 350	36	766
<b>37</b>	DMSO	668	44 600	754	3%	1 280	86	1 707
<b>48</b>	DMSO	711	66 600	749	23%	15 570	38	714
<b>53</b>	DMSO	700	77 900	735	18%	13 640	35	680
<b>54</b>	DMSO	700	78 500	735	29%	22 580	35	680
<b>55</b>	DMSO	704	83 200	738	33%	27 420	34	654
<b>57</b>	DMSO	700	77 300	735	20%	15 470	35	680
<b>58</b>	DMSO	704	74 200	739	29%	21 360	35	673
<b>44</b>	DMSO	702	86 700	738	27%	23 740	36	695
<b>60</b>	DMSO	693	71 400	725	18%	13 170	32	637
<b>61</b>	DMSO	691	80 400	724	20%	16 290	33	660
<b>62</b>	DMSO	694	61 500	727	27%	16 600	33	654
<b>64</b>	DMSO	691	62 700	724	22%	13 520	33	660
<b>65</b>	DMSO	696	58 800	726	32%	18 860	30	594
<b>65</b>	PBS	673	50 500	714	6%	3 230	41	853
<b>68</b>	DMSO	694	64 900	728	30%	19 330	34	673
<b>68</b>	PBS	677	51 400	715	5%	2 760	38	785
<b>66</b>	DMSO	703	79 700	731	41%	32 390	28	545
<b>66</b>	PBS	676	51 600	712	9%	4 690	36	748
<b>69</b>	DMSO	703	48 500	731	34%	16 300	28	545
<b>69</b>	PBS	682	30 300	717	6%	1 760	35	716

When looking at the data shown in Table 15, it is evident that indeed the introduction of alkyne substituents to the boron atom of the azaBODIPY does not adversely influence the photophysical properties of the obtained compounds. All three systems (hydroxy-azaBODIPY as well as 1,7-di(bromophenyl)-3,5-di(methoxyphenyl) 1,7-di(phenyl)-3,5-di(methoxyphenyl) substituted azaBODIPYs) retain the photophysical properties of their parent compounds.

### 2.4.6.1 1,7-Di(phenol)-3,5-di(phenyl)-E-azaBODIPYs

Both hydroxy azaBODIPYs **30** and **37** display molar absorption coefficients of ~42 000 and ~45 000 M<sup>-1</sup> cm<sup>-1</sup> and quantum yields of 4 and 3%. The absorption maximum of **37** experiences a slight hypsochromic shift (-10 nm compared to **30**), its emission maximum is

bathochromically shifted (+5 nm). The spectra of both compounds show very large peaks for both the absorption as well as emission spectra (Figure 143). The introduction of the alkyne-substituent results in an even larger Stokes-shift of 86 nm. This behavior may be advantageous for imaging-applications. When the Stokes shift of the used fluorophore increases the spectral overlap of absorption and emission spectra decreases. This results in very small auto-absorption of emitted photons. The other advantage is the possibility to use less expensive spectral filters.

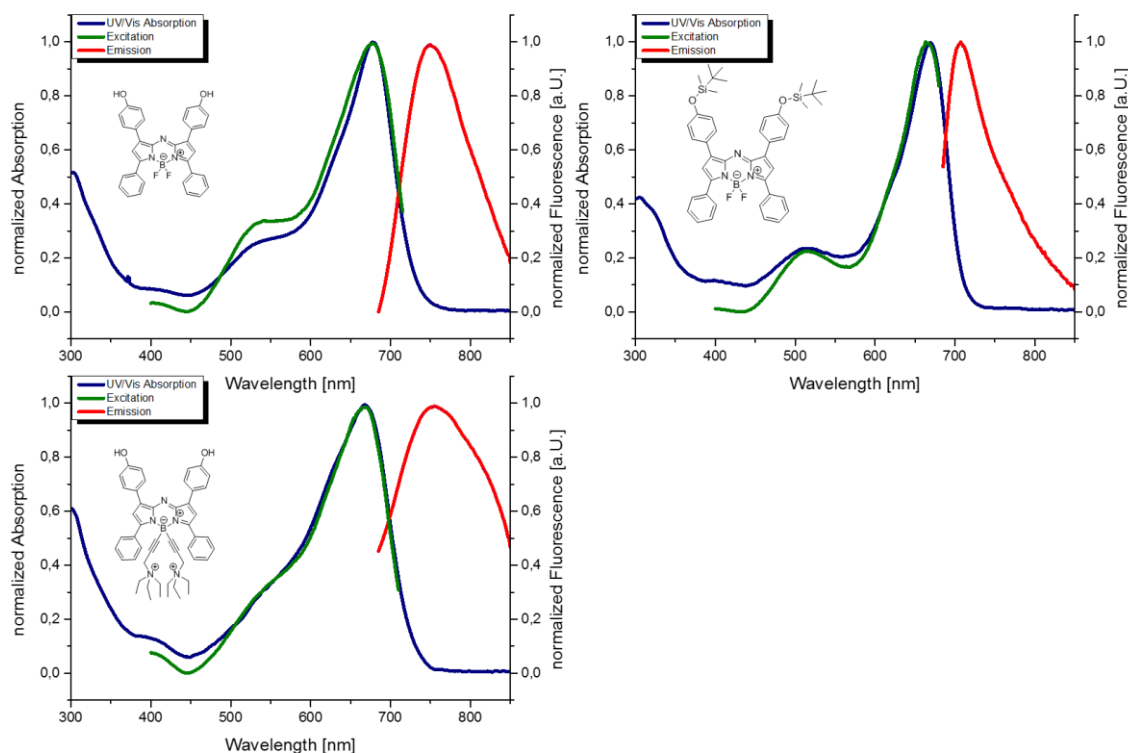


Figure 143: Absorption and Emission spectra of **30** (top left), **37** (bottom left) and **38** (top right) in DMSO. Blue: absorption, Green: excitation, Red: fluorescence. Spectra were recorded at  $10^{-6}$  M concentrations

The comparison of either **30** or **37** to the TBDMS-protected derivate **38** shows that the protection of the hydroxy groups improves all optical properties significantly. The molar absorption coefficient nearly doubles (from  $41\,900\text{ M}^{-1}\text{ cm}^{-1}$  for **30** to  $77\,400\text{ M}^{-1}\text{ cm}^{-1}$  for **38**), the quantum yield increases to 10% and both the maximum absorption and emission bands become thin (Figure 143). The Stokes shift reduces to 36 nm.

All these changes confirm that indeed the free hydroxy groups are responsible for the unfavourable photophysical properties. If we had not succeeded in developing the entirety of our platform around the boron-functionalization the masking of the free hydroxygroup (e.g. by propane sultone) would have been a viable option to improve the optical properties of the hydroxy-azaBODIPY series.

#### 2.4.6.2 1,7-Di(bromophenyl)-3,5-di(methoxyphenyl)-E-azaBODIPYs

The bromo-methoxy substituted compounds **53**, **54**, **55**, **57** and **58** all display excellent optical properties. The introduction of the aliphatic alkyne substituent does not change the form of neither absorption nor emission spectra of any of the compounds. Both absorption and emission bands of all boron-substituted compounds are slightly thinner than **48**'s. Aside from that all spectra remain basically the same as for the starting material azaBODIPY **48** (Figure 144).

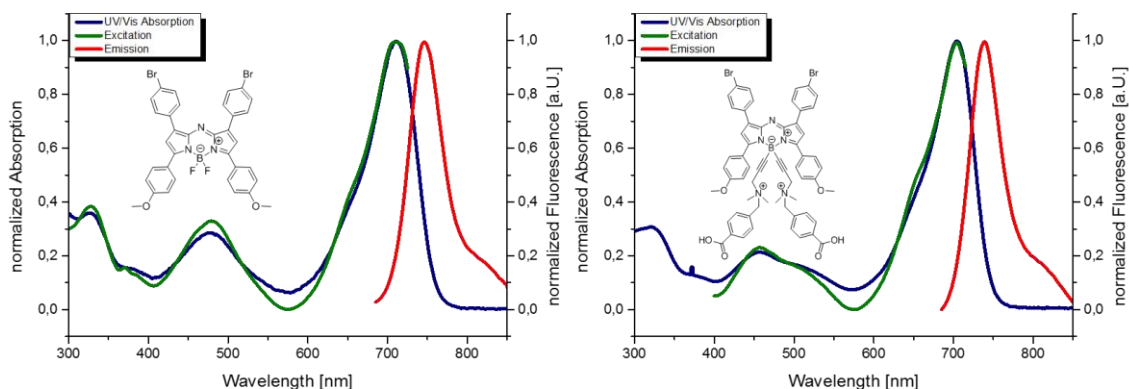


Figure 144: Absorption and Emission spectra of **48** (left) and **58** (right) in DMSO. The spectrum of **58** (right) is representative for **53**, **54**, **55** and **57**. Blue: absorption, Green: excitation, Red: fluorescence. Spectra were recorded at  $\sim 10^{-6}$  M concentrations

All of the obtained compounds display molar absorption coefficients of  $74\,200\text{--}83\,000\text{ M}^{-1}\text{ cm}^{-1}$  with absorption maxima of 700 and 704 nm and emission maxima of 735–739 nm. All five compounds have higher molar absorption coefficients than their parent **48** (which has a molar absorption coefficient of  $66\,600\text{ M}^{-1}\text{ cm}^{-1}$ ). The introduction of the alkyne substituent onto the boron atom results in a hypsochromic shift of  $\sim 10$  nm for the maximum absorption and  $\sim 12$  nm for the emission (as was the case for the 1,7-diphenol-azaBODIPY **37**).

The introduction of the alkyne substituent results in a decrease of the quantum yield from 23% (for **48**) to 18% for **53**. However, upon quaternization the quantum yield is recovered: the quaternization of one of the amines leads to an increase in quantum yield to 29% (**54**) and 20% (**57**) respectively, the quaternization of the second amine results in another increase to 33% (**55**) and 29% (**58**).

#### 2.4.6.3 1,7-Di(phenyl)-3,5-di(methoxyphenyl)-E-azaBODIPYs

As for the first and second system the introduction of the aliphatic alkyne onto the boron atom of **44** causes at maximum a hypsochromic shift of the absorption maximum of  $\sim 10$  nm (azaBODIPY **61**) to approximately 695 nm and of  $\sim 13$  nm for the emission maximum to approx. 725 nm (**61**, **62**, **64**, **65**) compared to the parent azaBODIPY **44**. All synthesized E-azaBODIPYs display excellent molar absorption coefficients that are comprised between  $48\,500\text{ M}^{-1}\text{ cm}^{-1}$  (**69**) and  $80\,400\text{ M}^{-1}\text{ cm}^{-1}$  (**61**). Taken together with their respective quantum yields of 18–41% (in DMSO) this results in excellent brightnesses of ca.  $17\,000\text{ M}^{-1}\text{ cm}^{-1}$ . As observed earlier for the second system the presence of amine results in a decrease in quantum yield to 18% (**60**, two free amines) which is recovered upon quaternization of the amines (to 20% (**61**) and up to 32% (**65**); **66** displays an exceptionally high quantum efficiency of 41%). This results in quantum yields that are higher for the totally quaternized E-azaBODIPYs **62**, **65**, **68**, **66** and **69** than the starting azaBODIPY **44**. The obtained compounds display Stokes-shifts of  $\sim 32$  nm (with several exceptions such as the propane sulfonated **66** and **69** (28 nm)).

As observed earlier the introduction of the alkyne does not change the spectral characteristics such as general shape and thinness of both the absorption and the emission peak (Figure 145).

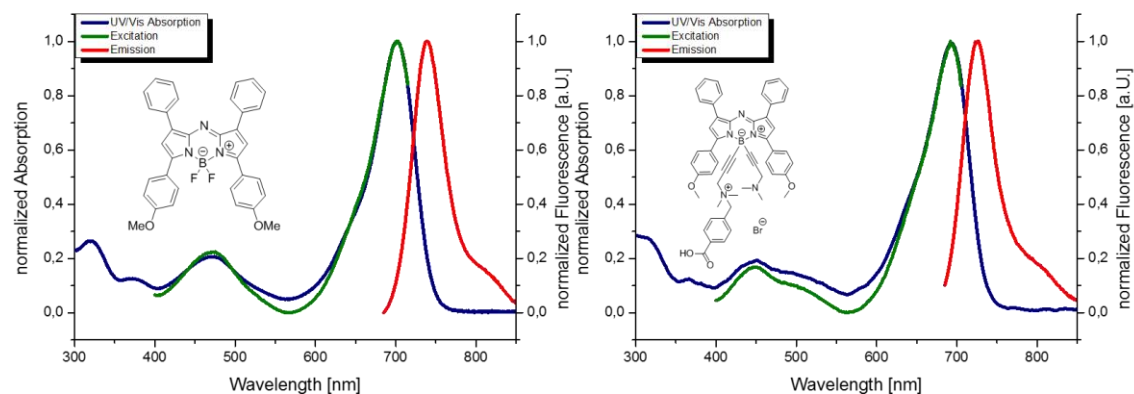


Figure 145: UV/Vis and fluorescence spectra of the model compound **44** and *E*-azaBODIPY **61**. The shown spectra are representative for all compounds obtained in this section. Spectra were recorded in DMSO at  $\sim 10^{-6}$  M concentrations

The results of all three systems validate the hypothesis that the introduction of the aliphatic alkyne does not (majorly) influence the spectral properties. This validates our hypothesis of the beginning of section 2.4.2 that the alkyne-substitution approach permits to choose the required spectral features of an azaBODIPY prior to functionalization since the introduction of substituents does not induce major changes (as opposed to e.g. the transformation of dialkylaniline-substituted azaBODIPYs into the corresponding ammonium).

#### 2.4.6.4 Photophysical properties in PBS

The bioconjugable compounds **68** and **69** as well as their precursors **65** and **66** were also characterized in PBS. The first property that we noticed during this characterization was the absence of solubility-related troubles – the preparation of PBS stock-solutions did not cause any problem.

The analysis of their spectral properties shows that the introduction of the compound into PBS results in a blue shift of the absorption maximum to ca 677 nm.

The use of PBS as solvent also causes a decrease in quantum yields to 5% (**68**), 6% (**65** and **69**) and 9% (**66**) respectively. This is expected due to a different polarity and motility of the solvent and salts which results in non-radiative relaxation into the ground state due to intermolecular collisions. (The same behavior is observed for oxygen that is dissolved in the solvent [261]) Even in PBS the bioconjugatable compounds exhibit satisfying brightnesses of  $2\,700\text{ M}^{-1}\text{cm}^{-1}$  (**68**) and  $1\,700\text{ M}^{-1}\text{cm}^{-1}$  (**69**) respectively, which is good enough for *in vitro* and even *in vivo* investigations.

The bottom left of Figure 146 shows the spectrum of **68**, which is representative of the *E*-azaBODIPYs that were analyzed in PBS. The comparison to its spectrum in DMSO shows the total absence of any stacking interaction.

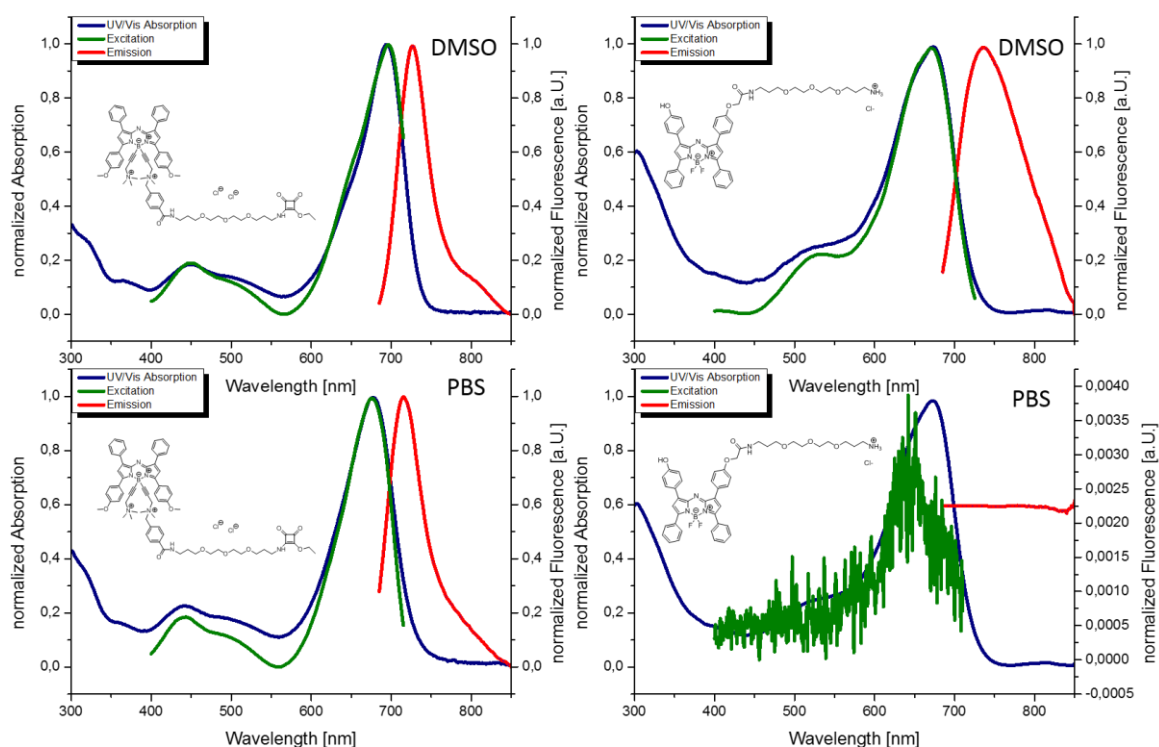


Figure 146: UV/Vis and Fluorescence spectra of *E*-azaBODIPY **68** (left) and azaBODIPY **34** (right). The spectra were recorded in DMSO (top) and PBS (bottom) at  $10^{-6}$  M concentrations. The spectral shape of *E*-azaBODIPY **68** in PBS is representative for all *E*-azaBODIPYs that we characterized in PBS.

Between the two solvents the spectral shape does not change whatsoever; no broadening of both the absorption as well as the emission peaks is discernable. The comparison of **68**'s spectra to **34** highlights the massive improvement of all aspects of the newly developed dyes. The bioconjugatable *E*-azaBODIPY **68** displays a higher molar absorption coefficient and quantum yield in PBS ( $51\,400\text{ M}^{-1}\text{cm}^{-1}$  and 5% respectively) than azaBODIPY **34** possesses in DMSO ( $50\,000\text{ M}^{-1}\text{cm}^{-1}$  and 4% respectively).

The absence of stacking even in PBS validated our second hypothesis of chapter 2.4.2. It stated that the introduction of bulky, charged substituents onto the boron atom would increase the solubility in water and prevent stacking interactions. This approach yielded a system that is superior to compounds that were developed previously in our research group such as the TrisDOTA-BODIPY **L63** shown in Figure 87 [132,222].

## 2.5 Biological investigations

In the previous section 2.4 - *E-aza-BODIPYs* we have synthesized several bioconjugable azaBODIPYs **67**, **68**, and **69** (Figure 147).

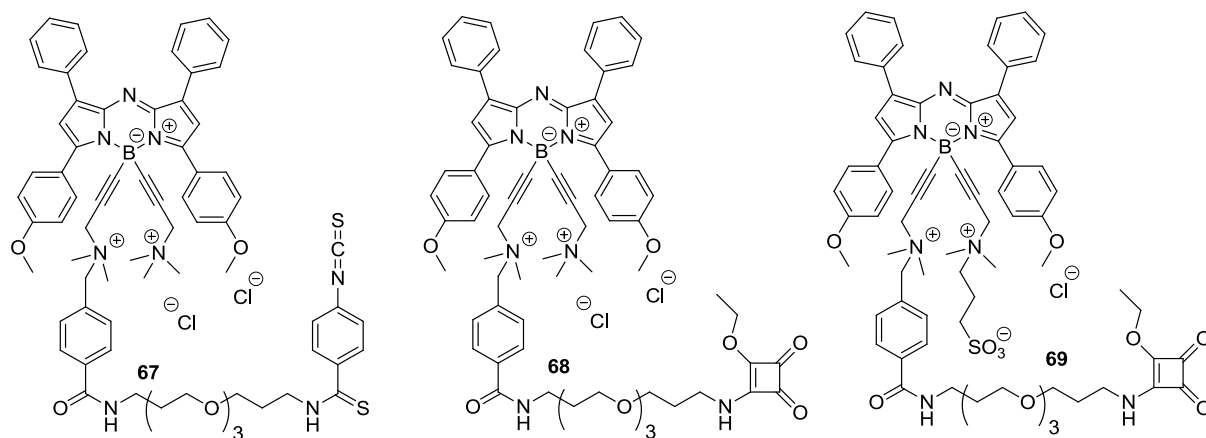


Figure 147: Activated, water-soluble, ready-to-conjugate azaBODIPYs that were obtained during this thesis

We have great hopes for the two last probes because they are synthesizable in satisfying yield and at the scale of several tens of milligrams. Having obtained these 3 compounds, we were interested to see how these probes would fare in biological systems, both *in vitro* as well as *in vivo*. In order to do so we had to choose a vector that would permit to aim our probes towards a specific target.

### 2.5.1 Choice of vector

In recent years, new treatment options have been discovered and developed until practical usability. Immunotherapy is one of these therapies, targeting the host's immune system to eliminate cancer. Indeed, as mentioned previously in the introduction (chapter 0.1), it is now well known that in order to become cancerous, cells need to acquire 10 hallmarks described by Hanahan and Weinberg in 2011 (see Figure 2)[10]. Escape to the host's immune system surveillance is one of those characteristics targeted by immunotherapies such as the antibodies (Ac) inhibiting the immune checkpoints. Immune checkpoints (i.e. PD-1, CTLA-4) are a variety of immune-inhibitory pathways that help maintain immune-homeostasis, prevent autoimmunity and control the amplitude of an immune response [262]. Blockade of these immune checkpoint has shown very impressive results in the treatments of various malignancies such as Hodgkin lymphoma, melanoma and especially in non-small cell lung cancer (NSLC, 75-80% of lung cancer cases). However, despite the strong contribution of anti-PD-1 (nivolumab) in cancer treatment, this immunotherapy is not effective in all patients, and predictive biomarkers of treatment efficacy are needed for efficient patient management. Traceable compounds (and especially theranostic compounds) can provide a valuable tool to immunotherapies that enable an early response assessment and thus improve therapy plans.



PD-L1 (also called CD274 or B7-H1) is a transmembrane protein that is the dominant inhibitory ligand for the PD-1 receptor. As shown in Figure 149, PD-L1 is expressed on type II macrophages, MDSC and the tumor itself. It plays a major role in the process of immune-evasion by tumors.

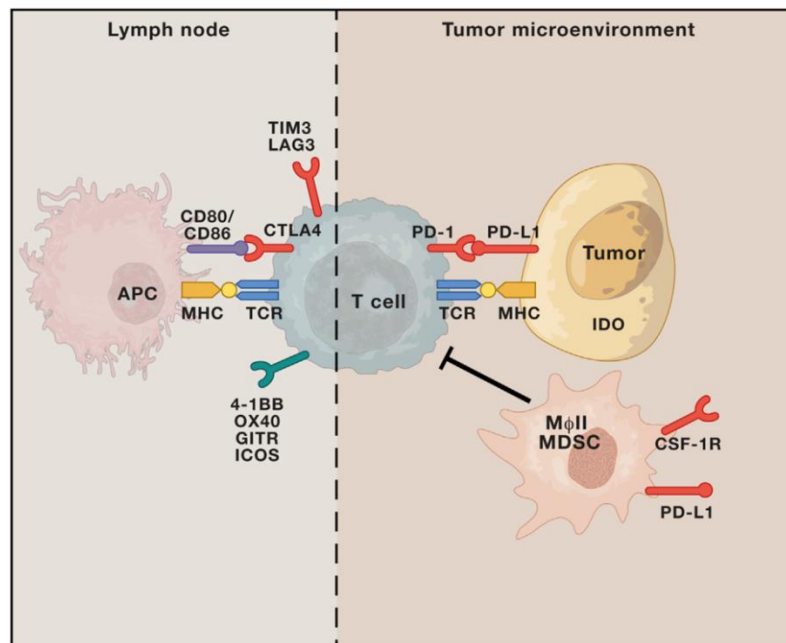


Figure 149: Mechanism of evading the immune system. Adapted from [265]

The expression of PD-L1 has been associated with bad prognosis and high aggressiveness [269] but also has predictive value in many (but not all) types of cancer [270].

Therapy targeting PD-L1 have also emerged and are in phase I clinical trials (BMS 936559, MPDL3280A), showing encouraging results [271,272].

Despite the strong contribution of these anti-immune checkpoints in the treatment of advanced cancers, 32-38% of patients treated with agents blocking the PD-1 / PD-L1 pathway will develop progressive disease [273].

The search for biomarkers and strategies to increase the response efficiency of these therapies remains a real challenge in the treatment of advanced cancers [274].

To date, no predictive biomarker for the efficacy of anti-PD-1 / PD-L1 therapies has been clearly and consensually identified. The search for tumor expression of PD-L1 in immunohistochemistry (IHC) has been proposed but does not seem to be the most appropriate for various reasons (choice of antibodies, availability of biopsies, spatio-temporal heterogeneity of PD-L1 expression, expression of other PD-1 ligands such as PD-L2). However, imaging PD-L1 non-invasively, using an antibody coupled to a fluorochrome or radioelement, seems to be the most promising way for obtaining a biomarker much more effective and reliable than the staining of PD-L1 by IHC. In addition, coupling these anti-PD-L1 antibodies with a cytotoxic agent may prove to be an interesting therapeutic strategy since they would target both the tumor cells but also immune cells, such as the myeloid cells whose role in the effectiveness these anti-immune checkpoint has just been shown [275]. We opted for the use of antibodies that block the PD-1/PD-L1 system to develop and evaluate their use in optical imaging agents.

## 2.5.2 Bioconjugation

Once we had obtained the activated azaBODIPYs (Figure 150) we attempted to conjugate those compounds to monoclonal antibodies.

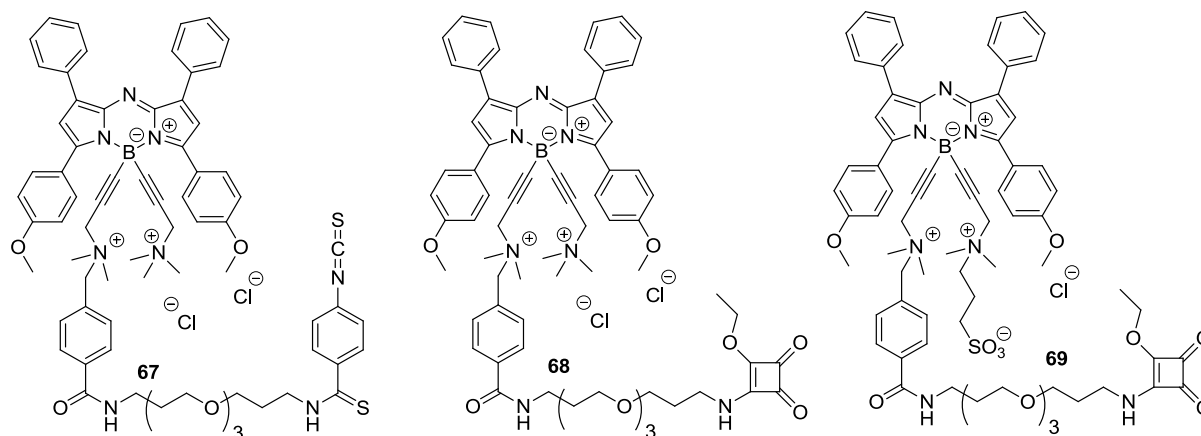


Figure 150: Activated, ready-to-conjugate azaBODIPYs that were obtained during this thesis

As targets we chose the mice-PD-L1 and mice PD-1; the corresponding antibodies are anti-PD-L1 (BioXcell) and anti-PD-1 (BioXcell) respectively. Both antibodies are IgG-antibodies and were coupled using the same conditions: the fluorophores were solubilized in DMSO and then reacted with the antibodies in carbonate buffer at pH=9.4 and 37°C. The general procedure is shown in Figure 151.

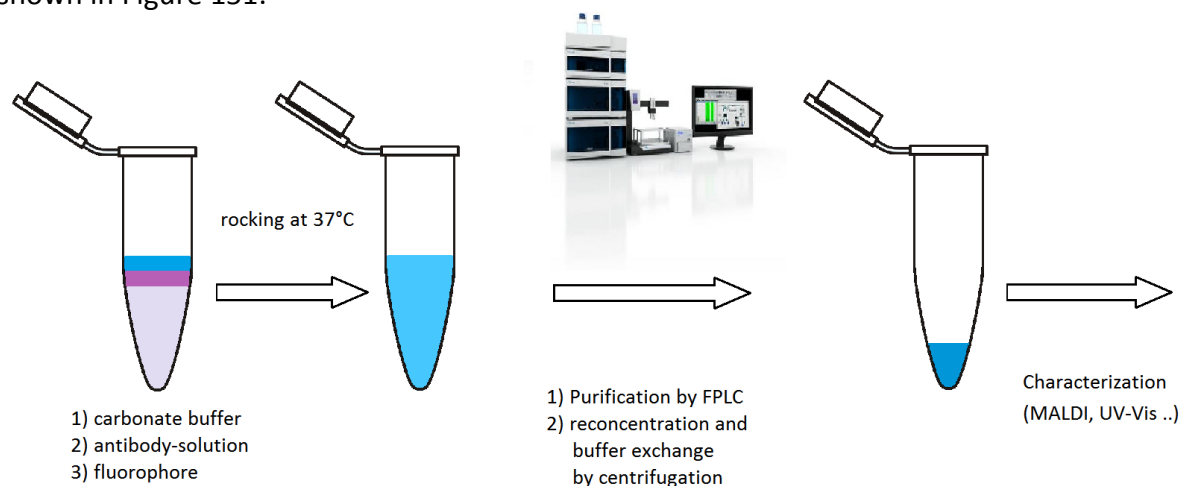


Figure 151: General steps involved in bioconjugation: Conjugation, Purification, Buffer-exchange and reconcentration

The antibodies are shipped in PBS-buffer, which meant they had to be prepared by buffer exchange against the correct buffer. All reactions took place at 37°C in the dark at a final antibody concentration of 3 mg/mL and a final fluorophore concentration of 200  $\mu$ M while not surpassing a DMSO content of 10%.

Test-runs on 100  $\mu$ g of protein were executed for each compound and antibody to determine if the chosen protocol is in general viable for this specific antibody/fluorophore combination and to establish the individual labelling efficiency of each reaction in order to permit the adjustment to amenable degrees of labelling.

### 2.5.2.1 Establishing the protocol and first attempts

#### 2.5.2.1.1 Bioconjugation of PDITC-activated azaBODIPYs **35** and **67**

We attempted bioconjugations with both PDITC activated azaBODIPYs. Just as at almost every step during synthesis of that probe AzaBODIPY **35** simply precipitated during our attempt to conjugate it to an antibody. This was ultimately the reason for our change in strategy towards the boron-functionalization.

AzaBODIPY **67** was soluble in the conjugation medium and did not precipitate during the bioconjugation. Unfortunately, during purification and buffer exchange the conjugate stuck to the membrane of the non-stick centrifugation tube which resulted in total loss of the conjugate. A second attempt where we used dialysis for reconcentration was not met with success either; these failures prompted us to modify the grafting function towards the more polar squarate linker.

#### 2.5.2.1.2 Bioconjugation of squarate-activated E-azaBODIPYs **68** and **69**

Having obtained the two new squarate-activated compounds **68** and **69** it was straightaway clear that they had far superior properties compared to their PDTIC-counterpart: they showed no signs of aggregation, were soluble in aqueous media, easily purifiable and stable towards hydrolysis. Heartened by the observed properties we repeated the conjugation on test-batches of anti-PD-L1 and obtained good results for **68**. Analysis by MALDI-TOF-Mass spectroscopy indicated that the bioconjugation using 5 and 10 equivalents of fluorophore overnight led to labelling degrees (DOL) of 0.9 and 2.6 respectively for the anti-PD-L1.

Using the same procedures we also tested sulfo-azaBODIPY **69**. Using again 5 and 10 equivalents we saw significant differences in labelling efficiency as seen in the DOL of 0.34 for 10 equivalents of azaBODIPY **69** and no labelling at all for 5 equivalents.

Although in principle this problem can be overcome by sheer quantity (e.g. reaction with 40 or 50 equivalents) of azaBODIPY **69** we decided to go ahead with the ammonium-azaBODIPY **68** as it not only shows better conjugation behavior, but is also easier to handle (far less hygroscopic) and possesses better optical properties.

These results in hand we executed a “production-batch” with 1.8 mg of antibody (anti-PD-L1) in order to isolate enough conjugate to permit *in vitro* and *in vivo* investigations. For the production-batch 10 equivalents of fluorophore were employed, resulting in a slightly lower DOL of 1.3 in 37% yield. We have no explanation for the lower DOL.

#### 2.5.2.1.3 Synthesis of a fluorophore-control

In order to have a control-antibody for the *in vitro* investigations and an *in vivo* proof of concept we decided to label the same anti-PD-L1 antibody using cyanine 5 as a reference. For this we activated cyanine 5 (provided by Prof. Anthony Romieu) as NHS-ester (Figure 152).

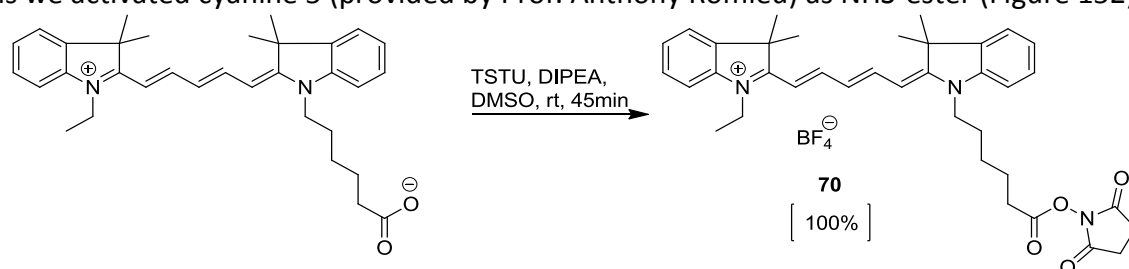


Figure 152: Activation of Cyanine 5 as NHS-ester

We followed the activation and verified the resulting compound's purity by HPLC. The activated intermediate **70** was not purified but used for bioconjugation as obtained at its reaction-concentration ( $2 \cdot 10^{-2} \text{M}$ ) and stored between uses at  $-18^\circ\text{C}$ . No degradation or changes in performance were observed over the course of 3 months and approximately a dozen freezing-thawing cycles.

The Cy5-NHS underwent the same conjugation assays as the activated azaBODIPY.

With 10 equivalents of fluorophore we obtained a DOL of 4.9, which is too high to maintain good antibody specificity. We therefore opted for the use of 4 equivalents of Cyanine 5 **70** during bioconjugation to aim at our target of approximately 2 molecules of fluorophore per antibody. Using 4 equivalents we were able to produce a production batch of Cy5-anti-PD-L1 with a DOL of 1.3.

The antibody-conjugates were then used in *in vitro* tests and an *in vivo*-proof of concept to test if both the choice of antibody and fluorophore are viable candidates for future development as molecular platform for antibody-drug conjugates. The results of these tests and characterizations are described in more detail in paragraph 2.5.3 and 2.5.4.1.

### 2.5.2.2 Enlarging the panel: anti-PD-1 and IgG2b-conjugates

For the preclinical study we repeated the anti-PD-L1 conjugation and widened the scope of our platform by the addition of a new target, mice PD-1 (the corresponding antibody is anti-PD-1 (BioXcell)) and rat-IgG2b (BioXCell) as negative isotype control antibody. Both antibodies are IgG-antibodies as well and were coupled using the same conditions. For each antibody a test-batch of  $100 \mu\text{g}$  was produced to confirm the viability of the previously established protocols for both the ammonium-azaBODIPY and the cyanine 5, followed by production batches when validated. The results are showcased in Table 16.

In general we observed good or acceptable reactivity of the azaBODIPY **68** towards all three antibodies whereas some weaknesses were observed for the cyanine 5 as the conjugation to IgG2b gave low yields. In the cases of anti-PD-L1 and isotype control, the protocol established earlier was sufficient for both fluorophores and gave very satisfying results that permitted the isolation of sufficient quantities of bioconjugate without alterations to the conjugation protocol.

Table 16: Labelling efficiencies and conjugation yields for the obtained bioconjugates

Bioconjugate	DOL	conjugate mass (yield)
azaBODIPY <b>68</b> - anti-PD-L1	2.9	772 $\mu\text{g}$ (43%)
Cy5 - anti-PD-L1	2.9	1109 $\mu\text{g}$ (62%)
azaBODIPY <b>68</b> - rat-IgG2b	2	349 $\mu\text{g}$ (70%)
Cy5 - rat-IgG2b	1.9	37 $\mu\text{g}$ (9%)
azaBODIPY <b>68</b> - anti-PD-1	1.3	143 $\mu\text{g}$ (25%)
Cy5 - anti-PD-1	2.7	99 $\mu\text{g}$ (33%)

In case of the anti-PD-1-antibody we suffered several backlashes. The initial tests gave good results, followed by production batches that showed very low DOLs (0.34 for 10eq. of azaBODIPY **68**). Thus we had to adjust the protocol by increasing the number of used equivalents from 10 to 15 for the azaBODIPY **68** and the conjugation time from 3.5-4 h to 6 h for the cyanine in order to be permit the isolation of at least some bioconjugate.

We were pleasantly surprised that the DOLs of all 6 conjugated antibodies were centered around 2.5 molecules of dye per antibody (with the exception of azaBODIPY-anti-PD-1). Moreover, each antibody pair had the same degree of labelling which renders them directly comparable.

### 2.5.3 Characterization of *in vitro*-properties of the obtained bioconjugates

All antibody-conjugates were characterized using MALDI-TOF-mass spectroscopy and UV/Vis spectroscopy to analyze their properties and determine the concentration of the conjugates. Whereas the cyanine aggregates in PBS when conjugated to the antibodies (as showcased by the apparition of an H-Type aggregate [276] with absorption wavelengths of around 590 nm compared to the Cy5 maximum of ca 660 nm) this behavior cannot be observed for the azaBODIPY.

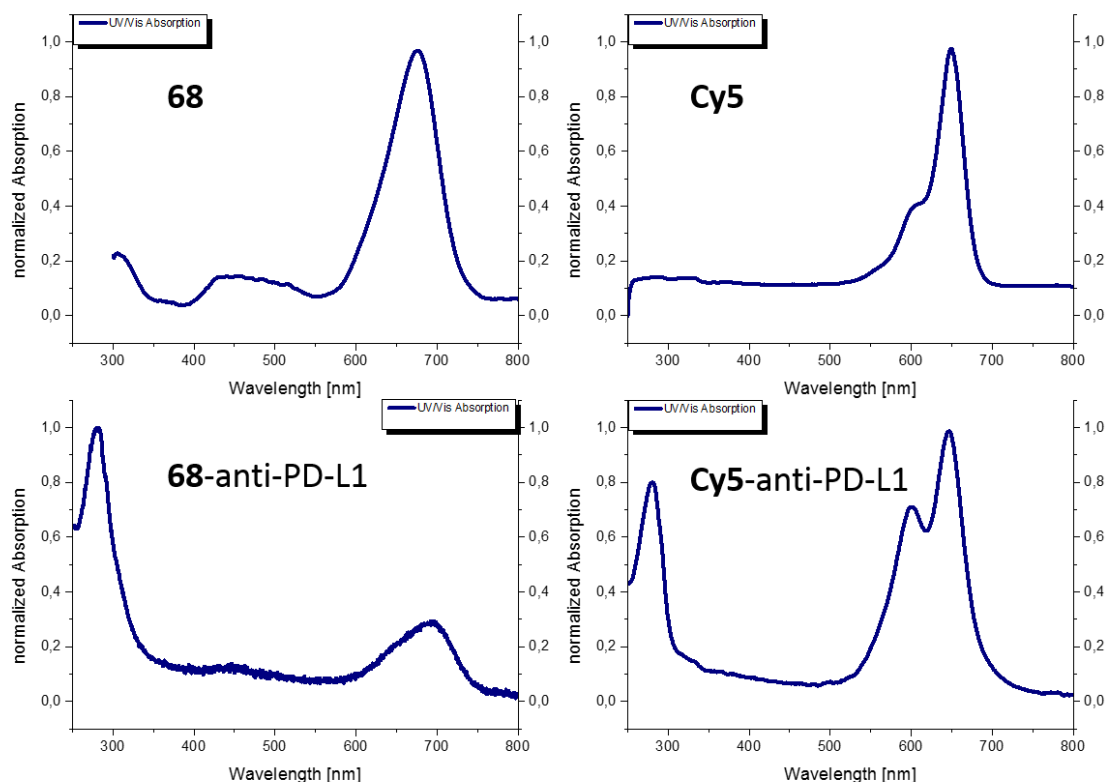


Figure 153: UV/Vis spectra of fluorophore and PD-L1-bioconjugates in PBS. Depicted spectra are representative for all obtained azaBODIPY/cyanine-mAb conjugates. Left: azaBODIPY 68, right: Cy5, top: fluorophore only, bottom: bioconjugate. Absorption peak at 280nm is caused by the antibody

Due to the small available quantities of antibody-conjugate we did not perform a full photophysical study.

In absence of stacking interactions, it is however reasonable to assume that the photophysical properties of the final conjugates resemble those of the unconjugated compound.

#### 2.5.3.1 Determination of purity and stability of the bioconjugates

Before the preclinical studies we tested all antibody conjugates for purity.

All conjugates were analyzed by electrophoresis on a sodium dodecyl sulfate polyacrylamide gel (SDS-PAGE analysis, 10% acrylamide gel) in non-reducing (loading buffer without dithiothreitol (DTT), or reducing conditions (with loading buffer with DTT and heating at 95°C during 5 minutes). A PageRuler™ Prestained Protein Ladders, 10 to 180 kDA was used for comparison. After protein migration in a running buffer the gels were analyzed on an Odyssey CLx Infrared Imaging System (LI-COR Biosciences) in pair filter mode (685/700 nm). The visualization was followed by Coomassie blue staining during 1 h after which the gels were

analyzed again on a Chemidoc XRS+ analyzer (BioRad). Coomassie Brilliant Blue binds electrostatically to charged protein complexes. This results in stained spots of proteins that allow their detection by UV-Vis absorption. The results of the gel electrophoresis are shown in Figure 154.

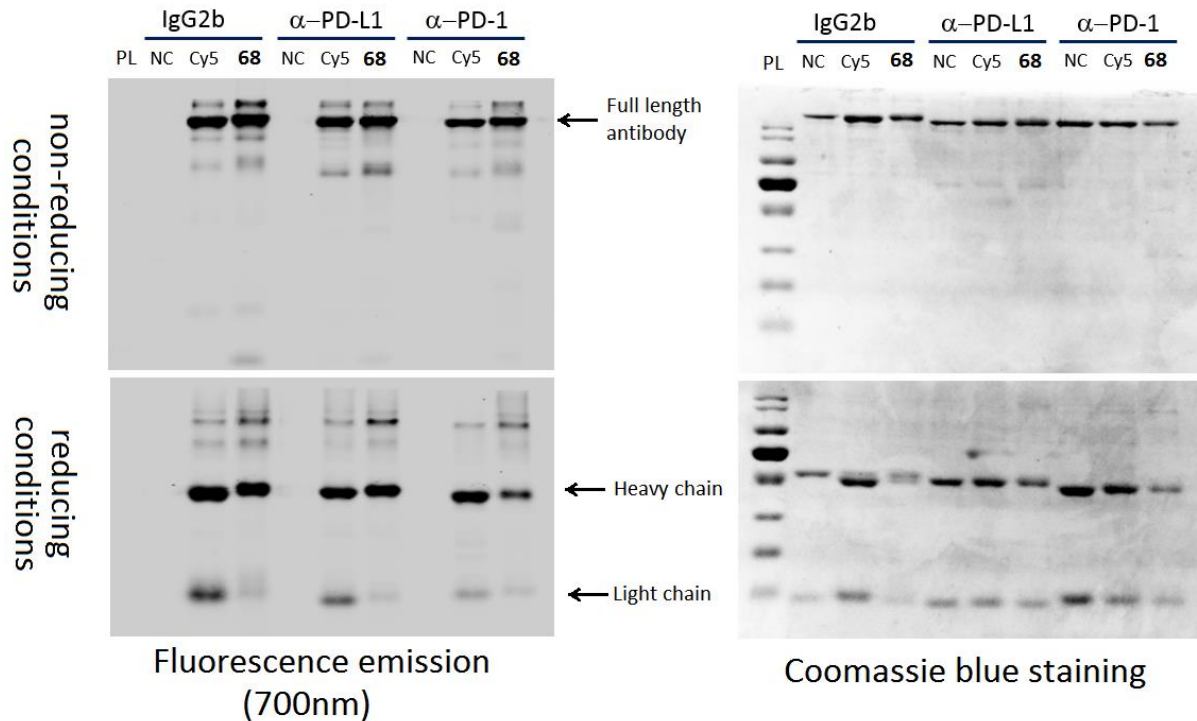


Figure 154: The anti-PD-L1 antibodies uncoupled (NC), coupled with cyanine 5 (Cy5) or azaBODIPY **68** were analyzed by electrophoresis on a SDS polyacrylamide gel (SDS-PAGE analysis, 10% acrylamide gel) in non-reducing (without DTT (dithiothreitol), top panels) or reducing conditions (with heating and DTT, bottom panels). The fluorescence analysis of the gels was performed on Odyssey CLx Infrared Imaging System (LI-COR Biosciences, left panels) in pair filter mode (685/700 nm). After Coomassie blue staining during 1h, the gels were visualized on a Chemidoc XRS+ analyzer (BioRad, right panels). PL: protein Ladders (130, 100, 70, 55, 40, 35, 25, 15 kDa).

The gel electrophoresis showed that the both dyes were conjugated to the respective antibodies. During electrophoresis the obtained antibody conjugates resolved into bands with a mass of approximately 150 kDa in native conditions and two bands of 50 and 25 kDa in denaturing conditions; this corresponds to the full length antibody and heavy/light chains respectively. Electrophoresis showed that the conjugates were pure and have not been degraded during conjugation and purification.

We were delighted to see that the use of the squarate function for activation had not only resulted in better solubility and good reactivity towards the chosen antibodies: Analysis of the gels under denaturing conditions showed that azaBODIPY **68** shows a strong preference for heavy-chain conjugation. The control-fluorophore cyanine 5 on the other hand also displays some conjugation to the light chain. Conjugation to the heavy chain is less likely to disturb the epitope responsible for antibody-antigen recognition and thus preferred.

The stability of azaBODIPY **68**-PD-L1 conjugate was investigated by incubation of the conjugate in mice plasma for up to 48h at 37°C, followed by analysis by electrophoresis using native SDS-PAGE gel electrophoresis (Figure 155).

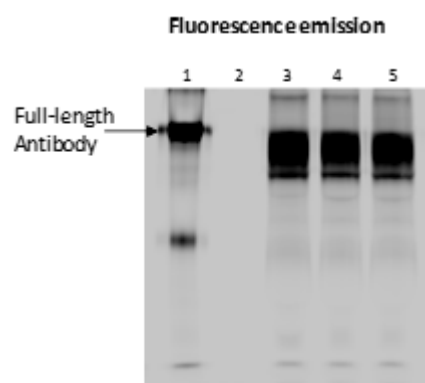


Figure 155: Investigation of the Stability of the **68**-anti-PD-L1 in mice plasma by electrophoresis on SDS-PAGE (7% acrylamide gel) in non-reducing conditions. The fluorescence analysis of the gel was performed on Odyssey CLx Infrared Imaging System (LI-COR Biosciences) in pair filter mode (685/700 nm). 1: **68**-anti-PD-L1 without incubation in mice plasma, 2: mice plasma without **68**-anti-PD-L1, 3 to 5: **68**-anti-PD-L1 incubated in mice plasma during respectively 0, 24 and 48h.

As is evidenced by the absence of evolution between 0 and 48h the compound is stable in mice plasma for at least 48h, making its biological stability very compatible with the relatively long timeframes required for antibody-based *in vivo* investigations.

### 2.5.3.2 Investigations of affinity and selection of target-cells

In order to check if the anti-PD-L1 conjugate had retained its binding affinity we tested the anti-PD-L1 conjugate in flow cytometry analysis against a commercial phycoerythrin-(PE) conjugated anti-PD-L1 antibody from BioLegend®. The antibody conjugates were tested on two cancer cell lines, the mouse colorectal carcinoma CT26 [277] and mammary carcinoma 4T1 [278].

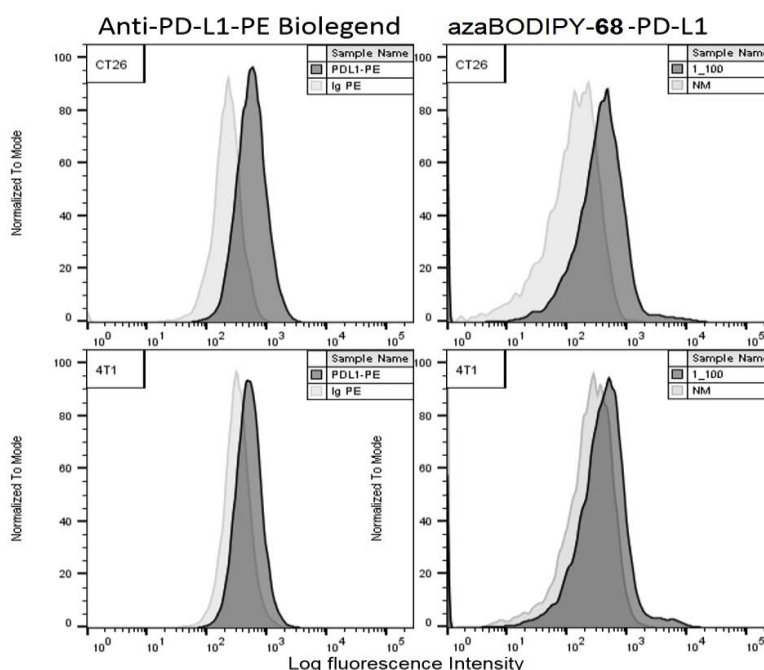


Figure 156: Flow cytometry analysis using a commercial PE-conjugated anti-PD-L1 antibody (left) and azaBODIPY **68**-conjugated anti-PD-L1 (right) on two different cancer cell lines, CT26 (top) and 4T1 (bottom). IgG2b-PE and untreated cells were used as negative controls respectively

This investigation showed that the labelled antibodies had retained an affinity for the PD-L1 ligand.

## 2.5.4 *In vivo* investigations

### 2.5.4.1 *Proof of concept*

4 BALB/c mice were injected with  $5 \times 10^6$  CT26 cells in the right flank. The xenografts were left to grow/mature for 14 days. After two weeks each mice was injected with either 25  $\mu\text{g}$  or 50  $\mu\text{g}$  of azaBODIPY **68**-anti-PD-L1, 25  $\mu\text{g}$  of Cy5-anti-PD-L1 or 0.384  $\mu\text{g}$  free azaBODIPY **68** (equivalent to 50  $\mu\text{g}$  azaBODIPY **68**-anti-PD-L1), followed by observation and imaging over 48h.

All tested compounds emitted an intense fluorescence signal with accumulation in the tumor and distinct pharmacokinetic behaviors that varied for each injected compound. No acute toxicity was detected in any of the treated mice. These results alone validate the designed azaBODIPYs as *in vivo* compatible fluorescent imaging probes.

#### 2.5.4.1.1 *Anti-PD-L1 conjugate*

When looking at the results obtained using 50  $\mu\text{g}$  of azaBODIPY labelled anti-PD-L1 a clear accumulation over the chosen timeframe is visible. The labelled antibody accumulates nicely in the xenograft and reaches its maximum concentration at the end of the observation period (Figure 157 and Figure 158).

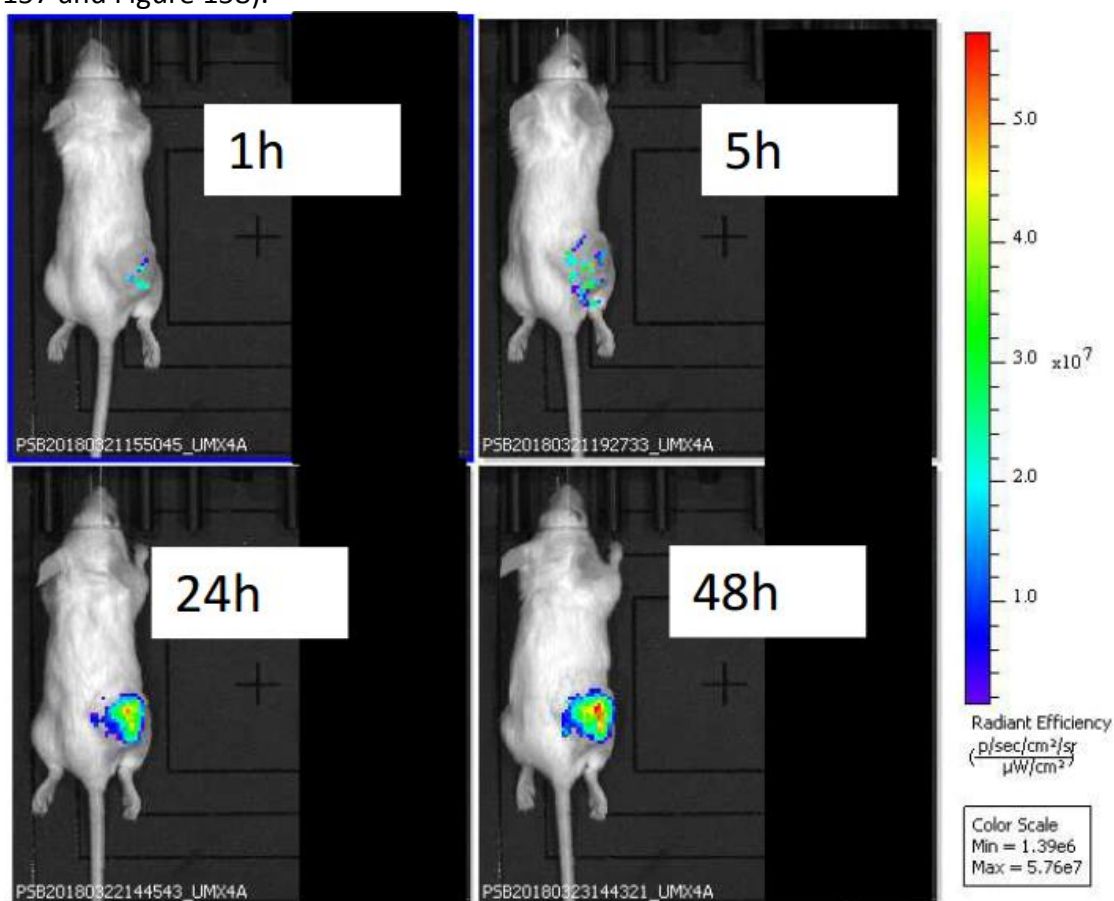


Figure 157: NIR fluorescence images of a subcutaneous CT26 tumor-bearing of BALB/c mouse injected with a single dose of 50  $\mu\text{g}$  azaBODIPY **68**-anti-PD-L1 (imaged from the back)

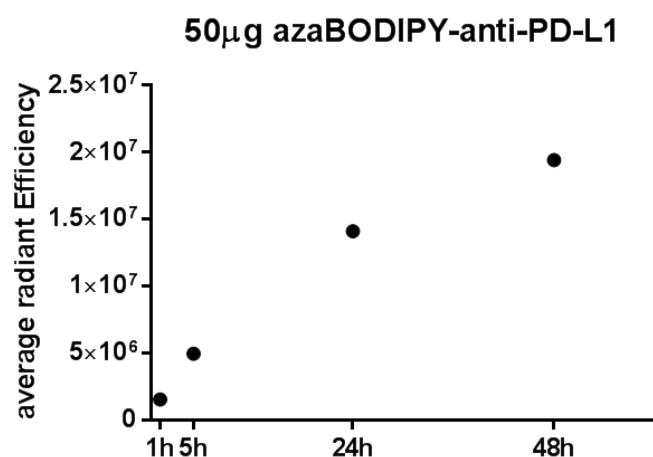


Figure 158: Corresponding fluorescence tumour uptake over time at 1, 5, 24 and 48 h post injection (bottom) (Ex/Em filters: 660/710 nm, IVIS Lumina, Perkin Elmer)

This is desirable in two ways: first this shows that the conjugate exhibits an affinity towards the tumor and seems to be biologically stable enough to not be metabolized to a too great extent. Secondly, the gradual accumulation permits clearance of unbound or non-specifically bound antibody conjugate from the organism which is desirable to remove background noise. Unfortunately, no whole-body images could be taken to quantify the body distribution of fluorophore (including the organs) due to the fur that covered the rest of the mouse.

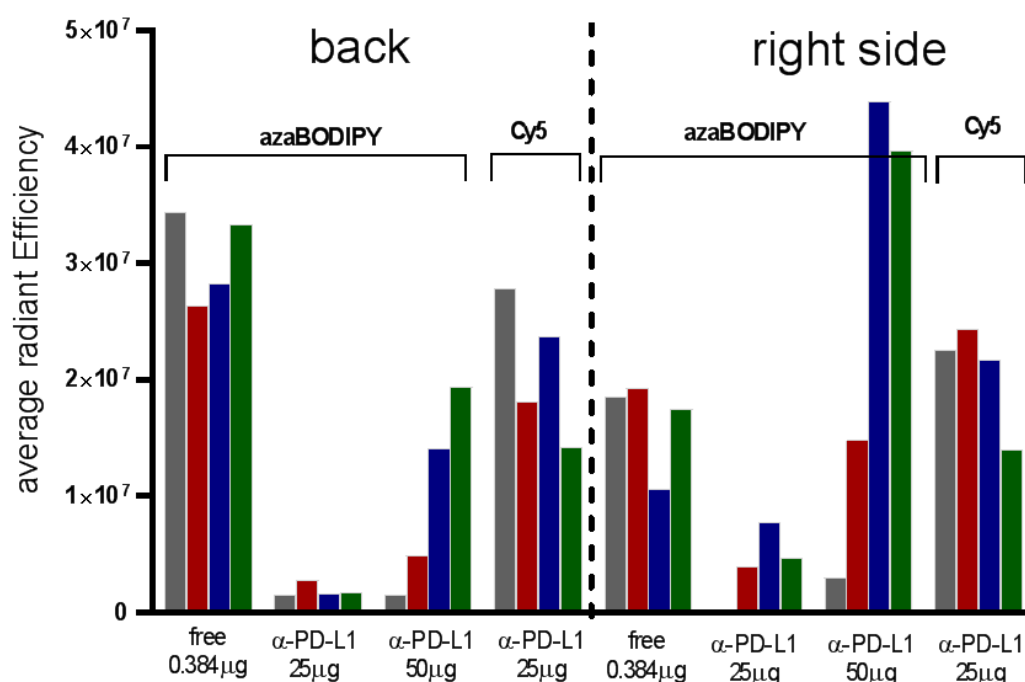


Figure 159: Development of absolute fluorescence intensities detected from 1-48h for all injected conjugates/compounds. Mice were imaged from the back and the right side. Grey: 1h, red: 5h, blue: 24h, green: 48h.

When looking at the development of each type of injected compound the 50  $\mu$ g injection of azaBODIPY-conjugate shows the clearest development over time and gives an overall excellent signal. The cyanine 5 does not exhibit an accumulation over time but remains at the same (high) fluorescence intensity. When solely the side-view is taken into account the Cy5-conjugate accumulates strongest at 5h and declines from thereon out.

#### 2.5.4.1.2 Conclusions

Other conclusions that can be drawn from this experiment are:

- As visible by the ratio of intensities between the 25 µg azaBODIPY **68**-conjugate injection and the 50 µg injection shown in Figure 159 the detected fluorescence does not scale linearly with the employed quantity of conjugate
- Free azaBODIPY **68** is not an appropriate candidate as a negative control: it shows strong fluorescence at all times in the xenograft. No conclusion can be drawn as to whether the free azaBODIPY has a preference for the tumor due to possible passive transportation mechanisms.

This study served as proof of concept and showed that neither the conjugates, nor the unconjugated probe caused acute toxicity in mice. For all cases a strong fluorescence signal could be detected which validated the designed fluorophore as *in vivo*-compatible NIR-fluorescent probe.

With these results in hand we designed a preclinical study that would use freshly prepared anti-PD-L1 conjugate, a correct negative control antibody and add an anti-PD-1 antibody to the study. [The syntheses of the antibody-conjugates were described in detail in paragraph 2.5.2.2.]

#### 2.5.4.2 Preclinical assay

Using the newly obtained antibody-conjugates a preclinical assay was designed using 2-3 mice per group (all azaBODIPY-conjugates are conjugates of azaBODIPY **68**). The 4 groups were prepared as previously and consisted of the following number of subjects:

- 3 mice for azaBODIPY-anti-PD-L1
- 3 mice for azaBODIPY-IgG2b
- 3 mice for Cy5-anti-PD-L1
- 2 mice for azaBODIPY-anti-PD-1

To exclude the autofluorescence caused by the food the mice received special non-fluorescent food starting 2 weeks prior to the experiment to allow for clearance of “normal” food. Aside from the food, nothing was changed in the experimental setup. The mice were injected once with 50 µg of antibody-conjugate and imaged after 1h, 6h, 24h and 48h for each group.

##### 2.5.4.2.1 Anti-PD-L1 conjugate

When looking at the fluorescence intensities of azaBODIPY-anti-PD-L1 the same accumulation over time is visible that was observed in the proof of concept, reaching a maximum at the end of the observation period (48h) (Figure 160).

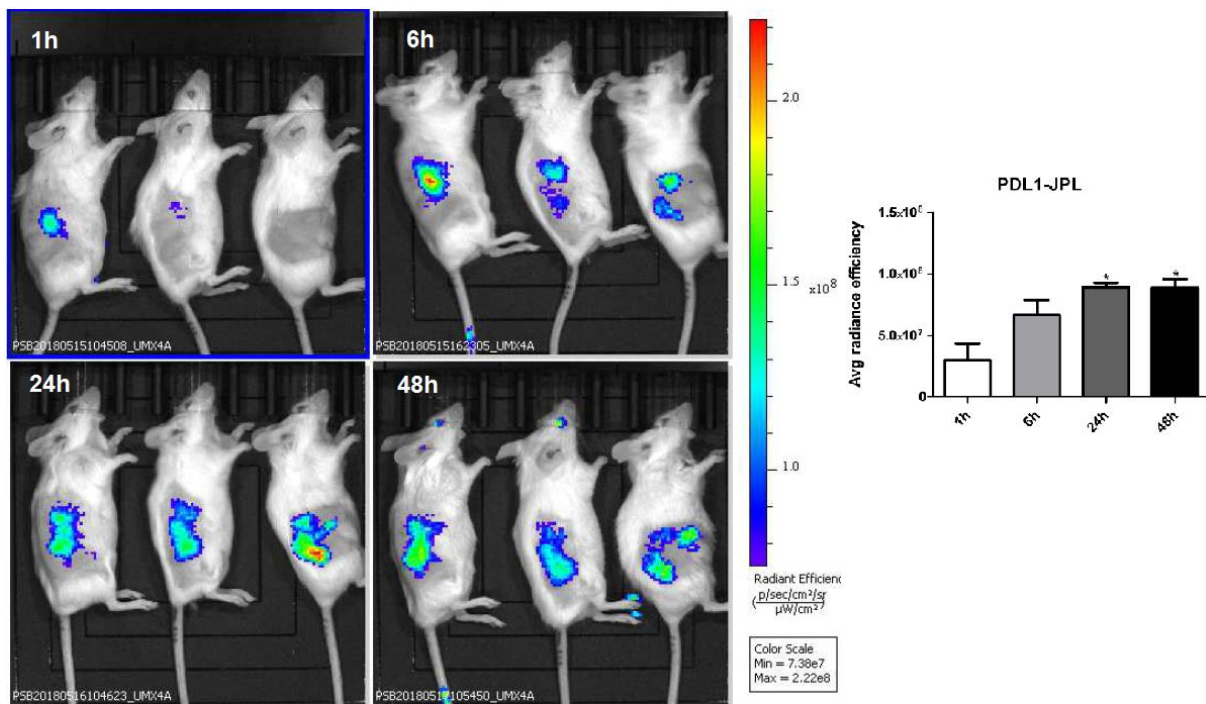


Figure 160: NIR fluorescence images of subcutaneous CT26 tumor-bearing mice at 1, 6, 24 and 48 h after a single injection of 50  $\mu\text{g}$  azaBODIPY **68**-anti-PD-L1 (Ex/Em filters: 660/710 nm, IVIS Lumina, Perkin Elmer) Right: Quantification of fluorescence tumour uptake over time. Results are presented as mean  $\pm$  SEM,  $n=3$ ,  $*p<0,05$ . Radiant efficiencies are also shown in Figure 164 below for direct comparison to other conjugates

The absolute intensities are in the same range as in the proof of concept, indicating a good repeatability of the experiment.

## 2.5.4.2.2 Isotype-control IgG2b conjugate

When mice were treated with the negative control azaBODIPY-IgG2b a strong accumulation of fluorescence was detected in the tumors (Figure 161) that surpassed the accumulation observed by treatment with azaBODIPY-anti-PD-L1 (The values are compared to each other in Figure 164).

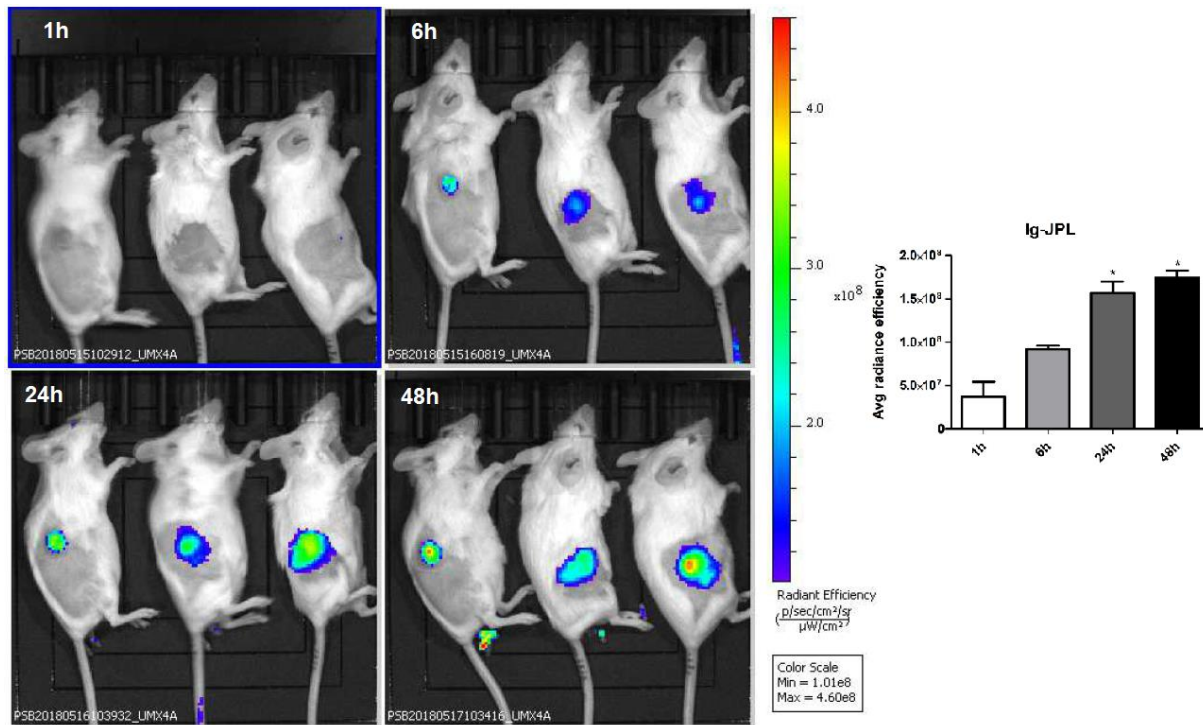


Figure 161: NIR fluorescence images of subcutaneous CT26 tumor-bearing mice at 1, 6, 24 and 48 h after a single injection of 50  $\mu\text{g}$  azaBODIPY 68-IgG2b (Ex/Em filters: 660/710 nm, IVIS Lumina, Perkin Elmer) Right: Quantification of fluorescence tumour uptake over time. Results are presented as mean  $\pm$  SEM,  $n=3$ ,  $*p < 0.05$ . Radiant efficiencies are also shown in Figure 164 below for direct comparison to other conjugates

The strong accumulation of the azaBODIPY-IgG2b isotype control was unexpected and needs to be investigated further. It is possible that the chosen isotype control antibody is incompatible with the targeted application of PD-L1 imaging; another clone or subtype may provide better results.

## 2.5.4.2.3 Anti-PD-1 conjugate

When the mice were injected with anti-PD-1 conjugate the measured fluorescence intensities are far lower than for anti-PD-L1 conjugates and followed a less clear increase over time (Figure 162).

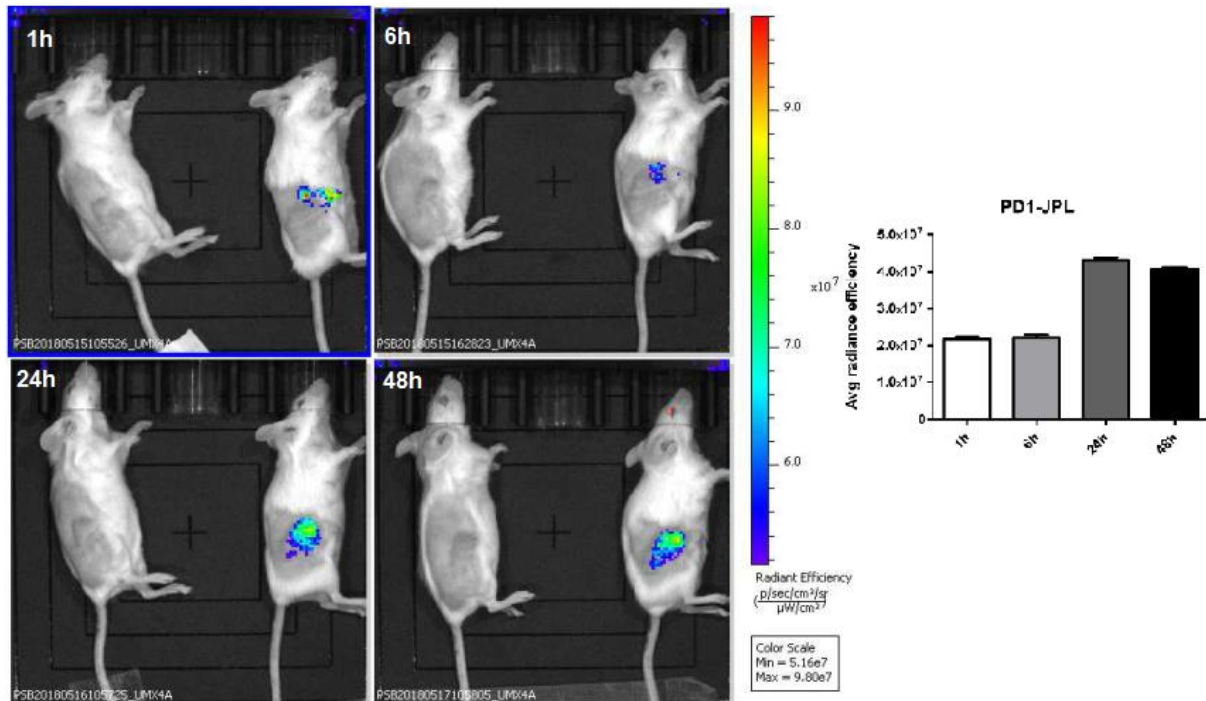


Figure 162: NIR fluorescence images of subcutaneous CT26 tumor-bearing mice at 1, 6, 24 and 48 h after a single injection of 50  $\mu$ g azaBODIPY 68-anti-PD-1 (Ex/Em filters: 660/710 nm, IVIS Lumina, Perkin Elmer) Right: Quantification of fluorescence tumour uptake over time. Results are presented as mean  $\pm$  standard error  $n=2$ . Radiant efficiencies are also shown in Figure 164 below for direct comparison to other conjugates

Interestingly the anti-PD-1 conjugate displays a dual evolvement: both the detected fluorescence intensity evolves over time as well as its localization in the xenograft. As shown in section 2.5.1 the PD-1 receptor is not expressed by the cancerous cells but by cells of the recruited immune system (T-lymphocytes, B-cells, macrophages etc.). The degree of recruitment varies from tumor to tumor (which is why the left mouse in Figure 162 did not display any fluorescence accumulation) and can be inhomogenous inside of a single tumor.

For the comparison of measured absolute fluorescence intensities of the anti-PD-1 conjugate and the anti-PD-L1 conjugate the fluorescence intensities have to be corrected for the respective DOLs of 1.3 (anti-PD-1 conjugate) compared to the 2.9 for the anti-PD-L1 conjugate. When the detected fluorescence intensity is multiplied by the factor 2.2 to adjust for the lower DOL it becomes clear that the PD-1 antibody accumulates as efficiently in the tumor as the anti-PD-L1 conjugate.

2.5.4.2.4 Cy5-anti-PD-L1 conjugate

Images of the 4<sup>th</sup> group that received Cy5-anti-PD-L1 are shown in Figure 163.

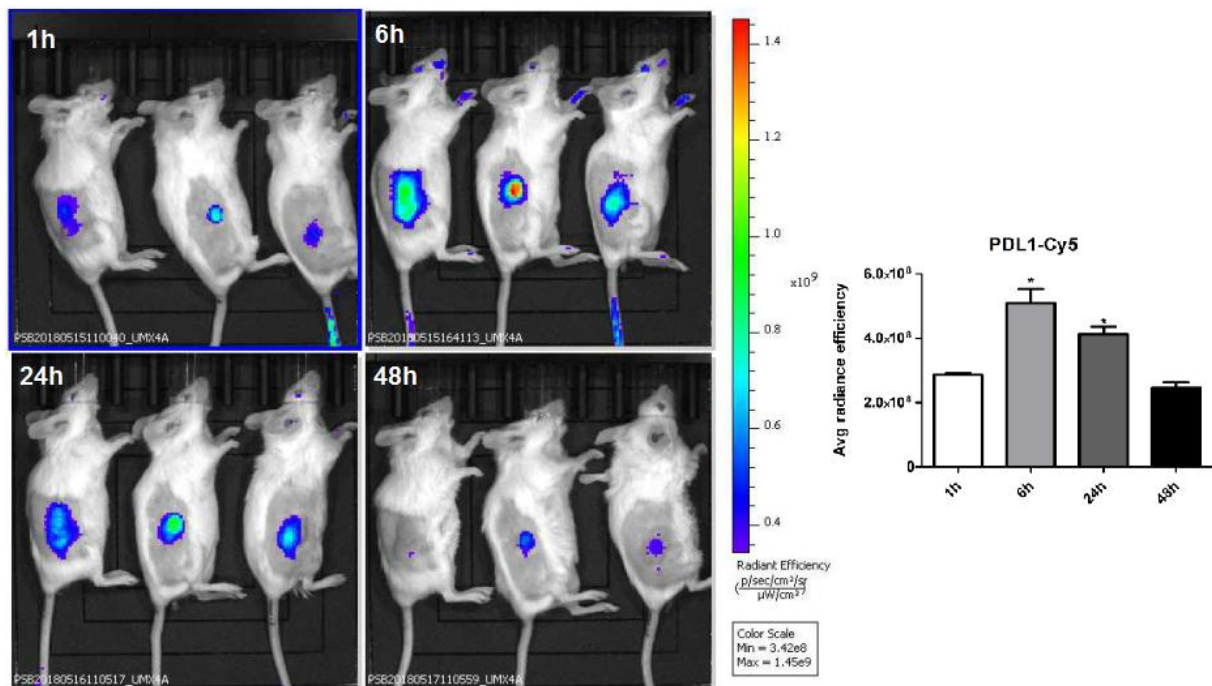


Figure 163: NIR fluorescence images of subcutaneous CT26 tumor-bearing mice at 1, 6, 24 and 48 h after a single injection of 50 µg Cy5-anti-PD-L1 (Ex/Em filters: 620/660 nm, IVIS Lumina, Perkin Elmer) Right: Quantification of fluorescence tumour uptake over time. Results are presented as mean ± SEM, n=3, \*p<0,05. Radiant efficiencies are also shown in Figure 164 below for direct comparison to other conjugate

As for the other conjugates the Cy5-anti-PD-L1 conjugate exhibited a strong fluorescence signal. The maximum fluorescence intensity is detected after 6h; from there on out the signal decreases. The same behavior was observed for the Cy5-conjugate in the first *in vivo* experiment when solely the side-view was taken into account.

2.5.4.2.5 Comparison

The direct comparison of the azaBODIPY-anti-PD-L1 results to the other used antibodies shows a clear accumulation behavior for each azaBODIPY-conjugated antibody whereas the Cy5 conjugate reaches its maximum after 6h and decreases afterwards (see Figure 164).

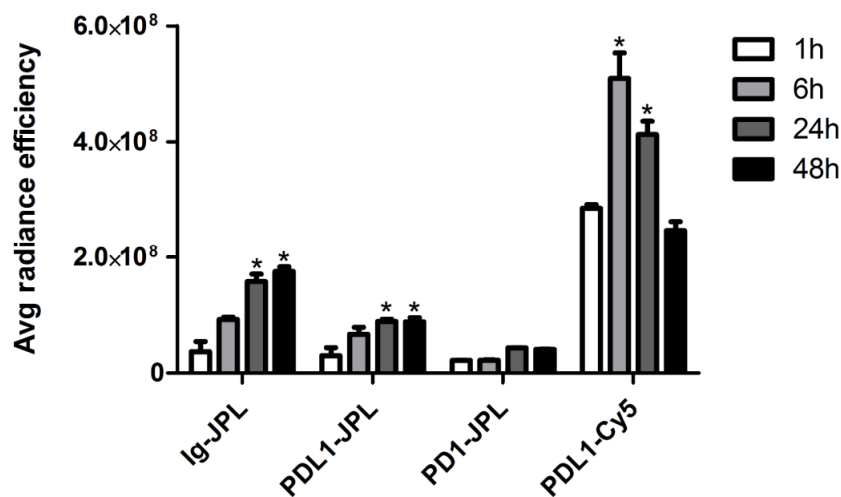


Figure 164: comparison of fluorescence accumulation over time for each cohort. JPL indicates use of azaBODIPY 72 as fluorophore

The Cyanine 5 conjugate shows the strongest absolute fluorescence. This however has to be viewed in conjunction with the optic properties of the Cyanine 5 which displays a higher brightness than azaBODIPY **68** (Cyanine 5 has a very high molar absorption coefficient of  $\epsilon=134\,000\text{ M}^{-1}\text{ cm}^{-1}$  and a quantum yield of 14% in PBS [279] . This results in a brightness of  $18\,800\text{ M}^{-1}\text{ cm}^{-1}$ , compared to  $2\,800\text{ M}^{-1}\text{ cm}^{-1}$  in PBS for azaBODIPY **68**). We have no information as to whether the decrease of Cy5-fluorescence is caused by elimination of the Cy5-antibody from the tumor, elimination of Cy5 from the antibody (unstable conjugate) or if the Cyanine 5 is simply degraded/metabolized over time due to biological influences or photobleaching (the mice are not kept in the dark).

#### 2.5.4.2.6 Ex-vivo images of organs

At the end of the 48h observation period the mice were euthanized and the organs extracted and imaged by fluorescence to obtain insight into the organ-distribution of the investigated compounds (Figure 165).

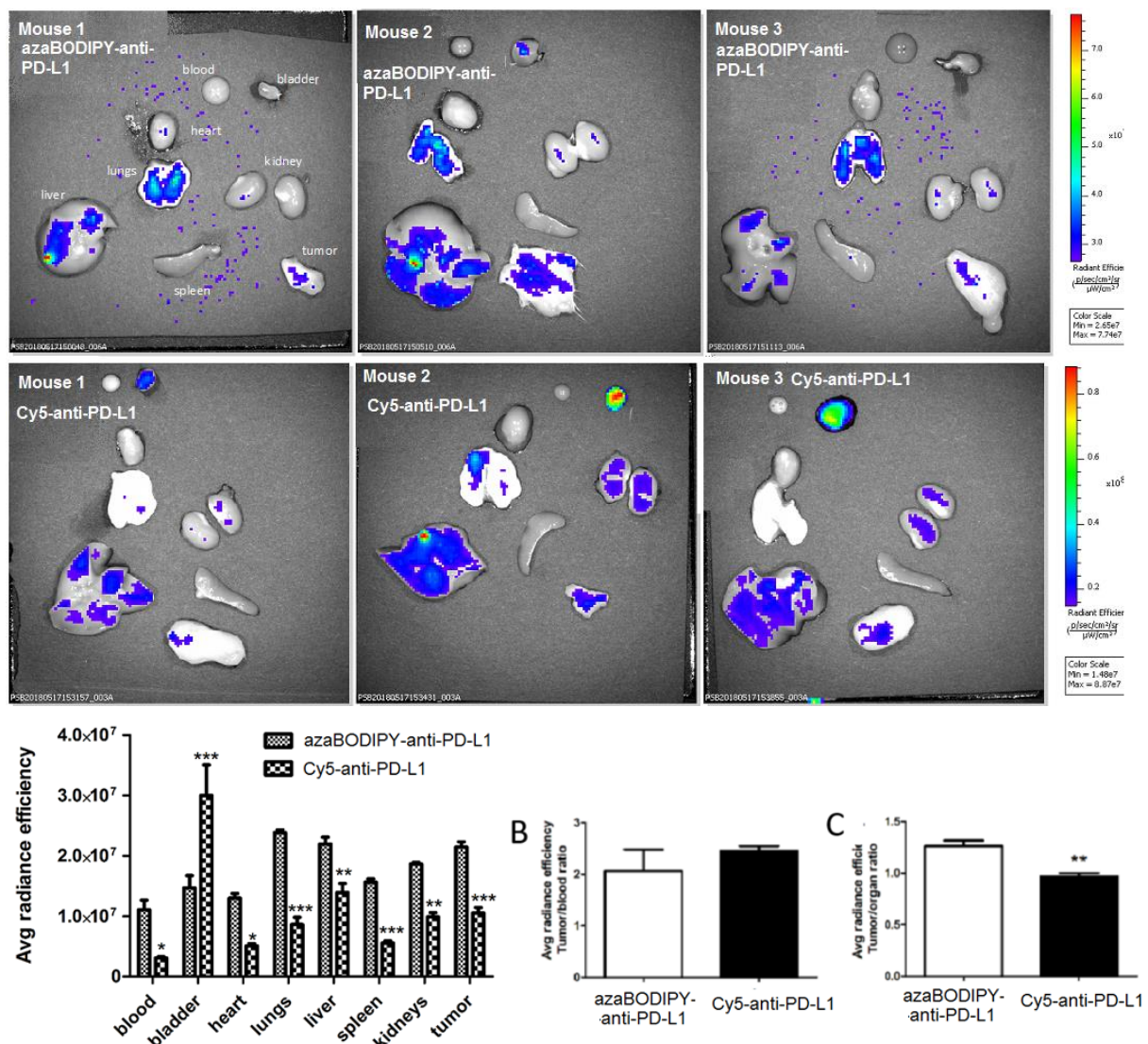


Figure 165: quantification of uptake of **azaBODIPY 68-anti-PD-L1** (Ex/Em filters: 660/710 nm) and **Cy5-anti-PD-L1** (Ex/Em filters: 620/660 nm) in organs collected 48h p.i. via ex vivo NIR fluorescence. Mice received a single injection (50  $\mu\text{g}$ ) of **azaBODIPY-68-anti-PD-L1** or **Cy5-anti-PD-L1**. Results are presented as mean  $\pm$  SEM, n=3, \*p<0,05; \*\*p<0.01 and \*\*\*p<0.001. B and C: Tumor/blood ratio (B) and tumor/organ ratio (C) of **azaBODIPY-68-anti-PD-L1** and **Cy5-anti-PD-L1** uptakes. Results are presented as mean  $\pm$  SEM, n=3, \*\*p<0,01

When azaBODIPY/Cy5-anti-PD-L1 are directly compared as shown in Figure 165 both compounds show distinct biodistributions: whereas the azaBODIPY conjugate is mainly found in the tumor, lungs and liver and to a high degree also in the kidneys; the Cy5-conjugate shows smaller tumor uptake and a preference for the liver combined with a high elimination through the urine (thus involving the kidneys and bladder).

Most importantly we were able to show that the azaBODIPY-conjugate displays a significantly higher tumor uptake than the Cy5-conjugate as well as a better tumor to organ distribution ratio after 48h. While the second is a very positive finding for pure imaging applications (reduced background noise) the higher tumor uptake is an excellent result for the development of trackable antibody-drug-conjugates (ADC). As the final goal of this project is the development of a multifunctional platform for the conception of trackable therapeutic agents (theranostic) the accumulation of antibody in the target tissue needs to be as high as possible in order to achieve good results. (Strictly speaking the fluorophore-antibody conjugates are already theranostics themselves since the antibody by itself will already have a therapeutic effect: by blocking the PD-L1 ligand it prevents or limits evasion of the host's immune system by the tumor).

#### 2.5.4.3 Conclusion

Using azaBODIPY **68**-antibody conjugates we were able to perform a proof of concept and a preliminary study on mice. In both studies no acute toxic effects were observed, both for the conjugates as well as the free azaBODIPY. All tested conjugates displayed a strong fluorescence signal *in vivo* which validated the chosen synthetic pathway and the resulting probe for further preclinical studies. The higher tumor uptake compared to the Cy5-conjugates showcases the positive contribution that both the developed platform-approach in general as well as the developed probe specifically have brought to the field.

## 2.6 Summary and Outlook

### 2.6.1 Summary

In the second part of this thesis I investigated the development of azaBODIPY-based molecular platforms, their functionalization and application for optical imaging in biological systems.

Three systems were investigated: 1,7-di(phenol)-3,5-di(phenyl)azaBODIPY **30**, di(bromophenyl)-di(methoxyphenyl)-azaBODIPYs **48** and **52** and 1,7-di(phenyl)-3,5-di(methoxyphenyl)-azaBODIPY **44**.

The synthetic know-how for their synthesis up to 5-10 g scale was successfully acquired and applied following procedures that are published in the scientific literature. Following the successful synthesis at multi-gram scale each system was modified in order to obtain a functionalizable, molecular platform.

Inspired by O'Shea's works, we investigated the functionalization of the hydroxy-group of azaBODIPY **30** in order to obtain a bioconjugable azaBODIPY that can be grafted onto antibodies. I successfully synthesized and characterized the desired compound **35**; due to very unfavorable solubility as well as photophysical properties in common solvents and especially in aqueous solution, we investigated the functionalization of the azaBODIPY's boron atom to increase the compounds solubility in water. Due to recurrent problems with hydroxy-azaBODIPY, we decided to investigate the feasibility of an entirely boron-based functionalization strategy; including desymmetrization, hydrosolubilization and vectorization

of the selected azaBODIPY. Towards that end we first turned our attention towards the 1,7-di(bromophenyl)-3,5-di(methoxyphenyl)-azaBODIPY **48**, followed by the final system 1,7-di(phenyl)-3,5-di(methoxyphenyl)-azaBODIPY **44**.

Using the bromine-substituted compound **53** a synthetic protocol was established that uses alkyne-Grignard agents and grants access to azaBODIPYs that are fully functionalizable, can (and have been) desymmetrized using two different carboxylic acids and possess excellent photophysical properties.

Next, the same transformations were executed for the 1,7-di(phenyl)-3,5-di(methoxyphenyl)-azaBODIPY **44**. Following the protocol that I established on the bromine substituted derivate I successfully synthesized azaBODIPYs that possess two functionalities on the substituent attached to the boron atom.

Using this versatile approach, I was able to synthesize three water-soluble, bioconjugable azaBODIPYs (**67-69**), two of which display excellent optical properties, are water-soluble and do not stack in aqueous solution.

The successful syntheses of these derivatives and the properties that they displayed validated several hypotheses that we had when we decided to use the boron-functionalization approach: the spectral properties of the selected azaBODIPYs are not changed by the introduction of aliphatic alkyne substituents and can thus be chosen beforehand. The functionalization of the boron atom also successfully prevented stacking of the dyes whereas the use of hydrosolubilizing groups rendered the azaBODIPYs soluble in aqueous solution.

I therefore managed to synthesize a new class of multifunctional, water-soluble molecular platform. The platform itself fulfills the task of being trackable by optical fluorescence imaging as it strongly absorbs and emits in the NIR I region. They also possess two versatile functions that I used during my thesis for the introduction of a water-solubilizing moiety (trimethylammonium and propane sulfone betaine) and a grafting function+vector.

The finished platforms were then conjugated to three different antibodies (anti-PD-L1, anti-PD-1 and IgG2b) using the uncommon diethylsquarate as grafting function.

We found that the synthesized probes showed a strong preference for (desirable) heavy chain labelling, retained recognition of the PD-L1 antigen as we determined by flow cytometry and remained stable in mice plasma for at least 48h.

Using the newly obtained bioconjugates we executed a proof of concept as well as a preliminary preclinical study on BALB/c mice that showed that

- the bioconjugates showed no acute toxicity
- the bioconjugates exhibited strong fluorescence *in vivo*
- remained stable during the observation period of 48h
- showed distinct biodistributions that differed from the Cy5-conjugate.

Additionally, we were able to obtain information about the biodistribution of the anti-PD-L1 conjugates.

Using the boron functionalization of azaBODIPYs we were able to develop a molecular probe from the initial idea all the way to a preclinical *in vivo* study.

The concept of the boron-based functionalization was further validated by the synthesis of a variety of other molecules (not detailed in this thesis) to assess the versatility of the newly developed platform approach by the introduction of other vectors (antibodies as well as small

molecular entities such as biotine and folic acid) as well as the symmetrical introduction of e.g. two hydrosolubilizing groups to improve the solubility even further ( Figure 166).

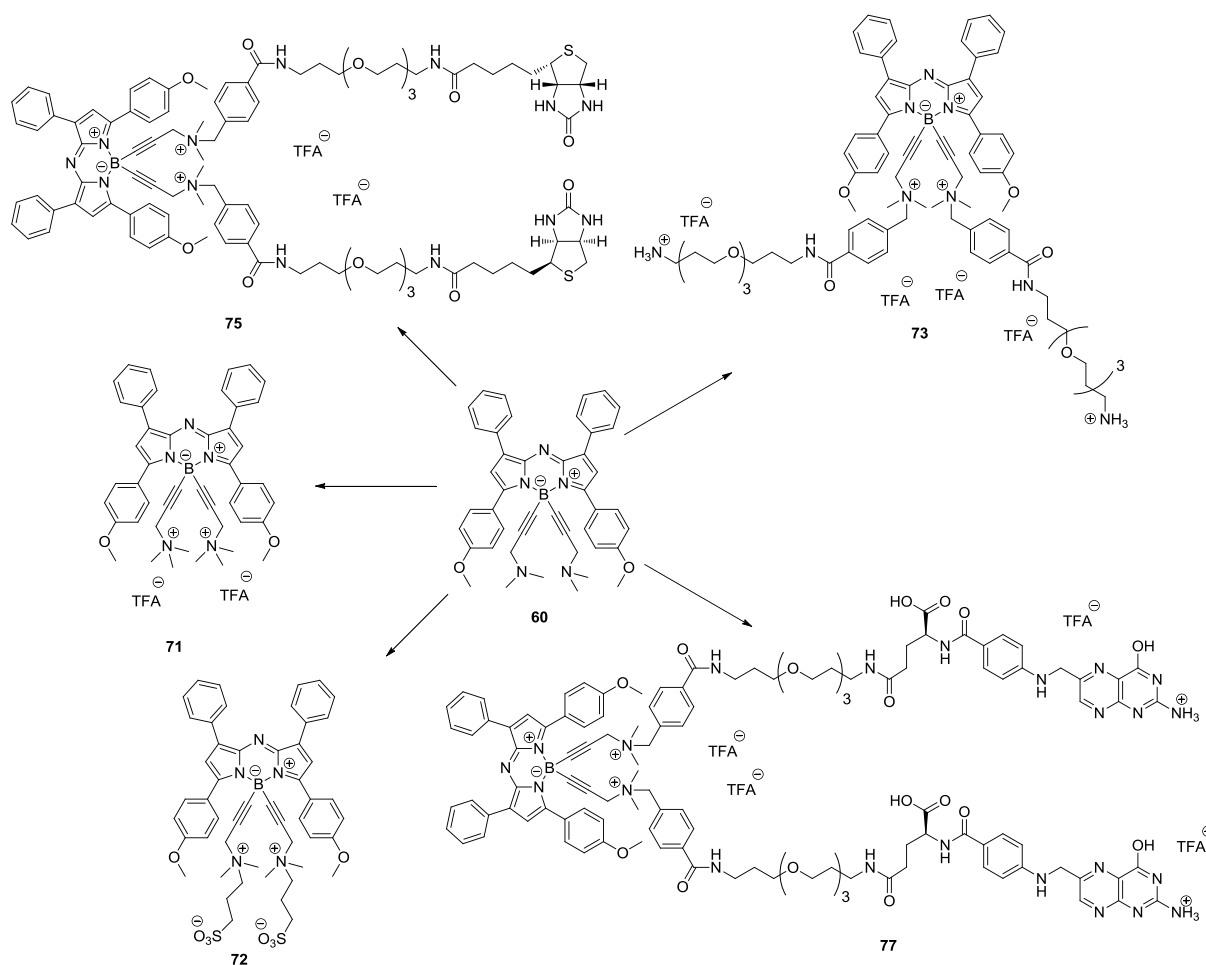


Figure 166: Further exploration of the developed platform

Starting from having no prior experience with azaBODIPYs in the group my thesis enabled us to establish viable synthetic protocols to access multifunctional azaBODIPYs that can be used as molecular platforms for a large variety of applications. The presented examples, as well as various other azaBODIPYs that were not presented but are currently subject to further studies in a variety of projects display the great potential of this approach and its general applicability to other azaBODIPY based platform molecules for future investigations.

## 2.6.2 Outlook

Although the synthesized system displays excellent properties in many aspects, it could be improved as well as developed further. Several suggestions will be briefly shown in the following.

### 2.6.2.1 Additional investigations for the existing system

Using the existing systems several additional properties should be investigated in the future. First of all, the LogP/LogD of the obtained dyes should be investigated to obtain an idea of their lipophilicity as well as identify desirable properties for future improvements. Additionally, all obtained conjugates as well as the unconjugated antibodies should undergo an evaluation of their binding affinity to their designated antigen. This should help to interpret the data obtained in the *in vivo* study.

Using the existing probes (azaBODIPY **68** and Cy5 **70**) new batches of conjugated antibody should be produced in order to obtain enough conjugate to execute an *in vivo* study that includes the entire panel of compounds – due to the poor labelling yields that we obtained for Cy5-IgG and Cy5-PD-1 we were unable to include these compounds into the *in vivo* studies. Especially the use of Cy5-IgG should yield additional information if the accumulation of azaBODIPY-IgG conjugate is caused by the fluorophore or if some property of the IgG causes this accumulation.

Additionally it would be interesting to execute tomographic imaging and high resolution imaging (e.g. intravital microscopy) of the couple PD-1/PD-L1 to investigate/confirm different localization and concentration of each of the two trackable antibodies for CT26-derived tumors.

Finally, in the interest of developing a trackable therapeutic agent a study should be performed to see if the application of the labelled antibody results in a recruitment of the host's immune system and shrinking of the tumoral masses. If this were the case this study would permit to officially relabel the obtained conjugates "theranostics" and also prove their value in therapy, as well as studying and monitoring the tumoral progression.

### 2.6.2.2 Desirable modifications, improvements and future studies

In order to investigate the results obtained for the IgG-conjugate it would be interesting to determine if the IgG itself suffers the same fate as the (fluorophore-)labelled antibody. The best way to study this would be to use either a tritium (where the tritium replaces a non-labile proton) or a <sup>35</sup>S-labelled IgG. This could be achieved using labelled amino acids during the production of the antibody. The antibodies that are labelled this way behave exactly like the unlabeled antibody and could be followed thanks to their radiation. However, this method would likely be rather costly. A cheaper way would be to replace labile protons in the finished IgG by either T<sub>2</sub>O or D<sub>2</sub>O (by incubating or simply storing the antibody in heavy or super heavy water). In order to yield useful data a baseline of tritium- or deuterium-loss from the antibody to the host's body would need to be established. T<sub>2</sub>O would again permit to follow the antibody using its radiation, D<sub>2</sub>O would need to be detected by mass spectrometry.

The development and validation of the azaBODIPY-platform during my thesis gave excellent results. However, both the results as well as the properties and versatility of the obtained compounds can of course be improved even further.

The first modification should be the use of one of the amine functions for something other than hydrosolubilization. Ideally it would serve for hydrosolubilization as well as a second function. Possibilities include

- the introduction of macrocyclic chelating agents (DOTA, NODAGA) in order to develop a multimodal imaging agent
- the introduction of a therapeutic moiety, e.g. metal based therapeutic agents such as the gold(I)-phosphine used in the first part of this thesis or agents such as doxorubicin, methotrexate and others.

The development of a multimodal imaging agent would combine the strengths of both modalities and enable the development of a tool that could be useful in the clinic both for non-invasive imaging to check e.g. tumor progression and during surgery for the development of a trackable agent that can be used in fluorescence guided surgery.

The introduction of a chelating agent in conjunction with radioactive isotopes could serve as a trackable therapeutic agent too when therapeutic  $\beta^-$ -emitters (e.g.  $^{90}\text{Y}$  or  $^{177}\text{Lu}$ ) are used.

The introduction of therapeutic moieties would permit to transform the azaBODIPY into an ADC (and thus again a trackable therapeutic agent).

The di(bromophenyl)azaBODIPYs should be investigated further in order to identify organometallic coupling conditions that yield the desired products – a variety of transformations such as Sonogashira cross coupling reactions has been published that successfully introduce functions on brominated compounds, hinting at their general feasibility.

Last but not least the azaBODIPY-core itself can be modified as well, both to increase the functionality even further and to enhance the properties.

The optical properties could be improved by restricting the rotation of the phenyl substituents or the use of totally different azaBODIPYs (such as thiophene fused azaBODIPYs which show molar absorption coefficients of  $180\,000\text{ M}^{-1}\text{ cm}^{-1}$  and quantum yields of up to 85% [213]).

Both the reduction of the molar mass as well as of the lipophilic character are desirable modifications. The synthesis of phenyl-free (unsubstituted) azaBODIPYs is desirable; up until now no group has however succeeded in developing this system. The synthesis of alkyl-substituted azaBODIPYs on the other hand should be possible and could greatly reduce both the lipophilic character as well as the molar mass of the resulting dye.

Finally, with the aim of developing therapeutically active trackable compounds a very simple modification would be the introduction of iodine atoms in the 2,6-pyrrolic positions. Iodo- and bromo-substituted azaBODIPY have already proven to be excellent  $^1\text{O}_2$ -sensitizers [280]. These photosensitizers currently lack solubility in water which limits their usefulness in biological systems. Using the strategy that was developed during this thesis to render a strong  $^1\text{O}_2$ -sensitizer soluble in water could prove valuable. Another modification that would be interesting for the development of agents aimed at photodynamic therapy would be a sort of “activatable” cytotoxic agent. In our group we have developed ruthenium-based compounds that possess no or little cytotoxicity when inactivated. Upon exposure to light these compounds turn active and become potent cytotoxic agents [182,281]. Both the iodine-based as well as the non-classic photoactivation strategies would permit the development of a targeted agent for photodynamic therapy (PDT) that unfold their cytotoxic properties only at the intended target, thus reducing the systemic stress that is usually involved in cancer

treatments. Additionally, the second approach is oxygen-independent which is especially interesting in hypoxic tumors.

As shown in the above paragraphs the methodologies and molecules developed in this thesis already possess great potential for current projects. In addition, this thesis provided valuable tools for future projects with biomedical orientation that require only minor changes to the existing structures.

It is worth noting that three theses have already begun in the team that deal with some of the listed approaches and propositions.



## General Conclusion



## General Conclusion

Molecular imaging is one of the cornerstones of modern medicine. In recent years optical imaging has emerged as promising modality for molecular imaging. Optical imaging describes a set of techniques that is based on the detection of radiation in the visible and near infrared part of the electromagnetic spectrum.

It has proven its potential in pre-clinical applications and is being developed more and more towards clinical use, mainly because of the recent emergence of fluorescence guided surgery. Currently the field of optical imaging is dominated by xanthene and cyanine dyes [42,43,48]. However, due to their susceptibility to photobleaching and difficult modifiability new and different dyes need to be developed towards practical usability. Due to their elaborateness most fluorophores lack the potential to be easily modified to suit the specific needs of the targeted application. BODIPYs and AzaBODIPYs are a viable alternatives for imaging applications due to their favorable optical properties, stability to biological, chemical and photophysical influences and most of all due to their easy modifiability.

This thesis sought to explore the potential of this dye-family in order to develop multifunctional, fluorescent platforms that can be easily, selectively and site-specifically modified at will to influence spectral properties, tune the solubility in aqueous media, and serve as probe for biomedical applications and more.

Towards that end two classes of fluorophores were investigated; BODIPY-Cl<sub>2</sub> and a variety of azaBODIPYs. For each class of dye we selected a specific application for which we planned to use the developed compounds.

The BODIPY-Cl<sub>2</sub> was explored for its potential in the development of *in vitro* applications. For that we designed a variety of trackable, metal based anti-cancer drugs. The fluorophore served as a multifunctional scaffold onto which we selectively added three different substituents in varying combinations and positions. The application of the platform-approach enabled us to develop 12 gold(I)-based theranostic compounds as well as 8 metal-free agents that are all based on the same base structure with relatively little effort. The entirety of the developed compounds was then characterized to establish structure-activity relationships for each substituent and its positioning in the molecule. For that all compounds underwent a study of their photophysical properties, followed by biological evaluation. Here each compound was tested for their antiproliferative properties (IC<sub>50</sub>) on two murine and one human cancer cell line, followed by confocal imaging on all three cell lines for up to 24h. Finally, each compounds lipophilic balance was evaluated. Using 11 of the 12 gold(I)-containing BODIPYs we performed a gold-uptake study on MDA-MB-231 cells to cross-correlate each property.

Thus the platform-approach enabled us to synthesize, characterize and evaluate a panel of 20 BODIPY-based compounds in a short amount of time and identify two to three molecules (**4b**, **9**, **13**) that display very promising activity on breast-cancer cell lines (EMT6, MDA-MB-231) and melanoma (B16-F10) as well as good optical properties.

These compounds will be investigated further in the future to establish their mode of action (cytotoxic/cytostatic) and the cellular targets that are affected by treatment with them.

Both the platform itself as well as the idea behind its development are applicable to any number of application that requires an easily accessible and highly modifiable fluorescent compound.

## General Conclusion

---

The second system we studied is based on the azaBODIPY-base structure.

This fluorophore was specifically chosen to develop a multifunctional platform that is applicable to *in vivo* applications.

Having no prior experience with this class of fluorophore we initially followed the strategy established by O'Shea and others [216,218,219,221], i.e. using a diphenol-azaBODIPY (1,7-di(phenol)-3,5-di(phenyl)-azaBODIPY in our case).

The choice of our particular fluorophore turned out to be a dismal failure: we successfully managed to functionalize the dye following our specific requirements (monofunctionalization, presence of a possible handle for a second functionalization, introduction of a spacer and a bioconjugation-function). However, the resulting dye **35** and all its preceding derivatives displayed very unfavourable solubility and stacking behavior. They were all difficult to purify and had unfavorable optical properties. Due to these properties we abandoned the chosen functionalization strategy and investigated means to render the dye more soluble in aqueous media and less prone to stacking.

The strategy that we selected is based around the introduction of cationic substituents onto the boron and was inspired by previous works of Ziessel and Ulrich on BODIPYs (e.g. [114]) and has until now been developed very little for azaBODIPYs. Using this approach we successfully managed to render the diphenol-azaBODIPY **30** soluble in water.

For this reason we decided to develop an entirely new strategy that, based on the functionalization of the boron atom introduces ALL substituents onto the boron center, thus increasing the bulkiness of the fluorophore-faces to prevent any stacking. This approach has never been done before. Using this approach we successfully modified two azaBODIPYs, **44** and **48**, and elaborated a large panel of dyes with increasing difficulty of functionalization.

All functionalizations of the boron atom were developed and optimized for bromine-substituted compound **48** and then successfully transposed onto the bromine-free azaBODIPY **44**.

Using this new strategy we managed to develop two entirely water soluble, activated azaBODIPYs (**68** and **69**) that can be conjugated to antibodies. All boron-functionalized azaBODIPYs that were developed during this thesis display excellent optical properties and are strongly fluorescent in the NIR-I region.

AzaBODIPY **68** was then successfully conjugated to an anti-PD-L1 antibody as well as several others and used both for an *in vitro*-study, as well as a proof of concept and preclinical study. The developed antibody-conjugates were stable for at least 48h in mice plasma.

In a preclinical study all antibody-conjugates were then tested in mice bearing CT26 xenografts. All conjugates displayed strong fluorescence emission in the NIR-I region during the *in vivo* study and showed a favorable, very distinct biodistribution without exhibiting any acute toxicity.

To conclude, the development of new and innovative tools for optical fluorescence imaging is of key interest for future advancements both in the development of imaging agents as well as for theranostic applications and tools in fluorescence guided surgery.

Due to the influence of the fluorophore on the properties of vectorized agents as well as trackable therapeutic agents (elimination behavior, specificity, biodistribution,...) the fluorophore needs to be an integral part of the molecule from the very beginning.

This requires highly versatile and stable fluorophores. The platforms that were developed during this thesis certainly possess these properties which is why we have high hopes for the further application of the developed methodology for future projects.

Especially since these projects do not need to be limited to biological uses but hold the potential for very broad application in a variety of fields.

## Materials and Methods



## Materials and Methods

### 4.1 Materials and Methods

Unless stated differently, reactions were carried out in technical grade solvents from Carlo Erba under normal atmosphere. Dry solvents were non-stabilized, purchased from Carlo Erba and dried using a MB-SPS-800 (MBraun) or PureSolv-MD-5 (Inert®). All reagents were purchased from SigmaAldrich or ACROS Organics™ and used as received without further purification. TOTA-Boc was purchased from Iris Biotech GmbH. Anti-PD-L1 and anti-PD-1 antibodies were purchased as PBS-solution from BioXCell. Column chromatography was carried out using silica gel (SigmaAldrich; 40-63  $\mu\text{m}$  230-400 mesh 60Å). Analytical thin-layer chromatography was performed with Merck 60 F254 silica gel (precoated sheets, 0.2 mm thick). Reactions were monitored by thin-layer chromatography, RP-HPLC-MS and  $^{31}\text{P}$ -NMR. Ion exchange was executed using a DOWEX basic ion-exchange resin.

#### 4.1.1 NMR spectra

( $^1\text{H}$ ,  $^{13}\text{C}$ ,  $^{11}\text{B}$ ,  $^{19}\text{F}$ ) were recorded at 300K on Bruker 300 Avance III, Bruker 500 Avance III or Bruker Avance III HD 600 MHz spectrometer (equipped with double resonance broad band probes). Chemical shifts are given relative to TMS ( $^1\text{H}$ ,  $^{13}\text{C}$ ),  $\text{BF}_3 \cdot \text{Et}_2\text{O}$  ( $^{11}\text{B}$ ),  $\text{CFCl}_3$  ( $^{19}\text{F}$ ) and were referenced to the residual solvent signal. High-resolution mass spectra were recorded on a Thermo LTQ Orbitrap XL ESI-MS spectrometer. NMR and Mass-analyses were performed at the "Plateforme d'Analyse Chimique et de Synthèse Moléculaire de l'Université de Bourgogne" (PACSMUB).

#### 4.1.2 Spectroscopic properties

BODIPYs were characterized using a JASCO V630BIO spectrometer. The steady - state fluorescence emission spectra were obtained using a JASCO FP8500 spectrofluorometer. All fluorescence spectra were corrected for apparatus response. Relative quantum efficiencies were obtained by comparing the areas under the corrected emission spectrum. Measurements were performed in DMSO (Sigma Aldrich, spectroscopic grade  $\geq 99.9\%$ ) at 298K. Rhodamine 6G ( $\Phi = 0.94$  in EtOH,  $\lambda_{\text{ex}} = 488$  nm) was used as the standard.

UV-Visible absorption spectra of azaBODIPYs were recorded on a Varian Cary 50 scan (single-beam). Data are reported as absorption maximum wavelength ( $[\lambda_{\text{max}}] = \text{nm}$ ) and molar absorption coefficient at the absorption maximum wavelength ( $[\epsilon] = \text{L mol}^{-1} \text{cm}^{-1}$ ). The steady - state fluorescence emission spectra of azaBODIPYs were obtained using a HORIBA Jobin Yvon Fluorolog spectrofluorometer (software FluorEssence). All fluorescence spectra were corrected for apparatus response. Quartz cuvettes (1.5 mL) with a path length of 1 cm were used. All solutions were prepared with spectroscopic grade solvents. Three different measurements (i.e. different solutions) were performed for each compound. The sample concentrations were chosen to obtain a maximum absorbance between 0.3 and 1.0 for UV spectra and between 0.035 and 0.1 at excitation wavelength for quantum yield measurements. Relative quantum efficiencies were obtained by comparing the areas under the corrected emission spectrum. All measurements were performed in DMSO (Sigma Aldrich, spectroscopic grade  $\geq 99.9\%$ ) and PBS at 298K. Aza-BODIPY **30** ( $\Phi = 0.36$  in  $\text{CHCl}_3$ ,  $\lambda_{\text{ex}} = 670$  nm) was used as the standard. In all  $\Phi_f$  determinations, correction for the solvent refractive index ( $\eta$ ) was applied [DMSO:  $\eta = 1.477$ ,  $\text{CHCl}_3$ :  $\eta = 1.4459$ , PBS:  $\eta = 1.337$ ]. The equation  $\Phi_x = \Phi_{\text{st}} (I_x/I_{\text{st}}) (A_{\text{st}}/A_x) (\eta_x^2/\eta_{\text{st}}^2)$  was used to calculate the quantum yield of the sample, in which

## Materials and Methods

$\Phi_{st}$  is the reported quantum yield of the standard, I is the integrated emission spectrum, A is the absorbance at excitation wavelength, and  $\eta$  is the refractive index of the solvent used. The X subscript denotes unknown, st denotes standard.

### 4.1.3 Analytical HPLC

HPLC-MS analyses were performed on a Thermo-Dionex Ultimate 3000 instrument (pump + autosampler at 20 °C + column oven at 25 °C) equipped with a diode array detector (Thermo-Dionex DAD 3000-RS) and a MSQ Plus single quadrupole mass spectrometer equipped with a Phenomenex Kinetex® column (2.6  $\mu\text{m}$  C18 100 Å, LC Column 50 x 2.1 mm).

The employed gradient for analyses is the following:

<b>Time</b> [min]	<b>%</b> <b>H<sub>2</sub>O + 0.1%</b> <b>formic acid</b>	<b>%</b> <b>ACN + 0.1%</b> <b>formic acid</b>	<b>Flow</b> [mL/min]
0	95	5	0.5
5	0	100	0.5
6.5	0	100	0.5
6.6	95	5	0.5
8.5	95	5	0.5
8.51	95	5	0.05

### 4.1.4 Semi preparative chromatography

Semi preparative separations were executed on a HPLC-system from Shimadzu that is equipped with 2 LC-20AT pumps, a SPD-20A UV/Vis detector, a FRC-10A fraction collector, a SIL-10AP sampler and a CBM-20A control unit. The column was a Shim-Pack GIST 5  $\mu\text{m}$  C18 10x250 mm column. The gradient (gradient A) that was used for purifications (unless mentioned otherwise) is the following:

<b>Time</b> [min]	<b>%</b> <b>H<sub>2</sub>O+0.1%TFA</b>	<b>%</b> <b>ACN+0.1%TFA</b>	<b>Flow</b> [mL/min]
0	95	5	5
10	0	100	5
13	0	100	5
13.1	95	5	5
15	95	5	5

### 4.1.5 MALDI

Matrix-assisted laser desorption ionization/time of flight (MALDI/TOF) mass spectra were obtained on a Bruker DALTONICS Ultra flex II (Bruker Daltonics, Bremen, Germany) mass spectrometer using sinapinic acid as matrix (Sigma-Aldrich, St. Quentin Falavier, France).

### 4.1.6 Determination of cytotoxic properties

5 mM stock solutions were prepared by dissolving the compounds in DMSO.  $10^5$  cells were seeded in 96-well flat-bottomed microplates (final volume 100  $\mu\text{L}$  per well) and incubated for

24h to allow for cell adherence. The medium was then replenished with 100  $\mu$ L fresh medium containing the compounds to be tested at increasing concentrations (final well concentrations ranging from 0.5 to 150  $\mu$ M) at 37°C for 48 h. The cytotoxic activity of compounds and drug references was determined using the MTS assay (Promega). The assay is based on the reduction of a tetrazolium compound [3-(4,5-dimethylthiazol-2-yl)-5-(3-carboxymethoxyphenyl)-2-(4-sulfophenyl)-2H-tetrazolium, inner salt] to a colored formazan in the presence of an electron coupling reagent (phenazine ethosulfate; PES) and NADH/NADPH produced by metabolically active cells. The cells were incubated with MTS for 3h. The amount of formazan produced is proportional to the cumulated metabolic activity present in the well and was detected by measurement of the absorbance at 490 nm on a ClarioStar microplate reader. IC<sub>50</sub> values (i.e., the concentration causing a half maximum response, i.e. either cell death, decrease of metabolic activity or inhibition of mitosis or a combination thereof) were calculated using GraphPad Prism 5.0 software. Each treatment was performed in three independent experiments.

#### 4.1.7 Determination of logP

An isocratic analysis (40 min) was performed by RP-HPLC (Phenomenex Kinetex® 2.6  $\mu$ m C18 100 Å, LC Column 30 x 2.1 mm) using an eluent of 35% of [H<sub>2</sub>O /0.1 % FA] and 65% of [ACN /0.1 % FA]. The dead time was determined using formamide. The capacity factor (k) was calculated with the equation  $k = (t_r - t_0) / t_0$ , in which  $t_r$  was the retention time and  $t_0$  the dead time. Benzoic acid, thymol, naphthalene, diphenyl ether and 2,6-diphenylpyridine were used as standards. Mean values of three injections were used to calculate the logP

#### 4.1.8 Cell lines and culture conditions

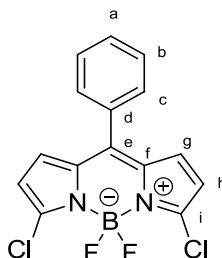
B16F10, MDA-MB-231, EMT6, CT26 and 4T1 cells were purchased from American Type Culture Collection (ATCC, Manassas, VA). The cells were routinely cultured in 75cm<sup>2</sup> tissue culture flasks (Nunc™) at 37 °C in a humidified, 5% CO<sub>2</sub> atmosphere in DMEM supplemented with 10% fetal bovine serum (FBS, D. Dutscher). Cells were sub cultured twice weekly using standard protocols.

## 4.2 Synthetic procedures

### 4.2.1 BODIPYs

#### 4.2.1.1 BODIPY-Cl<sub>2</sub> (**1**)

The target compound was synthesized following reported procedures [103].



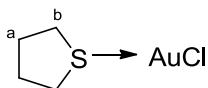
<sup>1</sup>H NMR (300 MHz, CDCl<sub>3</sub>)  $\delta$  (ppm) = 6.44 (d,  $J$  = 4.3 Hz, 2H, H<sub>h</sub>), 6.85 (d,  $J$  = 4.4 Hz, 2H, H<sub>g</sub>), 7.60 – 7.46 (m, 5H, H<sub>a,b,c</sub>).

<sup>11</sup>B NMR (96 MHz, CDCl<sub>3</sub>)  $\delta$  (ppm) = 0.48 (t,  $J_{B-F}$  = 27.9 Hz).

<sup>19</sup>F NMR (282 MHz, CDCl<sub>3</sub>)  $\delta$  (ppm) = -148.24 (q,  $J_{F-B}$  = 27.9 Hz).

4.2.1.2 (tht)AuCl (**2**)

1.003g (2.43mmol, 1eq) H<sub>2</sub>AuCl<sub>4</sub>\*xH<sub>2</sub>O were dissolved in 1.55 mL water and 7.7 mL EtOH, followed by the addition of 0.433 mL (5mmol, 2eq) THT and stirring for 15 minutes (formation of an off-white precipitate). The suspension was centrifuged and the supernatant discarded. The solid was washed using Et<sub>2</sub>O and sonicated repeatedly until the smell of THT was almost imperceptible. The solid was dried to yield 744 mg (2.32 mmol, yield = 96%) of the target compound as a grey-white powder.

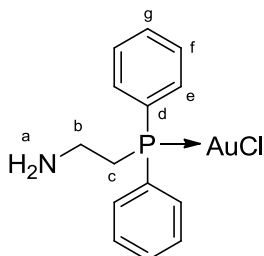


<sup>1</sup>H NMR (300 MHz, C<sub>6</sub>D<sub>6</sub>) δ (ppm) = 0.80 (s, vbr, 2H, H<sub>a</sub>), 1.04 (s, vbr, 2H, H<sub>a'</sub>), 1.98 (s, vbr, 2H, H<sub>b</sub>), 2.22 (s, vbr, 2H, H<sub>b'</sub>)

<sup>13</sup>C NMR (75 MHz, C<sub>6</sub>D<sub>6</sub>) δ (ppm) = 29.9 (s, C<sub>a</sub>), 39.6 (s, C<sub>b</sub>)

4.2.1.3 2-(Diphenylphosphino)ethylamine-aurichloride (**3**)

In a glovebox 500 mg (2.18 mmol, 1eq) 2-(diphenylphosphino)ethylamine were placed in a schlenktube and dissolved in 4mL (dry) DCM. 699 mg (2.18 mmol, 1eq) (tht)AuCl (**2**) were dissolved in 2mL dry DCM, added to the phosphine-solution and stirred over night at room temperature. Upon completion the solvents were evaporated to near dryness. The crude product was redissolved in a minute amount of DCM, precipitated twice with Et<sub>2</sub>O and thoroughly dried to obtain 936 mg (2.03 mmol, yield = 93%) of the target compound as a white, odorless powder.



<sup>1</sup>H NMR (500 MHz, CDCl<sub>3</sub>) δ (ppm) = 2.66 (td, *J* = 10.7, 7.8 Hz, 2H, H<sub>c</sub>), 3.15 – 3.01 (m, 2H, H<sub>b</sub>), 7.54 – 7.42 (m, 6H, H<sub>f,g</sub>), 7.67 (dd, *J* = 13.0, 7.1 Hz, 4H, H<sub>e</sub>).

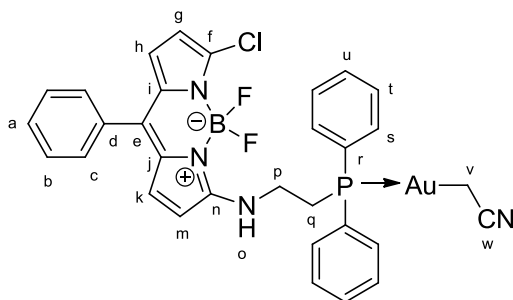
<sup>13</sup>C NMR (126 MHz, CDCl<sub>3</sub>) δ (ppm) = 32.1 (d, *J*<sub>C-P</sub> = 37.9 Hz, C<sub>b</sub>), 38.8 (d, *J*<sub>C-P</sub> = 6.9 Hz, C<sub>c</sub>), 129.0 (s, C<sub>d</sub>), 129.5 (d, *J*<sub>C-P</sub> = 11.7 Hz, C<sub>g</sub>), 132.2 (s, C<sub>f</sub>), 133.3 (d, *J*<sub>C-P</sub> = 13.3 Hz, C<sub>e</sub>).

<sup>31</sup>P NMR (202 MHz, CDCl<sub>3</sub>) δ (ppm) = 23.86

4.2.1.4 Compound **4a**

137 mg (0.376 mmol, 2eq) gold(I)-phosphine **3**, 50 mg (148.4 μmol, 1 eq) Dichloro-BODIPY **1** and 105 mg (0.742 mmol, 5 eq) K<sub>2</sub>CO<sub>3</sub> were placed in a 50 mL round bottom flask and put under argon. 15 mL dry ACN were added and the reaction heated under reflux for 26h.

The solvents were evaporated and the crude product was purified by column chromatography (eluent: Hexane/Et<sub>3</sub>N to Hexane/EtOAc/Et<sub>3</sub>N 97/3→60/40/3). After evaporation of solvents under reduced pressure the product was precipitated from DCM/pentane to yield 95 mg (123.9 μmol, 84%) of **4a** as an orange solid.



$^1\text{H}$  NMR (500 MHz, DMSO- $d_6$ )  $\delta$  (ppm) = 1.48 (d,  $J$  = 9.7 Hz, 2H,  $H_v$ ), 3.11 (td,  $J$  = 10.2, 5.9 Hz, 2H,  $H_q$ ), 3.72 (s, 2H,  $H_p$ ), 6.20 (d,  $J$  = 3.7 Hz, 1H,  $H_m$ ), 6.24 (d,  $J$  = 3.8 Hz, 1H,  $H_k$ ), 6.52 (d,  $J$  = 5.1 Hz, 1H,  $H_g$ ), 6.95 (d,  $J$  = 5.1 Hz, 1H,  $H_h$ ), 7.48 – 7.44 (m, 2H,  $H_c$ ), 7.54 – 7.50 (m, 3H,  $H_b$ ,  $H_a$ ), 7.59 – 7.54 (m, 6H,  $H_u$ ,  $H_t$ ), 7.83 – 7.77 (m, 4H,  $H_s$ ), 8.57 (t,  $J$  = 7.0 Hz, 1H,  $H_o$ )

$^{13}\text{C}$  NMR (126 MHz, DMSO- $d_6$ )  $\delta$  (ppm) = 6.0 (d,  $J$  = 87.6 Hz,  $C_v$ ), 27.4 (d,  $J$  = 30.2 Hz,  $C_p$ ), 41.1 (d,  $J$  = 10.5 Hz,  $C_q$ ), 111.8 (s,  $C_g$ ), 114.3 (s,  $C_m$ ), 117.5 (s,  $C_h$ ), 126.0 (s,  $C_i$ ,  $C_j$ ), 127.0 (d,  $J$  = 6.3 Hz,  $C_w$ ), 128.3 (s,  $C_e$ ), 128.5 (s,  $C_k$ ), 129.2 (s,  $C_a$ ), 129.4 (d,  $J$  = 10.8 Hz,  $C_u$ ), 130.1 (s,  $C_b$ ), 130.3 (d,  $J$  = 51.7 Hz,  $C_r$ ), 131.1 (s,  $C_d$ ), 131.7 (d,  $J$  = 1.8 Hz,  $C_t$ ), 133.2 (d,  $J$  = 13.3 Hz,  $C_s$ ), 133.3 (s,  $C_f$ ), 133.6 (d,  $J$  = 1.9 Hz,  $C_n$ ), 135.7 (s,  $C_c$ ).

$^{11}\text{B}$  NMR (160 MHz, DMSO- $d_6$ )  $\delta$  (ppm) = 0.65 (t,  $J$  = 32.7 Hz)

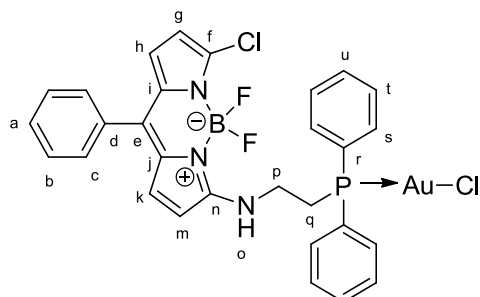
$^{19}\text{F}$  NMR (470 MHz, DMSO- $d_6$ )  $\delta$  (ppm) = -144.36 (q,  $J$  = 32.7 Hz)

$^{31}\text{P}$  NMR (202 MHz, DMSO- $d_6$ )  $\delta$  (ppm) = 32.46

HR-MS (ESI): calculated for  $\text{C}_{31}\text{H}_{26}\text{Au}_1\text{B}_1\text{Cl}_1\text{F}_2\text{N}_4\text{P}_1\text{Na}_1$  [ $\text{M}+\text{Na}$ ] $^+$  789.12025; found 789.12025

#### 4.2.1.5 Compound **4b**

173 mg (0.376 mmol, 1.2 eq) of gold(I)-phosphine **3**, 106 mg (0.314 mmol, 1eq) of BODIPY **1** and 203mg (1.47mmol, 5eq)  $\text{K}_2\text{CO}_3$  were placed in a 50 mL round bottom flask and put under argon. 15 mL dry THF were added and the reaction was refluxed for 70 minutes. The solvents were evaporated and the crude product was purified by column chromatography on silica gel using hexane/EtOAc/ $\text{Et}_3\text{N}$  (90/10/3 to 70/30/3) as eluent. After evaporation of the solvents under reduced pressure the crude product was dissolved in  $\text{CH}_2\text{Cl}_2$  and crushed out with pentane to yield 218 mg (285.74  $\mu\text{mol}$ , yield = 91%) of **4b** as an orange solid.



$^1\text{H}$  NMR (500 MHz, DMSO- $d_6$ )  $\delta$  (ppm) = 3.17 (ddd,  $J$  = 11.7, 7.8, 5.1 Hz, 2H,  $H_q$ ), 3.71 (s, 2H,  $H_p$ ), 6.19 (d,  $J$  = 3.8 Hz, 1H,  $H_m$ ), 6.24 (d,  $J$  = 3.8 Hz, 1H,  $H_k$ ), 6.57 (d,  $J$  = 5.1 Hz, 1H,  $H_g$ ), 6.96 (d,  $J$  = 5.1 Hz, 1H,  $H_h$ ), 7.47 – 7.43 (m, 2H,  $H_c$ ), 7.54 – 7.50 (m, 3H,  $H_b$ ,  $H_a$ ), 7.63 – 7.55 (m, 6H,  $H_{at}$ ,  $H_u$ ), 7.84 – 7.78 (m, 4H,  $H_s$ ), 8.58 (t,  $J$  = 5.9 Hz, 1H,  $H_o$ )

$^{13}\text{C}$  NMR (126 MHz, DMSO- $d_6$ )  $\delta$  (ppm) = 27.4 (d,  $J$  = 36.1 Hz,  $C_p$ ), 41.2 (d,  $J$  = 9.7 Hz,  $C_q$ ), 111.8 (s,  $C_g$ ), 114.4 (s,  $C_m$ ), 117.5 (s,  $C_h$ ), 126.0 (s,  $C_i$ ,  $C_j$ ), 128.4 (s,  $C_e$ ), 128.5 (s,  $C_k$ ), 128.9 (d,  $J$  = 60.7 Hz,  $C_r$ ), 129.2 (s,  $C_a$ ), 129.4 (d,  $J$  = 11.6 Hz,  $C_u$ ), 130.1 (s,  $C_b$ ), 131.1 (s,  $C_d$ ), 132.1 (d,  $J$  = 2.3 Hz,  $C_t$ ), 133.2 (d,  $J$  = 13.5 Hz,  $C_s$ ), 133.3 (s,  $C_f$ ), 133.7 (s,  $C_n$ ), 135.8 (s,  $C_c$ ),

$^{11}\text{B}$  NMR (160 MHz, DMSO- $d_6$ )  $\delta$  (ppm) = 0.64 (t,  $J$  = 32.7 Hz)

## Materials and Methods

$^{19}\text{F}$  NMR (470 MHz, DMSO- $d_6$ )  $\delta$  (ppm) = -144.48 (q,  $J$  = 32.7 Hz)

$^{31}\text{P}$  NMR (202 MHz, DMSO- $d_6$ )  $\delta$  (ppm) = 24.32 (s)

HR-MS (ESI): calculated for  $\text{C}_{29}\text{H}_{24}\text{Au}_1\text{B}_1\text{Cl}_2\text{F}_2\text{N}_3\text{P}_1\text{Na}_1$   $[\text{M}+\text{Na}]^+$  784.07037; found 784.07020

### Variation a)

164 mg (0.356 mmol, 3eq) gold(I)-phosphine **3**, 41 mg (0.119 mmol, 1eq) Dichloro-BODIPY **1** and 102 mg (1.187 mmol, 10eq)  $\text{NaHCO}_3$  were placed in a 50 mL round bottom flask and put under argon. 15 mL dry ACN were added and the reaction refluxed for 70 min.

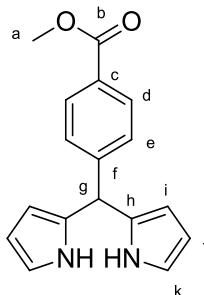
The solvents were evaporated and the crude product was purified by column chromatography (Hexane+3% $\text{Et}_3\text{N}$   $\rightarrow$  Hexane 6 : 4  $\text{EtOAc}$ +3% $\text{Et}_3\text{N}$ ). After evaporation of solvents under reduced pressure the product was precipitated from DCM/pentane to yield 76.5 mg (yield = 84%) of **4b** as an orange solid.

### 4.2.1.6 methyl 4- (di (1H-pyrrol-2-yl)methyl)benzoate (**5**)

68 mL of freshly distilled pyrrole were placed into a 500 mL round-bottom flask and degassed with  $\text{N}_2$ . 4 g (24.37 mmol, 1eq) methyl-4-formylbenzoate was added, followed by 0.1 mL (2.4 mmol, 0.1eq) TFA. The reaction was stirred under  $\text{N}_2$  for 1 h.

The solvents were evaporated to yield a violet-white precipitate. The precipitate was solubilized in DCM, precipitated by addition of heptane and filtered over a glass frit.

If the filtrate still contains particles the solvents were removed under reduced pressure, the resulting solid was resolubilized in MeOH, precipitated with heptane and filtered off to yield 4.9406 g (17.62 mmol, yield = 72%) of the target compound as a white to off-white solid.

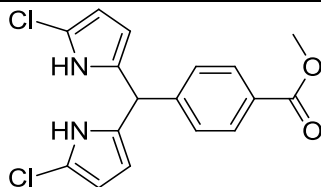


$^1\text{H}$  NMR (300 MHz,  $\text{CDCl}_3$ )  $\delta$  (ppm) = 3.91 (s, 3H,  $\text{H}_a$ ), 5.53 (s, 1H,  $\text{H}_g$ ), 5.90 (t,  $^3J$  = 2.7 Hz, 2H,  $\text{H}_i$ ), 6.16 (dd,  $^3J$  = 5.9,  $^4J$  = 2.7 Hz, 2H,  $\text{H}_j$ ), 6.72 (dd,  $^3J$  = 4.0 Hz,  $^4J$  = 2.6 Hz, 2H,  $\text{H}_k$ ), 7.29 (d,  $^3J$  = 8.1 Hz, 2H,  $\text{H}_e$ ), 7.98 (d,  $^3J$  = 8.4 Hz, 2H,  $\text{H}_d$ )

$^{13}\text{C}$  NMR (75 MHz,  $\text{CDCl}_3$ )  $\delta$  (ppm) = 44.2 (s,  $\text{C}_g$ ), 52.3 (s,  $\text{C}_a$ ), 107.7 (s,  $\text{C}_i$ ), 108.3 (s,  $\text{C}_j$ ), 117.2 (s,  $\text{C}_k$ ), 128.5 (s,  $\text{C}_h$ ), 129.1 (s,  $\text{C}_c$ ), 130.1 (s,  $\text{C}_d$ ), 131.7 (s,  $\text{C}_e$ ), 143.6 (s,  $\text{C}_f$ ), 167.0 (s,  $\text{C}_b$ ).

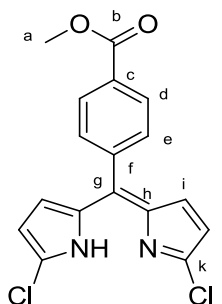
### 4.2.1.7 1,1'-Dichloro-5- (4- (methoxycarbonyl)phenyl)dipyrromethane

4.74 g (16.9 mmol, 1 eq) dipyrromethane (**5**) were placed into a round-bottom flask and dissolved in 50 mL THF. The solution was degassed and cooled to  $-78^\circ\text{C}$ . 4.95 g (37.2 mmol, 2.2 eq) NCS were suspended in several mL of THF and added to the reaction mixture. The reaction was stirred at  $-78^\circ\text{C}$  for 1 h, let to heat up to room temperature and stirred for another 3 h. The reaction was quenched by addition of 60 mL of water and extracted thrice with DCM. The organic layers were combined, dried over anhydrous  $\text{MgSO}_4$  and solvents removed under reduced pressure to yield the target-compound as a black solid that was directly engaged in the next step.



#### 4.2.1.8 1,1'-Dichloro-5-(4-(methoxycarbonyl)phenyl)dipyrromethene (**6**)

The crude product was dissolved in 200 mL dry DCM. 4.61 g (20.28 mmol, 1.2 eq) DDQ was added and the solution stirred overnight. Once TLC indicates completion (product is unstable on TLC!) the solvents were removed and the crude product purified by column chromatography using an eluent of heptane: EtOAc 100%--> 9:1. Product fractions were collected, evaporated to dryness and precipitated from hot DCM by addition of pentane. 5.12 g (14.75 mmol, yield = 87% over two steps) of the target compound were isolated as red-fluorescent crystals.

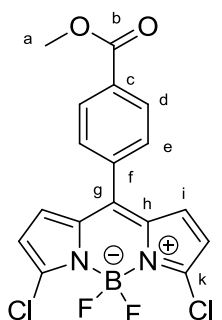


$^1\text{H NMR}$  (300 MHz,  $\text{CDCl}_3$ )  $\delta$  (ppm) = 3.97 (s, 3H,  $\text{H}_a$ ), 6.26 (d,  $^3J = 4.3$  Hz, 2H,  $\text{H}_j$ ), 6.46 (d,  $^3J = 4.3$  Hz, 2H,  $\text{H}_i$ ), 7.51 (d,  $^3J = 8.5$  Hz, 2H,  $\text{H}_e$ ), 8.12 (d,  $^3J = 8.5$  Hz, 2H,  $\text{H}_d$ )

$^{13}\text{C NMR}$  (75 MHz,  $\text{CDCl}_3$ )  $\delta$  (ppm) = 52.5 (s,  $\text{C}_a$ ), 117.5 (s,  $\text{C}_j$ ), 129.2 (s,  $\text{C}_i$ ), 130.0 (s,  $\text{C}_e$ ), 130.9 (s,  $\text{C}_c$ ), 131.1 (s,  $\text{C}_d$ ), 138.3 (s,  $\text{C}_f$ ), 138.5 (s,  $\text{C}_g$ ), 140.2 (s,  $\text{C}_h$ ), 142.5 (s,  $\text{C}_k$ ), 166.7 (s, C,  $\text{C}_b$ )

#### 4.2.1.9 BODIPY **7**

2.3422 g (6.75 mmol, 1 eq) dipyrromethene **6** was dissolved in 180mL dry DCM. 2.1 mL (14.85 mmol, 2.2eq)  $\text{Et}_3\text{N}$  and 4mL 48wt%- $\text{BF}_3 \cdot \text{Et}_2\text{O}$  were added and the mixture stirred for 24h at room temperature. The reaction mixture was extracted thrice with water and the organic fractions dried over anhydrous  $\text{MgSO}_4$ . After removal of solvents under reduced pressure the compound was purified by column chromatography on silica gel (gradient heptane 99 : 1 EtOAc  $\rightarrow$  heptane 1 : 4 EtOAc). The collected fractions were evaporated, the obtained solid was precipitated once from DCM/pentane to obtain 2.1976 g (5.56 mmol, yield = 82%) of the desired compound as a dark red- green metallic powder.



## Materials and Methods

$^1\text{H}$  NMR (300 MHz,  $\text{CDCl}_3$ )  $\delta$  (ppm) = 3.99 (s, 3H,  $\text{H}_a$ ), 6.45 (d,  $J = 4.3$  Hz, 2H,  $\text{H}_j$ ), 6.79 (d,  $J = 3.9$  Hz, 2H,  $\text{H}_i$ ), 7.57 (d,  $J = 8.5$  Hz, 2H,  $\text{H}_e$ ), 8.19 (d,  $J = 8.5$  Hz, 2H,  $\text{H}_d$ )

$^{13}\text{C}$  NMR (75 MHz,  $\text{CDCl}_3$ )  $\delta$  (ppm) = 52.7 ( $\text{C}_a$ ), 119.5 ( $\text{C}_j$ ), 129.8 ( $\text{C}_e$ ), 130.6 ( $\text{C}_c$ ), 131.5 ( $\text{C}_i$ ), 132.5 ( $\text{C}_h$ ), 133.7 ( $\text{C}_d$ ), 136.7 ( $\text{C}_g$ ), 142.4 ( $\text{C}_f$ ), 145.9 ( $\text{C}_k$ ), 166.2 ( $\text{C}_b$ )

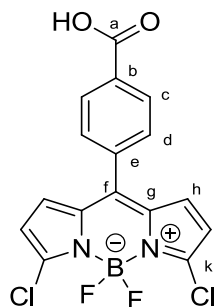
$^{11}\text{B}$  NMR (96 MHz,  $\text{CDCl}_3$ )  $\delta$  (ppm) = 0.46 (t,  $J_{\text{B-F}} = 27.7$  Hz)

$^{19}\text{F}$  NMR (282 MHz,  $\text{CDCl}_3$ )  $\delta$  (ppm) = -148.17 (q,  $J_{\text{F-B}} = 27.7$  Hz)

HR-MS (ESI): calculated for  $\text{C}_{17}\text{H}_{11}\text{B}_1\text{Cl}_2\text{F}_2\text{N}_2\text{O}_2\text{Na}_1$   $[\text{M}+\text{Na}]^+$  417.01509; found 417.01396

### 4.2.1.10 Compound **8**

0.5 g (1.27 mmol) BODIPY **7** were placed into a 100 mL round-bottom flask and dissolved in THF (20mL). 20mL 3M HCl were added and the mixture refluxed for 60h. Upon completion the solvents were removed under reduced pressure. The crude product was purified by column chromatography (eluent: DCM  $\rightarrow$  DCM/MeOH 95 : 5). The product fractions were combined and the solvents evaporated. The product was precipitated from DCM/pentane to obtain 0.2603 g (0.686 mmol, yield = 54%) of the target compound as a dark red solid.



$^1\text{H}$  NMR (500 MHz,  $\text{DMSO-d}_6$ )  $\delta$  (ppm) = 6.80 (d,  $^3J = 4.6$  Hz, 2H,  $\text{H}_i$ ), 7.08 (d,  $^3J = 4.4$  Hz, 2H,  $\text{H}_h$ ), 7.76 (dt,  $^3J = 8.5$  Hz,  $^4J = 3.5$  Hz, 2H,  $\text{H}_d$ ), 8.12 (dt,  $^3J = 8.5$  Hz,  $^4J = 3.5$  Hz, 2H,  $\text{H}_c$ ).

$^{13}\text{C}$  NMR (126 MHz,  $\text{DMSO-d}_6$ )  $\delta$  (ppm) = 119.7 ( $\text{C}_i$ ), 129.2 (deprotonated form,  $\text{C}_d$ ), 129.4 ( $\text{C}_d$ ), 130.5 (deprotonated form,  $\text{C}_c$ ), 131.0 ( $\text{C}_c$ ), 132.8 ( $\text{C}_h$ ), 133.0 ( $\text{C}_g$ ), 133.1 ( $\text{C}_f$ ), 135.4 ( $\text{C}_b$ ), 143.1 ( $\text{C}_e$ ), 143.9 ( $\text{C}_k$ ), 166.7 ( $\text{C}_a$ ), 167.1 ( $\text{C}_a$ , deprotonated form).

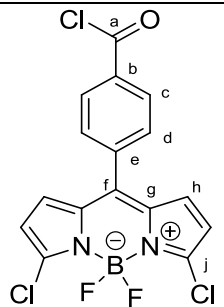
$^{11}\text{B}$  NMR (160 MHz,  $\text{DMSO-d}_6$ )  $\delta$  (ppm) = 0.30 (t,  $J_{\text{B-F}} = 28.1$  Hz).

$^{19}\text{F}$  NMR (470 MHz,  $\text{DMSO-d}_6$ )  $\delta$  (ppm) = -145.75 (q,  $J_{\text{F-B}} = 28.0$  Hz).

HR-MS (ESI): calculated for  $\text{C}_{16}\text{H}_9\text{BCl}_2\text{F}_2\text{N}_2\text{O}_2\text{Na}$   $[\text{M}+\text{Na}]^+$  402.99944; found 403.00080

### 4.2.1.11 BODIPY **8**-acyl chloride

51 mg (0.13 mmol, 1eq) of BODIPY **8** and 73 mg (50.3 mmol, 4eq) of  $\text{K}_2\text{CO}_3$  were placed into a 50 mL round bottom flask and dissolved in 30 mL DCM under argon. 23  $\mu\text{L}$  (0.26 mmol, 2eq) of oxalyl chloride were added, followed by a droplet of DMF. The reaction was stirred at room temperature for 45min. The solvents were evaporated under reduced pressure to yield the target compound quantitatively as a pink solid. The crude product was directly engaged in the next reaction without any further purification.



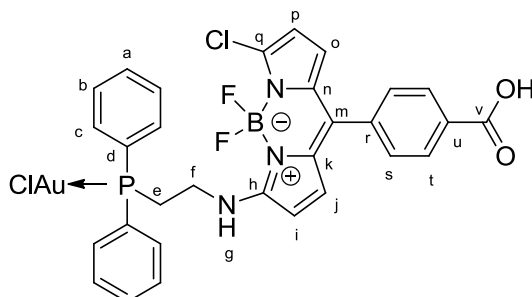
$^1\text{H}$  NMR (300 MHz,  $\text{CDCl}_3$ )  $\delta$  (ppm) = 6.47 (d,  $^3J = 4.4$  Hz, 2H,  $\text{H}_i$ ), 6.77 (d,  $^3J = 4.1$  Hz, 2H,  $\text{H}_h$ ), 7.66 (d,  $^3J = 8.6$  Hz, 2H,  $\text{H}_d$ ), 8.28 (d,  $^3J = 8.6$  Hz, 2H,  $\text{H}_c$ )

$^{11}\text{B}$  NMR (96 MHz,  $\text{CDCl}_3$ )  $\delta$  (ppm) = 0.45 (t,  $J_{\text{B-F}} = 27.6$  Hz)

$^{19}\text{F}$  NMR (282 MHz,  $\text{CDCl}_3$ )  $\delta$  (ppm) = -148.14 (q,  $J_{\text{F-B}} = 27.7$  Hz)

#### 4.2.1.12 Compound 9

Gold(I)-phosphine **3** (145 mg, 0.315 mmol, 1.2eq), BODIPY **8** (100 mg, 0.26mmol, 1eq) and  $\text{K}_2\text{CO}_3$  (181 mg, 1.96 mmol, 5eq) were placed in a 20 mL round bottom flask and put under argon. 15 mL dry THF were added and the reaction refluxed overnight. The solvents were evaporated and the crude product was purified by column chromatography using  $\text{CH}_2\text{Cl}_2/\text{MeOH}$  (100:0 to 80:20) as eluent. After evaporation of solvents under reduced pressure the product was dissolved in a minimal amount of  $\text{CH}_2\text{Cl}_2$  and precipitated by addition of pentane to obtain 202.2 mg (208  $\mu\text{mol}$ ; yield = 80%) of **9** as a red-orange solid.



$^1\text{H}$  NMR (500 MHz,  $\text{DMSO-d}_6$ )  $\delta$  (ppm) = 3.21 – 3.13 (m, 2H,  $\text{H}_e$ ), 3.78 – 3.65 (m, 2H,  $\text{H}_i$ ), 6.21 (d,  $J = 3.8$  Hz, 1H,  $\text{H}_i$ ), 6.25 (d,  $J = 3.8$  Hz, 1H,  $\text{H}_j$ ), 6.61 (d,  $J = 5.1$  Hz, 1H,  $\text{H}_p$ ), 7.01 (d,  $J = 5.2$  Hz, 1H,  $\text{H}_o$ ), 7.63 – 7.53 (m, 8H,  $\text{H}_{a,b}$ ,  $\text{H}_s$ ), 7.81 (ddd,  $J = 13.2, 7.8, 1.5$  Hz, 4H,  $\text{H}_c$ ), 8.06 (d,  $J = 8.3$  Hz, 2H,  $\text{H}_t$ ), 8.67 (s, 1H,  $\text{H}_g$ )

$^{13}\text{C}$  NMR (126 MHz,  $\text{DMSO-d}_6$ )  $\delta$  (ppm) = 27.4 (d,  $J = 35.6$  Hz,  $\text{C}_i$ ), 41.3 (d,  $J = 11.0$  Hz,  $\text{C}_e$ ), 111.9 (s,  $\text{C}_p$ ), 114.9 (s,  $\text{C}_i$ ), 117.3 (s,  $\text{C}_o$ ), 126.1 (s,  $\text{C}_n$ ,  $\text{C}_k$ ), 127.1 (s,  $\text{C}_m$ ), 128.9 (d,  $J = 60.7$  Hz,  $\text{C}_d$ ), 129.3 (s,  $\text{C}_j$ ), 129.4 (d,  $J = 11.5$  Hz,  $\text{C}_a$ ), 130.4 (s,  $\text{C}_s$ ), 130.7 (s,  $\text{C}_u$ ), 131.3 (s,  $\text{C}_r$ ), 132.1 (d,  $J = 2.3$  Hz,  $\text{C}_b$ ), 133.2 (d,  $J = 13.5$  Hz,  $\text{C}_c$ ), 133.8 (s,  $\text{C}_q$ ), 135.8 (s,  $\text{C}_t$ ), 137.6 (s,  $\text{C}_h$ ), 161.7 (s,  $\text{C}_v$ ),

$^{11}\text{B}$  NMR (160 MHz,  $\text{DMSO-d}_6$ )  $\delta$  (ppm) = 0.64 (t,  $J = 32.4$  Hz)

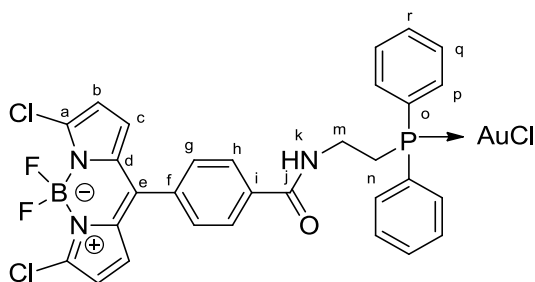
$^{19}\text{F}$  NMR (470 MHz,  $\text{DMSO-d}_6$ )  $\delta$  (ppm) = -144.38 (q,  $J_{\text{F-B}} = 32.3$  Hz)

$^{31}\text{P}$  NMR (202 MHz,  $\text{DMSO-d}_6$ )  $\delta$  (ppm) = 24.33

HR-MS (ESI): calculated for  $\text{C}_{30}\text{H}_{24}\text{Au}_1\text{B}_1\text{Cl}_2\text{F}_2\text{N}_3\text{O}_2\text{P}_1\text{Na}_1$   $[\text{M}+\text{Na}]^+$  828.06020; found 828.06136

4.2.1.13 Compound **10**

The crude acyl chloride of **8** was redissolved in 10 mL CH<sub>2</sub>Cl<sub>2</sub> and 60.4 mg (0.131 mmol, 1eq) of gold(I)-phosphine **3** was added. The resulting solution was stirred for 100 min at room temperature, the solvents were evaporated and the crude product purified by column chromatography on silica gel, using CH<sub>2</sub>Cl<sub>2</sub>/MeOH (100:0 to 99.2:0.8) as eluent. The solvents were removed under reduced pressure and the product dissolved in a minimal amount of CH<sub>2</sub>Cl<sub>2</sub>, followed by precipitation with pentane to yield pure **10** (60.1 mg, 71.5 μmol, yield = 55%) as a pink-orange solid.



<sup>1</sup>H NMR (500 MHz, CDCl<sub>3</sub>) δ (ppm) = 2.96 (dt, <sup>3</sup>J = 10.6, <sup>4</sup>J = 6.5 Hz, 2H, H<sub>n</sub>), 3.81 (dq, <sup>3</sup>J = 17.2, <sup>3</sup>J = 6.4 Hz, 2H, H<sub>m</sub>), 6.45 (d, <sup>3</sup>J = 4.4 Hz, 2H, H<sub>b</sub>), 6.80 (d, <sup>3</sup>J = 4.3 Hz, 2H, H<sub>c</sub>), 6.96 (t, <sup>3</sup>J = 5.8 Hz, 1H, H<sub>k</sub>), 7.55 – 7.46 (m, 8H, H<sub>g</sub>, H<sub>q</sub>, H<sub>r</sub>), 7.71 (ddd, J = 13.2, 8.0, 1.5 Hz, 4H, H<sub>p</sub>), 7.90 (d, <sup>3</sup>J = 8.3 Hz, 2H, H<sub>h</sub>)

<sup>13</sup>C NMR (126 MHz, CDCl<sub>3</sub>) δ (ppm) = 28.5 (d, J = 38.5 Hz, C<sub>m</sub>), 36.6 (d, J = 3.5 Hz, C<sub>n</sub>), 119.4 (s, (C<sub>b</sub>)), 127.5 (s, C<sub>c</sub>), 128.6 (d, J = 61.4 Hz, C<sub>o</sub>), 129.7 (d, J = 11.8 Hz, C<sub>r</sub>), 130.7 (s, C), 130.8 (s, C<sub>g</sub>), 131.6 (s, C<sub>h</sub>), 132.5 (d, J = 2.6 Hz, C<sub>q</sub>), 133.4 (d, J = 13.3 Hz, C<sub>p</sub>), 133.7 (s, C<sub>d</sub>, C<sub>e</sub>), 135.7 (s, C<sub>i</sub>), 142.4 (s, C<sub>f</sub>), 145.8 (s, C<sub>a</sub>), 166.7 (s, C<sub>j</sub>).

<sup>11</sup>B NMR (160 MHz, CDCl<sub>3</sub>) δ (ppm) = 0.46 (t, J<sub>B-F</sub> = 27.7 Hz).

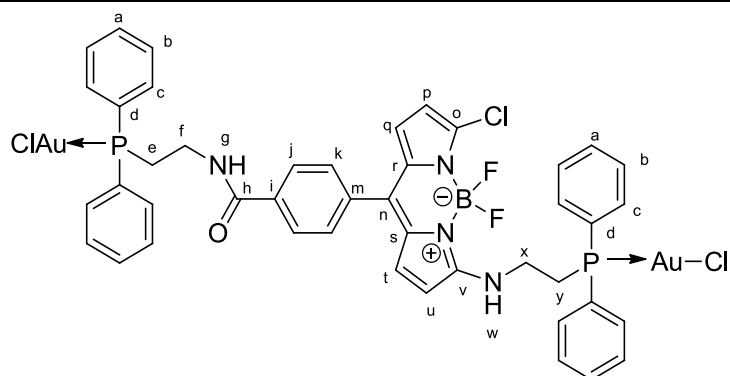
<sup>19</sup>F NMR (470 MHz, CDCl<sub>3</sub>) δ (ppm) = -148.10 (q, J = 27.8 Hz).

<sup>31</sup>P NMR (202 MHz, CDCl<sub>3</sub>) δ (ppm) = 23.47.

HR-MS (ESI): calculated for C<sub>30</sub>H<sub>23</sub>Au<sub>1</sub>B<sub>1</sub>Cl<sub>3</sub>F<sub>2</sub>N<sub>3</sub>O<sub>1</sub>P<sub>1</sub>Na<sub>1</sub> [M+Na]<sup>+</sup> 848.02337; found 828.02495

4.2.1.14 Compound **11**

100 mg (0.262 mmol, 1 eq) of BODIPY **8** were placed in a round bottom flask and dissolved in 10 mL DCM. 45 μL (0.524 mmol, 2 eq) oxalyl chloride were added, followed by a droplet of DMF. The reaction was stirred at room temperature for 1h before evaporation to dryness. The solid was redissolved in 10 mL THF. 181 mg (1.31 mmol, 5 eq) of K<sub>2</sub>CO<sub>3</sub> and 254 mg (0.551 mmol, 2.1eq) of gold(I)-phosphine **3** were added and the reaction refluxed for 80 min. Upon total consumption of the BODIPY starting material the solvents were evaporated and the product was purified by column chromatography on silica gel, using as eluent CH<sub>2</sub>Cl<sub>2</sub>/MeOH (99:1). The product fractions were collected, and evaporated to dryness. The product was dissolved in a minimal amount of CH<sub>2</sub>Cl<sub>2</sub> and crushed out with pentane twice to yield **11** (305 mg, 243.7 μmol, yield = 93%) as an orange powder.



$^1\text{H}$  NMR (500 MHz,  $\text{DMSO-d}_6$ )  $\delta$  (ppm) = 3.09 (dt,  $J$  = 11.0, 7.0 Hz, 2H,  $\text{H}_y$ ), 3.17 (dd,  $J$  = 15.9, 11.4 Hz, 2H,  $\text{H}_e$ ), 3.58 (dt,  $J$  = 20.3, 6.7 Hz, 2H,  $\text{H}_x$ ), 3.80 – 3.65 (m, 2H,  $\text{H}_f$ ), 6.20 (d,  $J$  = 3.9 Hz, 1H,  $\text{H}_u$ ), 6.26 (d,  $J$  = 3.8 Hz, 1H,  $\text{H}_t$ ), 6.65 – 6.59 (m, 1H,  $\text{H}_p$ ), 6.96 (t,  $J$  = 5.6 Hz, 1H,  $\text{H}_q$ ), 7.50 (d,  $J$  = 8.3 Hz, 2H,  $\text{H}_k$ ), 7.63 – 7.53 (m, 12H,  $\text{H}_{a,b}$ ), 7.85 – 7.77 (m, 8H,  $\text{H}_c$ ), 7.89 (d,  $J$  = 8.3 Hz, 2H,  $\text{H}_j$ ), 8.70 – 8.62 (m, 1H,  $\text{H}_w$ ), 8.86 (t,  $J$  = 5.6 Hz, 1H,  $\text{H}_g$ )

$^{13}\text{C}$  NMR (126 MHz,  $\text{DMSO-d}_6$ )  $\delta$  (ppm) = 26.4 (d,  $J$  = 37.7 Hz,  $\text{C}_f$ ), 27.4 (d,  $J$  = 39.3 Hz,  $\text{C}_x$ ), 35.8 (d,  $J$  = 6.2 Hz,  $\text{C}_e$ ), 41.3 (d,  $J$  = 10.6 Hz,  $\text{C}_y$ ), 111.9 (s,  $\text{C}_p$ ), 114.8 (s,  $\text{C}_u$ ), 117.3 (s,  $\text{C}_q$ ), 126.1 (s,  $\text{C}_r$ ,  $\text{C}_s$ ), 127.4 (s,  $\text{C}_j$ ), 128.9 (d,  $J$  = 60.8 Hz,  $\text{C}_d$ ), 129.0 (s,  $\text{C}_n$ ), 129.7 (s,  $\text{C}_t$ ), 129.4 (dd,  $J$  = 11.7, 3.5 Hz,  $\text{C}_a$ ), 130.0 (s,  $\text{C}_k$ ), 130.8 (s,  $\text{C}_i$ ), 132.1 (dd,  $J$  = 15.5, 2.1 Hz,  $\text{C}_b$ ), 133.2 (dd,  $J$  = 13.4, 3.5 Hz,  $\text{C}_c$ ), 133.8 (s,  $\text{C}_m$ ), 134.4 (s,  $\text{C}_o$ ), 136.1 (s,  $\text{C}_v$ ), 161.7 (s,  $\text{C}_h$ ).

$^{11}\text{B}$  NMR (160 MHz,  $\text{DMSO-d}_6$ )  $\delta$  (ppm) = 0.63 (t,  $J$  = 32.8 Hz).

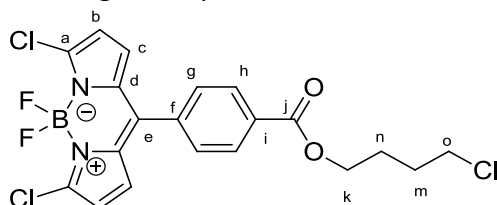
$^{19}\text{F}$  NMR (470 MHz,  $\text{DMSO-d}_6$ )  $\delta$  (ppm) = -144.40 (q,  $J$  = 32.2 Hz)

$^{31}\text{P}$  NMR (202 MHz,  $\text{DMSO-d}_6$ )  $\delta$  (ppm) = 24.52 – 24.13 (m), 25.35 – 24.84 (m)

$^{31}\text{P}$  { $^1\text{H}$ } NMR (202 MHz,  $\text{DMSO-d}_6$ )  $\delta$  (ppm) = 24.33, 25.09

HR-MS (ESI): calculated for  $\text{C}_{44}\text{H}_{38}\text{Au}_2\text{B}_1\text{Cl}_3\text{F}_2\text{N}_4\text{O}_1\text{P}_2\text{Na}_1$   $[\text{M}+\text{Na}]^+$  1273.08413; found 1273.08874

Unwanted byproduct (**12**) following incomplete removal of excess  $(\text{COCl})_2$ :



$^1\text{H}$  NMR (300 MHz,  $\text{CDCl}_3$ )  $\delta$  (ppm) = 1.98 (dt,  $J$  = 3.2, 6.3 Hz, 4H,  $\text{H}_n$ ,  $\text{H}_m$ ), 3.64 (ddd,  $J$  = 2.3, 3.6, 6.1 Hz, 2H,  $\text{H}_o$ ), 4.43 (ddd,  $J$  = 2.3, 3.5, 6.0 Hz, 2H,  $\text{H}_k$ ), 6.46 (d,  $J$  = 4.4 Hz, 2H,  $\text{H}_b$ ), 6.79 (d,  $J$  = 4.3 Hz, 2H,  $\text{H}_c$ ), 7.58 (d,  $J$  = 8.5 Hz, 2H,  $\text{H}_g$ ), 8.19 (d,  $J$  = 8.5 Hz, 2H,  $\text{H}_h$ ).

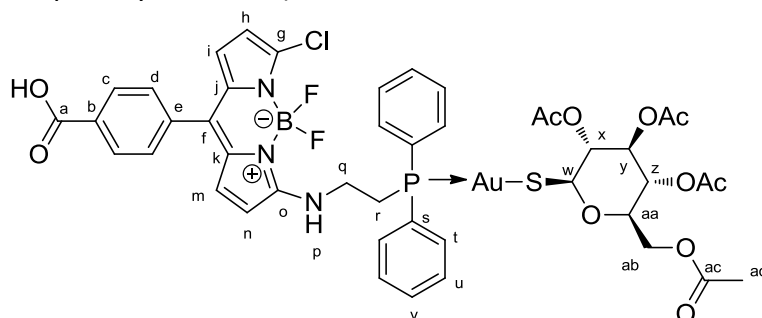
$^{11}\text{B}$  NMR (96 MHz,  $\text{CDCl}_3$ )  $\delta$  (ppm) = 0.46 (t,  $J$  = 27.8 Hz).

$^{19}\text{F}$  NMR (282 MHz,  $\text{CDCl}_3$ )  $\delta$  (ppm) = -148.18 (q,  $J$  = 27.7 Hz).

HR-MS (ESI): calculated for  $\text{C}_{20}\text{H}_{16}\text{B}_1\text{Cl}_3\text{F}_2\text{N}_2\text{O}_2\text{Na}_1$   $[\text{M}+\text{Na}]^+$  493.02329; found 493.02240

4.2.1.15 Compound **13**

18 mg (49.6  $\mu\text{mol}$ )  $\beta$ -thioglucose-tetraacetate (1 eq) was dissolved in acetone (1 mL). 49.6  $\mu\text{L}$  1M NaOH (1 eq) was added and the resulting solution stirred for 15 min. 40mg (49.6  $\mu\text{mol}$ ) BODIPY **9** was placed in a separate round bottom flask and dissolved in acetone (5 mL). The thioglucose solution was added at once and the reaction stirred for 30 min at room temperature. The solvents were evaporated,  $\text{CH}_2\text{Cl}_2$  (10 mL) was added, and the supernatant separated and evaporated. The resulting crude product was dissolved in a minimal amount of  $\text{CH}_2\text{Cl}_2$  and precipitated with pentane to obtain the pure target compound as a flaky orange powder 51 mg (45.1  $\mu\text{mol}$ , yield = 91%).



$^1\text{H}$  NMR (500 MHz,  $\text{CDCl}_3$ )  $\delta$  (ppm) = 1.94 (s, 3H,  $\text{H}_{\text{ad}}$ ), 1.96 (s, 3H,  $\text{H}_{\text{ad}}$ ), 2.02 (s, 3H,  $\text{H}_{\text{ad}}$ ), 2.11 (s, 3H,  $\text{H}_{\text{ad}}$ ), 2.91 (tdd,  $J$  = 10.2, 6.6, 3.3 Hz, 2H,  $\text{H}_{\text{r}}$ ), 3.77 (ddd,  $J$  = 9.4, 4.9, 2.4 Hz, 1H,  $\text{H}_{\text{ab}}$ ), 3.83 (dt,  $J$  = 16.1, 7.7 Hz, 2H,  $\text{H}_{\text{q}}$ ), 4.13 (dd,  $J$  = 12.2, 2.2 Hz, 1H,  $\text{H}_{\text{ab}'}$ ), 4.24 (dd,  $J$  = 12.2, 5.0 Hz, 1H,  $\text{H}_{\text{z}}$ ), 5.17 – 5.05 (m, 3H,  $\text{H}_{\text{x}}$ ,  $\text{H}_{\text{y}}$ ,  $\text{H}_{\text{aa}}$ ), 5.22 (d,  $J$  = 8.7 Hz, 1H,  $\text{H}_{\text{w}}$ ), 6.19 (d,  $J$  = 3.8 Hz, 1H,  $\text{H}_{\text{n}}$ ), 6.26 (d,  $J$  = 4.9 Hz, 1H,  $\text{H}_{\text{m}}$ ), 6.31 (d,  $J$  = 3.7 Hz, 1H,  $\text{H}_{\text{h}}$ ), 6.83 (d,  $J$  = 4.8 Hz, 1H,  $\text{H}_{\text{i}}$ ), 6.90 (s, 1H,  $\text{H}_{\text{p}}$ ), 7.62 – 7.37 (m, 8H,  $\text{H}_{\text{u,v}}$ ,  $\text{H}_{\text{d}}$ ), 7.84 – 7.67 (m, 4H,  $\text{H}_{\text{t}}$ ), 8.18 (d,  $J$  = 8.0 Hz, 2H,  $\text{H}_{\text{c}}$ ).

$^{13}\text{C}$  NMR (126 MHz,  $\text{CDCl}_3$ )  $\delta$  (ppm) = 20.8 (s,  $\text{C}_{\text{ad}}$ ), 20.8 (s,  $\text{C}_{\text{ad}}$ ), 20.9 (s,  $\text{C}_{\text{ad}}$ ), 21.3 (s,  $\text{C}_{\text{ad}}$ ), 29.9 (d,  $J$  = 31.7 Hz,  $\text{C}_{\text{q}}$ ), 41.3 (d,  $J$  = 12.3 Hz,  $\text{C}_{\text{r}}$ ), 63.0 (s,  $\text{C}_{\text{ab}}$ ), 69.1 (s,  $\text{C}_{\text{z}}$ ), 74.3 (s,  $\text{C}_{\text{y}}$ ), 76.0 (s,  $\text{C}_{\text{x}}$ ), 78.3 (s,  $\text{C}_{\text{aa}}$ ), 83.6 (s,  $\text{C}_{\text{w}}$ ), 111.4 (s,  $\text{C}_{\text{h}}$ ), 113.3 (s,  $\text{C}_{\text{n}}$ ), 120.7 (s,  $\text{C}_{\text{i}}$ ), 129.0 (dd,  $J$  = 55.4, 8.0 Hz,  $\text{C}_{\text{s}}$ ), 129.8 (dd,  $J$  = 11.4, 6.5 Hz,  $\text{C}_{\text{v}}$ ), 130.2 (s,  $\text{C}_{\text{m}}$ ), 130.3 (s,  $\text{C}_{\text{k}}$ ,  $\text{C}_{\text{j}}$ ), 130.6 (s,  $\text{C}_{\text{d}}$ ), 130.9 (s,  $\text{C}_{\text{f}}$ ), 131.5 (s,  $\text{C}_{\text{e}}$ ), 132.4 (dd,  $J$  = 8.3, 2.2 Hz,  $\text{C}_{\text{u}}$ ), 133.4 (t,  $J$  = 13.9 Hz,  $\text{C}_{\text{t}}$ ), 135.8 (s,  $\text{C}_{\text{c}}$ ), 139.2 (s,  $\text{C}_{\text{g}}$ ,  $\text{C}_{\text{o}}$ ), 161.6 (s,  $\text{C}_{\text{a}}$ ), 169.9 (s,  $\text{C}_{\text{ac}}$ ), 170.5 (s,  $\text{C}_{\text{ac}}$ ), 170.6 (s,  $\text{C}_{\text{ac}}$ ), 171.0 (s,  $\text{C}_{\text{ac}}$ ).

$^{11}\text{B}$  NMR (160 MHz,  $\text{CDCl}_3$ )  $\delta$  (ppm) = 0.83 (t,  $J$  = 32.7 Hz)

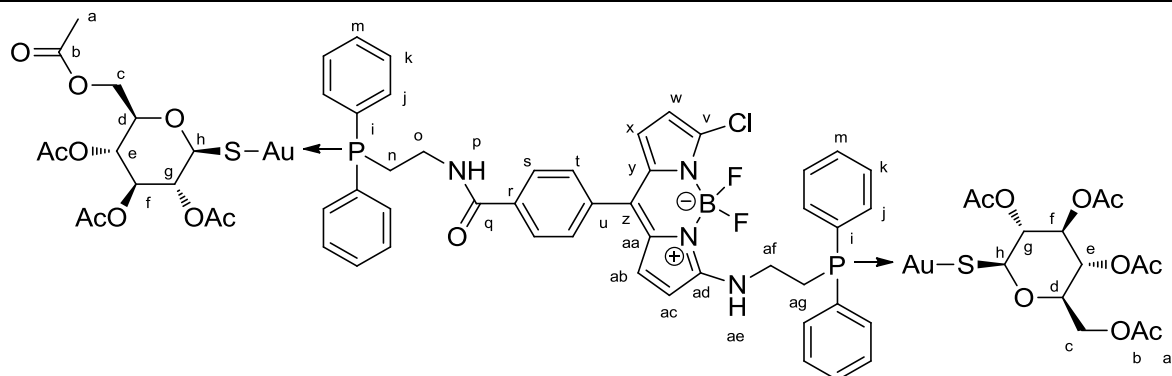
$^{19}\text{F}$  NMR (470 MHz,  $\text{CDCl}_3$ )  $\delta$  (ppm) = -147.78 (s, br)

$^{31}\text{P}$  NMR (202 MHz,  $\text{CDCl}_3$ )  $\delta$  (ppm) = 29.39. (s, br)

HR-MS (ESI): calculated for  $\text{C}_{44}\text{H}_{43}\text{Au}_1\text{B}_1\text{Cl}_1\text{F}_2\text{N}_3\text{O}_{11}\text{P}_1\text{S}_1\text{Na}_1$   $[\text{M}+\text{Na}]^+$  1156.16633; found 1156.16962

4.2.1.16 Compound **15**

26.2 mg (72  $\mu\text{mol}$ )  $\beta$ -thioglucose-tetraacetate (1 eq) was dissolved in acetone (1 mL). 72  $\mu\text{L}$  1M NaOH (1 eq) was added and the resulting solution stirred for 15 min. 45 mg (36  $\mu\text{mol}$ , 1 eq) of BODIPY **11** was placed in a separate round bottom flask and dissolved in acetone (5 mL). The thioglucose solution was added at once and the reaction stirred for 30 min at room temperature. The solvents were evaporated,  $\text{CH}_2\text{Cl}_2$  (10 mL) was added, and the supernatant separated and evaporated. The resulting crude product was dissolved in a minimal amount of  $\text{CH}_2\text{Cl}_2$  and precipitated with pentane to obtain the pure target compound as an orange powder (62 mg, 32.4  $\mu\text{mol}$ , yield = 90%).



$^1\text{H}$  NMR (500 MHz,  $\text{DMSO-d}_6$ )  $\delta$  (ppm) = 1.84 (s, 6H,  $\text{H}_a$ ), 1.88 (s, 6H,  $\text{H}_a$ ), 1.96 (s, 6H,  $\text{H}_a$ ), 1.97 (s, 6H,  $\text{H}_a$ ), 3.20 – 2.99 (m, 4H,  $\text{H}_{ag}$ ,  $\text{H}_n$ ), 3.60 (dt,  $J = 12.7, 6.9$  Hz, 2H,  $\text{H}_o$ ), 3.76 (s, 2H,  $\text{H}_{af}$ ), 3.99 (dt,  $J = 5.6, 2.6$  Hz, 4H,  $\text{H}_c$ ,  $\text{H}_d$ ), 4.08 (dd,  $J = 12.7, 5.7$  Hz, 2H,  $\text{H}_c$ ), 4.90 (dt,  $J = 18.8, 9.6$  Hz, 4H,  $\text{H}_g$ ,  $\text{H}_e$ ), 5.19 (t,  $J = 9.5$  Hz, 2H,  $\text{H}_i$ ), 5.33 (d,  $J = 9.4$  Hz, 2H,  $\text{H}_h$ ), 6.21 (d,  $J = 3.8$  Hz, 1H,  $\text{H}_{ac}$ ), 6.26 (d,  $J = 3.8$  Hz, 1H,  $\text{H}_{ab}$ ), 6.63 (d,  $J = 5.1$  Hz, 1H,  $\text{H}_w$ ), 6.97 (d,  $J = 5.1$  Hz, 1H,  $\text{H}_x$ ), 7.50 (d,  $J = 8.3$  Hz, 2H,  $\text{H}_s$ ), 7.61 – 7.54 (m, 12H,  $\text{H}_{k,m}$ ), 7.92 – 7.81 (m, 10H,  $\text{H}_j$ ,  $\text{H}_s$ ), 8.65 (t,  $J = 6.4$  Hz, 1H,  $\text{H}_{ae}$ ), 8.81 (t,  $J = 5.5$  Hz, 1H,  $\text{H}_p$ ).

$^{13}\text{C}$  NMR (126 MHz,  $\text{DMSO-d}_6$ )  $\delta$  (ppm) = 20.3 (s,  $\text{C}_a$ ), 20.3 (s,  $\text{C}_a$ ), 20.4 (s,  $\text{C}_a$ ), 20.8 (s,  $\text{C}_a$ ), 26.5 (d,  $J = 34.1$  Hz,  $\text{C}_o$ ), 27.4 (s,  $\text{C}_{af}$ ), 35.8 (d,  $J = 8.0$  Hz,  $\text{C}_n$ ), 41.3 (d,  $J = 10.2$  Hz,  $\text{C}_{ag}$ ), 62.4 (s,  $\text{C}_c$ ), 68.6 (s,  $\text{C}_e$ ), 73.2 (s,  $\text{C}_f$ ), 74.3 (s,  $\text{C}_g$ ), 77.4 (s,  $\text{C}_d$ ), 81.8 (s,  $\text{C}_h$ ), 111.9 (s,  $\text{C}_w$ ), 114.5 (s,  $\text{C}_{ac}$ ), 117.3 (s,  $\text{C}_x$ ), 126.1 (s,  $\text{C}_y$ ,  $\text{C}_{aa}$ ), 127.3 (s,  $\text{C}_{ab}$ ), 127.4 (s,  $\text{C}_r$ ), 129.3 (d,  $J = 11.1$  Hz,  $\text{C}_m$ ), 129.9 (d,  $J = 56.6$  Hz,  $\text{C}_i$ ), 130.0 (s,  $\text{C}_s$ ), 130.8 (s,  $\text{C}_z$ ), 132.0 – 131.5 (m,  $\text{C}_k$ ), 133.3 – 133.0 (m,  $\text{C}_j$ ), 133.4 (s,  $\text{C}_t$ ), 133.7 (s,  $\text{C}_u$ ), 134.4 (s,  $\text{C}_v$ ), 136.1 (s,  $\text{C}_{ad}$ ), 161.6 (s,  $\text{C}_q$ ), 165.6 (s,  $\text{CHCO}_3^-$ ), 169.1 (s,  $\text{C}_b$ ), 169.3 (s,  $\text{C}_b$ ), 169.5 (s,  $\text{C}_b$ ), 170.0 (s,  $\text{C}_b$ ).

$^{11}\text{B}$  NMR (160 MHz,  $\text{DMSO-d}_6$ )  $\delta$  (ppm) = 0.62 (t,  $J = 32.4$  Hz)

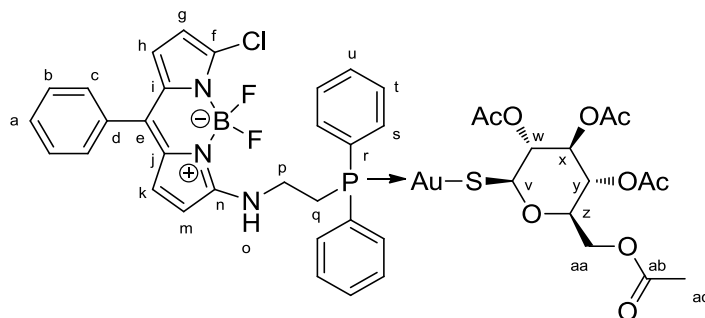
$^{19}\text{F}$  NMR (470 MHz,  $\text{DMSO-d}_6$ )  $\delta$  (ppm) = -144.45 (q,  $J = 32.3$  Hz)

$^{31}\text{P}$  NMR (202 MHz,  $\text{DMSO-d}_6$ )  $\delta$  (ppm) = 29.66

HR-MS (ESI): calculated for  $\text{C}_{72}\text{H}_{76}\text{Au}_2\text{B}_1\text{Cl}_1\text{F}_2\text{N}_4\text{O}_{19}\text{P}_2\text{S}_2\text{Na}_1$   $[\text{M}+\text{Na}]^+$  1927.30049; found 1927.30492

#### 4.2.1.17 Compound 16

19.1 mg (52.4  $\mu\text{mol}$ ) of  $\beta$ -Thioglucose tetraacetate was dissolved in acetone (1 mL). 52.4  $\mu\text{l}$  of 1M NaOH (1 eq) was added and the resulting solution stirred for 15 min. 40 mg (52.4  $\mu\text{mol}$ ) of BODIPY **4b** was placed in a separate round bottom flask and dissolved in acetone (5 mL). The thioglucose solution was added at once and the reaction stirred for 30 min at room temperature. The solvents were evaporated,  $\text{CH}_2\text{Cl}_2$  (10 mL) was added and the supernatant separated and evaporated. The resulting crude product was dissolved in a minimal amount of  $\text{CH}_2\text{Cl}_2$  and precipitated with pentane to obtain the pure target compound as a flaky orange powder. Yield: 56 mg (50.3  $\mu\text{mol}$ , 96%).



$^1\text{H}$  NMR (500 MHz,  $\text{DMSO-d}_6$ )  $\delta$  (ppm) = 1.85 (s, 6H,  $\text{H}_{ac}$ ), 2.00 – 1.94 (m, 6H,  $\text{H}_{ac}$ ), 3.19 – 3.07 (m, 2H,  $\text{H}_q$ ), 3.74 (ddd,  $J = 15.3, 12.5, 7.5$  Hz, 2H,  $\text{H}_p$ ), 4.03 – 3.96 (m, 2H,  $\text{H}_{aa}$ ,  $\text{H}_z$ ), 4.08 (dd,  $J = 12.7, 5.8$  Hz, 1H,  $\text{H}_{aa}$ ), 4.90 (ps-dt,  $J = 13.2, 9.6$  Hz, 2H,  $\text{H}_w$ ,  $\text{H}_y$ ), 5.18 (t,  $J = 9.5$  Hz, 1H,  $\text{H}_x$ ), 5.33 (d,  $J = 9.4$  Hz, 1H,  $\text{H}_v$ ), 6.20 (d,  $J = 3.8$  Hz, 1H,  $\text{H}_m$ ), 6.24

## Materials and Methods

(d,  $J = 3.8$  Hz, 1H, H<sub>k</sub>), 6.59 (d,  $J = 5.1$  Hz, 1H, H<sub>i</sub>), 6.96 (d,  $J = 5.1$  Hz, 1H, H<sub>g</sub>), 7.47 – 7.44 (m, 2H, H<sub>c</sub>), 7.54 – 7.48 (m, 3H, H<sub>b</sub>, H<sub>a</sub>), 7.62 – 7.55 (m, 6H, H<sub>at</sub>, H<sub>u</sub>), 7.92 – 7.80 (m, 4H, H<sub>s</sub>), 8.58 (t,  $J = 6.2$  Hz, 1H, H<sub>o</sub>)

<sup>13</sup>C NMR (126 MHz, DMSO-d<sub>6</sub>)  $\delta$  (ppm) = 20.3 (s, C<sub>ac</sub>), 20.3 (s, C<sub>ac</sub>), 20.4 (s, C<sub>ac</sub>), 20.8 (s, C<sub>ac</sub>), 27.5 (d,  $J = 32.6$  Hz, C<sub>p</sub>), 41.3 (d,  $J = 12.1$  Hz, C<sub>q</sub>), 62.4 (s, C<sub>aa</sub>), 68.6 (s, C<sub>y</sub>), 73.2 (s, C<sub>x</sub>), 74.3 (s, C<sub>w</sub>), 77.5 (s, C<sub>z</sub>), 81.8 (s, C<sub>v</sub>), 111.8 (s, C<sub>t</sub>), 114.1 (s, C<sub>m</sub>), 117.5 (s, C<sub>g</sub>), 126.0 (s, C<sub>h</sub>, C<sub>j</sub>), 128.4 (s, C<sub>i</sub>), 128.4 (s, C<sub>k</sub>), 129.2 (s, C<sub>a</sub>), 129.3 (d,  $J = 11.3$  Hz, C<sub>u</sub>), 129.8 (dd,  $J = 55.0, 26.9$  Hz, C<sub>r</sub>), 130.1 (s, C<sub>b</sub>), 131.1 (s, C<sub>d</sub>), 131.9 (dd,  $J = 9.4, 0.9$  Hz, C<sub>t</sub>), 133.2 (dd,  $J = 23.9, 13.7$  Hz, C<sub>s</sub>), 133.3 (s, C<sub>e</sub>), 133.6 (s, C<sub>n</sub>), 135.8 (s, C<sub>c</sub>), 169.2 (s, C<sub>ab</sub>), 169.3 (s, C<sub>ab</sub>), 169.4 (s, C<sub>ab</sub>), 170.0 (s, C<sub>ab</sub>)

<sup>11</sup>B NMR (160 MHz, DMSO-d<sub>6</sub>)  $\delta$  (ppm) = 0.63 (t,  $J = 32.6$  Hz)

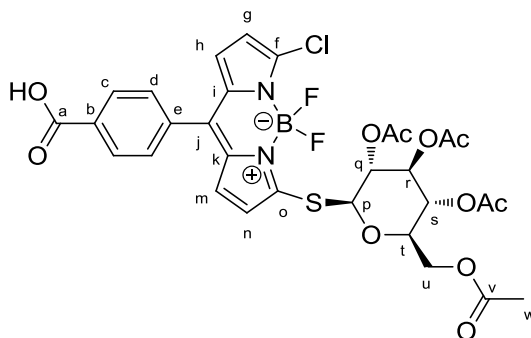
<sup>19</sup>F NMR (470 MHz, DMSO-d<sub>6</sub>)  $\delta$  (ppm) = -144.52 (q,  $J = 32.6$  Hz)

<sup>31</sup>P NMR (202 MHz, DMSO-d<sub>6</sub>)  $\delta$  (ppm) = 29.67

HR-MS (ESI): calculated for C<sub>43</sub>H<sub>43</sub>Au<sub>1</sub>B<sub>1</sub>Cl<sub>1</sub>F<sub>2</sub>N<sub>3</sub>O<sub>9</sub>P<sub>1</sub>S<sub>1</sub>Na<sub>1</sub> [M+Na]<sup>+</sup> 1112.1765; found 1112.17971

### 4.2.1.18 Compound 17

50 mg (0.13 mmol, 1eq) of BODIPY **8** and 22 mg (0.26 mmol, 2 eq) NaHCO<sub>3</sub> were placed in a round bottom flask and dissolved in acetone. In a separate vessel, 43 mg (0.124 mmol, 0.9eq) of  $\beta$ -thioglucose-tetraacetate were dissolved in 2 mL acetone, 124  $\mu$ L 1M NaOH were added and the mixture stirred at room temperature. After 10 min the thioglucose-solution was drawn into a syringe and added slowly (30 min) to the solution of BODIPY **8**. The resulting solution was stirred at room temperature for another hour and then evaporated to dryness. The crude product was purified by column-chromatography on silica gel using CH<sub>2</sub>Cl<sub>2</sub>/formic acid (99:1) as eluent. The product fractions were collected, evaporated to dryness, dissolved in a minimal amount of DCM and precipitated with pentane to yield 80mg (123.5  $\mu$ mol, yield = 95%) of the targeted compound as a pink powder.



<sup>1</sup>H NMR (500 MHz, DMSO-d<sub>6</sub>)  $\delta$  (ppm) = 1.98 (s, 3H, H<sub>w</sub>), 2.00 (s, 3H, H<sub>w</sub>), 2.01 (s, 3H, H<sub>w</sub>), 2.04 (s, 3H, H<sub>w</sub>), 4.06 (dd,  $J = 12.4, 2.4$  Hz, 1H, H<sub>u</sub>), 4.15 (dd,  $J = 12.4, 5.8$  Hz, 1H, H<sub>u</sub>), 4.29 (ddd,  $J = 10.1, 5.8, 2.3$  Hz, 1H, H<sub>t</sub>), 5.06 (t,  $J = 9.8$  Hz, 1H, H<sub>q</sub>), 5.14 (t,  $J = 9.7$  Hz, 1H, H<sub>s</sub>), 5.45 (t,  $J = 9.5$  Hz, 1H, H<sub>r</sub>), 5.82 (d,  $J = 10.1$  Hz, 1H, H<sub>p</sub>), 6.64 (d,  $J = 4.2$  Hz, 1H, H<sub>n</sub>), 6.85 (d,  $J = 4.2$  Hz, 1H, H<sub>m</sub>), 6.94 (d,  $J = 4.7$  Hz, 1H, H<sub>g</sub>), 7.19 (d,  $J = 4.7$  Hz, 1H, H<sub>h</sub>), 7.73 (d,  $J = 8.2$  Hz, 2H, H<sub>d</sub>), 8.11 (d,  $J = 8.3$  Hz, 2H, H<sub>c</sub>).

<sup>13</sup>C NMR (126 MHz, DMSO-d<sub>6</sub>)  $\delta$  (ppm) = 20.2 (C<sub>w</sub>), 20.2 (C<sub>w</sub>), 20.3 (C<sub>w</sub>), 20.5 (C<sub>w</sub>), 61.8 (C<sub>u</sub>), 67.8 (C<sub>s</sub>), 69.2 (C<sub>r</sub>), 72.6 (C<sub>q</sub>), 74.8 (C<sub>t</sub>), 80.7 (C<sub>p</sub>), 117.5 (C<sub>g</sub>), 120.9 (C<sub>n</sub>), 129.2 (C<sub>h</sub>), 129.4 (C<sub>m</sub>), 130.8 (C<sub>d</sub>), 132.2 (C<sub>b</sub>), 132.6 (C<sub>f</sub>), 133.2 (C<sub>c</sub>), 135.6 (C<sub>i</sub>), 136.1 (C<sub>j</sub>), 139.0 (C<sub>k</sub>), 139.7 (C<sub>e</sub>), 157.7 (C<sub>o</sub>), 166.7 (C<sub>a</sub>), 169.1 (C<sub>u</sub>), 169.2 (C<sub>u</sub>), 169.5 (C<sub>u</sub>), 169.9 (C<sub>u</sub>).

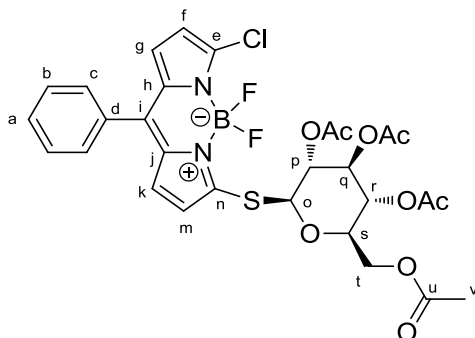
<sup>11</sup>B NMR (160 MHz, DMSO-d<sub>6</sub>)  $\delta$  (ppm) = 0.37 (t,  $J = 30.2$  Hz)

<sup>19</sup>F NMR (470 MHz, DMSO-d<sub>6</sub>)  $\delta$  (ppm) = -146.19 – -144.84 (m).

HR-MS (ESI): calculated for C<sub>30</sub>H<sub>28</sub>B<sub>1</sub>Cl<sub>1</sub>F<sub>2</sub>N<sub>2</sub>O<sub>11</sub>S<sub>1</sub>Na<sub>1</sub> [M+Na]<sup>+</sup> 731.10557; found 731.10681

4.2.1.19 Compound **18**

100 mg of  $\beta$ -thioglucose-tetraacetate (0.274 mmol, 0.95 eq) were dissolved in acetone (2 mL). 27.4  $\mu$ L of 1M NaOH were added and the resulting solution stirred for 15min at room temperature. In a separate flask 97.5mg (289  $\mu$ mol, 1 eq) BODIPY **1** and 48 mg NaHCO<sub>3</sub> (0.578mmol, 2eq) were dissolved in acetone (10 mL). The thioglucose-tetraacetate solution was added over the course of 1h30 at room temperature, followed by stirring for another 90min at room temperature. The solvents were then evaporated and the crude product was purified by column chromatography on silica gel, using CH<sub>2</sub>Cl<sub>2</sub> to CH<sub>2</sub>Cl<sub>2</sub>/MeOH 99:1 as eluent. Product fractions were evaporated to dryness. The resulting product was dissolved in a minimal amount of DCM and crushed out with pentane to obtain 80.9mg (121  $\mu$ mol, yield = 44%) of pure BODIPY **18** as a bright pink powder.



<sup>1</sup>H NMR (500 MHz, DMSO-d<sub>6</sub>)  $\delta$  (ppm) = 1.99, 2.01, 2.02, 2.05 (4x s, 4x 3H, H<sub>v</sub>), 4.08 (dd,  $J$  = 12.3, 2.0 Hz, 1H, H<sub>i</sub>), 4.17 (dd,  $J$  = 12.4, 5.9 Hz, 1H, H<sub>i</sub>), 4.30 (ddd,  $J$  = 10.0, 5.8, 2.2 Hz, 1H, H<sub>s</sub>), 5.07 (t,  $J$  = 9.8 Hz, 1H, H<sub>p</sub>), 5.15 (t,  $J$  = 9.7 Hz, 1H, H<sub>r</sub>), 5.47 (t,  $J$  = 9.4 Hz, 1H, H<sub>q</sub>), 5.83 (d,  $J$  = 10.1 Hz, 1H, H<sub>o</sub>), 6.63 (d,  $J$  = 4.2 Hz, 1H, H<sub>m</sub>), 6.83 (d,  $J$  = 4.1 Hz, 1H, H<sub>k</sub>), 6.94 (d,  $J$  = 4.6 Hz, 1H, H<sub>f</sub>), 7.16 (d,  $J$  = 4.5 Hz, 1H, H<sub>g</sub>), 7.63 – 7.57 (m, 4H, H<sub>b</sub>, H<sub>c</sub>), 7.66 (m, 1H, H<sub>a</sub>)

<sup>13</sup>C NMR (126 MHz, DMSO-d<sub>6</sub>)  $\delta$  (ppm) = 20.2 (C<sub>v</sub>), 20.2 (C<sub>v</sub>), 20.3 (C<sub>v</sub>), 20.5 (C<sub>v</sub>), 61.8 (C<sub>t</sub>), 67.8 (C<sub>r</sub>), 69.2 (C<sub>q</sub>), 72.6 (C<sub>p</sub>), 74.8 (C<sub>s</sub>), 80.8 (C<sub>o</sub>), 117.3 (C<sub>f</sub>), 120.6 (C<sub>m</sub>), 128.7 (C<sub>g</sub>), 129.2 (C<sub>k</sub>), 130.5 (C<sub>a</sub>), 130.8 (C<sub>b</sub>), 132.1 (C<sub>h</sub>), 132.5 (C<sub>j</sub>), 133.2 (C<sub>c</sub>), 135.7 (C<sub>i</sub>), 138.7 (C<sub>d</sub>), 141.1 (C<sub>e</sub>), 157.0 (C<sub>n</sub>), 169.1 (C<sub>u</sub>), 169.3 (C<sub>u</sub>), 169.6 (C<sub>u</sub>), 170.0 (C<sub>u</sub>)

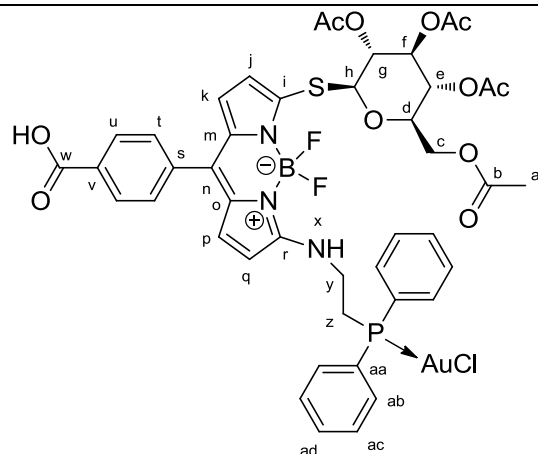
<sup>11</sup>B NMR (160 MHz, DMSO-d<sub>6</sub>)  $\delta$  (ppm) = 0.37 (t,  $J$  = 30.3 Hz)

<sup>19</sup>F NMR (470 MHz, DMSO-d<sub>6</sub>)  $\delta$  (ppm) = -146.20 – -144.82 (m)

HR-MS (ESI): calculated for C<sub>29</sub>H<sub>28</sub>B<sub>1</sub>Cl<sub>1</sub>F<sub>2</sub>N<sub>2</sub>O<sub>9</sub>S<sub>1</sub>Na<sub>1</sub> [M+Na]<sup>+</sup> 687.11574; found 687.11699

4.2.1.20 Compound **19**

32.2 mg (0.045 mmol, 1eq) of BODIPY **17** were dissolved in 8 mL dry THF. 25.2 mg (54  $\mu$ mol, 1.2 eq) of gold(I)-phosphine **3** and 31.4 mg (0.227 mmol, 5 eq) of K<sub>2</sub>CO<sub>3</sub> were added, and the reaction was refluxed for 60min. The solvent was evaporated, and the crude product was purified by column chromatography on silica gel, using CH<sub>2</sub>Cl<sub>2</sub>/MeOH (100:0 to 90:10) as eluent. Product fractions were collected and evaporated to dryness. After dissolution in a minimal amount of CH<sub>2</sub>Cl<sub>2</sub> the product was crushed out by addition of pentane (twice) to yield pure **19** (42 mg, 36.9  $\mu$ mol, 82% yield) as a red-pink powder.



$^1\text{H}$  NMR (500 MHz, DMSO- $d_6$ )  $\delta$  (ppm) = 1.94, 1.99, 2.00 (3s, 12H, H<sub>a</sub>), 3.22 – 3.07 (m, 2H, H<sub>z</sub>), 3.68 (s, 2H, H<sub>y</sub>), 4.05 (dd,  $J$  = 14.7, 5.2 Hz, 1H, H<sub>d</sub>), 4.16 (q,  $J$  = 5.3 Hz, 2H, H<sub>c</sub>), 4.95 (t,  $J$  = 9.7 Hz, 2H, H<sub>g</sub>, H<sub>e</sub>), 5.32 (d,  $J$  = 10.1 Hz, 1H, H<sub>h</sub>), 5.39 (t,  $J$  = 9.4 Hz, 1H, H<sub>i</sub>), 6.30 (d,  $J$  = 3.8 Hz, 1H, H<sub>q</sub>), 6.43 (d,  $J$  = 3.8 Hz, 1H, H<sub>p</sub>), 6.51 (d,  $J$  = 5.1 Hz, 1H, H<sub>j</sub>), 6.94 (d,  $J$  = 5.1 Hz, 1H, H<sub>k</sub>), 7.53 (d,  $J$  = 8.1 Hz, H<sub>at</sub>), 7.60 – 7.55 (m, 6H, H<sub>ac</sub>, H<sub>ad</sub>), 7.86 – 7.76 (m, 4H, H<sub>ab</sub>), 8.06 (d,  $J$  = 7.9 Hz, 2H, H<sub>u</sub>), 8.46 (s, 1H, H<sub>x</sub>)

$^{13}\text{C}$  NMR (126 MHz, DMSO- $d_6$ )  $\delta$  (ppm) = 20.3 (s, C<sub>a</sub>), 20.4 (s, C<sub>a</sub>), 20.4 (s, C<sub>a</sub>), 20.5 (s, C<sub>a</sub>), 27.5 (d,  $J$  = 35.5 Hz, C<sub>y</sub>), 41.2 (d,  $J$  = 10.5 Hz, C<sub>z</sub>), 61.9 (s, C<sub>c</sub>), 68.1 (s, C<sub>e</sub>), 69.3 (s, C<sub>f</sub>), 73.0 (s, C<sub>g</sub>), 74.3 (s, C<sub>d</sub>), 83.3 (s, C<sub>h</sub>), 113.3 (s, C<sub>q</sub>), 115.0 (s, C<sub>i</sub>), 118.6 (s, C<sub>p</sub>), 127.5 (s, C<sub>r</sub>), 128.7 (ps-d,  $J$  = 3.5 Hz, C<sub>aa</sub>, C<sub>o</sub>, C<sub>m</sub>), 129.2 (ps-d,  $J$  = 3.5 Hz, C<sub>n</sub>, C<sub>v</sub>), 129.3 (s, C<sub>k</sub>), 129.4 (d,  $J$  = 11.7 Hz, C<sub>ad</sub>), 130.1 (s, C<sub>t</sub>), 132.1 (d,  $J$  = 1.8 Hz, C<sub>ac</sub>), 132.5 (s, C<sub>r</sub>, C<sub>n</sub>), 133.2 (d,  $J$  = 12.6 Hz, C<sub>ab</sub>), 133.7 (s, br, C<sub>i</sub>, C<sub>s</sub>), 135.2 (s, C<sub>u</sub>), 161.2 (s, C<sub>w</sub>), 169.1 (s, C<sub>b</sub>), 169.3 (s, C<sub>b</sub>), 169.5 (s, C<sub>b</sub>), 170.0 (s, C<sub>b</sub>)

$^{11}\text{B}$  NMR (160 MHz, DMSO- $d_6$ )  $\delta$  (ppm) = 0.69 (t,  $J$  = 34.0 Hz)

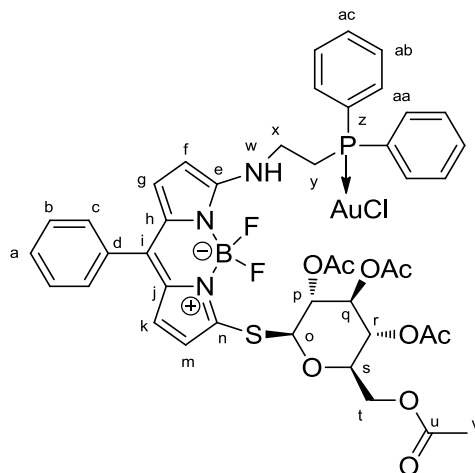
$^{19}\text{F}$  NMR (470 MHz, DMSO- $d_6$ )  $\delta$  (ppm) = -142.81 – -143.79 (m)

$^{31}\text{P}$  NMR (202 MHz, DMSO- $d_6$ )  $\delta$  (ppm) = 24.40 (s, br)

HR-MS (ESI): calculated for C<sub>44</sub>H<sub>43</sub>Au<sub>1</sub>B<sub>1</sub>Cl<sub>1</sub>F<sub>2</sub>N<sub>3</sub>O<sub>11</sub>P<sub>1</sub>S<sub>1</sub>Na<sub>1</sub> [M+Na]<sup>+</sup> 1156.16633; found 1156.17033

#### 4.2.1.21 Compound **20**

20 mg (30  $\mu\text{mol}$ , 1 eq) of BODIPY **18** were placed in a round bottom flask and suspended in 10 mL of dry THF. Gold(I)-phosphine **3** (15.3 mg, 33  $\mu\text{mol}$ , 1.1 eq) and NaHCO<sub>3</sub> (10.1 mg, 0.12 mmol, 4 eq) were added, and the reaction was refluxed for 1h. Upon total consumption of the starting BODIPY the solvents were evaporated and the crude product was purified by column chromatography on silica gel, using CH<sub>2</sub>Cl<sub>2</sub> as eluent. The product fractions were evaporated to dryness, dissolved in CH<sub>2</sub>Cl<sub>2</sub> and precipitated by addition of pentane twice to obtain BODIPY **20** (31 mg, 28.5  $\mu\text{mol}$ , 95% yield) as an orange-pink powder.



$^1\text{H}$  NMR (500 MHz, DMSO- $d_6$ )  $\delta$  (ppm) = 1.94 (s, 3H, H<sub>v</sub>), 1.99 (s, 3H, H<sub>v</sub>), 2.01 (s, 6H, H<sub>v</sub>), 3.15 (ddd,  $J$  = 11.0, 8.4, 5.2 Hz, 2H, H<sub>v</sub>), 3.68 (dt,  $J$  = 21.4, 7.8 Hz, 2H, H<sub>x</sub>), 4.05 (dd,  $J$  = 14.8, 5.2 Hz, 1H, H<sub>s</sub>), 4.16 (q,  $J$  = 5.3 Hz, 2H, H<sub>t</sub>), 4.94 (ps-tt,  $J$  = 9.6, 2.0 Hz, 2H, H<sub>r</sub>, H<sub>p</sub>), 5.32 (d,  $J$  = 10.1 Hz, 1H, H<sub>o</sub>), 5.40 (t,  $J$  = 9.4 Hz, 1H, H<sub>a</sub>), 6.28 (d,  $J$  = 3.8 Hz, 1H, H<sub>i</sub>), 6.42 (d,  $J$  = 3.8 Hz, 1H, H<sub>g</sub>), 6.48 (d,  $J$  = 5.1 Hz, 1H, H<sub>m</sub>), 6.90 (d,  $J$  = 5.1 Hz, 1H, H<sub>k</sub>), 7.46 – 7.43 (m, 2H, H<sub>c</sub>), 7.54 – 7.50 (m, 3H, H<sub>a</sub>, H<sub>b</sub>), 7.62 – 7.55 (m, 6H, H<sub>ab</sub>, H<sub>ac</sub>), 7.84 – 7.78 (m, 4H, H<sub>aa</sub>), 8.40 (s, 1H, H<sub>w</sub>)

$^{13}\text{C}$  NMR (126 MHz, DMSO- $d_6$ )  $\delta$  (ppm) = 20.3 (s, C<sub>v</sub>), 20.4 (s, C<sub>v</sub>), 20.4 (s, C<sub>v</sub>), 20.5 (s, C<sub>v</sub>), 27.4 (d,  $J$  = 35.6 Hz, C<sub>x</sub>), 41.2 (d,  $J$  = 10.8 Hz, C<sub>v</sub>), 61.9 (s, C<sub>t</sub>), 68.1 (s, C<sub>r</sub>), 69.3 (s, C<sub>q</sub>), 73.0 (s, C<sub>p</sub>), 74.3 (s, C<sub>s</sub>), 83.3 (s, C<sub>o</sub>), 113.0 (s, C<sub>r</sub>), 115.2 (s, C<sub>m</sub>), 118.7 (s, C<sub>g</sub>), 128.5 (s, C<sub>a</sub>), 128.7 (s, C<sub>h</sub>), 129.0 (d,  $J$  = 60.6 Hz, C<sub>z</sub>), 129.2 (s, C<sub>k</sub>), 129.2 (s, C<sub>i</sub>), 129.4 (d,  $J$  = 11.7 Hz, C<sub>ac</sub>), 130.1 (s, C<sub>b</sub>), 132.1 (d,  $J$  = 2.2 Hz, C<sub>ab</sub>), 132.8 (s, C<sub>j</sub>), 133.2 (d,  $J$  = 13.6 Hz, C<sub>aa</sub>), 133.6 (s, C<sub>d</sub>), 133.8 (s, C<sub>e</sub>), 135.2 (s, C<sub>c</sub>), 161.0 (s, C<sub>n</sub>), 169.1 (s, C<sub>u</sub>), 169.3 (s, C<sub>u</sub>), 169.5 (s, C<sub>u</sub>), 170.0 (s, C<sub>u</sub>)

$^{11}\text{B}$  NMR (160 MHz, DMSO- $d_6$ )  $\delta$  (ppm) = 0.72 (t,  $J$  = 33.7 Hz)

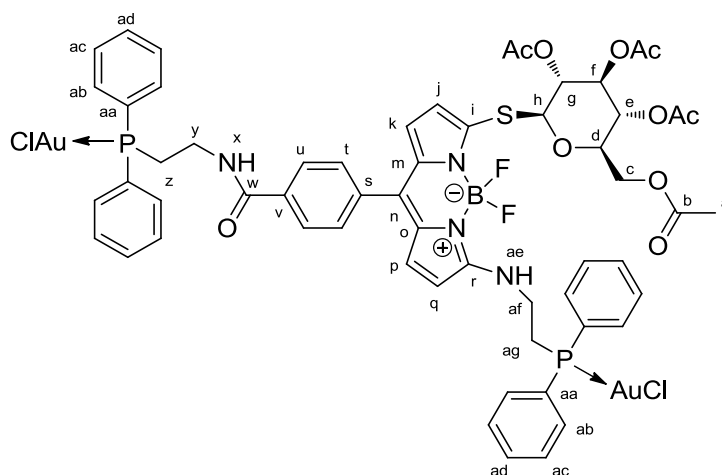
$^{19}\text{F}$  NMR (470 MHz, DMSO- $d_6$ )  $\delta$  (ppm) = -143.72 – -142.85 (m)

$^{31}\text{P}$  NMR (202 MHz, DMSO- $d_6$ )  $\delta$  (ppm) = 24.40

HR-MS (ESI): calculated for C<sub>43</sub>H<sub>43</sub>Au<sub>1</sub>B<sub>1</sub>Cl<sub>1</sub>F<sub>2</sub>N<sub>3</sub>O<sub>9</sub>P<sub>1</sub>S<sub>1</sub>Na<sub>1</sub> [M+Na]<sup>+</sup> 1112.17650; found 1112.17964

#### 4.2.1.22 Compound 21

50 mg (0.071 mmol, 1eq) of BODIPY **17** were dissolved in 5 mL CH<sub>2</sub>Cl<sub>2</sub>. 30  $\mu$ L (0.35 mmol, 5 eq) of (COCl)<sub>2</sub> and a droplet of DMF were added and the reaction was stirred at room temperature. After 45min the solvents were evaporated and the resulting solid was redissolved in 15 mL CH<sub>3</sub>CN. Gold(I)-chloride **3** (78 mg, 0.169 mmol, 2.4 eq) and NaHCO<sub>3</sub> (30 mg, 0.35mmol, 5eq) were added and the reaction was refluxed for 60min. The solvent was evaporated and the crude product purified by column chromatography on silica gel, using CH<sub>2</sub>Cl<sub>2</sub>/MeOH (100:0 to 90:10) as eluent. The different product fractions were collected and evaporated to dryness. The product was dissolved in a minimal amount of CH<sub>2</sub>Cl<sub>2</sub> and crushed out by addition of pentane (twice) to obtain 102mg (65.32  $\mu$ mol, yield = 92%) of the target compound as a red-pink powder.



$^1\text{H}$  NMR (500 MHz, DMSO- $d_6$ )  $\delta$  (ppm) = 1.91, 1.94, 2.00, 2.01 (4s, 12H, H<sub>a</sub>), 3.10 (dt,  $J$  = 11.0, 6.9 Hz, 2H, H<sub>z</sub>), 3.18 – 3.13 (m, 2H, H<sub>ag</sub>), 3.58 (dt,  $J$  = 20.6, 6.7 Hz, 2H, H<sub>v</sub>), 3.69 (dt,  $J$  = 15.3, 7.8 Hz, 2H, H<sub>af</sub>), 4.06 (q,  $J$  = 5.1 Hz, 1H, H<sub>d</sub>), 4.17 (q,  $J$  = 5.1 Hz, 2H, H<sub>c</sub>), 4.95 (t,  $J$  = 9.7 Hz, 2H, H<sub>g</sub>, H<sub>e</sub>), 5.32 (d,  $J$  = 10.1 Hz, 1H, H<sub>h</sub>), 5.40 (t,  $J$  = 9.4 Hz, 1H, H<sub>f</sub>), 6.28 (d,  $J$  = 3.8 Hz, 1H, H<sub>q</sub>), 6.44 (d,  $J$  = 3.8 Hz, 1H, H<sub>p</sub>), 6.52 (d,  $J$  = 5.1 Hz, 1H, H<sub>j</sub>), 6.91 (d,  $J$  = 5.1 Hz, 1H, H<sub>k</sub>), 7.49 (d,  $J$  = 8.3 Hz, 2H, H<sub>t</sub>), 7.63 – 7.53 (m, 12H, H<sub>ac</sub>, H<sub>ad</sub>), 7.84 – 7.77 (m, 8H, H<sub>ab</sub>), 7.89 (d,  $J$  = 8.3 Hz, 2H, H<sub>u</sub>), 8.47 (s, 1H, H<sub>ae</sub>), 8.86 (t,  $J$  = 5.4 Hz, 1H, H<sub>x</sub>)

$^{13}\text{C}$  NMR (126 MHz, DMSO- $d_6$ )  $\delta$  (ppm) = 20.23 (s, C<sub>a</sub>), 20.3 (s, C<sub>a</sub>), 20.4 (s, C<sub>a</sub>), 20.5 (s, C<sub>a</sub>), 26.4 (d,  $J$  = 37.8 Hz, C<sub>y</sub>), 27.4 (d,  $J$  = 35.7 Hz, C<sub>af</sub>), 35.8 (d,  $J$  = 5.4 Hz, C<sub>z</sub>), 41.2 (d,  $J$  = 9.4 Hz, C<sub>ag</sub>), 61.9 (s, C<sub>c</sub>), 68.1 (s, C<sub>e</sub>), 69.3 (s, C<sub>f</sub>), 73.0 (s,

## Materials and Methods

$^{13}\text{C}$ , 74.3 (s, C<sub>d</sub>), 83.2 (s, C<sub>h</sub>), 113.4 (s, C<sub>q</sub>), 115.3 (s, C<sub>i</sub>), 118.5 (s, C<sub>p</sub>), 127.3 (s, C<sub>k</sub>), 127.7 (s, C<sub>o</sub>), 128.9 (dd,  $J = 60.7$ , 3.2 Hz, C<sub>aa</sub>), 129.0 (s, C<sub>m</sub>), 129.4 (dd,  $J = 11.6$ , 2.6 Hz, C<sub>ad</sub>), 129.5 (s, C<sub>v</sub>), 129.9 (s, C<sub>u</sub>), 132.0 (d,  $J = 16.9$  Hz, C<sub>ac</sub>), 132.5 (s, C<sub>n</sub>), 133.1 (dd,  $J = 13.4$ , 1.6 Hz, C<sub>ab</sub>), 133.2 (s, C<sub>s</sub>), 134.3 (s, C<sub>r</sub>), 135.0 (s, C<sub>t</sub>), 136.5 (s, C<sub>i</sub>), 161.2 (s, C<sub>w</sub>), 169.0 (s, C<sub>a</sub>), 169.3 (s, C<sub>a</sub>), 169.4 (s, C<sub>a</sub>), 169.9 (s, C<sub>a</sub>)

$^{11}\text{B}$  NMR (160 MHz, DMSO- $d_6$ )  $\delta$  (ppm) = 1.04 – 0.40 (m)

$^{19}\text{F}$  NMR (470 MHz, DMSO- $d_6$ )  $\delta$  (ppm) = -142.79 – -143.80 (m)

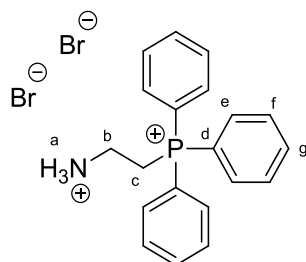
$^{31}\text{P}$  NMR (202 MHz, DMSO- $d_6$ )  $\delta$  (ppm) = 24.62 – 24.15 (m, 1P), 25.32 – 24.77 (m, 1P)

$^{31}\text{P}$  { $^1\text{H}$ } NMR (202 MHz, DMSO- $d_6$ )  $\delta$  (ppm) = 24.42, 25.05

HR-MS (ESI): calculated for C<sub>58</sub>H<sub>57</sub>Au<sub>2</sub>B<sub>1</sub>Cl<sub>2</sub>F<sub>2</sub>N<sub>4</sub>O<sub>10</sub>P<sub>2</sub>S<sub>1</sub>Na<sub>1</sub> [M+Na]<sup>+</sup> 1599.19321; found 1599.19617

### 4.2.1.23 Triphenylphosphonium-ethylammonium dibromide (**22**)

2 g (7.63 mmol, 1 eq) PPh<sub>3</sub> and 1.562 g (7.63 mmol, 1 eq) bromoethylamine hydrobromide were dissolved in 150 mL acetonitrile and refluxed for 72h. The reaction was stopped upon total consumption of PPh<sub>3</sub>. Acetonitrile was evaporated and the crude product redissolved in 10 mL of MeOH. The product was crushed out with ice-cold Et<sub>2</sub>O (300 mL). The solid was collected and the washing repeated twice to obtain 1.771 g (3.82 mmol, yield = 50%) of the target compound as a white powder.

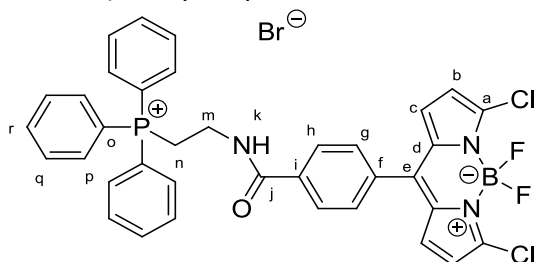


$^1\text{H}$  NMR (500 MHz, DMSO- $d_6$ )  $\delta$  (ppm) = 3.13 – 3.07 (m, 2H, H<sub>b</sub>), 4.05 – 3.97 (m, 2H, H<sub>c</sub>), 7.80 (td,  $J = 7.8$ , 3.7 Hz, 6H, H<sub>e</sub>), 7.86 (ddd,  $J = 13.0$ , 8.5, 1.4 Hz, 6H, H<sub>f</sub>), 7.94 (td,  $J = 7.3$ , 1.8 Hz, 3H, H<sub>g</sub>), 8.36 (s, 3H, H<sub>a</sub>).

$^{31}\text{P}$  NMR (202 MHz, DMSO- $d_6$ )  $\delta$  (ppm) = 21.39 (s).

### 4.2.1.24 Compound **23**

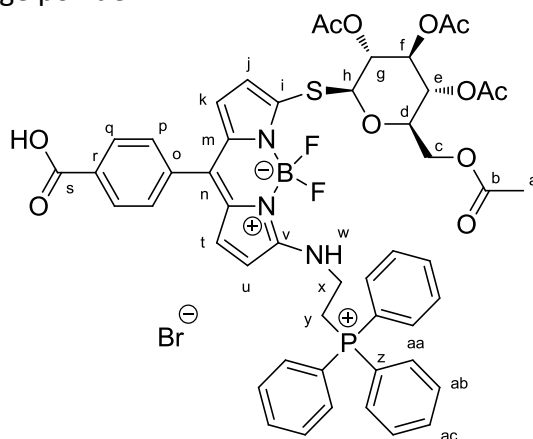
100 mg (0.262 mmol, 1 eq) of BODIPY **8** were dissolved in 15 mL CH<sub>2</sub>Cl<sub>2</sub>. 45  $\mu\text{L}$  (0.525 mmol, 2eq) oxalyl chloride and a droplet of DMF were added (vigorous development of gas) and the solution stirred for 1h at room temperature. Solvents were then evaporated and the solid redissolved in 20 mL acetonitrile. 110 mg (1.31 mmol, 5 eq) of NaHCO<sub>3</sub> and 123 mg (0.262 mmol, 1 eq) of phosphonium **22** were added and the resulting mixture was refluxed for 1h. Upon completion of the reaction, the crude product was purified by column chromatography on silica gel, using CH<sub>2</sub>Cl<sub>2</sub>/MeOH (95:5) as eluent. The resulting product was dissolved in a minimal amount of DCM and crushed out with pentane to yield pure BODIPY **23** (110 mg, 0.147 mmol, yield = 56%) as a pink powder.





4.2.1.26 Compound **25**

150.4 mg (0.21 mmol, 1 eq) of BODIPY **17** were placed in a round bottom flask and dissolved in acetonitrile. Phosphonium **22** (148 mg, 0.32 mmol, 1.5 eq) and NaHCO<sub>3</sub> (89 mg, 1.06 mmol, 5eq) were added and the resulting mixture was refluxed for 70 min. The solvent was then evaporated and the crude product purified by column chromatography on silica gel, using as eluent CH<sub>2</sub>Cl<sub>2</sub>/MeOH/formic acid (99:1:1 to 90:10:1). The product fractions were evaporated, dissolved in a minimal amount of MeOH and precipitated with Et<sub>2</sub>O. The procedure was repeated with CH<sub>2</sub>Cl<sub>2</sub> and pentane to obtain 135 mg (126 μmol, yield = 60%) of the target compound as a pink-orange powder.



<sup>1</sup>H NMR (500 MHz, DMSO-d<sub>6</sub>) δ (ppm) = 1.95 (s, 3H, H<sub>a</sub>), 2.00 (ps-d, 9H, H<sub>a</sub>), 3.76 (d, *J* = 6.0 Hz, 2H, H<sub>v</sub>), 4.09 – 3.95 (m, 3H, H<sub>c</sub>, H<sub>x</sub>), 4.23 – 4.13 (m, 2H, H<sub>c</sub>, H<sub>d</sub>), 4.96 (ps-td, *J* = 9.7, 2.9 Hz, 2H, H<sub>g</sub>, H<sub>e</sub>), 5.36 (d, *J* = 10.1 Hz, 1H, H<sub>h</sub>), 5.41 (t, *J* = 9.4 Hz, 1H, H<sub>f</sub>), 6.34 (d, *J* = 3.8 Hz, 1H, H<sub>u</sub>), 6.41 (d, *J* = 5.0 Hz, 1H, H<sub>t</sub>), 6.44 (d, *J* = 3.8 Hz, 1H, H<sub>j</sub>), 6.97 (d, *J* = 5.0 Hz, 1H, H<sub>k</sub>), 7.52 (d, *J* = 7.8 Hz, 2H, H<sub>p</sub>), 7.77 (ddd, *J* = 14.9, 7.4, 2.9 Hz, 6H, H<sub>aa</sub>), 7.85 (dd, *J* = 12.9, 7.5 Hz, 6H, H<sub>ab</sub>), 7.92 (t, *J* = 7.3 Hz, 3H, H<sub>ac</sub>), 8.05 (d, *J* = 7.8 Hz, 2H, H<sub>q</sub>), 8.24 (s, 1H, H<sub>w</sub>)

<sup>13</sup>C NMR (126 MHz, DMSO-d<sub>6</sub>) δ (ppm) = 20.4 (s, C<sub>a</sub>), 20.4 (s, C<sub>a</sub>), 20.4 (s, C<sub>a</sub>), 20.5 (s, C<sub>a</sub>), 22.1 (d, *J* = 48.4 Hz, C<sub>x</sub>), 38.6 (s, C<sub>v</sub>), 61.9 (s, C<sub>c</sub>), 68.0 (s, C<sub>e</sub>), 69.3 (s, C<sub>f</sub>), 72.9 (s, C<sub>g</sub>), 74.3 (s, C<sub>d</sub>), 83.0 (s, C<sub>h</sub>), 113.0 (s, C<sub>u</sub>), 114.9 (s, C<sub>j</sub>), 118.0 (d, *J* = 86.3 Hz, C<sub>z</sub>), 119.1 (s, C<sub>t</sub>), 128.5 (s, C<sub>n</sub>), 129.3 (s, C<sub>k</sub>), 130.1 (d, *J* = 12.9 Hz, C<sub>q</sub>), 130.3 (d, *J* = 12.7 Hz, C<sub>ac</sub>), 132.4 (s, C<sub>m</sub>, C<sub>n</sub>), 133.0 (s, C<sub>i</sub>, C<sub>v</sub>), 133.2 (d, *J* = 10.7 Hz, C<sub>p</sub>), 133.7 (d, *J* = 10.5 Hz, C<sub>ab</sub>), 134.6 (s, C<sub>o</sub>), 135.1 (d, *J* = 1.6 Hz, C<sub>aa</sub>), 161.0 (s, C<sub>s</sub>), 169.0 (s, C<sub>b</sub>), 169.3 (s, C<sub>b</sub>), 169.5 (s, C<sub>b</sub>), 170.0 (s, C<sub>b</sub>)

<sup>11</sup>B NMR (160 MHz, DMSO-d<sub>6</sub>) δ (ppm) = 0.70 (t, *J* = 32.7 Hz)

<sup>19</sup>F NMR (470 MHz, DMSO-d<sub>6</sub>) δ (ppm) = -143.45 (s, vbr)

<sup>31</sup>P NMR (202 MHz, DMSO-d<sub>6</sub>) δ (ppm) = 21.46

HR-MS (ESI): calculated for C<sub>50</sub>H<sub>48</sub>B<sub>1</sub>F<sub>2</sub>N<sub>3</sub>O<sub>11</sub>P<sub>1</sub>S<sub>1</sub> [M]<sup>+</sup> 978.28028; found 978.28403

4.2.1.27 Compound **26**

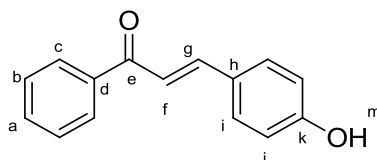
BODIPY **25** (50mg, 0.047mmol, 1eq) was placed in a dried round bottom flask and dissolved in 5 mL dry DMF. 0.1 mL of DIPEA and 27mg (0.071mmol, 1.5eq) of HBTU were added and the reaction stirred for 40 min at 30°C. Gold(I)-phosphine **3** (32.7mg, 0.071mmol, 1.5eq) was dissolved in 1 mL dry DMF and added to the solution. The reaction was stirred for 4h at 30°C. The solvent was then evaporated and the crude product purified by column chromatography on silica gel using CH<sub>2</sub>Cl<sub>2</sub>/MeOH/Formic acid (99:1:1 to 97:3:1) as eluent, was dissolved in a minimal amount of CH<sub>2</sub>Cl<sub>2</sub> and precipitated by addition of pentane to obtain BODIPY **26** at a purity of ≈ 85% (69.9 mg of a mixture containing ≈ 60 mg of BODIPY **26**, 38.3 μmol, equivalent to 81% yield) as an orange-pink solid.



## 4.2.2 AzaBODIPYs

4.2.2.1 (*E*)-3-(4-hydroxyphenyl)-1-phenylprop-2-en-1-one (**27**)

3 g (53.5 mmol, 3.2 eq) KOH were dissolved in 40 mL methanol. 2.033 g (16.65 mmol, 0.99 eq) 4-hydroxybenzaldehyde, followed by 1.95 mL (16.65 mmol, 1 eq) acetophenone were added. The reaction was stirred for 1.5 h at room temperature (formation of an orange-red solution). The solvents were evaporated and the crude product neutralized by addition of 4.58 mL conc. HCl in 20 mL water and solubilized by addition of 30 mL DCM. The aqueous phase was extracted twice with DCM. The organic layers were united, washed with brine, dried over anhydrous MgSO<sub>4</sub> and the solvents removed under reduced pressure to yield 3.398 g (15.15 mmol, yield = 91%) of the target-compound **27** as a fluffy yellow solid.

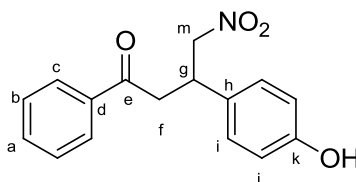


<sup>1</sup>H NMR (300 MHz, DMSO-d<sub>6</sub>) δ (ppm) = 6.81 – 6.88 (m, 2H, H<sub>j</sub>), 7.52 – 7.59 (m, 2H, H<sub>b</sub>), 7.64 (dt, *J* = 1.9, 2.8 Hz, 1H, H<sub>a</sub>), 7.69 (s, 1H, H<sub>g</sub>), 7.70 (s, 1H, H<sub>f</sub>), 7.71 – 7.76 (m, 2H, H<sub>i</sub>), 8.08 – 8.14 (m, 2H, H<sub>c</sub>), 10.07 (s, 1H, H<sub>m</sub>).

<sup>13</sup>C NMR (75 MHz, DMSO-d<sub>6</sub>) δ (ppm) = 115.8 (s, C<sub>j</sub>), 118.5 (s, C<sub>f</sub>), 125.8 (s, C<sub>h</sub>), 128.3 (s, C<sub>c</sub>), 128.7 (s, C<sub>b</sub>), 131.0 (s, C<sub>i</sub>), 132.8 (s, C<sub>a</sub>), 138.0 (s, C<sub>d</sub>), 144.5 (s, C<sub>g</sub>), 160.1 (s, C<sub>k</sub>), 189.0 (s, C<sub>e</sub>).

4.2.2.2 3-(4-hydroxyphenyl)-4-nitro-1-phenylbutan-1-one (**28**)

3.398 g of the chalcone **27** (15.15 mmol, 1 eq) were dissolved in 40 mL methanol, followed by addition of 5 mL DEA and 5 mL MeNO<sub>2</sub>. The reaction was refluxed for 18 h. The solvents were removed under reduced pressure to yield a brown, sticky liquid that was engaged into the next reaction without further purification or characterization.



<sup>1</sup>H NMR (300 MHz, CDCl<sub>3</sub>) δ (ppm) = 3.41 (dd, *J* = 2.9, 7.0 Hz, 2H, H<sub>f</sub>), 3.73 (q, *J* = 7.0 Hz, 1H, H<sub>g</sub>), 4.71 (ddd, *J* = 7.3, 12.3, 20.2 Hz, 2H, H<sub>m</sub>), 6.73 – 6.82 (m, 2H, H<sub>j</sub>), 7.08 – 7.17 (m, 2H, H<sub>i</sub>), 7.41 – 7.50 (m, 2H, H<sub>b</sub>), 7.53 – 7.62 (m, 1H, H<sub>a</sub>), 7.91 (m, 2H, H<sub>c</sub>).

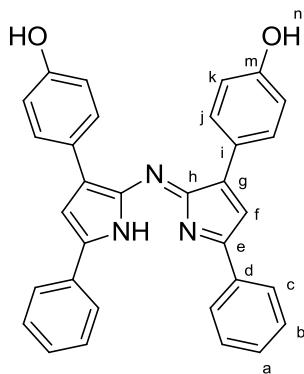
<sup>13</sup>C NMR (75 MHz, CDCl<sub>3</sub>) δ (ppm) = 38.9 (s, C<sub>g</sub>), 41.8 (s, C<sub>f</sub>), 80.0 (s, C<sub>m</sub>), 116.1 (s, C<sub>j</sub>), 128.2 (s, C<sub>i</sub>), 128.8 (s, C<sub>b</sub>), 128.9 (s, C<sub>c</sub>), 130.9 (s, C<sub>h</sub>), 133.7 (s, C<sub>a</sub>), 136.6 (s, C, C<sub>d</sub>), 155.7 (s, C<sub>k</sub>), 197.4 (s, C<sub>e</sub>).

4.2.2.3 Compound **29**

10 g of NH<sub>4</sub>OAc were added to the crude product **28**. After addition of 50 mL ethanol the reaction was refluxed for 18 hours. The solvents were then removed under reduced pressure and the resulting dark mass suspended in 20 mL of methanol.

The suspension was poured into 500 mL of water. The solids were filtered off, solubilized in a minimum amount of THF and precipitated by addition of heptane. The supernatant was discarded. The solid was purified over a 4 cm alumina (activity 5) plug (heptane 1 : 1 EtOAc). The solvents were removed under reduced pressure to obtain a compound that forms green-metallic mirrors. The solid was sonicated and washed repeatedly with a 10% EtOAc in heptane

solution and dried under reduced pressure to obtain 1.75 g (3.63 mmol, yield = 48% over two steps) of a dark blue solid.



$^1\text{H}$  NMR (300 MHz, DMSO- $d_6$ )  $\delta$  (ppm) = 6.87 (d,  $J$  = 8.8 Hz, 4H, H<sub>k</sub>), 7.49 (s,  $J$  = 8.0 Hz, 2H, H<sub>i</sub>), 7.54 (d,  $J$  = 7.2 Hz, 2H, H<sub>a</sub>), 7.62 (t,  $J$  = 7.4 Hz, 4H, H<sub>b</sub>), 7.97 (d,  $J$  = 8.8 Hz, 4H, H<sub>j</sub>), 8.06 (d,  $J$  = 7.2 Hz, 4H, H<sub>c</sub>), 9.76 (s,  $J$  = 47.8 Hz, 2H, H<sub>n</sub>).

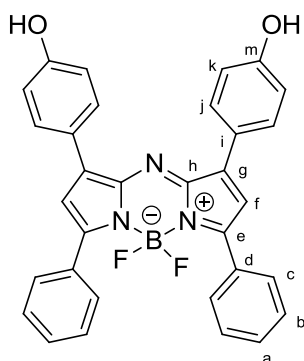
$^{13}\text{C}$  NMR (75 MHz, DMSO- $d_6$ )  $\delta$  (ppm) = 113.8 (s, C<sub>f</sub>), 115.3 (s, C<sub>k</sub>), 124.4 (s, C<sub>i</sub>), 126.5 (s, C<sub>a</sub>), 129.4 (s, C<sub>j</sub>), 130.2 (s, C<sub>b</sub>), 130.3 (s, C<sub>c</sub>), 131.5 (s, C<sub>d</sub>), 141.9 (s, C<sub>e</sub>), 148.7 (s, C<sub>g</sub>), 154.7 (s, C<sub>h</sub>), 158.0 (s, C<sub>m</sub>).

HR-MS (ESI): calculated for C<sub>32</sub>H<sub>24</sub>N<sub>3</sub>O<sub>2</sub> [M+H]<sup>+</sup> 482.18630; found 482.18508

#### 4.2.2.4 Compound **30**

1.5 g (3.11 mmol) Bis-hydroxy AzaDipyrromethene **29** were put into a round-bottom flask and dissolved in 100 mL of dry THF. The solution was stirred for 15 minutes at room temperature after addition of 2 mL dry DIPEA, followed by the addition of 2 mL 48% BF<sub>3</sub>·Et<sub>2</sub>O. The reaction was refluxed for 30 h, 2 mL BF<sub>3</sub>·Et<sub>2</sub>O were added every 6-8 hours until the reaction was complete.

Once finished, the solvents were removed under reduced pressure. The resulting solid was solubilized in EtOAc and washed 3 times with 3M HCl, followed by brine. The aqueous phase was discarded. The organic solvents were removed under reduced pressure and the resulting solid was washed and sonicated repeatedly with pentane. After drying 1.495 g (2.82 mmol, 91%) of the target compound **30** were obtained as a black-blue powder in sufficient purity for the following reactions. If necessary the compound can be further purified by column chromatography on silica gel (heptane 3 : 1 EtOAc → EtOAc), followed by precipitation from EtOAc/pentane.



$^1\text{H}$  NMR (300 MHz, CD<sub>3</sub>CN, 300K)  $\delta$  (ppm) = 6.93 (d,  $^3J$  = 8.9 Hz, 4H, H<sub>k</sub>), 7.07 (s, 2H, H<sub>i</sub>), 7.50 (dd,  $^3J$  = 5.3,  $^4J$  = 1.9 Hz, 6H, H<sub>a</sub>, H<sub>b</sub>), 8.00 (m, 8H, H<sub>c</sub>, H<sub>j</sub>)

## Materials and Methods

$^{13}\text{C}$  NMR (75 MHz, DMSO- $d_6$ )  $\delta$  (ppm) = 113.8 (s, C<sub>f</sub>), 115.3 (s, C<sub>k</sub>), 124.5 (s, C<sub>i</sub>), 126.5 (s, C<sub>a</sub>), 128.6 (s, br, C<sub>c</sub>), 129.4 (s, C<sub>j</sub>), 130.2 – 130.4 (m, C<sub>b</sub>), 131.5 (s, C<sub>d</sub>), 142.0 (s, C<sub>e</sub>), 148.7 (s, C<sub>g</sub>), 154.7 (s, C<sub>h</sub>), 158.0 (s, C<sub>m</sub>).

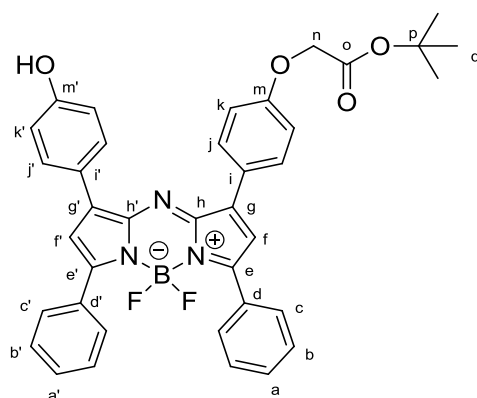
$^{11}\text{B}$  NMR (96 MHz, CD<sub>3</sub>CN, 300K)  $\delta$  (ppm) = 0.81 (t,  $J_{\text{B-F}}$  = 31.2 Hz)

$^{19}\text{F}$  NMR (282 MHz, CD<sub>3</sub>CN, 300K)  $\delta$  (ppm) = -130.19 (q,  $J_{\text{F-B}}$  = 31.3 Hz)

HR-MS (ESI): calculated for C<sub>32</sub>H<sub>22</sub>N<sub>3</sub>O<sub>2</sub>B<sub>1</sub>F<sub>2</sub>Na<sub>1</sub> [M+Na]<sup>+</sup> 552.16654; found 552.16550

### 4.2.2.5 Compound **31**

500 mg (945  $\mu\text{mol}$ , 1 eq) of **30** were dissolved in 4 mL of dry DMSO into a 10 mL flask. 574 mg (3.78 mmol, 4 eq) of CsF were added. The resulting mixture was stirred at room temperature for 10 min. 279  $\mu\text{L}$  (1.889 mmol, 2 eq) *t*-butyl-bromoacetic acid were added. After 2.5 minutes at room temperature the reaction was quenched by addition of 50 mL EtOAc and poured into 60 mL PBS-buffer. The organic layer was washed three times with 60 mL of PBS-buffer, followed by brine. Organic layer was dried over anhydrous MgSO<sub>4</sub> and evaporated under reduce pressure. The crude product was then purified by silica gel column chromatography (heptane 7: 3 EtOAc) to obtain a dark blue substance. Precipitation from EtOAc/pentane yields 318 mg of pure **31** (494  $\mu\text{mol}$ , 52% yield).



$^1\text{H}$  NMR (300 MHz, CDCl<sub>3</sub>)  $\delta$  (ppm) = 1.52 (s, 9H, H<sub>q</sub>), 4.59 (s, 2H, H<sub>n</sub>), 6.91 (d,  $J$  = 7.7 Hz, 4H, H<sub>f</sub>, H<sub>g</sub>, H<sub>k</sub>), 6.97 (d,  $J$  = 8.9 Hz, 2H, H<sub>k'</sub>), 7.45 – 7.49 (m, 6H, H<sub>j</sub>, H<sub>j'</sub>, H<sub>a</sub>, H<sub>a'</sub>), 7.97 (d,  $J$  = 8.6 Hz, 2H, H<sub>c</sub>), 7.99 – 8.04 (m, 6H, H<sub>b</sub>, H<sub>c'</sub>, H<sub>b'</sub>).

$^{13}\text{C}$  NMR (75 MHz, CDCl<sub>3</sub>)  $\delta$  (ppm) = 28.2 (s, C<sub>q</sub>), 65.8 (s, C<sub>n</sub>), 82.9 (s, C<sub>p</sub>), 114.9 (s, H<sub>f</sub>), 115.9 (s, H<sub>f</sub>), 117.7 (s, C<sub>k</sub>, k'), 125.4 (s, C<sub>i</sub>), 126.3 (s, C<sub>i'</sub>), 128.7 (s, C<sub>a</sub>, C<sub>a'</sub>), 129.7 (s, br, C<sub>c</sub>, C<sub>c'</sub>), 130.8 (s, C<sub>b</sub>), 130.9 (s, C<sub>b'</sub>), 131.0 (s, C<sub>j</sub>), 131.3 (s, C<sub>j'</sub>), 131.9 (s, C<sub>d'</sub>), 131.9 (s, C<sub>d</sub>), 143.6 (s, C<sub>e</sub>, C<sub>e'</sub>), 157.4 (s, C<sub>g</sub>, C<sub>g'</sub>), 159.2 (s, C<sub>h</sub>, C<sub>h'</sub>), 159.5 (s, C<sub>m</sub>, C<sub>m'</sub>), 168.0 (s, C<sub>o</sub>)

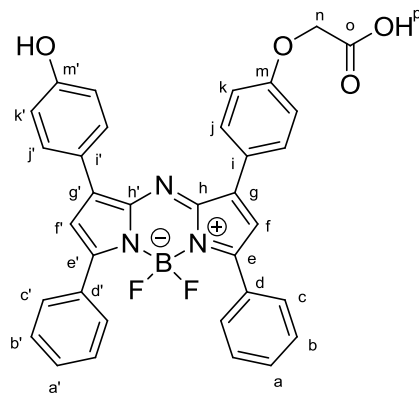
$^{11}\text{B}$  NMR (96 MHz, CDCl<sub>3</sub>)  $\delta$  (ppm) = 0.92 (t,  $J_{\text{B-F}}$  = 31.2 Hz)

$^{19}\text{F}$  NMR (282 MHz, CDCl<sub>3</sub>)  $\delta$  (ppm) = -130.92 (q,  $J_{\text{F-B}}$  = 31.2 Hz)

HR-MS (ESI): calculated for C<sub>38</sub>H<sub>32</sub>B<sub>1</sub>F<sub>2</sub>N<sub>3</sub>O<sub>4</sub>Na<sub>1</sub> [M+Na]<sup>+</sup> 666.23461; found 666.23338

4.2.2.6 Compound **32**

141 mg (0.219 mmol) of **31** were dissolved in 4 mL of THF. 2 mL of a solution of 6 M HCl in water were added and the solution was stirred at room temperature upon completion (7 h, followed by TLC). The solvents were evaporated under reduced pressure. The crude product was purified by RP-Flash-chromatography using a gradient of an aqueous, 50 mM TEAB (triethylammonium bicarbonate) solution and acetonitrile (10%ACN→100%ACN in 10 min, followed by 10 min 100% ACN). The collected product fractions were evaporated to dryness to yield 89 mg (152  $\mu$ mol, 69% yield) of the target compound **32** as a dark blue solid.



$^1\text{H}$  NMR (600 MHz, DMF- $d_7$ )  $\delta$  (ppm) = 4.95 (s, 2H, H<sub>n</sub>), 7.08 (d,  $J$  = 8.8 Hz, 2H, H<sub>k</sub>), 7.21 (d,  $J$  = 9.0 Hz, 2H, H<sub>k</sub>), 7.49 (s, 1H, H<sub>f</sub>), 7.51 (d,  $J$  = 0.8 Hz, 1H, H<sub>f</sub>), 7.55 – 7.59 (m, 6H, H<sub>b</sub>, H<sub>b'</sub>, H<sub>a</sub>, H<sub>a'</sub>), 8.17 – 8.21 (m, 4H, H<sub>c</sub>, H<sub>c'</sub>), 8.25 (d,  $J$  = 8.8 Hz, 2H, H<sub>j</sub>), 8.29 (d,  $J$  = 9.0 Hz, 2H, H<sub>j</sub>), 10.40 (s, 1H, H<sub>p</sub>).

$^{13}\text{C}$  NMR (151 MHz, DMF- $d_7$ )  $\delta$  (ppm) = 66.0 (s, C<sub>n</sub>), 116.1 (s, C<sub>f</sub>), 117.2 (s, C<sub>f</sub>), 119.1 (s, C<sub>k</sub>), 119.5 (s, C<sub>k'</sub>), 124.6 (s, C<sub>i</sub>), 126.7 (s, C<sub>i'</sub>), 129.7 (s, C<sub>a</sub>), 129.7 (s, C<sub>a'</sub>), 130.7 (t,  $J$  = 4.2 Hz, C<sub>c</sub>), 130.8 (t,  $J$  = 4.3 Hz, C<sub>c'</sub>), 131.9 (s, C<sub>b</sub>), 132.1 (s, C<sub>j</sub>), 132.1 (s, C<sub>b'</sub>), 132.5 (s, C<sub>j'</sub>), 132.9 (s, C<sub>d'</sub>), 133.0 (s, C<sub>d</sub>), 144.1 (s, C<sub>e</sub>), 145.6 (s, C<sub>e'</sub>), 146.0 (s, C<sub>g'</sub>), 146.6 (s, C<sub>g</sub>), 159.3 (s, C<sub>h</sub>), 160.7 (s, C<sub>h'</sub>), 160.9 (s, C<sub>m</sub>), 161.6 (s, C<sub>m'</sub>), 171.1 (s, C<sub>o</sub>).

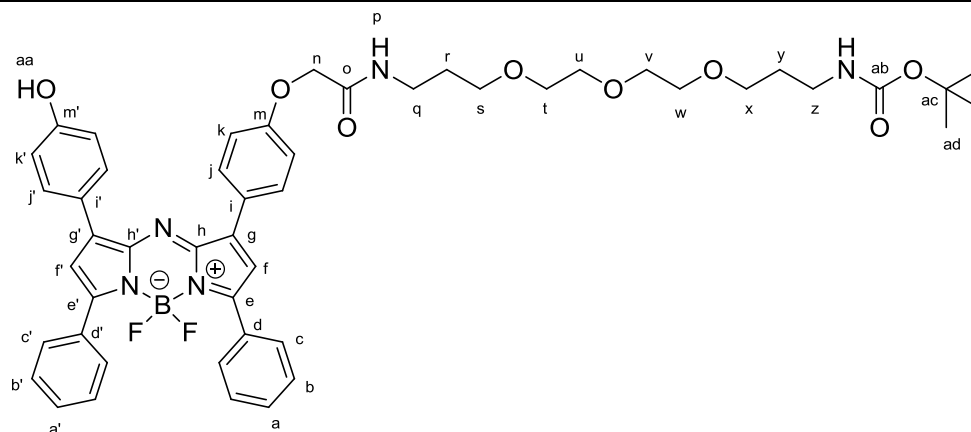
$^{11}\text{B}$  NMR (96 MHz, CD<sub>3</sub>CN)  $\delta$  (ppm) = 0.85 (t,  $J_{\text{B-F}}$  = 31.2 Hz).

$^{19}\text{F}$  NMR (282 MHz, CD<sub>3</sub>CN, 300K)  $\delta$  (ppm) = -130.32 (q,  $J_{\text{F-B}}$  = 31.3 Hz)

HR-MS (ESI): calculated for C<sub>35</sub>H<sub>25</sub>B<sub>1</sub>F<sub>2</sub>N<sub>3</sub>O<sub>4</sub> [M+H]<sup>+</sup> 588.19007; found 588.19042

4.2.2.7 Compound **33**

20 mg (34  $\mu$ mol, 1eq) of compound **32** were dissolved in 3 mL of DCM. Two droplets ( $m_{\text{theo}}=5$  mg,  $v_{\text{theo}}=3.5$   $\mu$ L, 1.2 eq) of oxalylchloride and one droplet of DMF were added. After the development of gas has seized, the reaction was stirred for one hour at room temperature. The solution was evaporated to dryness and the resulting residue was dissolved in DMF (1 mL). 13 mg (41  $\mu$ mol, 1.2 eq) of TOTA-Boc were dissolved in 1 mL of DMF and added to the Aza-BODIPY solution, followed by addition of 16 mg (41  $\mu$ mol, 1.2 eq) of HBTU in 1 mL of DMF and 0.1 mL of DIPEA. The reaction was further stirred for 16 h at room temperature (reaction control by HPLC). After total conversion of the starting material, the solvents were evaporated under reduced pressure. The crude product was washed three times with diluted HCl (pH=3) and neutralized by washing with NaHCO<sub>3</sub> solution. The organic fractions were gathered, dried over Na<sub>2</sub>SO<sub>4</sub> and solvents removed *in vacuo*. The product was dissolved in DCM and precipitated by addition of pentane. The resulting product was dried, resulting in pure **33** as dark blue solid in 73% yield (22 mg, 25  $\mu$ mol).



$^1\text{H}$  NMR (300 MHz,  $\text{CD}_3\text{CN}$ )  $\delta$  (ppm) = 1.37 (s, 9H,  $\text{H}_{\text{ad}}$ ), 1.61 (q,  $^3J = 6.4$  Hz, 2H,  $\text{H}_{\text{r}}$ ), 1.74 (q,  $^3J = 6.4$  Hz, 2H,  $\text{H}_{\text{v}}$ ), 3.05 (dd,  $^3J = 12.8$  Hz,  $^4J = 6.7$  Hz, 2H,  $\text{H}_{\text{q}}$ ), 3.33 (dd,  $J = 12.7$  Hz,  $^4J = 6.6$  Hz, 2H,  $\text{H}_{\text{z}}$ ), 3.40 (t,  $^3J = 6.1$  Hz, 2H,  $\text{H}_{\text{s}}$ ), 3.56 – 3.42 (m, 10H,  $\text{H}_{\text{t}}$ ,  $\text{H}_{\text{u}}$ ,  $\text{H}_{\text{v}}$ ,  $\text{H}_{\text{w}}$ ,  $\text{H}_{\text{x}}$ ), 4.50 (s, 2H,  $\text{H}_{\text{n}}$ ), 5.38 (s, 1H,  $\text{H}_{\text{aa}}$ ), 6.96 (d,  $^3J = 8.9$  Hz, 2H,  $\text{H}_{\text{k}}$ ), 7.06 (d,  $^3J = 9.0$  Hz, 2H,  $\text{H}_{\text{k}'}$ ), 7.10 (s, 2H,  $\text{H}_{\text{f}}$ ,  $\text{H}_{\text{f}'}$ ), 7.26 (t,  $J = 5.7$  Hz, 1H,  $\text{H}_{\text{p}}$ ), 7.57 – 7.42 (m, 6H,  $\text{H}_{\text{a}}$ ,  $\text{H}_{\text{a}'}$ ,  $\text{H}_{\text{b}}$ ,  $\text{H}_{\text{b}'}$ ), 8.04 – 7.95 (m, 6H,  $\text{H}_{\text{c}}$ ,  $\text{H}_{\text{c}'}$ ,  $\text{H}_{\text{j}}$ ), 8.08 (d,  $J = 9.0$  Hz, 2H,  $\text{H}_{\text{j}'}$ )

$^{13}\text{C}$  NMR (75 MHz,  $\text{CD}_3\text{CN}$ )  $\delta$  (ppm) = 28.6 (s,  $\text{C}_{\text{ad}}$ ), 30.1 (s,  $\text{C}_{\text{v}}$ ,  $\text{C}_{\text{r}}$ ), 37.4 (s,  $\text{C}_{\text{q}}$ ,  $\text{C}_{\text{z}}$ ), 57.4 (s,  $\text{C}_{\text{x}}$ ), 68.1 (s,  $\text{C}_{\text{n}}$ ), 69.6 (s,  $\text{C}_{\text{s}}$ ), 69.8, 70.6, 70.9, 71.0 (4x s,  $\text{C}_{\text{t}}$ ,  $\text{C}_{\text{u}}$ ,  $\text{C}_{\text{v}}$ ,  $\text{C}_{\text{w}}$ ), 75.4 (s,  $\text{C}_{\text{ac}}$ ), 116.0 (s,  $\text{C}_{\text{f}}$ ), 116.8 (s,  $\text{C}_{\text{k}}$ ), 124.9 (s,  $\text{C}_{\text{i}}$ ), 126.8 (s,  $\text{C}_{\text{i}'}$ ), 129.4 (s,  $\text{C}_{\text{a}}$ ), 129.4 (s,  $\text{C}_{\text{a}'}$ ), 130.5 (s, br,  $\text{C}_{\text{c}}$ ), 131.7 (s,  $\text{C}_{\text{j}}$ ), 131.9 (s,  $\text{C}_{\text{b}}$ ), 132.2 (s,  $\text{C}_{\text{b}'}$ ), 132.6 (s,  $\text{C}_{\text{d}'}$ ), 132.7 (s,  $\text{C}_{\text{d}}$ ), 144.4 (s,  $\text{C}_{\text{e}}$ ), 159.9 (s,  $\text{C}_{\text{h}}$ ), 160.3 (s,  $\text{C}_{\text{ab}}$ ), 160.6 (s,  $\text{C}_{\text{m}}$ ), 168.6 (s,  $\text{C}_{\text{o}}$ ).

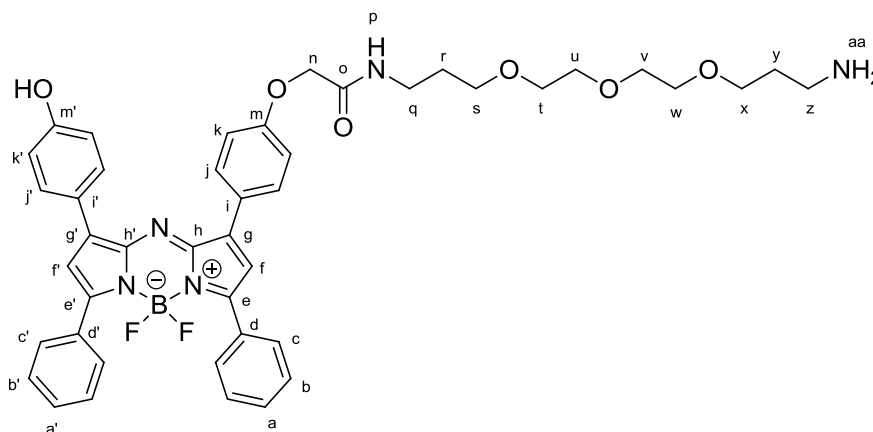
$^{11}\text{B}$  NMR (96 MHz,  $\text{CD}_3\text{CN}$ )  $\delta$  (ppm) = 0.81 (t,  $J_{\text{B-F}} = 31.2$  Hz)

$^{19}\text{F}$  NMR (282 MHz,  $\text{CD}_3\text{CN}$ )  $\delta$  (ppm) = -130.23 (q,  $J_{\text{F-B}} = 31.2$  Hz)

HR-MS (ESI): calculated for  $\text{C}_{49}\text{H}_{54}\text{B}_1\text{F}_2\text{N}_5\text{O}_8\text{Na}_1$   $[\text{M}+\text{Na}]^+$  912.39257; found 912.39411

#### 4.2.2.8 Compound 34

21 mg (24  $\mu\text{mol}$ ) of compound **33** were dissolved in THF (3 mL). 3 mL of 3 M HCl were then added and the reaction was stirred for 18h at room temperature, followed by 4 h at 35°C. The resulting crude product was evaporated to dryness at 30°C and purified by semi-preparative HPLC using as eluent, the following gradient:  $\text{H}_2\text{O}+0.1\%$  formic acid and  $\text{ACN}+0.1\%$  formic acid (30%ACN + 0.1FA to 90%ACN + 0.1%FA in 20 min). The fractions corresponding to the targeted product were evaporated to dryness and precipitated from DCM/pentane to obtain 16 mg (20  $\mu\text{mol}$ , 83%) of pure **34** as a dark blue powder.





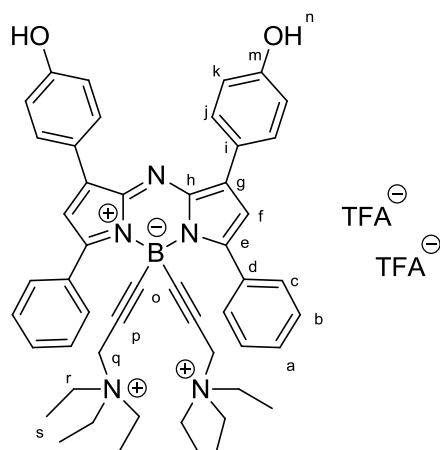
## Materials and Methods

$^1\text{H}$  NMR (300 MHz, MeOD, 300K)  $\delta$  (ppm) = 1.42 (t,  $^3J = 7.3$  Hz, 9H,  $\text{H}_a$ ), 3.53 (q,  $^3J = 7.3$  Hz, 6H,  $\text{H}_b$ ), 4.36 (s, 2H,  $\text{H}_c$ )

$^{13}\text{C}$  NMR (75 MHz, MeOD, 300K)  $\delta$  (ppm) = 8.0 (s,  $\text{C}_a$ ), 54.7 (s,  $\text{C}_b$ ), 71.7 (t,  $^2J_{\text{C-D}}=7.85\text{Hz}$ ,  $\text{C}_c$ ), 82.0 (t,  $^1J_{\text{C-D}}=39.30\text{Hz}$ ,  $\text{C}_e$ ), 82.3 (s,  $\text{C}_d$ ).

### 4.2.2.11 Compound **37**

61.6 mg (279.8  $\mu\text{mol}$ , 2.1 eq) propyne-ammonium **36** were dissolved in 15 mL of dry THF under argon and cooled to  $-78^\circ\text{C}$ . 165  $\mu\text{L}$  1.7M tBuLi in THF (279.8  $\mu\text{mol}$ , 2.1 eq) were added and the reaction stirred for 15min. 101 mg azaBODIPY **38** (133.2  $\mu\text{mol}$ ) were dissolved in 5mL dry THF, pulled into a syringe and added slowly to the reaction mixture. The reaction is stirred for 90min at  $-78^\circ\text{C}$  and then left to heat up to room temperature. The crude mixture is quenched by addition of EtOH, followed by 5 mL 1M HCl. The solution is stirred for 6 h until total consumption of TBDMS-protected products. The crude product is evaporated to dryness and purified by semi preparative HPLC using a gradient of ACN:  $\text{H}_2\text{O}+0.1\%\text{FA}$  (20%ACN+0.1%FA to 80% ACN+0.1%FA in 30 min). The product fractions are collected and lyophilized to yield 65.2 mg (37  $\mu\text{mol}$ , 49%) of the target compound as a dark blue powder.



$^1\text{H}$  NMR (300 MHz, MeOD- $d_4$ )  $\delta$  (ppm) = 1.04 – 1.15 (m, 18H,  $\text{H}_s$ ), 2.91 (dd,  $J = 7.2, 14.4$  Hz, 4H,  $\text{H}_r$  (inner)), 3.01 (q,  $J = 7.2$  Hz, 8H,  $\text{H}_r$  (outer)), 3.63 (d,  $J = 6.1$  Hz, 1H,  $\text{H}_q$ ), 3.81 (s, 4H,  $\text{H}_q$ ), 6.87 – 6.97 (m, 4H,  $\text{H}_k$ ), 7.09 – 7.17 (m, 2H,  $\text{H}_l$ ), 7.53 – 7.64 (m, 6H,  $\text{H}_a, \text{H}_b$ ), 8.04 (dd,  $J = 2.6, 8.8$  Hz, 4H,  $\text{H}_c$ ), 8.26 (dd,  $J = 2.2, 5.4$  Hz, 4H,  $\text{H}_j$ ), 8.38 (s, 2H,  $\text{H}_n$ ).

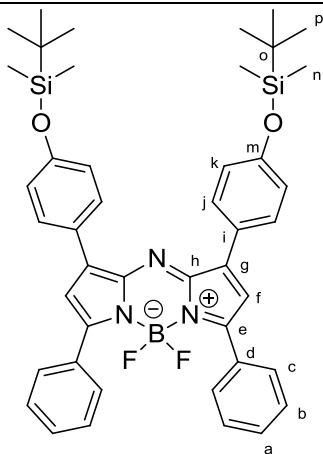
$^{13}\text{C}$  NMR (75 MHz, MeOD- $d_4$ )  $\delta$  (ppm) = 7.8 (s,  $\text{C}_s$ ), 9.9 (s), 33.3 (s,  $\text{C}_o$ ), 54.1 (s,  $\text{C}_q$ ), 54.2 (s,  $\text{C}_r$ ), 87.5 (s,  $\text{C}_p$ ), 116.9 (s,  $\text{C}_l$ ), 119.3 (s,  $\text{C}_k$ ), 125.0 (d,  $J = 4.6$  Hz,  $\text{C}_i$ ), 129.5 (d,  $J = 7.4$  Hz,  $\text{C}_b$ ), 131.4 (d,  $J = 4.9$  Hz,  $\text{C}_c$ ), 131.9 (d,  $J = 12.2$  Hz,  $\text{C}_a$ ), 132.3 (d,  $J = 3.0$  Hz,  $\text{C}_j$ ), 133.8 (d,  $J = 7.6$  Hz,  $\text{C}_d$ ), 144.2 (s,  $\text{C}_e$ ), 145.1 (d,  $J = 7.2$  Hz,  $\text{C}_g$ ), 159.6 (d,  $J = 5.9$  Hz,  $\text{C}_h$ ), 161.0 (d,  $J = 7.0$  Hz,  $\text{C}_m$ ).

$^{11}\text{B}$  NMR (96 MHz, MeOD- $d_4$ )  $\delta$  (ppm) = -12.97 (s, br).

HR-MS (ESI): calculated for  $\text{C}_{50}\text{H}_{56}\text{B}_1\text{N}_5\text{O}_2$   $[\text{M}]^{2+}$  384.72580; found 384.72604

### 4.2.2.12 Compound **38**

90 mg (170  $\mu\text{mol}$ , 1 eq) azaBODIPY **30** were dissolved in 10 mL of dry THF. 95  $\mu\text{L}$  (6.28  $\mu\text{mol}$ , 4 eq) of dry  $\text{Et}_3\text{N}$ , 102 mg (4 eq, 680  $\mu\text{mol}$ ) of TBDMSCl and one crystal of DMAP were added and the resulting solution stirred for 90 minutes at room temperature. Solvents were evaporated and the crude product purified by column chromatography on silica gel using an eluent of EtOAc/heptane (2:8), yielding 101 mg (133  $\mu\text{mol}$ , yield = 78%) of the desired product as a coppery, crystalline solid.



$^1\text{H}$  NMR (600 MHz,  $\text{CDCl}_3$ )  $\delta$  (ppm) = 0.24 – 0.30 (m, 12H,  $\text{H}_n$ ), 1.01 – 1.08 (m, 18H,  $\text{H}_p$ ), 6.92 (m, 6H,  $\text{H}_f$ ,  $\text{H}_k$ ), 7.47 (m, 6H,  $\text{H}_a$ ,  $\text{H}_b$ ), 7.96 – 8.05 (m, 8H,  $\text{H}_c$ ,  $\text{H}_j$ ).

$^{13}\text{C}$  NMR (151 MHz,  $\text{CDCl}_3$ )  $\delta$  (ppm) = -4.1 (s,  $\text{C}_n$ ), 18.5 (s,  $\text{C}_o$ ), 25.9 (s,  $\text{C}_p$ ), 117.7 (s,  $\text{C}_f$ ), 120.5 (s,  $\text{C}_k$ ), 126.1 (s,  $\text{C}_i$ ), 128.7 (s,  $\text{C}_a$ ), 129.7 (t,  $J = 3.9$  Hz,  $\text{C}_c$ ), 130.8 (s,  $\text{C}_b$ ), 131.1 (s,  $\text{C}_j$ ), 132.0 (s,  $\text{C}_d$ ), 144.0 (s,  $\text{C}_e$ ), 145.6 (s,  $\text{C}_g$ ), 157.6 (s,  $\text{C}_h$ ), 159.3 (s,  $\text{C}_m$ ).

$^{11}\text{B}$  NMR (96 MHz,  $\text{CDCl}_3$ )  $\delta$  (ppm) = 0.95 (t,  $J_{\text{B-F}} = 31.2$  Hz).

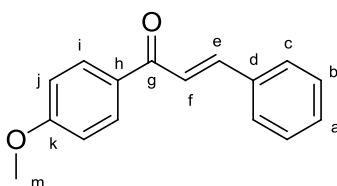
$^{19}\text{F}$  NMR (282 MHz,  $\text{CDCl}_3$ )  $\delta$  (ppm) = -131.00 (q,  $J_{\text{F-B}} = 31.2$  Hz).

$^{29}\text{Si}$  NMR (60 MHz,  $\text{CDCl}_3$ )  $\delta$  (ppm) = -110.07 (br).

HR-MS (ESI): calculated for  $\text{C}_{44}\text{H}_{51}\text{B}_1\text{F}_2\text{N}_3\text{O}_2\text{Si}_2$   $[\text{M}+\text{H}]^+$  758.35754; found 758.35665

#### 4.2.2.13 (*E*)-1-(4-methoxyphenyl)-3-phenylprop-2-en-1-one (**41**)

3 g KOH (53.47 mmol, 1.6 eq) KOH were dissolved in 40 mL methanol. 5 g (33.3 mmol, 1 eq) 4-methoxyacetophenone and 3.36 mL (32.97 mmol, 0.99 eq) were added and the reaction stirred for 1.5h at room temperature. The formed precipitate was filtered and washed twice with MeOH. The filtrate was reconcentrated and filtered as well, followed by washing with MeOH. The solids were collected to obtain 8.0029 g (5.7806 g (24.26 mmol, yield = 74%) + 2.2223 g (9.33 mmol, yield = 28%) that contains traces of KOH) of the target compound as a fluffy white solid.



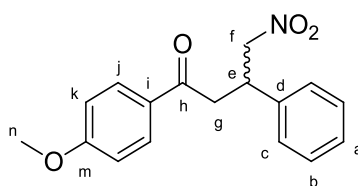
$^1\text{H}$ -NMR (300 MHz,  $\text{CDCl}_3$ , 300K):  $\delta$  (ppm) = 3.88 (s,  $\text{H}_m$ ), 7.00 (d,  $J = 8.8$  Hz, 2H,  $\text{H}_j$ ), 7.40 (m, 3H,  $\text{H}_a$ ,  $\text{H}_b$ ), 7.54 (d,  $J = 15.6$  Hz, 1H,  $\text{H}_i$ ), 7.63 (dd,  $J = 7.2$  Hz, 3.4 Hz, 2H,  $\text{H}_c$ ), 7.81 (d,  $J = 15.6$  Hz, 1H,  $\text{H}_e$ ), 8.04 (d,  $J = 8.8$  Hz, 2H,  $\text{H}_i$ )

#### 4.2.2.14 1-(4-methoxyphenyl)-4-nitro-3-phenylbutan-1-one (**42**)

5.7806 g (24.26 mmol, 1eq) chalcone **41** was suspended in 20mL MeOH. After addition of 8mL (76.56mmol, 3.2eq) DEA and 4mL (74.7 mmol, 3.1 eq)  $\text{MeNO}_2$  the reaction was refluxed for 6h. After total conversion the solvents were evaporated and the compound dried under fine vacuum for 18h to obtain 7.479 g of the target compound as a sticky yellow oil that still

## Materials and Methods

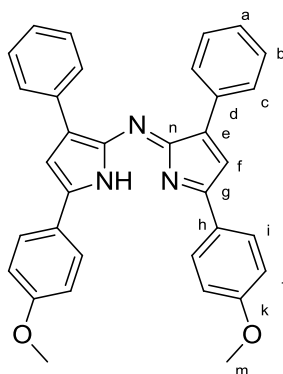
contains MeNO<sub>2</sub> (considered as 100%). The product was used in the next reaction without purification or characterization.



<sup>1</sup>H NMR (500 MHz, CDCl<sub>3</sub>, 300K): δ (ppm) = 3.39 (qd, <sup>3</sup>J = 17.4, <sup>4</sup>J = 7.0 Hz, 2H, H<sub>f</sub>), 3.87 (s, 3H, H<sub>n</sub>), 4.21 (q, <sup>3</sup>J = 7.1 Hz, 1H, H<sub>e</sub>), 4.32 (s, 1H), 4.68 (dd, <sup>3</sup>J = 12.5, <sup>4</sup>J = 8.1 Hz, 1H, H<sub>g</sub>), 4.84 (dd, <sup>3</sup>J = 12.5, 6.5 Hz, 1H, H<sub>g'</sub>), 6.93 (d, J = 8.9 Hz, 2H, H<sub>k</sub>), 7.23 – 7.30 (m, 3H, H<sub>a</sub>, H<sub>b</sub>), 7.37 – 7.30 (m, 2H, H<sub>c</sub>), 7.90 (d, J = 9.0 Hz, 2H, H<sub>j</sub>)

### 4.2.2.15 Compound **43**

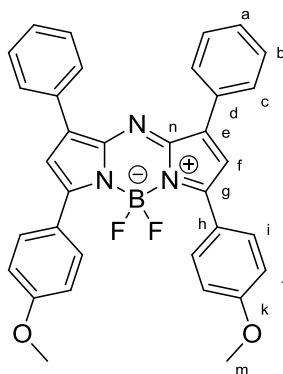
7.479 g of the product-oil **42** (considered as 24.26 mmol, 1 eq) were placed in 200 mL EtOH. After addition of 37.4 g NH<sub>4</sub>OAc (485.2 mmol, 20 eq) the mixture was refluxed for 8h. The solvents were evaporated until ½ of the original volume and then centrifuged. The supernatant was discarded, the solid resuspended and centrifuged again (3x repetitions until the supernatant stayed almost colorless). The blue black filtrate was dried to yield 3.2347 g (6.348 mmol, yield = 52% over 2 steps) of the target-compound as a dark blue solid.



<sup>1</sup>H NMR (500 MHz, CDCl<sub>3</sub>) δ (ppm) = 3.91 (s, 6H, H<sub>m</sub>), 7.05 (d, J = 8.8 Hz, 4H, H<sub>i</sub>), 7.13 (s, 2H, H<sub>f</sub>), 7.42 (t, J = 7.5 Hz, 4H, H<sub>b</sub>), 7.87-7.92 (m, 6H, H<sub>a</sub>, H<sub>j</sub>), 8.06 (d, J = 7.2 Hz, 4H<sub>c</sub>).

### 4.2.2.16 AzaBODIPY **44**

3.2347 g (6.347 mmol) of azadipyromethene **43** were dissolved/suspended in 200 mL dry THF. After addition of 10 mL (57.4 mmol, 9.04 eq) DIPEA and 12 mL 48% BF<sub>3</sub>·Et<sub>2</sub>O (45.5 mmol, 7.17 eq) the reaction was stirred at 60°C for 2.5 h (solution turns green). The reaction-mixture was evaporated to dryness. The crude product was redissolved in MeOH, stirred for 30 min and centrifuged. The solid was washed and centrifuged 3x with MeOH. The solid was dissolved in DCM (30 mL), followed by addition of MeOH (200 mL) and slowly evaporated to near dryness (formation of coppery solid). The remaining supernatant was removed *via* pipette and the solid dried to yield 2.6296 g (4.718 mmol, yield = 74%) of the target-compound as a coppery powder.



$^1\text{H}$  NMR (500 MHz, DMSO- $d_6$ )  $\delta$  (ppm) = 3.89 (s, 6H,  $H_m$ ), 7.15 (d,  $J$  = 9.0 Hz, 4H,  $H_j$ ), 7.48 (t,  $J$  = 7.3 Hz, 2H,  $H_a$ ), 7.54 (t,  $J$  = 7.4 Hz, 4H,  $H_b$ ), 7.61 (s, 2H,  $H_f$ ), 8.18 (ps-t,  $J$  = 8.4 Hz, 8H,  $H_c, H_i$ ).

$^{13}\text{C}$  NMR (126 MHz,  $\text{CDCl}_3$ )  $\delta$  (ppm) = 55.6 (s,  $C_m$ ), 114.4 (s,  $C_f$ ), 118.8 (s,  $C_j$ ), 124.3 (s,  $C_h$ ), 128.7 (s,  $C_a$ ), 129.4 (s,  $C_c$ ), 129.4 (s,  $C_b$ ), 131.8 (t,  $J$  = 4.8 Hz,  $C_i$ ), 132.7 (s,  $C_d$ ), 143.3 (s,  $C_e$ ), 145.5 (s,  $C_g$ ), 158.3 (s,  $C_n$ ), 162.1 (s,  $C_k$ ).

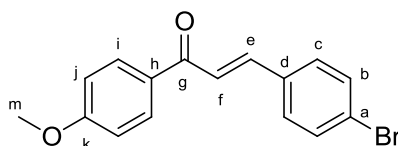
$^{11}\text{B}$  NMR (160 MHz, DMSO- $d_6$ )  $\delta$  (ppm) = 1.04 (t,  $J$  = 32.6 Hz).

$^{19}\text{F}$  NMR (470 MHz, DMSO- $d_6$ )  $\delta$  (ppm) = -130.41 (q,  $J$  = 32.6 Hz).

HR-MS (ESI): calculated for  $\text{C}_{34}\text{H}_{26}\text{B}_1\text{F}_2\text{N}_3\text{O}_2$   $[\text{M}]^+$  557.20807; found 557.20754

#### 4.2.2.17 (*E*)-3- (4-bromophenyl)-1-methoxyphenylprop-2-en-1-one **45**

7.5 g (133 mmol) KOH were dissolved in 150 mL of MeOH. 5g (33.29mmol, 1eq.) of 4-methoxyacetophenone and 6.159 g (33.29 mmol, 0.99 eq) of 4-bromobenzaldehyde were successively added and the mixture stirred for 1.5 h at room temperature. The solvents were evaporated to near dryness and the resulting slurry was dissolved in DCM (400 mL) and extracted once with water until the aqueous phase was colorless. The organic phase was dried with  $\text{Na}_2\text{SO}_4$ , filtered and evaporated to dryness to yield 9.334 g (yield = 88%) of the target compound as a pale yellow solid.



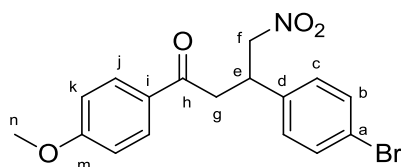
$^1\text{H}$  NMR (500 MHz,  $\text{CDCl}_3$ )  $\delta$  (ppm) = 3.89 (s, 3H,  $H_m$ ), 6.99 (d,  $J$  = 8.9 Hz, 2H,  $H_j$ ), 7.50 (d,  $J$  = 8.5 Hz, 2H,  $H_b$ ), 7.52 (d,  $J$  = 15.6 Hz, 1H,  $H_i$ ), 7.55 (d,  $J$  = 8.4 Hz, 2H,  $H_c$ ), 7.72 (d,  $J$  = 15.6 Hz, 1H,  $H_e$ ), 8.03 (d,  $J$  = 8.9 Hz, 2H,  $H_f$ ).

$^{13}\text{C}$  NMR (126 MHz,  $\text{CDCl}_3$ )  $\delta$  (ppm) = 55.7 (s,  $C_m$ ), 114.1 (s,  $C_j$ ), 122.6 (s,  $C_f$ ), 124.7 (s,  $C_a$ ), 129.8 (s,  $C_c$ ), 131.0 (s,  $C_h$ ), 132.3 (s,  $C_i$ ), 134.2 (s,  $C_b$ ), 142.6 (s,  $C_e$ ), 163.7 (s,  $C_k$ ), 188.5 (s,  $C_g$ ).

#### 4.2.2.18 3- (4-bromophenyl)-4-nitro-1-methoxyphenylbutan-1-one (**46**)

8.0174 g (25.28mmol) of chalcone **45** were suspended in 150 mL of MeOH. 20 mL of nitromethane (373.5 mmol, 14.8eq) and 20 mL of diethylamine (193 mmol, 7.6 eq) were added and the mixture refluxed for 48h.

The solvents were evaporated under fine vacuum to yield the target compound as a brown solid. The substance was engaged in the next reaction without further purification or characterization.

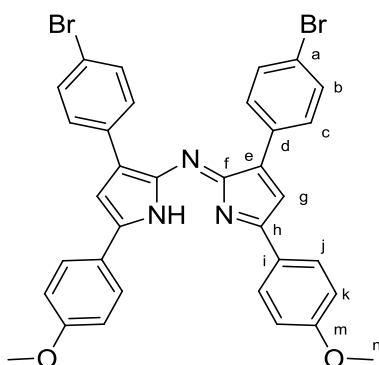


$^1\text{H}$  NMR (500 MHz,  $\text{CDCl}_3$ )  $\delta$  (ppm) = 3.36 (dd,  $J$  = 5.4, 6.9 Hz, 2H,  $\text{H}_f$ ), 3.87 (s, 3H,  $\text{H}_n$ ), 4.13 – 4.23 (m, 1H,  $\text{H}_e$ ), 4.65 (dd,  $J$  = 8.2, 12.6 Hz, 1H,  $\text{H}_g$ ), 4.81 (dd,  $J$  = 6.4, 12.6 Hz, 1H,  $\text{H}_g'$ ), 6.92 (d,  $J$  = 8.9 Hz, 2H,  $\text{H}_c$ ), 7.16 (d,  $J$  = 8.4 Hz, 2H,  $\text{H}_k$ ), 7.45 (d,  $J$  = 8.4 Hz, 2H,  $\text{H}_j$ ), 7.88 (d,  $J$  = 8.9 Hz, 2H,  $\text{H}_b$ ).

#### 4.2.2.19 Compound **47**

The oil **46** was dissolved in 250 mL EtOH and 30 g of  $\text{NH}_4\text{OAc}$  were added. The mixture was refluxed for 36 h. The solvents were evaporated to 1/4<sup>th</sup> of the original volume. The mixture was centrifuged and washed repeatedly (4-5 times) with EtOH until the washing phase stays (almost) colorless.

The obtained blue solid was suspended in pentane, decanted and the solid evaporated to dryness to yield 3.7843 g of the target compound as a dark blue solid. The discarded filtrates was reengaged following the same procedure to yield 0.627 g of the target compound. (6.61 mmol, yield = 52% over 2 steps)



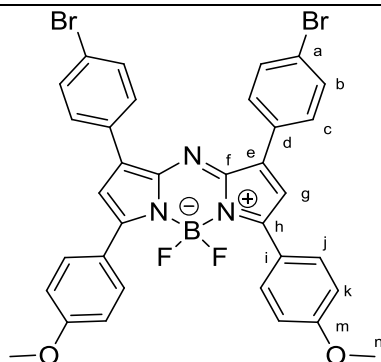
$^1\text{H}$  NMR (300 MHz,  $\text{DMSO}-d_6$ )  $\delta$  (ppm) = 3.90 (s, 6H,  $\text{H}_n$ ), 7.22 (d,  $J$  = 8.7 Hz, 4H,  $\text{H}_k$ ), 7.65 (s,  $J$  = 7.8 Hz, 2H,  $\text{H}_g$ ), 7.70 (d,  $J$  = 8.6 Hz, 4H,  $\text{H}_c$ ), 8.03 (t,  $J$  = 8.2 Hz, 8H,  $\text{H}_b$ ,  $\text{H}_j$ ).

#### 4.2.2.20 AzaBODIPY **48**

4.4113 g (6.61 mmol) azaDIPY **47** were dissolved in 200 mL of dry THF. 10 mL of dry DIPEA were added and the solution stirred for 20min at room temperature. After 20 min 6 mL of 48%  $\text{BF}_3 \cdot \text{Et}_2\text{O}$  (6 mL, 48.8 mmol, 7.4 eq) were added and the resulting solution refluxed for 24 h. After total consumption of starting materials (checked by TLC) the solvents were evaporated and the crude product partitioned thrice between DCM/1M HCl.

The organic fractions were collected, washed with brine and dried with  $\text{Na}_2\text{SO}_4$ .

The crude product was deposited on silica gel and purified on silica gel using an eluent of heptane /EtOAc (6:4  $\rightarrow$  1:2). 4.6 g (6.43 mmol, 97%) of the target compound were isolated as a fine crystalline, dark green powder.



$^1\text{H}$  NMR (500 MHz,  $\text{CDCl}_3$ )  $\delta$  (ppm) = 3.89 (s, 6H,  $\text{H}_m$ ), 7.01 (m, 6H,  $\text{H}_g$ ,  $\text{H}_k$ ), 7.59 (d,  $J$  = 7.3 Hz, 4H,  $\text{H}_c$ ), 7.90 (d,  $J$  = 7.2 Hz, 4H,  $\text{H}_b$ ), 8.08 (d,  $J$  = 7.4 Hz, 4H,  $\text{H}_j$ ).

$^{13}\text{C}$  NMR (75 MHz,  $\text{CDCl}_3$ )  $\delta$  (ppm) = 55.6 ( $\text{C}_n$ ), 114.5, ( $\text{C}_g$ ), 118.9 ( $\text{C}_k$ ), 124.0 ( $\text{C}_a$ ), 130.7 ( $\text{C}_i$ ), 131.4 ( $\text{C}_j$ ), 131.8 ( $\text{C}_c$ ), 131.9 ( $\text{C}_b$ ), 131.9 ( $\text{C}_d$ ), 141.8 ( $\text{C}_e$ ), 145.3 ( $\text{C}_f$ ), 158.5 ( $\text{C}_h$ ), 162.3 ( $\text{C}_m$ )

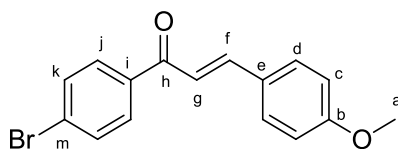
$^{11}\text{B}$  NMR (96 MHz,  $\text{CDCl}_3$ )  $\delta$  (ppm) = -1.05 (t,  $J_{\text{B-F}}$  = 31.7 Hz).

$^{19}\text{F}$  NMR (282 MHz,  $\text{CDCl}_3$ )  $\delta$  (ppm) = -132.07 (q,  $J$  = 31.7 Hz)

HR-MS (ESI): calculated for  $\text{C}_{34}\text{H}_{24}\text{B}_1\text{Br}_2\text{F}_2\text{N}_3\text{O}_2$  [ $\text{M}$ ] $^+$  713.02909; found 713.03150

#### 4.2.2.21 (*E*)-3-(4-Methoxyphenyl)-1-bromophenylprop-2-en-1-one (**49**)

7.5 g (133 mmol) of KOH were dissolved in 150 mL of MeOH. 7.31g (36.73 mmol, 1eq.) of 4-bromoacetophenone and 5 g (36.72 mmol, 0.99 eq) 4-methoxybenzaldehyde were successively added and the mixture stirred for 1.5 h at room temperature. The solvents were evaporated to near dryness, the resulting crude product was dissolved in DCM (400 mL) and extracted with water until the aqueous phase was colorless. The organic phase was dried with  $\text{Na}_2\text{SO}_4$  (5-10 g), filtered and evaporated to dryness to yield 10.25 g (32.32 mmol, 88%) of the target compound as a pale yellow solid.



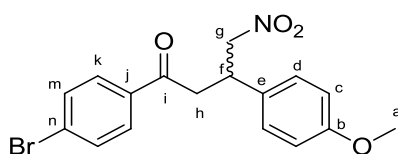
$^1\text{H}$  NMR (500 MHz,  $\text{CDCl}_3$ )  $\delta$  (ppm) = 3.85 (s, 3H,  $\text{H}_a$ ), 6.93 (d,  $J$  = 8.7 Hz, 2H,  $\text{H}_c$ ), 7.34 (d,  $J$  = 15.6 Hz, 1H,  $\text{H}_g$ ), 7.59 (d,  $J$  = 8.7 Hz, 2H,  $\text{H}_d$ ), 7.62 (d,  $J$  = 8.4 Hz, 2H,  $\text{H}_k$ ), 7.77 (d,  $J$  = 15.6 Hz, 1H,  $\text{H}_f$ ), 7.86 (d,  $J$  = 8.5 Hz, 2H,  $\text{H}_j$ ).

$^{13}\text{C}$  NMR (126 MHz,  $\text{CDCl}_3$ )  $\delta$  (ppm) = 55.6 (s,  $\text{C}_a$ ), 114.6 (s,  $\text{C}_c$ ), 119.3 (s,  $\text{C}_g$ ), 127.6 (s,  $\text{C}_e$ ), 127.7 (s,  $\text{C}_m$ ), 130.1 (s,  $\text{C}_j$ ), 130.5 (d,  $J$  = 2.6 Hz,  $\text{C}_d$ ), 132.0 (s,  $\text{C}_k$ ), 137.4 (s,  $\text{C}_i$ ), 145.5 (d,  $J$  = 3.4 Hz,  $\text{C}_f$ ), 162.0 (s,  $\text{C}_b$ ), 189.7 (s,  $\text{C}_h$ ).

#### 4.2.2.22 3-(4-Methoxyphenyl)-4-nitro-1-bromophenylbutan-1-one (**50**)

8.0174 g (25.28 mmol) of chalcone **49** were placed in a round bottom flask and suspended in 150mL of MeOH. 20mL of nitromethane (373.53 mmol, 14.8 eq) and 20 mL of diethylamine (193.33 mmol, 7.65 eq) were added and the mixture refluxed for 48h.

The solvents were evaporated to yield the target compound as a brown solid. The crude substance was engaged in the next reaction without further purification.



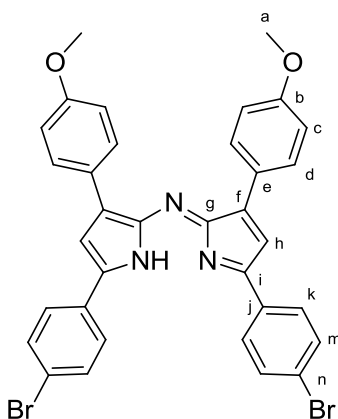
## Materials and Methods

$^1\text{H}$  NMR (500 MHz,  $\text{CDCl}_3$ )  $\delta$  (ppm) = 3.38 (dd,  $J$  = 3.3, 6.9 Hz, 2H,  $\text{H}_h$ ), 3.77 (s, 3H,  $\text{H}_a$ ), 4.15 (p,  $J$  = 7.1 Hz, 1H,  $\text{H}_i$ ), 4.64 (dd,  $J$  = 7.7, 12.4 Hz, 1H,  $\text{H}_g$ ), 4.77 (dd,  $J$  = 6.8, 12.4 Hz, 1H,  $\text{H}_g'$ ), 6.85 (d,  $J$  = 8.7 Hz, 2H,  $\text{H}_c$ ), 7.18 (d,  $J$  = 8.7 Hz, 2H,  $\text{H}_d$ ), 7.59 (d,  $J$  = 8.6 Hz, 2H,  $\text{H}_m$ ), 7.76 (d,  $J$  = 8.6 Hz, 2H,  $\text{H}_k$ ).

### 4.2.2.23 Compound **51**

Compound **50** was dissolved in 250mL of EtOH and 30g of  $\text{NH}_4\text{OAc}$  were added. The mixture was refluxed for 36h. The solution was concentrated and filtered. The recovered solid was further washed with EtOH (40 mL, 4-5times) until the supernatant remained colorless.

The obtained blue solid was suspended in pentane, decanted and dried to yield 6.1366 g of the target compound as a dark blue solid. The discarded filtrate was reengaged following the same procedure to yield 0.802 g of the target compound (10.40 mmol, yield = 82% over two steps).



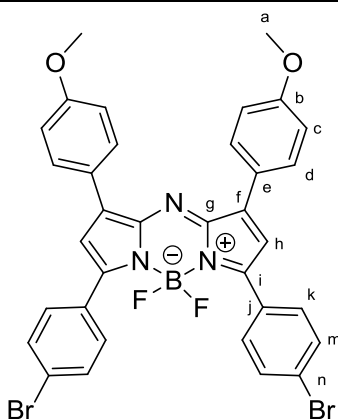
$^1\text{H}$  NMR (300 MHz,  $\text{CDCl}_3$ )  $\delta$  (ppm) = 3.89 (s, 6H,  $\text{H}_a$ ), 6.97 (m, 4H,  $\text{H}_c$ ), 7.07 (s, 2H,  $\text{H}_h$ ), 7.66 (m, 4H,  $\text{H}_d$ ), 7.77 (m, 4H,  $\text{H}_m$ ), 7.99 (m, 4H,  $\text{H}_k$ ).

### 4.2.2.24 AzaBODIPY **52**

5.8884 g (8.823 mmol, 1eq) of azaDIPY **51** were dissolved in 200 mL of dry THF. 10 mL of dry DIPEA were added and the solution stirred for 20min at room temperature. After 20 min 6 mL of 48%  $\text{BF}_3 \cdot \text{Et}_2\text{O}$  (6 mL, 48.8 mmol, 7.4 eq) were added and the resulting solution refluxed for 24 h. After total consumption of starting materials (checked by TLC) the solvents were evaporated and the crude product partitioned thrice between DCM/1M HCl.

The organic fractions were collected, washed with brine and dried with  $\text{Na}_2\text{SO}_4$ .

The crude product was deposited on silica gel and purified on silica gel using an eluent of heptane /EtOAc (6:4  $\rightarrow$  1:2). 4.54 g (6.35 mmol, yield = 72%) of the target compound were isolated as a fine crystalline, dark blue powder.



$^1\text{H}$  NMR (500 MHz,  $\text{CDCl}_3$ )  $\delta$  (ppm) = 3.90 (s, 6H,  $\text{H}_a$ ), 6.89 (s, 2H,  $\text{H}_h$ ), 6.99 (d,  $J$  = 8.7 Hz, 4H,  $\text{H}_c$ ), 7.61 (d,  $J$  = 8.5 Hz, 4H,  $\text{H}_k$ ), 7.89 (d,  $J$  = 8.6 Hz, 4H,  $\text{H}_m$ ), 8.04 (d,  $J$  = 8.7 Hz, 4H,  $\text{H}_d$ ).

$^{13}\text{C}$  NMR (75 MHz,  $\text{CDCl}_3$ )  $\delta$  (ppm) = 55.6 (s,  $\text{H}_a$ ), 114.5 (s,  $\text{C}_h$ ), 117.4 (s,  $\text{C}_c$ ), 125.3 (s,  $\text{C}_n$ ), 125.8 (s,  $\text{C}_e$ ), 130.8 (s,  $\text{C}_d$ ), 131.0 (s,  $\text{C}_i$ ), 131.1 (s,  $\text{C}_j$ ), 131.1 (s,  $\text{C}_k$ ), 132.0 (s,  $\text{C}_m$ ), 144.3 (s,  $\text{C}_i$ ), 145.8 (s,  $\text{C}_g$ ), 161.3 (s,  $\text{C}_b$ ).

$^{11}\text{B}$  NMR (160 MHz,  $\text{CDCl}_3$ )  $\delta$  (ppm) = 0.85 (t,  $J$  = 31.5 Hz).

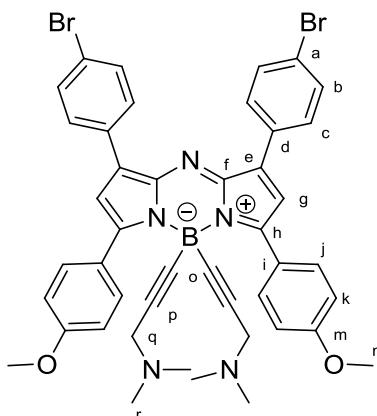
$^{19}\text{F}$  NMR (470 MHz,  $\text{CDCl}_3$ )  $\delta$  (ppm) = -130.63 (q,  $J$  = 31.5 Hz).

HR-MS (ESI): calculated for  $\text{C}_{34}\text{H}_{24}\text{B}_1\text{Br}_2\text{F}_2\text{N}_3\text{O}_2$   $[\text{M}]^+$  713.02909; found 713.03146

#### 4.2.2.25 Compound 53

(Dry glassware, solvents and protective atmosphere used)

151  $\mu\text{L}$  (1.349 mmol, 2eq) of propargyl amine were dissolved in 5 mL dry THF. 1.47 mL (2.1 eq) of  $\text{EtMgBr}$  (1M in THF) solution was added and the resulting mixture refluxed for 45 min. 500 mg (699.1  $\mu\text{g}$ , 1eq) of azaBODIPY **48** were dissolved in 5 mL in a separate flask and added to the reaction. The resulting mixture was refluxed for another 45 min and then quenched by addition of ethanol. The crude product was evaporated to dryness. After dissolution in  $\text{EtOAc}$  the compound was partitioned thrice in  $\text{EtOAc}/\text{water}$  and washed with brine. The organic fraction was dried with  $\text{Na}_2\text{SO}_4$  and evaporated to dryness. After precipitation from  $\text{DCM}/\text{pentane}$  the target compound (0.5824 g, 692.1  $\mu\text{mol}$ , yield = 99%) was isolated as a dark green solid.



$^1\text{H}$  NMR (600 MHz,  $\text{MeOD}$ )  $\delta$  (ppm) = 2.56 (s, 12H,  $\text{H}_r$ ), 3.72 (s, 4H,  $\text{H}_q$ ), 3.92 (s, 6H,  $\text{H}_n$ ), 7.14 (d,  $J$  = 8.8 Hz, 4H,  $\text{H}_k$ ), 7.36 (s, 2H,  $\text{H}_g$ ), 7.65 (d,  $J$  = 8.5 Hz, 4H,  $\text{H}_b$ ), 7.99 (d,  $J$  = 8.5 Hz, 4H,  $\text{H}_c$ ), 8.37 (d,  $J$  = 8.8 Hz, 4H,  $\text{H}_i$ ).

$^{13}\text{C}$  NMR (151 MHz,  $\text{MeOD}$ )  $\delta$  (ppm) = 42.4 (s,  $\text{C}_r$ ), 48.5 (s,  $\text{C}_q$ ), 56.2 (s,  $\text{C}_n$ ), 88.4 (s,  $\text{C}_p$ ), 115.0 (s,  $\text{C}_g$ ), 121.3 (s,  $\text{C}_k$ ), 124.9 (s,  $\text{C}_a$ ), 125.4 (s,  $\text{C}_i$ ), 131.8 (s,  $\text{C}_j$ ), 132.5 (s,  $\text{C}_d$ ), 133.0 (s,  $\text{C}_c$ ), 134.0 (s,  $\text{C}_b$ ), 142.4 (s,  $\text{C}_e$ ), 144.1 (s,  $\text{C}_h$ ), 159.4 (s,  $\text{C}_f$ ), 163.7 (s,  $\text{C}_m$ ).

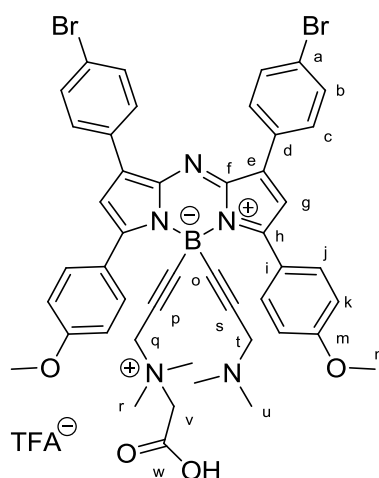
$^{11}\text{B}$  NMR (193 MHz, MeOD)  $\delta$  (ppm) = -12.39 (s).

HR-MS (ESI): calculated for  $\text{C}_{44}\text{H}_{41}\text{B}_1\text{Br}_2\text{N}_5\text{O}_2$   $[\text{M}+\text{H}]^+$  840.17146; found 840.17202

#### 4.2.2.26 Compounds **54** and **55**

100 mg (118.8  $\mu\text{mol}$ , 1 eq) of azaBODIPY **53** were placed into a round bottom flask and dissolved in 30 mL of dry  $\text{CHCl}_3$ . 18.2 mg (130.7  $\mu\text{mol}$ , 1.1 eq) of bromoacetic acid were added and the solution stirred overnight. Once finished the solvents were evaporated and the crude product purified by semi preparative HPLC using gradient A. Product fractions were collected and lyophilized to yield 66.2 mg (65.4  $\mu\text{mol}$ , yield = 55%) of the monoacid **54** and 20.6 mg (17.4  $\mu\text{mol}$ , yield = 15%) of the diacid **55** as dark green solids.

##### 4.2.2.26.1 Compound **54**

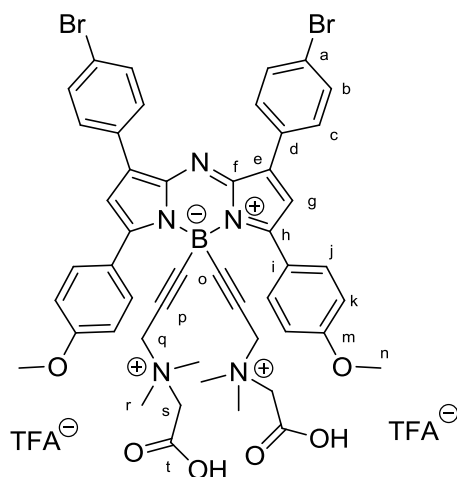


$^1\text{H}$  NMR (500 MHz,  $\text{CDCl}_3$ )  $\delta$  (ppm) = 2.25 (s, 6H,  $\text{H}_u$ ), 2.68 (s, 6H,  $\text{H}_r$ ), 3.28 (s, 2H,  $\text{H}_t$ ), 3.40 (s, 2H,  $\text{H}_q$ ), 3.77 (s, 2H,  $\text{H}_v$ ), 3.90 (s, 6H,  $\text{H}_n$ ), 6.99 (s, 2H,  $\text{H}_g$ ), 7.01 (d,  $J$  = 8.9 Hz, 4H,  $\text{H}_k$ ), 7.59 (d,  $J$  = 8.6 Hz, 4H,  $\text{H}_c$ ), 7.89 (d,  $J$  = 8.5 Hz, 4H,  $\text{H}_b$ ), 8.26 (d,  $J$  = 8.8 Hz, 4H,  $\text{H}_i$ ).

$^{13}\text{C}$  NMR (126 MHz,  $\text{CDCl}_3$ )  $\delta$  (ppm) = 43.8 (s,  $\text{C}_u$ ), 48.6 (s,  $\text{C}_t$ ), 50.4 (s,  $\text{C}_r$ ), 55.7 (s,  $\text{C}_q$ ), 55.9 (s,  $\text{C}_n$ ), 64.8 (s,  $\text{C}_v$ ), 85.9 (s,  $\text{C}_o$ ), 93.6 (s,  $\text{C}_p$ ,  $\text{C}_s$ ), 113.9 (s,  $\text{C}_g$ ), 119.6 (s,  $\text{C}_k$ ), 124.0 (s,  $\text{C}_a$ ), 124.5 (s,  $\text{C}_i$ ), 130.6 (s,  $\text{C}_j$ ), 131.4 (s,  $\text{C}_d$ ), 132.0 (s,  $\text{C}_c$ ), 132.6 (s,  $\text{C}_b$ ), 141.2 (s,  $\text{C}_e$ ), 143.1 (s,  $\text{C}_h$ ), 157.8 (s,  $\text{C}_f$ ), 161.9 (s,  $\text{C}_m$ ), 164.6 (s,  $\text{C}_w$ ).

$^{11}\text{B}$  NMR (160 MHz,  $\text{CDCl}_3$ )  $\delta$  (ppm) = -12.69 (s).

HR-MS (ESI): calculated for  $\text{C}_{46}\text{H}_{43}\text{BB}_2\text{N}_5\text{O}_4^+$   $[\text{M}]^+$  898.17694; found 898.17888

4.2.2.26.2 Compound **55**

$^1\text{H}$  NMR (600 MHz, MeOD)  $\delta$  (ppm) = 2.98 (s, 12H,  $H_r$ ), 3.86 (s, 4H,  $H_q$ ), 3.95 (s, 6H,  $H_n$ ), 4.25 (s, 4H,  $H_s$ ), 7.17 (d,  $J$  = 8.7 Hz, 4H,  $H_k$ ), 7.31-7.37 (m, 2H,  $H_g$ ), 7.57-7.66 (m, 4H,  $H_c$ ), 7.94-8.02 (m, 4H,  $H_b$ ), 8.33 (d,  $J$  = 8.7 Hz, 4H,  $H_i$ ).

$^{13}\text{C}$  NMR (151 MHz, MeOD)  $\delta$  (ppm) = 51.6 (s,  $C_r$ ), 56.3 (s,  $C_n$ ), 56.4 (s,  $C_q$ ), 62.4 (s,  $C_s$ ), 87.6 (s,  $C_p$ ), 115.3 (s,  $C_g$ ), 121.5 (s,  $C_k$ ), 125.0 (s,  $C_a$ ), 125.3 (s,  $C_i$ ), 131.9 (s,  $C_j$ ), 132.5 (s,  $C_d$ ), 132.9 (s,  $C_e$ ), 133.8 (s,  $C_b$ ), 142.5 (s,  $C_e$ ), 144.1 (s,  $C_h$ ), 159.5 (s,  $C_i$ ), 163.8 (s,  $C_m$ ), 167.3 (s,  $C_t$ ).

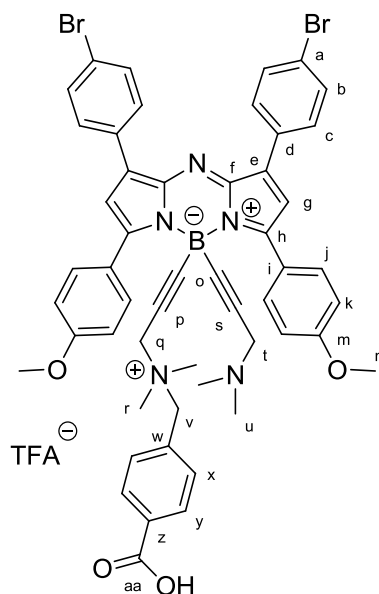
$^{11}\text{B}$  NMR (193 MHz, MeOD)  $\delta$  (ppm) = -12.41 (s).

HR-MS (ESI): calculated for  $\text{C}_{48}\text{H}_{44}\text{BBr}_2\text{N}_5\text{O}_6\text{Na}^+$  [ $\text{M}-2\text{H}+\text{Na}$ ] $^+$  978.16436; found 978.16585

4.2.2.27 Compounds **57** and **58**

100 mg (118.8  $\mu\text{mol}$ , 1eq) of azaBODIPY **53** were dissolved in 30mL of DCM. 25.6 mg (118.8  $\mu\text{mol}$ , 1eq) of bromomethyl benzoic acid were added and the reaction refluxed over night. The stirring was then cut and the solids left to decant. The supernatant was removed and the solids washed thrice with DCM (supernatant and washing solutions contain monoacid and starting materials). The product was dissolved in MeOH and precipitated with  $\text{Et}_2\text{O}$  to yield 68mg (53.5  $\mu\text{mol}$ , yield = 45%; 90% with regards to the carboxylic acid) of the diacid **58** as a dark green solid. The supernatant and washing solutions were evaporated to dryness and purified by semi preparative HPLC. Product fractions were collected and lyophilized to yield 11.7mg (10.7  $\mu\text{mol}$ , yield = 9%) of the monoacid **57** as the TFA-salt. The leftover starting azaBODIPY **53** can be recovered.

## 4.2.2.27.1 Compound 57



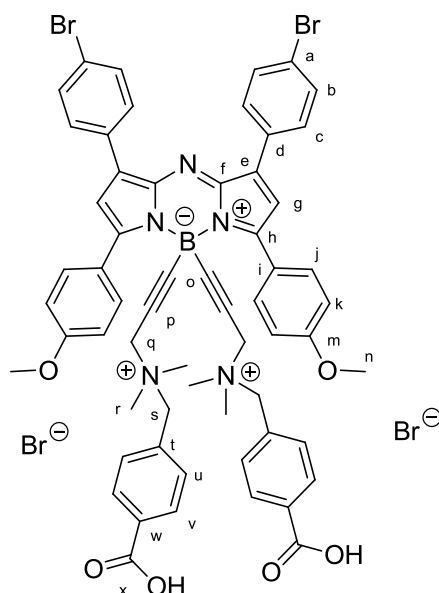
$^1\text{H}$  NMR (600 MHz, MeOD)  $\delta$  (ppm) = 2.71 (s, 6H,  $\text{H}_u$ ), 2.74 (s, 6H,  $\text{H}_r$ ), 3.65 (s, 2H,  $\text{H}_v$ ), 3.85 (s, 6H,  $\text{H}_n$ ), 3.99 (s, 2H,  $\text{H}_t$ ), 4.07 (s, 2H,  $\text{H}_q$ ), 7.13 (d,  $J = 8.5$  Hz, 4H,  $\text{H}_k$ ), 7.36 (d,  $J = 7.9$  Hz, 2H,  $\text{H}_x$ ), 7.40 (s, 2H,  $\text{H}_g$ ), 7.61 – 7.67 (m, 4H,  $\text{H}_b$ ), 8.00 (d,  $J = 8.2$  Hz, 4H,  $\text{H}_c$ ), 8.04 (d,  $J = 8.0$  Hz, 2H,  $\text{H}_y$ ), 8.41 (d,  $J = 8.6$  Hz, 4H,  $\text{H}_i$ ).

$^{13}\text{C}$  NMR (151 MHz, MeOD)  $\delta$  (ppm) = 42.6 (s,  $\text{C}_u$ ), 48.6 (s,  $\text{C}_t$ ), 50.7 (s,  $\text{C}_r$ ), 55.2 (s,  $\text{C}_q$ ), 56.2 (s,  $\text{C}_n$ ), 66.6 (s,  $\text{C}_v$ ), 88.2 (s,  $\text{C}_s$ ), 88.6 (s,  $\text{C}_p$ ), 115.2 (s,  $\text{C}_g$ ), 121.5 (s,  $\text{C}_k$ ), 125.0 (s,  $\text{C}_a$ ), 125.3 (s,  $\text{C}_i$ ), 131.4 (s,  $\text{C}_x$ ), 131.9 (s,  $\text{C}_j$ ), 132.5 (s,  $\text{C}_d$ ), 132.6 (s,  $\text{C}_z$ ), 133.0 (s,  $\text{C}_c$ ), 133.8 (s,  $\text{C}_y$ ), 134.0 (s,  $\text{C}_b$ ), 134.5 (s,  $\text{C}_w$ ), 142.5 (d,  $J = 2.7$  Hz,  $\text{C}_e$ ), 144.1 (s,  $\text{C}_h$ ), 159.3 (s,  $\text{C}_f$ ), 163.7 (s,  $\text{C}_m$ ), 168.5 (s,  $\text{C}_{aa}$ ).

$^{11}\text{B}$  NMR (193 MHz, MeOD)  $\delta$  (ppm) = -12.41 (s).

HR-MS (ESI): calculated for  $\text{C}_{52}\text{H}_{47}\text{BBr}_2\text{N}_5\text{O}_4$   $[\text{M}]^+$  974.20824; found 974.21085

## 4.2.2.27.2 Compound 58



$^1\text{H}$  NMR (600 MHz, MeOD)  $\delta$  (ppm) = 2.85 (s, 12H,  $\text{H}_r$ ), 3.82 (s, 6H,  $\text{H}_n$ ), 3.93 (s, 4H,  $\text{H}_q$ ), 4.23 (s, 4H,  $\text{H}_s$ ), 7.13 (d,  $J = 8.7$  Hz, 4H,  $\text{H}_k$ ), 7.42 (d,  $J = 8.0$  Hz, 4H,  $\text{H}_u$ ), 7.46 (s, 2H,  $\text{H}_g$ ), 7.65 (d,  $J = 7.8$  Hz, 4H,  $\text{H}_b$ ), 8.01 (d,  $J = 8.1$  Hz, 8H,  $\text{H}_c$ ,  $\text{H}_v$ ), 8.44 (d,  $J = 8.7$  Hz, 4H,  $\text{H}_i$ ).

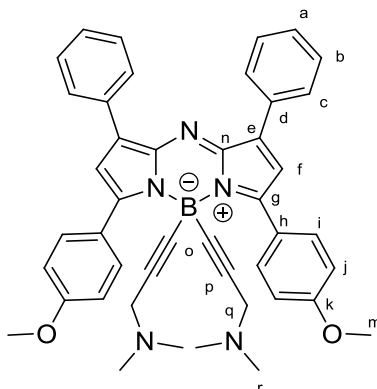
$^{13}\text{C}$  NMR (151 MHz, MeOD)  $\delta$  (ppm) = 50.8 (s, Cr), 55.5 (s, Cq), 56.2 (s, Cn), 66.8 (s, Cs), 88.5 (s, Cp), 115.3 (s, Cg), 121.6 (s, Ck), 125.1 (s, Ca), 125.2 (s, Ci), 131.4 (s, Cu), 131.9 (s, Cj), 132.4 (s, Cd), 132.6 (s, Cw), 133.0 (s, Cc), 133.8 (s, Cv), 134.0 (s, Cb), 134.5 (s, Ct), 142.7 (s, Ce), 144.1 (s, Ch), 159.2 (s, Cf), 163.9 (s, Cm), 168.4 (s, Cx).

$^{11}\text{B}$  NMR (193 MHz, MeOD)  $\delta$  (ppm) = -12.39 (s, br).

HR-MS (ESI): calculated for  $\text{C}_{60}\text{H}_{54}\text{BBr}_2\text{N}_5\text{O}_6$   $[\text{M}]^{2+}$  554.62615; found 554.62644

#### 4.2.2.28 Compound **60**

In a dried Schlenktube, 386  $\mu\text{L}$  (3.89 mmol, 2 eq) of 3-dimethylpropyne were dissolved in dry THF (3 mL). 4.503 mL (2.1 eq) of freshly dosed ethylmagnesiumbromide were added and the resulting solution was refluxed for 45 min. In a separate Schlenktube, 1 g (1.79 mmol, 1 eq) of aza-BODIPY **44** was dissolved in dry THF (15 mL) and added to the Grignard-solution *via* cannula. The mixture was refluxed for another 45 min. EtOH (5 mL) was then added, the solvents were evaporated and the crude product dissolved in EtOAc and washed twice with diluted bicarbonate aqueous solution. Organic fractions were collected, evaporated to dryness, adsorbed onto silica gel and purified using a short silica gel plug (eluent: EtOAc, followed by DCM/MeOH 80:20). Product fractions were collected, evaporated and precipitated once from DCM/pentane, yielding pure aza-BODIPY **60** (1.1 g, 1.61 mmol, 90% yield) as a dark green powder with coppery reflexes.



$^1\text{H}$  NMR (500 MHz,  $\text{CDCl}_3$ )  $\delta$  (ppm) = 2.10 (s, 12H, Hr), 3.05 (s, 4H, Ha), 3.87 (s, 6H, Hm), 6.97 (s, 2H, Hi), 6.99 (s, 4H, Hj), 7.40 (t,  $J = 7.3$  Hz, 2H, Ha), 7.45 (t,  $J = 7.3$  Hz, 4H, Hb), 8.06 (d,  $J = 7.3$  Hz, 4H, Hc), 8.31 (d,  $J = 8.7$  Hz, 4H, Hi).

$^{13}\text{C}$  NMR (126 MHz,  $\text{CDCl}_3$ )  $\delta$  (ppm) = 29.8 (s, Co) 43.0 (s, Cr), 48.2 (s, Cq), 55.6 (s, Cm), 91.7 (s, Cp), 113.5 (s, Cg), 119.4 (s, Ci), 125.2 (s, Ch), 128.6 (s, Ca), 129.1 (s, Cc), 129.3 (s, Cb), 132.7 (s, Ci), 132.8 (s, Cd), 142.2 (s, Ce), 143.3 (s, Cg), 157.8 (s, Cn), 161.4 (s, Ck).

$^{11}\text{B}$  NMR (160 MHz,  $\text{CDCl}_3$ )  $\delta$  (ppm) = -12.36 (s (vbr)).

HR-MS (ESI): calculated for  $\text{C}_{44}\text{H}_{43}\text{B}_1\text{N}_5\text{O}_2$   $[\text{M}+\text{H}]^+$  684.35043; found 684.34847

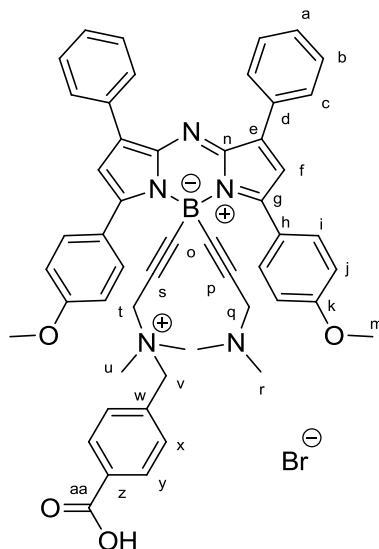
#### 4.2.2.29 Compounds **61** and **62**

194 mg (0.284 mmol, 1 eq) of aza-BODIPY **60** were dissolved in 200 mL of dry THF. 67 mg (0.312 mmol, 1.1 eq) of 4-(Bromomethyl) benzoic acid were added and the resulting solution was stirred overnight. The stirring was stopped and the supernatant decanted once all solids had sedimented. The sediment was washed three times with hot THF (supernatants contain Aza-BODIPY **61**) and dried to isolate **62**. All supernatants were gathered, evaporated to dryness and purified by column chromatography on a short silica gel column. Leftover starting material is eluted with toluene  $\rightarrow$  Tol:MeOH 8:2, followed by 100% MeOH to isolate Aza-BODIPY **61**. Product fractions of monoacid were reunited and evaporated to dryness. The product was dissolved in a minimum amount of MeOH, diluted in DCM and precipitated by

## Materials and Methods

addition of pentane to obtain 83 mg (91  $\mu\text{mol}$ , yield = 32%) of the target compound **61** as a dark green powder. Overall yield 58%, leftover starting material can be isolated and re-used.

### 4.2.2.29.1 Compound **61**



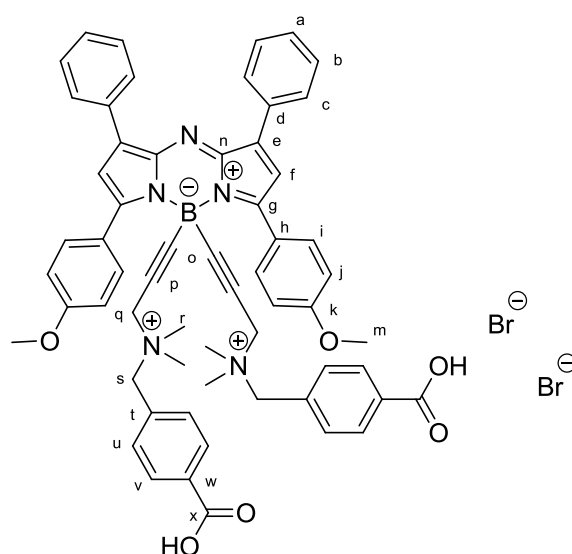
$^1\text{H}$  NMR (600 MHz, MeOD- $d_4$ )  $\delta$  (ppm) = 2.62 (d,  $J$  = 1.3 Hz, 6H,  $H_r$  (protonated form)), 2.68 (s, 6H,  $H_u$ ), 3.58 (s, 2H,  $H_a$ ), 3.86 – 3.76 (m, 8H,  $H_m+H_t$ ), 3.99 (s, 2H,  $H_v$ ), 7.10 (d,  $J$  = 8.8 Hz, 4H,  $H_j$ ), 7.32 (dd,  $J$  = 12.3, 4.2 Hz, 4H,  $H_f, H_x$ ), 7.51 – 7.40 (m, 6H,  $H_a, H_b$ ), 8.04 – 7.97 (m, 2H,  $H_y$ ), 8.14 – 8.08 (m, 4H,  $H_c$ ), 8.42 (dd,  $J$  = 8.8, 2.4 Hz, 4H,  $H_i$ ).

$^{13}\text{C}$  NMR (151 MHz, MeOD- $d_4$ )  $\delta$  (ppm) = 43.0 (s, br,  $C_r$ ), 50.6 (s,  $C_u$ ), 55.0 (s,  $C_t, C_q$ ), 56.2 (s,  $C_m$ ), 66.6 (s,  $C_v$ ), 87.9 (s,  $C_s$ ), 90.2 (s,  $C_p$ ), 115.1 (s,  $C_f$ ), 121.1 (s,  $C_j$ ), 125.6 (s,  $C_h$ ), 129.7 (s,  $C_c$ ), 130.4 (s,  $C_a$ ), 130.5 (s,  $C_b$ ), 131.1 (s,  $C_z$ ), 131.2 (s,  $C_x$ ), 133.5 (s,  $C_d$ ), 133.5 (s,  $C_y$ ), 133.9 (s,  $C_i$ ), 138.4 (s,  $C_w$ ), 143.9 (s,  $C_e$ ), 144.2 (s,  $C_g$ ), 159.1 (s,  $C_n$ ), 163.5 (s,  $C_k$ ), 171.4 (s,  $C_{aa}$ ).

$^{11}\text{B}$  NMR (160 MHz, MeOD- $d_4$ )  $\delta$  (ppm) = -12.11 (s, vbr).

HR-MS (ESI): calculated for  $\text{C}_{52}\text{H}_{49}\text{B}_1\text{N}_5\text{O}_4$   $[\text{M}]^+$  828.38721; found 828.38718

### 4.2.2.29.2 Compound **62**



$^1\text{H}$  NMR (500 MHz, MeOD- $d_4$ )  $\delta$  (ppm) = 2.87 (s, 12H,  $H_r$ ), 3.80 (s, 6H,  $H_m$ ), 3.96 (s, 4H,  $H_q$ ), 4.24 (s, 4H,  $H_s$ ), 7.13 (d,  $J$  = 8.9 Hz, 4H,  $H_j$ ), 7.42 (s, 2H,  $H_f$ ), 7.50 – 7.43 (m, 10H,  $H_a, H_b, H_u$ ), 8.04 (d,  $J$  = 8.1 Hz, 4H,  $H_v$ ), 8.13 (dd,  $J$  = 8.1, 1.4 Hz, 4H,  $H_c$ ), 8.45 (d,  $J$  = 8.9 Hz, 4H,  $H_i$ ).

$^{13}\text{C}$  NMR (126 MHz, MeOD- $d_4$ )  $\delta$  (ppm) = 50.8 (s, C<sub>r</sub>), 55.5 (s, C<sub>q</sub>), 56.2 (s, C<sub>m</sub>), 66.7 (s, C<sub>s</sub>), 88.3 (s, C<sub>p</sub>), 115.3 (s, C<sub>i</sub>), 121.4 (s, C<sub>j</sub>), 125.4 (s, C<sub>h</sub>), 129.8 (s, C<sub>c</sub>), 130.4 (s, C<sub>a</sub>), 130.7 (s, C<sub>b</sub>), 131.4 (s, C<sub>u</sub>), 131.9 (s, C<sub>w</sub>), 133.4 (s, C<sub>d</sub>), 133.7 (s, C<sub>v</sub>), 133.9 (s, C<sub>i</sub>), 144.1 (s, C<sub>g</sub>), 144.2 (s, C<sub>n</sub>), 159.1 (s, C<sub>k</sub>), 163.7 (s, C<sub>x</sub>)

$^{11}\text{B}$  NMR (160 MHz, MeOD- $d_4$ )  $\delta$  (ppm) = -11.93.

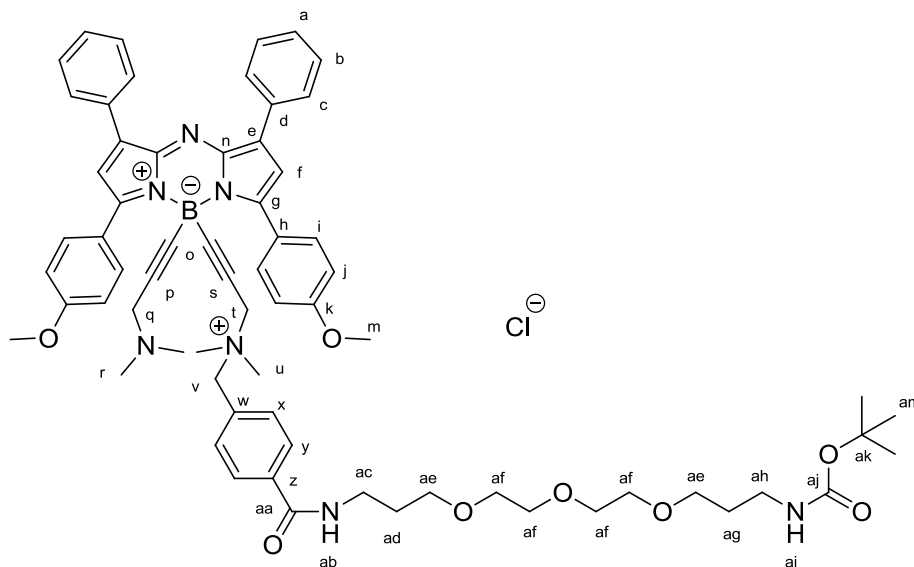
HR-MS (ESI): calculated for C<sub>60</sub>H<sub>56</sub>B<sub>1</sub>N<sub>5</sub>O<sub>6</sub> [M]<sup>2+</sup> 476.71563; found 476.71565

#### 4.2.2.30 Compound **64**

50 mg (56  $\mu\text{mol}$ , 1 eq) of **61** were placed in a round bottom flask and dissolved in dry DMF (5 mL). HBTU (25 mg, 67  $\mu\text{mol}$ , 1.2 eq) and DIPEA (0.3 mL, 1.8 mmol, 33 eq) were added and the mixture was stirred for 1 h at 30°C. 21 mg (67  $\mu\text{mol}$ , 1.2 eq) of TOTA-Boc in DMF (1 mL) were added, and the solution stirred at 30°C for 4 h (reaction control by HPLC). Once finished, the solvents were evaporated to dryness and the crude product purified by column chromatography on 5% deactivated alumina, using DCM: MeOH 100 $\rightarrow$ 97:3 as eluent. Product fractions were collected and evaporated. The product was dissolved in ACN/H<sub>2</sub>O (10 mL) and ion-exchange on a DOWEX basic resin performed. The eluate was evaporated and precipitated once from DCM/pentane to obtain the target compound **64** as a dark green solid. (20 mg, 17  $\mu\text{mol}$ , 31% yield).

Semi prep: the crude product was purified by semi preparative HPLC using gradient A. Product fractions were collected, evaporated to dryness/lyophilized. The product was redissolved in ACN/H<sub>2</sub>O to undergo ion exchange on a DOWEX basic ion-exchange resin; collected, and lyophilized to obtain the target compound as a green, hygroscopic sponge (32% yield)

HPLC yield: 90%



$^1\text{H}$  NMR (500 MHz, MeOD- $d_4$ )  $\delta$  (ppm) = 1.30 (t,  $J$  = 7.3 Hz, 6H), 1.40 (s, 9H, H<sub>am</sub>), 1.66 (dt,  $J$  = 12.9, 6.5 Hz, 2H, H<sub>ag</sub>), 1.87 (p,  $J$  = 6.4 Hz, 2H, H<sub>ad</sub>), 2.41 – 2.34 (m, 6H, H<sub>r</sub>), 2.72-2.67 (m, 6H, H<sub>u</sub>), 3.01 - 3.09 (m, 4H, H<sub>ae</sub>), 3.41 - 3.52 (m, 8H, 2H<sub>q</sub>, 2H<sub>ah</sub>, 2H<sub>ac</sub>, H<sub>ai</sub>, H<sub>ab</sub>), 3.54 (s, 2H, H<sub>t</sub>), 3.56 - 3.64 (m, 8H, H<sub>af</sub>), 3.82 (s, 6H, H<sub>m</sub>), 3.96 (s, 2H, H<sub>v</sub>), 7.09 (d,  $J$  = 8.8 Hz, 4H, H<sub>j</sub>), 7.33 (s, 2H, H<sub>i</sub>), 7.36 (d,  $J$  = 8.1 Hz, 2H, H<sub>x</sub>), 7.52 – 7.44 (m, 6H, H<sub>a</sub>, H<sub>b</sub>), 7.86 (d,  $J$  = 8.1 Hz, 2H, H<sub>y</sub>), 8.15 – 8.11 (m, 4H, H<sub>c</sub>), 8.46 (d,  $J$  = 8.8 Hz, 4H, H<sub>i</sub>).

$^{13}\text{C}$  NMR (151 MHz, MeOD- $d_4$ )  $\delta$  (ppm) = 28.8 (s, C<sub>am</sub>), 30.3 (s, C<sub>ag</sub>), 30.9 (s, C<sub>ad</sub>), 38.7 (s, C<sub>ac</sub>), 38.9 (s, C<sub>ah</sub>), 42.6 (s, C<sub>r</sub>), 48.7 (s, C<sub>o</sub>), 50.6 (s, C<sub>u</sub>), 55.1 (s, C<sub>t</sub>, C<sub>q</sub>), 56.2 (s, C<sub>m</sub>), 66.5 (s, C<sub>v</sub>), 69.8 (s, C<sub>ae</sub>), 70.3 (s, C<sub>ae</sub>), 71.2 (s, C<sub>af</sub>), 71.3 (s, C<sub>af</sub>), 71.5 (s, C<sub>af</sub>), 71.5 (s, C<sub>af</sub>), 79.8 (s, C<sub>ak</sub>), 88.1 (s, C<sub>s</sub>), 88.5 (s, C<sub>p</sub>), 115.1 (s, C<sub>f</sub>), 121.1 (s, C<sub>j</sub>), 125.5 (s, C<sub>h</sub>), 128.9 (s, C<sub>x</sub>), 129.1 (s, C<sub>x</sub>), 129.8 (s, C<sub>c</sub>), 130.4 (s, C<sub>a</sub>), 130.7 (s, C<sub>b</sub>), 131.2 (s, C<sub>z</sub>), 133.4 (s, C<sub>d</sub>), 133.9 (s, C<sub>v</sub>), 133.9 (s, C<sub>i</sub>), 138.2 (s, C<sub>w</sub>), 144.0 (s, C<sub>e</sub>), 144.2 (s, C<sub>g</sub>), 159.1 (s, C<sub>n</sub>), 162.0 (s, vbr, C<sub>aj</sub>), 163.6 (s, C<sub>k</sub>), 168.6 (s, C<sub>aa</sub>).

## Materials and Methods

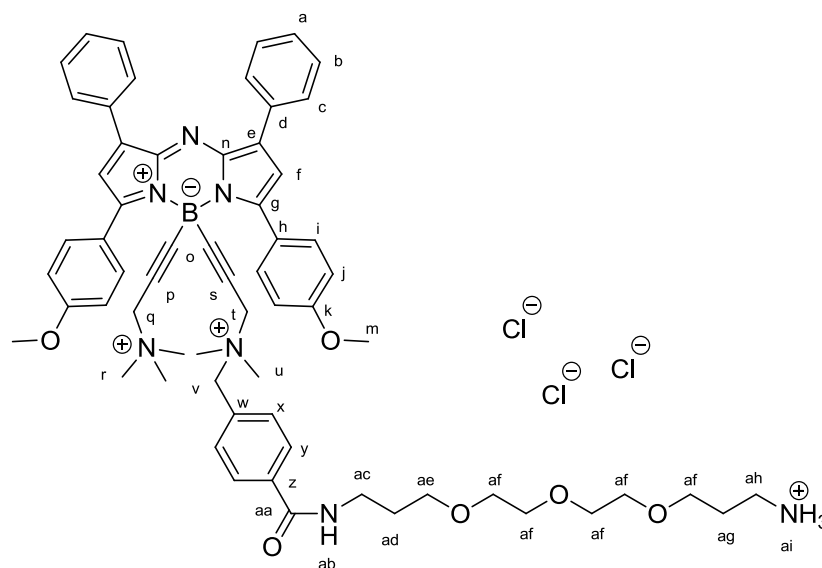
$^{11}\text{B}$  NMR (160 MHz, MeOD- $d_4$ )  $\delta$  (ppm) = -12.76 (s, br).

HR-MS (ESI): calculated for  $\text{C}_{67}\text{H}_{79}\text{B}_1\text{N}_7\text{O}_8$   $[\text{M}]^+$  1120.60777; found 1120.60905

### 4.2.2.31 Compound **65**

30 mg (26  $\mu\text{mol}$ ) of **64** were dissolved in DCM (5 mL). 0.5 mL of MeI were added and the solution was stirred at room temperature for 1h. The solution was evaporated to dryness and the residue was dissolved in ACN (8 mL). 16 mL of 1M HCl were added and the reaction was stirred for 8 h at 30-35°C. Solvents were then evaporated and the crude product was purified by semi preparative HPLC using gradient A. Product fractions were collected, evaporated to dryness/lyophilized and ion exchange was performed. The resulting solution was lyophilized, yielding **65** (Cl-salt) (23 mg, 20  $\mu\text{mol}$ , 78% yield) as a crystalline dark green solid.

HPLC-Yield: 90-100%



$^1\text{H}$  NMR (500 MHz, MeOD- $d_4$ )  $\delta$  (ppm) = 1.88 (dt,  $J$  = 12.7, 6.0 Hz, 2H,  $\text{H}_{\text{ad}}$ ), 1.92 (dt,  $J$  = 12.0, 6.5 Hz, 2H,  $\text{H}_{\text{ag}}$ ), 2.84 (s, 6H,  $\text{H}_{\text{u}}$ ), 2.94 (s, 9H,  $\text{H}_{\text{r}}$ ), 3.10 (t,  $J$  = 6.4 Hz, 2H,  $\text{H}_{\text{ah}}$ ), 3.46 (t,  $J$  = 7.1 Hz, 2H,  $\text{H}_{\text{ac}}$ ), 3.57 (t,  $J$  = 6.1 Hz, 2H,  $\text{H}_{\text{ae}}$ ), 3.67 – 3.59 (m, 10H,  $\text{H}_{\text{af}}$ ), 3.87 (s,  $J$  = 6.4 Hz, 6H,  $\text{H}_{\text{m}}$ ), 3.90 (s, 2H,  $\text{H}_{\text{t}}$ ), 4.13 (d,  $J$  = 3.6 Hz, 2H,  $\text{H}_{\text{q}}$ ), 4.21 (s, 2H,  $\text{H}_{\text{v}}$ ), 7.16 (d,  $J$  = 9.0 Hz, 4H,  $\text{H}_{\text{j}}$ ), 7.40 (s, 2H,  $\text{H}_{\text{f}}$ ), 7.53 – 7.42 (m, 8H,  $\text{H}_{\text{x}}$ ,  $\text{H}_{\text{a}}$ ,  $\text{H}_{\text{b}}$ ), 7.87 (d,  $J$  = 8.3 Hz, 2H,  $\text{H}_{\text{y}}$ ), 8.13 (dd,  $J$  = 8.1, 1.4 Hz, 4H,  $\text{H}_{\text{c}}$ ), 8.41 (d,  $J$  = 8.9 Hz, 4H,  $\text{H}_{\text{i}}$ ).

$^{13}\text{C}$  NMR (126 MHz, MeOD- $d_4$ )  $\delta$  (ppm) = 28.1 (s,  $\text{C}_{\text{ad}}$ ), 30.5 (s,  $\text{C}_{\text{ag}}$ ), 38.5 (s,  $\text{C}_{\text{ac}}$ ), 40.1 (s,  $\text{C}_{\text{ah}}$ ), 50.7 (s,  $\text{C}_{\text{u}}$ ), 53.0 (s,  $\text{C}_{\text{r}}$ ), 55.5 (s,  $\text{C}_{\text{t}}$ ), 56.3 (s,  $\text{C}_{\text{m}}$ ), 58.1 (s,  $\text{C}_{\text{q}}$ ), 66.7 (s,  $\text{C}_{\text{v}}$ ), 69.9 (s,  $\text{C}_{\text{ae}}$ ), 70.4 (s,  $\text{C}_{\text{af}}$ ), 71.0 (s,  $\text{C}_{\text{af}}$ ), 71.1 (s,  $\text{C}_{\text{af}}$ ), 71.4 (s,  $\text{C}_{\text{af}}$ ), 87.9 (s,  $\text{C}_{\text{p}}$ ), 88.1 (s,  $\text{C}_{\text{s}}$ ), 115.3 (s,  $\text{C}_{\text{f}}$ ), 121.3 (s,  $\text{C}_{\text{j}}$ ), 125.4 (s,  $\text{C}_{\text{h}}$ ), 129.2 (s,  $\text{C}_{\text{x}}$ ), 129.8 (s,  $\text{C}_{\text{c}}$ ), 130.4 (s,  $\text{C}_{\text{a}}$ ), 130.7 (s,  $\text{C}_{\text{b}}$ ), 131.4 (s,  $\text{C}_{\text{z}}$ ), 133.4 (s,  $\text{C}_{\text{d}}$ ), 133.9 (s,  $\text{C}_{\text{y}}$ ), 134.0 (s,  $\text{C}_{\text{i}}$ ), 138.0 (s,  $\text{C}_{\text{w}}$ ), 144.0 (s,  $\text{C}_{\text{e}}$ ), 144.2 (s,  $\text{C}_{\text{g}}$ ), 159.1 (s,  $\text{C}_{\text{n}}$ ), 163.7 (s,  $\text{C}_{\text{k}}$ ), 168.8 (s,  $\text{C}_{\text{aa}}$ ).

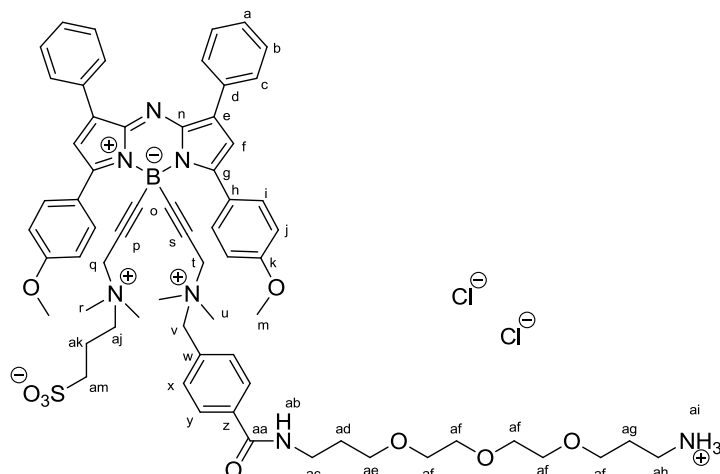
$^{11}\text{B}$  NMR (160 MHz, MeOD- $d_4$ )  $\delta$  (ppm) = -12.43 (s, br).

HR-MS (ESI): calculated for  $\text{C}_{63}\text{H}_{75}\text{B}_1\text{N}_7\text{O}_6$   $[\text{M}]^{3+}$  345.52851; found 345.52954

### 4.2.2.32 Compound **66**

40 mg (34  $\mu\text{mol}$ , 1 eq) aza-BODIPY **61** were placed in a round bottom flask and dissolved in 6mL of  $\text{CH}_3\text{CN}$ . 21 mg (172  $\mu\text{mol}$ , 5 eq) of 1,3-propane sultone and 14 mg (172  $\mu\text{mol}$ , 5 eq) of  $\text{NaHCO}_3$  were added and the reaction refluxed overnight. After cooling the solution, 1M HCl (10 mL) was added and the reaction was stirred at 30-35°C until complete hydrolysis. Solvents were evaporated and the crude product was purified by semi preparative HPLC using gradient A. Product fractions were collected and underwent ion exchange (Dowex basic resin) before

lyophilisation to yield 15 mg (12  $\mu\text{mol}$ , 38% yield) of the target compound **66** as a strongly hygroscopic dark green solid.



$^1\text{H}$  NMR (600 MHz, MeOD- $d_4$ )  $\delta$  (ppm) = 1.89 (dd,  $J$  = 13.0, 6.5 Hz, 2H,  $\text{H}_{\text{ad}}$ ), 1.93 (dt,  $J$  = 12.9, 6.6 Hz, 2H,  $\text{H}_{\text{ag}}$ ), 2.23 – 2.16 (m, 2H,  $\text{H}_{\text{ak}}$ ), 2.85 (s, 6H,  $\text{H}_{\text{u}}$ ), 2.91 – 2.89 (m, 2H,  $\text{H}_{\text{am}}$ ), 2.93 (s, 6H,  $\text{H}_{\text{r}}$ ), 3.12 (t,  $J$  = 6.3 Hz, 2H,  $\text{H}_{\text{ah}}$ ), 3.49 (t,  $J$  = 7.0 Hz, 2H,  $\text{H}_{\text{ac}}$ ), 3.55 – 3.51 (m, 2H,  $\text{H}_{\text{aj}}$ ), 3.58 (t,  $J$  = 6.0 Hz, 2H,  $\text{H}_{\text{ae}}$ ), 3.68 – 3.62 (m, 13H,  $\text{H}_{\text{af}}$ ,  $\text{H}_{\text{ai}}$ ), 3.88 (s, 6H,  $\text{H}_{\text{m}}$ ), 3.91 (s, 2H,  $\text{H}_{\text{t}}$ ), 4.01 (s, 2H,  $\text{H}_{\text{q}}$ ), 4.27 (s, 2H,  $\text{H}_{\text{v}}$ ), 7.25 (d,  $J$  = 8.7 Hz, 4H,  $\text{H}_{\text{j}}$ ), 7.42 (s, 2H,  $\text{H}_{\text{i}}$ ), 7.53 – 7.46 (m, 8H,  $\text{H}_{\text{x}}$ ,  $\text{H}_{\text{a}}$ ,  $\text{H}_{\text{b}}$ ), 7.89 (d,  $J$  = 8.0 Hz, 2H,  $\text{H}_{\text{y}}$ ), 8.14 (d,  $J$  = 7.5 Hz, 4H,  $\text{H}_{\text{c}}$ ), 8.48 (d,  $J$  = 8.7 Hz, 4H,  $\text{H}_{\text{i}}$ ).

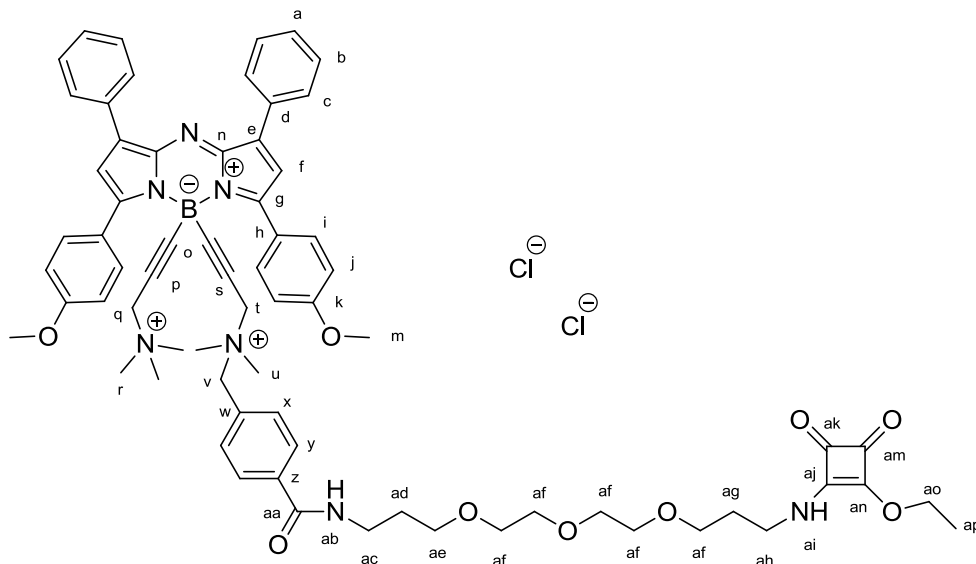
$^{13}\text{C}$  NMR (151 MHz, MeOD- $d_4$ )  $\delta$  (ppm) = 20.1 (s,  $\text{C}_{\text{ak}}$ ), 28.1 (s,  $\text{C}_{\text{ad}}$ ), 30.5 (s,  $\text{C}_{\text{ag}}$ ), 38.5 (s,  $\text{C}_{\text{ac}}$ ), 40.1 (s,  $\text{C}_{\text{ah}}$ ), 49.1 (s,  $\text{C}_{\text{o}}$ ), 51.0 (s,  $\text{C}_{\text{u}}$ ), 51.0 (s,  $\text{C}_{\text{r}}$ ), 55.5 (s,  $\text{C}_{\text{t}}$ ,  $\text{C}_{\text{q}}$ ), 56.0 (s,  $\text{C}_{\text{am}}$ ), 56.4 (s,  $\text{C}_{\text{m}}$ ), 63.7 (s,  $\text{C}_{\text{aj}}$ ), 66.9 (s,  $\text{C}_{\text{v}}$ ), 69.9 (s,  $\text{C}_{\text{ae}}$ ), 70.3 (s,  $\text{C}_{\text{af}}$ ), 70.4 (s,  $\text{C}_{\text{af}}$ ), 71.0 (s,  $\text{C}_{\text{af}}$ ), 71.1 (s,  $\text{C}_{\text{af}}$ ), 71.4 (s,  $\text{C}_{\text{af}}$ ), 87.5 (s,  $\text{C}_{\text{p}}$ ), 88.0 (s,  $\text{C}_{\text{s}}$ ), 115.5 (s,  $\text{C}_{\text{f}}$ ), 121.2 (s,  $\text{C}_{\text{j}}$ ), 125.3 (s,  $\text{C}_{\text{h}}$ ), 129.1 (s,  $\text{C}_{\text{x}}$ ), 129.8 (s,  $\text{C}_{\text{c}}$ ), 130.4 (s,  $\text{C}_{\text{a}}$ ), 130.6 (s,  $\text{C}_{\text{b}}$ ), 131.5 (s,  $\text{C}_{\text{z}}$ ), 133.5 (s,  $\text{C}_{\text{d}}$ ), 134.0 (s,  $\text{C}_{\text{i}}$ ), 138.0 (s,  $\text{C}_{\text{w}}$ ), 143.8 (s,  $\text{C}_{\text{e}}$ ), 144.1 (s,  $\text{C}_{\text{g}}$ ), 158.9 (s,  $\text{C}_{\text{n}}$ ), 163.7 (s,  $\text{C}_{\text{k}}$ ), 168.9 (s,  $\text{C}_{\text{aa}}$ ).

$^{11}\text{B}$  NMR (160 MHz, MeOD- $D_4$ )  $\delta$  (ppm) = -12.44 (s).

HR-MS (ESI): calculated for  $\text{C}_{65}\text{H}_{77}\text{B}_1\text{N}_7\text{O}_9\text{S}_1\text{Na}_1$  [ $\text{M}-\text{H}+\text{Na}$ ] $^{2+}$  582.77416; found 582.77359

#### 4.2.2.33 Compound **68**

17 mg (1 eq, 14  $\mu\text{mol}$ ) of **65** were dissolved in 2 mL of EtOH. After addition of diethyl squarate (12 mg, 5 eq, 73  $\mu\text{mol}$ ) and 20  $\mu\text{L}$  (8 eq, 118  $\mu\text{mol}$ ) DIPEA the reaction was stirred for 5 h at 30-35°C. The solvents were evaporated and the crude product purified by semi preparative HPLC using gradient A. Product fractions were collected and lyophilized, followed by ion exchange and lyophilization to yield 15 mg (12  $\mu\text{mol}$ , 84%) of the target compound **68** as a fluffy green solid (Cl $^-$ -salt).



## Materials and Methods

$^1\text{H}$  NMR (600 MHz, MeOD- $d_4$ )  $\delta$  (ppm) = 1.39 (td,  $J$  = 4.0, 7.0 Hz, 3H, H<sub>ap</sub>), 1.75 (dt,  $J$  = 6.2, 12.6 Hz, 1H, H<sub>ag</sub>), 1.81 (dt,  $J$  = 6.1, 12.2 Hz, 1H, H<sub>ag</sub>), 1.86 (p,  $J$  = 6.4 Hz, 2H, H<sub>ad</sub>), 2.83 (s, 6H, H<sub>u</sub>), 2.87 (s, 2H, H<sub>ah</sub>), 2.92 (s, 9H, H<sub>r</sub>), 3.44–3.47 (m, 4H, H<sub>ac</sub>), 3.52 (t,  $J$  = 6.0 Hz, 2H, H<sub>ae</sub>), 3.54–3.63 (m, 10H, H<sub>af</sub>), 3.85 (s, 2H, H<sub>t</sub>), 3.87 (s, 6H, H<sub>m</sub>), 3.93 (s, 1H, H<sub>ai</sub>), 4.01 (s, 1H), 4.08 (s, 2H, H<sub>d</sub>), 4.16 (d,  $J$  = 10.4 Hz, 2H, H<sub>v</sub>), 4.64 (dq,  $J$  = 7.0, 19.4 Hz, 2H, H<sub>ao</sub>), 7.14 (d,  $J$  = 9.0 Hz, 4H, H<sub>j</sub>), 7.40 (s, 2H, H<sub>f</sub>), 7.40–7.42 (m, 1H, H<sub>ab</sub>), 7.45–7.52 (m, 8H, H<sub>a</sub>, H<sub>b</sub>, H<sub>x</sub>), 7.82 (d,  $J$  = 7.7 Hz, 2H, H<sub>y</sub>), 8.14 (d,  $J$  = 6.9 Hz, 4H, H<sub>c</sub>), 8.41 (d,  $J$  = 8.8 Hz, 4H, H<sub>i</sub>).

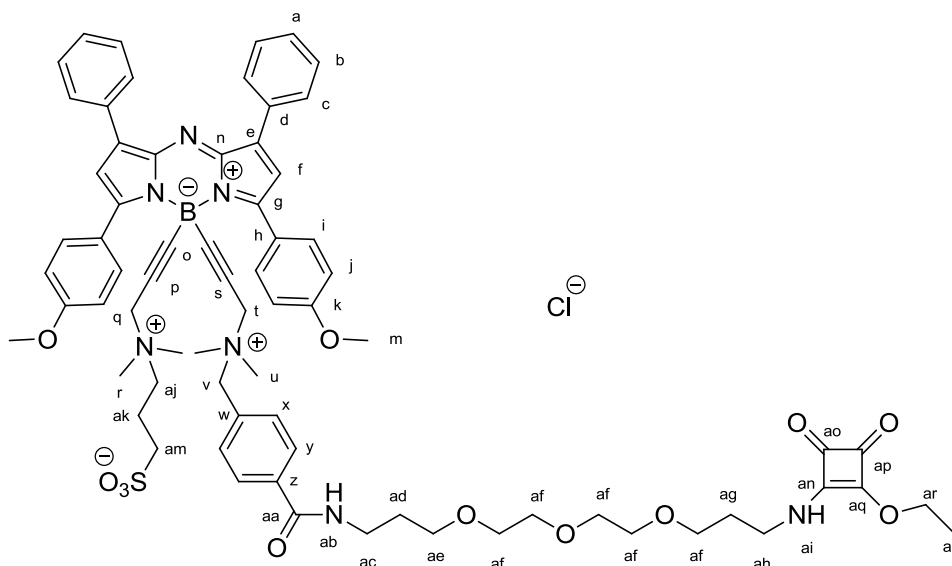
$^{13}\text{C}$  NMR (151 MHz, MeOD- $d_4$ )  $\delta$  (ppm) = 16.1 (d,  $J$  = 15.6 Hz, C<sub>ap</sub>), 30.3 (d,  $J$  = 22.2 Hz, C<sub>ad</sub>), 31.6 (d,  $J$  = 59.7 Hz, C<sub>ac</sub>), 38.9 (d,  $J$  = 40.2 Hz, C<sub>ag</sub>), 43.0 (d,  $J$  = 51.3 Hz, C<sub>ah</sub>), 50.7 (s, C<sub>u</sub>), 53.0 (s, C<sub>r</sub>), 55.3 (s, C<sub>t</sub>), 56.2 (s, C<sub>m</sub>), 58.1 (s, C<sub>q</sub>), 66.7 (s, C<sub>v</sub>), 69.2 (d,  $J$  = 25.2 Hz, C<sub>ae</sub>), 70.1 (s, C<sub>af</sub>), 70.4 (s, C<sub>af</sub>), 70.6 (d,  $J$  = 6.3 Hz, C<sub>ao</sub>), 71.1 (s, C<sub>af</sub>), 71.2 (s, C<sub>af</sub>), 71.5 (s, C<sub>af</sub>), 87.9 (s, C<sub>p</sub>), 88.2 (s, C<sub>s</sub>), 115.1 (d,  $J$  = 11.3 Hz, C<sub>i</sub>), 121.2 (d,  $J$  = 13.7 Hz, C<sub>j</sub>), 125.5 (s, C<sub>h</sub>), 129.1 (s, C<sub>x</sub>), 129.8 (s, C<sub>c</sub>), 130.4 (s, C<sub>a</sub>), 130.7 (s, C<sub>b</sub>), 131.3 (s, C<sub>z</sub>), 133.4 (s, C<sub>d</sub>), 133.8 (s, C<sub>y</sub>), 133.9 (d,  $J$  = 6.3 Hz, C<sub>i</sub>), 138.1 (s, C<sub>w</sub>), 144.0 (s, vbr, C<sub>e</sub>, C<sub>aj</sub>, C<sub>an</sub>), 144.2 (s, C<sub>g</sub>), 159.1 (s, C<sub>n</sub>), 163.7 (s, C<sub>k</sub>), 168.6 (s, C<sub>aa</sub>), 174.6 (s, C<sub>ak</sub>, C<sub>am</sub>).

$^{11}\text{B}$  NMR (193 MHz, MeOD- $d_4$ )  $\delta$  (ppm) = -12.28 (s, br).

HR-MS (ESI): calculated for C<sub>69</sub>H<sub>78</sub>B<sub>1</sub>N<sub>7</sub>O<sub>9</sub> [M]<sup>2+</sup> 579.79716; found 579.79812

### 4.2.2.34 Compound 69

16 mg (1 eq, 13  $\mu\text{mol}$ ) of **66** were dissolved in 1 mL of EtOH. After addition of 20  $\mu\text{L}$  (10 eq, 135  $\mu\text{mol}$ ) of diethyl squarate and 20  $\mu\text{L}$  (9 eq, 118  $\mu\text{mol}$ ) DIPEA the reaction was stirred at 30–35°C for 5 h. The solvents were evaporated and the crude product was purified by semi preparative HPLC using gradient A. Product fractions were collected and lyophilized, followed by ion-exchange and subsequent lyophilization to yield 15 mg (11  $\mu\text{mol}$ , 85%) of the target compound **69** as a fluffy dark green solid (Cl<sup>-</sup>-salt).



$^1\text{H}$  NMR (600 MHz, CD<sub>3</sub>CN)  $\delta$  (ppm) = 1.36 (t,  $J$  = 7.2 Hz, 3H, H<sub>as</sub>), 1.73–1.78 (m, 2H, H<sub>ad</sub>), 1.82 (dt,  $J$  = 6.2, 12.5 Hz, 2H, H<sub>ag</sub>), 2.10–2.16 (m, 2H, H<sub>ah</sub>), 2x 2.78 (s, 2x6H, H<sub>r</sub>, H<sub>u</sub>), 3.43 (dd,  $J$  = 6.5, 12.5 Hz, 10H, H<sub>af</sub>), 3.52–3.58 (m, 6H, H<sub>aj</sub>, H<sub>ac</sub>, H<sub>ae</sub>), 3.64 (s, 2H, H<sub>t</sub>), 3.79 (s, 6H, H<sub>m</sub>), 3.88 (s, 2H, H<sub>q</sub>), 4.06 (s, 2H, H<sub>v</sub>), 4.64 (m, 2H, H<sub>ar</sub>), 7.16 (d,  $J$  = 8.8 Hz, 4H, H<sub>j</sub>), 7.32 (s, 2H, H<sub>f</sub>), 7.38 (d,  $J$  = 7.9 Hz, 2H, H<sub>x</sub>), 7.46 (t,  $J$  = 7.3 Hz, 2H, H<sub>a</sub>), 7.51 (t,  $J$  = 7.4 Hz, 4H, H<sub>b</sub>), 7.87 (s, br, 2H, H<sub>y</sub>), 8.11 (d,  $J$  = 7.2 Hz, 4H, H<sub>c</sub>), 8.34 (t,  $J$  = 8.6 Hz, 4H, H<sub>i</sub>).

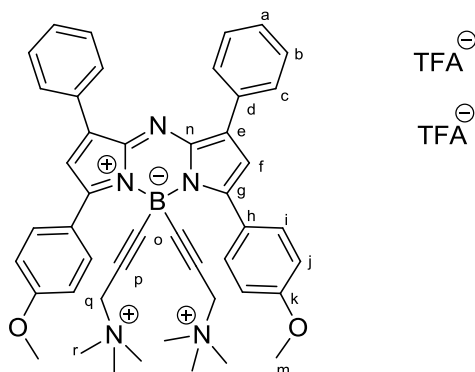
$^{13}\text{C}$  NMR (151 MHz, CD<sub>3</sub>CN)  $\delta$  (ppm) = 18.6 (s, C<sub>as</sub>), 20.0 (s, C<sub>ak</sub>), 30.1 (s, C<sub>ag</sub>), 31.0 (s, C<sub>ad</sub>), 38.6 (s, C<sub>ac</sub>), 43.0 (s, C<sub>ah</sub>), 48.8 (s, C<sub>o</sub>), 51.1 (s, C<sub>u</sub>), 51.2 (s, C<sub>r</sub>), 54.9 (s, C<sub>t</sub>, C<sub>q</sub>), 55.9 (s, C<sub>am</sub>), 56.5 (s, C<sub>m</sub>), 63.7 (s, C<sub>aj</sub>), 66.3 (s, C<sub>v</sub>), 69.1 (s, C<sub>af</sub>), 69.1 (s, C<sub>ar</sub>), 70.1 (s, C<sub>af</sub>), 70.7 (s, C<sub>af</sub>), 70.8 (s, C<sub>af</sub>), 70.9 (s, C<sub>af</sub>), 71.0 (s, C<sub>af</sub>), 86.8 (s, C<sub>s</sub>), 87.4 (s, C<sub>p</sub>), 115.2 (s, C<sub>i</sub>), 119.4 (s, C<sub>an</sub>), 121.4 (s, C<sub>j</sub>), 124.9 (s, C<sub>h</sub>), 128.8 (s, C<sub>x</sub>), 129.7 (s, C<sub>c</sub>), 130.2 (s, C<sub>a</sub>), 130.5 (s, C<sub>b</sub>), 130.6 (s, C<sub>z</sub>), 133.0 (s, C<sub>d</sub>), 133.6 (s, C<sub>i</sub>), 133.7 (s, C<sub>y</sub>), 137.8 (s, C<sub>w</sub>), 143.2 (s, br, C<sub>aq</sub>, C<sub>an</sub>), 143.8 (s, C<sub>e</sub>, C<sub>g</sub>), 158.7 (s, C<sub>n</sub>), 163.1 (s, C<sub>k</sub>), 166.8 (s, C<sub>aa</sub>), 173.8 (s, C<sub>ap</sub>, C<sub>ao</sub>).

$^{11}\text{B}$  NMR (160 MHz, CD<sub>3</sub>CN)  $\delta$  (ppm) = -12.56 (s)

HR-MS (ESI): calculated for  $C_{71}H_{81}B_1N_7O_{12}S_1$   $[M]^+$  1266.57515; found 1266.57764

#### 4.2.2.35 Compound **71**

40 mg of azaBODIPY **60** (58.5  $\mu$ mol, 1 eq) were dissolved in 10 mL of ACN. 0.3 mL of MeI (4.82 mmol) were added and the reaction stirred for 1h30 at room temperature. The solvents were then evaporated and the resulting crude product purified by semi preparative HPLC using a gradient A. Product fractions were collected and lyophilized to yield 36 mg (38.3  $\mu$ mol, 65%) of the target compound **71** as a green solid.



$^1H$  NMR (600 MHz, MeOD- $d_4$ )  $\delta$  (ppm) = 2.87 (s, 18H, Hr), 3.93 (s, 6H, Hm), 4.01 (s, 2H, Hq), 7.15 (d,  $J$  = 8.9 Hz, 4H, Hi), 7.36 (s, 2H, Hf), 7.45 – 7.51 (m, 6H, Ha, Hc), 8.12 (d,  $J$  = 6.9 Hz, 4H, Hb), 8.37 (d,  $J$  = 8.9 Hz, 4H, Hl).

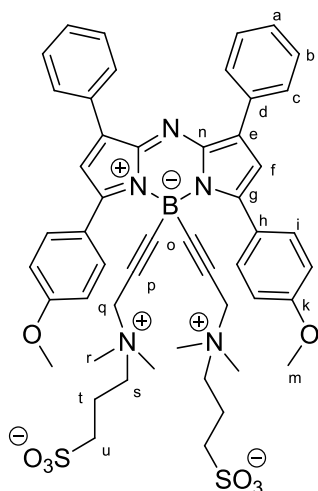
$^{11}B$  NMR (193 MHz, MeOD- $d_4$ )  $\delta$  (ppm) = -12.30 (s).

$^{13}C$  NMR (151 MHz, MeOD- $d_4$ )  $\delta$  (ppm) = 53.0 (s, Cr), 56.2 (s, Cm), 58.1 (s), 87.7 (s, Cp), 115.1 (s, Cf), 121.2 (s, Cj), 125.5 (s, Ch), 129.8 (s, Cc), 130.4 (s, Ca), 130.6 (s, Cb), 133.4 (s, Cd), 133.8 (s, Ci), 144.0 (s, Ce), 144.1 (s, Cg), 159.2 (s, Cn), 163.7 (s, Ck).

HR-MS (ESI): calculated for  $C_{46}H_{48}B_1N_5O_2$   $[M]^{2+}$  356.69450; found 356.69493

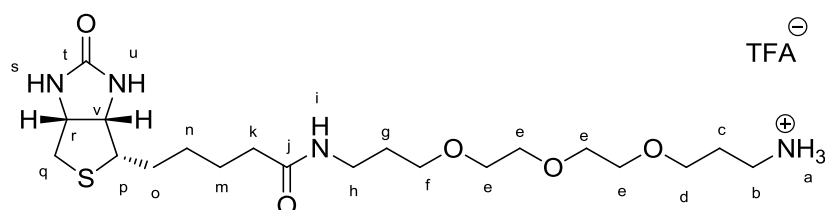
#### 4.2.2.36 Compound **72**

20 mg (29.3  $\mu$ mol, 1 eq) compound **60** were dissolved in 5 mL ACN. 14.3 mg (117  $\mu$ mol, 4 eq) propane sultone and  $NaHCO_3$  (12 mg, 146  $\mu$ mol, 5 eq) were added and the mixture refluxed for 18h. Upon completion the solvents were evaporated and the crude product purified using gradient A. Product fractions were collected and lyophilized to isolate 24 mg (25.9  $\mu$ mol, yield = 88%) of the target compound as a dark green solid.





100 mg (0.409 mmol, 1 eq) of biotin and 129.4 mg (0.428 mmol, 1.05 eq) of TSTU were dissolved in dry DMF (5 mL). 0.35 mL (2.04 mmol, 5 eq) of DIPEA was added and the solution stirred at 25°C for 1 h. After 1 h TOTA-Boc (131.1 mg, 0.409 mmol, 1eq) was dissolved in 1 mL DMF and added to the reaction. The solution was stirred for 4 h, followed by evaporation to dryness. The crude product was redissolved in a mixture of ACN (5 mL) and 1M HCl (10 mL) and stirred at roomtemperature overnight. After evaporation to dryness the crude product was purified by semi preparative HPLC using gradient A. Product fractions were collected and lyophilized to yield 189.5 mg (348  $\mu$ mol, yield = 85%) of the target compound as an off-white hygroscopic solid.



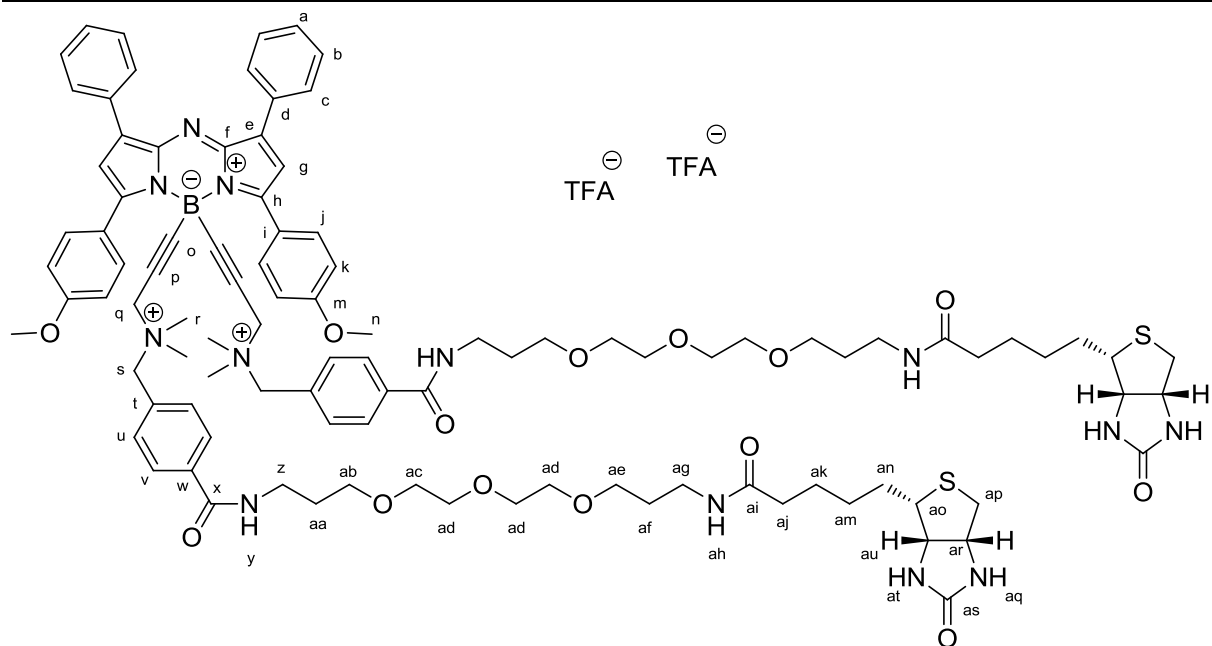
$^1\text{H}$  NMR (600 MHz,  $\text{D}_2\text{O}$ )  $\delta$  (ppm) = 1.39 – 1.48 (m, 2H,  $\text{H}_n$ ), 1.55 – 1.78 (m, 4H,  $\text{H}_o$ ,  $\text{H}_m$ ), 1.82 (p,  $J$  = 6.6 Hz, 2H,  $\text{H}_g$ ), 1.98 (p,  $J$  = 6.5 Hz, 2H,  $\text{H}_c$ ), 2.28 (t,  $J$  = 7.2 Hz, 2H,  $\text{H}_b$ ), 2.77 – 2.86 (m, 1H,  $\text{H}_k$ ), 3.02 (dd,  $J$  = 5.0, 13.1 Hz, 1H,  $\text{H}_l$ ), 3.14 (t,  $J$  = 7.0 Hz, 2H,  $\text{H}_h$ ), 3.29 (td,  $J$  = 2.9, 6.8 Hz, 2H,  $\text{H}_q$ ), 3.34 – 3.40 (m, 1H,  $\text{H}_p$ ), 3.60 (t,  $J$  = 6.4 Hz, 2H,  $\text{H}_d$ ), 3.66 – 3.76 (m, 10H,  $\text{H}_e$ ,  $\text{H}_f$ ), 4.45 (dd,  $J$  = 4.5, 7.9 Hz, 1H,  $\text{H}_v$ ), 4.64 (dd,  $J$  = 4.9, 7.8 Hz, 1H,  $\text{H}_r$ ).

$^{13}\text{C}$  NMR (151 MHz,  $\text{D}_2\text{O}$ )  $\delta$  (ppm) = 25.5 (s,  $\text{C}_o$ ), 26.8 (s,  $\text{C}_m$ ), 28.0 (s,  $\text{C}_n$ ), 28.2 (s,  $\text{C}_g$ ), 28.6 (s,  $\text{C}_c$ ), 35.8 (s,  $\text{C}_k$ ), 36.6 (s,  $\text{C}_b$ ), 38.0 (s,  $\text{C}_h$ ), 40.0 (s,  $\text{C}_q$ ), 55.7 (s,  $\text{C}_p$ ), 60.5 (s,  $\text{C}_v$ ), 62.4 (s,  $\text{C}_r$ ), 68.6 (s,  $\text{C}_f$ ), 68.7 (s,  $\text{C}_d$ ), 69.6 (s,  $\text{C}_e$ ), 69.7 (s,  $\text{C}_e$ ), 69.8 (s,  $\text{C}_e$ ), 69.9 (s,  $\text{C}_e$ ), 165.6 (s,  $\text{C}_t$ ), 177.0 (s,  $\text{C}_j$ ).

HR-MS (ESI): calculated for  $\text{C}_{20}\text{H}_{39}\text{N}_4\text{O}_5\text{S}_1$  [ $\text{M}$ ] $^{2+}$  447.26357; found 447.26233

#### 4.2.2.39 Compound 75

30 mg (26.9  $\mu$ mol, 1 eq) of compound **62**, 20.3 mg (67.3  $\mu$ mol, 2.5 eq) of TSTU and DIPEA (0.1 mL, 588  $\mu$ mol 21.8 eq) were dissolved in 4mL of dry DMF and stirred for 30 min at room temperature. 30.1 mg (53.6  $\mu$ mol, 2 eq) compound **74** were dissolved in 0.5 mL DMF, added and the reaction stirred for another 2h. Upon completion the solvents were evaporated and the compound purified by RP-flash-chromatography using  $\text{H}_2\text{O}+0.1\%\text{TFA} \rightarrow \text{ACN}+0.1\%\text{TFA}$  (20% ACN to 100% ACN in 15 min) as eluent. Product fractions were collected and lyophilized to yield 23.2 mg (11.6  $\mu$ mol, 43% yield) of the target compound as a fluffy powder.



$^1\text{H}$  NMR (600 MHz,  $\text{CD}_3\text{CN}$ )  $\delta$  (ppm) = 1.29 – 1.36 (m, 4H), 1.49 – 1.55 (m, 4H), 1.58 – 1.63 (m, 1H), 1.81 (dd,  $J$  = 6.0, 12.2 Hz, 1H), 2.08 (t,  $J$  = 7.3 Hz, 1H), 2.62 (d,  $J$  = 12.6 Hz, 1H), 2.75 (d,  $J$  = 13.0 Hz, 3H), 2.81 – 2.87 (m, 1H), 3.09 – 3.19 (m, 2H), 3.37 – 3.59 (m, 8H), 3.70 (dd,  $J$  = 3.3, 13.5 Hz, 1H), 3.78 (d,  $J$  = 3.9 Hz, 2H), 4.08 (d,  $J$  = 4.2 Hz, 1H), 4.10 (s, 1H), 4.20 – 4.25 (m, 1H), 4.40 (dt,  $J$  = 6.2, 14.0 Hz, 1H), 7.05 (d,  $J$  = 8.5 Hz, 5H), 7.33 – 7.39 (m, 7H), 7.44 – 7.50 (m, 4H), 7.52 (t,  $J$  = 7.4 Hz, 6H), 7.81 (dd,  $J$  = 4.8, 10.5 Hz, 4H), 7.85 (d,  $J$  = 8.2 Hz, 2H), 8.13 (d,  $J$  = 7.4 Hz, 4H), 8.30 – 8.36 (m, 4H).

$^{13}\text{C}$  NMR (151 MHz,  $\text{CD}_3\text{CN}$ )  $\delta$  (ppm) = 17.8 (s), 26.4 (s), 28.7 – 29.0 (m), 30.1 (s), 30.2 (s), 36.2 (d,  $J$  = 2.4 Hz), 37.6 (s), 38.3 (s), 38.7 (d,  $J$  = 3.4 Hz), 40.9 (s), 50.9 (s), 55.0 – 55.3 (m), 56.2 (d,  $J$  = 3.6 Hz), 56.3 – 56.4 (m,  $J$  = 3.0 Hz), 61.1 (s), 62.7 (s), 66.4 (d,  $J$  = 8.1 Hz), 69.6 (s), 70.1 (d,  $J$  = 3.0 Hz), 70.7 (s), 70.8 (s), 71.0 (d,  $J$  = 4.7 Hz), 87.5 (d,  $J$  = 16.7 Hz), 114.9 (s), 118.0 (s), 121.5 (s), 125.0 (d,  $J$  = 3.2 Hz), 128.8 (s), 129.2 (d,  $J$  = 4.3 Hz), 129.7 (s), 130.2 (s), 130.5 (s), 130.6 (s), 130.9 (d,  $J$  = 2.2 Hz), 133.0 (s), 133.6 (d,  $J$  = 3.2 Hz), 133.7 (d,  $J$  = 1.7 Hz), 137.1 (s), 138.0 (s), 143.4 (d,  $J$  = 4.4 Hz), 143.9 (s), 158.8 (d,  $J$  = 6.1 Hz), 163.0 (s).

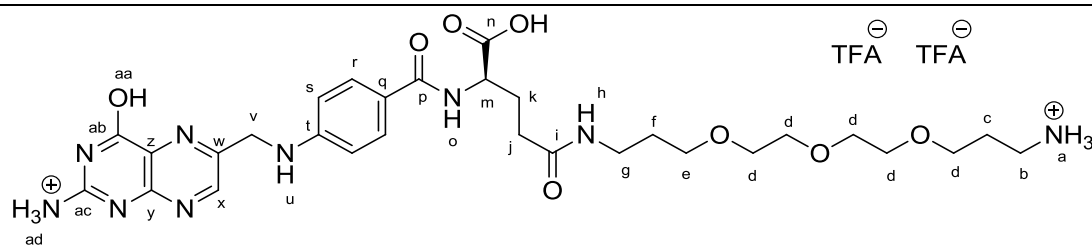
$^{11}\text{B}$  NMR (193 MHz,  $\text{CD}_3\text{CN}$ )  $\delta$  (ppm) = -12.33 (s).

HR-MS (ESI): calculated for  $\text{C}_{100}\text{H}_{128}\text{B}_1\text{N}_{13}\text{O}_{14}\text{S}_2$   $[\text{M}]^{2+}$  904.96136; found 904.96107

#### 4.2.2.40 Compound 76

100 mg (22.6  $\mu\text{mol}$ , 1 eq) of folic acid were dissolved in a mixture of dry DMF (20 mL) and dry DMSO (10 mL). 0.3 mL of DIPEA were added and the solution cooled to  $0^\circ\text{C}$ . 90.2 mg (23.8  $\mu\text{mol}$ , 1.05 eq) HBTU were added and the solution stirred for 1 h.

After 1 h 76.2 mg (23.8  $\mu\text{mol}$ , 1.05 eq) TOTA-Boc in 1 mL dry DMF were added. The solution was left to heat up to room temperature and stirred for another 3 h. Once HPLC indicated completion the raw product was precipitated by addition of water (40 mL). The precipitate was isolated by centrifugation, redissolved in 1M HCl and stirred for 3-4 h. Solvents were then evaporated and the crude product purified by RP-flash-chromatography using an eluent of  $\text{H}_2\text{O}+0.1\%\text{TFA} \rightarrow \text{ACN}+0.1\%\text{TFA}$  (10%ACN to 100%ACN in 10 minutes). Product fractions were lyophilized to yield 115 mg (60% yield) of the target compound as a pale yellow solid.



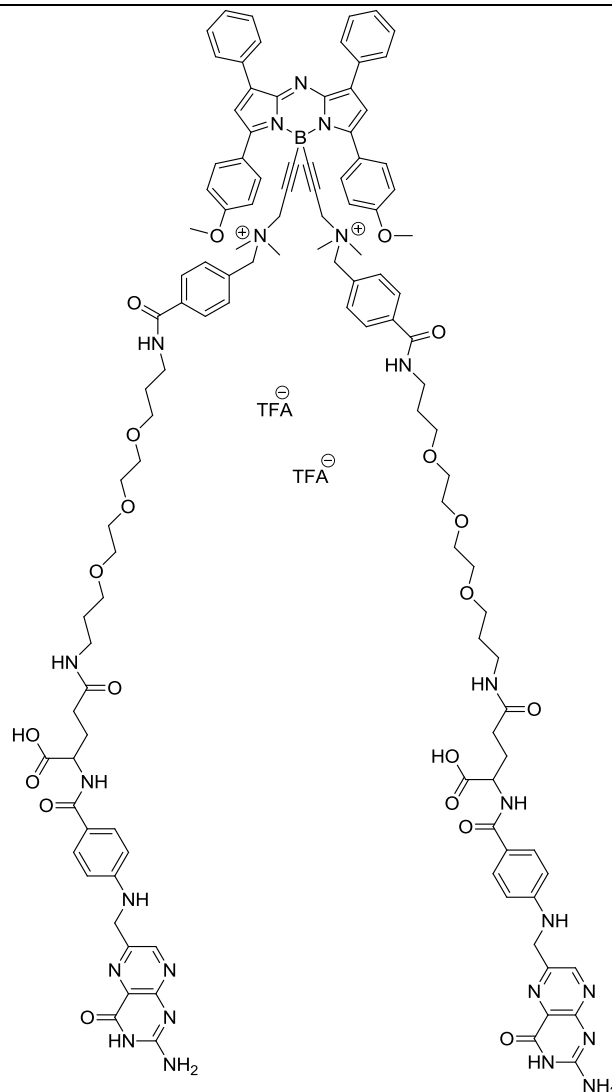
$^1\text{H}$  NMR (600 MHz, DMSO- $d_6$ )  $\delta$  (ppm) = 1.60 (tt,  $J$  = 6.7, 13.4 Hz, 2H,  $H_f$ ), 1.73 – 1.79 (m, 2H,  $H_c$ ), 1.82 – 1.93 (m, 1H,  $H_j$ ), 1.93 – 2.09 (m, 1H,  $H_k$ ), 2.18 (t,  $J$  = 7.9 Hz, 1H,  $H_{j'}$ ), 2.25 (dd,  $J$  = 7.3, 15.6 Hz, 1H,  $H_{k'}$ ), 2.85 (d,  $J$  = 5.3 Hz, 2H,  $H_g$ ), 3.01 – 3.13 (m, 2H,  $H_e$ ), 3.36 (dt, br,  $J$  = 6.4, 12.8 Hz, 2H,  $2H_b$  + HDO) 3.43 – 3.52 (m, 13H,  $3H_a$ ,  $H_d$ ) [wrong integration : HDO, PEG+ $\text{NH}_3$  interfere], 4.23 – 4.36 (m, 1H,  $H_m$ ), 4.48 (s, 2H,  $H_v$ ), 6.64 (dd,  $J$  = 3.2, 8.7 Hz, 2H,  $H_s$ ), 6.93 (s, 2H,  $H_u$ ,  $H_{aa}$ ), 7.65 (dd,  $J$  = 2.8, 8.7 Hz, 4H,  $2H_r$ ,  $H_h$ ,  $H_o$ ), 8.64 (d,  $J$  = 2.0 Hz, 1H,  $H_x$ ).

$^{13}\text{C}$  NMR (151 MHz, DMSO- $d_6$ )  $\delta$  (ppm) = 27.1 (d,  $J$  = 7.9 Hz,  $C_k$ ), 29.3 (d,  $J$  = 9.6 Hz,  $C_f$ ), 30.5 (s,  $C_c$ ), 32.0 (s,  $C_b$ ), 35.9 (d,  $J$  = 12.6 Hz,  $C_j$ ), 36.9 (d,  $J$  = 12.8 Hz,  $C_g$ ), 45.9 (s,  $C_v$ ), 52.5 (d,  $J$  = 101.9 Hz,  $H_m$ ), 67.4 (s,  $C_e$ ), 68.0 (s,  $C_d$ ), 69.5 (d,  $J$  = 3.4 Hz,  $C_d$ ), 69.6 (s,  $C_d$ ), 69.7 (s,  $C_d$ ), 69.7 (s,  $C_d$ ), 111.1 (s,  $C_s$ ), 116.2 (s), 118.2 (s), 121.3 (d,  $J$  = 5.5 Hz,  $C_q$ ), 127.9 (s,  $C_z$ ), 128.9 (s,  $C_r$ ), 129.0 (s,  $C_x$ ), 148.6 (s,  $C_w$ ), 150.8 (s,  $C_y$ ), 153.8 (s,  $C_t$ ), 157.9 (d,  $J$  = 30.9 Hz,  $C_{ac}$ ), 166.3 (d,  $J$  = 4.0 Hz,  $C_{ab}$ ), 171.5 (d,  $J$  = 20.8 Hz,  $C_n$ ), 173.8 (s,  $C_p$ ), 174.0 (s,  $C_i$ ).

HR-MS (ESI): calculated for  $\text{C}_{29}\text{H}_{43}\text{N}_9\text{O}_8$  [ $\text{M}+2\text{H}$ ] $^{2+}$  322.66118; found 322.66118  $\text{C}_{29}\text{H}_{42}\text{N}_9\text{O}_8$  [ $\text{M}+\text{H}$ ] $^+$  644.31509 found 644.31448

#### 4.2.2.41 Compound 77

17.0 mg (15.2  $\mu\text{mol}$ , 1 eq) compound **62** were dissolved together with 0.1 mL DIPEA (588  $\mu\text{mol}$ , 38.6 eq) and 11.2mg (37.3  $\mu\text{mol}$ , 2.4 eq) TSTU in 3 mL dry DMF and stirred for 30 min at 30°C. After 30min 26.5mg (30.5  $\mu\text{mol}$ , 2 eq) folic acid derivative **76** were dissolved in 0.5 mL DMF, added to the solution and stirred for another 2 h at room temperature. The crude product was evaporated to dryness and purified by semi preparative HPLC using gradient A. Product fractions were collected and lyophilized to obtain 9.4 mg (4.3  $\mu\text{mol}$ , 28% yield) of the target compound as a green sponge.

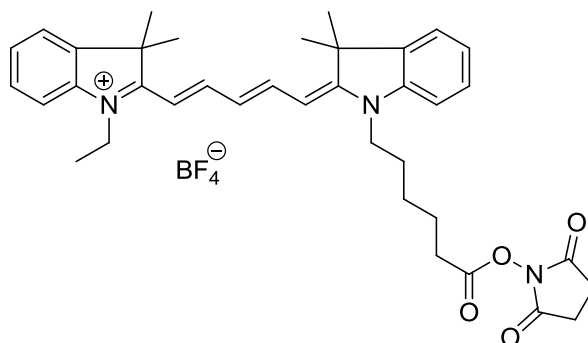


$^1\text{H}$  NMR (600 MHz, 0.7  $\text{D}_2\text{O}$ +0.3 $\text{CD}_3\text{CN}$ )  $\delta$  (ppm) = 1.69 – 1.75 (m, 2H), 1.75 – 1.81 (m, 2H), 2.36 – 2.44 (m, 2H), 2.52 (t,  $J$  = 7.3 Hz, 2H), 3.16 – 3.25 (m, 3H), 3.25 – 3.32 (m, 3H), 3.46 – 3.70 (m, 32H), 3.84 (s, 4H), 3.88 (d,  $J$  = 6.6 Hz, 6H), 4.20 (s, 4H), 4.62 (d,  $J$  = 13.1 Hz, 3H), 6.70 – 6.78 (m, 3H), 7.19 (t,  $J$  = 9.6 Hz, 4H), 7.45 (t,  $J$  = 12.2 Hz, 6H), 7.60 (tt,  $J$  = 7.0, 14.3 Hz, 6H), 7.70 (d,  $J$  = 8.5 Hz, 4H), 7.83 (d,  $J$  = 7.9 Hz, 4H), 8.19 (dd,  $J$  = 7.4, 17.0 Hz, 3H), 8.44 (t,  $J$  = 7.9 Hz, 4H), 8.76 (d,  $J$  = 9.9 Hz, 2H).

$^{13}\text{C}$  NMR (151 MHz, 0.7  $\text{D}_2\text{O}$ +0.3  $\text{CD}_3\text{CN}$ )  $\delta$  (ppm) = 26.2 (s), 28.0 (d,  $J$  = 16.9 Hz), 29.8 (s), 31.8 (s), 36.0 (d,  $J$  = 6.2 Hz), 36.9 (d,  $J$  = 4.2 Hz), 45.3 (s), 49.7 (s), 52.2 (s), 53.1 (s), 53.6 (s), 55.1 (s), 64.8 (s), 67.9 (d,  $J$  = 9.7 Hz), 68.3 (s), 69.0 (d,  $J$  = 4.3 Hz), 69.1 (s), 69.2 (d,  $J$  = 6.0 Hz), 69.3 (s), 86.5 (s), 111.6 (s), 111.7 (s), 113.6 (s), 119.9 (s), 120.7 (s), 123.5 (s), 126.8 (s), 127.4 (s), 128.4 (s), 128.7 (s), 128.7 (d,  $J$  = 4.2 Hz), 128.7 (s), 129.4 (s), 129.4 (s), 131.3 (s), 132.1 (s), 132.3 (s), 135.8 (s), 141.8 (s), 142.3 (s), 148.6 (s), 150.5 (s), 151.0 (d,  $J$  = 6.0 Hz), 152.4 (s), 157.3 (s), 161.0 (d,  $J$  = 4.2 Hz), 161.4 (s), 167.2 (s), 168.0 (s), 168.1 (s), 172.5 (s), 173.6 (s), 174.2 (s), 175.8 (s).

$^{11}\text{B}$  NMR (160 MHz, 0.7  $\text{D}_2\text{O}$ +0.3 $\text{CD}_3\text{CN}$ )  $\delta$  (ppm) = -12.36 (s).

HR-MS (ESI): calculated for  $\text{C}_{118}\text{H}_{134}\text{B}_1\text{N}_{23}\text{O}_{20}$   $[\text{M}]^{2+}$  1102.01288; found 1102.01708 calculated for  $\text{C}_{111}\text{H}_{129}\text{B}_1\text{N}_{18}\text{O}_{19}$   $[\text{M}-\text{C}_7\text{H}_5\text{N}_5\text{O}]^{2+}$  1014.48817; found 1014.49293

4.2.2.42 Cy5-NHS (**70**)

10 mg (20.13  $\mu\text{mol}$ , 1 eq) cyanine 5 was dissolved in 1 mL DMSO, followed by addition of 3.5  $\mu\text{L}$  (20.12  $\mu\text{mol}$ , 1eq) and 6.1 mg (20.1  $\mu\text{mol}$ , 1eq) TSTU. The reaction was stirred for 45min at room temperature until HPLC indicates completion. The activated Cy5 was used for bioconjugation as is without further purification

### 4.3 Gold uptake

MDA-MB-231 cells ( $1.0 \times 10^5/\text{mL}$ ) were seeded in 6 well plates and allowed to recover to ensure that the cells were adherent during the uptake experiment. After 24h, cells were treated for 4 h with 40  $\mu\text{M}$  of BODIPYs **4b**, **9**, **10**, **11**, **13**, **15**, **16**, **19**, **20**, **21**, **26**

And several controls: BODIPY **1**, BODIPY **8**, BODIPY **18**, BODIPY **25** as negative control; Auranofin as reference and DMSO (vector control)

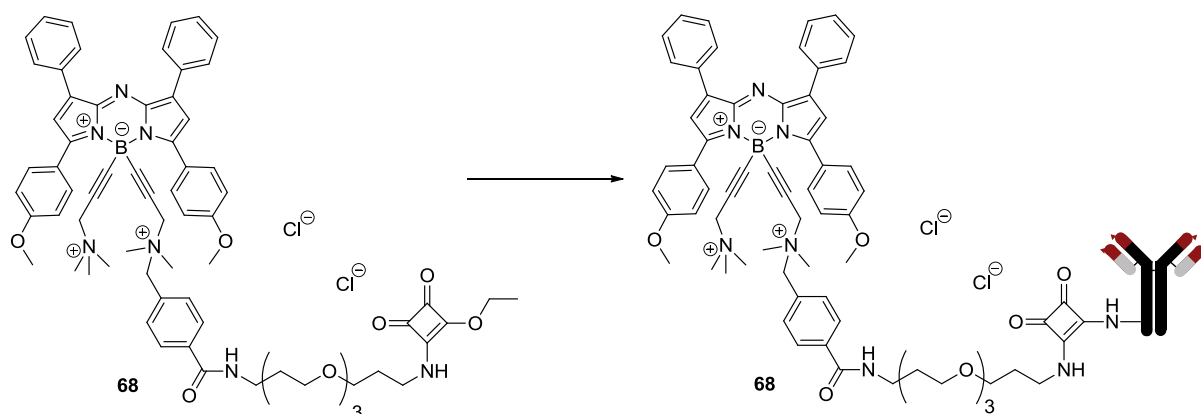
After treatment, cells were washed three times with phosphate buffer saline (PBS1X) in order to assure that each drug-exposed well was cleaned, then and lysed in water. The protein concentration were determined for each drug-exposed well. The protein concentration of each lysate was determined in a 96-well plate against BSA standards in PBS (ranging from 0–16  $\mu\text{g}$ ), applying the QuantiPro™ BCA Assay Kit (Sigma-Aldrich), and the total amount of proteins per well was calculated.

All samples were then digested in ICP-MS grade concentrated hydrochloric acid (OPTIMA Grade, Fisher Chemical) for 3h at room temperature and filled to a total volume of 5 mL with ultrapure water.

Iridium ( $^{193}\text{Ir}$ ) was added as an internal standard at a concentration of 1 ppb. Determinations of total metal contents were achieved using a Thermo Element 2 ICP-MS. The instrument was tuned daily using a solution provided by the manufacturer containing 1 ppb each of Ba, B, Co, Fe, Ga, In, K, Li, Lu, Na, Rh, Sc, Tl, U, and Y (Tune-Up Solution Element, Thermo Fisher Scientific, Bremen, Germany). The external standard was prepared gravimetrically in an identical matrix to the samples (with regard to the internal standard and hydrochloric acid) with a gold solution single element standard at 1000 ppm (Assurance, SPEX CertiPrep).

Results were expressed as % uptake or  $\mu\text{g}/\text{gold}/10^5$  cells.

## 4.4 Bioconjugation



10 equivalents of a 2mM stock solution of azaBODIPY X in DMSO or 4 equivalents of a 20 mM Cy5-NHS stock solution was added to a 3 mg/mL solution of antibody in NaHCO<sub>3</sub> buffer (0.2 M, pH=8.4). The amount of DMSO in the final aqueous reaction mixture was 10%. The solution was stirred overnight (azaBODIPY) or for 4h in a thermomixer (900 rpm, 37 °C). The bioconjugate was then purified by FPLC (Äkta Pure 25 M chromatography system, GE Healthcare Life Sciences) on a HiTrap<sup>®</sup> Protein G HP column (MabSelect resine, Protein G, cross-linked agarose, column I.D 7 mm, bed dimensions 7 x 25 mm, bed volume 1 mL). Excess probe was removed with 20 mM phosphate buffer (pH=7.3) as eluent and 0.1% Tween 80 in 20 mM phosphate buffer (pH 7.3). The IgG conjugates were eluted with acetic acid solution (50 mM, pH 3.0). Thereafter, the solution was transferred to an ultra-centrifugal filter device (Amicon Ultra 2 mL, Ultracel cut-off 30 kDa from Merck Millipore) and centrifuged at 4000 rpm for 3x30 min at 4°C in order to condition the mixture in 20 mM phosphate-buffered saline (pH 7.4). The recovered yields, concentrations and masses are listed below Table 17. The degree of labelling (amount of probe per IgG) was determined by MALDI-TOF mass spectrometry measurements.

Table 17: yields, DOL's, and concentrations of the obtained azaBODIPY-bioconjugates

Bioconjugate	DOL	IgG engaged	conjugate mass (yield)	concentration
<b>68</b> - anti-PD-L1	2.9	1.8 mg	772 µg (43%)	1.23 mg/mL
<b>Cy5</b> - anti-PD-L1	2.9	1.8 mg	1109 µg (62%)	2.21 mg/mL
<b>68</b> - rat-IgG2b	2	500 µg	349 µg (70%)	1.33 mg/mL
<b>Cy5</b> - rat-IgG2b	1.9	400 µg	37 µg (9%)	0.17 mg/mL
<b>68</b> - anti-PD-1	1.3	563 µg	143 µg (25%)	1.54 mg/mL
<b>Cy5</b> - anti-PD-1	2.7	300 µg	99 µg (33%)	0.82 mg/mL

## 4.5 In-vitro confocal microscopy experiments

Cells (B16F10, MDA-MB-231, EMT6 and CT26) were seeded on chambered cover glasses (24 well-plate) and allowed to recover. Cells were incubated with 10 µM of each compound at 37°C. After 1, 4 and 24 hours the cells were fixed and permeabilized with iced MeOH for 10 min at room temperature. Cells were then washed thrice with PBS (5 min each), counterstained with 5 µM DRAQ5 (or 1 µg.mL<sup>-1</sup> DAPI) for 5-10 min, washed with PBS and mounted with Fluoromount-G<sup>®</sup> (Southern Biotech). Confocal imaging was performed using a confocal laser-scanning microscope (Leica TCS SP8) with a × 63 HCX PL APO oil immersion (ON

1.4) objective lens that allowed to simultaneously obtain DIC (Differential Interference Contrast) and fluorescent images (1024 pixels × 1024 pixels), and LASX software (Leica Microsystems, Ltd).

The samples were excited using internal microscope lasers and emission intensity was recorded at the appropriate emission wavelength. Fluorescence images were sequentially acquired. For co-localization experiments, BODIPY compounds (green) was excited at 488 nm and its emission was recorded from 493 to 600 nm, whereas DRAQ5 (red) was excited at 638 nm and its emission was recorded from 661 nm to 778 nm. Image processing and analyses were carried out using Fiji/ImageJ.

## References

- [1] Raymond W., R. M. D., "*Cancer Biology*", Fourth Edition, Oxford University Press, Oxford, New York, (2007).
- [2] WHO | Cancer, <http://www.who.int/cancer/en/>, accessed 10/04/2018.
- [3] Stewart, B. W.; Wild, C.; International Agency for Research on Cancer; and World Health Organization, "*World cancer report 2014*", (2014).
- [4] The Nobel Prize in Physiology or Medicine 2018, <https://www.nobelprize.org/prizes/medicine/2018/summary/>, accessed 10/04/2018.
- [5] Mankoff, D. A., A definition of molecular imaging, *J. Nucl. Med. Off. Publ. Soc. Nucl. Med.* **48** (2007) 18N, 21N,.
- [6] Weissleder, R. and Pittet, M. J., Imaging in the era of molecular oncology, *Nature* **452** (2008) 580–589, <https://doi.org/10.1038/nature06917>.
- [7] James, M. L. and Gambhir, S. S., A Molecular Imaging Primer: Modalities, Imaging Agents, and Applications, *Physiol. Rev.* **92** (2012) 897–965, <https://doi.org/10.1152/physrev.00049.2010>.
- [8] Survival by stage, [http://ncin.org.uk/publications/survival\\_by\\_stage](http://ncin.org.uk/publications/survival_by_stage), accessed 05/07/2018.
- [9] Street, W., Cancer Prevention & Early Detection Facts & Figures 2017-2018, *Am. Cancer Soc.* (2017) 1–76,.
- [10] Hanahan, D. and Weinberg, R. A., Hallmarks of Cancer: The Next Generation, *Cell* **144** (2011) 646–674, <https://doi.org/10.1016/j.cell.2011.02.013>.
- [11] Nair, M.; Sandhu, S. S.; and Sharma, A. K., Cancer molecular markers: A guide to cancer detection and management, *Semin. Cancer Biol.* (2018) <https://doi.org/10.1016/j.semcancer.2018.02.002>.
- [12] Weissleder, R. and Mahmood, U., Molecular imaging, *Radiology* **219** (2001) 316–333, <https://doi.org/10.1148/radiology.219.2.r01ma19316>.
- [13] Rudin, M., "*Molecular imaging: basic principles and applications in biomedical research*", 2nd edition, World Scientific, London, (2013).
- [14] Morzycki, A.; Bhatia, A.; and Murphy, K. J., Adverse Reactions to Contrast Material: A Canadian Update, *Can. Assoc. Radiol. J.* **68** (2017) 187–193, <https://doi.org/10.1016/j.carj.2016.05.006>.
- [15] Granata, V.; Cascella, M.; Fusco, R.; dell'Aprovitola, N.; Catalano, O.; Filice, S. et al., Immediate Adverse Reactions to Gadolinium-Based MR Contrast Media: A Retrospective Analysis on 10,608 Examinations, *BioMed Res. Int.* **2016** (2016) 1–6, <https://doi.org/10.1155/2016/3918292>.
- [16] Haris, M.; Yadav, S. K.; Rizwan, A.; Singh, A.; Wang, E.; Hariharan, H. et al., Molecular magnetic resonance imaging in cancer, *J. Transl. Med.* **13** (2015) <https://doi.org/10.1186/s12967-015-0659-x>.
- [17] Electromagnetic spectrum, *Wikipedia* (2018).
- [18] Klán, P. and Wirz, J., "*Photochemistry of organic compounds: from concepts to practice*", Wiley, Chichester, West Sussex, U.K, (2009).
- [19] Lakowicz, J. R., "*Principles of Fluorescence Spectroscopy*", 3rd ed., Springer US, (2006).
- [20] Wykes, M.; Parambil, R.; Beljonne, D.; and Gierschner, J., Vibronic coupling in molecular crystals: A Franck-Condon Herzberg-Teller model of H-aggregate fluorescence based on quantum chemical cluster calculations, *J. Chem. Phys.* **143** (2015) 114116, <https://doi.org/10.1063/1.4930606>.

- [21] Valdes-Aguilera, O. and Neckers, D. C., Aggregation phenomena in xanthene dyes, *Acc. Chem. Res.* **22** (1989) 171–177, <https://doi.org/10.1021/ar00161a002>.
- [22] Renn, A.; Seelig, J.; and Sandoghdar, V., Oxygen-dependent photochemistry of fluorescent dyes studied at the single molecule level, *Mol. Phys.* **104** (2006) 409–414, <https://doi.org/10.1080/00268970500361861>.
- [23] Kamimura, M.; Yano, Y.; Kuraoka, S.; Suyari, S.; Ube, T.; Wortmann, L. et al., Near-Infrared to Visible Upconversion Emission Induced Photopolymerization: Polystyrene Shell Coated NaYF<sub>4</sub> Nanoparticles for Fluorescence Bioimaging and Nanothermometry, *J. Photopolym. Sci. Technol.* **30** (2017) 265–270, <https://doi.org/10.2494/photopolymer.30.265>.
- [24] He, S.; Song, J.; Qu, J.; and Cheng, Z., Crucial breakthrough of second near-infrared biological window fluorophores: design and synthesis toward multimodal imaging and theranostics, *Chem. Soc. Rev.* (2018) <https://doi.org/10.1039/C8CS00234G>.
- [25] Vogel, A. and Venugopalan, V., Mechanisms of Pulsed Laser Ablation of Biological Tissues, *Chem. Rev.* **103** (2003) 577–644, <https://doi.org/10.1021/cr010379n>.
- [26] Resch-Genger, U.; Grabolle, M.; Cavaliere-Jaricot, S.; Nitschke, R.; and Nann, T., Quantum dots versus organic dyes as fluorescent labels, *Nat. Methods* **5** (2008) 763–775, <https://doi.org/10.1038/nmeth.1248>.
- [27] Petryayeva, E.; Algar, W. R.; and Medintz, I. L., Quantum Dots in Bioanalysis: A Review of Applications across Various Platforms for Fluorescence Spectroscopy and Imaging, *Appl. Spectrosc.* **67** (2013) 215–252, <https://doi.org/10.1366/12-06948>.
- [28] Day, R. N. and Davidson, M. W., The fluorescent protein palette: tools for cellular imaging, *Chem. Soc. Rev.* **38** (2009) 2887, <https://doi.org/10.1039/b901966a>.
- [29] Chudakov, D. M.; Matz, M. V.; Lukyanov, S.; and Lukyanov, K. A., Fluorescent Proteins and Their Applications in Imaging Living Cells and Tissues, *Physiol. Rev.* **90** (2010) 1103–1163, <https://doi.org/10.1152/physrev.00038.2009>.
- [30] Lavis, L. D. and Raines, R. T., Bright Ideas for Chemical Biology, *ACS Chem. Biol.* **3** (2008) 142–155, <https://doi.org/10.1021/cb700248m>.
- [31] MitoTracker Green FM - Special Packaging - Thermo Fisher Scientific, <https://www.thermofisher.com/order/catalog/product/M7514>, accessed 09/25/2018.
- [32] LysoSensor Yellow/Blue DND-160 - Special Packaging - Thermo Fisher Scientific, <https://www.thermofisher.com/order/catalog/product/L7545>, accessed 09/25/2018.
- [33] DRAQ5 Fluorescent Probe Solution (5 mM) - Thermo Fisher Scientific, <https://www.thermofisher.com/order/catalog/product/62251>, accessed 09/25/2018.
- [34] DAPI (4',6-Diamidino-2-Phenylindole, Dihydrochloride) - Thermo Fisher Scientific, <https://www.thermofisher.com/order/catalog/product/D1306>, accessed 09/25/2018.
- [35] Walter, J.; Joffe, B.; Bolzer, A.; Albiez, H.; Benedetti, P. A.; Müller, S. et al., Towards many colors in FISH on 3D-preserved interphase nuclei, *Cytogenet. Genome Res.* **114** (2006) 367–378, <https://doi.org/10.1159/000094227>.
- [36] Gao, W.; Xing, B.; Tsien, R. Y.; and Rao, J., Novel Fluorogenic Substrates for Imaging  $\beta$ -Lactamase Gene Expression, *J. Am. Chem. Soc.* **125** (2003) 11146–11147, <https://doi.org/10.1021/ja036126o>.
- [37] Ho, N.-H.; Weissleder, R.; and Tung, C.-H., A Self-Immolative Reporter For  $\beta$ -Galactosidase Sensing, *ChemBioChem* **8** (2007) 560–566, <https://doi.org/10.1002/cbic.200600386>.
- [38] Jiang, G.; Zeng, G.; Zhu, W.; Li, Y.; Dong, X.; Zhang, G. et al., A selective and light-up fluorescent probe for  $\beta$ -galactosidase activity detection and imaging in living cells based on an AIE tetraphenylethylene derivative, *Chem. Commun.* **53** (2017) 4505–4508, <https://doi.org/10.1039/C7CC00249A>.

## References

---

- [39] Conic, S.; Desplancq, D.; Ferrand, A.; Fischer, V.; Heyer, V.; Reina San Martin, B. et al., Imaging of native transcription factors and histone phosphorylation at high resolution in live cells, *J. Cell Biol.* **217** (2018) 1537–1552, <https://doi.org/10.1083/jcb.201709153>.
- [40] Alexa® dyes, <https://www.atdbio.com/content/34/Alexa-dyes>, accessed 09/26/2018.
- [41] Ding, F.; Zhan, Y.; Lu, X.; and Sun, Y., Recent advances in near-infrared II fluorophores for multifunctional biomedical imaging, *Chem. Sci.* **9** (2018) 4370–4380, <https://doi.org/10.1039/C8SC01153B>.
- [42] Azzopardi, E. A.; Owens, S.-E.; Murison, M.; Rees, D.; Anne Sawhney, M.; Francis, L. W. et al., Chromophores in operative surgery: Current practice and rationalized development, *J. Controlled Release* **249** (2017) 123–130, <https://doi.org/10.1016/j.jconrel.2016.12.044>.
- [43] Martinić, I.; Eliseeva, S. V.; and Petoud, S., Near-infrared emitting probes for biological imaging: Organic fluorophores, quantum dots, fluorescent proteins, lanthanide(III) complexes and nanomaterials, *J. Lumin.* **189** (2017) 19–43, <https://doi.org/10.1016/j.jlumin.2016.09.058>.
- [44] Brouwer, A. M., Standards for photoluminescence quantum yield measurements in solution (IUPAC Technical Report), *Pure Appl. Chem.* **83** (2011) 2213–2228, <https://doi.org/10.1351/PAC-REP-10-09-31>.
- [45] Niu, E.; Ghiggino, K. P.; Mau, A. W.-H.; and Sasse, W. H. F., Fluorescence and photochemistry of dye sensitizers in nafion membrane, *J. Lumin.* **40–41** (1988) 563–564, [https://doi.org/10.1016/0022-2313\(88\)90331-6](https://doi.org/10.1016/0022-2313(88)90331-6).
- [46] Lozovaya, G. I.; Masinovsky, Z.; and Sivash, A. A., Protoporphyrin ix as a possible ancient photosensitizer: Spectral and photochemical studies, *Orig. Life Evol. Biosph.* **20** (1990) 321–330, <https://doi.org/10.1007/BF01808114>.
- [47] Markwardt, N. A.; Haj-Hosseini, N.; Hollnburger, B.; Stepp, H.; Zelenkov, P.; and Rühm, A., 405 nm versus 633 nm for protoporphyrin IX excitation in fluorescence-guided stereotactic biopsy of brain tumors, *J. Biophotonics* **9** (2016) 901–912, <https://doi.org/10.1002/jbio.201500195>.
- [48] Haque, A.; Faizi, M. S. H.; Rather, J. A.; and Khan, M. S., Next generation NIR fluorophores for tumor imaging and fluorescence-guided surgery: A review, *Bioorg. Med. Chem.* **25** (2017) 2017–2034, <https://doi.org/10.1016/j.bmc.2017.02.061>.
- [49] Clinical trials using IRDye 800 CW, <https://clinicaltrials.gov/ct2/results?cond=&term=irdye+800+cw&cntry=&state=&city=&dist=>, accessed 01/10/2019.
- [50] Fluorescence SpectraViewer - FR, <https://www.thermofisher.com/fr/fr/home/life-science/cell-analysis/labeling-chemistry/fluorescence-spectraviewer.html>, accessed 09/26/2018.
- [51] Boldyrev, I. A.; Zhai, X.; Momsen, M. M.; Brockman, H. L.; Brown, R. E.; and Molotkovsky, J. G., New BODIPY lipid probes for fluorescence studies of membranes, *J. Lipid Res.* **48** (2007) 1518–1532, <https://doi.org/10.1194/jlr.M600459-JLR200>.
- [52] Spangenburg, E. E.; Pratt, S. J. P.; Wohlers, L. M.; and Lovering, R. M., Use of BODIPY (493/503) to Visualize Intramuscular Lipid Droplets in Skeletal Muscle, <https://www.hindawi.com/journals/bmri/2011/598358/>, accessed 09/27/2018.
- [53] Pader, I.; Sengupta, R.; Cebula, M.; Xu, J.; Lundberg, J. O.; Holmgren, A. et al., Thioredoxin-related protein of 14 kDa is an efficient L-cystine reductase and S-denitrosylase, *Proc. Natl. Acad. Sci.* **111** (2014) 6964–6969, <https://doi.org/10.1073/pnas.1317320111>.

- [54] Bernhard, C.; Goze, C.; Rousselin, Y.; and Denat, F., First bodipy–DOTA derivatives as probes for bimodal imaging, *Chem. Commun.* **46** (2010) 8267, <https://doi.org/10.1039/c0cc02749a>.
- [55] Lhenry, D.; Larrouy, M.; Bernhard, C.; Goncalves, V.; Raguin, O.; Provent, P. et al., BODIPY: A Highly Versatile Platform for the Design of Bimodal Imaging Probes, *Chem. - Eur. J.* **21** (2015) 13091–13099, <https://doi.org/10.1002/chem.201501676>.
- [56] Duheron, V.; Moreau, M.; Collin, B.; Sali, W.; Bernhard, C.; Goze, C. et al., Dual Labeling of Lipopolysaccharides for SPECT-CT Imaging and Fluorescence Microscopy, *ACS Chem. Biol.* **9** (2014) 656–662, <https://doi.org/10.1021/cb400779j>.
- [57] Brizet, B.; Goncalves, V.; Bernhard, C.; Harvey, P. D.; Denat, F.; and Goze, C., DMAP-BODIPY Alkynes: A Convenient Tool for Labeling Biomolecules for Bimodal PET-Optical Imaging, *Chem. - Eur. J.* **20** (2014) 12933–12944, <https://doi.org/10.1002/chem.201402379>.
- [58] Ono, M.; Watanabe, H.; Ikehata, Y.; Ding, N.; Yoshimura, M.; Sano, K. et al., Radioiodination of BODIPY and its application to a nuclear and optical dual functional labeling agent for proteins and peptides, *Sci. Rep.* **7** (2017) 3337, <https://doi.org/10.1038/s41598-017-03419-z>.
- [59] Kowada, T.; Kikuta, J.; Kubo, A.; Ishii, M.; Maeda, H.; Mizukami, S. et al., In Vivo Fluorescence Imaging of Bone-Resorbing Osteoclasts, *J. Am. Chem. Soc.* **133** (2011) 17772–17776, <https://doi.org/10.1021/ja2064582>.
- [60] Rodríguez, G.; Nargoli, J.; López, A.; Moyna, G.; Álvarez, G.; Fernández, M. et al., Synthesis and in vivo proof of concept of a BODIPY-based fluorescent probe as a tracer for biodistribution studies of a new anti-Chagas agent, *RSC Adv.* **7** (2017) 7983–7989, <https://doi.org/10.1039/C6RA27851E>.
- [61] Xu, J.; Li, Q.; Yue, Y.; Guo, Y.; and Shao, S., A water-soluble BODIPY derivative as a highly selective “Turn-On” fluorescent sensor for H<sub>2</sub>O<sub>2</sub> sensing in vivo, *Biosens. Bioelectron.* **56** (2014) 58–63, <https://doi.org/10.1016/j.bios.2013.12.065>.
- [62] Kikuta, J.; Wada, Y.; Kowada, T.; Wang, Z.; Sun-Wada, G.-H.; Nishiyama, I. et al., Dynamic visualization of RANKL and Th17-mediated osteoclast function, *J. Clin. Invest.* (2013) <https://doi.org/10.1172/JCI65054>.
- [63] Landrum, M.; Smertenko, A.; Edwards, R.; Hussey, P. J.; and Steel, P. G., BODIPY probes to study peroxisome dynamics in vivo: BODIPY probes to study peroxisome function, *Plant J.* **62** (2010) 529–538, <https://doi.org/10.1111/j.1365-313X.2010.04153.x>.
- [64] Urano, Y.; Asanuma, D.; Hama, Y.; Koyama, Y.; Barrett, T.; Kamiya, M. et al., Selective molecular imaging of viable cancer cells with pH-activatable fluorescence probes, *Nat. Med.* **15** (2009) 104–109, <https://doi.org/10.1038/nm.1854>.
- [65] Zhang, H.-X.; Chen, J.-B.; Guo, X.-F.; Wang, H.; and Zhang, H.-S., Highly Sensitive Low-Background Fluorescent Probes for Imaging of Nitric Oxide in Cells and Tissues, *Anal. Chem.* **86** (2014) 3115–3123, <https://doi.org/10.1021/ac4041718>.
- [66] Vázquez-Romero, A.; Kielland, N.; Arévalo, M. J.; Preciado, S.; Mellanby, R. J.; Feng, Y. et al., Multicomponent Reactions for *de Novo* Synthesis of BODIPY Probes: *In Vivo* Imaging of Phagocytic Macrophages, *J. Am. Chem. Soc.* **135** (2013) 16018–16021, <https://doi.org/10.1021/ja408093p>.
- [67] Buyukcakil, O.; Bozdemir, O. A.; Kolemene, S.; Erbas, S.; and Akkaya, E. U., Tetrastyril-Bodipy Dyes: Convenient Synthesis and Characterization of Elusive Near IR Fluorophores, *Org. Lett.* **11** (2009) 4644–4647, <https://doi.org/10.1021/ol9019056>.
- [68] Arranja, C. T.; Aguiar, A.; Encarnação, T.; Fonseca, S. M.; Justino, L. L. G.; Castro, R. A. E. et al., Double-tailed long chain BODIPYs - Synthesis, characterization and preliminary

## References

- studies on their use as lipid fluorescence probes, *J. Mol. Struct.* **1146** (2017) 62–69, <https://doi.org/10.1016/j.molstruc.2017.05.119>.
- [69] Li, S.-J.; Fu, Y.-J.; Li, C.-Y.; Li, Y.-F.; Yi, L.-H.; and Ou-Yang, J., A near-infrared fluorescent probe based on BODIPY derivative with high quantum yield for selective detection of exogenous and endogenous cysteine in biological samples, *Anal. Chim. Acta* **994** (2017) 73–81, <https://doi.org/10.1016/j.aca.2017.09.031>.
- [70] Ono, M.; Watanabe, H.; Kimura, H.; and Saji, H., BODIPY-Based Molecular Probe for Imaging of Cerebral  $\beta$ -Amyloid Plaques, *ACS Chem. Neurosci.* **3** (2012) 319–324, <https://doi.org/10.1021/cn3000058>.
- [71] Kang, J.; Huo, F.; Ning, P.; Meng, X.; Chao, J.; and Yin, C., Two red-emission single and double ‘arms’ fluorescent materials stemmed from ‘one-pot’ reaction for hydrogen sulfide vivo imaging, *Sens. Actuators B Chem.* **250** (2017) 342–350, <https://doi.org/10.1016/j.snb.2017.04.180>.
- [72] Verwilt, P.; Kim, H.-R.; Seo, J.; Sohn, N.-W.; Cha, S.-Y.; Kim, Y. et al., Rational Design of *in Vivo* Tau Tangle-Selective Near-Infrared Fluorophores: Expanding the BODIPY Universe, *J. Am. Chem. Soc.* **139** (2017) 13393–13403, <https://doi.org/10.1021/jacs.7b05878>.
- [73] Ni, Y.; Kannadorai, R. K.; Yu, S. W.-K.; Chang, Y.-T.; and Wu, J., Push–pull type meso-ester substituted BODIPY near-infrared dyes as contrast agents for photoacoustic imaging, *Org. Biomol. Chem.* **15** (2017) 4531–4535, <https://doi.org/10.1039/C7OB00965H>.
- [74] Kue, C. S.; Ng, S. Y.; Voon, S. H.; Kamkaew, A.; Chung, L. Y.; Kiew, L. V. et al., Recent strategies to improve boron dipyrromethene (BODIPY) for photodynamic cancer therapy: an updated review, *Photochem. Photobiol. Sci.* (2018) <https://doi.org/10.1039/C8PP00113H>.
- [75] Lu, H.; Mack, J.; Yang, Y.; and Shen, Z., Structural modification strategies for the rational design of red/NIR region BODIPYs, *Chem Soc Rev* **43** (2014) 4778–4823, <https://doi.org/10.1039/C4CS00030G>.
- [76] Dubach, J. M.; Vinegoni, C.; Mazitschek, R.; Fumene Feruglio, P.; Cameron, L. A.; and Weissleder, R., In vivo imaging of specific drug–target binding at subcellular resolution, *Nat. Commun.* **5** (2014) <https://doi.org/10.1038/ncomms4946>.
- [77] THERANOSTICS an emerging tool in drug discovery and commercialisation, <http://www.ddw-online.com/personalised-medicine/p148484-theranostics-an-emerging-tool-in-drug-discovery-and-commercialisation-fall-02.html>, accessed 05/11/2018.
- [78] Funkhouser, J., Reintroducing pharma: Theranostic Revolution, *Current Drugs Discov* **2** (2002) 17–19,.
- [79] Armstrong-Gordon, E.; Gnjidic, D.; McLachlan, A. J.; Hosseini, B.; Grant, A.; Beale, P. J. et al., Patterns of platinum drug use in an acute care setting: a retrospective study, *J. Cancer Res. Clin. Oncol.* (2018) 1–8, <https://doi.org/10.1007/s00432-018-2669-6>.
- [80] Rosenberg, B.; Van Camp, L.; and Krigas, T., Inhibition of Cell Division in *Escherichia coli* by Electrolysis Products from a Platinum Electrode, *Nature* **205** (1965) 698–699, <https://doi.org/10.1038/205698a0>.
- [81] Chabner, B. A., Barnett Rosenberg: In Memoriam (1924–2009), *Cancer Res.* **70** (2010) 428–429, <https://doi.org/10.1158/0008-5472.CAN-09-4146>.
- [82] Cisplatin - Drug Information - Chemocare, <https://chemocare.com/chemotherapy/drug-info/cisplatin.aspx>, accessed 05/24/2018.

- [83] Shen, D.-W.; Pouliot, L. M.; Hall, M. D.; and Gottesman, M. M., Cisplatin Resistance: A Cellular Self-Defense Mechanism Resulting from Multiple Epigenetic and Genetic Changes, *Pharmacol. Rev.* **64** (2012) 706–721, <https://doi.org/10.1124/pr.111.005637>.
- [84] Heffeter, P.; Jungwirth, U.; Jakupec, M.; Hartinger, C.; Galanski, M.; Elbling, L. et al., Resistance against novel anticancer metal compounds: Differences and similarities, *Drug Resist. Updat.* **11** (2008) 1–16, <https://doi.org/10.1016/j.drug.2008.02.002>.
- [85] Muhammad, N. and Guo, Z., Metal-based anticancer chemotherapeutic agents, *Curr. Opin. Chem. Biol.* **19** (2014) 144–153, <https://doi.org/10.1016/j.cbpa.2014.02.003>.
- [86] Bruijninx, P. C. A. and Sadler, P. J., 'New Trends for Metal Complexes with Anticancer Activity,' *Curr. Opin. Chem. Biol.* **12** (2008) 197–206, <https://doi.org/10.1016/j.cbpa.2007.11.013>.
- [87] Ndagi, U.; Mhlongo, N.; and Soliman, M. E., Metal complexes in cancer therapy – an update from drug design perspective, *Drug Des. Devel. Ther.* **11** (2017) 599–616, <https://doi.org/10.2147/DDDT.S119488>.
- [88] Santini, C.; Pellei, M.; Gandin, V.; Porchia, M.; Tisato, F.; and Marzano, C., Advances in Copper Complexes as Anticancer Agents, *Chem. Rev.* **114** (2014) 815–862, <https://doi.org/10.1021/cr400135x>.
- [89] Sun, T.; Guan, X.; Zheng, M.; Jing, X.; and Xie, Z., Mitochondria-Localized Fluorescent BODIPY-Platinum Conjugate, *ACS Med. Chem. Lett.* **6** (2015) 430–433, <https://doi.org/10.1021/acsmchemlett.5b00041>.
- [90] Tasan, S.; Zava, O.; Bertrand, B.; Bernhard, C.; Goze, C.; Picquet, M. et al., BODIPY–phosphane as a versatile tool for easy access to new metal-based theranostics, *Dalton Trans* **42** (2013) 6102–6109, <https://doi.org/10.1039/C2DT32055J>.
- [91] Doulain, P.-E.; Décréau, R.; Racœur, C.; Goncalves, V.; Dubrez, L.; Bettaieb, A. et al., Towards the elaboration of new gold-based optical theranostics, *Dalton Trans.* **44** (2015) 4874–4883, <https://doi.org/10.1039/C4DT02977A>.
- [92] Zimbron, J. M.; Passador, K.; Gatin-Fraudet, B.; Bachelet, C.-M.; Plažuk, D.; Chamoreau, L.-M. et al., Synthesis, Photophysical Properties, and Living Cell Imaging of Theranostic Half-Sandwich Iridium–4,4-Difluoro-4-bora-3 *a*, 4 *a* -diazas-indacene (BODIPY) Dyads, *Organometallics* **36** (2017) 3435–3442, <https://doi.org/10.1021/acs.organomet.7b00250>.
- [93] Florès, O.; Trommenschlager, A.; Amor, S.; Marques, F.; Silva, F.; Gano, L. et al., In vitro and in vivo trackable titanocene-based complexes using optical imaging or SPECT, *Dalton Trans.* **46** (2017) 14548–14555, <https://doi.org/10.1039/C7DT01981E>.
- [94] Bhattacharyya, A.; Dixit, A.; Mitra, K.; Banerjee, S.; Karande, A. A.; and Chakravarty, A. R., BODIPY appended copper( II ) complexes of curcumin showing mitochondria targeted remarkable photocytotoxicity in visible light, *MedChemComm* **6** (2015) 846–851, <https://doi.org/10.1039/C4MD00425F>.
- [95] Bertrand, B.; Passador, K.; Goze, C.; Denat, F.; Bodio, E.; and Salmain, M., Metal-based BODIPY derivatives as multimodal tools for life sciences, *Coord. Chem. Rev.* **358** (2018) 108–124, <https://doi.org/10.1016/j.ccr.2017.12.007>.
- [96] Kue, C. S.; Ng, S. Y.; Voon, S. H.; Kamkaew, A.; Chung, L. Y.; Kiew, L. V. et al., Recent strategies to improve boron dipyrromethene (BODIPY) for photodynamic cancer therapy: an updated review, *Photochem. Photobiol. Sci.* (2018) <https://doi.org/10.1039/C8PP00113H>.
- [97] Sparey, T. J. and Harrison, T., Inverse electron demand Diels-Alder reactions of 3,6-dichloro-[1,2,4,5]tetrazine, *Tetrahedron Lett.* **39** (1998) 5873–5874, [https://doi.org/10.1016/S0040-4039\(98\)01186-1](https://doi.org/10.1016/S0040-4039(98)01186-1).

## References

- [98] Kumar, A.; Zhang, S.; Hao, G.; Hassan, G.; Ramezani, S.; Sagiya, K. et al., Molecular Platform for Design and Synthesis of Targeted Dual-Modality Imaging Probes, *Bioconjug. Chem.* **26** (2015) 549–558, <https://doi.org/10.1021/acs.bioconjchem.5b00028>.
- [99] Meimetis, L. G.; Boros, E.; Carlson, J. C.; Ran, C.; Caravan, P.; and Weissleder, R., Bioorthogonal Fluorophore Linked DFO—Technology Enabling Facile Chelator Quantification and Multimodal Imaging of Antibodies, *Bioconjug. Chem.* **27** (2016) 257–263, <https://doi.org/10.1021/acs.bioconjchem.5b00630>.
- [100] Grimm, J. B.; Gruber, T. D.; Ortiz, G.; Brown, T. A.; and Lavis, L. D., Virginia Orange: A Versatile, Red-Shifted Fluorescein Scaffold for Single- and Dual-Input Fluorogenic Probes, *Bioconjug. Chem.* **27** (2016) 474–480, <https://doi.org/10.1021/acs.bioconjchem.5b00566>.
- [101] Starkey, J. R.; Rebane, A. K.; Drobizhev, M. A.; Meng, F.; Gong, A.; Elliott, A. et al., New Two-Photon Activated Photodynamic Therapy Sensitizers Induce Xenograft Tumor Regressions after Near-IR Laser Treatment through the Body of the Host Mouse, *Clin. Cancer Res.* **14** (2008) 6564–6573, <https://doi.org/10.1158/1078-0432.CCR-07-4162>.
- [102] Trommenschlager, A.; Chotard, F.; Bertrand, B.; Amor, S.; Dondaine, L.; Picquet, M. et al., Gold(I)–BODIPY–imidazole bimetallic complexes as new potential anti-inflammatory and anticancer trackable agents, *Dalton Trans.* **46** (2017) 8051–8056, <https://doi.org/10.1039/C7DT01377A>.
- [103] Rohand, T.; Baruah, M.; Qin, W.; Boens, N.; and Dehaen, W., Functionalisation of fluorescent BODIPY dyes by nucleophilic substitution, *Chem Commun* (2006) 266–268, <https://doi.org/10.1039/B512756D>.
- [104] Treibs, A. and Kreuzer, F.-H., Difluoroboryl-Komplexe von Di- und Tripyrrylmethenen, *Justus Liebigs Ann. Chem.* **718** (1968) 208–223, <https://doi.org/10.1002/jlac.19687180119>.
- [105] Tram, K.; Yan, H.; Jenkins, H. A.; Vassiliev, S.; and Bruce, D., The synthesis and crystal structure of unsubstituted 4,4-difluoro-4-bora-3a,4a-diaza-s-indacene (BODIPY), *Dyes Pigments* **82** (2009) 392–395, <https://doi.org/10.1016/j.dyepig.2009.03.001>.
- [106] Arroyo, I. J.; Hu, R.; Merino, G.; Tang, B. Z.; and Peña-Cabrera, E., The Smallest and One of the Brightest. Efficient Preparation and Optical Description of the Parent Borondipyrromethene System, *J. Org. Chem.* **74** (2009) 5719–5722, <https://doi.org/10.1021/jo901014w>.
- [107] Schmitt, A.; Hinkeldey, B.; Wild, M.; and Jung, G., Synthesis of the Core Compound of the BODIPY Dye Class: 4,4'-Difluoro-4-bora-(3a,4a)-diaza-s-indacene, *J. Fluoresc.* **19** (2009) 755–758, <https://doi.org/10.1007/s10895-008-0446-7>.
- [108] Wu, L. and Burgess, K., A new synthesis of symmetric boraindacene (BODIPY) dyes, *Chem. Commun.* (2008) 4933, <https://doi.org/10.1039/b810503k>.
- [109] Boens, N.; Verbelen, B.; and Dehaen, W., Postfunctionalization of the BODIPY Core: Synthesis and Spectroscopy: Postfunctionalization of the BODIPY Core, *Eur. J. Org. Chem.* **2015** (2015) 6577–6595, <https://doi.org/10.1002/ejoc.201500682>.
- [110] Brellier, M.; Duportail, G.; and Baati, R., Convenient synthesis of water-soluble nitrilotriacetic acid (NTA) BODIPY dyes, *Tetrahedron Lett.* **51** (2010) 1269–1272, <https://doi.org/10.1016/j.tetlet.2009.12.126>.
- [111] Tomasulo, M.; Deniz, E.; Alvarado, R. J.; and Raymo, F. M., Photoswitchable Fluorescent Assemblies Based on Hydrophilic BODIPY–Spiropyran Conjugates, *J. Phys. Chem. C* **112** (2008) 8038–8045, <https://doi.org/10.1021/jp8009035>.

- [112] Schoenberg, A.; Bartoletti, I.; and Heck, R. F., Palladium-catalyzed carboalkoxylation of aryl, benzyl, and vinylic halides, *J. Org. Chem.* **39** (1974) 3318–3326, <https://doi.org/10.1021/jo00937a003>.
- [113] Kumaresan, D.; Thummel, R. P.; Bura, T.; Ulrich, G.; and Ziessel, R., Color Tuning in New Metal-Free Organic Sensitizers (Bodipys) for Dye-Sensitized Solar Cells, *Chem. – Eur. J.* **15** (2009) 6335–6339, <https://doi.org/10.1002/chem.200900518>.
- [114] Niu, S. L.; Ulrich, G.; Ziessel, R.; Kiss, A.; Renard, P.-Y.; and Romieu, A., Water-Soluble BODIPY Derivatives, *Org. Lett.* **11** (2009) 2049–2052, <https://doi.org/10.1021/ol900302n>.
- [115] Lhenry, D.; Larrouy, M.; Bernhard, C.; Goncalves, V.; Raguin, O.; Provent, P. et al., BODIPY: A Highly Versatile Platform for the Design of Bimodal Imaging Probes, *Chem. – Eur. J.* **21** (2015) 13091–13099, <https://doi.org/10.1002/chem.201501676>.
- [116] Haugland, R. P. and Kang, H. C., Chemically reactive dipyrrometheneboron difluoride dyes, Patent US4774339A, (1988).
- [117] Kang, H. C. and Haugland, R. P., Ethenyl-substituted dipyrrometheneboron difluoride dyes and their synthesis, Patent US5187288A, (1993).
- [118] Monsma, F. J.; Barton, A. C.; Kang, H. C.; Brassard, D. L.; Haugland, R. P.; and Sibley, D. R., Characterization of Novel Fluorescent Ligands with High Affinity for D1 and D2 Dopaminergic Receptors, *J. Neurochem.* **52** (1989) 1641–1644, <https://doi.org/10.1111/j.1471-4159.1989.tb09220.x>.
- [119] BODIPY Dye Series—Section 1.4 - FR, <https://www.thermofisher.com/fr/fr/home/references/molecular-probes-the-handbook/fluorophores-and-their-amine-reactive-derivatives/bodipy-dye-series.html>, accessed 05/30/2018.
- [120] Chen, T.; Boyer, J. H.; and Trudell, M. L., Synthesis of 2,6-diethyl-3-methacroyloxymethyl-1,5,7,8-tetramethylpyrromethene-BF<sub>2</sub> for the preparation of new solid-state laser dyes, *Heteroat. Chem.* **8** (1997) 51–54, [https://doi.org/10.1002/\(SICI\)1098-1071\(1997\)8:1<51::AID-HC7>3.0.CO;2-5](https://doi.org/10.1002/(SICI)1098-1071(1997)8:1<51::AID-HC7>3.0.CO;2-5).
- [121] Ulrich, G.; Ziessel, R.; and Haefele, A., A General Synthetic Route to 3,5-Substituted Boron Dipyrromethenes: Applications and Properties, *J. Org. Chem.* **77** (2012) 4298–4311, <https://doi.org/10.1021/jo3002408>.
- [122] Sathyamoorthi, G.; Wolford, L. T.; Haag, A. M.; and Boyer, J. H., Selective side-chain oxidation of peralkylated pyrromethene-BF<sub>2</sub> complexes, *Heteroat. Chem.* **5** (n.d.) 245–249, <https://doi.org/10.1002/hc.520050309>.
- [123] Yang, L.; Liao, D.-J.; Wu, A.; and Yan, H., Synthesis and fluorescent properties of azacrown ether tethered BODIPY fluorophores, *Tetrahedron Lett.* **58** (2017) 889–891, <https://doi.org/10.1016/j.tetlet.2017.01.058>.
- [124] Coskun, A. and Akkaya, E. U., Ion Sensing Coupled to Resonance Energy Transfer: A Highly Selective and Sensitive Ratiometric Fluorescent Chemosensor for Ag(I) by a Modular Approach, *J. Am. Chem. Soc.* **127** (2005) 10464–10465, <https://doi.org/10.1021/ja052574f>.
- [125] Dost, Z.; Atilgan, S.; and Akkaya, E. U., Distyryl-boradiazaindacenes: facile synthesis of novel near IR emitting fluorophores, *Tetrahedron* **62** (2006) 8484–8488, <https://doi.org/10.1016/j.tet.2006.06.082>.
- [126] Yu, Y.-H.; Descalzo, A. B.; Shen, Z.; Röhr, H.; Liu, Q.; Wang, Y.-W. et al., Mono- and Di(dimethylamino)styryl-Substituted Borondipyrromethene and Borondiindomethene Dyes with Intense Near-Infrared Fluorescence, *Chem. – Asian J.* **1** (2006) 176–187, <https://doi.org/10.1002/asia.200600042>.

## References

---

- [127] Lin, Q.; Gruskos, J. J.; and Buccella, D., Bright, red emitting fluorescent sensor for intracellular imaging of Mg <sup>2+</sup>, *Org. Biomol. Chem.* **14** (2016) 11381–11388, <https://doi.org/10.1039/C6OB02177H>.
- [128] Bozdemir, O. A.; Guliyev, R.; Buyukcakir, O.; Selcuk, S.; Kolemen, S.; Gulseren, G. et al., Selective Manipulation of ICT and PET Processes in Styryl-Bodipy Derivatives: Applications in Molecular Logic and Fluorescence Sensing of Metal Ions, *J. Am. Chem. Soc.* **132** (2010) 8029–8036, <https://doi.org/10.1021/ja1008163>.
- [129] Lin, Q. and Buccella, D., Highly selective, red emitting BODIPY-based fluorescent indicators for intracellular Mg <sup>2+</sup> imaging, *J. Mater. Chem. B* (2018) <https://doi.org/10.1039/C8TB01599F>.
- [130] Sozmen, F.; Kolemen, S.; Kumada, H.-O.; Ono, M.; Saji, H.; and Akkaya, E. U., Designing BODIPY-based probes for fluorescence imaging of  $\beta$ -amyloid plaques, *RSC Adv* **4** (2014) 51032–51037, <https://doi.org/10.1039/C4RA07754G>.
- [131] Mani, V.; Krishnakumar, V. G.; Gupta, S.; Mori, S.; and Gupta, I., Synthesis and characterization of styryl-BODIPY derivatives for monitoring in vitro Tau aggregation, *Sens. Actuators B Chem.* **244** (2017) 673–683, <https://doi.org/10.1016/j.snb.2016.12.104>.
- [132] Maindron, N.; Ipuy, M.; Bernhard, C.; Lhenry, D.; Moreau, M.; Carme, S. et al., Near-Infrared-Emitting BODIPY-trisDOTA <sup>111</sup>In as a Monomolecular Multifunctional Imaging Probe: From Synthesis to In Vivo Investigations, *Chem. - Eur. J.* **22** (2016) 12670–12674, <https://doi.org/10.1002/chem.201602886>.
- [133] Gilow, H. M. and Burton, D. E., Bromination and chlorination of pyrrole and some reactive 1-substituted pyrroles, *J. Org. Chem.* **46** (1981) 2221–2225, <https://doi.org/10.1021/jo00324a005>.
- [134] Lakshmi, V. and Ravikanth, M., Brominated boron dipyrrens: synthesis, structure, spectral and electrochemical properties, *Dalton Trans.* **41** (2012) 5903, <https://doi.org/10.1039/c2dt00019a>.
- [135] Feng, Z.; Jiao, L.; Feng, Y.; Yu, C.; Chen, N.; Wei, Y. et al., Regioselective and Stepwise Syntheses of Functionalized BODIPY Dyes through Palladium-Catalyzed Cross-Coupling Reactions and Direct C–H Arylations, *J. Org. Chem.* **81** (2016) 6281–6291, <https://doi.org/10.1021/acs.joc.6b00858>.
- [136] Duran-Sampedro, G.; Agarrabeitia, A. R.; Garcia-Moreno, I.; Costela, A.; Bañuelos, J.; Arbeloa, T. et al., Chlorinated BODIPYs: Surprisingly Efficient and Highly Photostable Laser Dyes, *Eur. J. Org. Chem.* **2012** (2012) 6335–6350, <https://doi.org/10.1002/ejoc.201200946>.
- [137] Leen, V.; Leemans, T.; Boens, N.; and Dehaen, W., 2- and 3-Monohalogenated BODIPY Dyes and Their Functionalized Analogues: Synthesis and Spectroscopy, *Eur. J. Org. Chem.* **2011** (2011) 4386–4396, <https://doi.org/10.1002/ejoc.201100324>.
- [138] Mirri, G.; Schoenmakers, D. C.; Kouwer, P. H. J.; Veranič, P.; Mušević, I.; and Štefane, B., Synthesis of Functional Fluorescent BODIPY-based Dyes through Electrophilic Aromatic Substitution: Straightforward Approach towards Customized Fluorescent Probes, *ChemistryOpen* **5** (2016) 450–454, <https://doi.org/10.1002/open.201600067>.
- [139] Li, L.; Nguyen, B.; and Burgess, K., Functionalization of the 4,4-difluoro-4-bora-3a,4a-diaza-s-indacene (BODIPY) core, *Bioorg. Med. Chem. Lett.* **18** (2008) 3112–3116, <https://doi.org/10.1016/j.bmcl.2007.10.103>.
- [140] Climent, E.; Biyikal, M.; Gawlitza, K.; Dropa, T.; Urban, M.; Costero, A. M. et al., A Rapid and Sensitive Strip-Based Quick Test for Nerve Agents Tabun, Sarin, and Soman Using BODIPY-Modified Silica Materials, *Chem. – Eur. J.* **22** (2016) 11138–11142, <https://doi.org/10.1002/chem.201601269>.

- [141] Gong, D.; Zhu, X.; Tian, Y.; Han, S.-C.; Deng, M.; Iqbal, A. et al., A Phenylselenium-Substituted BODIPY Fluorescent Turn-off Probe for Fluorescence Imaging of Hydrogen Sulfide in Living Cells, *Anal. Chem.* **89** (2017) 1801–1807, <https://doi.org/10.1021/acs.analchem.6b04114>.
- [142] Liu, X.-L.; Niu, L.-Y.; Chen, Y.-Z.; Zheng, M.-L.; Yang, Y.; and Yang, Q.-Z., A mitochondria-targeting fluorescent probe for the selective detection of glutathione in living cells, *Org. Biomol. Chem.* **15** (2017) 1072–1075, <https://doi.org/10.1039/C6OB02407F>.
- [143] Volkova, Y. A.; Brizet, B.; Harvey, P. D.; Averin, A. D.; Goze, C.; and Denat, F., BODIPY Dyes Functionalized with Pendant Cyclic and Acyclic Polyamines, *Eur. J. Org. Chem.* **2013** (2013) 4270–4279, <https://doi.org/10.1002/ejoc.201300414>.
- [144] Ali, M.; Dondaine, L.; Adolle, A.; Sampaio, C.; Chotard, F.; Richard, P. et al., Anticancer Agents: Does a Phosphonium Behave Like a Gold(I) Phosphine Complex? Let a “Smart” Probe Answer!, *J. Med. Chem.* **58** (2015) 4521–4528, <https://doi.org/10.1021/acs.jmedchem.5b00480>.
- [145] Dondaine, L.; Escudero, D.; Ali, M.; Richard, P.; Denat, F.; Bettaieb, A. et al., Coumarin-Phosphine-Based Smart Probes for Tracking Biologically Relevant Metal Complexes: From Theoretical to Biological Investigations, *Eur. J. Inorg. Chem.* **2016** (2016) 545–553, <https://doi.org/10.1002/ejic.201501304>.
- [146] Kean, W. F.; Hart, L.; and Buchanan, W. W., Auranofin, *Rheumatology* **36** (1997) 560–572, <https://doi.org/10.1093/rheumatology/36.5.560>.
- [147] WHO Drug Information, *WHO Drug Inf.* **2** (1988) 1–59,.
- [148] Huang, R.; Southall, N.; Wang, Y.; Yasgar, A.; Shinn, P.; Jadhav, A. et al., The NCGC Pharmaceutical Collection: A comprehensive resource of clinically approved drugs enabling repurposing and chemical genomics, *Sci. Transl. Med.* **3** (2011) 80ps16, <https://doi.org/10.1126/scitranslmed.3001862>.
- [149] Roder, C. and Thomson, M. J., Auranofin: Repurposing an Old Drug for a Golden New Age, *Drugs RD* **15** (2015) 13–20, <https://doi.org/10.1007/s40268-015-0083-y>.
- [150] Wiberg, N.; Holleman, A. F.; Wiberg, E.; and Fischer, G., "*Lehrbuch der Anorganischen Chemie*", 102., stark umgearb. u. verb., De Gruyter, Berlin New York, (2007).
- [151] Pearson, R. G., in ed. Scott, A. F., Hard and Soft Acids and Bases, *Surv. Prog. Chem.*, Elsevier, (1969), pp. 1–52.
- [152] Wu, C.-Y.; Horibe, T.; Jacobsen, C. B.; and Toste, F. D., Stable gold(III) catalysts by oxidative addition of a carbon–carbon bond, *Nature* **517** (2015) 449–454, <https://doi.org/10.1038/nature14104>.
- [153] Lewis, G. and Shaw, C. F., Competition of thiols and cyanide for gold(I), *Inorg. Chem.* **25** (1986) 58–62, <https://doi.org/10.1021/ic00221a016>.
- [154] Berthon, G., Critical evaluation of the stability constants of metal complexes of amino acids with polar side chains (Technical Report), *Pure Appl. Chem.* **67** (1995) 1117–1240, <https://doi.org/10.1351/pac199567071117>.
- [155] Kean, W. F.; Hart, L.; and Buchanan, W. W., Auranofin., *Rheumatology* **36** (1997) 560–572, <https://doi.org/10.1093/rheumatology/36.5.560>.
- [156] Teo, R. D.; Gray, H. B.; Lim, P.; Termini, J.; Domeshek, E.; and Gross, Z., A cytotoxic and cytostatic gold(III) corrole, *Chem Commun* **50** (2014) 13789–13792, <https://doi.org/10.1039/C4CC06577H>.
- [157] Che, C.-M.; Sun, R. W.-Y.; Yu, W.-Y.; Ko, C.-B.; Zhu, N.; and Sun, H., Gold(III) porphyrins as a new class of anticancer drugs: cytotoxicity, DNA binding and induction of apoptosis in human cervix epitheloid cancer cells, *Chem. Commun.* (2003) 1718, <https://doi.org/10.1039/b303294a>.

## References

- [158] Madeira, A.; de Almeida, A.; de Graaf, C.; Camps, M.; Zorzano, A.; Moura, T. F. et al., A Gold Coordination Compound as a Chemical Probe to Unravel Aquaporin-7 Function, *ChemBioChem* **15** (2014) 1487–1494, <https://doi.org/10.1002/cbic.201402103>.
- [159] Ribeiro, A. J. M.; Holliday, G. L.; Furnham, N.; Tyzack, J. D.; Ferris, K.; and Thornton, J. M., Mechanism and Catalytic Site Atlas (M-CSA): a database of enzyme reaction mechanisms and active sites, *Nucleic Acids Res.* **46** (2018) D618–D623, <https://doi.org/10.1093/nar/gkx1012>.
- [160] Kumar, S.; Kumar, N.; and Gaur, R. K., AMINO ACID FREQUENCY DISTRIBUTION AT ENZYMATIC ACTIVE SITE, *IIOAB J.* **2** (2011) 23–30.
- [161] Zou, T.; Lum, C. T.; Lok, C.-N.; Zhang, J.-J.; and Che, C.-M., Chemical biology of anticancer gold(III) and gold(I) complexes, *Chem. Soc. Rev.* **44** (2015) 8786–8801, <https://doi.org/10.1039/C5CS00132C>.
- [162] Yeo, C.; Ooi, K.; and Tiekink, E., Gold-Based Medicine: A Paradigm Shift in Anti-Cancer Therapy?, *Molecules* **23** (2018) 1410, <https://doi.org/10.3390/molecules23061410>.
- [163] Bertrand, B.; Williams, M. R. M.; and Bochmann, M., Gold(III) Complexes for Antitumor Applications: An Overview, *Chem. - Eur. J.* **24** (2018) 11840–11851, <https://doi.org/10.1002/chem.201800981>.
- [164] Jain, S.; Hirst, D. G.; and O’Sullivan, J. M., Gold nanoparticles as novel agents for cancer therapy, *Br. J. Radiol.* **85** (2012) 101–113, <https://doi.org/10.1259/bjr/59448833>.
- [165] Tsoli, M.; Kuhn, H.; Brandau, W.; Esche, H.; and Schmid, G., Cellular Uptake and Toxicity of Au<sub>55</sub> Clusters, *Small* **1** (2005) 841–844, <https://doi.org/10.1002/smll.200500104>.
- [166] Shi, P.; Jiang, Q.; Zhao, Y.; Zhang, Y.; Lin, J.; Lin, L. et al., DNA binding properties of novel cytotoxic gold(III) complexes of terpyridine ligands: the impact of steric and electrostatic effects, *JBIC J. Biol. Inorg. Chem.* **11** (2006) 745–752, <https://doi.org/10.1007/s00775-006-0120-y>.
- [167] Ronconi, L.; Marzano, C.; Zanello, P.; Corsini, M.; Miolo, G.; Maccà, C. et al., Gold(III) Dithiocarbamate Derivatives for the Treatment of Cancer: Solution Chemistry, DNA Binding, and Hemolytic Properties, *J. Med. Chem.* **49** (2006) 1648–1657, <https://doi.org/10.1021/jm0509288>.
- [168] Yeo, C. I.; Ooi, K. K.; Akim, A. M.; Ang, K. P.; Fairuz, Z. A.; Halim, S. N. B. A. et al., The influence of R substituents in triphenylphosphinegold(I) carbonimidothioates, Ph<sub>3</sub>PAu[SC(OR)=NPh] (R=Me, Et and iPr), upon in vitro cytotoxicity against the HT-29 colon cancer cell line and upon apoptotic pathways, *J. Inorg. Biochem.* **127** (2013) 24–38, <https://doi.org/10.1016/j.jinorgbio.2013.05.011>.
- [169] Casini, A. and Messori, L., Molecular mechanisms and proposed targets for selected anticancer gold compounds, *Curr. Top. Med. Chem.* **11** (2011) 2647–2660.
- [170] Hatfield, D. L. and Gladyshev, V. N., How Selenium Has Altered Our Understanding of the Genetic Code, *Mol. Cell. Biol.* **22** (2002) 3565–3576, <https://doi.org/10.1128/MCB.22.11.3565-3576.2002>.
- [171] Kuntz, A. N.; Davioud-Charvet, E.; Sayed, A. A.; Califf, L. L.; Dessolin, J.; Arnér, E. S. J. et al., Thioredoxin Glutathione Reductase from *Schistosoma mansoni*: An Essential Parasite Enzyme and a Key Drug Target, *PLoS Med.* **4** (2007) <https://doi.org/10.1371/journal.pmed.0040206>.
- [172] Saccoccia, F.; Angelucci, F.; Boumis, G.; Carotti, D.; Desiato, G.; Miele, A. E. et al., Thioredoxin reductase and its inhibitors, *Curr. Protein Pept. Sci.* **15** (2014) 621–646.
- [173] Conrad, M.; Jakupoglu, C.; Moreno, S. G.; Lippl, S.; Banjac, A.; Schneider, M. et al., Essential Role for Mitochondrial Thioredoxin Reductase in Hematopoiesis, Heart Development, and Heart Function, *Mol. Cell. Biol.* **24** (2004) 9414–9423, <https://doi.org/10.1128/MCB.24.21.9414-9423.2004>.

- [174] Karver, M. R.; Krishnamurthy, D.; Kulkarni, R. A.; Bottini, N.; and Barrios, A. M., Identifying Potent, Selective Protein Tyrosine Phosphatase Inhibitors from a Library of Au(I) Complexes, *J. Med. Chem.* **52** (2009) 6912–6918, <https://doi.org/10.1021/jm901220m>.
- [175] Quero, J.; Cabello, S.; Fuertes, T.; Mármol, I.; Laplaza, R.; Polo, V. et al., Proteasome versus Thioredoxin Reductase Competition as Possible Biological Targets in Antitumor Mixed Thiolate-Dithiocarbamate Gold(III) Complexes, *Inorg. Chem.* **57** (2018) 10832–10845, <https://doi.org/10.1021/acs.inorgchem.8b01464>.
- [176] Martins, A. P.; Ciancetta, A.; de Almeida, A.; Marrone, A.; Re, N.; Soveral, G. et al., Aquaporin Inhibition by Gold(III) Compounds: New Insights, *ChemMedChem* **8** (2013) 1086–1092, <https://doi.org/10.1002/cmdc.201300107>.
- [177] S. Allardyce, C. and J. Dyson, P., Metal-based drugs that break the rules, *Dalton Trans.* **45** (2016) 3201–3209, <https://doi.org/10.1039/C5DT03919C>.
- [178] Bertrand, B.; Stefan, L.; Pirrotta, M.; Monchaud, D.; Bodio, E.; Richard, P. et al., Caffeine-Based Gold(I) N-Heterocyclic Carbenes as Possible Anticancer Agents: Synthesis and Biological Properties, *Inorg. Chem.* **53** (2014) 2296–2303, <https://doi.org/10.1021/ic403011h>.
- [179] Wenzel, M.; Bigaeva, E.; Richard, P.; Le Gendre, P.; Picquet, M.; Casini, A. et al., New heteronuclear gold(I)–platinum(II) complexes with cytotoxic properties: Are two metals better than one?, *J. Inorg. Biochem.* **141** (2014) 10–16, <https://doi.org/10.1016/j.jinorgbio.2014.07.011>.
- [180] Bertrand, B.; Spreckelmeyer, S.; Bodio, E.; Cocco, F.; Picquet, M.; Richard, P. et al., Exploring the potential of gold(III) cyclometallated compounds as cytotoxic agents: variations on the C<sup>N</sup> theme, *Dalton Trans.* **44** (2015) 11911–11918, <https://doi.org/10.1039/C5DT01023C>.
- [181] Bertrand, B.; Bodio, E.; Richard, P.; Picquet, M.; Le Gendre, P.; and Casini, A., Gold(I) N-heterocyclic carbene complexes with an “activable” ester moiety: Possible biological applications, *J. Organomet. Chem.* **775** (2015) 124–129, <https://doi.org/10.1016/j.jorganchem.2014.03.020>.
- [182] Chotard, F.; Dondaine, L.; Balan, C.; Bettaïeb, A.; Paul, C.; Le Gendre, P. et al., Highly antiproliferative neutral Ru(II)-arene phosphine complexes, *New J. Chem.* **42** (2018) 8105–8112, <https://doi.org/10.1039/c7nj04442a>.
- [183] Emeljanenko, D.; Peters, A.; Vitske, V.; Kaifer, E.; and Himmel, H.-J., The First Cyanomethyl Complex of Gold, Synthesized by Reaction of a Au(I) Complex with Acetonitrile in the Presence of a New Guanidine N-Superbase, *Eur. J. Inorg. Chem.* **2010** (2010) 4783–4789, <https://doi.org/10.1002/ejic.201000691>.
- [184] Schmidbaur, H. and Schier, A., A briefing on aurophilicity, *Chem. Soc. Rev.* **37** (2008) 1931, <https://doi.org/10.1039/b708845k>.
- [185] Schmidbaur, H. and Schier, A., Aurophilic interactions as a subject of current research: an up-date, *Chem Soc Rev* **41** (2012) 370–412, <https://doi.org/10.1039/C1CS15182G>.
- [186] Nomiya, K.; Noguchi, R.; Ohsawa, K.; and Tsuda, K., Synthesis and crystal structure of gold(I) complexes with triazole and triphenylphosphine ligands: monomeric complex [Au(1,2,3-L)(PPh<sub>3</sub>)] and dimeric complex [Au(1,2,4-L)(PPh<sub>3</sub>)<sub>2</sub>] (HL = triazole) through an Au–Au bond in the solid state, *J. Chem. Soc. Dalton Trans.* (1998) 4101–4108, <https://doi.org/10.1039/a806283h>.
- [187] Leung, K. H.; Phillips, D. L.; Tse, M.-C.; Che, C.-M.; and Miskowski, V. M., Resonance Raman Investigation of the Au(I)–Au(I) Interaction of the  $1[\delta\sigma^*p\sigma]$  Excited State of Au<sub>2</sub>(dcpm)<sub>2</sub>(ClO<sub>4</sub>)<sub>2</sub> (dcpm = Bis(dicyclohexylphosphine)methane), *J. Am. Chem. Soc.* **121** (1999) 4799–4803, <https://doi.org/10.1021/ja990195e>.

## References

---

- [188] Dorh, N.; Zhu, S.; Dhungana, K. B.; Pati, R.; Luo, F.-T.; Liu, H. et al., BODIPY-Based Fluorescent Probes for Sensing Protein Surface-Hydrophobicity, *Sci. Rep.* **5** (2016) <https://doi.org/10.1038/srep18337>.
- [189] Boens, N.; Qin, W.; Baruah, M.; De Borggraeve, W. M.; Filarowski, A.; Smisdom, N. et al., Rational Design, Synthesis, and Spectroscopic and Photophysical Properties of a Visible-Light-Excitable, Ratiometric, Fluorescent Near-Neutral pH Indicator Based on BODIPY, *Chem. - Eur. J.* **17** (2011) 10924–10934, <https://doi.org/10.1002/chem.201002280>.
- [190] Hong, X.; Wang, Z.; Yang, J.; Zheng, Q.; Zong, S.; Sheng, Y. et al., Silylated BODIPY dyes and their use in dye-encapsulated silica nanoparticles with switchable emitting wavelengths for cellular imaging, *The Analyst* **137** (2012) 4140, <https://doi.org/10.1039/c2an35389j>.
- [191] Obondi, C. O.; Lim, G. N.; Karr, P. A.; Nesterov, V. N.; and D'Souza, F., Photoinduced charge separation in wide-band capturing, multi-modular bis(donor styryl)BODIPY–fullerene systems, *Phys. Chem. Chem. Phys.* **18** (2016) 18187–18200, <https://doi.org/10.1039/C6CP03479A>.
- [192] Fukui, K.; Yonezawa, T.; and Shingu, H., A Molecular Orbital Theory of Reactivity in Aromatic Hydrocarbons, *J. Chem. Phys.* **20** (1952) 722–725, <https://doi.org/10.1063/1.1700523>.
- [193] Zhuo, L.-G.; Liao, W.; and Yu, Z.-X., A Frontier Molecular Orbital Theory Approach to Understanding the Mayr Equation and to Quantifying Nucleophilicity and Electrophilicity by Using HOMO and LUMO Energies, *Asian J. Org. Chem.* **1** (2012) 336–345, <https://doi.org/10.1002/ajoc.201200103>.
- [194] Lincoln, R.; Greene, L. E.; Krumova, K.; Ding, Z.; and Cosa, G., Electronic Excited State Redox Properties for BODIPY Dyes Predicted from Hammett Constants: Estimating the Driving Force of Photoinduced Electron Transfer, *J. Phys. Chem. A* **118** (2014) 10622–10630, <https://doi.org/10.1021/jp5059148>.
- [195] Hansch, C.; Leo, A.; and Taft, R. W., A survey of Hammett substituent constants and resonance and field parameters, *Chem. Rev.* **91** (1991) 165–195, <https://doi.org/10.1021/cr00002a004>.
- [196] Hu, Z.; Sim, Y.; Kon, O. L.; Ng, W. H.; Ribeiro, A. J. M.; Ramos, M. J. et al., Unique Triphenylphosphonium Derivatives for Enhanced Mitochondrial Uptake and Photodynamic Therapy, *Bioconjug. Chem.* **28** (2017) 590–599, <https://doi.org/10.1021/acs.bioconjchem.6b00682>.
- [197] Fischer, M. and Georges, J., Fluorescence quantum yield of rhodamine 6G in ethanol as a function of concentration using thermal lens spectrometry, *Chem. Phys. Lett.* **260** (1996) 115–118, [https://doi.org/10.1016/0009-2614\(96\)00838-X](https://doi.org/10.1016/0009-2614(96)00838-X).
- [198] Varnes, A. W. and Dodson, B., Interactions of Transition-Metal Ions with Photoexcited States of Flavins. Fluorescence Quenching Studies, (n.d.) 5,.
- [199] Wang, P.; Henning, S. M.; and Heber, D., Limitations of MTT and MTS-Based Assays for Measurement of Antiproliferative Activity of Green Tea Polyphenols, *PLoS ONE* **5** (2010) e10202, <https://doi.org/10.1371/journal.pone.0010202>.
- [200] Vermes, I.; Haanen, C.; Steffens-Nakken, H.; and Reutellingsperger, C., A novel assay for apoptosis Flow cytometric detection of phosphatidylserine expression on early apoptotic cells using fluorescein labelled Annexin V, *J. Immunol. Methods* **184** (1995) 39–51, [https://doi.org/10.1016/0022-1759\(95\)00072-I](https://doi.org/10.1016/0022-1759(95)00072-I).
- [201] Galluzzi, L.; Vitale, I.; Abrams, J. M.; Alnemri, E. S.; Baehrecke, E. H.; Blagosklonny, M. V. et al., Molecular definitions of cell death subroutines: recommendations of the

- Nomenclature Committee on Cell Death 2012, *Cell Death Differ.* **19** (2012) 107–120, <https://doi.org/10.1038/cdd.2011.96>.
- [202] Galluzzi, L.; Bravo-San Pedro, J. M.; Vitale, I.; Aaronson, S. A.; Abrams, J. M.; Adam, D. et al., Essential versus accessory aspects of cell death: recommendations of the NCCD 2015, *Cell Death Differ.* **22** (2015) 58–73, <https://doi.org/10.1038/cdd.2014.137>.
- [203] Gamberi, T.; Magherini, F.; Fiaschi, T.; Landini, I.; Massai, L.; Valocchia, E. et al., Proteomic analysis of the cytotoxic effects induced by the organogold(III) complex Aubipyc in cisplatin-resistant A2780 ovarian cancer cells: further evidence for the glycolytic pathway implication, *Mol. Biosyst.* **11** (2015) 1653–1667, <https://doi.org/10.1039/C5MB00008D>.
- [204] Results for “Cell Fractionation Kits” | Abcam: antibodies, proteins, kits..., <https://www.abcam.com/products?selected.researchAreas=Kits%2f+Lysates%2f+Other--Kits--Molecular+Biology+Kits--Cell+Fractionation+Kits>, accessed 09/20/2018.
- [205] Yu, Z.; Huang, Z.; and Lung, M., Subcellular Fractionation of Cultured Human Cell Lines, *BIO-Protoc.* **3** (2013) <https://doi.org/10.21769/BioProtoc.754>.
- [206] Veličković, D. and Anderton, C. R., Mass spectrometry imaging: Towards mapping the elemental and molecular composition of the rhizosphere, *Rhizosphere* **3** (2017) 254–258, <https://doi.org/10.1016/j.rhisph.2017.03.003>.
- [207] Colvin, R. A.; Jin, Q.; Lai, B.; and Kiedrowski, L., Visualizing Metal Content and Intracellular Distribution in Primary Hippocampal Neurons with Synchrotron X-Ray Fluorescence, *PLOS ONE* **11** (2016) e0159582, <https://doi.org/10.1371/journal.pone.0159582>.
- [208] Vasiuta, R. and Plenio, H., Observing Initial Steps in Gold-Catalyzed Alkyne Transformations by Utilizing Bodipy-Tagged Phosphine–Gold Complexes, *Chem. – Eur. J.* **22** (2016) 6353–6360, <https://doi.org/10.1002/chem.201600264>.
- [209] Wada, M.; Ito, S.; Uno, H.; Murashima, T.; Ono, N.; Urano, T. et al., Synthesis and optical properties of a new class of pyromethene–BF<sub>2</sub> complexes fused with rigid bicyclo rings and benzo derivatives, *Tetrahedron Lett.* **42** (2001) 6711–6713, [https://doi.org/10.1016/S0040-4039\(01\)01299-0](https://doi.org/10.1016/S0040-4039(01)01299-0).
- [210] Rogers, M. A. T., 156. 2 : 4-Diarylpyrroles. Part I. Synthesis of 2 : 4-diarylpyrroles and 2 : 2' : 4 : 4'-tetra-arylazadipyrrromethines, *J Chem Soc* **0** (1943) 590–596, <https://doi.org/10.1039/JR9430000590>.
- [211] Rogers, M. a. T., Tetra-arylazadipyrrromethines: a New Class of Synthetic Colouring Matter, *Nature* **151** (1943) 504, <https://doi.org/10.1038/151504a0>.
- [212] Gorman, A.; Killoran, J.; O’Shea, C.; Kenna, T.; Gallagher, W. M.; and O’Shea, D. F., In Vitro Demonstration of the Heavy-Atom Effect for Photodynamic Therapy, *J. Am. Chem. Soc.* **126** (2004) 10619–10631, <https://doi.org/10.1021/ja047649e>.
- [213] Wang, J.; Li, J.; Chen, N.; Wu, Y.; Hao, E.; Wei, Y. et al., Synthesis, structure and properties of thiophene-fused BODIPYs and azaBODIPYs as near-infrared agents, *New J. Chem.* **40** (2016) 5966–5975, <https://doi.org/10.1039/C6NJ01011C>.
- [214] Ge, Y. and O’Shea, D. F., Azadipyrrromethenes: from traditional dye chemistry to leading edge applications, *Chem. Soc. Rev.* **45** (2016) 3846–3864, <https://doi.org/10.1039/C6CS00200E>.
- [215] Jiao, L.; Wu, Y.; Wang, S.; Hu, X.; Zhang, P.; Yu, C. et al., Accessing Near-Infrared-Absorbing BF<sub>2</sub>-Azadipyrrromethenes via a Push–Pull Effect, *J. Org. Chem.* **79** (2014) 1830–1835, <https://doi.org/10.1021/jo402160b>.
- [216] Tasior, M.; Murtagh, J.; Frimannsson, D. O.; McDonnell, S. O.; and O’Shea, D. F., Water-solubilised BF<sub>2</sub>-chelated tetraarylazadipyrrromethenes, *Org Biomol Chem* **8** (2010) 522–525, <https://doi.org/10.1039/B919546G>.

## References

- [217] Daly, H. C.; Sampedro, G.; Bon, C.; Wu, D.; Ismail, G.; Cahill, R. A. et al., BF<sub>2</sub>-azadipyromethene NIR-emissive fluorophores with research and clinical potential, *Eur. J. Med. Chem.* **135** (2017) 392–400, <https://doi.org/10.1016/j.ejmech.2017.04.051>.
- [218] Cheng, M. H. Y.; Maruani, A.; Savoie, H.; Chudasama, V.; and Boyle, R. W., Synthesis of a novel HER2 targeted aza-BODIPY–antibody conjugate: synthesis, photophysical characterisation and *in vitro* evaluation, *Org. Biomol. Chem.* **16** (2018) 1144–1149, <https://doi.org/10.1039/C7OB02957H>.
- [219] Grossi, M.; Morgunova, M.; Cheung, S.; Scholz, D.; Conroy, E.; Terrile, M. et al., Lysosome triggered near-infrared fluorescence imaging of cellular trafficking processes in real time, *Nat. Commun.* **7** (2016) 10855, <https://doi.org/10.1038/ncomms10855>.
- [220] Hu, X.; Zhang, J.; Yu, Z.; Xie, Y.; He, H.; Qi, J. et al., Environment-responsive aza-BODIPY dyes quenching in water as potential probes to visualize the *in vivo* fate of lipid-based nanocarriers, *Nanomedicine Nanotechnol. Biol. Med.* **11** (2015) 1939–1948, <https://doi.org/10.1016/j.nano.2015.06.013>.
- [221] Kim, E.-J.; Bhuniya, S.; Lee, H.; Kim, H. M.; Shin, W. S.; Kim, J. S. et al., *In Vivo* Tracking of Phagocytic Immune Cells Using a Dual Imaging Probe with Gadolinium-Enhanced MRI and Near-Infrared Fluorescence, *ACS Appl. Mater. Interfaces* **8** (2016) 10266–10273, <https://doi.org/10.1021/acsami.6b03344>.
- [222] Lhenry, D., Sondes fluorescentes multifonctionnelles pour le marquage de vecteurs biologiques pour une imagerie bimodale, Université de Bourgogne, (2015).
- [223] Wu, D.; Cheung, S.; Daly, R.; Burke, H.; Scanlan, E. M.; and O’Shea, D. F., Synthesis and Glycoconjugation of an Azido-BF<sub>2</sub>–Azadipyromethene Near-Infrared Fluorochrome, *Eur. J. Org. Chem.* **2014** (2014) 6841–6845, <https://doi.org/10.1002/ejoc.201402960>.
- [224] Jing, X.; Yu, F.; and Chen, L., Visualization of nitroxyl (HNO) *in vivo* via a lysosome-targetable near-infrared fluorescent probe, *Chem Commun* **50** (2014) 14253–14256, <https://doi.org/10.1039/C4CC07561G>.
- [225] Wu, D.; Cheung, S.; Devocelle, M.; Zhang, L.-J.; Chen, Z.-L.; and O’Shea, D. F., Synthesis and assessment of a maleimide functionalized BF<sub>2</sub> azadipyromethene near-infrared fluorochrome, *Chem. Commun.* **51** (2015) 16667–16670, <https://doi.org/10.1039/C5CC06137G>.
- [226] Loudet, A.; Bandichhor, R.; Wu, L.; and Burgess, K., Functionalized BF<sub>2</sub> chelated azadipyromethene dyes, *Tetrahedron* **64** (2008) 3642–3654, <https://doi.org/10.1016/j.tet.2008.01.117>.
- [227] Bhuniya, S.; Lee, M. H.; Jeon, H. M.; Han, J. H.; Lee, J. H.; Park, N. et al., A fluorescence off–on reporter for real time monitoring of gemcitabine delivery to the cancer cells, *Chem. Commun.* **49** (2013) 7141, <https://doi.org/10.1039/c3cc42653j>.
- [228] Clark, J. H., Fluoride ion as a base in organic synthesis, *Chem. Rev.* **80** (1980) 429–452, <https://doi.org/10.1021/cr60327a004>.
- [229] Koniev, O. and Wagner, A., Developments and recent advancements in the field of endogenous amino acid selective bond forming reactions for bioconjugation, *Chem Soc Rev* **44** (2015) 5495–5551, <https://doi.org/10.1039/C5CS00048C>.
- [230] Guo, S.; Ma, L.; Zhao, J.; Küçüköz, B.; Karatay, A.; Hayvali, M. et al., BODIPY triads triplet photosensitizers enhanced with intramolecular resonance energy transfer (RET): broadband visible light absorption and application in photooxidation, *Chem Sci* **5** (2014) 489–500, <https://doi.org/10.1039/C3SC52323C>.
- [231] Murtagh, J.; Frimannsson, D. O.; and O’Shea, D. F., Azide Conjugatable and pH Responsive Near-Infrared Fluorescent Imaging Probes, *Org. Lett.* **11** (2009) 5386–5389, <https://doi.org/10.1021/ol902140v>.

- [232] Gao, M.; Wang, R.; Yu, F.; You, J.; and Chen, L., A near-infrared fluorescent probe for the detection of hydrogen polysulfides biosynthetic pathways in living cells and in vivo, *The Analyst* **140** (2015) 3766–3772, <https://doi.org/10.1039/C4AN02366H>.
- [233] Rousseau, T.; Cravino, A.; Bura, T.; Ulrich, G.; Ziessel, R.; and Roncali, J., BODIPY derivatives as donor materials for bulk heterojunction solar cells, *Chem. Commun.* (2009) 1673, <https://doi.org/10.1039/b822770e>.
- [234] Niu, S.; Massif, C.; Ulrich, G.; Renard, P.-Y.; Romieu, A.; and Ziessel, R., Water-Soluble Red-Emitting Distyryl-Borondipyrromethene (BODIPY) Dyes for Biolabeling, *Chem. – Eur. J.* **18** (2012) 7229–7242, <https://doi.org/10.1002/chem.201103613>.
- [235] Shah, M.; Thangaraj, K.; Soong, M.-L.; Wolford, L. T.; Boyer, J. H.; Politzer, I. R. et al., Pyrromethene-BF<sub>2</sub> complexes as laser dyes:1., *Heteroat. Chem.* **1** (1990) 389–399, <https://doi.org/10.1002/hc.520010507>.
- [236] Li, L.; Han, J.; Nguyen, B.; and Burgess, K., Syntheses and Spectral Properties of Functionalized, Water-Soluble BODIPY Derivatives, *J. Org. Chem.* **73** (2008) 1963–1970, <https://doi.org/10.1021/jo702463f>.
- [237] Tokoro, Y.; Nagai, A.; and Chujo, Y., Nanoparticles via H-aggregation of amphiphilic BODIPY dyes, *Tetrahedron Lett.* **51** (2010) 3451–3454, <https://doi.org/10.1016/j.tetlet.2010.04.120>.
- [238] Brizet, B.; Bernhard, C.; Volkova, Y.; Rousselin, Y.; Harvey, P. D.; Goze, C. et al., Boron functionalization of BODIPY by various alcohols and phenols, *Org. Biomol. Chem.* **11** (2013) 7729, <https://doi.org/10.1039/c3ob41370e>.
- [239] O’Shea, D., Fluorescent near infra-red (nir) dyes, Patent US20120232282A1, (2012).
- [240] Reinhardt, C. J.; Zhou, E. Y.; Jorgensen, M. D.; Partipilo, G.; and Chan, J., A Ratiometric Acoustogenic Probe for *in Vivo* Imaging of Endogenous Nitric Oxide, *J. Am. Chem. Soc.* **140** (2018) 1011–1018, <https://doi.org/10.1021/jacs.7b10783>.
- [241] Wu, D.; Cheung, S.; Daly, R.; Burke, H.; Scanlan, E. M.; and O’Shea, D. F., Synthesis and Glycoconjugation of an Azido-BF<sub>2</sub>-Azadipyrromethene Near-Infrared Fluorochrome: Synthesis and Glycoconjugation of an Azido-BF<sub>2</sub>-Azadipyrromethene, *Eur. J. Org. Chem.* **2014** (2014) 6841–6845, <https://doi.org/10.1002/ejoc.201402960>.
- [242] Kamkaew, A. and Burgess, K., Aza-BODIPY dyes with enhanced hydrophilicity, *Chem. Commun.* **51** (2015) 10664–10667, <https://doi.org/10.1039/C5CC03649F>.
- [243] Bodio, E. and Goze, C., Investigation of B-F substitution on BODIPY and aza-BODIPY dyes: Development of B-O and B-C BODIPYs, *Dyes Pigments* **160** (2019) 700–710, <https://doi.org/10.1016/j.dyepig.2018.08.062>.
- [244] Ulrich, G.; Goze, C.; Guardigli, M.; Roda, A.; and Ziessel, R., Pyrromethene Dialkynyl Borane Complexes for “Cascatelle” Energy Transfer and Protein Labeling, *Angew. Chem.* **117** (2005) 3760–3764, <https://doi.org/10.1002/ange.200500808>.
- [245] Harriman, A.; Izzet, G.; and Ziessel, R., Rapid Energy Transfer in Cascade-Type Bodipy Dyes, *J. Am. Chem. Soc.* **128** (2006) 10868–10875, <https://doi.org/10.1021/ja0631448>.
- [246] Goze, C.; Ulrich, G.; and Ziessel, R., Unusual Fluorescent Monomeric and Dimeric Dialkynyl Dipyrromethene–Borane Complexes, *Org. Lett.* **8** (2006) 4445–4448, <https://doi.org/10.1021/ol061601j>.
- [247] Goze, C.; Ulrich, G.; Mallon, L. J.; Allen, B. D.; Harriman, A.; and Ziessel, R., Synthesis and Photophysical Properties of Borondipyrromethene Dyes Bearing Aryl Substituents at the Boron Center, *J. Am. Chem. Soc.* **128** (2006) 10231–10239, <https://doi.org/10.1021/ja062405a>.
- [248] Ulrich, G.; Goze, C.; Goeb, S.; Retailleau, P.; and Ziessel, R., New fluorescent aryl- or ethynylaryl-boron-substituted indacenes as promising dyes, *New J. Chem.* **30** (2006) 982, <https://doi.org/10.1039/b604830g>.

## References

- [249] Duran-Sampedro, G.; Esnal, I.; Agarrabeitia, A. R.; Bañuelos Prieto, J.; Cerdán, L.; García-Moreno, I. et al., First Highly Efficient and Photostable *E* and *C* Derivatives of 4,4-Difluoro-4-bora-3a,4a-diaza-*s*-indacene (BODIPY) as Dye Lasers in the Liquid Phase, Thin Films, and Solid-State Rods, *Chem. - Eur. J.* **20** (2014) 2646–2653, <https://doi.org/10.1002/chem.201303579>.
- [250] Gabe, Y.; Ueno, T.; Urano, Y.; Kojima, H.; and Nagano, T., Tunable design strategy for fluorescence probes based on 4-substituted BODIPY chromophore: improvement of highly sensitive fluorescence probe for nitric oxide, *Anal. Bioanal. Chem.* **386** (2006) 621–626, <https://doi.org/10.1007/s00216-006-0587-y>.
- [251] Yang, L.; Simionescu, R.; Lough, A.; and Yan, H., Some observations relating to the stability of the BODIPY fluorophore under acidic and basic conditions, *Dyes Pigments* **91** (2011) 264–267, <https://doi.org/10.1016/j.dyepig.2011.03.027>.
- [252] Jiang, X.-D.; Zhang, J.; Furuyama, T.; and Zhao, W., Development of Mono- and Di-AcO Substituted BODIPYs on the Boron Center, *Org. Lett.* **14** (2012) 248–251, <https://doi.org/10.1021/ol2030229>.
- [253] Jiang, X.-D.; Fu, Y.; Zhang, T.; and Zhao, W., Synthesis and properties of NIR aza-BODIPYs with aryl and alkynyl substituents on the boron center, *Tetrahedron Lett.* **53** (2012) 5703–5706, <https://doi.org/10.1016/j.tetlet.2012.08.056>.
- [254] Berhe, S. A.; Rodriguez, M. T.; Park, E.; Nesterov, V. N.; Pan, H.; and Youngblood, W. J., Optoelectronic Tuning of Organoborylazadipyrromethenes via Effective Electronegativity at the Metalloid Center, *Inorg. Chem.* **53** (2014) 2346–2348, <https://doi.org/10.1021/ic402596u>.
- [255] Maligaspe, E.; Pundsack, T. J.; Albert, L. M.; Zatsikha, Y. V.; Solntsev, P. V.; Blank, D. A. et al., Synthesis and Charge-Transfer Dynamics in a Ferrocene-Containing Organoboryl aza-BODIPY Donor–Acceptor Triad with Boron as the Hub, *Inorg. Chem.* **54** (2015) 4167–4174, <https://doi.org/10.1021/acs.inorgchem.5b00494>.
- [256] 陈志坚; 王后臣; 高锋; 刘勇; 刘平; 李芬 et al., Quaternary ammonium salt type water-soluble Aza-BODIPY (Boron Dipyrromethene Dye) and synthesis method, Patent CN106699786A, (2017).
- [257] Mallan, J. M. and Bebb, R. L., Metalations by organolithium compounds, *Chem. Rev.* **69** (1969) 693–755, <https://doi.org/10.1021/cr60261a006>.
- [258] Jones, A. C.; Sanders, A. W.; Bevan, M. J.; and Reich, H. J., Reactivity of Individual Organolithium Aggregates: A RINMR Study of *n*-Butyllithium and 2-Methoxy-6-(methoxymethyl)phenyllithium, *J. Am. Chem. Soc.* **129** (2007) 3492–3493, <https://doi.org/10.1021/ja0689334>.
- [259] Gessner, V. H.; Däschlein, C.; and Strohmann, C., Structure Formation Principles and Reactivity of Organolithium Compounds, *Chem. - Eur. J.* **15** (2009) 3320–3334, <https://doi.org/10.1002/chem.200900041>.
- [260] Ximenis, M.; Bustelo, E.; Algarra, A. G.; Vega, M.; Rotger, C.; Basallote, M. G. et al., Kinetic Analysis and Mechanism of the Hydrolytic Degradation of Squaramides and Squaramic Acids, *J. Org. Chem.* **82** (2017) 2160–2170, <https://doi.org/10.1021/acs.joc.6b02963>.
- [261] Valeur, B. and Berberan-Santos, M. N., "*Molecular fluorescence: principles and applications*", Second edition, Wiley-VCH Verlag GmbH & Co. KGaA, Weinheim, Germany, (2013).
- [262] Pardoll, D. M., The blockade of immune checkpoints in cancer immunotherapy, *Nat. Rev. Cancer* **12** (2012) 252–264, <https://doi.org/10.1038/nrc3239>.

- [263] Kim, R.; Emi, M.; and Tanabe, K., Cancer immunoediting from immune surveillance to immune escape, *Immunology* **121** (2007) 1–14, <https://doi.org/10.1111/j.1365-2567.2007.02587.x>.
- [264] Vesely, M. D.; Kershaw, M. H.; Schreiber, R. D.; and Smyth, M. J., Natural Innate and Adaptive Immunity to Cancer, *Annu. Rev. Immunol.* **29** (2011) 235–271, <https://doi.org/10.1146/annurev-immunol-031210-101324>.
- [265] Sharma, P.; Hu-Lieskovan, S.; Wargo, J. A.; and Ribas, A., Primary, Adaptive, and Acquired Resistance to Cancer Immunotherapy, *Cell* **168** (2017) 707–723, <https://doi.org/10.1016/j.cell.2017.01.017>.
- [266] Hodi, F. S.; O’Day, S. J.; McDermott, D. F.; Weber, R. W.; Sosman, J. A.; Haanen, J. B. et al., Improved Survival with Ipilimumab in Patients with Metastatic Melanoma, *N. Engl. J. Med.* **363** (2010) 711–723, <https://doi.org/10.1056/NEJMoa1003466>.
- [267] Lee, N.; Zakka, L. R.; Mihm, M. C.; and Schatton, T., Tumour-infiltrating lymphocytes in melanoma prognosis and cancer immunotherapy, *Pathology (Phila.)* **48** (2016) 177–187, <https://doi.org/10.1016/j.pathol.2015.12.006>.
- [268] Borghaei, H.; Paz-Ares, L.; Horn, L.; Spigel, D. R.; Steins, M.; Ready, N. E. et al., Nivolumab versus Docetaxel in Advanced Nonsquamous Non–Small-Cell Lung Cancer, *N. Engl. J. Med.* **373** (2015) 1627–1639, <https://doi.org/10.1056/NEJMoa1507643>.
- [269] Thompson, R. H.; Gillett, M. D.; Cheville, J. C.; Lohse, C. M.; Dong, H.; Webster, W. S. et al., Costimulatory B7-H1 in renal cell carcinoma patients: Indicator of tumor aggressiveness and potential therapeutic target, *Proc. Natl. Acad. Sci.* **101** (2004) 17174–17179, <https://doi.org/10.1073/pnas.0406351101>.
- [270] Sun, C.; Mezzadra, R.; and Schumacher, T. N., Regulation and Function of the PD-L1 Checkpoint, *Immunity* **48** (2018) 434–452, <https://doi.org/10.1016/j.immuni.2018.03.014>.
- [271] Brahmer, J. R.; Tykodi, S. S.; Chow, L. Q. M.; Hwu, W.-J.; Topalian, S. L.; Hwu, P. et al., Safety and Activity of Anti–PD-L1 Antibody in Patients with Advanced Cancer, *N. Engl. J. Med.* **366** (2012) 2455–2465, <https://doi.org/10.1056/NEJMoa1200694>.
- [272] Herbst, R. S.; Soria, J.-C.; Kowanetz, M.; Fine, G. D.; Hamid, O.; Gordon, M. S. et al., Predictive correlates of response to the anti-PD-L1 antibody MPDL3280A in cancer patients, *Nature* **515** (2014) 563–567, <https://doi.org/10.1038/nature14011>.
- [273] Robert, C.; Long, G. V.; Brady, B.; Dutriaux, C.; Maio, M.; Mortier, L. et al., Nivolumab in Previously Untreated Melanoma without *BRAF* Mutation, *N. Engl. J. Med.* **372** (2015) 320–330, <https://doi.org/10.1056/NEJMoa1412082>.
- [274] Patel, S. P. and Kurzrock, R., PD-L1 Expression as a Predictive Biomarker in Cancer Immunotherapy, *Mol. Cancer Ther.* **14** (2015) 847–856, <https://doi.org/10.1158/1535-7163.MCT-14-0983>.
- [275] Tang, H. and Fu, Y.-X., Immune Evasion in Tumor’s Own Sweet Way, *Cell Metab.* **27** (2018) 945–946, <https://doi.org/10.1016/j.cmet.2018.03.013>.
- [276] Ogawa, M.; Kosaka, N.; Choyke, P. L.; and Kobayashi, H., H-Type Dimer Formation of Fluorophores: A Mechanism for Activatable, in Vivo Optical Molecular Imaging, *ACS Chem. Biol.* **4** (2009) 535–546, <https://doi.org/10.1021/cb900089j>.
- [277] Castle, J. C.; Loewer, M.; Boegel, S.; de Graaf, J.; Bender, C.; Tadmor, A. D. et al., Immunomic, genomic and transcriptomic characterization of CT26 colorectal carcinoma, *BMC Genomics* **15** (2014) 190, <https://doi.org/10.1186/1471-2164-15-190>.
- [278] 4T1 ATCC<sup>®</sup> CRL-2539<sup>™</sup> Mus musculus mammary gland This tumor i, [https://www.lgcstandards-atcc.org/Products/All/CRL-2539.aspx?geo\\_country=fr](https://www.lgcstandards-atcc.org/Products/All/CRL-2539.aspx?geo_country=fr), accessed 07/06/2018.

## References

---

- [279] Pisoni, D. S.; Todeschini, L.; Borges, A. C. A.; Petzhold, C. L.; Rodembusch, F. S.; and Campo, L. F., Symmetrical and Asymmetrical Cyanine Dyes. Synthesis, Spectral Properties, and BSA Association Study, *J. Org. Chem.* **79** (2014) 5511–5520, <https://doi.org/10.1021/jo500657s>.
- [280] Gut, A.; Łapok, Ł.; Drelinkiewicz, D.; Pędziński, T.; Marciniak, B.; and Nowakowska, M., Visible-Light Photoactive, Highly Efficient Triplet Sensitizers Based on Iodinated Aza-BODIPYs: Synthesis, Photophysics and Redox Properties, *Chem. - Asian J.* **13** (2018) 55–65, <https://doi.org/10.1002/asia.201701485>.
- [281] Chotard, F.; Malacea-Kabbara, R.; Balan, C.; Bodio, E.; Picquet, M.; Richard, P. et al., Atom Transfer Radical Addition Catalyzed by Ruthenium–Arene Complexes Bearing a Hybrid Phosphine–Diene Ligand, *Organometallics* **37** (2018) 812–820, <https://doi.org/10.1021/acs.organomet.7b00851>.
- [282] Frisch, M. .; Trucks, G. W.; Schlegel, H. B.; Scuseria, G. E.; Robb, M. A.; and Cheeseman, J. R., "Gaussian 09. Revision D", Gaussian Inc., Wallingford CT, (2009).
- [283] Zhao, Y. and Truhlar, D. G., The M06 suite of density functionals for main group thermochemistry, thermochemical kinetics, noncovalent interactions, excited states, and transition elements: two new functionals and systematic testing of four M06-class functionals and 12 other functionals, *Theor. Chem. Acc.* **120** (2008) 215–241, <https://doi.org/10.1007/s00214-007-0310-x>.
- [284] Chéron, N.; Jacquemin, D.; and Fleurat-Lessard, P., A qualitative failure of B3LYP for textbook organic reactions, *Phys. Chem. Chem. Phys.* **14** (2012) 7170, <https://doi.org/10.1039/c2cp40438a>.
- [285] Chéron, N.; Ramozzi, R.; Kaïm, L. E.; Grimaud, L.; and Fleurat-Lessard, P., Challenging 50 Years of Established Views on Ugi Reaction: A Theoretical Approach, *J. Org. Chem.* **77** (2012) 1361–1366, <https://doi.org/10.1021/jo2021554>.
- [286] Tomasi, J.; Mennucci, B.; and Cammi, R., Quantum Mechanical Continuum Solvation Models, *Chem. Rev.* **105** (2005) 2999–3094, <https://doi.org/10.1021/cr9904009>.
- [287] Mennucci, B.; Tomasi, J.; Cammi, R.; Cheeseman, J. R.; Frisch, M. J.; Devlin, F. J. et al., Polarizable Continuum Model (PCM) Calculations of Solvent Effects on Optical Rotations of Chiral Molecules, *J. Phys. Chem. A* **106** (2002) 6102–6113, <https://doi.org/10.1021/jp020124t>.
- [288] Chemcraft - Graphical program for visualization of quantum chemistry computations, <https://www.chemcraftprog.com/>, accessed 07/18/2018.

## Table of Figures

Figure 1: 1-year survival vs stage of initial diagnosis for the NHS (UK) from 2012-2014 for selected cancers. Red denominates % survival, blue % of cancers diagnosed at that stage. Figure adapted from [8] .....	17
Figure 2: The Hallmarks of cancer. Adapted from [10].....	18
Figure 3: Attenuation of electromagnetic radiation by biological tissue [13].....	19
Figure 4: The Electromagnetic spectrum. Adapted from [17] .....	22
Figure 5: A Jablonski Diagram of a given optically active system [18] 1- Absorption, 2- Internal Conversion, 3,4-Intersystem crossing, 5-vibrational relaxation, 6-Fluorescence, 7- Phosphorescence .....	23
Figure 6: Double logarithmic plot of absorption coefficients of biological tissues in the UV/Vis - infrared range. The optical therapeutic window is highlighted in orange. Hb: Hemoglobin, HbO <sub>2</sub> : oxygenated hemoglobin. Adapted from [25] .....	25
Figure 7: Plot of brightness vs. emission wavelength for various fluorophores [30] .....	26
Figure 8: Examples for commercial, organelle specific dyes: MitoTracker™ Green specifically labels mitochondria, LysoTracker Red DND-99 fluoresces in acidic organelles (usually Lysosomes), DRAQ5 stains DNA through intercalation; DAPI intercalates into the minor groove of DNA and thus stains the nucleus [31–34].....	26
Figure 9: Multi-color fluorescence in situ hybridization of human chromosomes in the cells nucleus. Top row: untreated images for each channel; arrows indicate channel –bleed through. Bottom: spectrally unmixed channels and overlay of unmixed channels [35]. Except for Cy5 all used dyes are Xanthene-derivates.....	27
Figure 10: Turn-on fluorescent probe for the detection of $\beta$ -Galactosidase activity. Image bottom left: fluorescence image of $\beta$ -Gal negative HeLa cells; bottom right: fluorescence image of $\beta$ -Gal-positive OVCAR-3 cells. Both were incubated with 10 $\mu$ M <b>L1</b> for 40min [38].	27
Figure 11: Some examples for fluorophores or fluorescent motives that are currently used in the clinic or in clinical trials (photophysical data of cyanines taken from [43], Fluorescein from [44], methylene blue from [45]) . n.r.= not reported.....	28
Figure 12: Nomenclature of BODIPYs.....	29
Figure 13: Spectral comparison of the commercial dyes BODIPY-FI(cyan) and Alexa 488 (green) [48] .....	29
Figure 14: Examples for BODIPY based bimodal probes that combine the advantages of BODIPYs in vitro and strengths of PET in vivo: <b>L2</b> [53] <b>L3</b> [55], <b>L4</b> [56].....	30
Figure 15: Examples for BODIPY-use in in vivo studies. <b>L5</b> : on/off-probe for studying osteoclasts in intravital microscopy on mice [57](intravital microscopic image of <b>L5</b> beneath); middle: whole body imaging in mice to track anti-Chagas agent <b>L6</b> in vivo [58] (whole body mice images of <b>L6</b> beneath; left mouse 120min p.i. with <b>L6</b> -vesicle emulsion, middle mouse 120min p.i. with <b>L6</b> -DMSO/H <sub>2</sub> O-solution, right mouse: control mouse injected with PBS). <b>L7</b> : selective in vivo detection of H <sub>2</sub> O <sub>2</sub> in angelfish [59] .....	30
Figure 16: Fine-tuning of optical properties BODIPYs by Knoevenagel reaction. Photophysical data for <b>L8</b> in EtOH [66], styrylBODIPYs <b>L9-L12</b> in CHCl <sub>3</sub> [65] .....	31
Figure 17: Fluorescence anisotropy imaging of a BODIPY-Biotin derivate ( <b>L13</b> ). Binding of <b>L13</b> reduces molecular movement which results in increased fluorescence anisotropy. Green: unbound fluorophore, red: bound fluorophore [74].....	32
Figure 18: Some Platinum-based drugs that are currently used in therapy or in clinical trials [83] .....	33

## Table of Figures

---

Figure 19: Some lead-motives of therapeutically active metals other than Platinum that are currently in clinical trials [83,85] or showing interesting in vivo activity [86] .....	33
Figure 20: Examples of BODIPY theranostics that have been developed using the leads of Figure 19. Pt-BODIPY [87], BODI-Ru-0 [88], BODI-Au-2 [89], IrBODIPY[90], BODI-Ti-1 [91], Cu-Curcumin-BODIPY for PDT [92] .....	34
Figure 21: Influence of trackable moiety on cellular localization [93]. Cellular localizations: CP-Au-1: raft domains; MC-Bio-Au-1: nucleus ; BODI-Au-0: membranes; BODI-Au-1 (in green, DAPI in blue): cytosol ; Porph-Au-2: membranes .....	34
Figure 22: Platform approach .....	36
Figure 23: Examples for molecular platforms [95,96].....	36
Figure 24: rare examples of fluorophores that are used as platforms: BODIPY( <b>L21</b> , top left) [97] Virginia Orange( <b>L23</b> , top right) [98] porphyrin ( <b>L26</b> , bottom) [99].....	37
Figure 25: The multifunctional platform approach.....	41
Figure 26: dichloro-BODIPY - the selected multifunctional platform .....	42
Figure 27: First synthesis of BODIPY-dyes [102] .....	42
Figure 28: Nomenclature of BODIPYs.....	42
Figure 29: General Synthesis of symmetrical BODIPYs .....	43
Figure 30: Synthesis of unsymmetrical BODIPYs.....	43
Figure 31: Accessing symmetric BODIPYs via decarbonylation reaction [106].....	43
Figure 32: Possible functionalizations of the BODIPY-base structure [107] .....	44
Figure 33: Accessing BODIPY-carboxylates via Pd-catalyzed carboalkoxylation [111,112].....	44
Figure 34: Use of BODIPY-carboxylic acid in previous studies from our group [55,88,89]. BBN= Bombesine.....	45
Figure 35: Functionalized BODIPY-dyes by pyrrole decoration [114,116].....	45
Figure 36: Use of $\alpha$ -pyrrolic methyl oxidation of BODIPY to increase solubility [119] .....	46
Figure 37: Accessing styryl and distyryl-BODIPYs by Knoevenagel-reaction. Discovery by Akaya in 2005 ( <b>L44</b> ) [122]. First accounts of distyryl-BODIPY ( <b>L46</b> ) [123,124].....	46
Figure 38: Application of distyryl-trisDOTA-BODIPY <b>L48</b> in molecular imaging [130] .....	47
Figure 39: Substitution order during halogenation. The order of halogenation is shown in black, the IUPAC-conform molecular positions are given in blue. Dipyrromethane is shown on the left, bora-dipyrromethene (BODIPY) on the right .....	47
Figure 40: Nucleophilic aromatic substitutions using a variety of nucleophiles [101] .....	48
Figure 41: Previous uses of BODIPY-Cl <sub>2</sub> <b>1</b> in our group[141,100]. The fluorescence image on the right shows the merged image of BODIPY <b>L50</b> and organelle-stains for colocalization....	48
Figure 42: Structure of Auranofin .....	49
Figure 43: DNA-damaging gold-based agents. <b>L51</b> [164] <b>L52a-e</b> [155], <b>L53</b> [165], <b>L54a,b</b> [166] .....	51
Figure 44: Au(III)-pyridiniums that have been shown to inhibit aquaporines and can interact with zinc-finger enzymes [174] .....	52
Figure 45: Synthesis of dichloro-BODIPY <b>1</b> starting material following established protocols. Synthesis executed by Dr. Martin Ipuay and Dr Julia Volkova following the procedure published in [101] .....	53
Figure 46: Synthesis of gold(I)-amine phosphine <b>3</b> [89] .....	54
Figure 47: Attempt at double substitution of dichloro-BODIPY <b>1</b> using gold(I) amino phosphine <b>3</b> .....	54
Figure 48: <sup>1</sup> H-NMR-spectra of the starting materials gold(I)amino phosphine <b>3</b> (top), BODIPY-Cl <sub>2</sub> <b>1</b> (middle). The bottom <sup>1</sup> H-NMR shows the spectrum obtained for the product that we obtained for the attempted double substitution of dichloro-BODIPY <b>1</b> . All spectra were recorded in CDCl <sub>3</sub> at 300MHz and 300K.....	55

Figure 49: HRMS spectrum of the reaction product of the attempted double substitution of <b>1</b> .....	56
Figure 50: Introduction of Gold(I)-amino phosphine <b>3</b> onto the BODIPY core of <b>1</b> by nucleophilic aromatic substitution in acetonitrile .....	56
Figure 51: Modified reaction conditions for the synthesis of monosubstituted BODIPY.....	57
Figure 52: X-Ray structure of BODIPY <b>4b</b> . The circled part is shown in the bottom right along its B→ meso-C→ meso-phenyl axis (molecule is flipped, view direction is indicated by the arrow). The ellipsoids are drawn at 50% probability level. Hydrogen atoms and solvent molecules are omitted for clarity. The molecule was drawn using CIF data .....	57
Figure 53: <sup>31</sup> P-NMR-spectra of BODIPY <b>4b</b> . Overlay of NMR recorded at different temperatures. The traces are <b>not</b> stacked at an angle or x-offset. The NMR was recorded in DCM-D <sub>2</sub> at 500MHz .....	58
Figure 54: Double substitution of the BODIPY-Cl <sub>2</sub> <b>1</b> with gold(I)-amino phosphine.....	59
Figure 55: Synthesis of BODIPY-Cl <sub>2</sub> acid <b>8</b> .....	60
Figure 56: X-Ray diffraction of dipyrromethene <b>6</b> (left) and BODIPYs <b>7</b> (middle), <b>8</b> (right) ....	61
Figure 57: Synthesis of BODIPY <b>9</b> .....	61
Figure 58: Functionalization of meso-acyl by activation as acyl chloride to synthesize BODIPY <b>10</b> .....	62
Figure 59: Double substitution of BODIPY <b>8</b> with two gold(I)-amino phosphine moieties .....	62
Figure 60: Opening of THF with subsequent chlorination by HCl .....	63
Figure 61: Introduction of thioglucose tetraacetate onto the gold bearing moiety .....	64
Figure 62: Intended reaction (left) and one of the observed products ( <b>14b</b> , right).....	64
Figure 63: Reaction of BODIPY <b>8</b> with thioglucose tetraacetate .....	65
Figure 64: LUMO energies (eV) for some model systems.....	66
Figure 65: Some hypothetical reactions involving the model system .....	67
Figure 66: Monosubstitution of BODIPY-Cl <sub>2</sub> <b>8</b> using HSGLu(OAc) <sub>4</sub> .....	68
Figure 67: Substitution of BODIPY-Cl <sub>2</sub> <b>1</b> with HSGLu(OAc) <sub>4</sub> . Yields are given with regard to BODIPY. Using thioglucose tetraacetate as reference the yields are 44% and 56% respectively .....	68
Figure 68: Secondary substitution of the thioglucose-functionalized BODIPYs .....	69
Figure 69: Attempt at introduction of the gold-bearing moiety onto the carboxylic acid function .....	69
Figure 70: Synthesis of phosphonium <b>22</b> .....	70
Figure 71: Formation of amid between BODIPY-Cl <sub>2</sub> <b>8</b> and phosphonium <b>23</b> and synthesis of BODIPY <b>24</b> .....	70
Figure 72: Introduction of phosphonium <b>22</b> in the 5-position of thioglucose-tetraacetate-substituted BODIPY <b>17</b> .....	71
Figure 73: Introduction of the third substituent.....	71
Figure 74: Analytical RP-HPLC/MS-Chromatogram from purification attempt of <b>26</b> . The first product is continuously formed during semipreparative RP-HPLC purification and corresponds to [ <b>26</b> -Ph]. The shown UV-Channel (top) is recorded at 220nm. ....	72
Figure 75: Simplified depiction of the obtained BODIPYs.....	73
Figure 76: Representative spectra for all obtained BODIPYs. Substitution pattern: top left: Cl/Cl ( <b>8</b> ), top right: Cl/N ( <b>9</b> ), bottom left: Cl/S ( <b>17</b> ), bottom right: S/N ( <b>19</b> ).....	75
Figure 77: Resonance-structures of. Dichloro-substituted BODIPYs show only resonance structure I and II whereas for amine-substituted BODIPYs the nitrogen can participate in the conjugation (III)[141].....	75

## Table of Figures

Figure 78: Interatomic distances in the pyrroles of BODIPY <b>4b</b> . All distances are given in Å. The black rectangle highlights the shown part of the molecule. Hydrogens and solvent molecules are omitted for clarity. Drawn with CIF data .....	76
Figure 79: LUMO-energies of 3 model-BODIPYs. The LUMO-coefficients are shown as blue and orange isosurfaces for each atom. ....	76
Figure 80: IC <sub>50</sub> Values for all tested BODIPYs. For better readability the compounds structures are shown using the simplified depictions introduced in chapter 2.4.1. The values are mean+SD of 3 independent experiments. All values are given in μM and were determined by MTS assay; data treatment was executed using GraphPad Prism 5.0.....	79
Figure 81: Confocal immunofluorescent analysis (merge) of MDA-MB-231 labelled with BODIPY <b>4b</b> . Cells were incubated with 10 μM BODIPY <b>4b</b> (green) for 1, 4 and 24h at 37°C, then fixed, followed by permeabilization with iced methanol. The nuclei are counterstained with DRAQ5 (red, fluorescent DNA dye) .....	80
Figure 82: Confocal immunofluorescent analysis (merge) of MDA-MB-231 labelled with the different BODIPY derivatives. Cells are incubated with 10 μM BODIPY derivatives (green) for 4h at 37°C then fixed, permeabilized with iced methanol. The nuclei are counterstained with DRAQ5 (red, fluorescent DNA dye) .....	81
Figure 83: Influence of gold uptake on IC <sub>50</sub> (for MDA-MB-231). Black dots represent gold-free compounds, red dots compounds carrying 1 gold atom and green dots compounds carrying 2 gold atoms .....	84
Figure 84: Influence of logD on IC <sub>50</sub> (left) and gold uptake (right). Both IC <sub>50</sub> and gold uptake were determined for MDA-MB-231 cells. Black dots are gold-free, red dots represent compounds that contain 1 gold atom, green dots represent compounds with 2 gold atoms	84
Figure 85: Proposition for a phosphine-gold(I) smart-probe. For R=H the molecule has been synthesized by [206].....	88
Figure 86: Absorbance of various tissues and biomolecules in the visible, red/infrared spectrum. The position of optical transparency windows has been added as orientation. Adapted from [25].....	91
Figure 87: Examples for π-extended BODIPYs: isoindoline-based BODIPY by retro-Diels-Alder reaction ( <b>L61</b> , left) by Wada et al. 2001 [207], access to styryl and distyryl-BODIPYs by Knoevenagel-reaction ( <b>L62</b> , middle) by Akaya in 2005 [122] and example for a distyryl-BODIPY carrying polyazamacrocycles developed by our group [130] ( <b>L63</b> , right).....	92
Figure 88: Structure and nomenclature of BODIPYs and azaBODIPYs.....	92
Figure 89: Base-structure of azaBODIPYs.....	93
Figure 90: General synthetic pathways to azaBODIPYs. Left: chalcone based synthetic access to symmetrical azaBODIPY dyes. Right: access to unsymmetrical azaBODIPYs using nitrosylation reactions .....	93
Figure 91: Selection of the first platform molecule (left). Right: commonly employed dihydroxy-azaBODIPY <b>L64</b> [217,216].....	95
Scheme 92: Preparation of azaBODIPY <b>30</b> starting from hydroxy-benzaldehyde and acetophenone .....	95
Figure 93: Envisioned formation of acetic acid ester <b>31</b> by simple nucleophilic substitution using a carbonate source as base .....	96
Figure 94: Principle of activation of aromatic hydroxy groups through CsF.....	96
Figure 95: Optimization of monofunctionalization of <b>30</b> using CsF and tButyl bromoacetic acid. The channel shown is the UV/Vis channel at 625 nm.....	97
Figure 96: Acidic hydrolysis of the t-Butyl ester <b>31</b> .....	98
Figure 97: Introduction of TOTA-Boc using peptide coupling conditions.....	99
Figure 98: Removal of Boc from azaBODIPY <b>33</b> using 3M HCl.....	99

Figure 99: UV/Vis and fluorescence spectra of di(phenol)-azaBODIPY <b>30</b> in DMSO. Blue: Absorption spectrum, Green: excitation, Red: fluorescence Spectrum. Spectra were recorded at $\sim 10^{-6}$ M concentrations .....	100
Figure 100: UV/Vis and Fluorescence spectra of azaBODIPY <b>34</b> . Left: Spectra recorded in DMSO, Right: spectra recorded in PBS. Blue: UV/Vis absorption. Green: Excitation spectra. Red: Fluorescence Emission. Spectra were recorded at $\sim 10^{-6}$ M concentrations .....	101
Figure 101: Reactions of isothiocyanates with nucleophiles that are present in biological media .....	102
Figure 102: Activation of azaBODIPY <b>34</b> using PDITC.....	102
Figure 103: Hydrosolubilization of BODIPY-dyes. <b>L66</b> (top-Left): example for a strategy employing exclusively PEGs [231]. <b>L69</b> (right): an extreme example combining PEGs, sulfobetaines and sulfonated amino acids for hydrosolubilization [232]. <b>L67</b> (bottom left): first example of core-sulfonated BODIPY [233]; <b>L68</b> (bottom middle): example from Li et al. for functionalizable, water soluble core-sulfonated BODIPY-dyes [234] .....	104
Figure 104: example for B-O functionalized BODIPYs for hydrosolubilization purposes. <b>L70</b> (left) [235], <b>L71</b> (middle) and <b>L72</b> (right) examples from our group [236] .....	105
Figure 105: Hydrosolubilization of azaBODIPYs using PEG of small ( <b>L73</b> , left, [237]) and very large ( <b>L74</b> , right, [217]) masses .....	105
Figure 106: Hydrosolubilization of azaBODIPYs through introduction of polar groups such as sulfones ( <b>L75</b> ), carboxylic acids ( <b>L76</b> ) or ammoniums ( <b>L77</b> ) to the periphery of the azaBODIPY [214] .....	105
Figure 107: Hybridic hydrosolubilization strategies that employ various solubility enhancing groups: PEG+ammonium (top left) [238], Sulfone, PEG and various sugars (right) [239] and sulfone and amino acids or short peptide sequences [223] .....	106
Figure 108: B-functionalization of BODIPY using organolithium compounds [242–244].....	107
Figure 109: Hydrosolubilization strategy employed by Niu et al. [112] .....	107
Figure 110: Synthesis of the ammoniumalkyne <b>36</b> .....	108
Figure 111: Synthesis of B-functionalized azaBODIPY <b>37</b> .....	108
Figure 112: Protection of Hydroxy-groups of <b>30</b> using TBDMSCl to obtain <b>38</b> .....	109
Figure 113: Boron functionalization of TBDMS-protected azaBODIPY <b>38</b> .....	109
Figure 114: Color change upon addition of azaBODIPY to the lithium-alkyne. From left to right: Li-alkyne <b>36</b> , dropwise addition of (blue) azaBODIPY <b>38</b> to organolithium solution after 1-4 minutes.....	110
Figure 115: Evolution of HPLC-profiles observed during boron functionalization of TBDMS-protected azaBODIPY <b>38</b> .....	110
Figure 116: O-functionalization of the hydrosoluble azaBODIPY <b>37</b> .....	111
Figure 117: New base compounds for the development of E-azaBODIPY-platforms .....	112
Figure 118: Formation of Michael-adduct <b>42</b> .....	112
Figure 119: Formation of the azadipyrromethene core .....	113
Figure 120: Introduction of the BF <sub>2</sub> -moiety to form the model-compound azaBODIPY <b>44</b> ..	113
Figure 121: Synthesis of Br-MeO functionalized azaBODIPYs <b>48</b> and <b>52</b> .....	114
Figure 122: Comparison of the <sup>1</sup> H-NMR-spectra of the aromatic zone of bromo-methoxy-substituted azaBODIPYs <b>52</b> , <b>48</b> and their comparison to methoxy-azaBODIPY <b>44</b> . The signal of the β-pyrrolic hydrogens are highlighted by flashes. The NMR were recorded in CDCl <sub>3</sub> at 500MHz .....	115
Figure 123: UV/Vis and fluorescence spectra of azaBODIPY <b>44</b> in DMSO. Spectra were recorded at $\sim 10^{-6}$ M concentrations .....	116
Figure 124: Absorption (blue), excitation (green) and emission spectra(red) for ( <b>52</b> , left) and ( <b>48</b> , right) in DMSO. Spectra were recorded at $\sim 10^{-6}$ M concentrations.....	117

## Table of Figures

Figure 125: Comparison of azaBODIPY <b>52</b> (left) and azaBODIPY <b>48</b> in DCM .....	117
Figure 126: Frontier orbitals of aza-BODIPY <b>44</b> [213] .....	117
Figure 127: Fluorescence lifetime measurements of <b>48</b> and <b>52</b> in DCM. Green shows azaBODIPY <b>48</b> (methoxy substituent in the 3,5-phenylic positions), blue azaBODIPY <b>52</b> (methoxy-substituent in the 1,7-phenylic positions). Left: Y-values plotted linearly, right: logarithmic plot. Both graphs show the same data. ....	118
Figure 128: Boron functionalization of azaBODIPY <b>48</b> using organolithium agents.....	119
Figure 129: Improved synthesis of boron-functionalized azaBODIPYs using Grignard-agents .....	119
Figure 130: Desymmetrization of azaBODIPY <b>53</b> using 1 equivalent of bromoacetic acid....	120
Figure 131: <sup>1</sup> H-NMR-spectrum of the successfully desymmetrized azaBODIPY <b>54</b> . The NMR was recorded in CDCl <sub>3</sub> at 500 MHz.....	120
Figure 132: Reaction of azaBODIPY <b>55</b> with benzylamine .....	121
Figure 133: Desymmetrization of azaBODIPY <b>53</b> using 4-(bromomethyl)benzoic acid.....	121
Figure 134: Successful activation of <b>58</b> and conjugation to TOTA-Boc.....	122
Figure 135: Introduction of 3-dimethylamino propyne onto azaBODIPY <b>44</b> .....	122
Figure 136: Desymmetrization of azaBODIPY <b>60</b> by reaction with 4-(bromomethyl)benzoic acid .....	123
Figure 137: Introduction of 4-methyl benzoic acid as handle for further functionalization .	124
Figure 138: Synthesis of Boc-spacer containing azaBODIPY <b>64</b> .....	124
Figure 139: N-quaternization of azaBODIPY <b>64</b> using methyl iodide (top) and propane sultone (bottom) .....	125
Figure 140: Activation of azaBODIPY <b>65</b> using PDITC.....	126
Figure 141: Activation of azaBODIPY <b>65</b> using diethyl squarate to obtain bioconjugable azaBODIPY <b>68</b> .....	127
Figure 142: Activation of azaBODIPY <b>66</b> with diethylsquarate .....	127
Figure 143: Absorption and Emission spectra of <b>30</b> (top left), <b>37</b> (bottom left) and <b>38</b> (top right) in DMSO. Blue: absorption, Green: excitation, Red: fluorescence. Spectra were recorded at 10 <sup>-6</sup> M concentrations .....	129
Figure 144: Absorption and Emission spectra of <b>48</b> (left) and <b>58</b> (right) in DMSO. The spectrum of <b>58</b> (right) is representative for <b>53</b> , <b>54</b> , <b>55</b> and <b>57</b> . Blue: absorption, Green: excitation, Red: fluorescence. Spectra were recorded at ~10 <sup>-6</sup> M concentrations .....	130
Figure 145: UV/Vis and fluorescence spectra of the model compound <b>44</b> and E-azaBODIPY <b>61</b> . The shown spectra are representative for all compounds obtained in this section. Spectra were recorded in DMSO at ~10 <sup>-6</sup> M concentrations .....	131
Figure 146: UV/Vis and Fluorescence spectra of E-azaBODIPY <b>68</b> (left) and azaBODIPY <b>34</b> (right). The spectra were recorded in DMSO (top) and PBS (bottom) at 10 <sup>-6</sup> M concentrations. The spectral shape of E-azaBODIPY <b>68</b> in PBS is representative for all E-azaBODIPYs that we characterized in PBS. ....	132
Figure 147: Activated, water-soluble, ready-to-conjugate azaBODIPYs that were obtained during this thesis .....	133
Figure 148: Mechanism of immunoediting. Adapted from [262].....	134
Figure 149: Mechanism of evading the immune system. Adapted from [263].....	135
Figure 150: Activated, ready-to-conjugate azaBODIPYs that were obtained during this thesis .....	136
Figure 151: General steps involved in bioconjugation: Conjugation, Purification, Buffer-exchange and reconcentration .....	136
Figure 152: Activation of Cyanine 5 as NHS-ester.....	137

Figure 153: UV/Vis spectra of fluorophore and PD-L1-bioconjugates in PBS. Depicted spectra are representative for all obtained azaBODIPY/cyanine-mAb conjugates. Left: azaBODIPY <b>68</b> , right: Cy5, top: fluorophore only, bottom: bioconjugate. Absorption peak at 280nm is caused by the antibody .....	139
Figure 154: The anti-PD-L1 antibodies uncoupled (NC), coupled with cyanine 5 (Cy5) or azaBODIPY <b>68</b> were analyzed by electrophoresis on a SDS polyacrylamide gel (SDS-PAGE analysis, 10% acrylamide gel) in non-reducing (without DTT (dithiothreitol), top panels) or reducing conditions (with heating and DTT, bottom panels). The fluorescence analysis of the gels was performed on Odyssey CLx Infrared Imaging System (LI-COR Biosciences, left panels) in pair filter mode (685/700 nm). After Coomassie blue staining during 1h, the gels were visualized on a Chemidoc XRS+ analyzer (BioRad, right panels). PL: protein Ladders (130, 100, 70, 55, 40, 35, 25, 15 kDa).....	140
Figure 155: Investigation of the Stability of the <b>68</b> -anti-PD-L1 in mice plasma by electrophoresis on SDS-PAGE (7% acrylamide gel) in non-reducing conditions. The fluorescence analysis of the gel was performed on Odyssey CLx Infrared Imaging System (LI-COR Biosciences) in pair filter mode (685/700 nm). 1: <b>68</b> -anti-PD-L1 without incubation in mice plasma, 2: mice plasma without <b>68</b> -anti-PD-L1, 3 to 5: <b>68</b> -anti-PD-L1 incubated in mice plasma during respectively 0, 24 and 48h. ....	141
Figure 156: Flow cytometry analysis using a commercial PE-conjugated anti-PD-L1 antibody (left) and azaBODIPY <b>68</b> -conjugated anti-PD-L1 (right) on two different cancer cell lines, CT26 (top) and 4T1 (bottom). IgG2b-PE and untreated cells were used as negative controls respectively .....	141
Figure 157: NIR fluorescence images of a subcutaneous CT26 tumor-bearing of BALB/c mouse injected with a single dose of 50µg azaBODIPY <b>68</b> -anti-PD-L1 (imaged from the back) .....	142
Figure 158: Corresponding fluorescence tumour uptake over time at 1, 5, 24 and 48 h post injection (bottom) (Ex/Em filters: 660/710 nm, IVIS Lumina, Perkin Elmer) .....	143
Figure 159: Development of absolute fluorescence intensities detected from 1-48h for all injected conjugates/compounds. Mice were imaged from the back and the right side. Grey: 1h, red: 5h, blue: 24h, green: 48h.....	143
Figure 160: NIR fluorescence images of subcutaneous CT26 tumor-bearing mice at 1, 6, 24 and 48 h after a single injection of 50 µg azaBODIPY <b>68</b> -anti-PD-L1 (Ex/Em filters: 660/710 nm, IVIS Lumina, Perkin Elmer) Right: Quantification of fluorescence tumour uptake over time. Results are presented as mean ± SEM, n=3, *p<0,05. Radiant efficiencies are also shown in Figure 164 below for direct comparison to other conjugates .....	145
Figure 161: NIR fluorescence images of subcutaneous CT26 tumor-bearing mice at 1, 6, 24 and 48 h after a single injection of 50 µg azaBODIPY <b>68</b> -IgG2b (Ex/Em filters: 660/710 nm, IVIS Lumina, Perkin Elmer) Right: Quantification of fluorescence tumour uptake over time. Results are presented as mean ± SEM, n=3, *p<0,05. Radiant efficiencies are also shown in Figure 164 below for direct comparison to other conjugates .....	146
Figure 162: NIR fluorescence images of subcutaneous CT26 tumor-bearing mice at 1, 6, 24 and 48 h after a single injection of 50 µg azaBODIPY <b>68</b> -anti-PD-1 (Ex/Em filters: 660/710 nm, IVIS Lumina, Perkin Elmer) Right: Quantification of fluorescence tumour uptake over time. Results are presented as mean ± standard error n=2. Radiant efficiencies are also shown in Figure 164 below for direct comparison to other conjugates .....	147
Figure 163: NIR fluorescence images of subcutaneous CT26 tumor-bearing mice at 1, 6, 24 and 48 h after a single injection of 50 µg Cy5-anti-PD-L1 (Ex/Em filters: 620/660 nm, IVIS Lumina, Perkin Elmer) Right: Quantification of fluorescence tumour uptake over time. Results are presented as mean ± SEM, n=3, *p<0,05. Radiant efficiencies are also shown in Figure 164 below for direct comparison to other conjugate.....	148

## Table of Figures

---

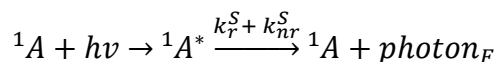
Figure 164: comparison of fluorescence accumulation over time for each cohort. JPL indicates use of azaBODIPY <b>72</b> as fluorophore.....	148
Figure 165: quantification of uptake of <b>azaBODIPY 68-anti-PD-L1</b> (Ex/Em filters: 660/710 nm) and <b>Cy5-anti-PD-L1</b> (Ex/Em filters: 620/660 nm) in organs collected 48h p.i. via ex vivo NIR fluorescence. Mice received a single injection (50 µg) of <b>azaBODIPY-68-anti-PD-L1</b> or <b>Cy5-anti-PD-L1</b> . Results are presented as mean ± SEM, n=3, *p<0,05; **p<0.01 and ***p<0.001. B and C: Tumor/blood ratio (B) and tumor/organ ratio (C) of <b>azaBODIPY-68-anti-PD-L1</b> and <b>Cy5-anti-PD-L1</b> uptakes. Results are presented as mean ± SEM, n=3, **p<0,01.....	149
Figure 166:Further exploration of the developed platform .....	152
Figure 167: LUMO energies (eV) for some model systems.....	245
Figure 168: some hypothetical reactions involving the model system .....	246
Figure 169: Calibration curve of logK vs logP for the chosen calibration agents.....	248
Figure 170: Absorption and emission spectra of BODIPYs <b>1</b> (left) and <b>4a</b> (right) in DMSO...	250
Figure 171: Absorption and emission spectra of <b>4b</b> (top, left), <b>7</b> (top, right), <b>8</b> (bottom, left) and <b>9</b> (bottom, right) in DMSO.....	250
Figure 172: Absorption and emission spectra of <b>10</b> (top, left), <b>11</b> (top, right), <b>13</b> (bottom, left) and <b>15</b> (bottom, right) in DMSO.....	251
Figure 173: Absorption and emission spectra of <b>16</b> (top, left), <b>17</b> (top, right), <b>18</b> (bottom, left) and <b>20</b> (bottom, right) in DMSO.....	251
Figure 174: Absorption and emission spectra of <b>21</b> (top, left), <b>23</b> (top, right), <b>24</b> (middle, left), <b>25</b> (middle, right) and <b>26</b> (bottom, left) in DMSO.....	252
Figure 175: Absorption (blue), excitation (green) and emission (red) spectra of <b>30</b> (top, left), <b>31</b> (top, right), <b>32</b> (middle, left), <b>34</b> (middle, right) and <b>37</b> (bottom right) in DMSO and Absorption (blue), excitation (green) and emission (red) spectra of <b>34</b> (bottom left) in PBS .....	253
Figure 176: Absorption (blue), excitation (green) and emission (red) spectra of <b>38</b> (top, left), <b>44</b> (top, right), <b>48</b> (middle, left), <b>52</b> (middle, right), <b>53</b> (bottom left) and <b>54</b> (bottom right) in DMSO.....	254
Figure 177: Absorption (blue), excitation (green) and emission (red) spectra of <b>55</b> (top, left), <b>57</b> (top, right), <b>58</b> (middle, left), <b>60</b> (middle, right), <b>61</b> (bottom left) and <b>62</b> (bottom right) in DMSO.....	255
Figure 178: Absorption (blue), excitation (green) and emission (red) spectra of <b>64</b> (top, left), <b>65</b> (top, right), <b>68</b> (middle left), <b>66</b> (middle right) and <b>69</b> (bottom) in DMSO.....	256
Figure 179: Absorption (blue), excitation (green) and emission (red) spectra of <b>65</b> (top, left), <b>68</b> (top, right), <b>66</b> (bottom left) and <b>69</b> (bottom right) in PBS.....	257
Figure 180: Absorption (blue), excitation (green) and emission (red) spectra of <b>71</b> (top, left), <b>72</b> (top, right), <b>73</b> (middle left), <b>75</b> (middle right) and <b>77</b> (bottom) in DMSO.....	258

## ANNEX I

### 7.1 Quantum Yield

(derivation done as shown in Valeur and Berberan-Santos, 2013 [261] )

For a given absorptive and radiative process



the the excited species  ${}^1A^*$  in response to a short ( $\delta$ -)light pulse decays exponentially from the excited state to the ground state. Its concentration is thus given by

$$-\frac{d[{}^1A^*]}{dt} = (k_r^S + k_{nr}^S)[{}^1A^*] \quad (\text{V})$$

Inegration of the above expression leads to

$$[{}^1A^*] = [{}^1A^*]_0 \exp\left(-\frac{t}{\tau_s}\right) \quad (\text{VI})$$

where the excited state lifetime  $\tau_s$  is given by the reciprocal sum of the radiative ( $k_r$ ) and nonradiative ( $k_{nr}$ ) processes:

$$\tau_s = \frac{1}{k_r + k_{nr}} \quad (\text{VII})$$

The measured fluorescence intensity is directly proportional to the concentration of the excited species and thus given by

$$i_F(t) = k_r^S [{}^1A^*] = k_r^S [{}^1A^*]_0 \exp\left(-\frac{t}{\tau_s}\right) \quad (\text{VIII})$$

The fluorescence quantum yield is defined as the ratio of emitted to absorbed photons

$$\phi = \frac{N_{emitted}}{N_{absorbed}} \quad (\text{IX})$$

As seen in equation (VIII) the amount of emitted photons in response to a  $\delta$ -pulse is always proportional to the concentration of remaining excited species; a rearrangement and integration from 0 to infinity thus yields the total amount of emitted photons relative to the absorbed photons:

$$\frac{i_F(t)}{[{}^1A^*]_0} = k_r^S \exp\left(-\frac{t}{\tau_s}\right) \quad (\text{X})$$

$$\frac{1}{[{}^1A^*]_0} \int_0^\infty i_F(t) dt = k_r^S \tau_s = \Phi \quad (\text{XI})$$

When time resolved measurements are performed the lifetimes of the involved processes can be used to calculate the quantum yield using equation (XII)

$$\phi = \frac{k_r}{k_r + k_{nr}} = \frac{\tau_s}{\tau_r} \quad (\text{XII})$$

Measurement of fluorescence lifetimes poses high demands on the used apparatus and requires sophisticated mathematical data-treatment. These measurements are interesting when a deeper understanding of the involved photophysical processes is required.

A simplified approach can be taken: the fluorescent properties of the compound can be determined using steady-state rather than time-resolved measurements. As seen previously absorptive processes are very fast. Using irradiation times that are long in comparison the excited lifetimes leads to saturation and equilibrium of the excited species. The amount of excited species  $^1A^*$  is thus kept constant and its change over time is 0:

$$-\frac{d[{}^1A^*]}{dt} = 0 = k_a \alpha N_0 - (k_r^S + k_{nr}^S)[{}^1A^*] \quad (\text{XIII})$$

$k_a \alpha N_0$  represents the amount of photons absorbed per unit volume and time, it can also be expressed as  $\alpha I_0$  where  $I_0$  is the absorbed intensity of the incident light and  $\alpha$  the unit volume. Rearrangement leads to

$$[{}^1A^*] = \frac{\alpha I_0}{(k_r^S + k_{nr}^S)} \quad (\text{XIV})$$

As seen in equation (VIII) the fluorescence intensity is proportional to the concentration of excited species; rearrangement therefore leads to the quantum yield for steady-state measurements:

$$i_F = k_r^S [{}^1A^*] = \alpha I_0 \frac{k_r^S}{(k_r^S + k_{nr}^S)} = \alpha I_0 \Phi \quad (\text{XV})$$

As derived above the fluorescence quantum yield can be determined using both time resolved and steady state measurements. For fluorophores that strongly suffer from photobleaching time resolved measurements should be the method of choice as they remove the error that is introduced by photobleaching. For the use of a fluorophore as probe and for imaging purposes a deeper understanding of the processes involved is usually not necessary; the only real requirement for the user is the observability of the probe. Thus steady-state measurements are often sufficient.

In practical terms the quantum yield is determined by comparison of the unknown compound to a known standard. The standards quantum yield has been determined using an integration sphere or calorimetric measurements.  $i_F$  in equation XV is the fluorescence intensity at a specific wavelength; for practical reasons the fluorescence intensity is integrated over the entire emission spectrum. For  $I_0$  the molar absorption at excitation wavelength is employed. Using a correctional term for the refractive indices  $n$  of the used solvents the quantum yield of an unknown compound can then be calculated by

$$\Phi_{uk} = \frac{I_{0,k} \int i_{F,uk} n_{uk}^2}{I_{0,uk} \int i_{F,k} n_k^2} \Phi_k \quad (\text{XVI})$$

where uk denominates unknown and k known.

## 7.2 Computational Details

All DFT calculations were carried out Gaussian 09 [282], tightening self-consistent field convergence thresholds ( $10^{-10}$  a.u.). A 6-31G (d) basis set and the hybrid functional M06-2X [283] were employed given the good performance of such scheme in other studies [284,285]. The DMSO solvent effects were included according to the Polarizable Continuum Model [286,287]. The LUMO isosurfaces have been plotted with the Chemcraft code [288] considering a contour threshold of 0.05 a.u.

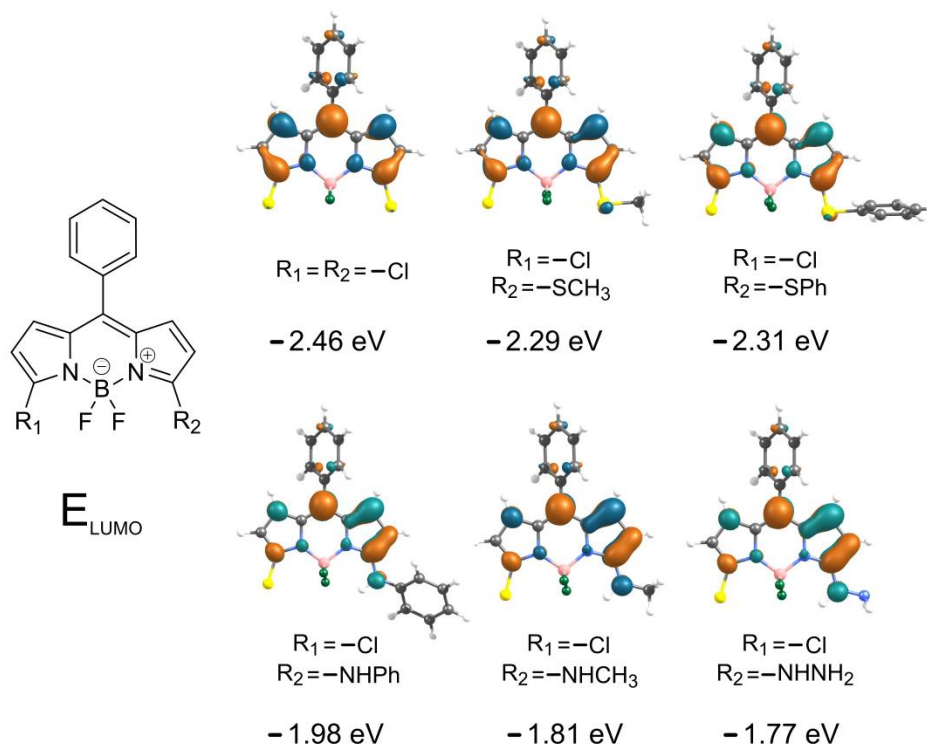


Figure 167: LUMO energies (eV) for some model systems

### 7.2.1 Results and Discussion

We conducted DFT calculations at the M06-2X/6-31G(d) level to determine the lowest unoccupied molecular orbital energy ( $E_{\text{LUMO}}$ ) for some model systems containing amino- and thio- groups. This value can be associated with the electrophilicity of the molecule [192,193]. Therefore, the higher  $E_{\text{LUMO}}$ , the lower the probability of the molecule to experience a nucleophilic attack.

In Figure 167 we can observe the graphical representation of the LUMO, which is mainly distributed over the dipyrromethene core in all systems. Remarkably, the small contribution of the phenyl ring at the *meso* position evidences the poor conjugation between this fragment and the boron-dipyrromethene moiety given the broad dihedral angle between them.

The replacement of a chlorine atom by an amino-/thio- substituent leads to an  $E_{\text{LUMO}}$  increase with respect to the dichloride- starting compound. This effect is more pronounced for the

## ANNEX I

amino-substituted BODYPYs ( $\Delta E_{\text{LUMO}} \sim 0.61$  eV) than for their thio-substituted counterparts ( $\Delta E_{\text{LUMO}} \sim 0.16$  eV). These calculated values are in good agreement with the experimental data showcasing the great difficulty/unfeasibility to incorporate a second primary amine to the amino-substituted BODIPYs.

Additionally, the reaction energies for (a) the incorporation of an aminomethyl group in the thio-substituted BODIPY and (b) the incorporation of a thiomethyl in the amino-substituted BODIPY were estimated, both processes leading to the same products. We found that reaction (a) is the more exothermic process releasing more than three times the energy of (b).

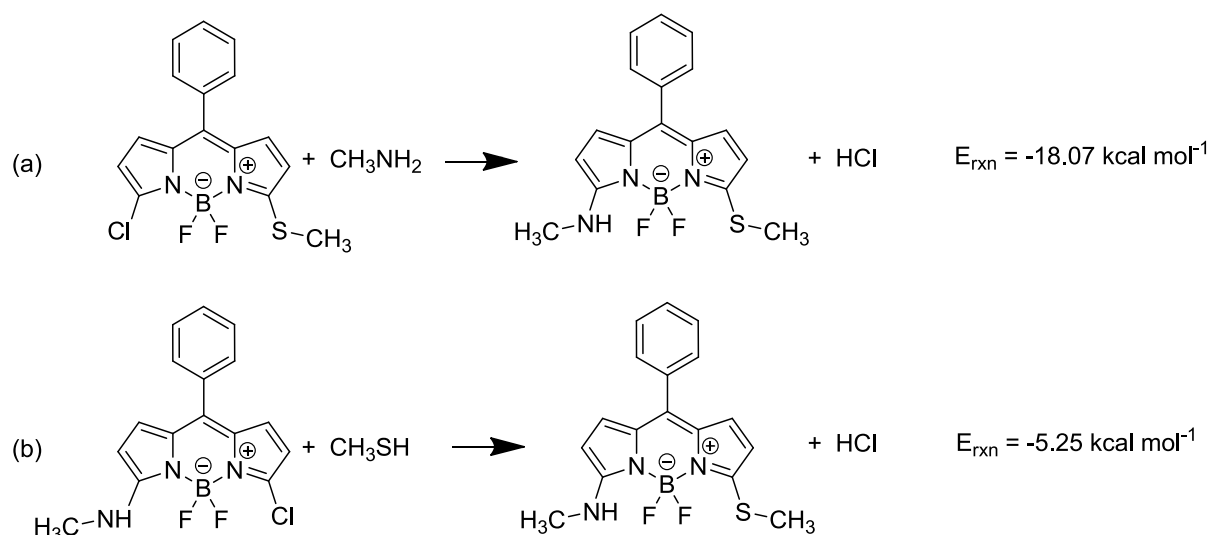


Figure 168: some hypothetical reactions involving the model system

These results evidence how the higher electron-donor behavior of the amino-substituents increases the LUMO energy in a larger extent than the thio- groups, resulting in a minor reactivity of the BODIPY toward a nucleophilic substitution. Also, the energy release associated to the substituents incorporation is calculated, resulting in a more exothermic process when the thiomethyl is first added to the BODIPY, followed by the aminomethyl.

### 7.3 Details for the determination of distribution coefficients (logD)

In order to check for correlations between the compounds hydro/lipophilicity and the observed cytotoxicity distribution coefficients were determined. Distribution coefficients describe the ratio of concentrations of a compound dissolved in two solvents at equilibrium. Any system of two immiscible solvents can be used, the most common however is the system water/1-octanol. When the investigated compound is unionizable or only the unionized part of the compound is used to calculate the ratio of concentrations, the obtained value is called partition coefficient logP and calculated as follows (equation III)

$$\log P = \log \left( \frac{c_{\text{solute octanol}}^{\text{un-ionized}}}{c_{\text{solute water}}^{\text{un-ionized}}} \right) \quad (\text{III})$$

When the investigated compound is ionizable and/or all forms of the compound are included in the ratio the obtained value is called distribution coefficient logD and calculated as follows (equation IV):

$$\log D = \log \left( \frac{C_{solute_{octanol}}^{un-ionized} + C_{solute_{octanol}}^{ionized}}{C_{solute_{water}}^{un-ionized} + C_{solute_{water}}^{ionized}} \right) \quad (IV)$$

In case of octanol and water the solvents are a good approximation of the aqueous cytosol and the lipid-based cell membranes. The obtained value therefore correlates with the lipophilicity of a compound and is a useful tool to predict its pharmacological behavior:

The lipophilicity of a compound will influence its bioavailability and elimination behavior.

For a compound that does not experience directed transport into a cell or a given compartment of the body (e.g. the brain) its distribution coefficient gives an idea of how well the compound will enter that compartment by unspecific transport (mostly diffusion).

Two general experimental procedures exist to reliably determine the concentration ratios:

- shake flask-method
- HPLC-method

The shake-flask-method is the original method. Here the compound is partitioned in a separation funnel at a given temperature between precise amounts of solvents. Once a pseudo-equilibrium between the phases is obtained the concentration of the compound in each phase is determined, using for example colorimetry or scintigraphy. The ratio is calculated and the experiment repeated at least three times for statistical confidence. There are several major sources for errors for this method:

- solvents that are not mutually pre-saturated are used
- insufficient control of temperatures
- the used compound is too lipophilic/hydrophilic
- the compound did not reach a (pseudo-)equilibrium
- insufficient control of pH
- determination of concentrations by subtraction

When done correctly the method yields very reliable values. However, the procedure is very time consuming and labor intensive due to a multitude of manual operations (including the washing and drying of glassware) and lengthy equilibration times. Also, this method can become very compound-consuming.

When the used detection method is scintigraphy the used concentrations can be far lower than for colorimetric detection due to higher sensitivity. The major drawback of this detection method obviously is the necessity for a radioactive element to be present in the investigated agent.

The second method relies on the determination of retention times of an investigated agent on a given chromatographic system. The thusly obtained retention time is then compared to a calibration curve that has been established prior to that. This method is highly automatable and applicable to a wide range of logD's. Also, only a very small quantity of compound is needed to execute the analysis.

Due to it being automatable, less compound-consuming and having less sources of errors we adopted the second method to determine the distribution coefficients of the obtained BODIPYs.

## ANNEX I

First, an appropriate eluent was established: neither must the analysis take too long (a compound having a logP of 5 is usually eluted inside of 30 minutes using an isocratic eluent of 50% ACN / 50% H<sub>2</sub>O), nor must the compound be detected with the injection peak. Use of 60% ACN/40% water and 0.1% formic acid enabled us to obtain reasonable retention times ( $t_R \leq 20$  min) for all compounds.

Once the eluent had been chosen a calibration curve was established using well described, common chemicals. For calibration, we used:

- benzoic acid (logP=1.9)
- thymol (logP=3.3)
- naphthalene (logP=3.6)
- diphenyl ether (logP=4.2)
- 2,6-diphenylpyridine (logP=4.9)

The dead-time  $t_0$  of the system was determined using formamid.

For each compound a capacity factor  $k$  was determined using equation (XVII)

$$k = \frac{t_R - t_0}{t_0} \quad (\text{XVII})$$

Next, the decadic logarithm of  $K$  was traced against the logP's of the calibration agents to obtain the corresponding equation (Figure 169).

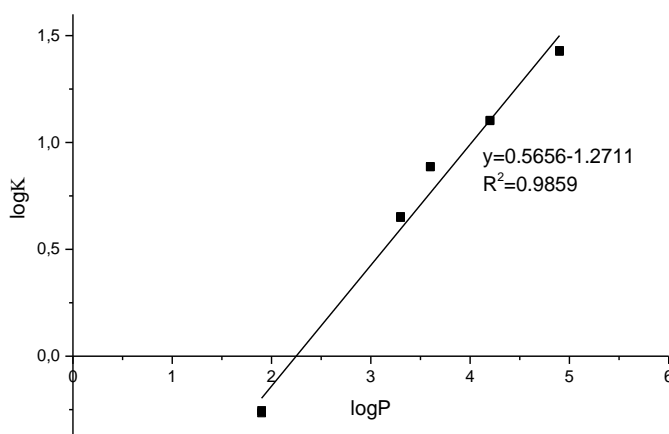


Figure 169: Calibration curve of logK vs logP for the chosen calibration agents

Once the calibration curve was established all BODIPYs were analyzed and the distribution coefficients calculated using the values of the calibration equation and the equation XVIII

$$\log K = a * \log D + b \quad (\text{XVIII})$$

A small amount of BODIPY was dissolved in 0.6 mL ACN, followed by addition of 0.4 mL water. When necessary the solution/suspension was sonicated. Each analysis was executed as follows:

- i) Washing step (two-pump gradient)
- ii) Equilibration (one pump; premixed isocratic eluent)
- iii) 3 injections of analyte (one pump; premixed isocratic eluent)

The washing step was necessary to avoid/limit cross-contaminations between different runs. Especially very lipophilic compounds tended to reappear even several injections later when no washing step was executed. To facilitate the elimination of a compound a solution of equal volumes of DMSO/ACN was injected.

During first trials cross contaminations of analyses were observed that originated from flakes of poorly solubilized compound that stuck to the injection needle as well as incomplete elution from the analytical column. The use and frequent change of the washing solution remedied this problem.

The second step, equilibration, was made necessary by the fact that the built-in equilibration time was insufficient, leading to heavy variations of up to 1 minute of observed retention times between the first and second analyte-injection.

Surprisingly, when equilibration was done using a 10 minute, two-pump isocratic program retention times still varied significantly. When equilibration was performed with one pump using the premixed eluent the retention times of analytes did not vary significantly between each run.

Once each compound was injected 3 times a mean value of its retention times was calculated which in turn was used to calculate the logD.

During the *in vitro* investigations the culture medium is buffered to pH=7.4. At pH=7.4 carboxylic acid functions are completely deprotonated and therefore increase the hydrophilicity and bioavailability of the compound in an aqueous solution.

The logD's however were determined at pH=2.7 (corresponding to an aqueous solution containing 0.1% formic acid), calling for a reevaluation of the distribution coefficients at a neutral pH to account for the influence of ionizable groups in physiological solutions.

Towards that end BODIPYs carrying a carboxylic acid function were deprotonated with Et<sub>3</sub>N in ACN containing 20% water, followed by evaporation to dryness and analysis using a neutral eluent (water/ACN without formic acid).

The use of neutral eluents did not significantly influence the retention times of the calibration agents, the calibration equation was kept throughout the experiment.

## ANNEX II – Photophysical Spectra

## 8.1 Spectra of BODIPYs

BODIPYs were characterized using a JASCO V630BIO spectrometer. The fluorescence emission spectra were obtained using a JASCO FP8500 spectrofluorometer, all compounds were measured in DMSO.

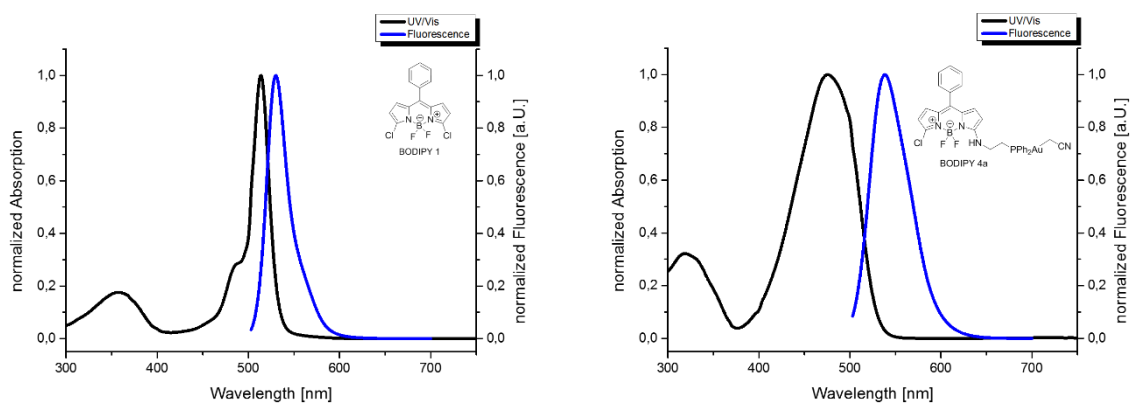


Figure 170: Absorption and emission spectra of BODIPYs **1** (left) and **4a** (right) in DMSO

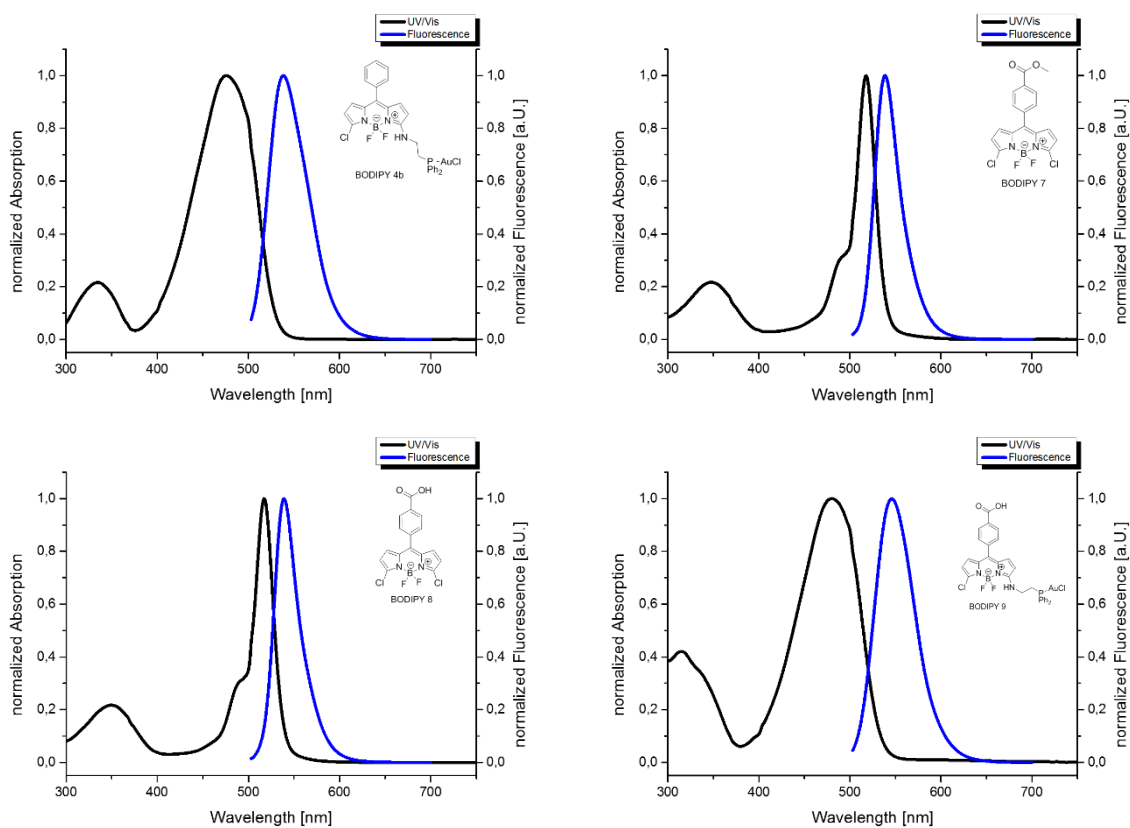


Figure 171: Absorption and emission spectra of **4b** (top, left), **7** (top, right), **8** (bottom, left) and **9** (bottom, right) in DMSO

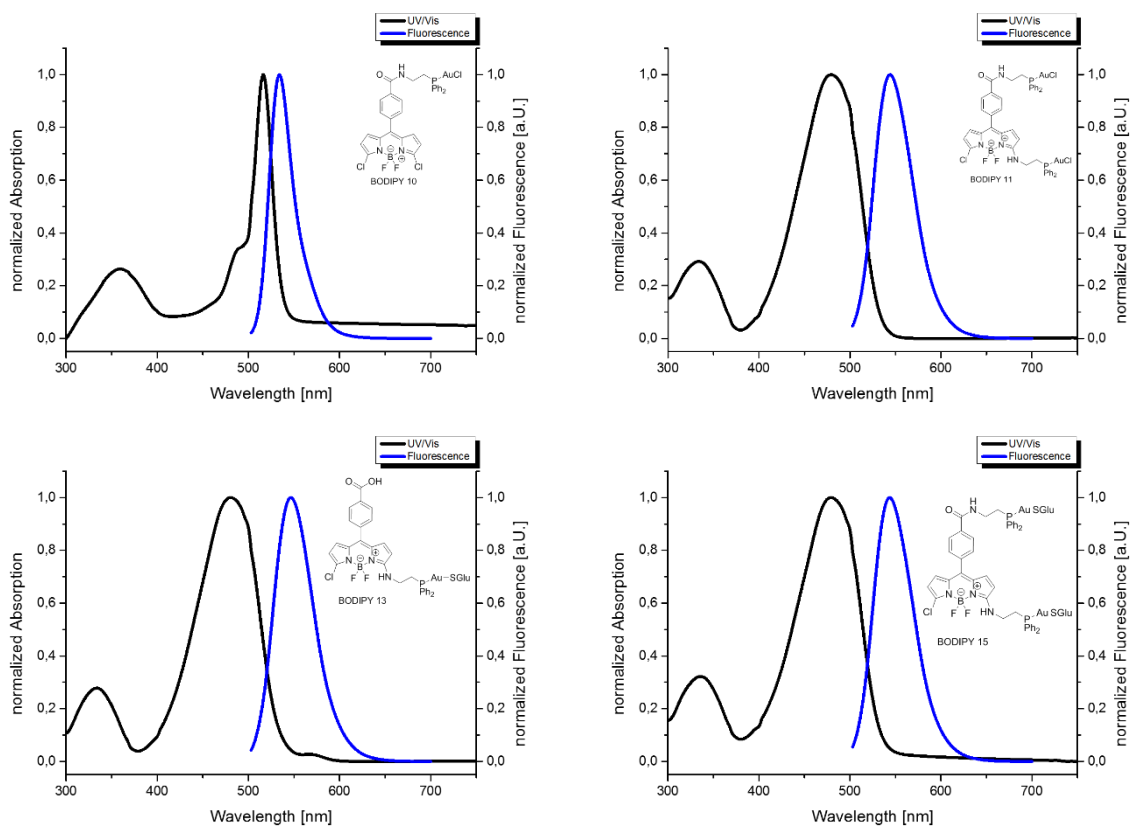


Figure 172: Absorption and emission spectra of **10** (top, left), **11** (top, right), **13** (bottom, left) and **15** (bottom, right) in DMSO

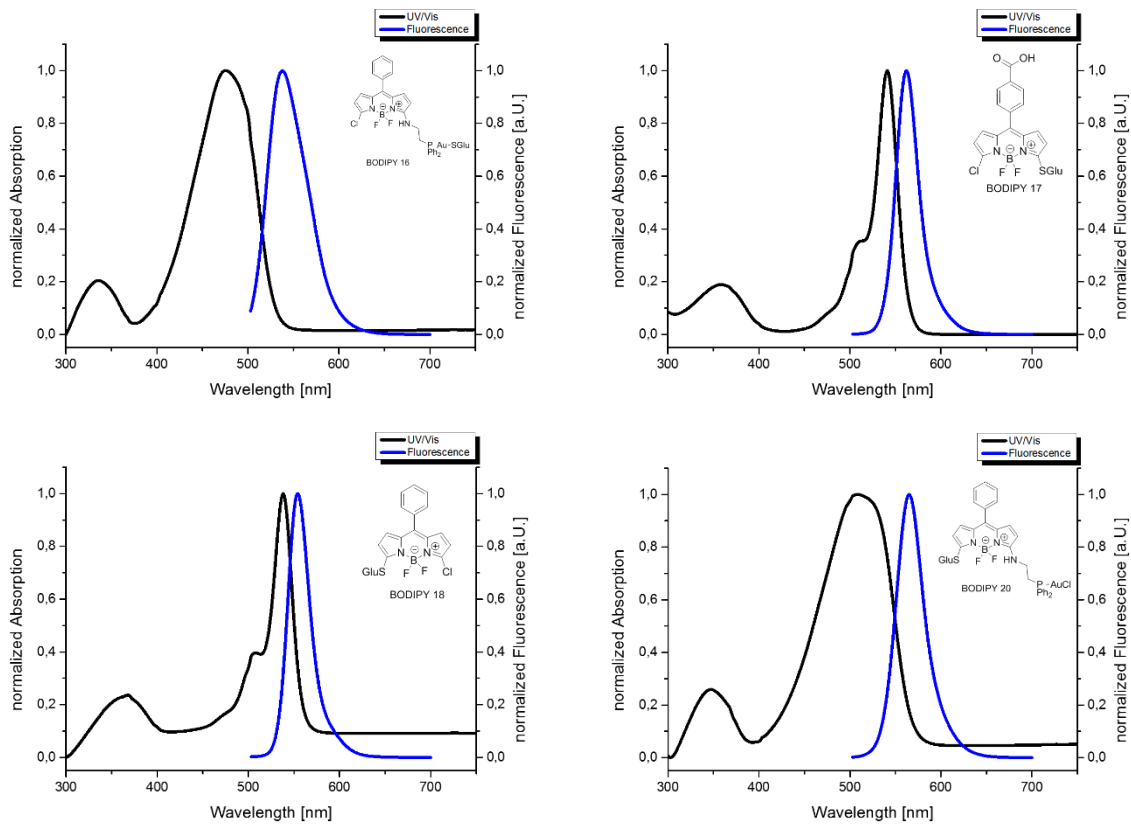


Figure 173: Absorption and emission spectra of **16** (top, left), **17** (top, right), **18** (bottom, left) and **20** (bottom, right) in DMSO

## ANNEX II – Photophysical Spectra

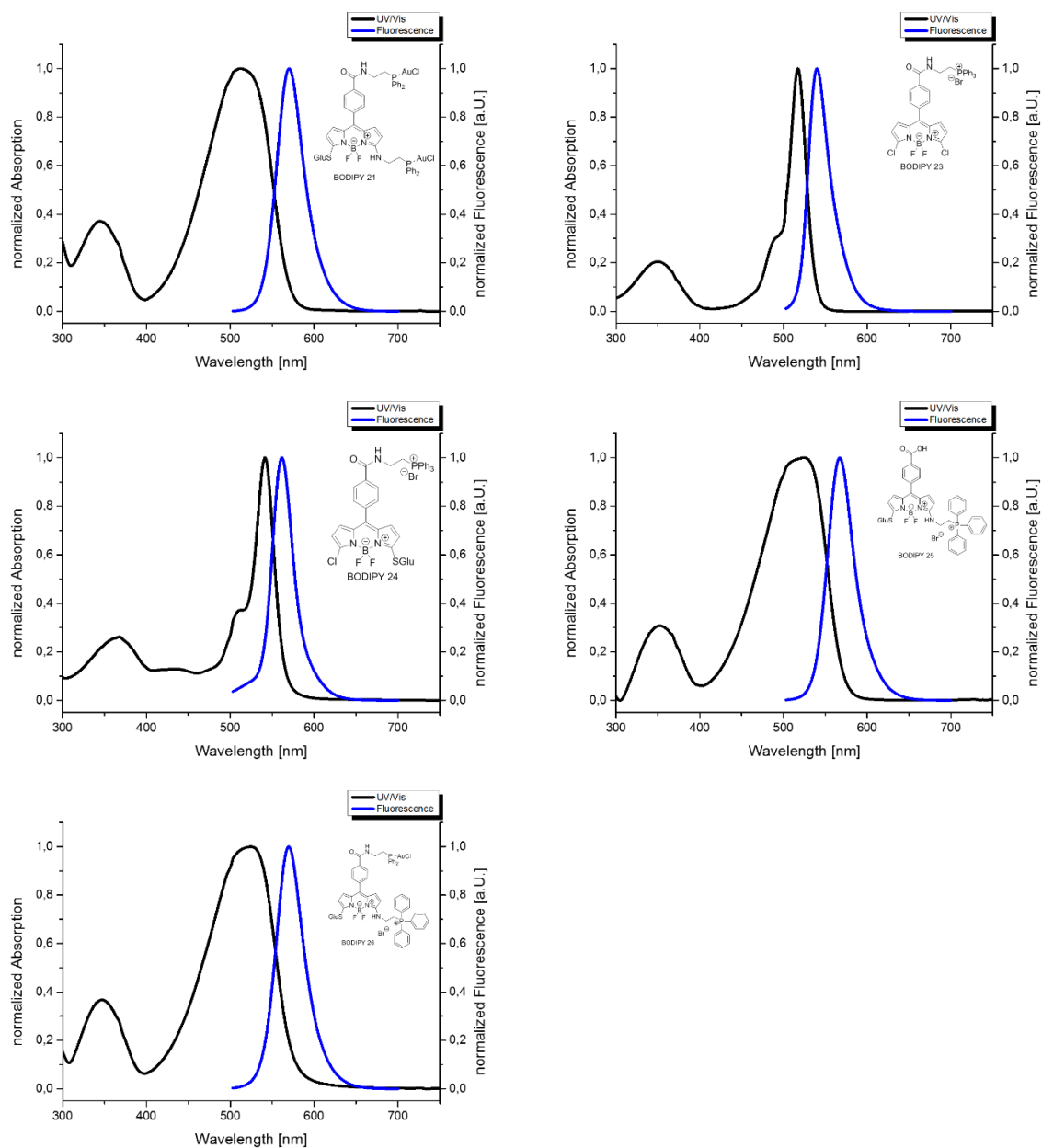


Figure 174: Absorption and emission spectra of **21** (top, left), **23** (top, right), **24** (middle, left), **25** (middle, right) and **26**(bottom, left) in DMSO

## 8.2 Spectra of azaBODIPYs

UV-Visible absorption spectra of azaBODIPYs were recorded on a Varian Cary 50 scan (single-beam). The steady - state fluorescence emission and excitation spectra of azaBODIPYs were obtained using a HORIBA Jobin Yvon Fluorolog spectrofluorometer (software FluorEssence). All spectra were recorded in DMSO unless mentioned otherwise.

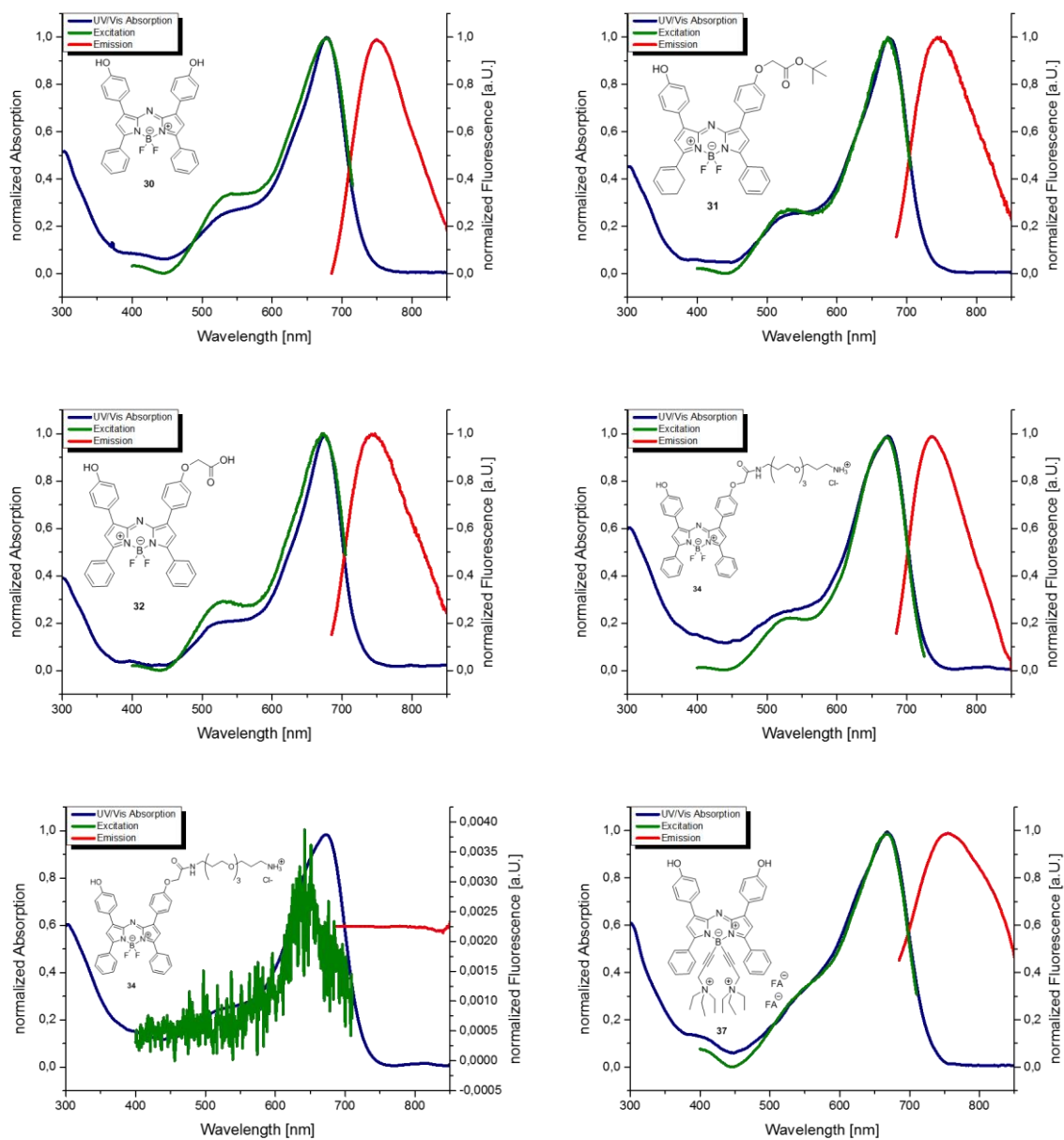


Figure 175: Absorption (blue), excitation (green) and emission (red) spectra of **30** (top, left), **31** (top, right), **32** (middle, left), **34** (middle, right) and **37** (bottom right) in DMSO and Absorption (blue), excitation (green) and emission (red) spectra of **34** (bottom left) in PBS

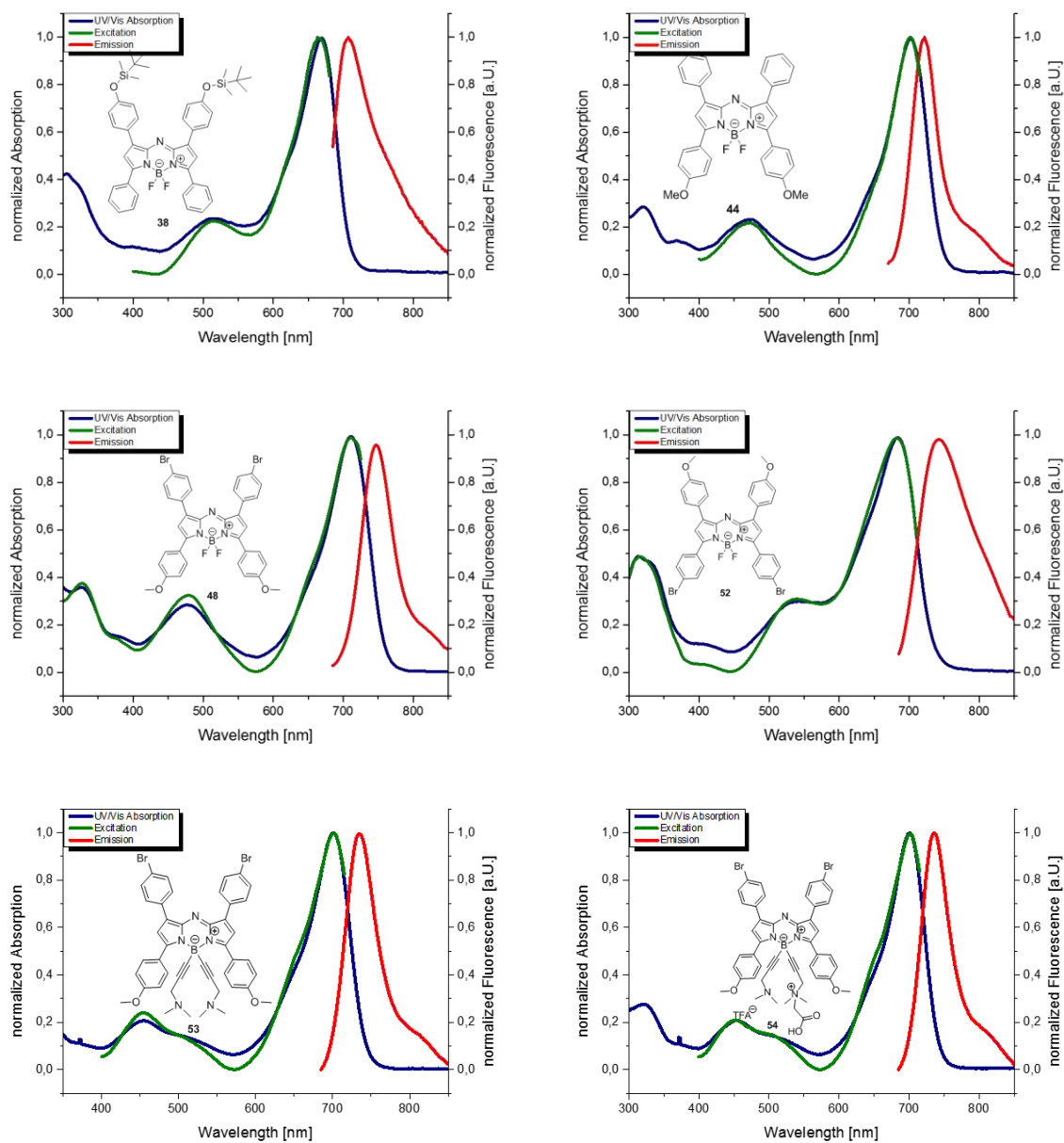


Figure 176: Absorption (blue), excitation (green) and emission (red) spectra of **38** (top, left), **44** (top, right), **48** (middle, left), **52** (middle, right), **53** (bottom left) and **54** (bottom right) in DMSO

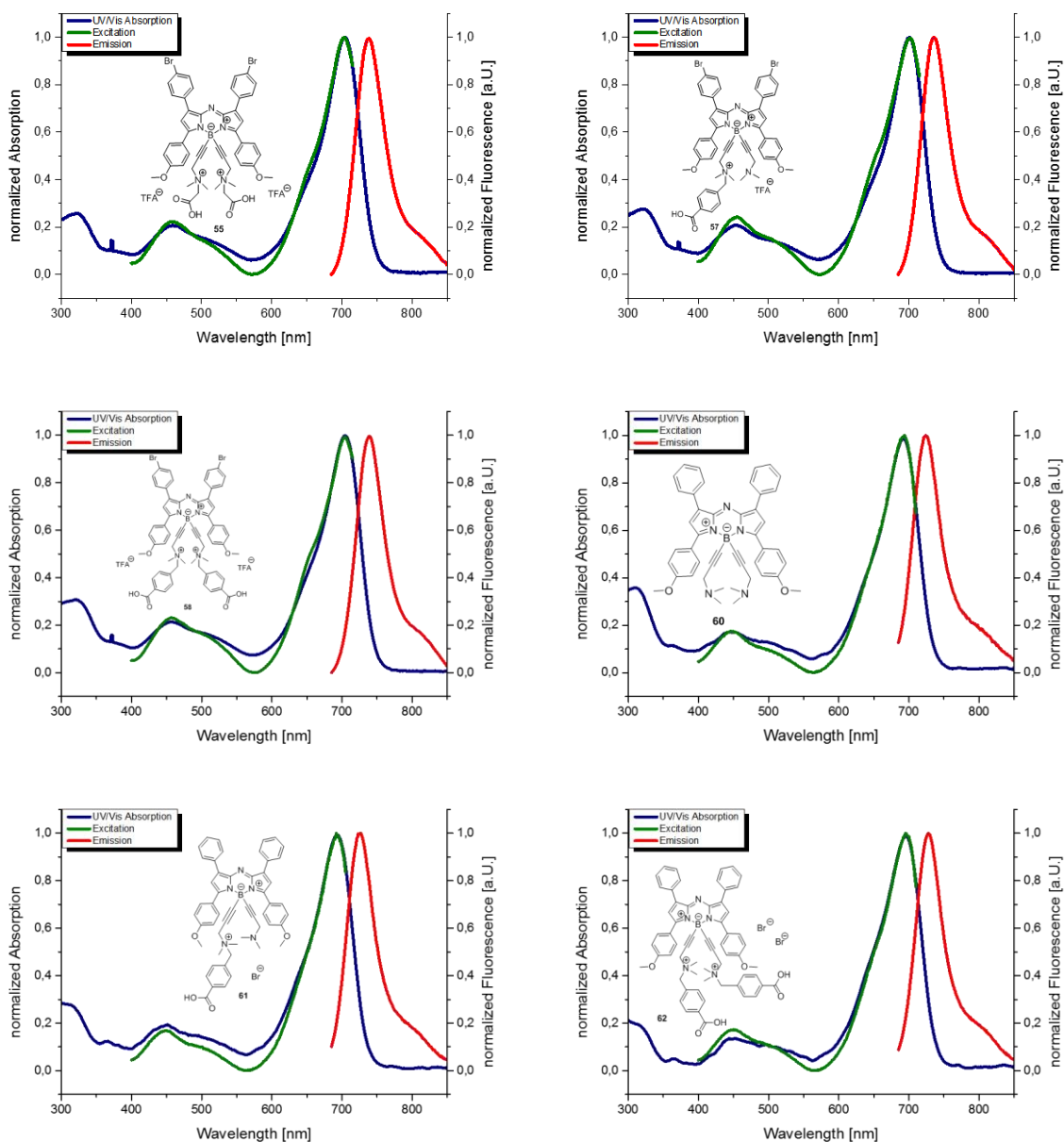


Figure 177: Absorption (blue), excitation (green) and emission (red) spectra of **55** (top, left), **57** (top, right), **58** (middle, left), **60** (middle, right), **61** (bottom left) and **62** (bottom right) in DMSO

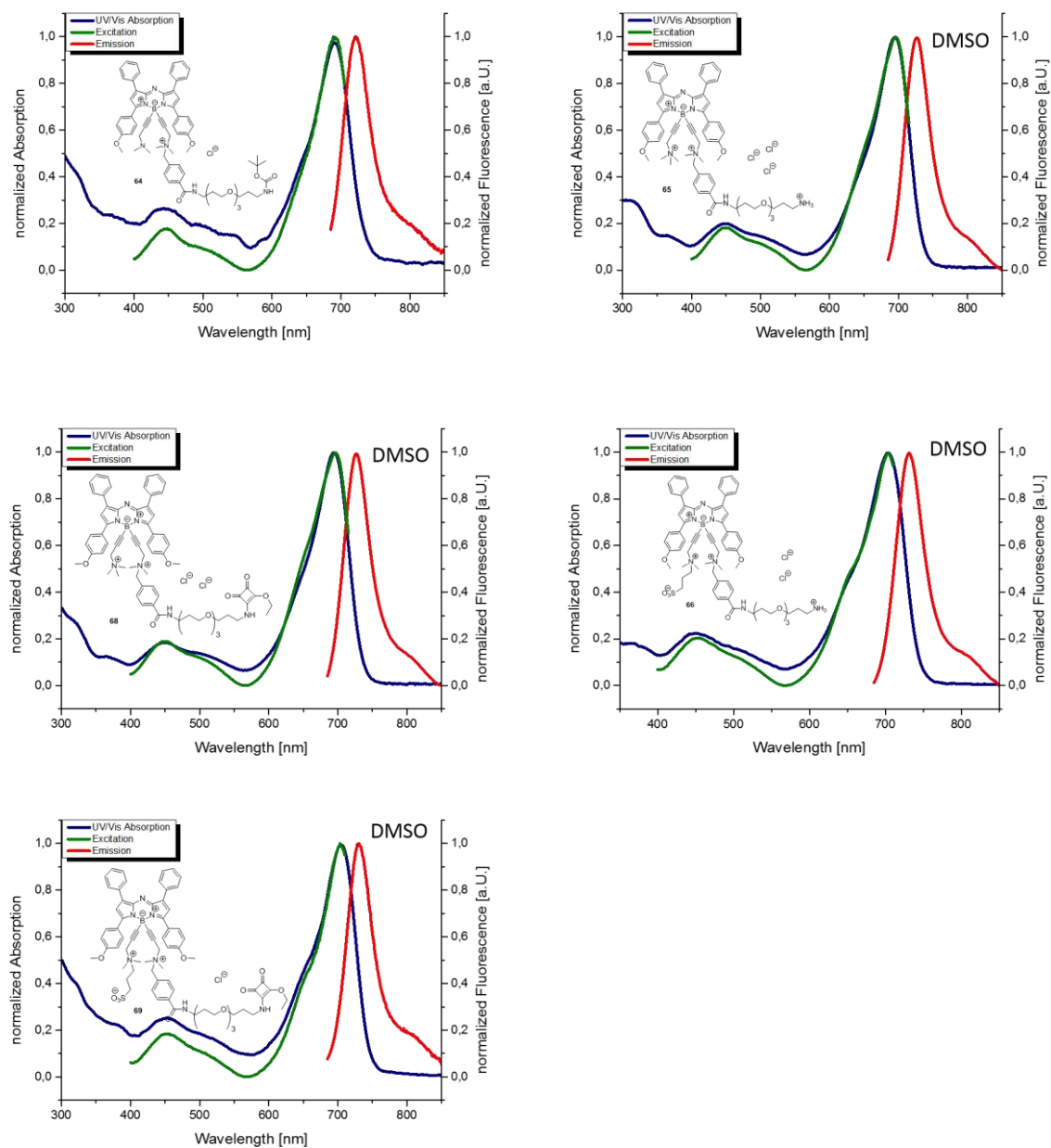


Figure 178: Absorption (blue), excitation (green) and emission (red) spectra of **64** (top, left), **65** (top, right), **68** (middle left), **66** (middle right) and **69** (bottom) in DMSO

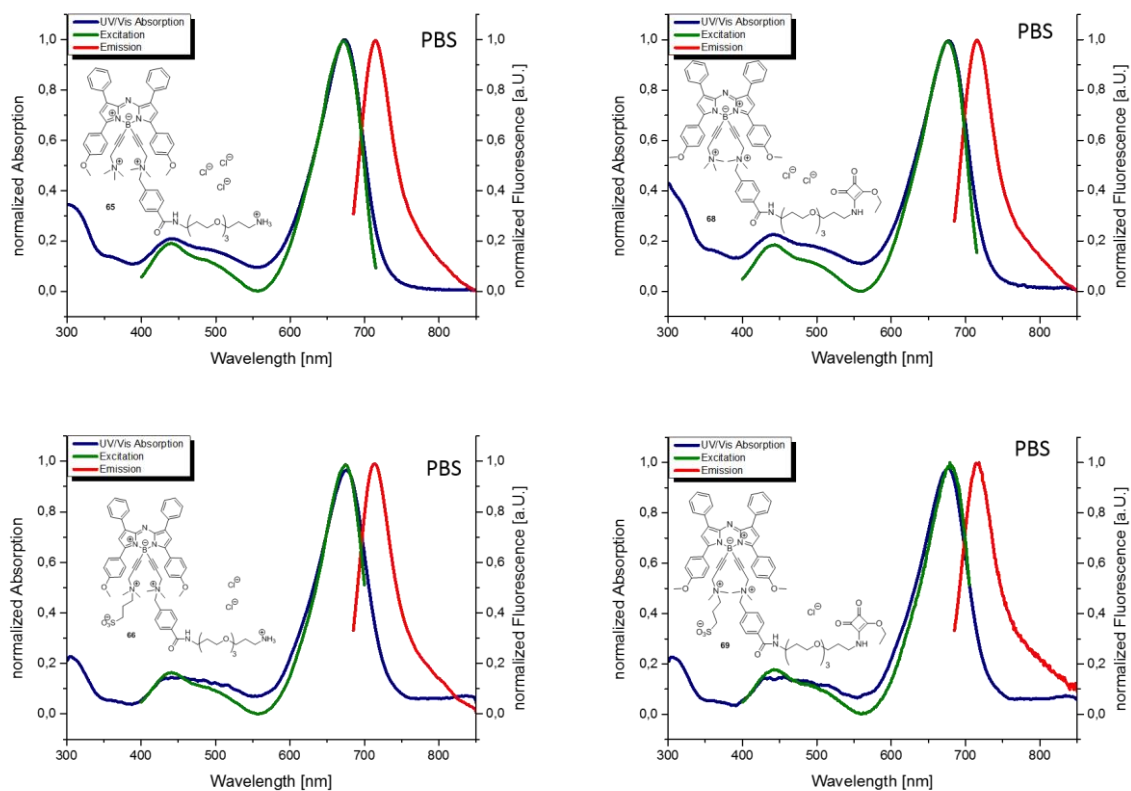


Figure 179: Absorption (blue), excitation (green) and emission (red) spectra of **65** (top, left), **68** (top, right), **66** (bottom left) and **69** (bottom right) in PBS

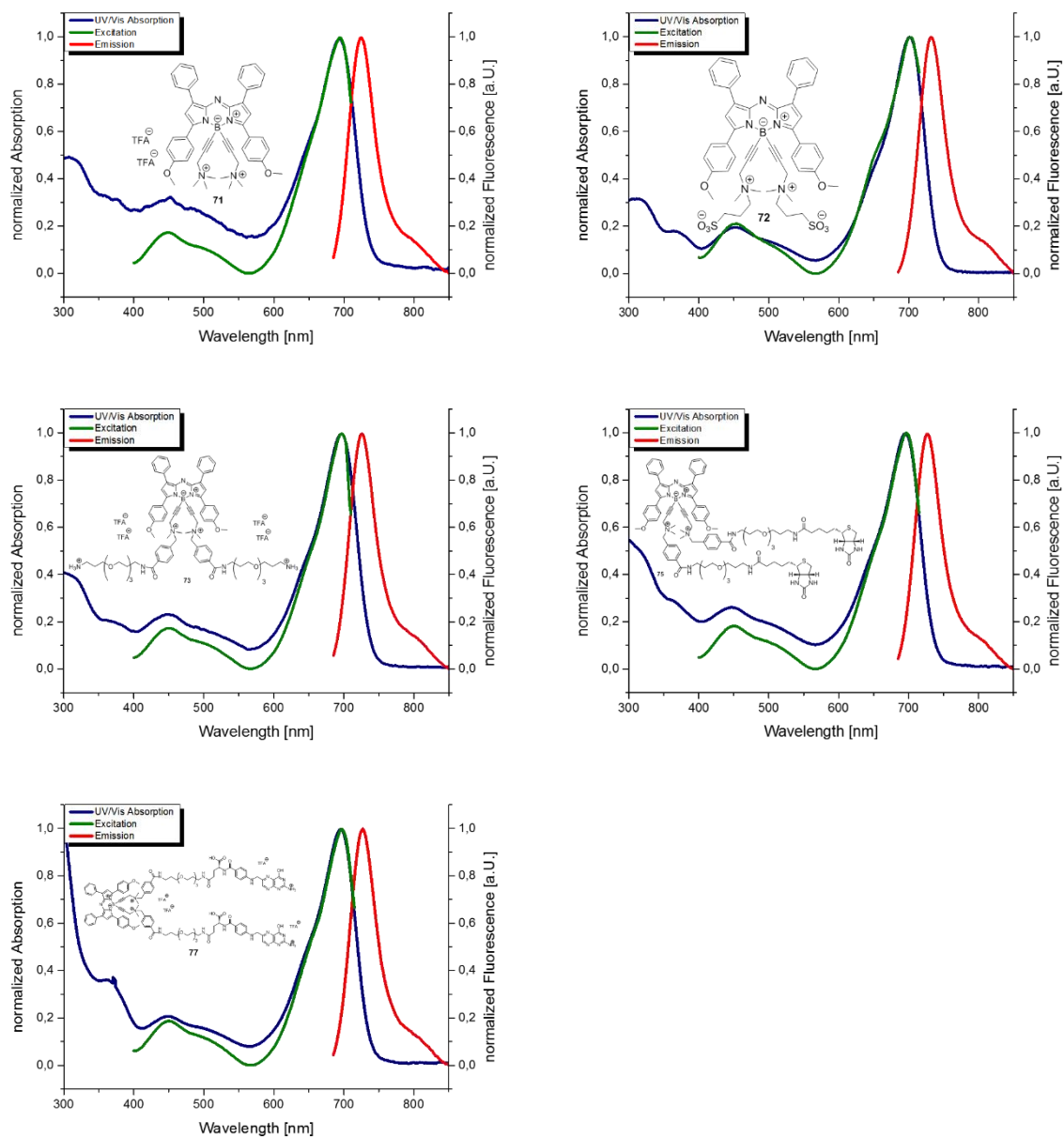
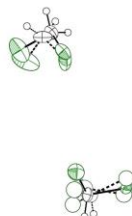
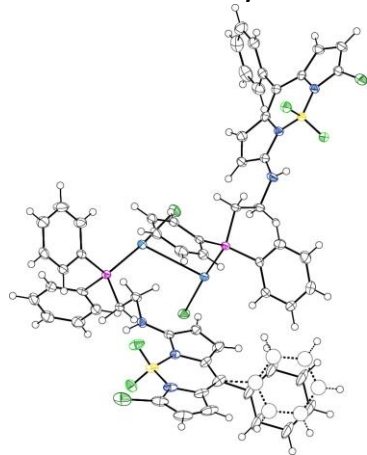


Figure 180: Absorption (blue), excitation (green) and emission (red) spectra of **71** (top, left), **72** (top, right), **73** (middle left), **75** (middle right) and **77** (bottom) in DMSO

## Annex III – single crystal X-Ray data

## 9.1 Compound 4b

## 9.1.1 Summary



**Crystal Data:**  $C_{30}H_{26}AuBCl_4F_2N_3P$ ,  $M_r = 847.08$ , monoclinic,  $P2_1/c$  (No. 14),  $a = 13.9927(4)$  Å,  $b = 29.9994(8)$  Å,  $c = 15.2788(5)$  Å,  $\beta = 95.500(2)^\circ$ ,  $\alpha = \gamma = 90^\circ$ ,  $V = 6384.1(3)$  Å<sup>3</sup>,  $T = 115$  K,  $Z = 8$ ,  $Z^0 = 2$ ,  $\mu(\text{MoK}\alpha) = 5.031$ , 113257 reflections measured, 14774 unique ( $R_{\text{int}} = 0.0503$ ) which were used in all calculations. The final  $wR2$  was 0.0530 (all data) and  $R_1$  was 0.0247 ( $I > 2\sigma(I)$ ).

**Experimental:** Single clear light orange prismshaped crystals of compound 4b were recrystallised from a mixture of DCM and hexane by slow evaporation. A suitable crystal ( $0.39 \times 0.25 \times 0.18$ ) was selected and mounted on a MITIGEN holder oil on a Nonius Kappa Apex II diffractometer. The crystal was kept at  $T = 115$  K during data collection. Using Olex2 (Dolomanov et al., 2009), the structure was solved with the ShelXT (Sheldrick, 2015) structure solution program, using the Direct Methods solution method. The model was refined with version of ShelXL (Sheldrick, 2008) using Least Squares minimisation.

Compound	4b
Formula	$C_{30}H_{26}AuBCl_4F_2N_3P$
$D_{\text{calc.}}/\text{gcm}^{-3}$	1.763
$\mu/\text{mm}^{-1}$	5.031
Formula Weight	847.08
Colour	clear light orange
Shape	prism
Max Size/mm	0.39
Mid Size/mm	0.25
Min Size/mm	0.18
$T/\text{K}$	115
Crystal System	monoclinic
Space Group	$P2_1/c$
$a/\text{Å}$	13.9927(4)
$b/\text{Å}$	29.9994(8)
$c/\text{Å}$	15.2788(5)
$\alpha/^\circ$	90
$\beta/^\circ$	95.500(2)
$\gamma/^\circ$	90
$V/\text{Å}^3$	6384.1(3)
$Z$	8
$Z'$	2
$\Theta_{\text{min}}/^\circ$	2.438
$\Theta_{\text{max}}/^\circ$	27.617
Measured Refl.	113257
Independent Refl.	14774
Reflections Used	12297
$R_{\text{int}}$	0.0503
Parameters	773
Restraints	24
Largest Peak	1.309
Deepest Hole	-0.739
GooF	1.028
$wR2$ (all data)	0.0530
$wR2$	0.0479
$R_1$ (all data)	0.0390
$R_1$	0.0247

## 9.1.2 Extended Experimental

**Experimental Extended:** A clear light orange prism-shaped crystal with dimensions  $0.39 \times 0.25 \times 0.18$  was mounted on a MITIGEN holder oil. Data were collected using a Nonius Kappa Apex II diffractometer equipped with an Oxford Cryosystems low-temperature apparatus operating at  $T = 115$  K. Data were measured using  $\varphi$  and  $\omega$  scans of  $0.60^\circ$  per frame for 7.00 s using  $\text{MoK}\alpha$  radiation (X-ray tube, 50 kV, 32 mA). The total number of runs and images was based on the strategy calculation from the program APEX3 (Bruker, 2015). The

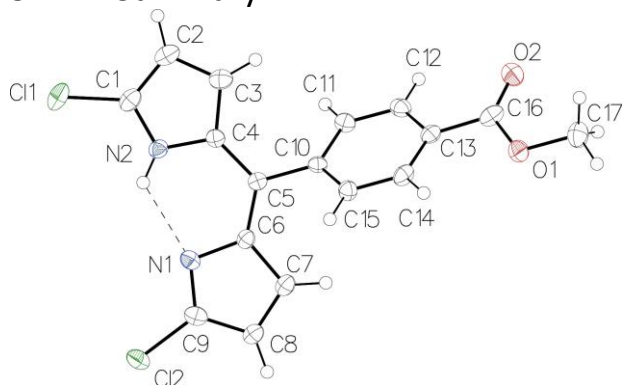
actually achieved resolution was  $\Theta = 27.617$ . Cell parameters were retrieved using the SAINT (Bruker, 2013) software and refined using SAINT (Bruker, 2013) on 9812 reflections, 9% of the observed reflections. Data reduction was performed using the SAINT (Bruker, 2013) software which corrects for Lorentz polarisation. The final completeness is 99.90% out to 27.617 in  $\Theta$ . The absorption coefficient ( $\mu$ ) of this material is 5.031 and the minimum and maximum transmissions are 0.4541 and 0.7456. The structure was solved in the space group  $P2_1/c$  (# 14) by Direct Methods using the ShelXT (Sheldrick, 2015) structure solution program and refined by Least Squares using version of ShelXL (Sheldrick, 2008). All nonhydrogen atoms were refined anisotropically. Hydrogen atom positions were calculated geometrically and refined using the riding model. The value of  $Z'$  is 2. This means that there are two independent molecules in the asymmetric unit. Two DCM molecules and one phenyl group from main complex were found disordered over two or three positions. Some SHELXL constraints (EADP) and restraints (SADI, RIGU) were employed to maintain a reasonable model.

### 9.1.3 Reflection Statistics

Total reflections (after filtering)	114708
Unique reflections	14774
Completeness	0.996
Mean $I/\sigma$	22.91
$hkl_{\max}$ collected	(18, 39, 19)
$hkl_{\min}$ collected	(-18, -38, -18)
$hkl_{\max}$ used	(18, 39, 19)
$hkl_{\min}$ used	(-18, 0, 0)
Lim $d_{\max}$ collected	100.0
Lim $d_{\min}$ collected	0.36
$d_{\max}$ used	15.21
$d_{\min}$ used	0.77
Friedel pairs	24662
Friedel pairs merged	1
Inconsistent equivalents	0
$R_{\text{int}}$	0.0503
$R_{\text{sigma}}$	0.0323
Intensity transformed	0
Omitted reflections	0
Omitted by user (OMIT hkl)	103
Multiplicity	(19232, 17510, 10918, 5008, 1372, 135)
Maximum multiplicity	19
Removed systematic absences	1348
Filtered off (SHEL/OMIT)	0

## 9.2 Compound 6

### 9.2.1 Summary



**Crystal Data:**  $C_{17}H_{12}Cl_2N_2O_2$ ,  $M_r = 347.19$ , monoclinic,  $P2_1/c$  (No. 14),  $a = 7.7609(3)$  Å,  $b = 13.7354(5)$  Å,  $c = 14.4706(6)$  Å,  $\beta = 98.464(3)^\circ$ ,  $\alpha = \gamma = 90^\circ$ ,  $V = 1525.75(10)$  Å<sup>3</sup>,  $T = 100(2)$  K,  $Z = 4$ ,  $Z' = 1$ ,  $\mu(\text{CuK}\alpha) = 3.925$ , 9973 reflections measured, 2696 unique ( $R_{\text{int}} = 0.0559$ ) which were used in all calculations. The final  $wR2$  was 0.1568 (all data) and  $R_1$  was 0.0624 ( $I > 2\sigma(I)$ ).

**Experimental:** Single clear light orange blockshaped crystals of compound **6** were recrystallised from DCM by slow evaporation. A suitable crystal (0.28×0.21×0.21) was selected and mounted on a MITIGEN holder oil on a Bruker D8 VENTURE diffractometer. The crystal was kept at  $T = 100(2)$  K during data collection. Using Olex2 (Dolomanov et al., 2009), the structure was solved with the ShelXT (Sheldrick, 2015) structure solution program, using the Direct Methods solution method. The model was refined with version of 2014/7 ShelXL (Sheldrick, 2008) using Least Squares minimisation.

### 9.2.2 Extended Experimental

**Experimental Extended:** A clear light orange block-shaped crystal with dimensions 0.28×0.21×0.21 was mounted on a MITIGEN holder oil. Data were collected using a Bruker D8 VENTURE diffractometer equipped with an Oxford Cryosystems low-temperature apparatus operating at  $T = 100(2)$  K. Data were measured using  $\varphi$  and  $\omega$  scans of  $2.00^\circ$  per frame for 10.00 s using  $\text{CuK}\alpha$  radiation (sealed X-ray tube, 50 kV, 1 mA). The total number of runs and images was based on the strategy calculation from the program APEX3 (Bruker, 2015). The actually achieved resolution was  $\Theta = 66.951$ . Cell parameters were retrieved using the SAINT (Bruker, 2013) software and refined using SAINT (Bruker, 2013) on 5160 reflections, 52% of the observed reflections. Data reduction was performed using the SAINT (Bruker, 2013) software which corrects for Lorentz polarisation. The final completeness is 99.10% out to 66.951 in  $\Theta$ . The

Compound	6
CCDC	?
Formula	$C_{17}H_{12}Cl_2N_2O_2$
$D_{\text{calc.}}/\text{gcm}^{-3}$	1.511
$\mu/\text{mm}^{-1}$	3.925
Formula Weight	347.19
Colour	clear light orange
Shape	block
Max Size/mm	0.28
Mid Size/mm	0.21
Min Size/mm	0.21
$T/\text{K}$	100(2)
Crystal System	monoclinic
Space Group	$P2_1/c$
$a/\text{Å}$	7.7609(3)
$b/\text{Å}$	13.7354(5)
$c/\text{Å}$	14.4706(6)
$\alpha/^\circ$	90
$\beta/^\circ$	98.464(3)
$\gamma/^\circ$	90
$V/\text{Å}^3$	1525.75(10)
$Z$	4
$Z'$	1
$\Theta_{\text{min}}/^\circ$	4.461
$\Theta_{\text{max}}/^\circ$	66.951
Measured Refl.	9973
Independent Refl.	2696
Reflections Used	1898
$R_{\text{int}}$	0.0559
Parameters	209
Restraints	0
Largest Peak	0.732
Deepest Hole	-0.380
Goof	1.040
$wR2$ (all data)	0.1568
$wR2$	0.1385
$R_1$ (all data)	0.0973
$R_1$	0.0624

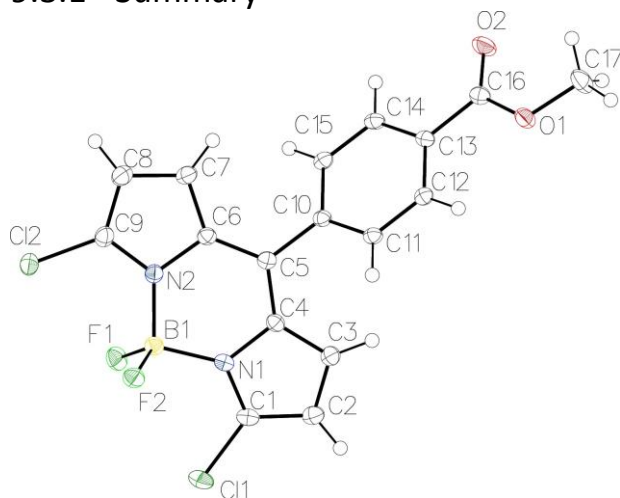
absorption coefficient ( $\mu$ ) of this material is 3.925 and the minimum and maximum transmissions are 0.6128 and 0.7528. The structure was solved in the space group  $P2_1/c$  (# 14) by Direct Methods using the ShelXT (Sheldrick, 2015) structure solution program and refined by Least Squares using version 2014/7 of ShelXL (Sheldrick, 2008). All non-hydrogen atoms were refined anisotropically. Hydrogen atom positions were calculated geometrically and refined using the riding model.

### 9.2.3 Reflection Statistics

Total reflections (after filtering)	10297
Unique reflections	2696
Completeness	0.991
Mean $I/\sigma$	10.91
$hkl_{\text{sub}_{\text{max}}}$ collected	(9, 15, 12)
$hkl_{\text{sub}_{\text{min}}}$ collected	(-8, -16, -17)
$hkl_{\text{max}}$ used	(9, 16, 17)
$hkl_{\text{min}}$ used	(-9, 0, 0)
Lim $d_{\text{max}}$ collected	100.0
Lim $d_{\text{min}}$ collected	0.77
$d_{\text{max}}$ used	14.31
$d_{\text{min}}$ used	0.84
Friedel pairs	1554
Friedel pairs merged	1
Inconsistent equivalents	1
$R_{\text{int}}$	0.0559
$R_{\text{sigma}}$	0.0625
Intensity transformed	0
Omitted reflections	0
Omitted by user (OMIT hkl)	1
Multiplicity	(3439, 1781, 938, 118, 2)
Maximum multiplicity	13
Removed systematic absences	323
Filtered off (SHEL/OMIT)	0

## 9.3 Compound 7

### 9.3.1 Summary



**Crystal Data:**  $C_{17}H_{11}BCl_2F_2N_2O_2$ ,  $M_r = 394.99$ , triclinic,  $P\bar{1}$  (No. 2),  $a = 7.8312(3) \text{ \AA}$ ,  $b = 10.3013(5) \text{ \AA}$ ,  $c = 10.4618(4) \text{ \AA}$ ,  $\alpha = 96.577(2)^\circ$ ,  $\beta = 101.739(2)^\circ$ ,  $\gamma = 97.026(2)^\circ$ ,  $V = 811.63(6) \text{ \AA}^3$ ,  $T = 100(2) \text{ K}$ ,  $Z = 2$ ,  $Z^0 = 1$ ,  $\mu(\text{MoK}\alpha) = 0.437$ , 28837 reflections measured, 3731 unique ( $R_{\text{int}} = 0.0303$ ) which were used in all calculations. The final  $wR2$  was 0.0902 (all data) and  $R_1$  was 0.0361 ( $I > 2\sigma(I)$ ).

**Experimental:** Single clear light orange plateshaped crystals of compound **7** were recrystallised from DCM by slow evaporation. A suitable crystal ( $0.46 \times 0.40 \times 0.21$ ) was selected and mounted on a MITIGEN holder oil on a Bruker D8 VENTURE diffractometer. The crystal was kept at  $T = 100(2) \text{ K}$  during data collection. Using Olex2 (Dolomanov et al., 2009), the structure was solved with the ShelXT (Sheldrick, 2015) structure solution program, using the Direct Methods solution method. The model was refined with version 2014/7 of ShelXL (Sheldrick, 2008) using Least Squares minimisation.

### 9.3.2 Extended Experimental

**Experimental Extended:** A clear light orange plate-shaped crystal with dimensions  $0.46 \times 0.40 \times 0.21$  was mounted on a MITIGEN holder oil. Data were collected using a Bruker D8 VENTURE diffractometer equipped with an Oxford Cryosystems low-temperature apparatus operating at  $T = 100(2) \text{ K}$ .

Data were measured using  $\varphi$  and  $\omega$  scans of  $2.00^\circ$  per frame for 10.00 s using  $\text{MoK}\alpha$  radiation (X-ray tube, 50 kV, 30 mA). The total number of runs and images was based on the strategy calculation from the program APEX3 (Bruker, 2015). The actually achieved resolution was  $\Theta = 27.560$ .

Compound	7
Formula	$C_{17}H_{11}BCl_2F_2N_2O_2$
$D_{\text{calc.}}/\text{gcm}^{-3}$	1.616
$\mu/\text{mm}^{-1}$	0.437
Formula Weight	394.99
Colour	clear light orange
Shape	plate
Max Size/mm	0.46
Mid Size/mm	0.40
Min Size/mm	0.21
$T/\text{K}$	100(2)
Crystal System	triclinic
Space Group	$P\bar{1}$
$a/\text{ \AA}$	7.8312(3)
$b/\text{ \AA}$	10.3013(5)
$c/\text{ \AA}$	10.4618(4)
$\alpha/^\circ$	96.577(2)
$\beta/^\circ$	101.739(2)
$\gamma/^\circ$	97.026(2)
$V/\text{ \AA}^3$	811.63(6)
$Z$	2
$Z'$	1
$\Theta_{\text{min}}/^\circ$	2.979
$\Theta_{\text{max}}/^\circ$	27.560
Measured Refl.	28837
Independent Refl.	3731
Reflections Used	3256
$R_{\text{int}}$	0.0303
Parameters	236
Restraints	0
Largest Peak	0.485
Deepest Hole	-0.284
GooF	1.046
$wR2$ (all data)	0.0902
$wR2$	0.0831
$R_1$ (all data)	0.0439
$R_1$	0.0361

Cell parameters were retrieved using the SAINT Bruker, 2013) software and refined using SAINT Bruker, 2013) on 9970 reflections, 35% of the observed reflections. Data reduction was performed using the SAINT

Bruker, 2013) software which corrects for Lorentz polarisation. The final completeness is 99.90% out to 27.560 in  $\Theta$ . The absorption coefficient ( $\mu$ ) of this material is 0.437 and the minimum and maximum transmissions are 0.6844 and 0.7456.

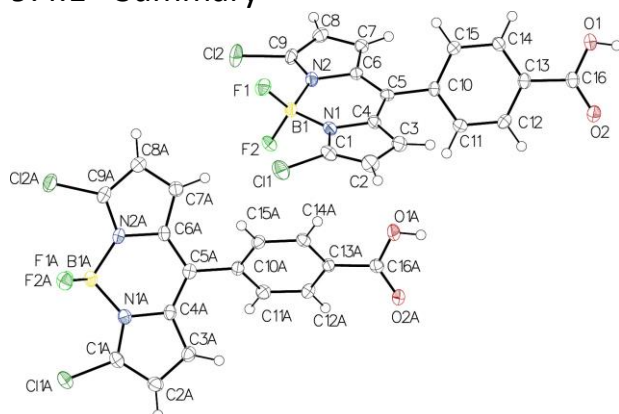
The structure was solved in the space group  $P\bar{1}$  (# 2) by Direct Methods using the ShelXT (Sheldrick, 2015) structure solution program and refined by Least Squares using version 2014/7 of ShelXL (Sheldrick, 2008). All non-hydrogen atoms were refined anisotropically. Hydrogen atom positions were calculated geometrically and refined using the riding model.

### 9.3.3 Reflection Statistics

Total reflections (after filtering)	28837
Unique reflections	3731
Completeness	0.998
Mean $I/\sigma$	37.48
$hkl_{\max}$ collected	(10, 13, 13)
$hkl_{\min}$ collected	(-10, -13, -13)
$hkl_{\max}$ used	(9, 13, 13)
$hkl_{\min}$ used	(-10, -13, 0)
Lim $d_{\max}$ collected	100.0
Lim $d_{\min}$ collected	0.36
$d_{\max}$ used	6.84
$d_{\min}$ used	0.77
Friedel pairs	3682
Friedel pairs merged	1
Inconsistent equivalents	0
$R_{\text{int}}$	0.0303
$R_{\text{sigma}}$	0.0165
Intensity transformed	0
Omitted reflections	0
Omitted by user (OMIT hkl)	0
Multiplicity	(348, 290, 1401, 3353, 1832, 189)
Maximum multiplicity	12
Removed systematic absences	0
Filtered off (SHEL/OMIT)	0

## 9.4 Compound 8

### 9.4.1 Summary



**Crystal Data:** C<sub>16</sub>H<sub>9</sub>BCl<sub>2</sub>F<sub>2</sub>N<sub>2</sub>O<sub>2</sub>,  $M_r = 380.96$ , triclinic,  $P\bar{1}$  (No. 2),  $a = 10.9208(5) \text{ \AA}$ ,  $b = 11.1413(5) \text{ \AA}$ ,  $c = 14.0873(6) \text{ \AA}$ ,  $\alpha = 69.876(3)^\circ$ ,  $\beta = 75.945(3)^\circ$ ,  $\gamma = 75.941(3)^\circ$ ,  $V = 1537.13(12) \text{ \AA}^3$ ,  $T = 100 \text{ K}$ ,  $Z = 4$ ,  $Z' = 2$ ,  $\mu(\text{MoK}\alpha) = 0.458$ , 37992 reflections measured, 7170 unique ( $R_{\text{int}} = 0.0456$ ) which were used in all calculations. The final  $wR_2$  was 0.1144 (all data) and  $R_1$  was 0.0379 ( $I > 2\sigma(I)$ ).

**Experimental:** Single clear light pink needleshaped crystals of compound **8** were recrystallised from a mixture of DCM and methanol by slow evaporation. A suitable crystal ( $0.60 \times 0.41 \times 0.27$ ) was selected and mounted on a MITIGEN holder oil on a Nonius Kappa Apex II diffractometer. The crystal was kept at  $T = 100 \text{ K}$  during data collection. Using Olex2 (Dolomanov et al., 2009), the structure was solved with the ShelXT (Sheldrick, 2015) structure solution program, using the Direct Methods solution method. The model was refined with version of ShelXL (Sheldrick, 2008) using Least Squares minimisation.

### 9.4.2 Extended Experimental

**Experimental Extended:** A clear light pink needleshaped crystal with dimensions  $0.60 \times 0.41 \times 0.27$  was mounted on a MITIGEN holder oil. Data were collected using a Nonius Kappa Apex II diffractometer equipped with an Oxford Cryosystems low-temperature apparatus operating at  $T = 100 \text{ K}$ .

Data were measured using  $\varphi$  and  $\omega$  scans of  $2.00^\circ$  per frame for 10.00 s using MoK $\alpha$  radiation (X-ray tube, 50 kV, 32 mA). The total number of runs and images was based on the strategy calculation from the program APEX3 (Bruker, 2015). The actually achieved resolution was  $\Theta = 27.740$ .

<b>Compound</b>	<b>8</b>
Formula	C <sub>16</sub> H <sub>9</sub> BCl <sub>2</sub> F <sub>2</sub> N <sub>2</sub> O <sub>2</sub>
$D_{\text{calc}}/\text{gcm}^{-3}$	1.646
$\mu/\text{mm}^{-1}$	0.458
Formula Weight	380.96
Colour	clear light pink
Shape	needle
Max Size/mm	0.60
Mid Size/mm	0.41
Min Size/mm	0.27
$T/\text{K}$	100
Crystal System	triclinic
Space Group	$P\bar{1}$
$a/\text{ \AA}$	10.9208(5)
$b/\text{ \AA}$	11.1413(5)
$c/\text{ \AA}$	14.0873(6)
$\alpha/^\circ$	69.876(3)
$\beta/^\circ$	75.945(3)
$\gamma/^\circ$	75.941(3)
$V/\text{ \AA}^3$	1537.13(12)
$Z$	4
$Z'$	2
$\Theta_{\text{min}}/^\circ$	1.564
$\Theta_{\text{max}}/^\circ$	27.740
Measured Refl.	37992
Independent Refl.	7170
Reflections Used	5077
$R_{\text{int}}$	0.0456
Parameters	453
Restraints	0
Largest Peak	0.364
Deepest Hole	-0.309
GooF	1.049
$wR_2$ (all data)	0.1144
$wR_2$	0.0906
$R_1$ (all data)	0.0679
$R_1$	0.0379

Cell parameters were retrieved using the SAINT (Bruker, 2013) software and refined using SAINT (Bruker, 2013) on 9455 reflections, 25% of the observed reflections. Data reduction was performed using the SAINT (Bruker, 2013) software which corrects for Lorentz polarisation. The final completeness is 100.00% out to 27.740 in  $\Theta$ . The absorption coefficient ( $\mu$ ) of this material is 0.458 and the minimum and maximum transmissions are 0.6759 and 0.7456.

The structure was solved in the space group  $P\bar{1}$  (# 2) by Direct Methods using the ShelXT (Sheldrick, 2015) structure solution program and refined by Least Squares using version of ShelXL (Sheldrick, 2008). All non-hydrogen atoms were refined anisotropically. Hydrogen atom positions were calculated geometrically and refined using the riding model.

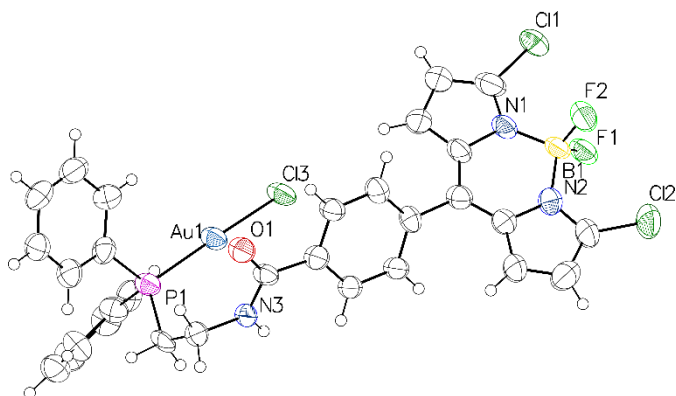
The value of  $Z'$  is 2. This means that there are two independent molecules in the asymmetric unit.

### 9.4.3 Reflection Statistics

Total reflections (after filtering)	37992
Unique reflections	7170
Completeness	0.989
Mean $I/\sigma$	18.62
$hkl_{\max}$ collected	(14, 14, 18)
$hkl_{\min}$ collected	(-14, -14, -18)
$hkl_{\max}$ used	(14, 14, 18)
$hkl_{\min}$ used	(-13, -13, 0)
Lim $d_{\max}$ collected	100.0
Lim $d_{\min}$ collected	0.36
$d_{\max}$ used	13.02
$d_{\min}$ used	0.76
Friedel pairs	6968
Friedel pairs merged	1
Inconsistent equivalents	0
$R_{\text{int}}$	0.0456
$R_{\text{sigma}}$	0.0416
Intensity transformed	0
Omitted reflections	0
Omitted by user (OMIT hkl)	0
Multiplicity	(2285, 5067, 3479, 1749, 1245, 279, 31, 3)
Maximum multiplicity	13
Removed systematic absences	0
Filtered off (SHEL/OMIT)	0

## 9.5 Compound 10

### 9.5.1 Summary



**Crystal Data.**  $C_{127}H_{106}Au_4B_4Cl_{26}F_8N_{12}O_4P_4$ ,  $M_r = 3892.92$ , orthorhombic, *Pbca* (No. 61),  $a = 25.643(4)$  Å,  $b = 9.4006(16)$  Å,  $c = 30.308(5)$  Å,  $\alpha = \beta = \gamma = 90^\circ$ ,  $V = 7306(2)$  Å<sup>3</sup>,  $T = 115$  K,  $Z = 2$ ,  $Z' = 0.25$ ,  $\mu(MoK\alpha) = 4.588$ , 151102 reflections measured, 6424 unique ( $R_{int} = 0.0918$ ) which were used in all calculations. The final  $wR_2$  was 0.1979 (all data) and  $R_1$  was 0.0732 ( $I > 2(I)$ ).

**Experimental.** Single clear light pink plate-shaped crystals of compound **10** were recrystallised from DCM by slow evaporation. A suitable crystal ( $0.51 \times 0.13 \times 0.05$  mm<sup>3</sup>) was selected and mounted on a MITIGEN holder oil on a Nonius Kappa Apex II diffractometer. The crystal was kept at  $T = 115$  K during data collection. Using **Olex2** (Dolomanov et al., 2009), the structure was solved with the **ShelXT** (Sheldrick, 2015) structure solution program, using the Intrinsic Phasing solution method. The model was refined with version 2016/6 of **ShelXL** (Sheldrick, 2015) using Least Squares minimisation.

### 9.5.2 Extended experimental

A clear light pink plate-shaped crystal with dimensions  $0.51 \times 0.13 \times 0.05$  mm<sup>3</sup> was mounted on a MITIGEN holder oil. X-ray diffraction data were collected using a Nonius Kappa Apex II diffractometer equipped with a Oxford Cryosystems low-temperature device, operating at  $T = 115$  K.

Data were measured using  $\phi$  and  $\omega$  scans of  $0.60^\circ$  per frame for 243.00 s using  $MoK\alpha$  radiation (X-ray tube, 50 kV, 32 mA). The total number of runs and images was based on the strategy calculation from the program APEX3 (Bruker, 2015). The maximum resolution achieved was  $\Theta = 25.000^\circ$ .

Cell parameters were retrieved using the **SAINT** (Bruker, V8.38A, after 2013) software and refined using **SAINT** (Bruker, V8.38A, after 2013) on 9817 reflections, 6 % of the observed reflections. Data reduction was performed using the **SAINT** (Bruker, V8.38A, after 2013)

Compound	10
Formula	$C_{127}H_{106}Au_4B_4Cl_{26}F_8N_{12}O_4P_4$
$D_{calc.}/g\ cm^{-3}$	1.770
$\mu/mm^{-1}$	4.588
Formula Weight	3892.92
Colour	clear light pink
Shape	plate
Size/mm <sup>3</sup>	0.51x0.13x0.05
$T/K$	115
Crystal System	orthorhombic
Space Group	<i>Pbca</i>
$a/\text{Å}$	25.643(4)
$b/\text{Å}$	9.4006(16)
$c/\text{Å}$	30.308(5)
$\alpha/^\circ$	90
$\beta/^\circ$	90
$\gamma/^\circ$	90
$V/\text{Å}^3$	7306(2)
$Z$	2
$Z'$	0.25
Wavelength/Å	0.710730
Radiation type	$MoK\alpha$
$\Theta_{min}/^\circ$	2.671
$\Theta_{max}/^\circ$	25.000
Measured Refl.	151102
Independent Refl.	6424
Reflections Used	4993
$R_{int}$	0.0918
Parameters	415
Restraints	0
Largest Peak	2.462
Deepest Hole	-2.994
Goof	1.168
$wR_2$ (all data)	0.1979
$wR_2$	0.1845
$R_1$ (all data)	0.0907
$R_1$	0.0732

software which corrects for Lorentz polarisation. The final completeness is 99.90 out to 25.000 in  $\theta$ . The absorption coefficient  $\mu$  of this material is 4.588 at this wavelength ( $\lambda = 0.71073$ ) and the minimum and maximum transmissions are 0.0041 and 0.0206.

The structure was solved in the space group *Pbca* (# 61) by Intrinsic Phasing using the **ShelXT** (Sheldrick, 2015) structure solution program and refined by Least Squares using version 2016/6 of **ShelXL** (Sheldrick, 2015). All non-hydrogen atoms were refined anisotropically. Hydrogen atom positions were calculated geometrically and refined using the riding model. SADABS-2016/2 (Bruker, 2016/2) was used for absorption correction.  $wR_2(\text{int})$  was 0.1173 before and 0.0831 after correction. The Ratio of minimum to maximum transmission is 0.1990. The value of  $Z'$  is 0.25.

### 9.5.3 Reflection Statistics

Total reflections (after filtering)	161317
Completeness	0.999
$hkl_{\text{max}}$ collected	(33, 10, 39)
$hkl_{\text{max}}$ used	(30, 11, 36)
Lim $d_{\text{max}}$ collected	100.0
$d_{\text{max}}$ used	25.64
Friedel pairs	25777
Inconsistent equivalents	0
$R_{\text{sigma}}$	0.0282
Omitted reflections	0
Multiplicity	(6368, 12582, 14535, 15028, 9624, 763, 216, 127, 54, 23, 78)
Removed systematic absences	10171
Unique reflections	6424
Mean $I/\sigma$	20.37
$hkl_{\text{min}}$ collected	(-33, -12, -39)
$hkl_{\text{min}}$ used	(0, 0, 0)
Lim $d_{\text{min}}$ collected	0.84
$d_{\text{min}}$ used	0.84
Friedel pairs merged	1
$R_{\text{int}}$	0.0918
Intensity transformed	0
Omitted by user (OMIT $hkl$ )	44
Maximum multiplicity	41
Filtered off (Shel/OMIT)	30732

## Résumé

Cette thèse s'inscrit dans le développement et l'évaluation de nouvelles plateformes moléculaires pour une application en imagerie optique par fluorescence. Nous avons cherché à développer de nouveaux outils multifonctionnels et modifiables à façon. Cette approche est nécessaire car l'introduction d'un fluorophore peut fortement influencer les propriétés du composé final. Cela signifie que l'introduction du fluorophore sur l'agent sélectionné doit avoir été réalisé dès le départ. Pour cela deux axes principaux ont été étudiés ; le premier consiste à utiliser des BODIPY pour le développement d'agents thérapeutiques traçables pour une application principalement *in vitro*; le deuxième cible sur la conception de plateformes à base d'AzaBODIPY compatibles avec l'imagerie *in vivo*.

Dans la première partie deux fluorophores à base de 3,5-dichloro-BODIPY ont été identifiés comme plateformes prometteuses. Ils ont été fonctionnalisés sélectivement par un agent or(I)-phosphine, un thiosucre et un phosphonium afin de pouvoir étudier l'influence du positionnement de chaque substituant sur les propriétés finales. Nous avons pu démontrer qu'une fonctionnalisation sélective et spécifique est possible avec ces substituants fragiles ; cela nous a permis de développer 12 agents théranostiques à base d'or(I). Les propriétés photophysiques et biologiques ont ensuite été évaluées ; pour cela nous avons déterminé leurs propriétés anti-prolifératives (3 lignées cellulaires), la balance hydrophile, l'accumulation d'or dans les cellules et la localisation des composés par microscopie confocale. Cette stratégie de plateforme multifonctionnelle nous a permis de développer un panel de composés traçables ayant des activités mixtes ainsi que des distributions cellulaires distinctes. Cette étude a permis l'identification et la sélection de trois ou quatre composés qui feront l'objet d'une étude approfondie.

Dans la deuxième partie de cette thèse, nous avons développé des plateformes multifonctionnelles compatibles avec l'imagerie *in vivo* ; pour cela nous avons poursuivi deux approches différentes. La première était l'utilisation de 1,7-di(phénol)3,5-di(phényl)-azaBODIPY, suivi par sa fonctionnalisation sur les groupements OH afin de développer un traceur bioconjugué fluorescent dans le proche infrarouge (NIR-I). Malheureusement, ce traceur possède des propriétés optiques très défavorables. Nous avons alors développé une approche innovante basée sur la fonctionnalisation de l'atome de bore. En s'appuyant sur cette approche deux traceurs fortement fluorescents dans le proche infrarouge et solubles dans l'eau ont été développés. Ces fluorophores ont été conjugués sur un anticorps innovateur afin de permettre l'imagerie optique du ligand PD-L1. Les traceurs se sont montrés stables pour au moins 48h dans le plasma murin et possèdent de très bonnes propriétés optiques. Comme preuve de concept nous avons conduit une étude préclinique *in vivo*. Cette étude a montré que les traceurs sont fortement fluorescents (NIR-I) et ne possèdent pas de toxicité aiguë.

La méthodologie développée pendant cette thèse présente un grand potentiel pour des études allant plus loin et des futures applications ; il est possible d'appliquer les principes et outils développés sur d'autres fluorophores ; la méthodologie permet une fonctionnalisation très riche avec une grande variété de substituants d'intérêt. Son utilisation n'est pas limitée aux applications biologiques, biochimiques et médicinales.

### Mots clés :

	<b>PD-L1</b>	<b>Fonctionnalisation du bore</b>	<b><i>in vitro/in vivo</i></b>
<b>BODIPY</b>	<b>gold(I)-theranostique</b>	<b>Imagerie par fluorescence</b>	<b>hydrosolubilisation</b>
<b>AzaBODIPY</b>	<b>multifonctionnel</b>	<b>Plateforme moléculaire</b>	

## Abstract

The objective of this thesis was the development and evaluation of new molecular platforms for optical fluorescence imaging applications. This work sought to develop new tools that can easily be modified and adapted to the specific needs of the intended use. This is required as the fluorophore will influence the final properties and should thus be incorporated *before* structural optimization of the selected agent rather than at the very end. Two main axes were explored; the use of BODIPYs for the development of trackable therapeutic agents that are primarily intended for *in vitro* applications and the use of azaBODIPYs for the design of an *in vivo* compatible fluorescent platform.

In the first part two fluorophores on the basis of a 3,5-dichloro-BODIPY were identified as promising platforms. These platform molecules were selectively functionalized using a gold(I)-phosphine moiety, a thiosugar and a phosphonium to explore their selective functionalization and investigate the influence of each substituents position on the final properties. We showed that a site-specific, selective functionalization with these fragile substituents is possible and developed 12 gold(I)-bearing therapeutic agents. We evaluated the photophysical properties of all obtained compounds which was followed by a characterization of their biological properties (antiproliferative properties on 3 cancer cell lines, lipophilic balance and cellular gold accumulation as well as fluorescence imaging on 3 cell lines for up to 24h). We succeeded in developing a panel of closely related trackable compounds that display mixed activity in cells and distinct cellular localization. This investigation permitted the selection of three to four hits that will be studied further.

In the second part we developed an *in vivo*-compatible multifunctional platform following two strategies: the first was the use of 1,7-di(phenol)-3,5-di(phenyl)-azaBODIPY and the functionalization of the hydroxy groups for the development of a bioconjugable NIR-I probe. Unfortunately the developed probe displayed very unfavourable optical properties; we therefore developed a new strategy that is entirely based on the functionalization of the boron atom. Using this approach we successfully synthesized 2 watersoluble, strongly fluorescent (NIR-I) molecular platforms that were conjugated to an innovative antibody to image the PD-L1 ligand. The developed probes displayed excellent optical properties, are stable for at least 48h in mice plasma and were validated in a preclinical study on mice. The developed probes displayed strong fluorescence *in vivo* and showed no acute toxicity.

The developed methodology shows great potential for further investigations and future studies; it can be transposed onto other closely related fluorophores and permits versatile functionalization with a large variety of compounds of interest. Its use is thus not limited to biological, biochemical and medical applications.

### Keywords:

<b>BODIPY</b>	<b>Molecular platform</b>	<b>boron- functionalization</b>	<b><i>in vitro/in vivo</i> evaluation</b>
<b>AzaBODIPY</b>	<b>multifunctional</b>	<b>fluorescence imaging</b>	
<b>PD-L1</b>	<b>gold(I)-theranostic</b>	<b>hydrosolubilization</b>	